IAEA-TECDOC-777

Mathematical models and their applications to isotope studies in groundwater hydrology

Proceedings of a final Research Co-ordination Meeting held in Vienna, 1–4 June 1993

INTERNATIONAL ATOMIC ENERGY AGENCY IAEA

The IAEA does not normally maintain stocks of reports in this series. However, microfiche copies of these reports can be obtained from

INIS Clearinghouse
International Atomic Energy Agency
Wagramerstrasse 5
P.O. Box 100
A-1400 Vienna, Austria

Orders should be accompanied by prepayment of Austrian Schillings 100,– in the form of a cheque or in the form of IAEA microfiche service coupons which may be ordered separately from the INIS Clearinghouse.

The originating Section of this document in the IAEA was:

Isotope Hydrology Section
International Atomic Energy Agency
Wagramerstrasse 5
P.O. Box 100
A-1400 Vienna, Austria

MATHEMATICAL MODELS AND THEIR APPLICATIONS TO ISOTOPE STUDIES IN GROUNDWATER HYDROLOGY

IAEA, VIENNA, 1994
IAEA-TECDOC-777
ISSN 1011–4289

Printed by the IAEA in Austria
December 1994

FOREWORD

During the last few decades, the use of tracer techniques in dealing with a variety of hydrological and hydrogeological problems have proved their value in improving the assessment, development and management of water resources. In this regard, the methodologies based on observations of temporal and spatial variations of naturally occurring isotopes, often referred to as 'environmental isotope techniques', are widely employed as an integral part of the routine investigations related to various hydrological systems, and particularly in regional groundwater aquifers.

A substantial amount of isotope data so far collected and published from hydrogeological applications of natural isotopes, however, is often used for qualitative inferences to be made of the system under study, and improved understanding of processes and dynamics of water circulation. The need for improved methodologies for quantitative evaluations to be made from isotope data as regards the relevant physical parameters of the system has been recognized and a co-ordinated research programme (CRP) was initiated by the IAEA for this purpose in 1990. The main objective of the CRP during 1990–1993 was to intensify co-ordinated international efforts into appraisal of existing models and development of further mathematical formulations as a basis for quantitative interpretation of isotope data in groundwater hydrology.

This publication is the result of the CRP and compiles papers summarizing the results and findings of the work undertaken by the participating institutes. Both theoretical aspects of mathematical modelling approaches and their applications to isotope data on actual field results are covered.

Mr. Y. Yurtsever, Division of Physical and Chemical Sciences, was the IAEA officer in charge of designing and implementing the CRP.

It is expected that the information provided will be useful guidance material to scientists involved in research/development of isotope applications in hydrology, as well as to engineers and professionals involved in field applications of environmental isotopes in groundwater systems.

EDITORIAL NOTE

In preparing this document for press, staff of the IAEA have made up the pages from the original manuscripts as submitted by the authors. The views expressed do not necessarily reflect those of the governments of the nominating Member States or of the nominating organizations.

Throughout the text names of Member States are retained as they were when the text was compiled.

The use of particular designations of countries or territories does not imply any judgement by the publisher, the IAEA, as to the legal status of such countries or territories, of their authorities and institutions or of the delimitation of their boundaries.

The mention of names of specific companies or products (whether or not indicated as registered) does not imply any intention to infringe proprietary rights, nor should it be construed as an endorsement or recommendation on the part of the IAEA.

The authors are responsible for having obtained the necessary permission for the IAEA to reproduce, translate or use material from sources already protected by copyrights.

CONTENTS

SUMMARY OF THE CO-ORDINATED RESEARCH PROGRAMME

INTRODUCTION AND BACKGROUND

Environmental isotope methods in water sciences have already reached a stage of routine application to a wide spectrum of hydrological problems encountered in water resources assessment, development and management. The field, often referred to as 'isotope hydrology', is presently a recognized scientific discipline and methodologies so far developed are employed as an integral part of investigations of water resources.

At present, the environmental isotope data collected from field applications, particularly for regional groundwater systems, is often employed for improved understanding of the various processes involved in the occurrence, source and flow dynamics of the groundwater. Need for a more efficient use of the 'information content' of the isotope data for estimating the relevant physical parameters of the hydrological system through formulation and development of appropriate mathematical models for isotope transport in hydrological systems is recognized. This has been the main motivation for the IAEA to initiate and implement a Co-ordinated Research Programme (CRP) on Mathematical Models for Quantitative Evaluation of Isotope Data in Hydrology. The programme had the main objective of co-ordinating joint efforts of interested national institutions in development of modelling formulations for isotope transport processes in hydrological systems and verifying their applicability.

The scope and modality of carrying out the CRP was initially designed at a consultants meeting organized by the IAEA from 4–8 December, 1989 on the topic, during which the present state-of-the-art in available model formulations was reviewed and further research needs were delineated. Subsequently, the IAEA initiated the CRP on the topic during 1990. A total of ten institutions took part in the CRP. The first co-ordination meeting of the programme was held in Vienna from 18–22 November, 1991 to which all chief scientific investigators (CSI) of the contracts/agreements attended, to review the progress made and plan further required work. The second (final) co-ordination meeting was also held in Vienna (1–4 June 1993), during which the overall achievements were reviewed in detail and the programme was concluded. The final manuscripts prepared by each participating institute on the results of their work were also presented and discussed at this final meeting. The final manuscripts are compiled into this technical document.

SCOPE AND ACHIEVEMENTS

Considering that model formulations for different hydrological subsystems (i.e. surface waters, unsaturated zone moisture transport, saturated groundwater flow and transport for different media, etc.) would need different approaches due to different nature of transport processes, the subject matter of the CRP was limited to saturated flow in groundwater systems, where the natural isotopes are most frequently employed. The general modelling formulations included within the scope of the CRP are:

- Linear lumped parameter models,
- Stochastic models for fractured media transport,
- Distributed parameter numerical models of flow and transport with geochemical coupling,
- Compartmental modelling approach,
- Numerical solution algorithms for transport modelling.

The scope of the programme included all above theoretically possible types of formulations, and work undertaken by the participating institutions was related to one or several aspects of these formulations. The work undertaken was both related to theoretical considerations of development of conceptual models and relevant mathematical formulations as well as to their application to actual field data to assess their applicability and data requirements.

Results of the work undertaken and detailed discussions led to the following conclusions as an overview of the capabilities and contributions of different mathematical modelling approaches in isotope data evaluations for groundwater systems.

Lumped parameter models, which are based on tracer input–output concentration relationships, have been developed sufficiently and can be used in practice for interpretation of environmental tracer data. While the simple one parameter models of this type can be employed for systems with inadequate basic hydrogeological data, more complex multi-parameter models can be adopted on the basis of available information. The approach is also useful for systems with multi-component flows when data on more than one environmental tracer are available (i.e. tritium and stable isotope data for two component flow system). The output information of this type of model is always related to the mean transit time of the tracer through the system. Thus, additional data (tracer interactions in the system for non-conservative tracers, porosities of mobile and immobile fractions in double porosity systems) are required to relate transit time obtained from the tracer to that of water. While improvements on the approach could be envisaged through further research, the methodology of lumped-parameter modelling is sufficiently developed now to be widely used in practice. Preparation of user friendly computer codes are most desirable for this purpose.

Distributed parameter models have the advantage of offering a capability for many different and complex processes to be included into isotope transport process description, and their use should be considered whenever feasible. One of the major limitations of the approach is the high spatial and temporal density of the required data. Model development and data collection should be interactive processes linked to each other. Incorporation of the double porosity medium concept into distributed parameter modelling, particularly for isotope data interpretations would be required, and development of efficient algorithms to handle such formulations is desirable. There are presently a good number of computer codes that could be readily transferred for wider scale use in practice. Strong requirements on both computer capabilities and data collection imposed by distributed parameter models to be developed for isotope data evaluations may be a significant limitation for its wide scale use.

Considering the overall tracer and isotope methods in conjunction with data requirements for modelling purposes, the data would probably never be sufficient to truly characterize the system (costs involved, complex spatial distributions observed in natural systems, etc.) and in principle, validation of a model is not possible in its strict sense, since all the data are essentially used to create/improve the model of the system. Best strategy for data collection should include reconnaissance review of all available data and preliminary assessment (discriminating) to identify data that includes real information on the system and processes under investigation (i.e. multi-variate statistical analyses). Data collection should follow such a preliminary stage and the objective of model making should be development of a consistent explanation (or explanations) that will work for all types of data collected, through model simulation trials.

As regards the coupled geochemical transport modelling through distributed parameter modelling, equilibrium models are already available and can be used for long time reactions. Sufficient data and understanding of basic systems exist. These do not include, however, thermodynamic data, such as ion exchange, high concentration trace metals, and isotopes. For systems with chemical transition zone, kinetic controlled reaction models are required. However, lack of data on reaction kinetics in natural settings limits the usefulness of these

models at present. Today, the reliance would need to be on equilibrium models that enable mass balance computations. In this regard, evaluation of data for commonly used natural isotopes of C-14 should be based on understanding of the geochemical processes which control the movement of this isotope in a given hydrological system. Mathematical formulation of the adjustment of C-14 activities should be based on geochemical equilibrium process description.

Multi-compartmental (or multi-cell) modelling formulation facilitates incorporation of available data (hydrogeological, hydrochemical, natural isotopes) into quantitative assessment of hydrological systems. They are particularly useful for cases where the amount of existing data would not justify the use of a distributed parameter numerical modelling approach. Thus, the methodology is more appropriate for regional scale studies to which detailed flow and transport models cannot be applied due to lack of sufficient data, or it can be employed for preliminary quantitative assessment prior to such detailed modelling. At the present stage of development, this approach should be considered as a means of quantitative evaluation methodology rather than an approach to provide a validated transport model for prediction purposes. Advantages of the multi-cell approach are:

- it can easily be adopted to non-steady state cases,
- essential parameters related to mass transport (i.e. dispersivities) are implicitly included in the approach,
- the methodology can also be employed for solution of the inverse problem, i.e. to estimate the distribution of aquifer parameters from tracer data.

This methodology, at the present stage of development, can readily be transferred to the user for the objectives cited above. Incorporation of non-conservative processes into the approach and development of improved solution algorithms would be a desirable improvement on this approach.

New theoretical approaches as regards the formulation of conceptual models of mass transport which are not based on the classical dispersion equation, involve incorporation of tracer data in stochastic transport models, use of stochastic differential equations with averaging procedure, Monte Carlo simulation and channeling concept to describe solute transport in fractured media and role of multi-variate statistical analyses. The new theoretical developments to simulate mass transport in groundwater systems may prove effective to overcome some of the difficulties and limitations inherent in the classical formulation of transport process description, i.e. random character of the observed transit time distributions of water in natural systems, description of various retardation processes and/or retention phenomena and their adequate incorporation in an explicit form into formulations, and description of complex and/or non-stationary boundary conditions.

Based on the results achieved during this CRP, the following are the most important issues delineated to be highest priority areas for further development and research needed in this field:

- Isotopes are necessary mainly to understand the system and enable quantitative estimates of relevant physical parameters of dynamics of transport. The methodology should be made more readily available, through field projects, and applied demonstration studies. A particularly important aspect will be to apply different models on actual 'test cases', where sufficient data are available. This will also enable intercomparison of different approaches.
- Consideration of non-steady state cases is an important aspect to be further developed in the formulations. In this regard palaeoclimatic evidence points to vast changes in the hydrological cycle on temporal scales ranging from diurnal to millennium. Isotopic

studies are the only tool presently available, which can verify the validity of the steady-state assumptions in temporal scale.

- Incorporation of geochemical–chemical processes during transport, particularly for kinetic controlled reactions, needs further experimental data and research.
- Continued work on the use of isotopes as a tool not only for verification but also for calibration of continuum and mixing-cell (compartmental) models is needed.
- Improved understanding of transport processes in the unsaturated zone, and models coupling unsaturated and saturated flow will be a desirable development.

It is expected that the results of the work presented in this publication will be a useful contribution to the scientific community in reflecting the present stage of development in isotope transport modelling as well as indicating some of the important issues still to be considered for further research and development.

ON CALIBRATION AND VALIDATION OF MATHEMATICAL MODELS FOR THE INTERPRETATION OF ENVIRONMENTAL TRACER DATA IN AQUIFERS

A. ZUBER
Institute of Nuclear Physics,
Cracow, Poland

Abstract

Calibration and validation of mathematical models for the interpretation of environmental tracer data in aquifers are reviewed. Definitions of basic terms are recalled and the importance of calibration and validation processes for obtaining satisfactory results is discussed. Due to insufficient data, it is usually difficult to obtain a unique calibration. Even a properly calibrated model does not necessarily supply the required information due the influence of hidden parameters. The ages of ideal tracers are understood as those corresponding to the ages of water molecules, whereas the water ages are understood as those defined by the water flux in Darcy's law. In fissured rocks, flow and tracer velocities (or exit ages) differ by retardation factor caused by matrix diffusion (R_p) which is equal to the ratio of total to fissure porosity, and in a good approximation to the ratio of matrix to fissure porosity. Thus, tracer ages must not be interpreted in terms of water ages. In consequence, though the environmental tritium as well as the stable isotopes of oxygen and hydrogen can be regarded as ideal groundwater tracers, their ages in fractured rocks may exceed by orders of magnitudes the water ages. Useful interpretation and validation possibilities are offered by a modified version of Darcy's law in which the tracer age (t_t) at a given distance (x) can be related to the hydraulic conductivity (k) and gradient (i) at regional scale, if the matrix porosity (n_p) is known from laboratory determinations ($k \cong n_p x/t_t i$). In the case of ^{14}C, additional retardation is caused by interactions between dissolved carbonate species and solid carbonates in the matrix. Due to high values of the interaction coefficients in carbonate rock systems, the movement of ^{14}C is much delayed by factors difficult to estimate, which makes quantitative age determinations by the ^{14}C method unreliable. In porous rocks the tracer age obtained from calibrated models may also differ from the water age due to the use of an inadequate model and/or to other reasons, e.g. due to exchange of tracer(s) between the aquifer and aquiclude. Therefore, model validation should be attempted whenever possible.

1. INTRODUCTION

The present paper is based on several works performed within the Coordinated Research Programme (CRP) of the IAEA on the Mathematical Modelling of Environmental Tracer Data in Groundwaters and devoted to the interpretation of either environmental tracer data [1, 2], or artificial tracer experiments and pollutant movement at different scales [3, 4], or both types of data [5, 6]. Parameters of fissured rocks, which can be determined from artificial tracer experiments and/or pollutant movement, are also of importance for the interpretation of environmental tracer data. Therefore, properly designed artificial tracer experiments can be expected to be useful in some cases for the interpretation of environmental tracer data. Both groups of papers are also related by discussion of the differences between tracer ages (or velocities) and water ages (or velocities), which are of particular importance for fissured rocks. Following the original works [1, 2, 5, 6], the present paper is addressed to the modellers of environmental tracer data in groundwater systems as well as to those who make use of the tracer data, but are not sufficiently familiar with the limitations of the mathematical models commonly applied. The aim of the paper is to discuss the major difficulties and pitfalls of the calibration and validation processes as well as to clarify problems which are often omitted by the modellers and, which, consequently, escape the attention of the users of tracer data. The common sins of the modellers are the application of inadequate models, satisfaction with obtained fit without proving that the calibration is unique, the lack of distinction between fitted (sought) and known parameters, the application of models with too large numbers of sought parameters (which yields ambiguous solutions), and no attempts at performing the validation process.

For determining the parameters of the flow system, or for prediction of its response from environmental tracer data, a quantitative approach is needed and a mathematical model must be employed. The parameters of the model are related to the input-output tracer relations by making use of one, or more, of the following principles: (a) decrease of tracer concentration due to the radioactive decay along flow paths, (b) transfer of variable tracer input by the system, and (c) mass balance of flow and tracer(s) components. Principle (a) is usually employed when individual tracer determinations are available and the tracer input is constant. Principle (b) is employed for tracers with variable concentrations at the entry to a system, and a time record of tracer concentrations at the outlet is available. Principle (c), often in combination with (a) and (b), is particularly applicable when availability of a large number of tracer data distributed in space permits to

model the structure of the system, e.g. by a network of cells or by analytical or numerical solutions to the solute transport equation(s) in which the parameters are allowed to vary in space. Models based on principles (a) and (b) are usually simple, especially when employed to solving the inverse problem, i.e. the values of parameters are sought by calibration (fitting). Models based on principle (c) are usually characterized by a large number of parameters. If the number of independent model equations is equal to the number of parameters, or if parameters can be determined by independent methods, their large number is to the advantage of the model. However, if the number of sought (fitted) parameters is larger than the number of independent equations a unique solution is not available, even if a good fit was obtained. A better fit obtained owing to an increased number of fitted parameters is trivial and such a way for improving the calibration should not be attempted, unless additional parameters are unavoidable and a unique calibration is still available.

Some of the terms and/or their definitions discussed within this paper are not generally known or accepted, and, therefore, they are recalled in the following sections after [1, 3, 7].

2. DEFINITIONS RELATED TO CALIBRATION AND VALIDATION PROCESSES

Conceptual model is a qualitative description of a system and its representation (e.g. geometry, parameters, initial and boundary conditions) relevant to the intended use of the model.

Mathematical model is a mathematical representation of a conceptual model for a physical, chemical, and/or biological system by expressions designed to aid in understanding and/or predicting the behaviour of the system under specified conditions.

Verification of a mathematical model, or its computer code, is obtained when it is shown that the model behaves as intended, i.e. that it is a proper mathematical representation of the conceptual model and that the equations are correctly encoded and solved. A model should be verified prior to calibration.

Model calibration is a process in which the mathematical model assumptions and parameters are varied to fit the model to observations. Usually, calibration is carried out by a trial-and-error procedure. The calibration process can be quantitatively described by the goodness of fit. *Model calibration* is a process in which the inverse problem is solved, i.e. from known input-output relations the values of parameters are determined. The direct problem is solved if for known or assumed parameters the output results are calculated (model prediction).

Validation is a process of obtaining assurance that a model is a correct representation of the process or system for which it is intended. Ideally, validation is obtained if the predictions derived from a calibrated model agree with new observations, preferably for other conditions than those used for calibration. Contrary to calibration, the validation process is a qualitative one based on the modeller's judgment. In the case of the tracer method the validation is often performed by comparison of the values of parameters obtained from the models with those obtainable independently (e.g. flow velocity obtained from a model fitted to tracer data is shown to agree with that calculated from the hydraulic gradient and conductivity known from conventional observations [1, 3, 4, 5]).

Partial validation can be defined as validation performed with respect to some properties of a model [1, 3, 4, 5]. For instance, models represented by solutions to the transport equation yield proper solute velocities (i.e. can be validated in that respect - a partial validation), but usually do not yield proper dispersivities for predictions at larger scales.

Another useful term which can be used either instead of validation or in addition to that term is *identifiability* [8]. A lack of *identifiability* means that it is not possible to corroborate or refute all the constituent hypotheses of a model. If a model cannot be identified there will be little confidence in the model's parameter values [8].

Definitions of validation and the validation process arise a lot of controversies discussed recently in an excellent paper [9] which is recommended to all those interested in mathematical modelling and/or in the results of modelling, though in the present paper somewhat different approach is accepted. Konikow and Bredehoeft [9] stated: "We believe the terms *validation* and *verification* have little or no place in ground-water science; these terms lead to to a false impression of model capability. More meaningful descriptors of the process include *model testing*, *model evaluation*, *model calibration*, *sensitivity testing*, *benchmarking*, *history matching*, and *parameter estimation.*" In the opinion of the present author, the criticism of the validation process is mainly related to improper definitions of that term (which lead to false impressions that the model represents reality) and to a wrong practice in which the calibration process (or its part) is applied as validation (i.e. improper operational definitions of validation are commonly applied in hydrology). The cited authors claim that the models cannot be validated, but only invalidated. However, it is difficult to agree with some of the opinions and arguments expressed in that paper. First of all, if the hydrogeologists do not see the difference between calibration and validation, an effort is needed in a proper education but not in the reduction of the vocabulary. Secondly, if the models cannot be validated but only invalidated, as claimed by the cited authors, it means that either all the models are invalid (can one use invalid models?), or some models cannot be shown to be invalid, and such models should be applied. This seems to be a semantic problem. Finally, the strongest argument against validation is based on its unprecise definitions related to the modeller's judgment. Therefore, Konikow and Bredehoeft [9] are right in stating that *model testing*, *model evaluation*, *sensitivity testing*, and *parameter*

estimation should be included in the process of validation. However, it seems that *model calibration* should be regarded as a separate process which must precede *model validation. History matching* is a term for calibration when time records of data are available. Validation can be obtained if either the parameters of a model found by calibration agree with the values of parameters found independently (within the accuracy satisfying the modeller's needs), or the prediction yielded by a model is checked against new data. However, then the model results and experimental data are compared but not matched. In other words, it is stressed once more that the calibration process should not be identified with validation, which seems to be a common mistake in hydrology.

In order to avoid possible misunderstandings which can be caused by the above given definition that "a model is a correct representation of the process or system for which it is intended", the following definition can be suggested: *Validation is* a process of obtaining assurance that a model satisfies the modeller's needs for the process or system for which it is intended, within an assumed or requested accuracy. If such freedom of choice is not allowed, all the efforts directed at the development of models which "cannot be validated" should be regarded as useless and the models developed should not be applied.

Tracer methods are usually applied in reconnaissance stages of aquifer investigations when neither results at larger time and/or space scales for comparison with predictions, nor results obtained by other methods are available. In such cases, the validation process cannot be performed. In the lack of other choices, the assurance that a model satisfactorily describes the investigated system must be based on experience gained in earlier studies of other systems. However, when new data are available, either recalibration of the model or its validation should be performed.

3. DEFINITIONS RELATED TO THE TRACER METHOD AND THE RELATIONS BETWEEN TRACER AND HYDRAULIC PARAMETERS

3.1. General

The *tracer method* is a technique for obtaining information about a system or some part of a system by observing the behaviour of a specific substance, the tracer, that has been added to the system [10]. In the case of environmental tracers they are added (injected) to the system by natural processes, whereas their production is either natural or results from the global activity of man.

An *ideal tracer* is a substance that behaves in the system exactly as the traced material as far as the sought parameters are concerned, and which has one property that distinguishes it from the traced material [11]. This definition means that for an ideal tracer there should be neither sources nor sinks in the system other than those adherent to the sought parameters. In practice even substances which have other sources or sinks are regarded as tracers, if these sources and sinks can be properly accounted for, or if their influence is negligible within the measurement accuracy [11]. The main

difficulty in the use of some environmental tracers results from the existence of additional sources and sinks. Hydrochemical models which are supposed to account for some of these sources and sinks are usually not well defined due to the complexity of natural systems and the lack of sufficient data.

The definitions of the turnover time (water age), conservative tracer age, and radioisotope age are commonly accepted, though it is not necessarily always well understood when and why they are, or are not, compatible.

The *turnover time* of water in a steady state system (or *mean age* of water leaving a system, or *mean transit time of water*, or *mean residence time of mobile water)* is defined as:

$$t_w = V_m/Q \tag{1}$$

where Q is the volumetric flow rate through the system, V_m is the volume of mobile water. For unidimensional flow systems, which can be approximated by piston flow or dispersion model (discussed further), $t_w = x/v$, where x is the length of the system, and v is the mean transit velocity of water. The same relation holds if the age of water along a chosen flow line is considered. This latter definition is useful for direct comparisons of water ages deduced from tracer ages with flow parameters available from conventional methods (e.g. with flow velocity calculated as Darcy's velocity divided by porosity). For variable flow systems, the mean water age (t_w) is a function of time. For large groundwater systems which contain water recharged under different climatic conditions, Eq. (1) is usually understood as that representing either the present situation, or the reconstruction to the time before an intensive exploitation has been started.

The *mean transit time* of a conservative tracer (t_t), or the *age of tracer leaving the system*, or the *mean residence time of tracer*, is defined by:

$$t_t = \int_0^\infty tc_I(t)dt \Big/ \int_0^\infty c_I(t)dt \tag{2}$$

where $c_I(t)$ is the concentration of tracer resulting from its instantaneous injection at the entrance to the system at t = 0. The tracer age defined by Eq. (2) is equal to the water age defined by Eq. (1) for any model of flow, if the tracer is injected and measured in flux of water, i.e. if it is injected and measured proportionally to the volumetric flow rates of individual flow paths [11, 12, 13, 14], and if there are no stagnant zones

accessible to tracer. In groundwater systems with active flow but containing old waters recharged during the Pleistocene, periods of no recharge probably existed. In such cases the tracer age is expected to be larger than the water ages defined by Eq. (1). Then, the mean tracer velocity ($v_t = x/t_t$) is an apparent quantity, lower than the mean water velocity.

Equation (2) is of basic importance in artificial tracing, whereas in environmental tracing it can be useful for a better understanding of some problems. For a radioisotope tracer, Eq. 2 yields the same value of age as for a conservative tracer, if the correction factor for radioactive decay is introduced.

In the case of steady flow through a groundwater system, the output concentration, c(t), can be related to the input concentration (c_{in}) of any tracer by the well known convolution integral:

$$c(t) = \int_0^\infty c_{in}(t-t')\, g(t')\, \exp(-\lambda t')\, dt' \qquad (3)$$

where g(t') is the system response function ($g(t) = c_I(t)Q/M$, M is the injected mass or activity of the tracer) which describes the residence time (t') distribution of tracer at the outlet [11, 14], and λ is the radioactive decay constant. The type of the model (e.g. the piston flow model, or dispersion model) is defined by the g(t') function chosen by the modeller. The main parameter of any g(t') function is the mean transit time of tracer (age) which is denoted here as t_t for both a conservative tracer and a radioisotope tracer corrected for the radioactive decay [6].

The *radioisotope age* (t_a) is usually defined by the radioactive decay equation for a system with a constant input concentration:

$$c/c_o = \exp(-\lambda t_a) \qquad (4)$$

where c and c_o are the measured and initial radioisotope tracer concentrations, respectively.

Equation (4) is meaningful only in two cases: (a) if a portion of water has been separated since the recharge time, and (b) if the piston flow model (PFM) can be accepted as a good approximation of flow in a given aquifer. Case (a) is self-evident, whereas in case (b) it can easily be shown from Eq. (3) that $t_a = t_t = t_w$, if diffusion of tracer from mobile to stagnant water zones is negligible.

In unconfined homogeneous aquifers the transit times between the recharge area and discharge site along different flow lines have the

exponential distribution, i.e. the exponential model applies (EM). The radioisotope tracer age (t'_a) which is supposed to represent the mean transit time value is then given by [11, 14, 15, 16]:

$$c/c_o = 1/(1 + \lambda t'_a) \qquad (5)$$

It may be shown again that $t'_a = t_t = t_w$, if diffusion is negligible. Evidently, the same c/c_o ratio values yield different ages (t_a or t'_a) depending on the type of flow. It is also evident that the radioisotope age can be defined in different ways depending on the flow model. It is a common practice to regard Eq. (4) as the definition of the radioisotope age, which differs from the water age when the piston flow model (PFM) does not apply. Even if the PFM is applicable, diffusion should be negligible as shown further. Therefore, it is strongly suggested that a radioisotope age, or more generally a tracer age, should be defined by both the tracer and the model employed. For instance, "the piston flow ^{14}C age is....", or "the exponential model tritium age is...". When a tracer age is reported without a reference to the model it is understood that Eq. (4) was employed, but then the age value may have little meaning. Similarly, if the initial tracer concentration (c_o) is not directly measurable but estimated from a special model, and if that model is not reported, the age may also be of little value. Unfortunately, it is a common practice to report ^{14}C ages without reporting the concentrations measured, the hydrochemical model applied for the initial concentration, and the model of flow pattern in the system.

For large groundwater systems which had periods of no recharge in the past, the tracer age is always larger than the water age defined by Eq. (1), unless the mean value of t_w would be calculated for the time span considered. Unfortunately, the data needed for the calculation of the mean water age are not available. Therefore, for such systems, the tracer age may yield lower flow velocities than the real values observed for the flow field which existed before an intensive exploitation. Exploitation of an aquifer may change the flow velocities and directions, which makes comparison with tracer velocities even more difficult.

3.2. Fissured rocks

A number of recent studies have shown that stagnant water in the micropores of matrix material of fissured rocks is an important hold-up reservoir for solutes transported by mobile water in fissures and fractures. The delay of solute movement in caused by diffusion exchange between the fissures and matrix.

The conservative tracer age is much greater than the water age, as shown by the following equation [17, 18]:

$$R_p = t_t/t_w = (V_p + V_f)/V_f = (n_p + n_f)/n_f - n_p \cong (n_p + n_f)/n_f \qquad (6)$$

where R_p is the retardation factor resulting from matrix diffusion, n_p and n_f are the matrix and fissure porosities, respectively; V_p and V_f are the stagnant water volume in the micropores of the matrix and the mobile water volume in fissures, respectively. According to Eq. (6) the tracer age corresponds to the total water volume accessible to tracer, whereas the water age is defined by the mobile water volume, assumed to be in fissures only. If a non-ideal tracer exchanges with the solid matter, a large surface available for exchange in the matrix contributes to its increased delay and greater age as discussed further for the ^{14}C method.

Theoretically Eq. (6) does not depend on the scale. However, the mean transit time of tracer (t_t) is not measurable at small scales due to a high asymmetry of tracer response curves (the g(t) functions), which is caused by matrix diffusion. It is very difficult to define the scale at which Eq. (6) becomes practically applicable [6]. Theoretical tracer curves calculated for different assumed parameters [6, 18] and experience gained in some case studies [5] suggest that for densely fissured rocks, say, several fissures per m^2, the time scale of several months is probably sufficient. For sparsely fissured rocks, a large scale may be difficult to obtain even for the flow along the whole system.

Equation (6) holds for conservative substances. For decaying tracers its applicability is limited because they are usually unable to penetrate the matrix deep enough to occupy homogeneously the whole matrix. The reader is referred to [17, 18, 19] for the derivations of formulas, given in Appendix I, which show that $t_t > t_a > t_w$. It means that in fissured rocks the radioisotope tracer age (t_a) is always greater than the water age (t_w) but usually smaller than the conservative tracer age (t_t). For long-lived radioisotopes in densely fissured rocks (e.g. in the case of ^{14}C in rocks with several fissures per m^2), $t_a \cong t_t$ in a good approximation [2, 19]. Theoretically, for short-lived radioisotopes, e.g. for the pre-bomb era tritium interpreted with the aid of Eq. (4) or (5), t_a (or t'_a) is smaller than t_t and its relation to t_w can be difficult to determine [19].

As mentioned, if Eq. (3) is applied to determine the tracer age for a variable input of a radioisotope (e.g. tritium), the correction factor for the radioactive decay causes that Eq. (3) works as if a conservative tracer were used and yields the mean value of the conservative tracer age, t_t.

From Eq. (6) it follows that Darcy's velocity (v_f) is related to the conservative tracer velocity by [5, 18, 20]:

$$v_f = n_f v = (n_p + n_f)v_t \cong n_p v_t = n_p x/t_t \qquad (7)$$

which means that contrary to the flux of water (mass transport), which takes place in fissures containing the mobile water, the stagnant water in the matrix is the main reservoir for tracer transport (usually $n_p >> n_f$). The following formula results directly from Eq. (7) inserted into Darcy's law [5, 20]:

$$k = v_f/i = (n_p + n_f)v_t/i \cong n_p v_t/i = n_p x/(t_t i) \qquad (8)$$

where k is the hydraulic conductivity and i is the hydraulic gradient. Matrix porosities are usually distinctly larger than 1 % whereas fissure porosities are very often much smaller. Therefore, in practice, the approximate form of Eq. (8), i.e. without n_f, is applicable. Then, the hydraulic conductivity can be found from the solute velocity (or tracer age) and matrix porosity, without any information on the fracture system. Equation (8) differs from the common form of Darcy's law by n_p which replaced n_f, and by t_t (age of tracer, mean transit time of tracer) which replaced t_w (age of water, mean transit time of water).

It is evident that Eqs (7) and (8) are particularly useful for validation of models by comparison of Darcy's velocity or hydraulic conductivity obtained from mathematical modelling of tracer data with those obtained by conventional methods.

The tracer age models are commonly calibrated without taking into account Eq. (6) because the influence of matrix diffusion can be found out only in the process of validation. In general, a number of examples can be given to illustrate the importance of matrix diffusion for solute transport in fissured rocks, e.g. [2-7, 17, 18, 21-23]. Its importance for age determinations and for the validation of the models employed for the interpretation of environmental tracer data has been exemplified in several recent studies [5, 24]. Similarly, it seems that "tracer ages that may exceed the computed hydrologic ages by orders of magnitude" reported in [25] and [26] also result from the matrix diffusion, though other reasons were originally given. In any case, the referred works supply additional arguments that the tracer ages and hydraulic ages may differ by orders of magnitudes, and therefore their definitions must be well understood, and the models employed for their determinations properly calibrated and validated.

Unfortunately, the influence of matrix diffusion on the tracer ages, known since early works of a number of authors (e.g. [17, 18, 21, 22] and approximated for fissured rocks by Eqs (6) and (7), is commonly neglected by modellers. Such practice may lead to serious errors in the interpretation of tracer data in terms of hydrogeologic parameters.

3.3. The ^{14}C method in fissured carbonate rocks

In spite of many limitations, the importance of the ^{14}C dating as a routine method is beyond any doubts for the majority of aquifer lithologies. The main limitation of the method is related to the exchange between the dissolved carbonate species and solid carbonates of the rock material. Low contents of carbonate material in many rocks allows to apply the ^{14}C method with a sufficient degree of confidence. Unfortunately, in fissured carbonate rocks the surface area available for exchange is so large in small micropores of the matrix that the delay of ^{14}C cannot be neglected. For densely fissured rocks with neglected exchange in the fissures, the total retardation factor (R), i.e. the ratio of the ^{14}C-PFM age to the water age, is:

$$t_a/t_w = R \cong [n_f + (R_{ap} + R_{ak})n_p]/n_f = [n_f + R_a n_p]/n_f \qquad (9)$$

where R_{ap} and R_{ak} are the retardation factors caused by instantaneous and kinetic exchange reactions, respectively (Appendix II). The R_{ap}-factor may have values about 3 and the R_{ak}-factor about 20 [2]. For a rock of a moderate porosity, say, 0.05, and the fissure porosity of about 0.01, the retardation due to matrix diffusion only is equal to 6 [R_p = (0.01+0.05)/0.01]. However, for a carbonate rock, if $R_a = R_{ap} + R_{ak} \cong 20$, the total retardation factor is about 100. For chalks and marls, which have average porosities about 0.40, the retardation factor for a conservative tracer is equal to about 40 (for fissure porosity as above), and for ^{14}C it is equal to about 800. For lower fissure porosities than that assumed above, the retardation factors can be larger.

The ^{14}C method has another limitation which is usually tacitly neglected by the modellers. When water flows with differert concentrations of dissolved carbon species meet, the resulting concentration depends not only on ^{14}C concentrations and on volumetric flow rates but also on the concentrations of total inorganic carbon (TIC), or total organic carbon (TOC). In the lumped-parameter approach this effect cannot be taken into account. However, in the MCM approach and the distributed-parameter models it should not be neglected.

3.4. Granular aquifers

The intergranular porosity of granular aquifers is usually much larger than the microporosity of grains, and, therefore the R_p-factor is negligible. However, it may happen that the grains are of high porosity and the R_p-factor should be taken into account (then, the intergranular porosity, n, replaces the fissure porosity in Eq. 6). However, for granular aquifers, the retardation factor is easy to determine because both the intergranular porosity and matrix porosity of grains are measurable.

In confined aquifers of large extend and slow flow, the diffusion exchange between the aquifer and aquiclude may also influence the concentration of tracer along the flow lines [27, 28, 29], and, then, the piston flow model represented by Eq. (4) may yield the tracer age which differs from the water age as discussed further.

4. THE MODELS AND THEIR CALIBRATION AND VALIDATION

An effort was made to use terms more or less generally applied. The classification of the models given below is a modified version of that chosen in [1] to fit the aims of the paper.

4.1. Lumped-parameter models [11, 14]

In the lumped parameter approach the groundwater system is treated as a whole and the variations of parameters within the system are not allowed (e.g. [11, 14]). For a constant tracer input, only single parameter models can yield unique solutions, i.e. Eqs (4) and (5), for the piston flow model (PFM) and the exponential flow model (EM), respectively. When Eqs (4) and (5) are applied to interpret single determinations, unique values of tracer ages are directly obtainable, without any calibration, providing the initial concentration is known. Calibration is performed when a number of individual determinations in a given system are interpreted to obtain isochrones and/or average velocities along chosen flow lines.

In general, the applicability of the lumped-parameter models for the interpretation of tracer data was proved in chemical engineering. In hydrogeology, the validity of Eq. (4) was obtained in a number of case studies of confined, granular, and non-carbonate aquifers. Validation can be regarded as obtained for cases in which the the ^{14}C ages agreed either with conventional flow data (e.g. [31]), or with 10,000 years' isochrone supposed to be represented by the position of the middle of the $\delta^{18}O$ and δD shifts caused by climatic changes at the end of the last glacial period (e.g. see [32]). Note that for the ^{14}C PFM age a constant input is assumed and the

decay of the tracer along the flow lines, whereas for the stable isotopes their step-like change about 10 ka ago and its transfer through the aquifer.

For fissured rocks, it is easy to check that in none of the case studies the ^{14}C ages (or velocities) agreed well with the conventional ages (or velocities). In all these cases an effective porosity was put in Darcy's law to obtain "a good comparison". That effective porosity was never defined nor measured. The values of the effective porosity usually assumed were of the order of 10 %, whicch clearly shows that they were close to the matrix porosity. Therefore, in fact, the approximate form of Eq. 8 was applied, though its meaning was never explained. In the case of the ^{14}C method in carbonate rocks, the effective porosity most probably includes in a hidden form the retardation factor resulting from exchange reactions (see Eq. 9), and, consequently, can even be larger than the matrix porosity.

In the case of the ^{14}C ages an additional difficulty results from the nonconservative behaviour of that tracer and complex hydrochemistry of carbon species. The problem is usually simplified to the determination of the initial activity (C_o), which, sometimes, is included in the calibration process, as discussed in the next section for the ^{36}Cl method.

For a variable tracer input, numerical solutions to Eq. (3) are sought, i.e. the type of the g(t') function and the values of its parameters have to be found by fitting (calibration) of the calculated output concentrations to the experimental values. In addition to the PFM and EM, two other models models are commonly applied, i.e. the dispersion model (DM) and the combined exponential and piston flow model (EPM). The mean tracer age (t_t) is the only parameter of the single parameter models and the main parameter of other models. The dispersion parameter which describes the distribution of transit times is the second parameter of the DM. A proper solution to unidimensional transport equation gives the g(t') function for the DM, but the dispersion parameter, i.e. the distribution of flow times, mainly results from different flow path lengths and velocities between the recharge area and the sampling site, and has nothing to do with the dispersivity known from artificial tracer tests or pollutant transport (exceptions are discussed in Sect. 4.8). The ratio of the total volume of the groundwater system to the volume of its part with the exponential distribution of flow lines is the second parameter of the EPM.

In general, the longer the time record of tracer data, the more reliable are the values of model parameters found by calibration. For a reliable interpretation of tritium data with the aid of lumped-parameter models, several years' record of output concentrations is required. Unfortunately, in practice, hydrogeologists request from modellers the determination of water

age either from a single tritium analysis or from a short record of data, which is not possible in a unique way because a number of models can equally well be fitted (calibrated). Even when several years' record of data is available, a unique calibration cannot be obtained if the number of fitted (sought) parameters exceeds two. The number of parameters is sometimes increased by the modeller when a more sophisticated model is assumed (because of the lack of a good fit for two-parameter models [30], or if the input function is not well known and its determination is included into the calibration process [30]). Two case studies discussed in [30], and a revised interpretation of one of them given in [1], demonstrate the difficulties encountered in searching for a unique calibration even when several years' record of tritium data is available. In general, for the lumped-parameter approach, the lower the number of fitted parameters, the more reliable the model [33].

Lumped-parameter models developed for a variable flow [34] were shown to yield better fits [35] than the models developed for a steady flow and applied for variable flow conditions. However, when the periods of variations are much shorter than the mean tracer age, the gain in the accuracy of calibration is not sufficient to justify the effort required.

References to examples of the validation of the PFM were given above for granular aquifers. Other examples of the validations of the PFM, EPM and EM with the aid of Eq. (8) can be found in [5], where the regional hydraulic conductivities of fissured rocks calculated from the tracer ages were shown to be equal, or close, to those determined by other methods. One of the examples given in [5] is briefly discussed below.

Consider the carbonate system of the Czatkowice karstic springs near Cracow, Poland [5], with a long record of tritium data. For the Nowe spring, the EPM tritium age was 300 years, which for the known matrix porosity of 0.030±0.005 (mean value for the Carboniferous dolomites and Jurassic limestones weighed by contribution of these two formations to the length of the flow system), the mean flow distance of 8,000±2,000 m, and the mean hydraulic gradient of 0.006±0.001 yielded from Eq. (8) $k = (4.2\pm1.5)\times10^{-6}$ m/s, which is in a good agreement with $(4.1\pm1.1)\times10^{-6}$ m/s estimated from Darcy's law for the mean flow rate through the middle of aquifer. For a young component in the Chuderski spring, the EM tritium age was 11±4 years, which for the known matrix porosity of 0.021±0.002, the mean flow distance of 1500±300 m, and the mean hydraulic gradient of 0.07 yielded the hydraulic conductivity of $(1.3\pm0.6)\times10^{-6}$ m/s which is in a good agreement with $k = 1.7\times10^{-6}$ m/s found from numerical modelling of inflow to a nearby quarry.

The carbonate system of Czatkowice is an exception because not only the matrix porosity is known but also the fissure porosity of the Carboniferous dolomites, which is equal to about 0.0015 [5]. Therefore, the R_p-factor is $(n_p + n_f)/n_f = (0.021 + 0.0015)/0.0015 = 15$, which means that the age of water for the groundwater system of the Chuderski spring is $t_w = t_t/R_p = 11/15 \cong 0.7$ a. Assuming the fissure porosity of the Jurassic limestones to be equal to that of dolomites, the R_p-factor for the system of the Nowe spring is $(0.030 + 0.0015)/0.0015 \cong 20$, and the water age is $300/20 \cong 15$ a. Of course, these two water ages applied in the common version of Darcy's law yield similar values of the hydraulic conductivity as those obtained from Eq. (8). However, if the tracer age is applied in the common version of Darcy's law, the hydraulic conductivity completely disagrees with other estimates.

The case study of the Czatkowice springs proves that serious errors are introduced if tracer ages in fissured rocks are identified with water ages without taking into account the retardation factor caused by matrix diffusion. It is also obvious that a large retardation factor can be observed even for a relatively low matrix porosity. Calibration curves shown in [1] demonstrate that a unique calibration is sometimes impossible to obtain even for long records of tritium data. The selection of the proper mathematical model can be obtained only by identification of the conceptual model. In that particular case the identification was obtained on the basis of geological data which allowed to reject the earlier hypothesis on the presence of a tritium free component in both springs, and to assume that the older water component in the Chuderski spring contains the same water as the Nowe spring [1, 5].

4.2. Lumped-parameter models combined with hydrochemical models

Single parameter models, especially the PFM, are often combined with hydrochemical models which take into account the underground production and other losses than that caused by the radioactive decay. As mentioned, for the ^{14}C method, a hydrochemical model for the initial ^{14}C content is sometimes included in the process of calibration, i.e. the type of the model and its parameters are chosen to obtain a better fit.

The PFM combined with simple hydrochemical models is also applied for the ^{36}Cl dating method [36, 37, 38]. In the case of the Great Australian Basin [35, 36] the PFM (Eq. 4) was corrected for secular in situ production of ^{36}Cl, and the calibration procedure consisted of the selection of the most adequate model of $^{36}Cl^-$ and Cl^- hydrochemistry to obtain a good fit of the $^{36}Cl^-$ isochrones to the isochrones calculated from the conventional hydrologic data. Different hydrochemical models yielded "the best fits"

in particular recharge areas, supplying information on the origin of salinity and their relative importance for the whole basin. However, in that case the conventional ages were applied to calibrate the models, therefore the comparison with them cannot be regarded as validation. The agreement between tracer and conventional ages up to 1 million years means that the system was recharged without major breaks under different climatic conditions of the Quaternary, which is difficult to explain considering constant and little scattered values of $\delta^{18}O$ and δD observed along the flow lines [39].

As mentioned, Eq. (4) combined with a simple model of $^{36}Cl^-$ and Cl^- hydrochemistry, which was based on an assumed ion filtration enrichment, was also applied for the Milk River Aquifer [38]. That model yielded a good fit of the $^{36}Cl/Cl^-$ contours to the experimental data, whereas other simple models yielded unacceptable results. The ion filtration model was also shown to explain changes in δD values along the flow lines. The ages obtained yielded flow velocities in agreement with hydraulic determinations. All these facts could be regarded as the validation of the ^{36}Cl age model. However, other mathematical models based on quite different conceptual models yielded equally good fits, which makes the problem of validation unsolved, as discussed further.

4.3. Continuum approaches in unidimensional flow

Some groundwater systems can be approximated by unidimensional flow with exchange of mass along a chosen flow line. Tracer exchange without any change in water flow may result from diffusion between the aquifer and aquiclude [27, 28, 29] whereas changes both in flow and in tracer concentration result either from seepage through the aquitard in confined aquifers [40], or by recharge and irrigation in unconfined systems [41]. Changes in tracer content also result, as mentioned earlier, from retardation and/or underground production, which are most properly considered as continuous processes in differential transport equations (e.g. [42]). The models discussed within this section could be equally well regarded as lumped parameter models. However, it seems that a separate category is convenient for models based on the assumption of a unidimensional flow with a constant, or linearly decreasing or increasing velocity, i.e. for models with lumped flow parameters, and reactions occurring along the flow lines.

The Milk River Aquifer (MRA), which was investigated by several scientific teams, may serve as a good example of difficulties encountered in the validation of mathematical models and in identification of conceptual models. The MRA was initially regarded as a simple hydrodynamic and hydrochemical system because it dips gently from the recharge area, and some

its chemical components are either constant or change their concentrations in a monotonic way [28]. The following discussion does not include some earlier conceptual models of the MRA hydrochemistry based on mixing of two different types of water due to megascopic dispersion and limited recharge area [43]. The ion filtration model for the distribution of $^{36}Cl/Cl^-$ and $\delta^{18}O$ in the MRA was already discussed in Sect. 4.2. The conceptual model of aquiclude diffusion served as a basis for two similar mathematical models, which were calibrated in different ways. Hendry and Schwartz [28] considered diffusion of ^{36}Cl and ^{18}O whereas Nolte et al. [29] also included the underground production of ^{36}Cl in the aquifer and diffusion of inactive Cl^- from the aquiclude. In both cases the transient state was considered, i.e. the active flow through the aquifer was assumed to start in the past (the step input function). The fitted age of the active front in the aquifer corresponds to that past event. The age obtained in [28] for the active inflow of meteoric water was 1-2 Ma whereas the age for inflow of water with a different isotopic composition than those originally contained in the aquifer was 0.25-0.5 Ma. This discrepancy in ages is difficult to explain.

The model of Nolte et al. [29] with the flow parameters found originally was also calibrated to $\delta^{18}O$ and δD data by Małoszewski and Zuber [1] by fitting only the diffusion coefficient of water molecules in the aquiclude (the diffusion coefficient was 1×10^{-10} m/s^2 for H_2O and 6.3×10^{-12} m/s^2 for Cl^-). In [28] the dispersivity was accounted for, though its influence for the assumed value of 100 m was negligible, whereas in [29] the dispersivity was already omitted in the departure equation. The mean flow velocities found in [28] by calibration were 0.10 m/a for flow path 1 (eastern) and 0.07 m/a for flow path 2 (western). They are lower than the values known from hydraulic estimates (0.3 m/a and 0.15 m/a, respectively), which should be expected considering the possible periods of no recharge during the Quaternary. It should be noted that the calibration obtained in [29] and extended to $\delta^{18}O$ and δD data in [1] is free of the discrepancy mentioned above because the age of active flow and the age of inflow of water with a different isotopic composition are the same (0.7 Ma for path 1 and 1.0 Ma for path 2).

Uranium dating is particularly difficult even for aquifers approximated by the PFM because a number of geochemical parameters should be known from independent determinations as shown by the general model of Fröhlich et al. [42]. In spite of a large number of parameters, the calibration is not easy to obtain because of a large scatter of experimental data [42]. The comparison given in [42] of uranium concentrations along flow lines with the ^{14}C ages indicate that ^{234}U and ^{238}U concentrations depend on the age only in

the oxidizing and transition zones of the investigated aquifer (up to about 2 ka). In the reducing zone their concentrations do not seem to depend on the age up to about 14 ka. Much more promising results were obtained for the MRA [44], where for the age range of about 0.01-1.5 Ma the uranium method was shown to yield good agreement with hydraulic data. For the flow path 1, it was 0.2-0.6 m/a and 0.3 m/a, respectively, and for the flow path 1 it was 0.1-0.4 m/a and 0.15 m/a, respectively (The uranium ratio method, which rather yields the uranium migration velocity than the flow velocity [42], yielded 0.1-0.2 m/a [44]). However, that "good agreement" was obtained for the rate constants determined for another aquifer [45]. Without the knowledge of these rate constants the flow velocity cannot be obtained even for a calibrated model. Therefore, it is evident that in the case of the uranium method the calibration cannot yield the flow velocity (age of water) even in granular aquifers without an independent determination of the rate constants.

In general, for large systems as that of the MRA, the tracer ages can be larger than the water age due to possible periods of no recharge during the glaciations, i.e. the tracer ages yield mean apparent tracer velocities which are lower than the mean water velocity, as explained in Sect.3.1.

Two models considered by Nolte et al. [29] for ^{36}Cl and several other models for other radioisotopes [46] yield similar tracer ages which slightly depend on the conceptual model of the MRA hydrochemistry. This means that the tracer ages obtained are reliable, but the conceptual model of the hydrochemistry remains unidentified. It should be noted that Fabryka-Martin et al. [47] proposed another conceptual model, mainly based on the concentrations and concentration ratios of halogens in the MRA and in the Bow Island Sandstone (BIS). They came to a conclusion that the hydrochemistry of the MRA can be explained by diffusion exchange with shale beds within the aquifer, which contain halogens derived from the diagenesis of organic matter in the sediments. The arguments of these authors against the exchange of water and its constituents between the MRA and the BIS are very convincing. Unfortunately, no data were given from the Colorado shales about 600 m thick, which separate the MRA from the BIS and from the Pakowki formation about 120 m thick, which overlies the MRA. The models of Hendry and Schwartz [28] and Nolte et al. [29] were based on the assumption of diffusional exchange with aquicludes in which the initial concentrations of Cl^-, ^{18}O and D were assumed to be similar to those in the BIS, which does not imply that exchange with water in the BIS takes place. There is no doubt that the conceptual model of diffusion exchange with the aquicludes [28] and the mathematical model developed in [29] and its calibration presented both in [29] and [1] give the best quantitative description available for several species in the MRA. On

the other hand, all the models applied so far can be regarded as validated in respect to tracer ages. However, as mentioned above, they are not sensitive enough to other parameters to identify the conceptual model of the MRA hydrochemistry. In fact, the models developed in [28] and [29] also describe the conceptual model of hydrochemistry governed by diffusion from shale beds within the MRA [47], especially if the beds are sufficiently thick to support diffusional exchange for the time span involved. In such a case, the main problem for obtaining a unique calibration is most probably related to determining the initial concentrations in the shale beds. Unfortunately, no data are available from the Colorado shales and Pakowki formation as well as from shale beds within MRA to support or reject any of the available models. The required data would be the diffusion coefficients and tracer profiles in the discussed formations, including observed or extrapolated initial concentrations. Most probably all the discussed phenomena govern the MRA hydrochemistry, i.e. ion filtration through the Pakowki formation, diffusion exchange between the MRA and the aquiclude(s), and diffusion exchange within the shale beds and more permeable parts of the MRA. Only if one of these processes dominates over the others, there is a possibility for its identification by modelling the tracer data.

4.4. Distributed-parameter models with lumping for time records of data

The principles of the multi-cell models (MCM) for the interpretation of environmental tracer data in hydrology were described in [48]. By modelling the cell sizes and flow routes it is possible to account for some variations of parameters in the system. Therefore, this category of models is called here the distributed models with lumping. Its popularity results from an easy conceptual and mathematical formulation. On the other hand, an easy formulation of a model with a large number of cells may lead to too large number of fitting parameters, which, in turn, may lead to an unnoticed ambiguous calibration. The use of this approach for solving the inverse problem from time record of data at a given site seems to be little justified because one- and two-lumped-parameter models give equally good fits [14].

The multi-cell models are also applicable to tracer data in variable flow. They seem to have a distinct advantage over the lumped-parameter models because the are able to model both the concentration and flow variations [49, 50].

4.5. Distributed-parameter models with lumping for space records of data

The multi-cell models (MCM) are particularly suitable for modelling the tracer and inflow (recharge) distributions in space. It is the only method

available at the operational level, for the interpretation of scarce data in large systems which due to the complexity of flow networks cannot be approximated either by the PFM or by continuous flow models discussed earlier, or by distributed parameter models discussed further. The design of a given cell network is determined by a prior knowledge of the flow system, or by calibration procedure, or by both [48]. However, several early case studies are probably not free of doubts related to the lack of unique calibration [1].

The power and some limitations of the MCM-s can be learnt from a recent study of a regional carbonate-alluvial system in Nevada [51]. Conservative tracer, deuterium, was used under assumptions of invariant tracer concentration and recharge rates. Thirty-four deuterium values were used for recharge components and 40 to represent the mean values in cells. It should be positively stressed that contrary to many earlier studies, the number of cells was smaller than the number of deuterium determinations in groundwater. Due to to the lack of constrains three scenarios (models) were considered with somewhat different cell arrangements in three-dimensional cell networks (17 to 20 cells arranged in 2 tiers), recharge distributions and flow routes. The arrangements of the cell networks, cell volumes and recharge/discharge rates were based on earlier hydrogeological investigations. The flow model was calibrated with deuterium to obtain the flow rates between the cells. Once the models were calibrated it was possible to calculate the mean and median ages as well as age distributions. However, it should be noted that due to the conservative character of the tracer and the assumed steady state, the ages obtained depend on known or assumed cell volumes, i.e. they do not represent independent estimates. A radioisotope tracer, or a conservative tracer in a transient state would yield independent age determinations.

For the carbonate part of the system, the effective porosity of 3 % was assumed. As stated in [1], if this value is close to the mobile water porosity (fractures, solution channels, conducting fault zones), the calculated ages correspond to the water ages as defined in the present paper. However, if this value is close to the matrix porosity, the calculated ages correspond to the tracer ages. In the latter case, the mobile water volumes in the carbonate cells are much smaller than those originally estimated.

In spite of a large number of tracer data, the three scenarios considered demonstrate that unique calibration was not possible. It was also clearly stated that it was virtually impossible to verify (validate in the terminology of the present paper) the numbers obtained, especially for the carbonate system [51]. For the mean age of the system of the order of 10 ka, and maximum ages in some cells approaching 100 ka, the assumptions on

invariant recharge rates and concentrations are very weak. Therefore, the parameters obtained by calibration were viewed as first approximations, which can serve as starting points for more sophisticated models or planning purposes [51].

4.6. Multi-tracer multi-cell models (MTMCM)

A novel approach to the multi-cell modelling of environmental tracer data was presented in a series of papers [52, 53, 54, 55, 56]. The principle of this approach is as follows [53]:

"The aquifer is divided into cells within which the isotopes and dissolved constituents are assumed to undergo complete mixing. For each mixing cell, mass balance equations expressing the conservation of water isotopes and dissolved chemicals are written. These equations are solved simultaneously for unknown rates of recharge into the various cells by quadratic programming. The degree to which individual dissolved constituents may be considered conservative is tested a priori by means of equilibrium model such as WATEQF. Constituents which do not pass this test are either disregarded or suitably assigned a small weight in the quadratic program."

The idea is to obtain the flow model for systems without hydrologic information where the hydrochemical data are available from a sufficient number of wells. The number of equations must exceed the number of unknown flows. For the aquifer parameter estimation from additional incorporation of periodic variations of the water table, the wells are also used to measure the hydraulic heads [55]. The method is applied in a constrained way, which means that the number of cells cannot exceed the number of sampling sites. Similarly to the MCM approach, the dispersion in the aquifer is automatically modelled by the number of cells and their arrangement. The general validity of multi-tracer multi-cell modelling (MTMCM) was proved on synthetic data [53].

Similarly to other tracer methods and models, the MTMCM approach is particularly applicable to systems where conventional data hydraulic data are unavailable or inadequate. Therefore, it would be unrealistic to expect a possibility for its validation in each case. It seems that the validity of a given MTMCM approach, whether tested or not, will mainly depend on the presence of a sufficient number of conservative constituents, on the accuracy of assumptions related to the conservative behaviour of nonconservative constituents, and on the validity of assumptions on invariant flow and concentration inputs. In addition, even such conservative tracers as ^{18}O, D, Cl^- and Br^- may change their concentration due to either ion filtration through ion membranes or diffusion exchange with aquicludes. The MTMCM approach in its present form does not account for such effects, which in some cases may lead to false results in spite of a unique calibration.

4.7. Distributed-parameter models based on flow equations

Numerical solutions to the equations of flow conservation and tritium balance were obtained for a phreatic aquifer, which was approximated by unidimensional flow with inflows and outflows caused by recharge and irrigation [41]. The model was well calibrated, similarly as the earlier developed unidimensional MCM approach [57], and both models yielded the same recharge rates, in agreement with conventional estimates.

Numerical model of flow in the carbonate fissured formations of the Paris Basin was partially validated by the comparison of ^{14}C concentrations calculated from the equation of advective flow (a modified version of the PFM) with the observed values [58]. However, the flow rate was calculated for adjusted effective porosity of 15 %, which was not defined. According to Eq. (7) this effective porosity should be understood as $n_f + n_p$. As stated in [1], depending on the modeller's needs and required accuracy, that porosity can be assumed either to be known and the model regarded as validated, or unknown and its value obtained from calibration. However, in the latter case one cannot claim that the model was validated. Quite to the contrary, if laboratory measurements on core samples yielded, say, $n_p = 1\ \% \cong n_{total}$(effective), the model would be invalidated. As stated in Sect. 3.3, the radiocarbon method in fissured carbonate formations yields tracer ages larger than the conservative tracer ages due to the delay caused by exchange reactions. Consequently, in the discussed case the total porosity is most probably much less than the adjusted value of 15 %, and that value involves the R_a-factor (see Eq. 9). Undoubtedly, this interesting study clearly demonstrates some pitfalls of the calibration and validation processes adherent to the tracer method in general, and to the ^{14}C method in particular.

4.8. Distributed-parameter models based on transport equation

As mentioned, the distributed-parameter approach requires a lot of data which can be obtained only in favourable situations. For instance, for a small granular aquifer situated at a flow divide between two watersheds, a dense line of borings and the installation of bundle-type piezometers, each consisting of nine individual piezometers with short slotted and screened tips, permitted to obtain detailed observations of the hydraulic heads and to perform hydraulic tests and tritium sampling at desired depths [58]. A numerical flow model was constructed for the observed cross-section as a prerequisite for the modelling of tritium transport. A known analytical unidimensional solution to the dispersion equation was used and calibrated by selecting the flow velocities and dispersivities along chosen flow lines to obtain fits with the spatial distribution of tritium data along flow lines at

different sites. The dispersion model can be regarded as validated because it yielded flow velocities close to those known from the flow model. The best fit was obtained for the dispersivity of 0.02 m, which for flow velocities of the order of 1 m/a corresponds in approximation to the coefficient of molecular diffusion in granular medium ($D/\tau_p = D_p \cong \alpha_L v$, where D is the coefficient of molecular diffusion in free water, $\tau_p = 1.5$ is the tortuosity factor). The agreement of the observed dispersivity with that expected from the coefficient of diffusion can also be regarded as validation. Note that the parameters of the dispersion model were lumped, however the use of the model for individual flow lines defined by the numerical flow model allows to consider the whole approach as the distributed type. Such low dispersivity is obtained only for individual flow lines. Other types of sampling would lead to much higher dispersivities.

The same aquifer was also modelled by applying two-dimensional solution to the dispersion equation. Calibration and validation were obtained in the way as in the case of the analytical model.

Point sampling of ^{85}Kr [59] along chosen flow lines was also applied in the Bordon aquifer. The piston flow model was used to calculate the ages for these lines. Two-dimensional model dispersion model was also applied. Similar piston flow model was used for environmental Freons observed along chosen flow lines in another aquifer [60].

In all these cases the tracer method was not applied in order to find some hydrologic parameters, but rather to validate the transport models which can in turn be used for prediction of pollutant movement.

5. CONCLUSIONS

Environmental tracer data in groundwater systems can be used in mathematical models either for finding some flow and/or rock parameters of the system or for calibration of flow and/or pollutant transport models. Mathematical modelling can be improved by execution of proper calibration process, and, whenever possible, by validation or partial validation of the model employed.

The relations between flow and tracer parameters should be well understood and taken into account either directly in models or in the interpretation of the results of modelling. In fissured rocks the influence of matrix diffusion leads to tracer ages which may exceed by orders of magnitudes the water ages. This effect, known for more than a decade, is unfortunately seldom taken into account in practice for the interpretation of environmental tracer data, though its importance is commonly accepted for pollutant transport modelling.

For the interpretation of tracer data in fissured rocks, the matrix porosity has been shown to be the most important parameter because tracer data can be related to Darcy's velocity or hydraulic conductivity without any knowledge on the fissure network parameters. Therefore, matrix porosity data of typical rocks should be useful for the interpretation of environmental tracer data. Unfortunately, there is little understanding among the hydrogeologists on the importance of the matrix porosity as the most important transport parameter in fissured rocks.

APPENDIX I.

RELATIONS BETWEEN RADIOISOTOPE TRACER AGES AND CONSERVATIVE TRACER AGES

Equation (4) is usually regarded by hydrogeologists as a general definition of the tracer age, and often wrongly identified with the water age. As discussed in the main text, that equation is meaningful only for aquifers in which the flow pattern can be approximated by the piston flow model. In such cases, the radioisotope age is equal to the mean transit time of water (t_w) only for nonsorbable tracers, and if there are no stagnant water zones into which the tracer is able to diffuse. In fractured rocks, $t_a > t_w$ because of stagnant water in the micropores of the rock matrix. If the fractured network is approximated by a model of parallel fractures of equal aperture and spacing, the solution of the advection equation combined with matrix diffusion equation and with eq. (4) leads to [16, 17 18]:

$$t_a/t_w = 1 + n_p \tanh(p)/(n_f p) \qquad (I.1)$$

with

$$p = (\lambda/D_p)^{1/2}(L/2 - b) \qquad (I.2)$$

where, D_p is the coefficient of molecular diffusion in the matrix, L is the distance between the fractures (axis to axis) and b is the half fracture aperture. For $p \leq 0.25$, Eq. (I.1) simplifies to Eq. (6) with t_t replaced by t_a, whereas for $p \geq 2$ [17, 18]:

$$t_a/t_w = 1 + n_p/(pn_f) \qquad (I.3)$$

In the case of piston flow and an instantaneous injection the solution is [18]:

$$t_{td}/t_w = \frac{n_p(L-2b)}{2b}\left\{\frac{\tanh(p)}{2p} + 0.5\cosh^{-2}(p)\right\} \qquad (I.4)$$

where t_{td} is the mean transit time of decaying tracer. For L >> 2b and p ≤ 0.25, Eq. (I.4) simplifies to Eq. (6), whereas for p ≥ 3

$$t_{td}/t_w = 1 + n_p/(2pn_f) \qquad (I.5)$$

Equations (I.1) to (I.5) differ from Eq. (6) because in the case of a decaying tracer its particles decay during the diffusion process in the matrix and are unable to penetrate the whole depth [17, 18, 19, 27]. Therefore, in general, $t_t \geq t_a > t_w$, which means that a radioisotope age is larger than the the water age, but it can be lower than the conservative tracer age.

A simple estimation of the condition p ≤ 0.25 shows that for the radiocarbon method any spacing not greater than about 0.8 m leads to $t_a/t_w \cong R_p$, if $D_p \geq 10^{-11}$ m^2s^{-1}. Therefore, Eq. (6) can also be accepted as an approximation for the radiocarbon method in densely fissured rocks [2]. Of course, for rocks with higher values of the diffusion coefficient than that assumed above, the fissure spacing can be larger.

Equation (5) was also sometimes applied for the tritium of the pre-bomb era. It can easily be shown that for tritium the condition p ≤ 0.25 is more difficult to satisfy than for the radiocarbon. However, since the beginning of the thermonuclear bomb tests the tritium age is usually determined with the aid of Eq. (3), as the main parameter of the g(t') function found by fitting. Then, due to the correction for the radioactive decay, Eq. (6) is applicable, i.e. the same results are obtained for decaying and nondecaying tracers. It means that similarly to the ^{14}C method, the R_p-factor must be known in order to calculate the water age (mean transit time) from the tritium age. As the retardation factor is seldom known, the water age usually remains unknown. However, other interpretation possibilities are offered by approach discussed in the main text.

APPENDIX II.

RETARDATION FACTORS CAUSED BY EXCHANGE REACTIONS

Assuming that the exchange reactions are governed in part by an instantaneous equilibrium and in part by a kinetic process, the retardation factors caused by exchange reactions in the matrix can be expressed as follows [2, 61]:

$$R_{ap} = 1 + (1 - n_p)\rho k_3/n_p \qquad (II.1)$$

where ρ is the density of the rock matrix and k_3 is the distribution constant

for an instantaneous equilibrium reaction, expressed in units of water volume per unit weight of the solid material [k_3 = (C in solid material in g/g)/(C in water in g/ml) at instantaneous equilibrium]. The retardation factor caused by kinetic reactions is [2, 61]:

$$R_{ak} = k_1/k_2 \qquad (II.2)$$

where k_1 and k_2 are the forward and backward rate constants (dimensions - T^{-1}), respectively. The distribution coefficient (k_d) obtained at the final equilibrium is:

$$k_d = k_3 + \frac{n_p}{(1 - n_p)\rho} \frac{k_1}{k_2} \qquad (II.3)$$

which means that if k_d is used in (II.1) instead of k_3, the R_{ap} factor represents the previous $R_{ap} + R_{ak}$ factor in Eq. (9). The choice of the approach is a matter of convenience depending on which parameters are easier to measure. For instance, in a laboratory experiment the equilibrium was not reached even after 800 hours [62].

It seems that the reaction constants and retardation factors can be measured either in laboratory on rock samples, or in field experiments with artificial tracers [61]. However, it remains an unsolved problem if such experiments can be useful for obtaining conservative tracer ages from ^{14}C ages. Considering large values of the adsorption retardation factors and the expected low accuracy of their determinations, a satisfactory solution does not seem to be easy to obtain.

REFERENCES

[1] MALOSZEWSKI, P. and ZUBER, A., Principles and practice of calibration and validation of mathematical models applied for the interpretation of environmental tracer data in aquifers, Adv. Water Resour. **16** (1993) 173-190.

[2] MAŁOSZEWSKI, P. and ZUBER, A., Influence of matrix diffusion and exchange reactions on radiocarbon ages in fissured carbonate aquifers, Water Resour. Res. **27** 8 (1991) 1937-1945.

[3] MAŁOSZEWSKI, P. and ZUBER, A., On the calibration and validation of mathematical models for the interpretation of tracer experiments in groundwater, Adv. Water Resour. **15** (1992) 47-62.

[4] MALOSZEWSKI, P. and ZUBER, A., Tracer experiments in fissured rocks: Matrix diffusion and the validity of models, Water Resour. Res. **29** 8 (1993) 2723-2735.

[5] ZUBER, A. and MOTYKA, J., Matrix porosity as the most important parameter of fissured rocks for solute transport at regional scales, J. Hydrol. **158** (1994) 19-46.
[6] MALOSZEWSKI, P., Mathematical modelling of tracer experiments in fissured aquifers (PhD dissertation), Freiburger Schriften zur Hydrologie, University of Freiburg (1994).
[7] THE INTERNATIONAL HYDROCOIN PROJECT, LEVEL 2: MODEL VALIDATION, Nuclear Energy Agency, Paris (1990).
[8] KLEISSEN, F.M., BECK, M.B. and WHEATHER, H.S., The identifiability of conceptual hydrochemical models, Water Resour. Res. **28** (1990) 2979-2992.
[9] KONIKOW, L.F., and BREDEHOEFT, J.D., Ground-water models cannot be validated, Adv. Water Resour. **15** 1 (1992) 75-83.
[10] GARDNER, R.P., and ELY, R.L., Radioisotope Measurement Applications in Engineering, Reinhold, New York (1967).
[11] ZUBER, A., Mathematical models for the interpretation of environmental radioisotopes in groundwater systems, Handbook of Environmental Isotope Geochemistry, Vol. 2, Part B (FRITZ, P., FONTES, J-CH., Eds), Elsevier, Amsterdam (1986) 1-59.
[12] KREFT, A., and ZUBER, A., On the physical meaning of the dispersion equation and its solution for different initial and boundary conditions, Chem. Eng. Sci. **33** (1978) 705-708.
[13] KREFT, A., ZUBER, A., Comments on "Flux-averaged and volume-averaged concentrations in continuum approaches to solute transport" by J.C. Parker and M.Th. Genuchten, Water Resour. Res. **22** (1986) 1157-1158.
[14] MAŁOSZEWSKI, P. and ZUBER, A., Determining the turnover time of groundwater systems with the aid of environmental tracers: I. Models and their applicability, J. Hydrol. **57** (1982) 207-231.
[15] ERIKSSON, E., The possible use of tritium for estimating groundwater storage, Tellus, **10** (1958) 472-478.
[16] FRÖHLICH, K, Current aspects in grounwater dating. Freiberger Forschungshefte C417 (1986) 18-32.
[17] NERETNIEKS, I., Age dating of groundwater in fissured rock: Influence of water volume in micropores, Water Resour. Res. **17** (1981) 421-422.
[18] MAŁOSZEWSKI, P. and ZUBER, A., On the theory of tracer experiments in fissured rocks with a porous matrix, J. Hydrol. **79** (1985) 333-358.
[19] MAŁOSZEWSKI, P. and ZUBER, A., Interpretation of artificial and environmental tracers in fissured rocks with a porous matrix, Isotope Hydrology 1983, IAEA, Vienna (1984) 635-651.
[20] ZUBER, A., Review of existing mathematical models for the interpretation of tracer data in hydrology, Mathematical Models for Interpretation of tracer Data in Groundwater Hydrology, IAEA-TECDOC 381, IAEA, Vienna (1986) 69-116.

[21] GRISAK, G.E., PICKENS, J.F., and CHERRY, J.A., Solute transport through fractured media, 2. Column study of fractured till, Water Resour. Res. **20** (1980) 731-739.
[22] FOSTER, S.S.D., The chalk groundwater tritium anomaly - a possible explanation, J. Hydrol. **25** (1975) 159-165.
[23] BIBBY, R., Mass transport of solutes in dual-porosity media, Water Resour. Res. **17** (1981) 1075-1081.
[24] CIĘŻKOWSKI, W., GRÖNING, M., LEŚNIAK, P.M., WEISE S.M., and ZUBER, A., Origin and age of thermal waters in Cieplice Spa, Sudeten, Poland, inferred from isotope, chemical and noble gas data, J. Hydrol. **140** (1992) 89-117.
[25] MAZOR, E., and BOSCH, A., Noble gases in formation fluids from deep sedimentary basins: a review, Applied Geochemistry **2** (1987) 621-627.
[26] MAZOR, E., and KROITORU, L., Phreatic-confined discontinuities and restricted flow in confined groundwater systems, Isotope Techniques in Water Resources Development 1987, IAEA, Vienna (1987) 427-437.
[27] SUDICKY, E.M. and FRIND, E.M., Carbon 14 dating of groundwater in confined aquifers: Implications of aquitard diffusion, Water Resour. Res. **17** 4 (1981) 1060-1064.
[28] HENDRY, M.J. and SCHWARTZ, F.W., An alternative view on the origin of chemical and isotopic patterns in groundwater from the Milk River aquifer, Canada, Water Resour. Res. **24** (1988) 1747-1763.
[29] NOLTE, E., KRAUTHAN, P., KORSCHINEK, G., MAŁOSZEWSKI, P., FRITZ, P. and WOLF, M., Measurements and interpretations of ^{36}Cl in grounwater, Milk River aquifer, Alberta, Canada, Applied Geochemistry **6** (1991) 435-445.
[30] GRABCZAK, J., MAŁOSZEWSKI, P., RÓŻAŃSKI, K. and ZUBER, A., Estimation of the tritium input function with the aid of stable isotopes, Catena **11** (1984) 105-114.
[31] PEARSON, F.J.Jr. and WHITE, D.E., Carbon 14 ages and flow rates of water in Carizo Sand, Atascosa County, Texas, Water Resour. Res. **3** (1967) 251-261.
[32] BLAVOUX, B. and OLIVE, Ph., Radiocarbon dating of groundwater of the aquifer confined in the Lower Triassic sandstones of the Lorraine region, France, J. Hydrol. **54** (1981) 167-183.
[33] HIMMELBLAU, D.M. and BISCHOFF, K.B., Process Analysis and Simulation: Deterministic Systems, Wiley, New York (1968).
[34] ZUBER, A., On the interpretation of tracer data in variable flow systems, J. Hydrol. **86** (1986) 45-57.
[35] ZUBER, A., MAŁOSZEWSKI, P., HERRMANN, A. and STICHLER, W., Tracer relations in variable flow, 5th International Symposium on Underground Water Tracing, IGME (Inst. of Geol. and Mineral Explor.), Athens (1986) 355-360.

[36] BENTLEY, H.W., PHILLIPS, F.M. and DAVIS, S.N., Chlorine-36 in the terrestrial environment, Hanbook of Environmental Isotope Geochemistry, Vol. 2, Part B (Eds P. FRITZ and J.Ch. FONTES) Elsevier, Amsterdam (1986) 427-480.

[37] BENTLEY, H.W., PHILLIPS, F.M., DAVIS, S.N. HABERMEHL, M.A., AIREY, P.L., CALF, G.M., ELMORE, D., GOVE, H.E. and TORGERSEN, T., Chlorine 36 dating of very old groundwater, 1. The Great Artesian Basin, Australia, Water Resour. Res. **22** (1986) 1991-2001.

[38] PHILLIPS, F.M., BENTLLEY H.W., DAVIS, S.N., ELMORE, D. and SWANICK, G.B., Chlorine 36 dating of very old groundwater, 2. Milk River aquifer, Alberta, Canada, Water Resour. Res. **22** (1986) 2003-2016.

[39] AIREY, P.L., CALF, G.E., CAMPBELL, B.L., HARTLEY, P.E., ROMAN, D. and HABERMEHL, M.A., Aspects of the isotope hydrology of the Great Artesian Basin, Australia, Isotope Hydrology 1978, Vol. I, IAEA, Vienna (1979) 205-219.

[40] GEY, M.A., and BACKHAUS, G., Hydrodynamic aspects of carbon-14 dating, Isotope Hydrology 1978, Vol. II, IAEA, Vienna (1979) 631-643.

[41] COLVILLE, J.S., Estimation of aquifer recharge on flow from natural tritium content of groundwater, J. Hydrol. **67** (1984) 195-222.

[42] FRÖHLICH, K., GELLERMAN, R. and HEBERT, D., Uranium isotopes in a sandstone aquifer, Isotope Hydrology 1983, IAEA, Vienna (1984) 447-466.

[43] HENDRY, M.J., SCHWARTZ, F.W. and ROBERTSON, C., Hydrogeology and hydrochemistry of the Milk River aquifer system, Alberta, Canada: a review, Applied Geochem. **6** 4 (1991) 369-380.

[44] IVANOVICH, M., FRÖHLICHh, K. and HENDRY, M.J., Uranium-series radionuclides in fluids and solids, Milk River aquifer, Alberta, Canada, Applied Geochem. **6** 4 (1991) 405-418.

[45] FRÖHLICH, K., Uranium isotope studies combined with groundwater dating as a natural analogue, Natural Analogues in Performance Assessments for the Disposal of Long-lived Radioactive Wastes, IAEA, Tech. Rept Ser. No 304, Vienna (1989) 46-50.

[46] IVANOVICH, M., FRÖHLICH, K., HENDRY, M.J., ANDREWS, J.N., DAVIS, S.N., DRIMMIE, R.J., FABRYKA-MARTIN, J., FLORKOWSKI, T., FRITZ, P., LEHMANN, B.E., LOOSLI, H.H. and NOLTE, E., Evaluation of isotopic methods for the dating of very old groundwaters, a case study of the Milk River Aquifer, Isotope Techniques in Water Resources Development 1991, IAEA, Vienna (1992) 229-244.

[47] FABRYKA-MARTIN, J., WHITTEMORE, D.O., DAVIS, S.N., KUBIK, P.W. and SHARMA, P., Geochemistry of halogens in the Milk River aquifer, Alberta, Canada, Applied Geochem. **6** 4 (1991) 447-464.

[48] SIMPSON, E.S. and DUCKSTEIN, L., Finite state mixing-cell models, Karst Hydrology and Water Resources, Vol. 2, Water Resources Publications, Fort Collins, Colorado (1976) 489-508.
[49] YURTSEVER, Y. and PAYNE, B.R., A digital simulation approach for a tracer case in hydrological systems: multi-compartmental mathematical model, Second Intern. Conf. on Finite Elements in Water Resources, London (1978) 4.165.
[50] YURTSEVER, Y. and PAYNE, B.R., Mathematical models based on compartmental simulation approach for quantitative interpretation of tracer data in hydrological systems, 5th Intern. Symp. on Underground Water Tracing, IGME (Inst. of Geol. and Mineral Explor.), Athens (1986) 341-353.
[51] KIRK, S.T. and CAMPANA. M.E., A deuterium-calibrated groundwater flow model of a regional carbonate-alluvial system, J. Hydrol. **119** (1990) 357-388.
[52] ADAR, E.M. and NEUMAN, S.P., The use of environmental tracers (isotopes and hydrochemistry) for quantification of natural recharge and flow components in arid basins, 5th Intern. Symp. on Underground Water Tracing, IGME (Inst. Of Geol. and Mineral Explor.), Athens (1986) 235-253.
[53] ADAR, E.M., NEUMAN, S.P. and WOOLHISER, D.A., Estimation of spatial recharge distribution using environmental isotopes and hydrochemical data, I. Mathematical model and application to synthetic data, J. Hydrol. **97** (1988) 251-276.
[54] ADAR, E.M. and NEUMAN, S.P., Estimation of spatial recharge distribution using environmental isotopes and hydrochemical data, II. Application to Avaraipa Valley in Southern Arizona, USA, J. Hydrol. **97** (1988) 279-302.
[55] ADAR, E.M. and SOREK, S., Multi-compartmental modelling for aquifer parameter estimation using natural tracers in non-steady flow, Adv. Water Resour. **12** (1989) 84-89.
[56] ADAR, E.M., ROSENTHAL, E., ISSAR, A.S. and BATELAAN, O., Quantitative assessment of the flow pattern in the southern Arava Valley (Israel) by environmental tracers and a mixing cell model, J. Hydrol. **136** (1992) 333-352.
[57] ALLISON, G.H. and HUGHES, M.W., The use of environmental to estimate recharge to a South-Australian aquifer, J. Hydrol. **26** (1975) 245-254.
[58] ROBERTSON, W.D. and CHERRY, J.A., Tritium as an of recharge and dispersion in groundwater system in Central Ontario, Water Resour. Res. **25** (1990) 1097-1109.
[59] SMETHIE, W.M. Jr., SOLOMON, D.K., SCHIFF, S.L. and MATHIEU, G.G., Tracing groundwater flow in the Bordon aquifer using krypton-85, J. Hydrol. **130** (1992) 279-297.

[60] BUSENBERG, E. and PLUMMER, L.N., Use of chlorofluorocarbons (CCl_3F and CCl_2F_2) as hydrologic tracers and age-dating tools: the alluvium and teracce system of central Oklahoma, Water Resour. Res. **28** 9 (1992) 2257-2283.

[61] MAŁOSZEWSKI, P. and ZUBER, A., Mathematical modeling of tracer behavior in short-term experiments in fissured rocks, Water Resour. Res. **26** 7 (1990) 1517-1528.

[62] MOZETO, A.A., FRITZ, P. and REARDON, E.J., Experimental observations on carbon isotope exchange in carbonate-water systems, Geochim. Cosmochim. Acta **48** (1984) 495-504.

A NEW APPROACH TO THE TRANSPORT PROBLEM

N. LIMIĆ, T. LEGOVIĆ
Rudjer Bošković Institute,
Zagreb, Croatia

Abstract

In the first part the assumptions of stochastic transport, from which the conventional dispersion equation is derived, are reconsidered. From more general assumptions on velocity fluctuations an equation that generalizes the conventional dispersion equation is derived. The two equations, conventional and generalized dispersion equations, are compared and properties discussed. Conditions are examined under which use of conventional dispersion equation is allowed.

In the second part, the velocity fluctuations are assumed to have bounded realizations and a new class of models of transport in the mean is derived. This new class essentially differs from the conventional dispersion equation. The basic feature of models is a finite velocity of spreading of substance from source. Finally the transport of substance in groundwaters is studied using the new class of models. A simpler subclass of models is derived and applied for the description of tracer in karstic groundwaters of the Istra peninsula.

List of symbols

b_k, $b_k(\lambda)$, $b_k(\lambda,t)$	amplitudes of dispersion velocity
D	dispersion constant
$\mathbf{v}$, $\mathbf{v}(t)$, $\mathbf{v}(t,x)$	random velocity fields
$\mathbf{w}$, $\mathbf{w}(t)$, $\mathbf{w}(t,x)$	mean fields $\mathbf{w} = \mathbf{E}(\mathbf{v})$
$\mathbf{E}$	operator of the mean over ensemble
$\mathbf{f}$, $\mathbf{f}(t)$, $\mathbf{f}(t,x)$	velocity fluctuations $\mathbf{f} = \mathbf{v} - \mathbf{w}$
c, $c(t)$, $c(t,x)$	random concentration field
C, $C(t)$, $C(t,x)$	mean concentration field $C = \mathbf{E}(c)$
$C(\lambda)$, $C(\lambda,t)$, $C(\lambda,t,x)$	concentration field with the probability $p(\lambda)\,d\lambda$
p, $p(\lambda)$	probability density distribution
q, $q(t,x)$	distribution of input
Φ_k, $\Phi_k(x)$	derministic velocity fields
g_k, $g_k(t)$	random processes
$S(\lambda)$	spectral function

1. INTRODUCTION

In the present article the term conventional dispersion equation is reserved for the linear dispersion equation with advection. The conventional dispersion equation is usually derived from the mass balance equation by applying to it a relationship connecting the flux and concentration gradient by the Fick's law. This approach is basically deterministic because the dispersion is described by average quantities: the average flux of substance and average concentration. On the other side, Fick's law is basically phenomenological. In a fundamental approach to transport, we must start with transport models in

random velocity fields. We know that the conventional dispersion equation describes an average motion in the case that the random velocity field is defined by the Brownian motion. Hence, the random counterpart of the dispersion equation is

$$\frac{d}{dt}\boldsymbol{r}(t) = \boldsymbol{v}(t,\boldsymbol{r}(t)), \qquad (1.1)$$

describing the random motion $\mathbf{r}(t)$ of a particle in the random velocity field $\mathbf{v}$. So far no other stochastic model is known that results in the dispersion equation after the statistical averaging is carried out. Therefore, we must think of the Brownian motion in a wider sense than in the case of molecular diffusion. Since, here, the dispersion equation is used for describing transport on a much larger scale, we must anticipate that the Brownian motion is the underlying random motion of water masses. As far as the dispersion equation is the basic model for describing transport in the mean, the Brownian motion is the basic model for the corresponding random motion of water. In this wider sense the term Brownian motion is used here.

There are several drawbacks of the conventional dispersion equation that are often noted and discussed. After an analysis of assumptions about the random nature of transport, from which the conventional dispersion equation is derived, the following two drawbacks can be particularly marked:

(a) Spreading of tracer around locations of sources i.e. immediately after the release of substance, has been observed to follow the linear law, while the conventional dispersion equation predicts the quadratic law.

(b) Substance spreads with a finite velocity from a source through the space. This apparent fact contradicts the infinite velocity that follows from the conventional dispersion equation.

It is well known that the conventional dispersion equation does not contain information about the spectral function of velocity fluctuations. This fact can be related closely to the drawback (a).

The encountered shortcomings of the dispersion equation have forced researchers to try other methods. Monte Carlo methods (to be denoted by M.C.) are most often exploited among new approaches to this problem. Unfortunately, from the theoretical point of view, this is a step back in the overall study of transport problem. Let us explain this statement.

A M.C. method can be applied if necessary statistics are defined. Schematically, this step is illustrated by the first box in Figure 1. After defining necessary statistics of the stochastic transport one can use a M.C. method to simulate paths of particles and calculate the average concentration in a portion of the medium. The other way is to derive an equation for the average concentration field. The equation must be derived from a stochastic model of transport and defined statistics of velocity fluctuations. This step is theoretical. After an equation is derived, the average concentration field is obtained by solving the equation as illustrated by the box "MODEL SOLUTION".

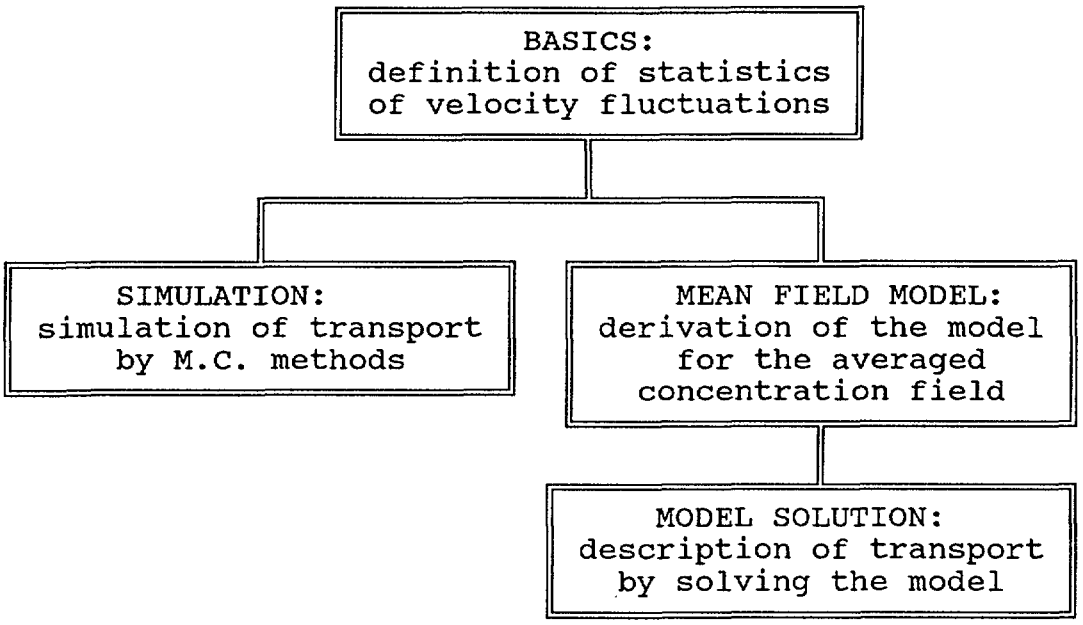

Figure 1. A schematic illustration of two approaches to the transport problem in a random velocity field.

Obtaining an efficient and accurate mean field model, i.e. the step "MEAN FIELD MODEL", is the most difficult part and it is not surprising that up to the present only one exact model has been found and used systematically. Unfortunately, this model is the conventional dispersion equation that exhibits undesirable features which are mentioned in (a) and (b).

To accept or reject the conventional dispersion equation as a transport model seems to be the matter of experience rather than some basic theoretical principle. Therefore, it is of a considerable interest to look for theoretical criteria to make a better judgement about a possible applicability of the conventional dispersion equation.

This article is devoted to 1) reconsideration of principles that are unavoidable in our cognition of transport in a random velocity field, 2) understanding consequences of any simplification that is made in order to derive tractable transport models, and 3) an attempt to derive transport models without simplifications in order to relate drawbacks (a) and (b) to the usually supposed simplifications of the basic principles.

The Brownian motion is defined by the random process with independent increments. Each increment has a normal distribution with zero mean and variance proportional to time. Due to independent increments we have the drawback a) (Limić [1,2]). Because increments are independent the covariance function of velocity fluctuations is proportional to the Dirac δ-function. By removing the independency of increments the drawback (a) can be eliminated. Unfortunately, some other nice features of the conventional dispersion equation are lost. Therefore, in the first part of our study we consider the transport in a random velocity field for which fluctuations are normally distributed but the covariance function is non-trivial, i.e. we assume that the spectral function of velocity fluctuations is general. By keeping unchanged the assumption about normal distribution of velocity fluctuations we are allowed to call the derived equation

the generalized dispersion equation. In Section 3. this generalized equation is studied. Our emphasis is on the comparison of properties of solutions of conventional and generalized dispersion equations rather than their derivations so that details of derivation are omitted.

The drawback (b) is caused by the fact that increments are normally distributed (see [2]). It is naturally, therefore, to omit the assumption about normally distributed velocity fluctuations in order to have a finite velocity of transport. In the new approach the content of steps "BASICS", "MEAN FIELD MODEL" and "MODEL SOLUTION" of Figure 1. differ from the classical derivation of the dispersion equation. In this approach the random process has non-trivial covariance functions and the fluctuations are bounded almost surely. Due to these features the drawback (b) is avoided. This new class of models is studied in the remaining part of this work.

The new class of models that is derived here resembles formally the wave or telegraph equation. It seems that Goldstein [3] was the first to utilize the telegraph equation for description of transport of substance in a turbulent medium. The model was generalized to the case of more dimensions by Bourett [4]. Results of the present work are more general. They are derived from a unique supposition on velocity fluctuations by a method which is developed in [2]. The method is quite general so that it reproduces the conventional dispersion equation as a special case.

2. CONVENTIONAL DISPERSION EQUATION AND BROWNIAN MOTION

To simplify notations and focus our discussion to basic principles of transport in a random velocity field it is admissible to consider the transport in one space dimension.

Let us remind first what is the Brownian motion in one space dimension and what is the meaning of velocity implied by the Brownian motion.

The Brownian motion is the random process $x(t)$ on $[0,\infty)$, $x(t) \in \mathbb{R}$, that is defined by

(i) $x(0) = 0$,

(ii) For $0 \le t_1 < t_2 < \cdots < t_n$, the random variables $x(t_k) - x(t_{k-1})$ are normally distributed and independent,

(iii) For any pair s, t, such that $t > s \ge 0$, the random variable $x(t) - x(s)$ has the zero mean and variance

$$Var[x(t) - x(s)] = 2D(t-s),$$

where D is a positive number that is called the dispersion constant.

The covariance function of this process is $B(t,s) = \min\{s,t\}$. The finite-dimensional characteristic functions can be easily derived. Let $t_o = 0$, $n \in \mathbb{N}$, and $t_o < t_1 < t_2 < \cdots < t_n$. Then

$$\varphi_{t_1,t_2,\ldots,t_n}(p) =$$

$$\exp\left\{-\frac{D}{2}\left[(p_1+p_2+p_3+\cdots p_n)^2 t_1 + (p_2+p_3+\cdots p_n)^2 (t_2-t_1) + p_n^2 (t_n-t_{n-1})\right]\right\}.$$

To the Brownian motion $x(t)$ there corresponds a velocity fluctuation $f(t) = dx(t)/dt$. From the properties (ii) and (iii)

we have $C(t,s) = \mathbf{E}[f(t)f(s)] = 2D\delta(t-s)$ where $\delta(t)$ is the Dirac delta function. Hence, the spectral function of $f(t)$ is $S(\lambda) = 2D$ for all $\lambda \in (-\infty,\infty)$. Realizations of the Brownian motion $x(t)$ are continuous in $\mathbf{R}$, and start form the origin. Let us call them paths. However, time derivatives of these paths, representing velocity fluctuation, are defined only as generalized functions.

To get a feeling about smoothness of paths that are generated by the Brownian motion consider the following example in $\mathbf{R}^2$. Let $D = 1$, $\mathbf{x}(t)$ be generated by the Brownian motion and let us consider another process $\mathbf{y}(t)$, for which the covariance and spectral functions are $K(t) = 2\rho/[\pi(\rho^2+t^2)]$ and $S(\lambda) = 2\exp(-\rho|\lambda|)$. An illustration of paths for both processes is given in Figure 2. For the second process the choice of parameter is $\rho = 2$. The spectral function tends to the value $S(0) = 2$ as ρ tends to zero. To a smaller value of this parameter there corresponds a less smooth path in Figure 2.

If the velocity v in Equation (1.1) is defined by w + f, where w is the mean velocity, $w = \mathbf{E}[v]$, and f is the velocity of the Brownian motion, then the corresponding transport in the mean is described by the conventional dispersion equation

$$\left\{ \frac{\partial}{\partial t} + w(t,x)\frac{\partial}{\partial x} - D\frac{\partial^2}{\partial x^2} + k \right\} c(t,x) = q(t,x). \qquad (2.1)$$

This equation must be supplied with an initial condition at $t = 0$ in order to have a unique solution.

If the mean field w is t- and x-independent solutions of (2.1) can be easily represented by means of the fundamental solution Y that is also known as the Green function. For a constant w the fundamental solution has the form

$$Y(t,x) = \frac{1}{\sqrt{4\pi Dt}} \exp\left(-\frac{(x-tw)^2}{4Dt} - kt \right). \qquad (2.2)$$

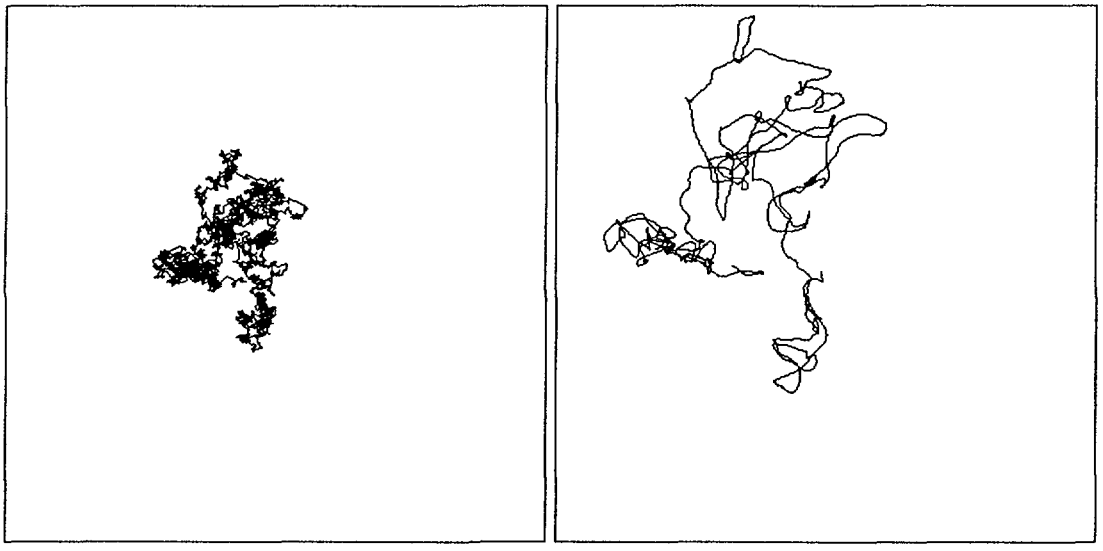

Figure 2. A path (left) generated by the Brownian motion with D =1, and a path (right) generated by the Gaussian process having the spectral function $S(\lambda) = 2\exp(-2|\lambda|)$.

The fundamental solution of the dispersion equation can be interpreted as the mean concentration field resulting from the source at x = 0, differing from zero only for t = 0, i.e. $q(t,x) = \delta(t)\delta(x)$. A general solution of (2.1) can be represented by means of the fundamental solution. Let $c_0(x)$ be the initial condition at $t = t_0$. Then the corresponding solution of (2.1) has the following form

$$c(t,x) = \int_{-\infty}^{\infty} dy\, Y(t-t_0, x-y)\, c_0(y) + \int_{-\infty}^{\infty} dy \int_{t_0}^{t} ds\, Y(t-s, x-y)\, q(s,y). \tag{2.3}$$

In the case of two space dimensions, instead of (2.2) we have

$$Y(t,\mathbf{x}) = \frac{1}{4\pi Dt} \exp\left\{ -\frac{(x_1-w_1t)^2}{4Dt} - \frac{(x_2-w_2t)^2}{4Dt} \right\} \tag{2.4}$$

where x_1, x_2 are components of $\mathbf{x}$ and w_1, w_2 are components of the drift velocity $\mathbf{w}$. The expression (2.3) is valid for the two-dimensional case as well, after Y of (2.4) is substituted and the integration with respect to y is changed into the double integration with respect to y_1 and y_2.

Drawbacks a) and b) can be directly seen from (2.4). Let us consider the process in $\mathbb{R}^2$, $\mathbf{w} = \{w,0\}$, and assume that the process starts at t = 0, so that $c_0(x) = 0$. If q is a "puff" at t = 0 and $\mathbf{x} = 0$, i.e. $q(t,\mathbf{x}) = q_0\delta(t)\delta(\mathbf{x})$, $q_0 > 0$, the resulting concentration field is $c(t,\mathbf{x}) = q_0 Y(t,\mathbf{x})$. This concentration field has isolines in the x_1,x_2- plane, that differ slightly from the curves defined by

$$\frac{(x_1-wt)^2 + x_2^2}{4Dt} = \alpha,$$

where α is the parameter of isolines. These curves are circles having centres at $\{wt,0\} \in \mathbb{R}^2$, moving downstream with the velocity w, and having redia $2(Dt\alpha)^{1/2}$. This behaviour can be easily observed further from source. Around source the radii are proportional to t rather than the square root of t. The drawback (b) can be demonstrated even by simpler arguments. Let the input distribution q(t,x) be zero for $t < 0$ and localized to a bounded domain for all $t > 0$. Then the solution (2.3) of (2.1) is positive on the whole $\mathbb{R}$ for any $t > 0$. The only possible explanation of this fact is by concluding that transport in the mean carries away substance with velocities that are arbitrarily large. Heuristically, we use to say that the dispersion equation allows an infinite velocity of spreading.

3. GENERALIZED DISPERSION EQUATION

The velocity fluctuation f(t,x) is again a Gaussian field, i.e. for fixed $t \in [0,\infty)$ random variables f(t,x) are normally distributed with zero means. In contrast to the previous section,

the random field f(t,x) is not related to the Brownian motion. It is general in the sense that its covariances C(s,t,x,y) = $\mathbf{E}$[f(t,x)f(s,y)] are smooth functions of t, s, x and y. The velocity fluctuation is defined by

$$f(t,x) = \sum_k g_k(t)\ \varphi_k(x), \tag{3.1}$$

where ϕ_k are velocity modes and $g_k(t)$ are random processes on $[0,\infty)$ for which statistics must be defined. The representation (3.1) can be understood as a decomposition of velocity fluctuation into a linear combination of local fluctuations ϕ_k. Each local fluctuation has a random amplitude $g_k(t)$ depending on time. Statistics for g_k are defined by:

$$\sigma_{k_1 k_2 \cdots k_n}(t_1, t_2, \ldots, t_n) = \mathbf{E}[g_{k_1}(t_1)\, g_{k_2}(t_2) \cdots g_{k_n}(t_n)] =$$

$$\int_\Lambda \rho(\lambda)\, d\lambda\ \mu_n(\lambda, t_1, t_2, \ldots, t_n) \prod_{i=1}^{n} b_{k_i}(\lambda, t_i),$$

where b_k are real valued functions, Λ is a set, and $\mu_n(\lambda,t,\ldots,s)$ are statistical moments of a Gaussian process. Again, for the sake of simplicity, the integral over Λ is omitted in the course of our discussion. At the final step the integral over Λ can be included in order to get a general representation of results. Furthermore, the stationarity of processes g_k in the strict sense is assumed so that the statistical moments μ_n depend only on differences $t_i - t_j$. Then the functions b_k become constant, i.e. real numbers. In this way, statistical moments, to be used in our derivations, have the form:

$$\sigma_{k_1 k_2 \cdots k_n}(t_1, t_2, \ldots, t_n) = \mu_n(t_1, t_2, \ldots, t_n) \prod_{i=1}^{n} b_{k_i}. \tag{3.2}$$

The real numbers b_k are still unspecified. In order to match the conventional dispersion equation as closely as possible the numbers b_k are defined by imposing a condition on the covariance function of velocity fluctuations. The second order statistical moment of velocity fluctuations or covariance function is defined by

$$Cov(s,t,x,y) = K(t-s) \left(\sum_k b_k \phi_k(x) \right) \left(\sum_l b_l \phi_l(y) \right), \tag{3.3}$$

where $K(t-s) = \mu_2(t,s)$. The covariance function (3.3) does not depend on space variables if the numbers b_k are chosen in such a way that $\Sigma b_k \phi_k(x)$ is constant on $\mathbf{R}$. Therefore we choose b_k to make the function $\Sigma b_k \phi_k(x)$ equal to 1 on $\mathbf{R}$. Then the standard deviation of velocity fluctuations is t- and x-independent, $\sigma = (\mu_2(0))^{1/2}$.

In the velocity field v, either deterministic or random, the transport problem has a known form that is equivalent to the mass balance for the concentration of considered substance:

$$\begin{aligned} \frac{\partial}{\partial t} C(t,x) + \frac{\partial}{\partial x} (v(t,x)\, C(t,x)) &= q(t,x), \\ C(t_0,x) &= C_0(x). \end{aligned} \tag{3.4}$$

By inserting the representation (3.1) into (3.4) we get

$$\frac{\partial}{\partial t}C(t,x) + \frac{\partial}{\partial x}(w(t,x)\,C(t,x)) + \frac{\partial}{\partial x}(f(t,x)\,C(t,x)) = q(t,x)\,. \tag{3.5}$$

Solutions of (3.4) can be obtained by using a family of stochastic evolution operators U(t,s). The operators U(t,s) are uniquely defined by the following system

$$U(t,t) = I, \quad U(s,t)^{-1} = U(t,s), \quad U(t,\tau)\,U(\tau,s) = U(t,s),$$
$$\frac{\partial}{\partial t}U(t,s) = -\frac{\partial}{\partial x}\,[(w(t,x) + f(t,x))\;U(t,s)]\,, \tag{3.6}$$

Their random nature follows from the randomness of f(t,x). After the evolution operators U(t,s) are calculated, any solutions of (3.4) is represented by

$$C(t,x) = U(t,t_0)\;C_0(x) + \int_{t_0}^{t} U(t,s)\;q(s,x)\;ds. \tag{3.7}$$

In particular, the mean value c(t,x) = E[C(t,x)] can be obtained as

$$c(t,x) = \mathbf{E}[U(t,t_0)]\;C_0(x) + \int_{t_0}^{t} \mathbf{E}[U(t,s)]\;q(s,x)\;ds. \tag{3.8}$$

The representation (3.8) is very similar to (2.3). Much more, these two expressions must be the same if the velocity fluctuation f(t,x) is defined by a Brownian motion. Hence, in this particular case we would have

$$\mathbf{E}[U(t,s)]\,q(t,x) = \int_{-\infty}^{\infty} dy\;Y(t-s,x-y)\;q(s,y)\,,$$

i.e. an integral operator with the kernel equal to the fundamental solution Y of the conventional dispersion equation. For the velocity fluctuations f(t,x) of this section E[U(t,s)] is again an integral operator. Its kernel is proportional to the fundamental solution Z of the following differential equation:

$$\frac{\partial}{\partial t}Z(t,x) = h(t)\;D\;\frac{\partial^2}{\partial x^2}Z(t,x)\,, \quad t > 0, \tag{3.9}$$

where

$$D = \int_0^{\infty} d\tau\;K(\tau)\,, \qquad h(t) = \frac{1}{D}\int_0^{t} d\tau\;K(\tau)\,, \tag{3.10}$$

We have to define another function:

$$e(t) = 2D \int_0^t h(\tau)\, d\tau = 2 \int_0^t dt_1 \int_0^{t_1} dt_2\, K(t_2)\,. \qquad (3.11)$$

With notations, just introduced, the solution of (3.9) is

$$Z(t,x) = \frac{1}{\sqrt{2\pi e(t)}} \exp\left(-\frac{x^2}{2e(t)}\right). \qquad (3.12)$$

The scaling factor $(2\pi)^{-1/2}$ is introduced in order to have

$$\int_{-\infty}^{\infty} Z(t,x)\, dx = 1, \qquad Z(0,x) = \delta(x)\,.$$

The function

$$X(t,x) = \exp(-kt)\; Z(t,x-wt) \qquad (3.13)$$

is evidently a solution of

$$\left\{\frac{\partial}{\partial t} + w\frac{\partial}{\partial x} - h(t)\; D\frac{\partial^2}{\partial x^2} + k\right\} X(t,x) = 0, \qquad t > 0, \qquad (3.14)$$

and can be called the fundamental solution of this equation. The resemblance of the function (3.13) with the fundamental solution of dispersion equation (2.2) is striking. The function (3.13) would be equal to the fundamental solution of dispersion equation (2.2) if the function e(t) in (3.12) had the form e(t) = 2Dt.

Three particular cases of the covariance function K are interesting to discuss:

(a) $\int_0^{\infty} K(s)\, ds \sim t^{-\rho}, \quad \rho > 1,$

(b) $\int_0^{\infty} K(s)\, ds = D > 0$

(c) $\int_0^{t} K(s)\, ds \to \infty.$

In all three cases e(t) behaves as t^2 for small t. As time tends to infinity, the function e(t) in (a) tends to a positive number, in (b) it behaves as Dt, and in (c) it increases to the infinity. The case (b) corresponds to the conventional dispersion law.

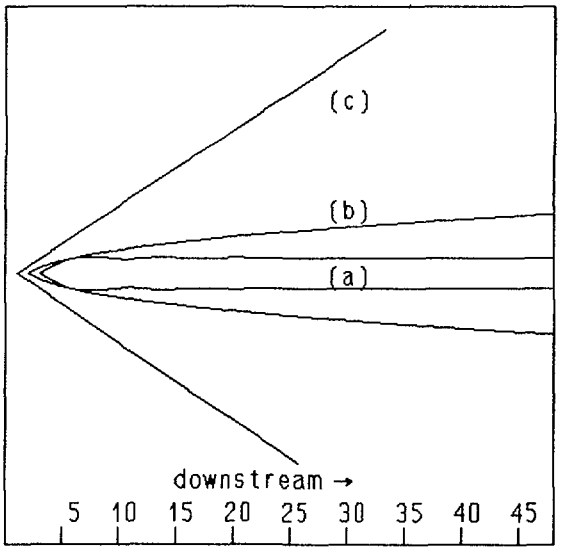

Figure 3. Examples of isolines corresponding to the three cases in (3.15)

The number D can be interpreted as an asymptotic dispersion constant. The solution (3.12) exhibits the linear law for small times and the standard quadratic law for larger times. This property stresses the non-triviality of the obtained model (3.9) in the class of exactly derivable models for the transport of substance in a random velocity field. Thus, (3.9) is an extension of the conventional dispersion law for which the covariance function of velocity fluctuations is a smooth function.

An illustration of properties (a) - (c) is given in Figure 3. Let K(t) be the covariance functions, defined by $K(t) = (2\pi)^{-1} \int \exp(it\lambda)\, S(\lambda)\, d\lambda$, where

$$(a)\quad S(\lambda) = \frac{3}{2}\,\lambda^2\,\theta(1-\lambda^2), \qquad e_1(t) = \frac{3}{\pi}\left(1-\frac{\sin t}{t}\right)$$

$$(b)\quad S(\lambda) = \frac{1}{\pi}\,\frac{1}{1+\lambda^2}, \qquad e_2(t) = \frac{1}{\pi}\left(t - 1 + \exp(-t)\right) \qquad (3.15)$$

$$(c)\quad S(\lambda) = \delta(\lambda), \qquad e_3(t) = \frac{1}{2\pi}\,t^2.$$

With k = 0 and $\mathbf{w} = \{w,0\}$, the straightforward extension of the function (3.13) to the space dimension n = 2 is

$$X(t,x_1,x_2) = \frac{1}{2\pi e(t)}\,\exp\left\{-\frac{(x_1-wt)^2+x_2^2}{2e(t)}\right\}.$$

The curves $X(t,x_1,x_2) = \text{const}$ are drawn in Figure 3.

By using the fundamental solution (3.13) in (3.8), solutions of transport in the mean can be written as a sum of two terms, one including the initial state and the other including input distribution. Let us assume that the process had started at $t = -\infty$, so that an initial state is absent. Then we have

$$c(t,x) = \int_{-\infty}^{t} ds\, \exp\{-k(t-s)\} \int_{-\infty}^{\infty} dy\, Z(t-s,x-y-w(t-s))\; q(s,y)\,. \qquad (3.16)$$

This is a solution of the following integro-differential equation

$$\left\{\frac{\partial}{\partial t} + w\frac{\partial}{\partial t} - D\frac{\partial^2}{\partial x^2} + k\right\} c(t,x) = q(t,x) - D\,\frac{\partial^2}{\partial x^2} \int_{-\infty}^{t} ds \int_{-\infty}^{\infty} dy \qquad (3.17)$$

$$[\,1 - h(t-s)\,]\, Z(t-s,x-w(t-s)-y)\, \exp(-k(t-s))\; q(s,y)\,.$$

The left hand side and the first term on the right hand side of this equation form a conventional dispersion equation. The second term on the right hand side is an additional term which may be interpreted as a correction to the conventional dispersion equation.

4. COMPARISON OF EQUATIONS

An advantage of the conventional dispersion equation to the generalized is, obviously, the simplicity of the former one. This cannot be the crucial point for ruling out the generalized dispersion equation. Their properties must be compared before we make a decision wether to use one or the other. A comparison

reduces to an analysis of the additional term of (3.17). A general discussion is not necessary in order to expose basic features of the term.

Although the conventional dispersion equation (2.1) and the generalized dispersion equation (3.17) are very similar in structure they differ significantly in important features that are listed in Table I.

TABLE I.

prop-erty	conventional dispersion equation (c.d.e.)	generalized dispersion equation
1	time-locality	time non-locality
2	quadratic law of spreading around source	linear law of spreading around source
3	D = S(0)	asymptotically tends to c.d.e. with D =S(0), after switching off the input term
4	time non-reversibility	time non-reversibility

Let us discuss these features one by one.

Time non-reversibility. We start our discussion with the fourth feature because only this feature is shared by both equations. Time non-reversibility means generally that the past cannot be reconstructed from the present (or future). Let us point out that this property is not a mere consequence of taking statistical average (or mean) of stochastic transport models. The class of models of transport in the mean, to be developed in the following section, are time reversible. Hence, the time non-reversibility is a consequence a random nature of fluctuations. Fluctuations are normally distributed so that there is positive probability that their amplitudes are larger than any fixed number. Speaking vaguely, a portion of substance is removed beyond any boundary and cannot be recovered.

Time locality. A system fulfils time locality if its knowledge at t_1 is sufficient for its description at any later time $t_2 > t_1$. In other words, the history of system untill $t = t_1$ does not need to be known for its reconstruction at $t > t_1$. Only its knowledge at $t = t_1$ is necessary and sufficient for such reconstruction. Systems that are defined by differential equations are obviously time local. The generalized dispersion equation is not a differential equation. It is an integro-differential equation that is not equivalent to a system of a finite number of differential equations. Hence, time non-locality is its inherent property. This fact is known for years and can be traced back to the fundamental work of Taylor [5]. There, the turbulent dispersion (or diffusion), is described by means of covariance function of locations of fluid elements (particles) in the Lagrangean picture of motion. The main point is that the complete history of motion of fluid elements must be known in order to calculate the covariance function.

For the present purpose we demonstrate the non-locality of the generalized dispersion equation by using a particular form of the covariance function of velocity fluctuations. The choice enables us to make analytical calculations in close form and obtain solutions as a series. Therefore, we assume that $K(t) = \rho D \exp(-\rho|t|)$ so that $h(t,s) = (1-\exp(-\rho|t-s|)$ and $h(t,s) - 1 = -\exp(-\rho|t-s|)$. A general covariance function can be represented by using the Laplace transform, $K(t) = \int P(\rho)\exp(-\rho|\lambda|)d\rho$, so that the considered covariance function is a basis for a general discussion. The use of the formal operator calculus has some advantage in present derivation. Let us define

$$\Delta = \frac{\partial^2}{\partial x^2}, \qquad L_k = \frac{\partial}{\partial t} + w\frac{\partial}{\partial x} - D\Delta + k$$

and let $c = L_k^{-1}q$ represent formally the expression

$$c(t,x) = \int_{-\infty}^{t} ds\, \exp\{-k(t-s)\} \int_{-\infty}^{\infty} dy\, Y(t-s, x-y-w(t-s))\, q(s,y),$$

i.e. a solution of (2.1) on $\mathbb{R}$. In terms of the defined formal operators the equation (3.17) can be rewritten as

$$L_k c_k = q - D\,\Delta c_{k+\lambda},$$

where the index k in L_k and c_k reminds us that the extinction constant in these expressions is k. The unique solution of this equation is defined by the series

$$c_k = L_k^{-1} \sum_{n=0}^{\infty} (-1)^n \prod_{m=0}^{n} \left(D\,\Delta L_{k+m\lambda}^{-1} \right) q. \tag{4.1}$$

The function c_k is defined for all t and x, so there exists its Fourier transform

$$\hat{c}_k(p_0,p) = \frac{1}{i(p_0+wp) + k + Dp^2} \times \left\{ 1 + \sum_{n=0}^{\infty} \prod_{m=1}^{n} \frac{Dp^2}{i(p_0+wp) + k + m\rho + Dp^2} \right\} \hat{q}(p_0,p) \tag{4.2}$$

The non-locality follows from this expression. The representation (4.2) proves that it is impossible to define a differential equation for the function $c_k(t,x)$. The existence of a differential equation would imply the existence of a polynomial $P(p_o,p)$ in p_o, with coefficients that are general functions of p, such that

$$P(p_0,p)\ \hat{c}_k(p_0,p) = \hat{q}(p_0,p).$$

Obviously that (4.2) does not allow such polynomial.

Law of spreading around a source. This law has been discussed in the previous section for the conventional dispersion equation. The discussion can be completed now by describing the behaviour of solutions of the generalized dispersion equation

around a source. The law of spreading is implied by the form of exponent of the fundamental solution. In the present case, Equation (3.13) must be used. Assumptions about parameters are the same as those at the end of the previous section. For the problem in $\mathbb{R}^2$, isolines of the fundamental solution are very close to the curves

$$(x_1 - wt)^2 + x_2 = 2e(t) = \alpha 4D \int_0^t dt_1 \int_0^{t_1} dt_2 \; h(t_2),$$

where α is a parameter. The right hand side behaves as t^2 for small t, implying that the defined curves are circles, moving downstream with velocity w, and having radii proportional to t for small t.

Dispersion constant and spectral function. From comparison of two equations in terms of the third property in Table I., we can draw the most serious critical remark regarding the applicability of conventional dispersion equation. We dare say that this comparison is fundamental in determining verges beyond which an application of the conventional dispersion equation is meaningless. The present discussion tries to answer the following basic question:

Let velocity fluctuations be normally distributed and have the stationary covariance function K(t) with spectral function S(λ). Is the conventional dispersion equation an adequate tool for describing transport in the mean?

With random nature of velocity fluctuation so assumed, there is no doubt that the average concentration field is given by Expression (3.16). On the other hand, if the conventional dispersion equation were valid, then the average concentration field would be given by (2.3), i.e. as

$$c_{cde}(t,x) = \int_{-\infty}^{t} ds \int_{-\infty}^{\infty} dy \; Y(t-s, x-y) \; q(s,y).$$

Hence, the difference of c of (3.16) and c_{cde} must be estimated in order to answer the formulated basic question.

Two situations are discussed separately, one admitting the applicability of the conventional dispersion equation and the other conflicting it.

The first situation is characterized by switching off input at t = 0. A simple estimate can be derived if we assume that the covariance function has the same form as in discussion of the previous property, q is spatially localized at the origin, i.e. $q(t,x) = q_0(t)\theta(-t)\delta(x)$, and w = 0. Hence

$$c_{cde}(t,x) = \int_{-\infty}^{0} ds \; Y(t-s, x) \; q_0(s).$$

Then, for any t, that is positive and large enough, $c_{cde}(x) > c(x)$ and we have the following estimate

$$c_{cde}(t,x) - c(t,x) = \int_{-\infty}^{0} ds\ [\ Y(t-s,x) - X(t-s,x)\ ]\ q_0(s) \leq$$

$$\int_{-\infty}^{0} ds\ Y(t-s,x) \left\{ \frac{x^2}{4D(t-s)} - \frac{x^2}{2e(t-s)} + \frac{1}{2} \ln\left(\frac{4D(t-s)}{2e(t-s)} \right) \right\} \times$$

$$\frac{X(t-s,x)}{Y(t-s,x)}\ q_0(s)\ .$$

For t positive and large enough we have X < Y so that

$$c_{cde}(t,x) - c(t,x) \leq \left[\frac{(1+4D)x^2}{8\rho Dte(t)} + \frac{2}{\rho t} \right] c_{cde}(t,x),$$

and the corresponding asymptotic behaviour of the relative error is

$$\frac{c_{cde}(t,x) - c(t,x)}{c_{cde}(t,x)} \sim \frac{2}{\rho t}.$$

From the definition of dispersion constant D in (3.10) there follows the identity $2D = \int k(t)\ dt = S(0)$ and, thus, the property 3 of Table I. is established for this particular case of covarinece function. However, the same is true for a general form of covariance function K(t). For the corresponding proof details of the asymptotic behaviour of X(t,x)/Y(t,x) must be derived first.

In the second situation, contrary to the first one, the input is different from zero for all t > 0. We assume that the input is constant with respect to t so that stationary conditions of the transport can be achieved at t = ∞. Again, an example of the covariance function is discussed because general case can give no new essential features. The assumption about the covariance function, drift velocity w, and input q are the same as in the previous case. Only the input term is not switched off at t = 0. With so accepted parameters of generalized dispersion equation, its solutions tend to time independent functions as t → ∞. Let us denote the corresponding limit by $c_k(x)$. Formally, $c_k(x)$ is represented by (4.1) where $L_k = -D\Delta + k$. Hence, the Fourier transform of $c_k(x)$ is

$$\hat{c}_k(p) = \frac{1}{k+Dp^2} \left\{ 1 + \sum_{n=1}^{\infty} \prod_{m=1}^{n} \frac{Dp^2}{k+m\rho+Dp^2} \right\} \hat{q}(p)\ .$$

Because of $\hat{q}(p) = 2\pi q_o$, we have

$$c_k(0) > 2\pi q_0 \int_{-\infty}^{\infty} dp\ \frac{1}{k+Dp^2} + 2\pi q_0 \int_{-\infty}^{\infty} dp\ \frac{Dp^2}{(k+Dp^2)\ (k+\rho+Dp^2)}\ .$$

The first term on the right hand side is the unique solution of stationary, conventional dispersion equation $L_k c_{cde} = q$, so that

$$\frac{c_k(0) - c_{cde}(0)}{C_{cde}(0)} > \frac{\sqrt{k}}{\sqrt{k+\rho} + \sqrt{k}}. \qquad (4.3)$$

A striking conclusion is implied by this inequality. The relative error between stationary solutions of the conventional and generalized dispersion equations can be close to 50%.

To larger values of ρ there corresponds a better approximation by the conventional dispersion equation. As ρ tends to infinity the spectral function tends to a constant, i.e. to the spectral function of velocity fluctuations induced by the Brownian motion.

There is another interesting result of the present analysis. For the same random model of velocity fluctuations, i.e. for the same ρ in terms of our example, reliability of results of the conventional dispersion equation depends on the extinction constant k. Let $\mu = \rho/k$. If $\mu \geq 100$, the relative error (4.3) is less than 10%. On the other hand, for $\mu \approx 1$, the relative error can be up to 30%.

The following example of transport in a bay can illustrate better this dependence on extinction. A spectral function of velocity fluctuations in a bay cannot be fitted with the function $S(\lambda) = 2D\rho^2/(\lambda^2+\rho^2)$ because of many local minima and maxima in a real spectrum. Such a fit can be understood, as a zero order approximation. With this assumption, we can say that the parameter ρ has a value in the range 0.05 - 0.1 h^{-1}. A coliform bacteria in the sea has the extinction constant $k = 0.3$ h^{-1} while hydrocarbons (dissolved oil components) have $k = 0.005$ h^{-1}. It follows from our analysis that the conventional dispersion equation can be used for the description of transport of hydrocarbons in the sea, while the use of this equation for transport of coliform bacteria is dubious. It is worthwhile to point out that a reliable description of the transport around sources for short-lived pollutants is crucial in applications.

Results obtained so far regarding comparison of the conventional and generalized dispersion equation were derived by using one class of covariance functions, $K(t) = \rho D\exp(-\rho|t|)$. Now we can derive indirectly a conclusion which is valid for general covariance function. The considered class of covariance functions is defined by two parameters, D and ρ. The first parameter, D, is the dispersion constant, while the second parameter, ρ. is a measure of extinction of the correlation between fluctuations at a time s and time s+t. This is a simple consequence of the fact that the correlation coefficient is $\exp(-\rho|t|)$. Hence $T = \ln 2/\rho$ is the half-life of correlation in the same way as $E = \ln 2/k$ is the half-life of extinction of the dissolved substance. The ratio $\mu = \rho/k$ can be expressed in terms of half-lives:

$$\mu = \frac{E}{T}. \qquad (4.4)$$

Thus, if this ratio is large then the approximation by conventional dispersion equation is good. Such conclusion is wholly plausible. In terms of the transport it follows that to a larger ratio there corresponds a larger amount of substance surviving in a new realization of velocity field which is not correlated with the previous realization. The conventional dispersion equation describes the transport precisely in such realizations of velocity fields, i.e. in velocity fields with uncorrelated fluctuations. Now a generalization of this simple result is straightforward. It suffices to determine the half-life of the covariance function of velocity fluctuations. This

quantity can be obtained by various methods. One is proposed here by defining the zero order fit of the spectral function. After the half-life of correlation is determined the dimensionless parameter μ is used as an indicator of reliability of results obtained by the conventional dispersion equation.

5. A SIMPLIFIED APPROACH

Let us consider the transport of substance through a duct spreading along the x-axis. We assume that the cross section of the duct does not change so that all parameters and fields depend only on time, t, and one space variable, x.

Here, we consider a simplified stochastic transport. A particle is moved through the duct with a random velocity v(t) depending only on time. This is the first step in simplification because v generally depends on time and space variables. We can define the mean value of velocity $w(t) = \mathbf{E}(v(t))$ and fluctuation $f(t) = v(t) - w(t)$. The next simplification consists in defining the fluctuation by $f(t) = \nu\, w(t)$ where ν is a random variable. Thus, we assume that the random nature of f(t) is completely defined by the time-independent random variable ν. This simplification may appear drastic since we are aware that general velocity fluctuations depend on time and space in a more complex way. Let the random variable ν have the probability density p, which is positive on the interval (-1,1). The probability that the fluctuation f has values in a sub-interval (λ_1,λ_2) is equal

$$\mathbf{P}\{f\epsilon(\lambda_1,\lambda_2)\} = \int_{\lambda_1}^{\lambda_2} d\lambda\; p(\lambda)\,.$$

With this simple definition of velocity fluctuation f(t), the velocity has the form $v(t) = (1+\nu)w(t)$. Its realizations have always the direction of w(t) and the amplitudes are proportional to w(t).

Now we can describe the transport in the following way. A particle can have the velocity $(1+\lambda)w(t)$ with the probability $p(\lambda)\,d\lambda$. A cloud of particles that is initially defined by the distribution $C_0(x)$ at t=0, changes in t so that its realization at a time moment t>0 has the form:

$$C(\lambda,t,x) = \frac{1}{2}\left[C_0(x-(1-\lambda)z(t)) + C_0(x-(1+\lambda)z(t))\right],$$
$$z(t) = \int_0^t w(s)\; ds, \tag{5.1}$$

with the probability $p(\lambda)\,d\lambda$. Hence, the expected concentration field at t is

$$c(t,x) = \mathbf{E}(C(t,x)) = \frac{1}{2}\int_{-1}^{1} d\lambda\; p(\lambda)\; C(\lambda,t,x)\,. \tag{5.2}$$

If the initial distribution C_0 is proportional to the Dirac δ-function, this expression has a simple form. Let $C_0(x) = A\delta(x)$. Then

$$c(t,x) = \frac{A}{2\,z(t)}\,\left[\,p\left(\frac{x}{z(t)}-1\right) + p\left(-\frac{x}{z(t)}+1\right)\right]. \qquad (5.3)$$

In the case of a conservative tracer, the mean transient time t_0, at a position x, is defined by

$$t_0 = \frac{\int c(t,x)\; t\; dt}{\int c(t,x)\; dt}.$$

Assuming the symmetry of the function p we have the following expressions

$$\int c(t,x)\; t\; dt = \frac{Ax}{w^2}\int_0^1 (1-\lambda)^{-2} p(\lambda)\, d\lambda,$$

$$\int c(t,x)\; t\; dt = \frac{A}{w}\int_0^1 (1-\lambda)^{-1} p(\lambda)\, d\lambda,$$

and consequently

$$t_0 = \kappa\,\frac{x}{w}, \qquad \kappa = \frac{\int_0^1 (1-\lambda)^{-2} p(\lambda)\, d\lambda}{\int_0^1 (1-\lambda)\, p(\lambda)\, d\lambda}.$$

Since $(1-\lambda) > (1-\lambda)^2$ for $\lambda \in (-1,1)$ we have $\kappa > 1$.

Let us illustrate the obtained results by two simple examples. Relevant quantities for the first and second example are denoted by subscript 1 and 2, respectively. Let:

$$p_1(\lambda) = \frac{3}{4d}\left(1-\frac{\lambda^2}{d^2}\right)\,\theta\left(1-\frac{\lambda^2}{d^2}\right),$$
$$p_2(\lambda) = \frac{2}{d^4}\left(|\lambda|-d\right)^2\left(|\lambda|+\frac{d}{2}\right)\,\theta\left(|\lambda|-d\right), \qquad (5.4)$$

where d is a parameter defining the interval [-d,d] outside which the densities p_i are zero. The graphs of p_i are illustrated in Figure 4. The corresponding functions $c_i(t,x)$ can be expressed by means of rational functions. We have

$$c_1(t,x) = \left\{ \begin{array}{cc} \frac{3}{4d^3wt}\,A\,\left(\frac{3}{2}-\frac{r}{t}\right)\left(\frac{r}{t}-\frac{1}{2}\right), & \frac{2r}{3} \le t \le 2r, \\ 0 \qquad otherwise & \end{array} \right\}, \qquad (5.5)$$

$$c_2(t,x) = \left\{ \begin{array}{cc} \frac{2}{d^4wt}\,A\,\left(\left|\frac{r}{t}-1\right|-d\right)^2\left(\left|\frac{r}{t}-1\right|+\frac{d}{2}\right), & \left|\frac{r}{t}-1\right| \le d, \\ 0 \qquad otherwise & \end{array} \right\}, \qquad (5.6)$$

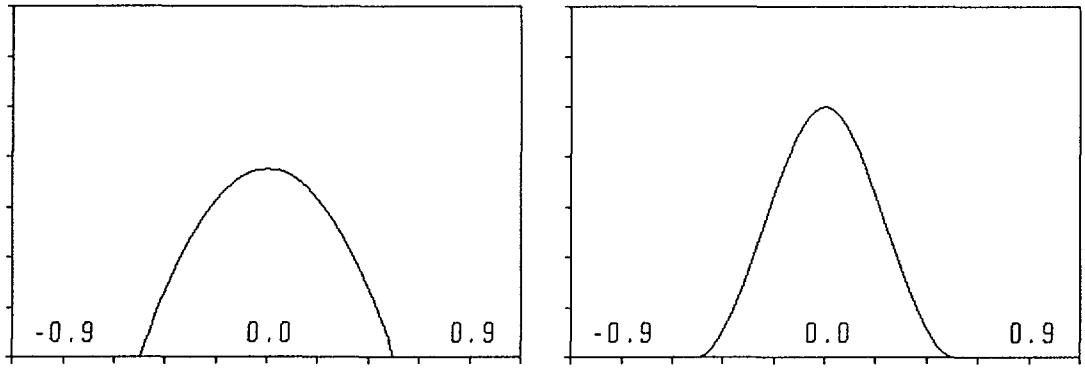

Figure 4. Probability densities p_1 and p_2.

where r = x/w. For w=0.1 and r = x/w = 9 the graphs of these functions are illustrated in Figure 5.

The expression (5.1) represents a travelling wave along the x-axis. The wave is initially defined by the distribution c_0 and after initial moment it splits into two components. One component travels with the velocity (1+λ) w(t), and the other travels with velocity (1-λ)w(t). Therefore, it is not surprising that the function (5.1) is a solution of the following telegraph (wave) equation:

The construction of the concentration field (5.1) was easily carried out because the velocity v(t) was x-independent. For a

$$\left(\frac{\partial}{\partial t} + w(t)\frac{\partial}{\partial x}\right)^2 C(\lambda,t,x) - \lambda^2 w(t)^2 \frac{\partial^2}{\partial x^2} C(\lambda,t,x) - w^{-1}(t)\frac{\partial}{\partial t}w(t)\left(\frac{\partial}{\partial t} + w(t)\frac{\partial}{\partial x}\right) C(\lambda,t,x) = 0. \tag{5.7}$$

velocity fluctuation depending on x the concentration field c(t,x) cannot be constructed by the present simple technique. The derivation of the field must follow the path: "BASICS", "MEAN

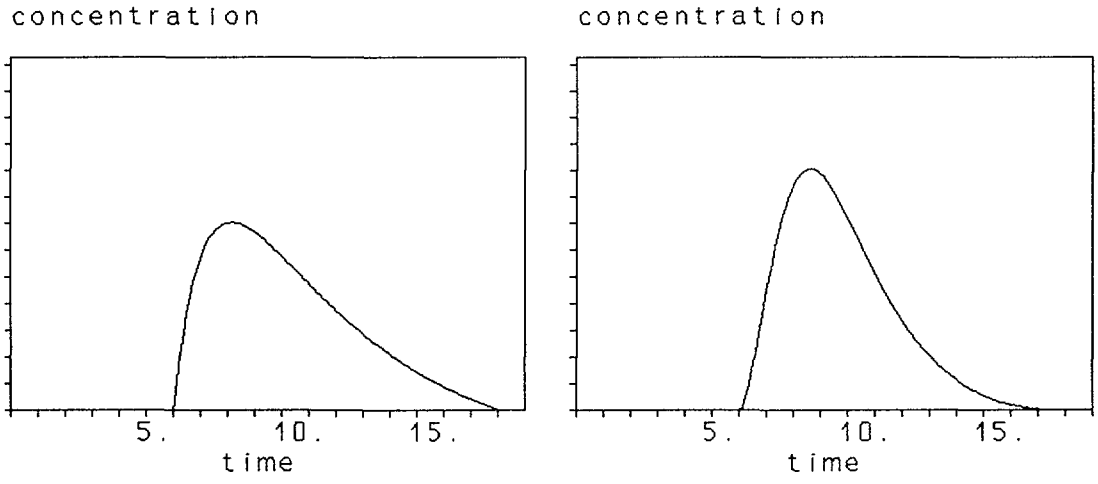

Figure 5. Graphs of concentration fields (4.5), (4.6) measured at the point x = 0.9 units downstream from the source.

FIELD MODEL", and "MODEL SOLUTION" of Figure 1. This means that a family of models such as (5.7) must be derived first and then solutions $C(\lambda,t,x)$ can be obtained by a numerical method. This program can be carried out for a general case of transport problem in a random velocity field as described in [1,2]. Due to a larger number of details of mathematical nature we prefer to avoid an exposition of this rather theoretical problem.

6. A CASE STUDY

Results of an experiment [6] in which tracer is transported through groundwaters of the Istra peninsula (Figure 6.) are analyzed. The terrain is karstic. Tritium was used as a tracer. Tritium was injected on 16.03.1976. into a cave at Čiže (Figure 7). At the end of experiment 99.87 % of the injected tracer was recovered at the Gradole spring. First occurrence of the tracer appeared 5.72 days after release. The peak of the tracer concentration was recorded 7.42 days after the injection (Figure 8). Tracer was also monitored at two other springs in the vicinity (100 m and 250 m) of Gradole but no tritium was found. This indicates that the flow resembles an underground "river". Geographical distance between Čiže and Gradole is 14 km. The corresponding difference in elevation is 260 m. It follows from this data that the velocity of water corresponding to the peak

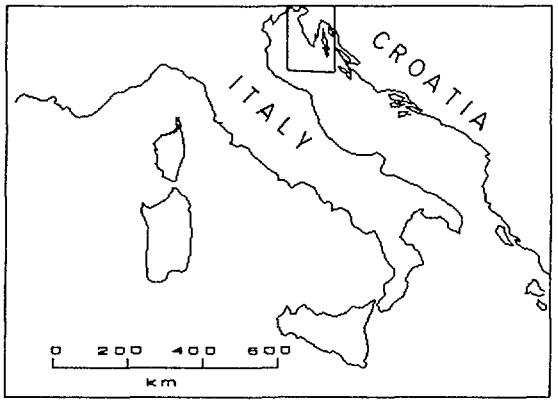

Figure 6. Northern Mediterranean Sea. Istra peninsula is located in the rectangle.

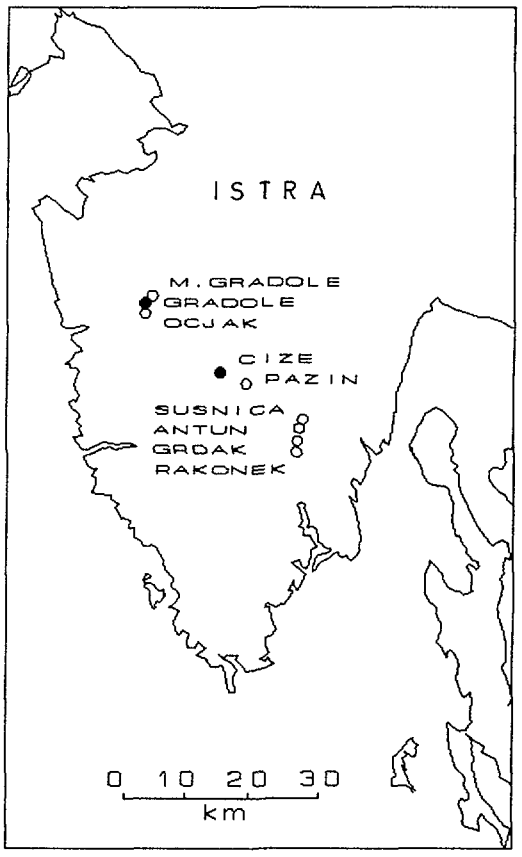

Figure 7. Istra peninsula. Tracer was injected into cave at CIZE and recovered at the spring GRADOLE.

is equal or larger than 1.96 cm/s. On 16.03.1991. the flow rate of water at Gradole was 7.58 m^3/s while at the end of experiment it was 3.5 m^3/s. The flow was nearly constantly decreasing during the experiment (Figure 8).

Let us apply results of the previous section to data which are illustrated in Figure 8. We try to find out the probability density p of (5.4) so that the solution (5.6) reproduces results of the measurement.

The assumptions of the model (5.1)-(5.3) are practically satisfied: (a) the measured flow rate during the experiment was changing slowly with nearly constant gradient, and (b) the transport is not branching i.e the total amount of tracer, injected at the beginning of the path, is carried until the point of measurement. The model is used to calculate the probability density function, p, (Figure 4). From this result a general theoretical model for p (5.4) is proposed. A model for p is necessary for our further study.

Since the water outflow at Gradole spring was decreasing during the measurements with a constant gradient, initially the mean velocity w(t) is approximated by

$$w(t) = w_0(a_0 + a_1\frac{t}{T}), \quad 0 \le t \le T, \qquad (6.1)$$

where w_o = 1.74 cm/s, a_0 = 1.5, a_1= -0.5 and T = 372 h. Neither the precise distance, x, between the injection point and measurement point nor the value of w_o are known. Because the solution in (5.6) depends on $r = x/w_o$ it is sufficient to determine one of the two parameters, x or w_o, while the other parameter has to be determined from data. We assume x = 14 km and obtained w_o = 1.5 cm/s. The criterion for the determination of w_o is the symmetry of probability density p, i.e. the constraint:

$$\Delta p = \left| \int_{-1}^{0} d\lambda\, p(\lambda) - \int_{0}^{1} d\lambda\, p(\lambda) \right| \to \min.$$

We obtained this velocity with Δp = 0.01, i.e. with the relative error of 1%. The graph of probability density p is illustrated in Figure 9.

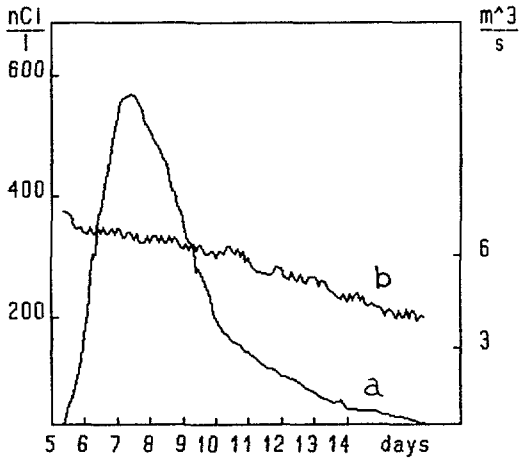

Figure 8. (a) Tritium concentration and (b) flow rate of water at Gradole spring.

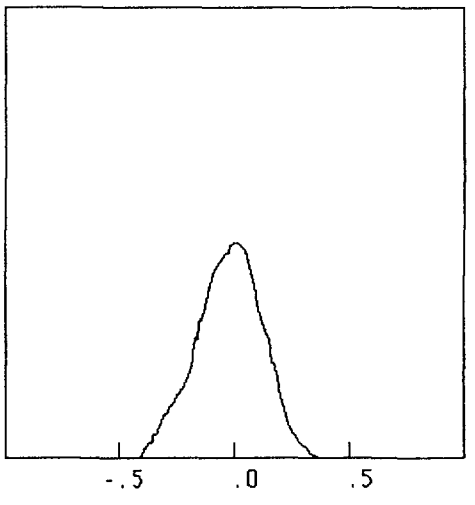

Figure 9. Probability density function from data.

From the obtained results the following model of the probability density p is proposed

$$p(x) = \left\{ \begin{array}{ll} \frac{6}{a^4}\left(\frac{x^3}{3} - a\frac{x^2}{2} + \frac{1}{6}a^3\right), & |x| \le a, \\ 0 \quad otherwise & \end{array} \right\}$$

with a single parameter a, representing the maximum ratio of diffusion to mean velocities.

How such a simple model of fluctuations is able to give plausible results? The model (5.3) is not trivial, although its derivation is based on a simplified model of fluctuations. The model can be derived from a general transport model for a stochastic velocity field and with all parameters depending on space and time [1,2]. An illustration of this general approach is given in Figure 10. A restriction of the general transport model to the one-dimensional transport, where the mean velocity is independent of x and external sources are omitted, is defined by (5.3). The assumptions of the model are practically satisfied: (a) data on flow rate suggest that velocity is a slow changing function during the experiment, and (b) branchings of flow are absent. Therefore, it is reasonable to assume that the flow rate is also a slowly changing with position x.

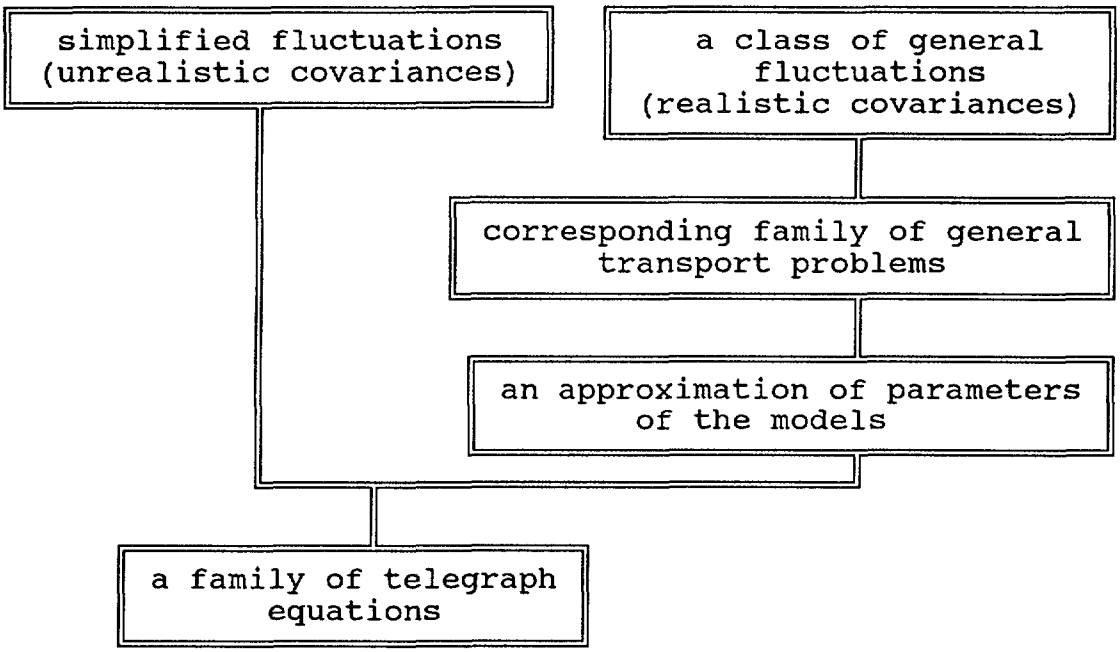

Figure 10. Steps in the derivation of the same type of model from different assumptions on statistics

7. DISCUSSION

Main properties of solutions c(t,x) of (5.3) or (5.7) are briefly described in Section 5. Let us recapitulate the two most important properties.

(A) The function $c(t,x)$, defining the mean concentration field, is equal identically to zero if the quantity $|x - tw(t,x)|$ is sufficiently large, i.e. the velocity of spreading of "the cloud" $c(t,x)$ is finite. This feature is illustrated in Figure 5.

(B) The function $c(t,x)$ describes the average motion of "fluid elements". Each "fluid element" travels along the x-direction with its own velocity, $w(t,x) + \lambda w(t)$. Actually, "fluid elements" travel in pairs, one with the velocity $w + \lambda w$ and the other with $w - \lambda w$. The averaging procedure is carried out with respect to the weight p over all the possible values of velocity λw. Therefore, the velocity $\lambda w(t)$ is called the dispersion velocity with the probability $d\lambda p(\lambda)$.

Conclusion

In principle, deterministic transport models describe transport in the mean. To each model of velocity fluctuation there corresponds a model of transport in the mean. Unfortunately, this choice is strictly limited. If a user accepts the hypothesis that velocity fluctuations are normally distributed then the conventional and generalized dispersion equations are at the user's disposal for a description of transport in the mean. If the hypothesis on normally distributed fluctuations must be rejected then only one limited class of models of transport in the mean can be used. The other possibility is to withdraw from modelling transport in the mean and turn back to M.C. methods and consider the stochastic transport problem.

Normally distributed velocity fluctuation.

1) Normally distributed velocity fluctuations can be non-correlated and correlated. They define a Brownian motion in the former case and a general Gaussian process in the latter case. The conventional dispersion equation describes transport in the mean for which the fluctuations are defined by the Brownian motion. For fluctuations defined by a general Gaussian process the transport problem is described by the generalized dispersion equation of Section 4.

2) If the sources are switched off the conventional dispersion equation describes the transport reliably.

3) The conventional dispersion equation cannot describe the transport reliably in the vicinity of sources.

4) The conventional dispersion equation induces highly underestimated net inputs in the case of small values of μ in (4.4), $\mu \sim 1$. In such cases the conventional dispersion equations cannot describe the transport reliably.

5) If μ is large, $\mu \gtrsim 100$, the net balance by the conventional dispersion equation is in a good agreement with the net balance of exact model for the assumed velocity fluctuations. In this case the conventional dispersion equation is an acceptable model.

6) The generalized dispersion equation describes the transport correctly for normally distributed velocity fluctuations. Unfortunately, the modelling is complex because the equation is not a differential equation and solutions must be constructed by iterations, solving a conventional dispersion equation at each iteration step.

Uniformly bounded velocity fluctuation.

For a class of uniformly bounded velocity fluctuations and the case of one space dimension, the model of transport in the mean has been derived. It is defined by a partial differential equation of the hyperbolic type. The model has been used for the description of tracer experiments in groundwaters. If the flow rate changes slowly, so that the velocity of flow can be approximated by a function which does not depend on position, predicted concentrations are in excellent agreement with data. For flows which change significantly during the experiment, predictions cannot describe all changes in concentration field. In this case models with spatially varying velocity must be used.

REFERENCES

[1] Limić, N., Models of velocity fluctuations and exactly derivable diffusion laws, Appl. Math Model. **14** (1990) 549-552.

[2] Limić, N., A new approach to the problem of transport in aquatic ecosystems, FIZIKA **1B** (1992) 7-31.

[3] Goldstein, I., On diffusion by discontinues movements and on the telegraph equation, Quart. J. Mech. and Appl. Math. **4** (1951) 129-156.

[4] Bourett, R., An hypothesis concerning turbulent diffusion, Canad. J. Phys. **38** (1960) 665-676.

[5] Taylor, The statistical theory of isottropic turbulence, J. Aeronaut. Sci., **4** (1937) 311-315

[6] V. Kubelka, Application of isotopes for determining quality of karstic groundwaters in Istra, Report of The Rudjer Bošković Institute, 1979

ELLAM: AN EFFECTIVE TOOL FOR MODELLING SHARP FRONTS IN QUANTITATIVE ISOTOPIC HYDROLOGY

I. HERRERA
National University of Mexico,
Mexico City, Mexico

Abstract

The main topic of study of Quantitative Isotopic Hydrology is the transport of isotopes by water flowing in a porous medium, and their interactions. The mathematical models of such processes are based in the advection-diffusion equation or systems of such equations. Until recently, effective mass conservative algorithms capable of modeling advection-dominated transport were lacking. However, many of the difficulties encountered previously have been overcome by ELLAM methods, recently developed by the author and coworkers. Here, the different implementations of ELLAM methods that exist at present, are presented and evaluated, with the purpose of making them more readible available to the scientific community working in Quantitative Isotopic Hydrology.

1. INTRODUCTION

The numerical solution of the advection-diffusion equation, is a problem of great importance in the study of transport of solutes by a liquid phase. A particular case of this general problem, is the study of the transport of a tracer by water flowing in a porous medium. The central problem of Quantitative Isotopic Hydrology, is precisely this problem.

The numerical treatment of the advection-diffusion equation, when advection is dominant, has been a challenging problem for a long time, specially if sharp fronts are present. A feature that is required from algorithms in order to be able to model effectively advection dominated transport, is that its performance be independent of the Courant number, to a large extent. Another feature which is essential, specially in Quantitative Isotopic Hydrology, is that the algorithms be mass-conservative, even when significant boundary behavior is present.

A general class of methods that has been quite successful and is being applied extensively, is the Eulerian-Lagrangian Localized Adjoint Method (ELLAM)[1-20]. One important feature of ELLAM methods, is that they are the only characteristic methods thus far developed, that are mass conservative. This property enhances

further the potential applications of ELLAM methods to mathematical models of Quantitative Isotopic Hydrology.

This paper is devoted to explain and discuss the ELLAM methodology with the intention of making it more readily available to the scientific community working in Quantitative Isotopic Hydrology. In addition, a brief critical comparison of the different ELLAM implementations that have been developed, is made.

The methods available to treat the advective-diffusive transport equation, are usually classified into: Eulerian, Lagrangian and Eulerian-Lagrangian. A method is called Eulerian, when the spatial grid is kept fixed in time. It is called Lagrangian or characteristic method, when the time derivatives are discretized following the motion of the fluid particles and it is called Eulerian-Lagrangian, when the fluid particles are tracked, but the spatial grid is kept fixed through time.

When applied to advection dominated transport, the salient features of approximations which derive from an Eulerian approach, may be summarized as follows: (i) The time truncation error dominates the solutions, (ii) The solutions are characterized by significant numerical diffusion and some phase errors, (iii) The Courant number ($Cu \equiv \frac{V\Delta t}{\Delta x}$) is generally restricted to be less than one, and sometimes much less than one. Among such procedures, one may distinguish Optimal Spatial Methods (OSM), in which an accurate solution of the spatial problem is developed.

Other Eulerian methods seek to cancel the errors introduced by the time discretization with the errors produced by the spatial discretization (see, for exmple [21-24]). Some of such methods actually improve to some extent, the inconvenient features of Eulerian methods in general, mentioned above. However, they still suffer from severe Courant number limitations [ ].

In Lagrangian methods in general, the problem is solved step by step in time. The process of obtaining the solution at the new time level from the solution at the previous one, in turn, is carried out in two teps: one in which fluid particles are tracked and a second one in which a purely spatial elliptic problem is solved. This latter step is frequently called the "diffusive step", because the elliptic character of the problem is induced by the presence of diffusion (usually Fickian).

Methods which are purely Lagrangian carry out the particle tracking forward in time. This introduces distorsions of the spatial

grid, which complicate the implementation of the diffusive step and lead to inacuracies of the solution. In Eulerian-Lagrangian approaches the grid is kept fixed at all times, avoiding in this manner the grid distorsions. To this end, the particles are tracked backwards in time. Thus, such procedures profit from the structure of characteristic curves when carrying out the time-discretization, but in addition they profit of having kept fixed the spatial grid, when carrying out the diffusive step. Eulerian-Lagrangian methods have the significant advantage that Courant number restrictions of Eulerian methods are overcome to a large extent, since the advection term is eliminated from the elliptic problems to be solved at each time step.

On the other hand, the Localized Adjoint Method (LAM) is a methodology for discretizing partial differential equations which was introduced by the author [25-30]. This procedure is based on Herrera's Algebraic Theory of Boundary Value Problems [31-35] (also [25]). Applications have successively been made to ordinary differential equations, for which highly accurate algorithms were developed [25-27], multidimensional steady state problems [28] and optimal spatial methods for advection-diffusion equations [29-30].

Recently, Localized Adjoint Method (LAM) has been applied in space-time, in an Eulerian-Lagrangian manner to problems of advective-diffusive transport, using specialized test functions [1-3,7-9]. These functions locally satisfy the homogeneous adjoint equation within each element. The general methodology so obtained is the Eulerian-Lagrangian Localized Adjoint Method (ELLAM).

Like characteristic methods in general [36-43], ELLAM methods have the advantage that Courant number restrictions of purely Eulerian methods are removed to a large extent, but in addition they present other important advantages. Until ELLAM was developed, characteristic methods had had three kinds of limitations: inability to rigorously treat boundary fluxes when characteristics intersect inflow or outflow boundaries, inability to ensure mass conservation and the introduction of numerical dispersion for some methods, due to low order interpolation or integration [44].

On the other hand, the general framework of ELLAM, as has been presented in [2] (see also [6]), is quite wide. In contrast to other characteristic methods, ELLAM allows systematic treatments of boundary conditions and the resulting algorithms are mass

conservative [1]. In addition, it provides a unification of characteristic methods (CM's).

The general methodology of ELLAM [2], can be implemented in many different manners. Up to now two kinds of implementations have been developed. They derive from the application of two different classes of test functions. In [1], bilinear functions which are defined as "chapeau" functions at level time t^{n+1} and constant along characteristic curves, were applied and in this manner the first mass conservative Eulerian-Lagrangian scheme for the general transport equations, was developed. This method is referred to as BELLAM [7].

An alternative manner of implementing ELLAM, is to use test functions which are piece-wise constant, and are advected with the transport velocity of the problem. In [7,8], under the title of "ELLAM Cells" (CELLAM), a very effective implementation of ELLAM using this kind of test functions, has been developed. CELLAM has the advantages of ELLAM methods described above, but in addition it ensures local mass conservation and yields algorithms which are more convenient for existing solute-transport codes which are based on finite differences. Thus far, the numerical performance of CELLAM has been slightly better than that of BELLAM [7-9]. Also, the simplicity of the implementation of the method, is appealing.

In passing, we mention that an implementation (FVELLAM) using similar test functions was intended in [45], but the authors reported numerical difficulties which severely limit the applicability of their results.

2. BILINEAR ELLAM (BELLAM)

This approach was first presented in a sequence of two papers [1,2]. Consider the one-dimensional transient advection-diffusion equation in conservative form:

$$\mathcal{L}u \equiv \frac{\partial u}{\partial t} - \frac{\partial}{\partial x}(D\frac{\partial u}{\partial x} - Vu) + Ru = f_{\Omega}(x,t), \text{ in } \Omega \qquad (2.1)$$

$$x \in \Omega_x = [0, l]$$

$$t \in \Omega_t = [t^n, t^{n+1}]$$

$$(x,t) \in \Omega = \Omega_x X\ \Omega_t$$

subject to initial conditions

$$u(x,t^n) = u^n(x), \qquad (2.2)$$

and suitable boundary conditions, at x=0 and l. The following development accommodates any combination of boundary conditions. The

manner in which the region Ω and the initial conditions are chosen in Eqs. (2.1) and (2.2), is suitable for applying a step by step solution procedure.

To make the exposition more readable, only the case of constant coefficients will be explained here, although variable coefficients have already been treated (see for example [11]). For simplicity, we proceed in an ad-hoc manner. More systematic expositions placing the procedures discussed in this article in the general frame-work of the Localized Adjoint Method (LAM), are given in [2] and [5].

For the case when the coefficients of Eq. (2.1) are constant, the source term vanishes ($R\equiv 0$) and the partition is uniform, the test functions used are:

$$w^i(x,t) = \begin{cases} \dfrac{x-x_{i-1}}{\Delta x} + V\dfrac{t^{n+1}-t}{\Delta x}, & (x,t)\in\Omega_1^i \\ \dfrac{x_{i+1}-x}{\Delta x} + V\dfrac{t^{n+1}-t}{\Delta x}, & (x,t)\in\Omega_2^i \\ 0, \quad \text{all other } (x,t) \end{cases} \tag{2.3}$$

where Ω_1^i and Ω_2^i are as is shown in Fig.1. Such weighting functions satisfy $\mathcal{L}^* w^i = 0$ and are continuous (i.e $[w]=0$), but have discontinuous first derivatives (i.e.; $[dw/dx]\neq 0$). The jumps are

$$\left[\frac{\partial w}{\partial x}\right]_{i-1} = \frac{1}{\Delta x}\ ; \quad \left[\frac{\partial w}{\partial x}\right]_{i} = \frac{-2}{\Delta x}; \quad \left[\frac{\partial w}{\partial x}\right]_{i+1} = \frac{1}{\Delta x}. \tag{2.4}$$

DISCRETIZATION IN THE INTERIOR OF Ω

When the region Ω^i does not intersect the lateral boundaries, integration over Ω^i, yields

$$\int_{x_{i-1}}^{x_{i+1}} u(x,t^{n+1})w^i(x,t^{n+1})dx - \frac{D}{\Delta x}\left\{\int_{t^n}^{t^{n+1}} u(\sigma_{i-1}(t),t)dt - 2\int_{t^n}^{t^{n+1}} u(\sigma_i(t),t)dt + \int_{t^n}^{t^{n+1}} u(\sigma_{i+1}(t),t)dt\right\}$$
$$= \int_{x_{i-1}^*}^{x_{i+1}^*} u(x,t^n)w^i(x,t^n)dx + \int_\Omega f_\Omega w^i dxdt, \tag{2.5}$$

where the unknowns have been collected in the left-hand member of the equation while the data is included in the right one. In Eq. (2.5), it is assumed that $x=\sigma_i(t)$ is the characteristic curve passing through x_i at time t_{n+1} (Fig. 1).

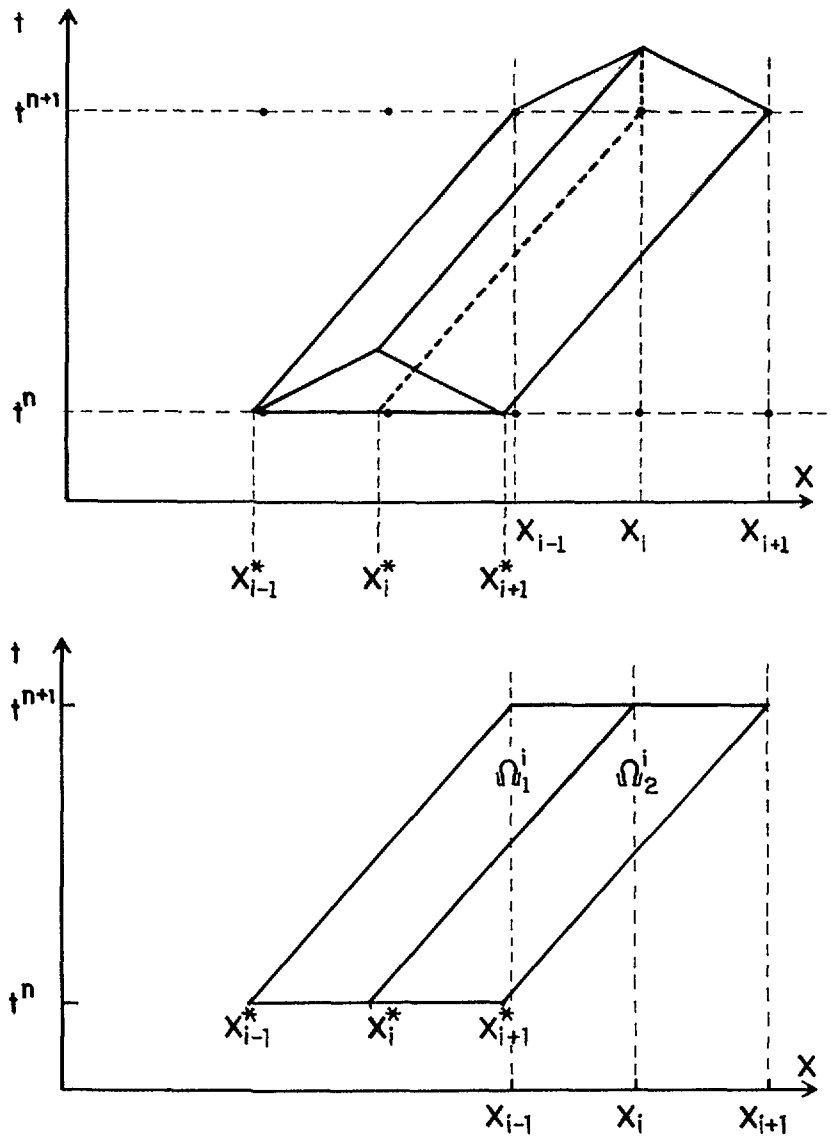

Figure 1.- Test functions used in BELLAM.

Notice that the unknown function u(x,t) has not yet been approximated by any specific functional form. The time integrals may be approximated using a Backward-Euler (fully implicit) scheme. Then the spatial integrals that appear in Eq. (2.5), may be approximated in many different ways, using the nodal values of u at the discrete time levels t^n and t^{n+1}, exclusively, so that the unknowns in the equation ultimately correspond to nodal values at time t^{n+1}. Different approximations of these integrals lead to different CM algorithms reported in the literature [1]. For example, piecewise linear spatial interpolation of u at time levels t^n and t^{n+1}, coupled with a one-point (at $t=t^{n+1}$) fully implicit approximation to the temporal integral, leads to the modified method of characteristics of Douglas and Russell [40].

BOUNDARY CONDITIONS

When a region Ω^i intersects the inflow boundary, several cases can occur. As an example, we discuss the case illustrated in Fig. 2. Then, integrating Eq. (2.1) over the region Ω_i, it is obtained:

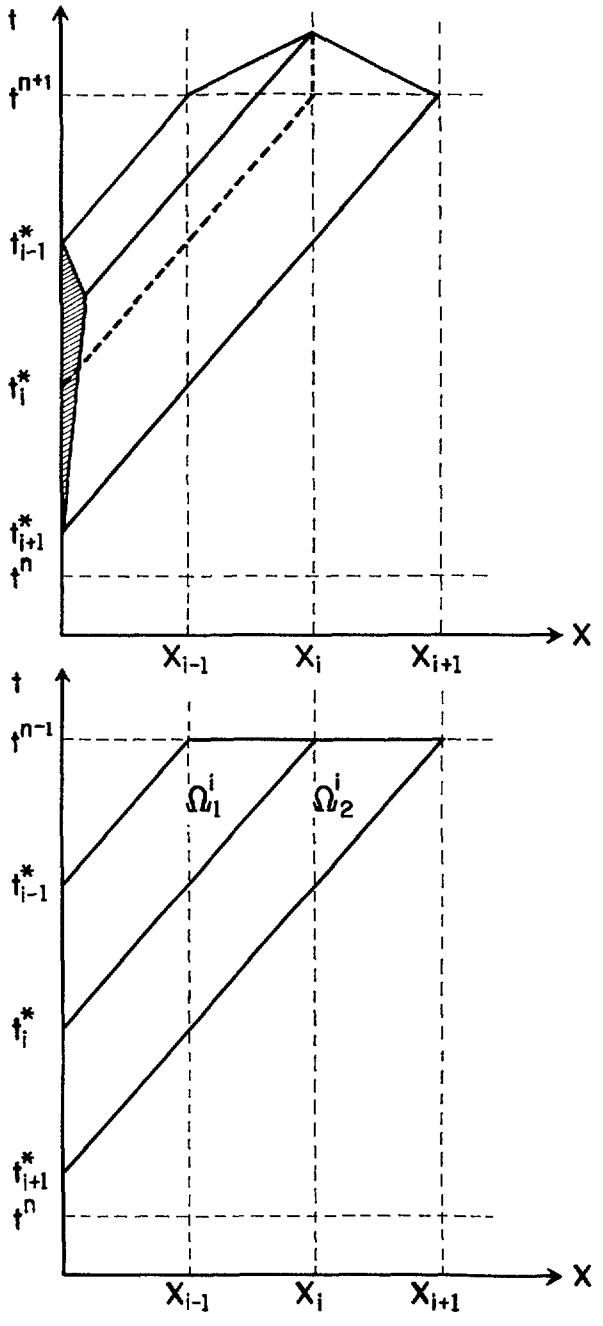

Figure 2.- Case when the domain of the test functions intesects the inflow boundary (BELLAM).

$$\int_{x_{i-1}}^{x_{i+1}} u(x,t^{n+1})w^i(x,t^{n+1})dx - \frac{D}{\Delta x}\left\{\int_{t^*_{i-1}}^{t^{n+1}} u(\sigma_{i-1}(t),t)dt - 2\int_{t^*_i}^{t^{n+1}} u(\sigma_i(t),t)dt\right.$$

$$\left. + \int_{t^*_{i+1}}^{t^{n+1}} u(\sigma_{i+1}(t),t)dt\right\} + \int_{t^*_{i+1}}^{t^*_{i-1}} w^i\left\{D\frac{\partial u}{\partial x}(0,t) - Vu(0,t)\right\}dt =$$

$$\frac{D}{\Delta x}\left\{\int_{t^*_i}^{t^*_{i-1}} u(0,t)dt - \int_{t^*_{i+1}}^{t^*_i} u(0,t)dt\right\} + \int_\Omega f_\Omega w^i dxdt \qquad (2.6)$$

The integrals along characteristics appearing in Equ. (2.6), can again be evaluated by means of a fully implicit approximation.

However, the fact that each of these three integrals has a different length, introduces problems for achieving consistency in the order of accuracy of the approximations, for some classes of boundary conditions, at least. Suitable combinations of the integrals just mentioned, with the last integral of the left-hand side of Eq. (2.6), may overcome the problem. However, whether this is feasible or not, depends on the type of boundary conditions to be satisfied. To exhibit this problem, it is necessary to develop a more careful derivation in which the order of the errors introduced at each step, is explicitly stated. Thus, the reader is referred to Section 5, where a more careful derivation of a similar equation is presented for CELLAM.

The last term in the left-hand side of Equ. (2.6) must be handled with special care, to obtain an algorithm with satisfactory properties. If we simply apply the Backward-Euler scheme to the unknown boundary flux along the time direction, the discretization will be unsatisfactory for large Courant numbers ($Cu=V\Delta t/\Delta x$), since many characteristic lines will be crossed. Thus, instead, one can evaluate the contribution to the integral of the term containing $u(0,t)$, since this is Dirichlet data, and transpose it to the right side of the equation. In [1], the remaining part of the integral was approximated in a way which, as indicated in [8], is equivalent to:

$$\int_{t^*_{i+1}}^{t^*_{i-1}} w^i D\frac{\partial u}{\partial x}(0,t)dt \cong \frac{D}{V}\int_{x_{i-1}}^{x_{i+1}} w^i\frac{\partial u}{\partial x}(x,t^{n+1})dx \qquad (2.7)$$

This approximation however, as pointed out in [7], is not necessarily consistent with the order of approximation that is required in the formulation: $O(\Delta x\Delta t^2)$. This latter order of

approximation can be achieved, using relations similar to Eq. (2.7), only if the expressions under the integrals, are suitably combined with the integrals along characteristics present in Eq. (2.6), and this is possible, as has been already been mentioned, only for some kinds of boundary conditions [7].

For outflow boundary conditions of Dirichlet type, the outflow boundary contributions vanish for all the test functions. This is due to the fact that all the weighting functions vanish in the characteristic Σ_E, which passes through (x_E, t^{n+1}), and beyond it. Also, the system of equations that is obtained in the manner explained above, is closed, because u_E^{n+1} is datum. If additional information is desired at the outflow boundary, it can be obtained applying procedures which amount essentially to post-processing [1].

3. SOME REMARKS ON DISCRETE METHODS

There are two basic tasks that every numerical method for partial differential equations has to accomplish [2,6,7]:

i).- Gathering information about the sought solution; and

ii).- Interpolating or, more generally, processing such information.

These two processes are distinct, although in many numerical methods they are not differentiated clearly. In procedures which are derived from the method of weighted residuals, the information about the exact solution that is gathered, is determined mainly by the weighting functions used. Since this information does not determine uniquely the sought solution, some procedure for extending it is required, in order to fill the gaps of information and exhibit at the end, a unique approximate solution.

Different methods of solution follow different strategies for accomplishing this latter task of extending the information that is available. In general, interpolation and extrapolation procedures are applied. For example, in finite element methods some basis functions are chosen and the approximate solution is assumed to be a superposition of such functions. In this case, the information about the exact solution which is gathered by the weighting functions, is interpolated in a manner which is determined by the family of basis functions chosen.

Clearly, it is not convenient to carry out the process of extending the information blindly, ignoring what is the actual information that is available. However, this is what is usually

done. On the contrary, it is advantageous to make use of the insight gained when the available information has been identified, since the selection of the best procedure for extending it, is strongly dependent on the information that is at hand.

Due to these facts, in recent works [6,7] the author has advocated an approach for developing numerical methods, in which the processes i) and ii) are clearly separated. Firstly, the information about the sought solution that is at hand, is identified and secondly, using that insight, a procedure for extending such information is defined.

Herrera's Algebraic Theory of Boundary Value Problems [25,31-35], which permits localizing the adjoint, has shown to be quite suitable for identifying the information contained in approximate solutions. The use of this theory has clear advantages over other options, such as the standard theory of distributions, because of two reasons at least: the use of the algebraic theory permits the localization of the adjoint, and the simultaneous use of discontinuous trial and test functions is feasible. Then, depending on the information that is identified, interpolation procedures suitable for handling it efficiently, are selected and applied. This is what should be properly called Localized Adjoint Method. The introduction of basis functions is not required and, even more, their use is inconvenient in some cases. In [7] and [8], this approach was applied quite successfully to derive CELLAM.

4 ELLAM CELLS (CELLAM)

This method was presented originally in [7] and [8] (see also [9]). The notations adopted conform with those which are usual for cell approaches. A partition $\{x_1, x_{3/2}, x_{5/2}, \ldots, x_{E-1/2}, x_E\}$, is introduced, which induces a partition of Ω into subregions $\{\Omega^1, \Omega^2, \ldots, \Omega^E\}$, if for each $i=2,\ldots,E-1$, Ω^i is defined as the subregion of Ω, limited by the characteristic curves $\Sigma_{i-1/2}$ and $\Sigma_{i+1/2}$ (see Fig. 3), while Ω^1 is that part of Ω which lies to the left of $\Sigma_{3/2}$ and Ω^E is the subregion of Ω which lies to right of $\Omega_{E-1/2}$. The subregions of the partition are called "cells" and they are said to be "uniform" when

$$x_{i+1/2}-x_{i-1/2} = h, \text{ for } i=2,\ldots,E-1;\ x_{3/2}-x_1=h/2, x_E-x_{E-1/2}=h/2 \quad (4.1)$$

A system of constant weighting functions is applied. These are the characteristic functions of the subregions that constitute this

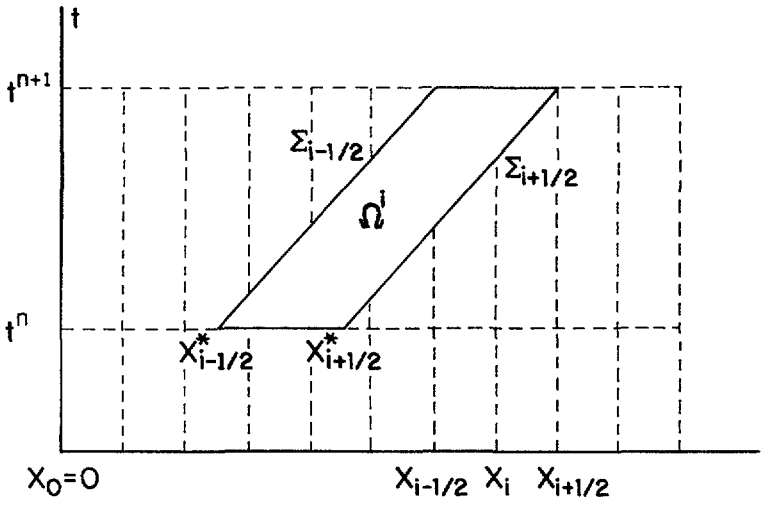

Figure 3.- Test functions used in CELLAM.

partition. Actually, not all of them are required. The system of weighting functions applied to derive CELLAM [7], is:

$$w^{\alpha}(x,t) = \begin{cases} 1, & \text{if } (x,t)\in\Omega^{\alpha} \\ 0, & \text{if } (x,t)\notin\Omega^{\alpha} \end{cases}, \quad \alpha=2,\ldots,E-1, \qquad (4.2)$$

DISCRETIZATION IN THE INTERIOR OF Ω

In the case when Ω^{α} does not intersect the lateral boundaries of the region $\Omega=[0,1]X[t_n,t_{n+1}]$, integration of Eq. (2.1) over Ω^{α}, yields:

$$\int_{x_{\alpha-1}}^{x_{\alpha+1}} u^{n+1}dx + \int_{tn}^{tn+1} (D\frac{\partial u}{\partial x})_{\Sigma_{\alpha+1/2}} dt - \int_{tn}^{tn+1} (D\frac{\partial u}{\partial x})_{\Sigma_{\alpha-1/2}} dt$$

$$= \int_{x^*_{\alpha-1}}^{x^*_{\alpha+1}} u^n dx \qquad (4.3)$$

Equation (4.3) and a modified version of it designed to incorporate boundary terms when the lateral boundaries of Ω are intersected by Ω^{α}, is the starting point of the numerical treatment. Observe that

$$\int_{x_{\alpha-1}}^{x_{\alpha+1}} u^{n+1}dx - \int_{x^*_{\alpha-1}}^{x^*_{\alpha+1}} u^n dx = O(hk) \qquad (4.4a)$$

and

$$\int_{tn}^{tn+1} (D\frac{\partial u}{\partial x})_{\Sigma_{\alpha+1/2}} dt - \int_{tn}^{tn+1} (D\frac{\partial u}{\partial x})_{\Sigma_{\alpha-1/2}} dt = O(hk) \qquad (4.4b)$$

where $h = \max(h_{i+1/2}-h_{i-1/2})$ and $k = t_{n+1}-t_n$. Thus, in the developments it is required that integrals such as those appearing in Equs. (4.4), be evaluated to a precision of $O(hk^2)$, at least. It will be assumed that $h \approx k$, so that $O(hk^2)=O(h^2k)=O(k^3)=O(h^3)$.

Equation (4.3) supplies information about the sought solution in the interval $[x_{\alpha-1/2}, x_{\alpha+1/2}]$ at time t_{n+1} and about its x-derivative on the characteristics $\Sigma_{\alpha-1/2}$ and $\Sigma_{\alpha+1/2}$. In the CELLAM approach [7], the goal of the information processing is to concentrate all of it, in the value of the solution at the "cell center" x_α, at time $t=t_{n+1}$. To this end, in Eq. (4.3), the integrals from t_n to t_{n+1}, are firstly approximated in a fully implicit manner (i.e., by a one-step Backward-Euler approximation at t_{n+1}). Thus

$$\int_{t_n}^{t_{n+1}} \left\{ \left(D\frac{\partial u}{\partial x}\right)_{\Sigma_{\alpha+1/2}} - \left(D\frac{\partial u}{\partial x}\right)_{\Sigma_{\alpha-1/2}} \right\} dt =$$

$$\left\{ \left(D\frac{\partial u^{n+1}}{\partial x}\right)_{\alpha+1/2} - \left(D\frac{\partial u^{n+1}}{\partial x}\right)_{\alpha-1/2} \right\} k + O(hk^2) \qquad (4.5)$$

For a uniform spacing and constant coefficients, a central difference approximation yields:

$$\left\{ \left(\frac{\partial u^{n+1}}{\partial x}\right)_{\alpha+1/2} - \left(\frac{\partial u^{n+1}}{\partial x}\right)_{\alpha-1/2} \right\} k = \frac{u_{\alpha+1}^{n+1} + u_{\alpha-1}^{n+1} - 2u_\alpha^{n+1}}{h} k + O(h^3 k) \qquad (4.6)$$

The extension of this formula to the case of a non-uniform partition, can be done in a similar manner. However, the order of precision is reduced by one and the overall error in (4.6), becomes $O(h^2k)$.

In characteristic methods, most of the numerical diffusion is due to the interpolations in space, which are required because in general, characteristics do not cross the t_n time level at nodes. Thus, all the approximations in space have to be carried out with special care. A special feature of the approximations used in the derivation of CELLAM [7], is that no assumption is made about the shape of the solution.

The first integral in (4.3), is approximated by

$$\int_{x_{\alpha-1}}^{x_{\alpha+1}} u^{n+1} dx = u_\alpha^{n+1} h_\alpha + \frac{1}{24}\left(\frac{\partial^2 u^{n+1}}{\partial x^2}\right)_\alpha h_\alpha^3 + O(h^5) \qquad (4.7)$$

and only the second order derivative requires a numerical approximation, since the information is being concentrated in the "cell centers". To get a tri-diagonal structure for the matrix, it

is necessary to use three-point approximations only. In the case of a "uniform partition", a central difference approximation yields

$$\int_{x_{\alpha-1}}^{x_{\alpha+1}} u^{n+1}dx = \left(\frac{u^{n+1}_{\alpha+1} + u^{n+1}_{\alpha-1} + 22u^{n+1}_{\alpha}}{24}\right)h + O(h^5) \qquad (4.8)$$

If the partition is non-uniform, the approximation to the second order derivative by a three-point scheme is only first order, and the error in the evaluation of the integral in (4.8), is only order four.

There is greater freedom for the choice of the approximations to be used in the evaluation of the integrals at time t_n, since they do not affect the structure of matrix of the final system of algebraic equations. In [7], the integral appearing in the right-hand side of Eq. (4.3) was approximated using an approach similar to the one used for deriving Equ. (4.7); i.e., integrating the Taylor series expansion of u^n around the mid-point of the interval $[x^*_{\alpha-1}, x^*_{\alpha+1}]$. However, since such point is not a "cell center", u^n is not known there and an interpolation must be used to evaluate it. Using three-point formulas, u^n and its second order derivative can be evaluated to orders three and one, respectively. This yields an approximation which is fourth order in h.

5. BOUNDARY CONDITIONS

The numerical approximations presented thus far, apply only when the subregion $\Omega^\alpha \subset \Omega$ does not intersect the lateral boundaries $\partial_o\Omega \cup \partial_\ell\Omega$, of the region Ω. When this is not the case, boundary conditions must be included. This Section is devoted to presenting the CELLAM procedures for dealing with them.

In Eulerian-Lagrangian approaches, the analyst does not have control of the discretization at an inflow boundary, since it is completely determined by the spatial discretization. However, the situation in this respect is a little better at an outflow boundary. Thus, when dealing with boundary conditions, specially at an inflow boundary, numerical diffusion is due to a large extent, to the fact that characteristics do not cross the boundaries of the space-time region Ω, at times levels belonging to the partition of the time interval. Thus, just as in the interior of the spatial region, the approximatinos in space have to be performed with special care to minimize numerical diffusion, when dealing with boundary conditions the time integrals on the boundaries have to be treated with special care.

There is an additional reason which enhances this effect at an inflow boundary. The information that is supplied at an inflow boundary has a larger effect on the solution than that coming from an outflow boundary, specially in the case of advection-dominated transport, because the former is transmitted to the interior of the spatial region by advection and diffusion, while the latter is only transmitted by diffusion.

In [7], it was pointed out that in some cases, it is more difficult to achieve the desired degree of accuracy in the integrals with respect to time at the boundary, than in the integrals with respect to x, at the different time levels. For Dirichlet boundary conditions, the different terms occur in a combination which is suitable for obtaining the desired degree of accuray. However, when the total flux is prescribed or when considering boundary conditions of Neuman type, this is not the case [7].

A.- Dirichlet Conditions

For this case, we use E-2 test functions; namely, those associated with subregions $\Omega^2,\ldots,\Omega^{E-1}$. In particular, no test function is applied on the first subregion (Ω^1) or on the last one (Ω^E). See Fig. 4.

Inflow Boundary

Dirichlet boundary conditions are incorporated in the numerical equations in two manners: directly, through the boundary terms and indirectly, imposing the condition that in the numerical approximations, some of the variables take the prescribed boundary values.

Assume Ω^α intersects the inflow boundary, as illustrated in Fig. 4. Then

$$\int_{\Omega^\alpha}\mathcal{L}u\,d\sigma = \int_{x_{\alpha-1/2}}^{x_{\alpha+1/2}} u^{n+1}dx - \int_{t^*_{\alpha-1/2}}^{t^{n+1}}\left\{(D\frac{\partial u}{\partial x})_{\Sigma_{\alpha+1/2}} - (D\frac{\partial u}{\partial x})_{\Sigma_{\alpha-1/2}}\right\}dt -$$

$$\int_{t^*_{\alpha+1/2}}^{t^*_{\alpha-1/2}}\left\{(D\frac{\partial u}{\partial x})_{\Sigma_{\alpha+1/2}} - (D\frac{\partial u}{\partial x})_{x=0}\right\}dt - \int_{t^*_{\alpha+1/2}}^{t^*_{\alpha-1/2}} Vu(0,t)dt \qquad (5.1)$$

The first two integrals of the right-hand member are like those appearing in Equs. (4.8) and (4.5), and can be handled similarly. In addition, the last one in this equation is easy to deal with, since u(0,t) is the prescribed boundary value. The third integral, however, requires a special treatment.

Firstly, observe that $(D\frac{\partial u}{\partial x})_{\Sigma_{\alpha+1/2}} - (D\frac{\partial u}{\partial x})_{x=0}$ is $O(h)$. Thus, for any $x\in[x_{\alpha-1/2}, x_{\alpha+1/2}]$, one has

$$(D\frac{\partial u}{\partial x})(x_{\Sigma_{\alpha+1/2}}(t^*), t^*) - (D\frac{\partial u}{\partial x})(0, t^*) = D\frac{\partial u^{n+1}}{\partial x}(x_{\alpha+1/2}) - D\frac{\partial u^{n+1}}{\partial x}(x) + O(hk) \quad (5.2)$$

where, for brevity, we have written t^* instead of $t^*(x)$. The approximation implied by Equ. (5.2), has the property that the values of the functions involved, at time t^*, are approximated by their values at time t_{n+1}, on the same characteristic. In this manner, crossing of characteristics is avoided. Such property is important in order to preserve the advantages of characteristic methods.

Equ. (5.2), can be used to obtain

$$\int_{t^*_{\alpha+1/2}}^{t^*_{\alpha-1/2}} \left\{ (D\frac{\partial u}{\partial x})_{\Sigma_{\alpha+1/2}} - (D\frac{\partial u}{\partial x})_{x=0} \right\} dt = (t^*_{\alpha-1/2} - t^*_{\alpha+1/2})(D\frac{\partial u^{n+1}}{\partial x})_{\alpha+1/2} +$$

$$\int_{x_{\alpha-1/2}}^{x_{\alpha+1/2}} D\frac{\partial u^{n+1}}{\partial x}(x)\frac{dt^*}{dx}(x)dx + O(hk^2) \quad (5.3)$$

As an illustration of the numerical implementation for this equation, we explain the case of constant coefficients. In this case

$$t^*(x) = t_{n+1} - \frac{x}{V} \quad (5.4)$$

so that

$$\frac{dt^*}{dx} = -\frac{1}{V} \quad (5.5)$$

and Equ. (5.3), becomes

$$\int_{t^*_{\alpha+1/2}}^{t^*_{\alpha-1/2}} \left\{ (D\frac{\partial u}{\partial x})_{\Sigma_{\alpha+1/2}} - (D\frac{\partial u}{\partial x})_{x=0} \right\} dt = \frac{x_{\alpha+1/2} - x_{\alpha-1/2}}{V}(D\frac{\partial u^{n+1}}{\partial x})_{\alpha+1/2} -$$

$$\frac{D}{V}(u^{n+1}_{\alpha+1/2} - u^{n+1}_{\alpha-1/2}) + O(hk^2) \quad (5.6)$$

In Equ. (5.6), the derivative $\partial u^{n+1}/\partial x$ at $x_{\alpha+1/2}$ ($\alpha=2,\ldots,E-1$), must be approximated to order $O(h^2)$, to be consistent with the order of approximation. For a non-uniform mesh, this requires a three-point scheme.

For $\alpha=2$, the boundary value u_1^{n+1}, occurs in equations such as (4.6) and (4.8), and it must be required that at each time level, u_1^{n+1} be equal to the prescribed boundary value. This is the indirect manner of imposing the boundary conditions that we referred to at the beginning of this section.

Outflow Boundary

Observe that the last test function to be applied is w^{E-1}. The support of this test function is Ω^{E-1}, which does not intersect the lateral boundary $x=l$. Thus, none of the boundary terms involving the outflow boundary occur in the numerical equations and the prescribed boundary values are incorporated in the numerical equations in an indirect manner exclusively; i.e., introducing them instead of u_E^{n+1} in approximations such as (4.6) and (4.8).

B.- Flux Conditions

For this case, we use E test functions. Thus, the test functions associated with regions Ω^1 and Ω^E, which were omitted when dealing with Dirichlet boundary conditions, are applied when dealing with this kind of boundary condition, and the values of u^{n+1} at zero and at l are treated as unknowns.

Inflow Boundary

Fig. 4, illustrates a case in which Ω^α intersects the inflow boundary. For flux boundary conditions, it is more convenient to write Equ. (5.1) in the form:

$$\int_{\Omega^\alpha} \mathcal{L}u\,d\sigma = \int_{x_{\alpha-1/2}}^{x_{\alpha+1/2}} u^{n+1}dx - \int_{t^*_{\alpha-1/2}}^{t^{n+1}} \left\{ \left(D\frac{\partial u}{\partial x}\right)_{\Sigma_{\alpha+1/2}} - \left(D\frac{\partial u}{\partial x}\right)_{\Sigma_{\alpha-1/2}} \right\} dt -$$

$$\int_{t^*_{\alpha+1/2}}^{t^*_{\alpha-1/2}} \left(D\frac{\partial u}{\partial x}\right)_{\Sigma_{\alpha+1/2}} dt - \int_{t^*_{\alpha+1/2}}^{t^*_{\alpha-1/2}} F(t)dt \qquad (5.7)$$

Here, $F \equiv \left(Vu - D\frac{\partial u}{\partial x}\right)_{x=0}$, is prescribed.

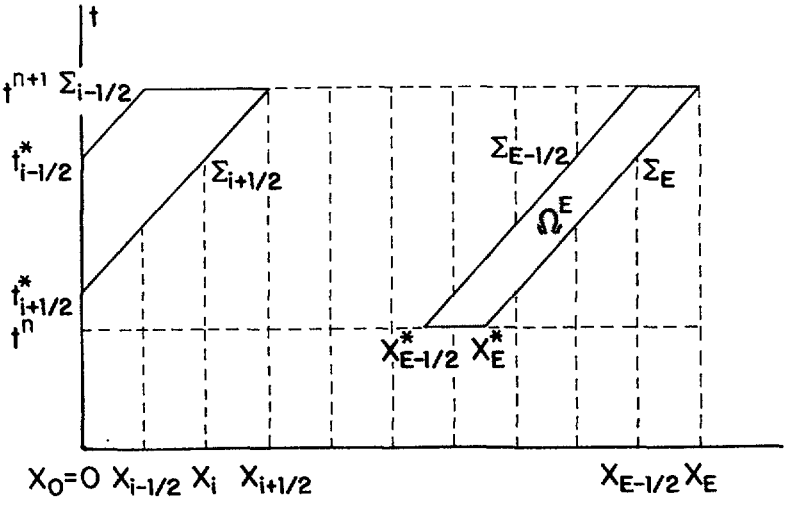

Figure 4.- Cases when the domain of the test functions intersects the lateral boundaries (CELLAM).

Since F(t) is a datum, the corresponding integral offers no special difficulty in being approximated to any desired order of accuracy. The other integrals can be treated in a manner similar to what was done in the case of Dirichlet conditions. The approximation

$$\int_{t^*_{\alpha+1/2}}^{t^*_{\alpha-1/2}} (D\frac{\partial u}{\partial x})_{\Sigma_{\alpha+1/2}} dt \cong (t^*_{\alpha-1/2} - t^*_{\alpha+1/2})(D\frac{\partial u^{n+1}}{\partial x})_{\alpha+1/2} \qquad (5.8)$$

is similar to one used in Equ. (5.3). However, the term $(D\frac{\partial u}{\partial x})_{x=0}$ which appears in Equ. (5.3), is missing here, because it was incorporated in the flux F. Due to this fact, approximation (5.8) is only $O(k^2)$, which is not consistent with the order of approximation that has been used in all other terms.

However, such a shortcoming has not been manifested in the numerical applications, which use Equ. (5.8). In particular, all the numerical experiments reported in this article, use this approximation. The development of an algorithm fully consistent with the order of accuracy that was set at the beginning of our discussion, would require a procedure, considerably more elaborate, which would not be justified at this point.

In addition, it must be mentioned that when the support of a weighting function intersects any of the corners of the domain Ω, the treatment presented requires slight modifications, whose details we leave out. At the inflow boundary, this happens for two test functions. One is w^1 and there is one more, whose support intersects the corner $(0, t_n)$, as shown in Fig. 4.

Outflow Boundary

The only weighting function whose support intersects the outflow boundary is w^E. Applying it, we get

$$\int_{\Omega^E} \mathcal{L}u\,d\sigma = \int_{x_{E-1/2}}^{l} u^{n+1}dx - \int_{x^*_{E-1/2}}^{l} u^n dx - \int_{t_n}^{t_{n+1}} F(t)dt + \int_{t_n}^{t_{n+1}} (D\frac{\partial u}{\partial x})_{\Sigma_{E-1/2}} dt \qquad (5.9)$$

Using three points approximations, one can evaluate the first two integrals of the right-hand side of this equation to $O(h^4)$. The third one offers no difficulty, since F(t) are data. Finally, an approximating procedure analogous to Equ. (5.8), can be applied to the last integral. However, the comments that were made immediately after Equ. (5.8), apply here too.

6 NUMERICAL COMPARISONS

The efficiencies of the BELLAM and CELLAM procedures have been compared. In [7], numerical examples that involve significant boundary behavior were solved, using these two methods. The results obtained there, are described next. The following change in the notation is noticed: In this Section, instead of taking the spatial region to be the interval $[0,1]$, as we did in the theoretical discussions, we set $\Omega_x=[a,b]$.

Consider an advancing Gaussian hill that may cross an inflow or an outflow boundary. Its general expression is

$$u_a(x,t) = \frac{1}{(1+4\pi Dt)^{1/2}}\exp\left(\frac{-\pi(x-Vt)^2}{1+4\pi Dt}\right) \qquad (6.1)$$

and the initial and boundary conditions are chosen in such a way that the exact solution of the problem is (6.1). Thus, the initial conditions are

$$u_I(x) = \exp(-\pi x^2) \qquad (6.2)$$

while the boundary conditions are

$$u(a,t) = u_a(a,t) \qquad (6.3a)$$

and

$$u(b,t) = u_a(b,t) \qquad (6.3b)$$

whenever Dirichlet conditions are considered. In addition, they are

$$\left(Vu - D\frac{\partial u}{\partial x}\right)(a,t) = \left(Vu_a - D\frac{\partial u_a}{\partial x}\right)(a,t) \qquad (6.4a)$$

and

$$\left(Vu - D\frac{\partial u}{\partial x}\right)(b,t) = \left(Vu_a - D\frac{\partial u_a}{\partial x}\right)(b,t) \qquad (6.4b)$$

whenever total flux boundary conditions are considered. In the numerical examples, only Dirichlet and total flux boundary conditions will be treated.

Several combinations of initial and boundary conditions are prescribed for Equ. (2.1), but in such a manner that for any of them the exact solution is given by Equ. (6.1). Also, domains considered were: $I=[2^1/_3,9]$, $O=[-3,2^1/_3]$ and $N=[-3,9]$. For them, the pulse crosses an inflow boundary, an outflow boundary and neither, respectively.

A. Comparison based on the Euclidean Norm

As explained in previous sections, in the CELLAM method the information about the sought solution is concentrated exclusively in the cell-centers and no base functions are used. This implies that no assumptions are made about the shape of the solution. This is in

contrast with other ELLAM procedures, in which the shape of the solution is assumed [1].

One consequence of this way of handling the information, is that some of the standard procedures for measuring the errors of approximate solutions, are not appropriate. In [1], for example, in which bilinear basis functions were used (the space of such functions, which are piece-wise linear and continuous in Ω_x, will be denoted be $\mathcal{S}$), the L^2 error of the approximate solution that BELLAM yields (and such approximate solution necessarily belongs to $\mathcal{S}$), was compared with the L^2 error of the projection of the exact solution on $\mathcal{S}$. This ratio is necessarily greater or equal to one, because of the minimal property of the projection.

When all the information is concentrated at the cell-centers, the best we can do is to obtain the exact values at those points. This, however, does not define a function of the space $\mathcal{S}$, and a direct comparison using the L^2 norm, is not possible. Of course, one could try to use linear interpolation of the approximate values at the cell-centers, to associate an element of $\mathcal{S}$ to the approximate solution. However, if one proceeds in that manner, even the optimal solution (i.e., that whose values at the cell-centers are the exact values) would give an L^2 error that in general, will be greater than that of the projection, again because of the minimal property of the projection. To illustrate this fact and its importance in the different cases tested, Table 1 compares the L^2 error of the linear interpolation, when the values at the cell-centers are the exact ones, with the error of the projection of the exact solution, on $\mathcal{S}$. It can be seen that in all cases, the L^2 error of the linear

Table 1. Comparison of L^2 errors between the projection of the exact solution on the space of piecewise linear functions and the function of this space, whose values are exact at the nodes ("interpolation").

DOMAIN	ΔX	ERROR PROJECTION	ERROR INTERPOLATION
N	0.267	0.715E-02	0.159E-01
N	0.053	0.265E-03	0.646E-03
I	0.267	0.715E-02	0.159E-01
I	0.053	0.265E-03	0.646E-03
O	0.267	0.497E-02	0.102E-01
O	0.053	0.177E-03	0.429E-03

interpolation of the exact values, is at least twice that of the projection on $\mathcal{S}$. Thus, if this measure of the error is used, one would not be able to discriminate between different methods on the basis of performance.

Before leaving this point, we would like to remark that when the information about the exact solution consists of the exact values at the cell centers exclusively, the extension of this information to the entire interval can be done in manners which are more efficient than using linear interpolation. For example, one could use a high order interpolation procedure, or solve a local problem (this is a kind of post-processing), to mention just a few of the possibilities for processing such information.

Therefore, a norm that directly compares the values at the cell centers was used to compare the errors of the different methods. The norm chosen was the "average Euclidean norm"

$$\|u-\hat{u}\| = \left(\frac{1}{E} \sum_{1}^{E} (u_i - \hat{u}_i)^2 \right)^{1/2}$$

Here, u_i are the values of the exact solution at the cell centers, while $\hat{u}_i$ are those of the approximate one.

Table 2 summarizes the numerical results. As in [1], the final time $t_f=0.5$, Δx is taken to be $4/15 \cong 0.267$ ($Pe=26\frac{2}{3}$) and $\Delta x=\frac{4}{75} \cong 0.0533$ ($Pe=5\frac{1}{3}$). For $\Delta x=\frac{4}{15}$, $\Delta t=0.25$ was used ($Cu=9\frac{3}{8}$). For $\Delta x=4/75$, the values 0.25, 0.05 and 0.01 of Δt, were used, which correspond to $Cu=46\frac{7}{8}$, $9\frac{3}{8}$ and $1\frac{1}{7}$, respectively. The integrals involving initial or boundary conditions were evaluated using Gauss-Kronrod rules to a high degree of precision. In Table 2, the Euclidean errors associated with the approximate solutions that were derived using CELLAM are compared with those obtained with BELLAM [1]. In all cases the errors listed correspond to the final time $t_f=0.5$.

TABLE 2. Comparison of errors between ELLAM-Cells and Bilinear-ELLAM

Run	DOM	Bound.Cond		ΔX	ΔT	Euclidean Error		Maximun Value		
		IN	OUT			Cells	Bilinear	Cells	Bilin	Exact
1	N	D	F	0.267	0.25	0.501E-02	0.652E-02	0.804	0.813	0.784
2	N	D	F	0.053	0.25	0.442E-02	0.446E-02	0.803	0.803	0.784
3	N	D	F	0.053	0.05	0.103E-02	0.105E-02	0.788	0.788	0.784
4	N	D	F	0.053	0.01	0.353E-03	0.265E-03	0.785	0.785	0.784
5	I	D	F	0.267	0.25	0.315E-02	0.695E-02	0.791	0.806	0.784
6	I	D	F	0.053	0.25	0.276E-02	0.289E-02	0.793	0.793	0.784
7	I	D	F	0.053	0.05	0.727E-03	0.822E-03	0.786	0.786	0.784
8	I	D	F	0.053	0.01	0.232E-03	0.289E-03	0.784	0.785	0.784
9	I	F	F	0.267	0.25	0.302E-02	0.684E-02	0.791	0.807	0.784
10	I	F	F	0.053	0.25	0.275E-02	0.287E-02	0.793	0.793	0.784
11	I	F	F	0.053	0.05	0.718E-03	0.821E-03	0.786	0.786	0.784
12	I	F	F	0.053	0.01	0.247E-03	0.293E-03	0.784	0.785	0.784
13	O	D	D	0.267	0.25	0.298E-02	0.452E-02	0.816	0.816	0.816
14	O	D	D	0.053	0.25	0.258E-02	0.262E-02	0.816	0.816	0.816
15	O	D	D	0.053	0.05	0.557E-03	0.614E-03	0.816	0.816	0.816
16	O	D	D	0.053	0.01	0.264E-03	0.202E-03	0.816	0.816	0.816

In general terms, one may conclude that in these examples, CELLAM performed slightly better than BELLAM. Runs 1 to 4 do not involve significant boundary contributions. When this is the case, BELLAM and the Modified Method of Characteristics (MMOC), become identical [1]. From the results shown in Table 2, it follows that in the examples treated, CELLAM is slightly more precise than MMOC. On the other hand, when the boundary contributions are important, MMOC is considerably less accurate than CELLAM and BELLAM.

B. Comparison Based on the Maximum Value

In [1], the maximum of the numerical solution was compared with the maximum of the exact solution. Thus, for completeness, the same comparison is made here and the results are also illustrated in Table 2. Inspecting this table, it is seen that also when the performance is judged according to this criterium, the results obtained with CELLAM are at least as good as BELLAM.

Observe that when the domain is $O=[-3, 2\frac{1}{3}]$, the maximum of the Gaussian distribution (6.1) has already crossed the outflow boundary of the spatial domain, so that when the boundary conditions are of Dirichlet type, the maximum values of the approximate and the exact solutions are equal. Hence, this comparison is not informative in those cases.

7 DISCUSSION AND CONCLUSIONS

The central subject of Quantitative Isotopic Hydrology, consists in studying the transport of tracers by water flowing in a porous medium and the interactions that take place between the solid matrix and the solutes. The corresponding mathematical models, derive from the advection-diffusion equation. The numerical solution of this equation, is a problem of great importance in many other scientific and technical fields, as well and it is being the subject of intensive research.

The numerical treatment of the advection-diffusion equation when advection is dominant, has been a challenging problem for a long time, specially if a sharp front is present. A feature that is required from algorithms in order to be able to model effectively advection dominated transport, is that its performance be independent of the Courant number, to a large extent. Another feature which is essential, specially in Quantitative Isotopic Hydrology, is that the algorithms be mass-conservative, even when significant boundary behavior is present.

It has been recognized that in order for the performance of an algorithm to be independent of the Courant number, it is necessary to incorporate in its formulation the structure of characteristic lines. Methods which are based in the characteristic structure of the differential equations, are known as "characteristic" or "Lagrangian" methods. Until recently, characteristic methods had had three important limitations: inability to ensure mass conservation, inability to treat boundary fluxes effectively and the introduction of numerical dispersion, due to low order interpolation or integration.

With the developmenmt by the author and coworkers, of Eulerian-Lagrangian Localized Adjoint Methods (ELLAM), which are based in the general LAM methodology introduced by the author, the limitations of characteristic methods mentioned above, have been overcome to a large extent.

The ELLAM approach can be implemented in several manners. Up to now two such implementations have been developed: BELLAM and CELLAM. Evidence has been presented, which indicates that CELLAM is at least as accurate as BELLAM and in some cases, more accurate. In addition, CELLAM is easier to implement and more general, since it is applicable to the general advection-diffusion equation with non-constant coefficients.

Here BELLAM and CELLAM have been explained and discussed, making them more readibly available to the scientific community which works in Quantitative Isotopic Hydrology.

REFERENCES

1 Celia, M.A., Russel, T.F., Herrera, I., and Ewing, R., "An Eulerian-Lagrangian Localized Adjoint Method for the Advection-Diffusion Equation", Advances in Water Resources, 13(4), pp.187-206, 1990.

2 Herrera, I., Ewing., R.E., Celia, M.A., and Russell, T.F., Eulerian-Lagrangian Localized Adjoint Method: The Theoretical Framework.- Numerical Methods for Partial Differential Equations 9(4), pp 431-457, 1993.

3 Herrera, I., Localized Adjoint Methods: A New Discretization Methodology, Chapter 6 of the book: "Computational Methods in Geosciences", W.E. Fitzgibbon & M.F. Wheeler Eds., SIAM, pp 66-77, 1992 (Invited paper).

4 Herrera, I., Localized Adjoint Methods in Water Resources Problems, In Computational Methods in Surface Hydrology, G. Gambolati, A. Rinaldo and C.A. Brebbia, Eds., Springer-Verlag, 433-440, 1990 (invited paper).

5 Herrera, I.,"Localized Adjoint Method: An Overview", **Advances in Computer Methods for Partial Differential Equations VII**, R. Vichnevetsky, et al. (Editors), *International Association for Mathematics and Computers in Simulation (IMACS)*, pp 342-348, 1992 (invited paper).

6 Herrera, I., "Innovative Discretization Methodologies Based on LAM", FEMIF93, Barcelona, 1993. (To appear).

7 Herrera, G. and I. Herrera, "An Eulerian-Lagrangian Method of Cells, Based on the Localized Adjoint Method", Num. Methods for Partial Differential Equations, 1994 (In press).

8 Herrera, G.,"Tratamiento Numérico de Transporte Dominado por Advección, Thesis, Instituto de Geofísica, UNAM, México, 1992.

9 Herrera, G.S., I. Herrera and A. Galindo, "ELLAM Procedures for Advection Dominated Transport", **Advances in Computer Methods for Partial Differential Equations VII**, R. Vichnevetsky, et al. (Editors), *International Association for Mathematics and Computers in Simulation (IMACS)*, pp 333-341, 1992 (invited paper).

10 Herrera, G.S. and I. Herrera, "Application of LAM to Advection Dominated Transport", FEMIF93, Barcelona, 1993. (To appear).

11 Russell, T.F and R.V. Trujillo., "Eulerian-Lagrangian Localized Adjoint Methods with Variable Coefficients in Multiple Dimensions", Computational Methods in Surface Hydrology, Eds. G. Gambolati et al., Computational Mechanics Publications, Springer Verlag, pp. 357-363. 1990.

12 Ewing, R. E.,"Operator Splitting and Eulerian-Lagrangian Localized Adjoint Methods for Multiphase Flow", J. Whiteman Ed., MAFELAP 1990, Academic Press, San Diego, pp. 215-232, 1991.

13 Herrera , I. , R.E. Ewing.,"Localized Adjoint Methods: Applications to Multiphase Flow Problems." Proceedings Fifth Wyoming Enhanced Oil Recovery Symposium, Mayo 10-11, 1989, Enhanced Oil Recovery Institute, University of Wyoming, pp. 155-173, 1990.

14 Ewing, R.E. and Celia. M.A., "Multiphase Flow Simulation in Groundwater Hydrology and Petroleum Engineering". Computational Methods in Subsurface Hydrology, Eds, G. Gambolati et al., Computational Mechanics Publications, Springer Verlag, pp. 195-202. 1990.

15 Zisman, S., "Simulation of contaminant transport in groundwater systems using Eulerian-Lagrangian localized adjoint methods," MS Thesis, Dept. Civil Eng., MIT, 1989.

16 Celia, M.A and Zisman S,"Eulerian-Lagrangian Localized Adjoint Method for Reactive Transport in Groundwater" Computational Methods in Subsurface Hydrology, Eds, G. Gambolati et al., Computational Mechanics Publications, Springer Verlag, pp. 383-390. 1990.

17 Neuman, S.P.,"Adjoint Petrov-Galerkin Method with Optimum Weight and Interpolation Functions Defined on Multi-dimensional Nested Grids", Computational Methods in Surface Hydrology, Eds G. Gambolati et al., Computational Mechanics Publications, Springer Verlag, pp. 347-356, 1990.

18 Espedal, N.S., and Ewing, R.E., "Characteristic Petrov-Galerkin subdomain methods for two-phase immiscible flow", Comp. Meth. Appl. Mech. Engng., (64) pp 113-135, 1987.

19 Dahle, H.K., Espedal, N.S., and Ewing, R.E., "Characteristic Petrov-Galerkin subdomain methods for convection diffusion problems", IMA Numerical Simulation in Oil Recovery, M.F., Wheeler (ed), Springer-Verlag, Berlin, (11), pp 77-88, 1988.

20 Wang H., R.E. Ewing, and T.F. Russell, "Eulerian-Lagrangian localized adjoint methods for convection-diffusion equations and their convergence analysis", IMA J. Numer. Anal., 1992. (to appear).

21 Cantekin, M.E. and Westerink J.J. "Non-Diffusive N+2 degree Petrov-Galerkin methods for two-dimensional transient transport computations, Int. J. Num. Meth. Engrg., 30 (1990), 397-418.

22 Westerink, J.J., and D. Shea, "Consistent higher degree Petrov-Galerkin Methods for the Solution of the Transient Convection-Diffusion Equation, Int. J. Num. Meth. Engng., 28 (1989), 1077-1102.

23 Bouloutas, E.T. and Celia, M.A., "An analysis of a Class of Petrov Galerkin and Optimal Test Functions Methods", Numerical Methods for Transport and Hydrologic Processes, Vol. 2, M.A. Celia et al., Eds., Vol. 36 of the Series Development in Water Science, Elsevier, Amsterdam, 1988, pp 15-20, 1988.

24 Bouloutas, E.T. and Celia, M.A., "An improved cubic Petrov-Galerkin Method for Advection-Dominated flows in rectangularly decomposable domains", to appear in Comp. Meth. Appl. Mech. & Engng., 1993.

25 Herrera, I., L. Chargoy y G. Alduncin., "Unified Approach to Numerical Methods. Part 3. Finite Differences and Ordinary Differential Equations, Journal of Numerical Methods for Partial Differrential Equations, 1,241-258 (1985)

26 Herrera, I., The algebraic theory approach for ordinary differential equations: Highly accurate finite differences, Journal of Numerical Methods for Partial Differential Equations, 3(3), pp 199-218, 1987.

27 Celia, M.A. and I. Herrera, Solution of general differential equations using the Algebraic Theory approach, Journal of Numerical Methods for Partial Differential Equations, 3(1), pp 117-129, 1987

28 Celia, M.A., Herrera, I., and Bouloutas, E.T., "Adjoint Petrov-Galerkin Methods for Multi-Dimensional Flow Problems", In Finite Element Analysis in Fluids, T.J. Chung and Karr R., Eds., UAH Press, Huntsville Alabama. pp. 953-958, 1989.

29 Celia.,M,A. Herrera,I., Bouloutas I.E. and Kindred, J.S.,"A New Numerical Approach for The Advective Diffusive Transport Equations", Numer. Methods for Partial Differential Equations, 5(3), 203-226, 1989.

30 Celia, M.A., Kindred, J.S., and Herrera, I., "Contaminant Transport and Biodegradation: 1. A Numerical Model for Reactive Transport in Porous Media", Water Resources Research, 25(6) PP 1141-1148, 1989.

31 Herrera, I., "Boundary methods: An algebraic theory", Pitman Advanced Publishing Program, Boston, London, Melbourne, 1984

32 Herrera, I., "Unified Approach to Numerical Methods. Part 1. Green's Formulas for Operators in Discontinuous Fields", Journal of Numerical Methods for Partial Differential Equations, 1(1), pp 12-37, 1985.

33 Herrera, I., "Unified Approach to Numerical Methods, Part 2. Finite Elements, Boundary Methods, and its coupling", Numerical Methods for Partial Differential Equations, 3, pp 159-186, 1985.

34 Herrera, I., "Some unifying concepts in applied mathematics", En "The Merging of Disciplines: New Directions in Pure, Applied, and Computational Mathematics". Edited by R.E. Ewing, K.I. Gross and C.F. Martin. Springer-Verlag, New York, pp 79-88, 1986 (invited paper).

35 Herrera, I., "On Operator Extensions: The Algebraic Theory Approach", Proceedings of VII Taller IIMAS-UNAM, Oaxaca, January, 1992 (invited paper).

36 Neuman, S.P., "An Eulerian-Lagrangian Numerical Scheme for the Dispersion-Convection Equation using Conjugate Space-time Grids", Jr. Computational Phys. 41, 270-294, 1981.

37 Neuman, S.P., "Adaptive Eulerian-Lagrangian Finite-element Method for Advection-dispersion, International Journal Numerical Meth Engng. 20, 321-337, 1984.

38 Garder, A.O., Peaceman, D.W. and Pozzi, A.L., "Numerical Calculations of multidimensional miscible displacement by the method of Characteristics", Soc. Pet. Eng. Journal 4(1), 26-36, 1964

39 Konikow, L.F., and Bredehoeft, J.D., "Computer Model of Two-dimensional Solute Transport and Dispersion in Groundwater", Journal of Tech of Water-Resources. Inv of the U.S. Geol. Surv, Book 7 Chapter C2, 90p 1978.

40 Douglas, J Jr, and Russell, T.F., Numerical Methods for Convection-dominated Diffusion Problems Based on Combining the Method of Characteristics with Finite Element or Finite Difference Procedures, SIAM, J Numerical Analysis 19, 871-885, 1982.

41 Russell, T.F. Wheeler, M.F., and Chiang, C.Y., "Large-scale Simulation of Micible Displacement by Mixed Characteristic Finite Element Methods, in Mathematical and Computational Methods in Seismic Exploration and Reservoir Modeling", W.E. Fitzgibbon, Piladelphia, SIAM 85-107, 1986.

42 Espedal, M.S., and Ewing, R.,E., "Characteristic Petrov-Galerkin Subdomain Methods for Two-phase Immerscible Flow", Computational Methods. Appl. Mech. Engng. 64, 113-136, 1987.

43 Pinder, G.F., and Cooper, H.H. "A Numerical technique for calculating the transient position of the saltwater front, Water Resources Research, 6 (3), pp 875-882 1970.

44 Healy, R.W., and Russell, T.F., "Efficient Implementation of the Modified Method of Characteristics in Finite-Difference Models of Solute Transport", Proceedings of Conference in Solving Ground Water Problems with Models, edited by J. Lehr, Indianapolis, NWWA, pp 483-491, 1989.

45 Healy, R.W., and Russell, T.F., "A Finite-Volume Eulerian-Lagrangian Localized Adjoint Method for Solution of the Advection-Dispersion Equation", Water Resour. Res., to appear, 1993.

ASSESSMENT OF GROUNDWATER FLUXES AND TRANSMISSIVITIES BY ENVIRONMENTAL TRACERS: SUMMARY OF THEORY, APPLICATION AND SENSITIVITY ANALYSIS

E.M. ADAR
Ben-Gurion University of the Negev,
Sede Boker, Israel

Abstract

This paper demonstrates the implementation of a novel mathematical model for assessing groundwater fluxes and distribution of transmissivities in groundwater basin with several sources of recharge. It is based on the assumption that each source is associated with unique characteristics of isotopic ratios and dissolved constituents. The model applies to basins with complex hydrogeological structures for which scarce physical hydrologic information is available. The model is based on spatial distribution of environmental tracers and relies heavily on stable isotopes of oxygen and hydrogen. It is assumed that spatial variations of dissolved constituents and isotopic ratios in the aquifer can be attributed to mixing and dilution of several sources of groundwater recharge. Tracers are assumed to be conservative along the flow path. The flow domain is discretized into mixing cells based on the distribution of the dissolved constituents. Environmental tracers are then used to write a set of water and mass balance equations in a compartmental flow system, such that the unknowns are transmissivities and groundwater fluxes. Quadratic programming is used for a unique assessment of the unknowns. The model has been tested for two multi-cell flow systems with synthetic data for which a precise analytical solution is available. The model was later implemented for a steady flow system to estimate recharge, internal fluxes and transmissivities in an arid alluvial basin of the southern Arava Valley, Israel. Results indicate that the calculated transmissivities for the alluvial aquifer of the southern Arava are close to what was obtained with interference pumping tests. Sensitivity analysis indicates that (1). the model is extremely sensitive to the accuracy of the chemical and isotope constituents assigned to the external flow components and to each aquifer compartment, and (2). the accuracy of the assessed transmissivities is highly related to both precise tracers' concentrations and to the assigned geometry of the cells.

1. INTRODUCTION

To properly manage groundwater resources, there is a need for accurate information about inflows (recharge), outflows (discharge) and the physical characteristics of aquifers. Yet it has been common to exploit aquifers based only on partial information concerning the hydrologic characteristics of many semi-arid and arid basins. A major source of uncertainty stems from the hydrologist's inability to reliably estimate the spatial and temporal distribution of recharge rates, groundwater fluxes, transmissivities and storativities. It is highly related to the obscure knowledge of the subsurface geohydrological system.

Quantitative assessment of recharge and groundwater flow components is often complicated in basins with scarce hydrological information and having a

puzzling geological structure. Therefore, an analytical solution is usually out of the question. However, the lack of precise geohydrological information along external and internal boundaries exclude even the implementation of numerical solutions.

Knowledge of the spatial distribution of groundwater fluxes, recharge components and the physical parameters of an aquifer such as transmissivities, are essential for the development of groundwater resources. Fluxes through external boundaries (recharge and discharge) and along stream lines can be assessed by numerical solution of the flow equation, provided that the piezometric and the aquifer's parameters distribution are known for well determined subsurface flow system. In general, transmissivity can be calculated from interference and recovery pumping tests. Various methods have been developed for the interpretation of pumping tests, and most rely on the Theis [1] method for applying the flow equation to simple infinite confined aquifers. However, methods can vary according to the geometry and type of aquifer and also according to the geometry of the pumping and monitoring wells. The main methods are listed in Kruseman and De Ridder [2]. The assumptions behind the analytical Theis solution, and the interpretation of the well function from pumping test data, restrict the utilization of such methods to very simple and local hydrological systems. Another, more practical, approach for the evaluation of the spatial distribution of transmissivities relies on the so-called inverse method of numerical solution for the flow equation (i.e., Carrera and Neuman, [3] and [4]). In this method, precise boundary conditions are required for the assessment of transmissivities, and accurate initial conditions are needed for the evaluation of storativities. Wittmeyer and Neuman [5] used quadratic estimation criteria for a set of hydraulic conductivity data to meet the hydraulic head distribution. An adaptive method applied to an elliptic PDE for simultaneous identification of aquifer parameters was suggested by Hoffman et. al. [6] for Dirichlet boundary conditions. Carrera and Glorioso [7] demonstrated a geostatistical formulation of the inverse problem of groundwater flow. Whi, Leodoux and Marsily [8] used the inverse method for parameter estimation in deep aquifers in Paris basin via a calibration process of a numerical model of a transient flow equation. All the above mentioned methods, however, can rarely be implemented in remote and undeveloped basins due to lack of basic hydrological information.

In basins with a limited number of wells and hence limited knowledge of the hydrogeological structure, it is often difficult to precisely define the flow system or the boundary conditions. Furthermore, the lack of observation wells and pumping test data eliminate the possibility of proper calibration processes. To improve the ability of modelling groundwater flow systems, environmental tracers have long been used to further illuminate on the subsurface flow pattern.

In the past, hydrologists have used chemical and isotope data for recharge studies primarily in a qualitative sense. Environmental isotopes played a dominant role in such studies, as exemplified by the works of Verhagen, et al. [9], Gat and Dansgaard [10], Mazor, et. al. [11], Levin, et. al. [12], and Rosenthal et. al. [13]. In other studies, tritium was used to obtain quantitative estimates of recharge (Eriksson [14], Bredenkamp, et al.,[15], Vogel, et al., [16], and Allison and Hughes [17]). Different conceptual modeling of hydrological systems relies on a lumped parameter modeling in a continuum approach using the so-called convolution integral. This concept can be exemplified by a series of papers by Maloszewski and Zuber (i.e. [18] and [19]), and Zuber et al. [20]. A comprehensive

review of the implementation of the above mentioned approach can be found in Nir [21], Zuber [22] and [23], and in Goblet [24]. These methods can be only implemented for a pronounced stream line for the evaluation of an average flow velocity, storage coefficient and transmissivity. An attempt to incorporate natural tracers in hydrological modeling in a combined hydrologic and hydrochemical mathematical model for the purpose of source identification and quantification was presented by Gorelick, et al. [25] and Wagner and Gorelick [26]. They deal with the question of identifying the location and magnitude of pollution sources that might have contributed to the contamination of an aquifer. For this, they utilize a two-dimensional, numerical model of solute transport in the aquifer, coupled with various optimization techniques.

Attempts to extract quantitative information concerning the groundwater flow system from hydrochemical data often rely on statistical analyses. As an example, Lawrence and Upchurch [27] used factor analysis to identify the recharge source for certain groups of dissolved chemical species in an aquifer. In all such works, the authors either evaluate the magnitude of a given recharge source, or evaluated the potential of recharge without providing quantitative estimates of recharge rates. Rosenthal et al., [13] and Adar et al. [28] used cluster analyses to classify groundwater units to be later incorporated in a numerical model for a quantitative assessment of recharge.

Environmental tracers have long been used to elaborate on groundwater flow systems. Recently, however, environmental tracers have been applied to a quantitative hydrological modeling of a regional aquifer. For this, the so-called Mixing Cell Approach (Simpson and Duckstein [29]), has been adapted. For basins with a complex geological structure and with scarce hydrologic information, this paper introduces a method for incorporating environmental tracers and mixing cell approach for the quantitative assessment of transmissivities and fluxes. This paper briefly describes the theory and presents results obtained from synthetic data and from an alluvial basin with an extremely complicated hydrogeological system, such as the southern Arava Rift Valley, eighty kilometers north of the Gulf of Eilat (Figure 4).

2. THEORY

Adar and Neuman [30] and Adar et al. [31] have demonstrated the utilization of environmental tracers for quantitative evaluation of various sources of recharge. Adar and Sorek [32] extended this approach and presented a theory which enabled to assess the physical parameters of the aquifer from the piezometric head distribution and the spatial distribution of natural dissolved tracers.

The model relies on two types of conceptual approaches applied in groundwater hydrology:

1. Evaluation of the motion of water and dissolved constituents in a multi-compartmental mixing cell model, as suggested initially by Simpson and Duckstein [29[and Yurtsever and Payne [33].
2. Quantitative assessment of groundwater flow components by optimizing a set of mass balance equations of water, ions and environmental isotopes in a multi-cell aquifer system. This approach assumes a steady flow system and fully conservative dissolved tracers (Adar et al., [31]).

Campana and Simpson [34] and Campana and Mahin [35] used the distribution of stable isotopes in multi-compartmental modeling to calculate

internal fluxes, rates of recharge and groundwater storage, respectively. Van Ommen [36], found a good agreement between a mixing-cell model with a one-dimensional convection/diffusion equation in transport of reactive and non reactive constituents in groundwater flow system. Yurtsever and Payne [37] and Yurtsever et al. [38] formulated a mathematical models for the interpretation of isotope distribution in a regional compartmental aquifer to quantitatively evaluate the groundwater flow system. A similar model was successfully implemented for the Bangkok Basin in Thailand (Yurtsever and Buapeng [39]).

In the following model, the steady flux for every flow component can be estimated providing that the general flow pattern and the spatial distribution of environmental tracers are known, and the number of mass balance equations over the entire flow system is much greater than the number of unknown fluxes. A solution is obtained utilizing an optimizing quadratic programming scheme, as suggested by Woolhiser et al. [40]. For a periodic transient flow system, Adar and Sorek [32] and [41] showed that if in addition to the tracer distribution, the spatial hydraulic head distribution is also available, the model can be used to assess the cell's storage coefficient and transmissivity across every permeable cell boundary. This paper describes a method for assessing the transmissivities in a steady flow system where the Darcian expression is directly embedded into the mass balance expressions. Results from the southern Arava Valley, Israel are compared with transmissivity values obtained from evaluation of pumping tests. Comprehensive sensitivity analyses is followed, taking into account possible errors in isotopic and chemical data, as well as the assessment of the geometry of the cell's configuration.

The model is designed in order to account for natural tracers, such as dissolved chemicals and minerals (ions and trace elements), electrical conductivity, and environmental stable isotopes. Knowledge of the accurate flow pattern and the piezometric water head potential in every cell is essential for obtaining the transmissivities across the permeable boundaries. These water characteristics and hydrogeological information are relatively easily attained, even in undeveloped basins with limited hydrogeological data. This model conceptualizes an aquifer system that can be discretized into a finite number of cells, such that each cell can be assigned with a unique representative value of the piezometric head and concentrations of tracers. This implies complete dilution and, hence, a complete mixing of all water sources entering each cell. With the mixing cell approach, we assume that at each segment (compartment) of the aquifer gradients of ions and isotopes concentrations and water head potentials are small and hence negligible. Therefore, the concentrations of solutes within cells and the hydraulic head are assumed to be constant for a specific time step. For each cell and potential source (contributor), one should be able to determine the same representative values of all accounted tracers and hydraulic heads. Similarly, in every compartment, the same information must be known for sinks and sources, if they exist. Therefore, it is assumed that enough observation wells and/or springs are available for head measurements and water sampling.

Mass balance expressions for water and solutes are written for each compartment, taking into account all the potential sources of water that may contribute to the subsurface reservoir enclosed by each cell's boundaries. Therefore, all the flow components entering and leaving the specific compartment must be known, at least qualitatively. Most sink or point source terms can be assessed quantitatively. Fluxes are described by a Darcian type of

expression that includes terms related to transmissivities via the geometry of the compartments.

2.1 Quantitative assessment of transmissivities

With regard to the above ideas, we will now write a set of balance equations for the flux and solutes within a given time period Δt and for each cell **n**. It is assumed that the flow system is steady at least within the time period Δt. For a fluid with constant density, the mass balance for the **n**-th compartment is expressed by the following equation:

$$So_n + \sum_{i=1}^{I_n} Q_{in} - \left(\sum_{j=1}^{J_n} Q_{nj} + Pm_n \right) = S_n^* \frac{dh_n}{dt} \qquad (1)$$

where I_n and J_n denote the number of sources and/or compartments from which the flow enters and leaves the **n**-th compartment, respectively. Q_{in} and Q_{nj} denote the fluxes from the **i**-th source (or compartment) into the **n**-th , and from the **n**-th compartment into the **j**-th compartment, respectively. So_n and Pm_n denote the fluid sources and sinks (pumping), respectively, in the **n**-th compartment. S_n^* represents the storage capacity within cell **n** and h_n denotes the hydraulic head associated with that compartment.

As the head (h_n) for each compartment varies, we may identify points in time, say t_1 and t_2 ($t_2 > t_1$), at which the hydraulic heads are the same (e.g., at the beginning and end of a specific season). This means that over that time interval $\tau = t_2 - t_1$ (regardless of the sequence of changes in heads during this time interval), the total magnitude of the derivatives dh_n/dt in each compartment has not changed. Hence, since $S_n^* \neq S_n^*(t)$, we obtain:

$$\frac{1}{t} \int_{t_1}^{t_2} S_n^* \frac{dh_n}{dt} = 0 \quad ; \quad h_n(t_1) \cong h_n(t_2) \qquad (2)$$

Thus, by integrating equation (2) over a time period $\tau = t_2 - t_1$ and dividing by τ we obtain accordingly:

$$\overline{So}_n - \overline{Pm}_n + \sum_{i=1}^{I_n} \overline{Q}_{in} - \sum_{j=1}^{J_n} \overline{Q}_{nj} = 0 \qquad (3)$$

where $\overline{Q}_{in}$ and $\overline{Q}_{nj}$ denote the average values of Q_{in} and Q_{nj}, respectively, i.e.:

$$\overline{Q}_n = \frac{1}{t} \int_{t_1}^{T} Q_{in} dt \qquad (4)$$

Likewise, the time averaged values of the source and sink fluxes in cell **n** are $\overline{So}_n$ and $\overline{Pm}_n$ respectively. Note that equation (3) expresses a quasi-steady state situation resulting from the time averaging process.

Following Darcy's flow expression for a steady flow, every flux term in equation (3) leaving or entering cell **n** can be written in terms of the cell's

geometry, transmissivity and hydraulic head difference across the active boundary.

$$Q_{nj} = T_{nj} \underbrace{w_{nj}(h_n - h_j)/Dl_{nj}}_{F_{nj}} = T_{nj} F_{nj} \tag{5}$$

where T_{nj} is the transmissivity across the boundary between cells **n** and **j**, respectively. w_{nj} is the width of the boundary normal to the flow path, and l_{nj} is the length of the stream line between the geometric centers in cells **n** and **j**. The term F_{nj} includes hydraulic head difference between cell **n** and **j**, and all the known parameters related to the geometry of the cell.

From this point, let I_n designate only the number of inflows into cell **n** from external sources, and M_n designate the number of inflows into cell **n** from nearby cells. It is assumed that in addition to pumping, all outflow components from cell **n** enter the nearby cell **j** ($j=1,2,.....,J_n$). Therefore from equations (3) and (5) the water balance expression can be rewritten as follows:

$$So_n + \sum_{i=1}^{I_n} Q_{in} + \sum_{m=1}^{M_n} F_{mn} T_{mn} - \left(\sum_{j=1}^{J_n} Q_{nj} + Pm_n \right) = \varepsilon_n \tag{6}$$

where F_{mn} is a factor which includes the geometric parameters between cells **m** and **n** and the head difference across the **m-n** boundary as expressed in equation (5). ε_n is an error term for a possible deviation from the water balance due to the misunderstanding of the appropriate flow pattern and/or disregarding one or more of the flow components. Water balance (equation (6)) might not hold because of an error in identifying and measuring of fluxes or rates of pumping.

Assuming only small variations in the concentrations of the dissolved constituents during the time period Δt, one can write a mass balance expression for the average concentration of every species (tracer) **k** in cell **n**.

For quasi steady-state variations of concentrations, when the mixing cell concept is applied, using the above mentioned assumptions and equation (6), we write a mass balance expression for a dissolved constituent **k** in cell **n**.

$$Cs_{nk} So_n + \sum_{i=1}^{I_n} Ci_{ink} Q_{in} + \sum_{m=1}^{M_n} Ct_{mnk} F_{mn} T_{mn} - Cn_k \left(\sum_{j=1}^{J_n} Q_{nj} + Pm_n \right) = \varepsilon_{nk} \qquad k=1,2,....,K \tag{7}$$

where Cs_{nk} is the average concentration of **k** associated with source So_n; Ci_{ink} is the average concentration of solute **k** entering cell **n** together with the flux coming from cell I. Ct_{mnk} is the concentration of **k** entering **n** through the m^{th} boundary, and Cn_k denotes average concentration of the k^{th} constituent within cell **n**. When constructing mass balance equations from field measurements, ε_{nk} is the deviation from the solute balance in cell **n**. The mass balance of solutes (equation 7) may be affected by analytical errors in measuring concentrations, especially when quantifying cell concentrations. For every cell **n**, there are K+1 equations: one for the water balance and **K** more for every **k** species ($k=1,2,.....,K$). This is demonstrated in equation 8.

$$
\begin{aligned}
&Q_{1n} + \ldots + Q_{Inn} + F_{1n}T_{1n} + \ldots + F_{Mnn}T_{Mnn} - Q_{n1} - \ldots - Q_{nJn} - \mathrm{Pm}_n + \mathrm{So}_n = \varepsilon_n \\
&Ct_{1n1}Q_{1n} + \ldots + Ct_{Inn1}Q_{Inn} + Ct_{1n1}F_{1n}T_{1n} + \ldots + Ct_{Mnn1}F_{Mnn}T_{Mnn} - Cn_{n1}Q_{n1} - \ldots - Cn_{n1}Q_{nJn} - Cn_{n1}\mathrm{Pm}_n + Cs_{n1}\mathrm{So}_n = \varepsilon_{n1} \\
&Ct_{1n2}Q_{1n} + \ldots + Ct_{Inn2}Q_{Inn} + Ct_{1n2}F_{1n}T_{1n} + \ldots + Ct_{Mnn2}F_{Mnn}T_{Mnn} - Cn_{n2}Q_{n1} - \ldots - Cn_{n2}Q_{nJn} - Cn_{n2}\mathrm{Pm}_n + Cs_{n2}\mathrm{So}_n = \varepsilon_{n2} \qquad (8) \\
&Ct_{1nk}Q_{1n} + \ldots + Ct_{Innk}Q_{Inn} + Ct_{1nk}F_{1n}T_{1n} + \ldots + Ct_{Mnnk}F_{Mnn}T_{Mnn} - Cn_{nk}Q_{n1} - \ldots - Cn_{nk}Q_{nJn} - Cn_{nk}\mathrm{Pm}_n + Cs_{nk}\mathrm{So}_n = \varepsilon_{nk}
\end{aligned}
$$

Upon combining equations (6) and (7) to a matrix form for each compartment **n**, we obtain:

$$\underline{\underline{\mathbf{C}}}_{\mathbf{n}}\underline{\mathbf{X}}_{\mathbf{n}} + \underline{\mathbf{D}}_{\mathbf{n}} = \underline{\mathbf{E}}_{\mathbf{n}} \qquad (9)$$

where $\underline{\underline{\mathbf{C}}}_{\mathbf{n}}$ is a matrix with known concentrations associated with every flux entering or leaving cell **n**. $\underline{\mathbf{X}}_{\mathbf{n}}$ is a vector of the unknown fluxes through the boundaries of cell **n**. $\underline{\mathbf{D}}_{\mathbf{n}}$ is a vector containing elements that are measured and known quantitatively in cell **n**, such as known fluxes of sink (pumping) and sources. $\underline{\mathbf{E}}_{\mathbf{n}}$ is the error vector in cell **n**. A comprehensive description of the above mentioned vectors and matrices is given in equation 10.

$$
\begin{bmatrix}
1 + \ldots + 1 + F_1 + \ldots + F_{Mn} - 1 - \ldots - 1 \\
Ct_{11} + \ldots + Ct_{In1} + Ct_{11}F_1 + \ldots + Ct_{Mn1}F_{Mn} - Cn_1 - \ldots - Cn_1 \\
Ct_{12} + \ldots + Ct_{In2} + Ct_{12}F_1 + \ldots + Ct_{Mn2}F_{Mn} - Cn_2 - \ldots - Cn_2 \\
\vdots \\
Ct_{1k} + \ldots + Ct_{Ink} + Ct_{1k}F_1 + \ldots + Ct_{Mnk}F_{Mn} - Cn_k - \ldots - Cn_k
\end{bmatrix}
\begin{bmatrix}
Q_{1n} \\ \vdots \\ Q_{In\,n} \\ T_{1n} \\ \vdots \\ T_{Mn\,n} \\ Q_{n1} \\ \vdots \\ Q_{n\,Jn}
\end{bmatrix}
+
\begin{bmatrix}
So_n - Pm_n \\
Cs_{n1}So_n - Cn_{n1}Pm_n \\
\vdots \quad \vdots \\
\vdots \quad \vdots \\
\vdots \quad \vdots \\
Cs_{nk}So_n - Cn_{nk}Pm_n
\end{bmatrix}
=
\begin{bmatrix}
\varepsilon_n \\ \varepsilon_{n1} \\ \varepsilon_{n2} \\ \vdots \\ \vdots \\ \varepsilon_{nK}
\end{bmatrix}
\qquad (10)
$$

$$
\begin{array}{cccc}
[(K+1)(In+Mn+Jn)] & [(In+Mn+Jn)(1)] & [(K+1)(1)] & [(K+1)(1)] \\
\underline{\underline{C}} & \underline{X} & \underline{D} & \underline{E}
\end{array}
$$

All flux components in the aquifer can now be estimated by a minimization of the square error sums **J**. Similar to a procedure suggested by Adar et al. (31), by virtue of equation (6) and by assembling the square error terms over all **N** cells we obtain:

$$\mathbf{J} = \sum_{\mathbf{n=1}}^{\mathbf{N}} \left[\underline{\mathbf{E}}_{\mathbf{n}}^{\mathbf{T}}\,\underline{\underline{\mathbf{W}}}\,\underline{\mathbf{E}}_{\mathbf{n}}\right] = \sum_{\mathbf{n=1}}^{\mathbf{N}} \left[\left(\underline{\underline{\mathbf{C}}}_{\mathbf{n}}\underline{\mathbf{X}}_{\mathbf{n}} + \underline{\mathbf{D}}_{\mathbf{n}}\right)^{\mathbf{T}}\underline{\underline{\mathbf{W}}}\left(\underline{\underline{\mathbf{C}}}_{\mathbf{n}}\underline{\mathbf{X}}_{\mathbf{n}} + \underline{\mathbf{D}}_{\mathbf{n}}\right)\right] \qquad (11)$$

where $(\,)^{\mathbf{T}}$ denotes transpose matrix. $\underline{\underline{\mathbf{W}}}$ represents a diagonal matrix comprised of weighting values for estimated errors (independent of each other) expected for each of the terms building the mass balance for the fluid and the dissolved constituents. The weighting matrix, $\underline{\underline{\mathbf{W}}}$, also reflects the degree of confidence to

which the tracers are assumed conservative and the degree of accuracy of the chemical and isotope analyses. For the solution of equation (11) for $\mathbf{X_n}$ (a vector with $I_n+M_n+J_n$ unknowns), the objective function J is decomposed into linear and non-linear parts. For example, J can now be minimized to evaluate $\mathbf{X_n}$ by quadratic programming with an algorithm developed by Wolf [42].

3. TESTING THE MODEL AND THE COMPUTER CODE WITH SYNTHETIC DATA

The conceptual model and the computer code were tested with a set of synthetic data which was generated for a hypothetical aquifer divided into mixing cells. These tests were conducted in order to evaluate the ability of the computer code to solve simultaneously the mathematical model for unknown fluxes and transmissivities. The first test was conducted using four cells. The configuration of the cell set-up and the assigned fluxes, sinks, sources (volume per unit time), and transmissivities (area per unit time) for the internal boundaries are given in Figure. 1. Cell I has a sink (pumping) term and receives four inflows through external boundaries without a source term. Fluxes leaving Cell I contribute water

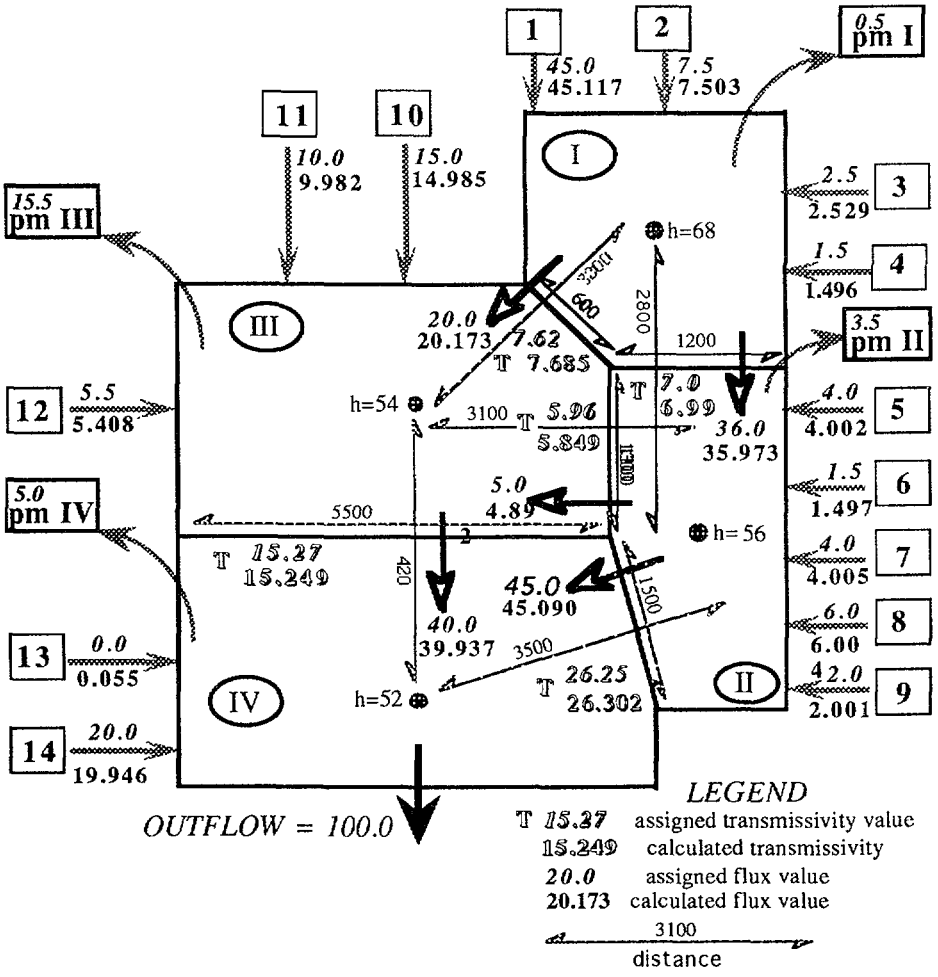

Figure 1 Schematic compartmental aquifer used for testing the mathematical algorithm. P_m is the rate of discharge (in volume per unit time). The upper numbers are the assigned values and the lower numbers designate the result obtained by quadratic programming.

to Cells **II** and **III** [36 and 20 (l^3/t), respectively]. Cell **II** also receives water from five external sources (Nos. 5 to 9 in Figure 1) and has both sink and source terms . Subsurface fluxes leave Cell **II** and flow into Cells **III** [5(l^3/t)] and **IV** [45(l^3/t)]. Cell **III** has three external sources with a sink term, and water leaves this cell and flows only into Cell **IV** [40(l^3/t)]. Cell **IV** has two external sources with a sink term and the total subsurface outflow is 100 (l^3/t). In Figure 1 the upper numbers designate the assigned fluxes or transmissivities used to calculate the concentration of the tracers for every cell, and the lower numbers are the results obtained from the model. The result indicates a precise evaluation of both fluxes and transmissivities.

To test the ability of the model to evaluate transmissivities and fluxes across active boundaries in a more realistic flow pattern, a complicated synthetic aquifer structure with a multi-cell flow system was used. In this test the aquifer was divided into twelve cells in a 3-D flow pattern, as illustrated in Figure. 2. Fifteen unknown internal fluxes and transmissivities were assigned for the internal active (permeable) boundaries. Fourteen different types of water were assigned as sources for external recharge. Two sources contribute the same type of water to more than one cell. Sources #13 and #16 are the same type of water which recharge Cells **X** and **XII**, respectively. Sources #10, #14 and #15 are also the same and contribute the same type of water to cells **IX**, **XI** and **XII**, respectively. In total seventeen unknown external sources. The total number of unknowns is 47 (17 external inflows, 15 internal fluxes and 15 transmissivities). Some of the cells: **VI**, **VII**, **VIII**, **X**, **XI** and **XII** were also assigned sink (pumping rates) terms. The numbers in the ellipsoids designate rates of inflows (recharge) from external sources. The upper numbers are the assigned values, while the lower ones are the computed results. Also in Figure 2, the numbers in the trapezoids specify the rates of internal fluxes between cells, and in Figure 3 these numbers specify the values of transmissivities. Here also the upper numbers designate assigned values, while the lower ones show the calculated values. Though internal fluxes and transmissivities are illustrated in different figures, it is important to emphasize that they were both obtained simultaneously. These values, while arbitrarily chosen (so as to maintain an isotopic and chemical balance for each species are nevertheless in accordance with actual data from the Aravaipa Valley in southern Arizona (Adar et al. [28]). With the flow rates in Figures 1 and 2, and with an appropriate concentration in the cell that follows the mixing cell approach, the error terms in equations (6) and (7) should be zero, and the minimization of **J.** in equation (11) should yield a zero value for the optimum solution. The noticeable, small variations between assigned and calculated values for fluxes and transmissivities are attributed to computer round off errors, as these small deviations vary slightly among different computers.

4. RESULTS FROM THE SOUTHERN ARAVA RIFT VALLEY.

The model has been used in an arid alluvial basin in the southern Arava Valley. The southern Arava Valley is a narrow down faulted rift valley about 20 km wide and extending about 80 km north of the Gulf of Eilat. It is an extremely arid basin with an average annual precipitation of about 50 mm. Due to its geological and geophysical nature, the rift forms a low base level into which surface, as well as subsurface, flows drain from the surrounding mountains. In the valley, water was found in (a) sandstone of Paleozoic age, (b) sandstone of

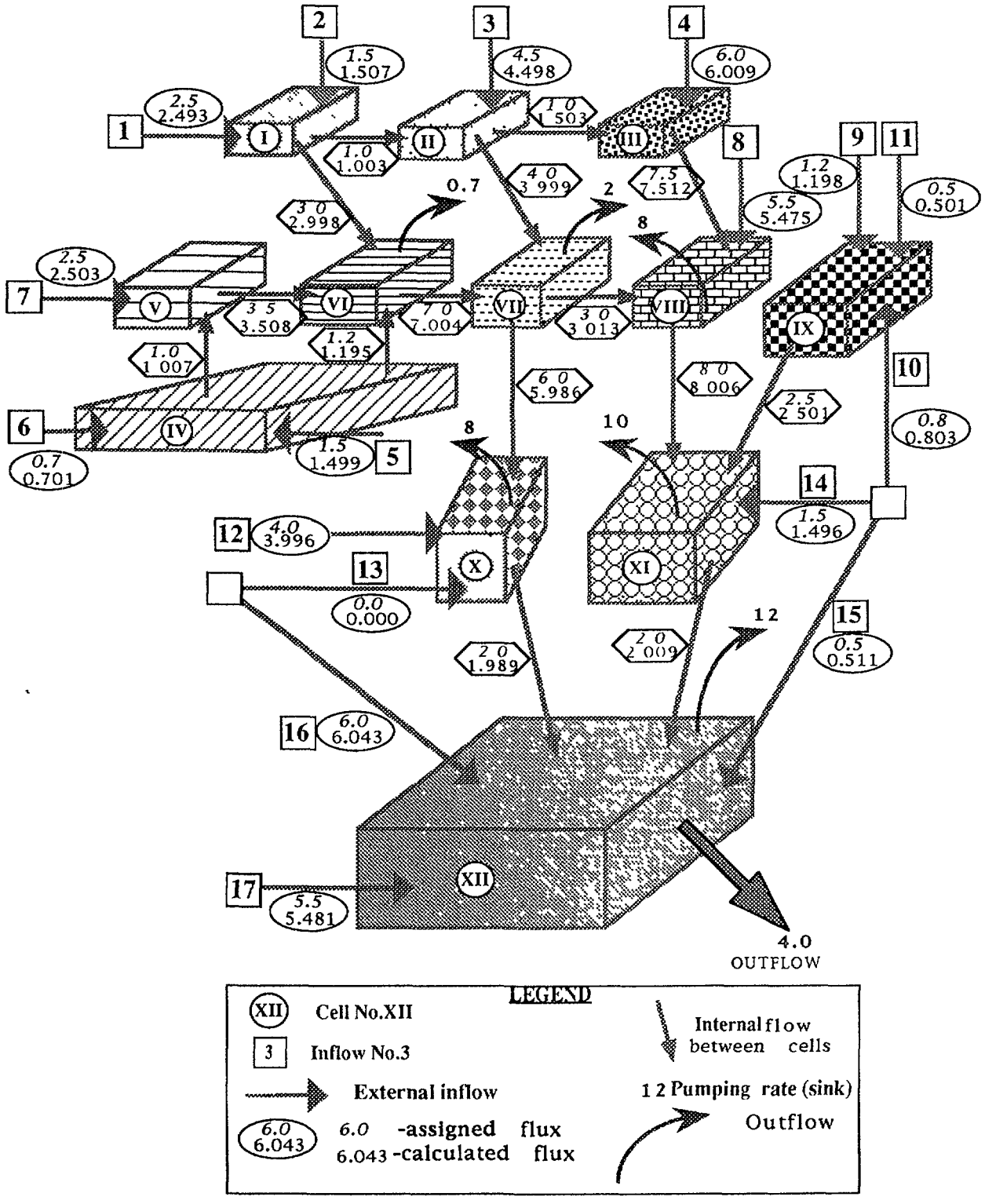

Figure 2. Estimating fluxes versus assigned values as obtained from a schematic multi-cell compartmental aquifer.

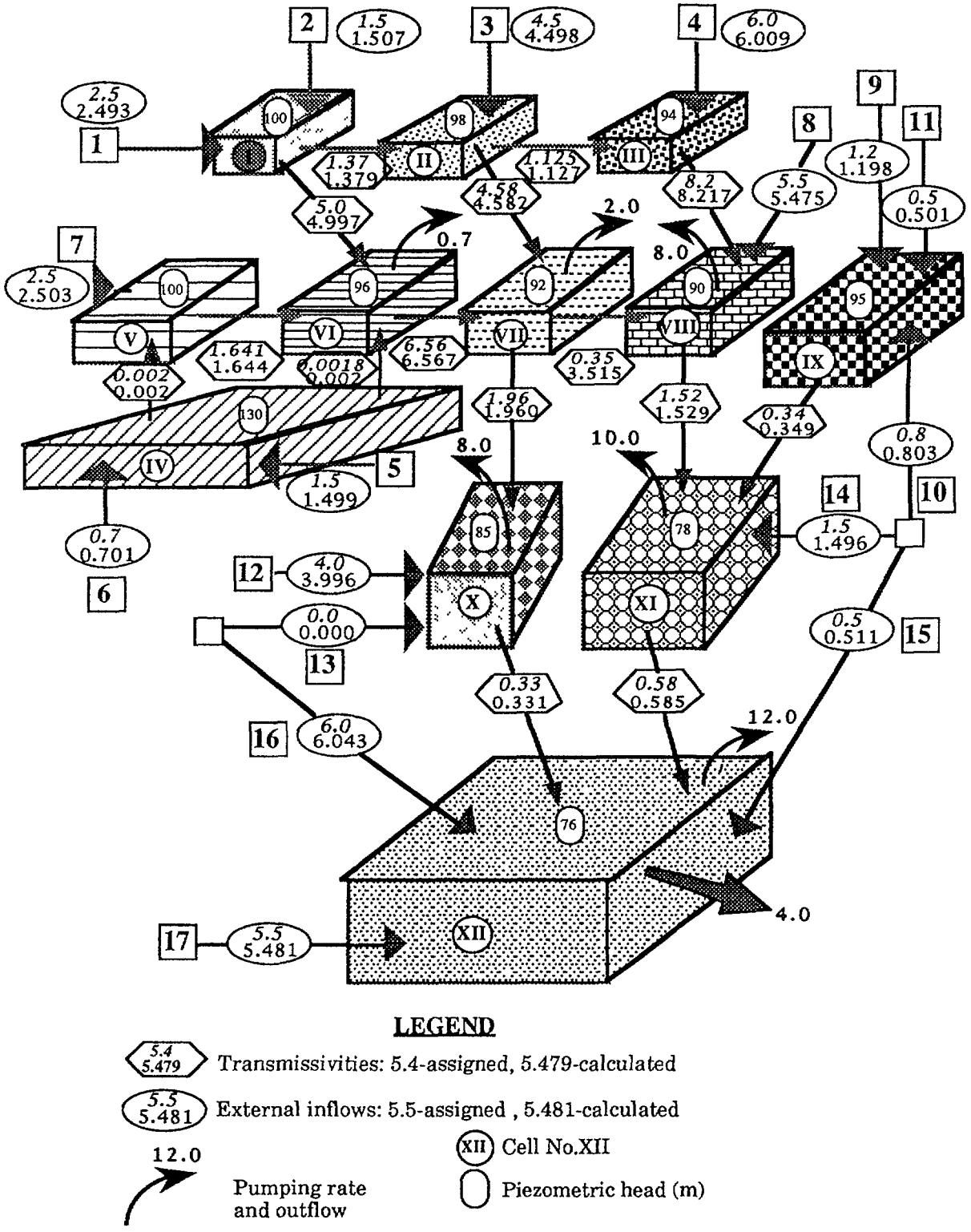

LEGEND

5.4 / 5.479 — Transmissivities: 5.4-assigned, 5.479-calculated

5.5 / 5.481 — External inflows: 5.5-assigned , 5.481-calculated

12.0 — Pumping rate and outflow

XII — Cell No.XII

Piezometric head (m)

Figure 3. Estimated transmissivities versus assigned values as calculated by the model for internal boundaries of the aquifer system.

Lower Cretaceous, (c) limestone of Cretaceous age, and (d) alluvial fill of Quaternary age. Figure 4 illustrates the geography, various geological outcrops and location of well fields along the valley. Due to extremely complex hydrogeologic structures caused by tilted faults, followed by upward and/or downward movement of blocks, it was almost impossible to obtain detailed and reliable information on the physical properties of each structural component of the aquifer system. The hydrogeological complexity is exemplified with two geological cross sections given in Figure 5. An attempt to determine the spatial distribution of transmissivities from pumping tests did not reveal reliable results. Interference tests which were performed in one pumping well related to several observation holes provided a wide range of transmissivity values. A review of the draw down and the recovery curves versus time suggests the existence of unknown impermeable and/or permeable boundaries that interfere with the classic Theis tests. The same phenomenon was observed in several well fields along the valley. Hence, it was impossible to assess the appropriate transmissivity values. Therefore a quantitative assessment of the flow system by numerical modelling is not possible at this stage.

Groundwater of varying chemical and isotopic qualities are exploited by wells drilled in the valley and along its margins. Wells drilled into different blocks and layers and springs showed that due to differences in lithology and mineralogy, each source of recharge provides the alluvial aquifer with water of a specific chemical composition. Also, the isotopic ratios of oxygen-18 to oxygen-16, and deuterium to hydrogen are determined by the geographic location, including prevailing temperatures and the altitude of the area in which recharge occurs. The spatial isotopic and ionic distribution within the alluvial aquifer along the southern Arava Valley seems to be affected mainly by the relative proportion of recharge contribution from each source. Hence, dilution and mixing are assumed to be the major mechanisms which control the hydrochemical and isotopic composition of the alluvial groundwater reservoir.

The temporal distribution of dissolved ions have revealed almost constant concentrations over the last twelve years. Furthermore, the piezometric head distribution and the pumping regime also seem to be constant for that period. Hence, changes in heads and concentrations of most species within cell **n** during time period Δt turned out to be very small and thus negligible for modeling purposes. This implies an almost steady state hydrological flow regime, at least for the past decade. For a further hydrogeological description and for the detailed flow pattern, as suggested by the distribution of environmental tracers, the reader is referred to Rosenthal et al. [13].

Six ions, TDI, deuterium (D) and oxygen-18 (^{18}O) parameters were finally isolated by multi-variable cluster analyses to characterize 12 major potential sources of recharge and divide the alluvial aquifer into 6 homogeneous compartments. Several close configurations of cells and potential inflows were modeled. For only four close configurations, the Wolf algorithm provided a solution. For the remainder, unbounded or no solutions were obtained. A comprehensive description of the quantitative assessment of subsurface fluxes within the southern Arava basin is given in Adar et al. [28].

Figure 6 presents the results for 12 potential inflows obtained with 7 dissolved ions and 2 isotopes. Subsurface recharge components and internal fluxes are given in $10^6\ m^3$/year. Transmissivities are given in m^2/day. The range of calculated fluxes as appears in Figure 6, represent the minimum and maximum

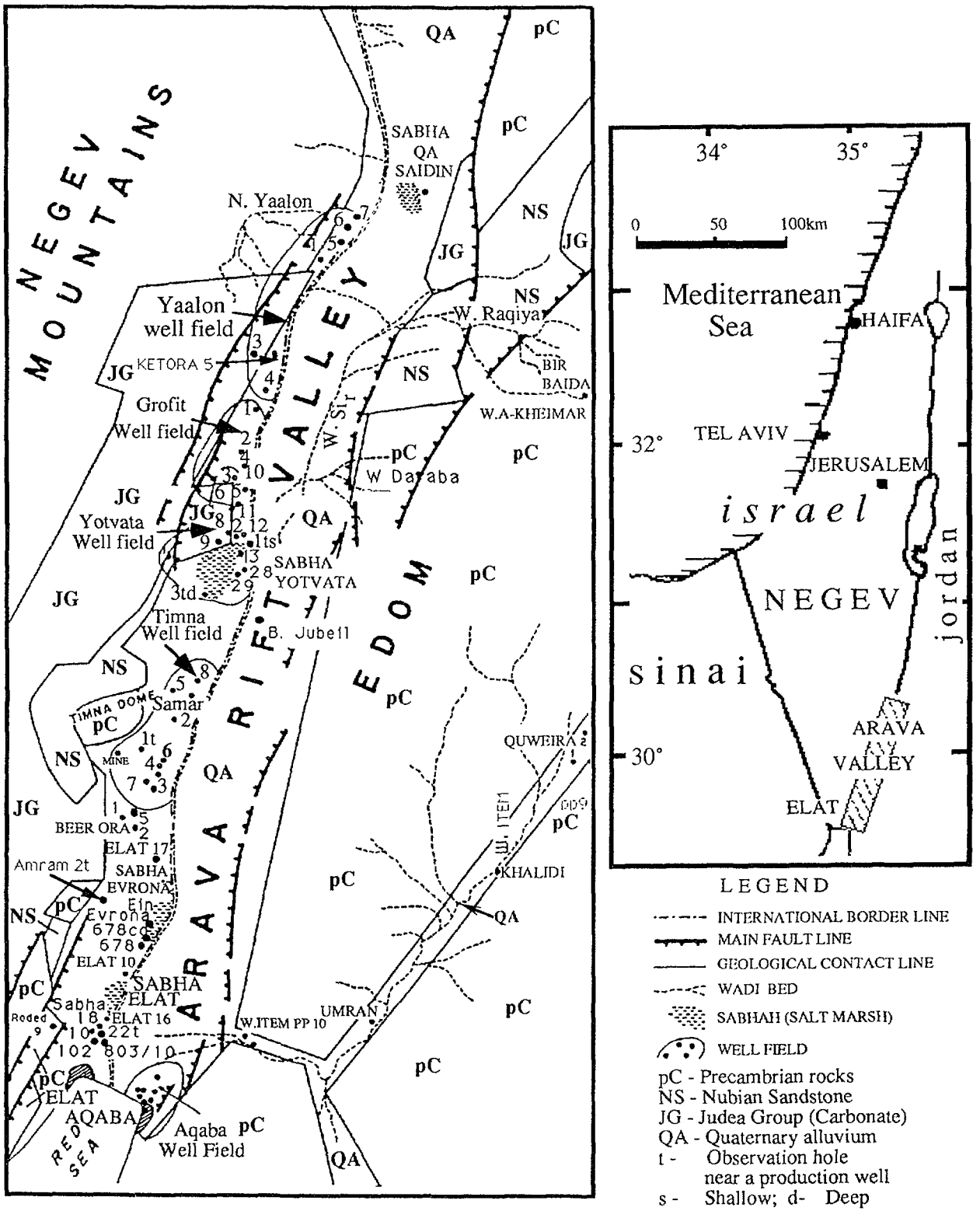

Figure 4 A map of the southern Arava basin showing the location of the main well fields and a schematic appearance of major geological units (After Rosenthal et al. [13]).

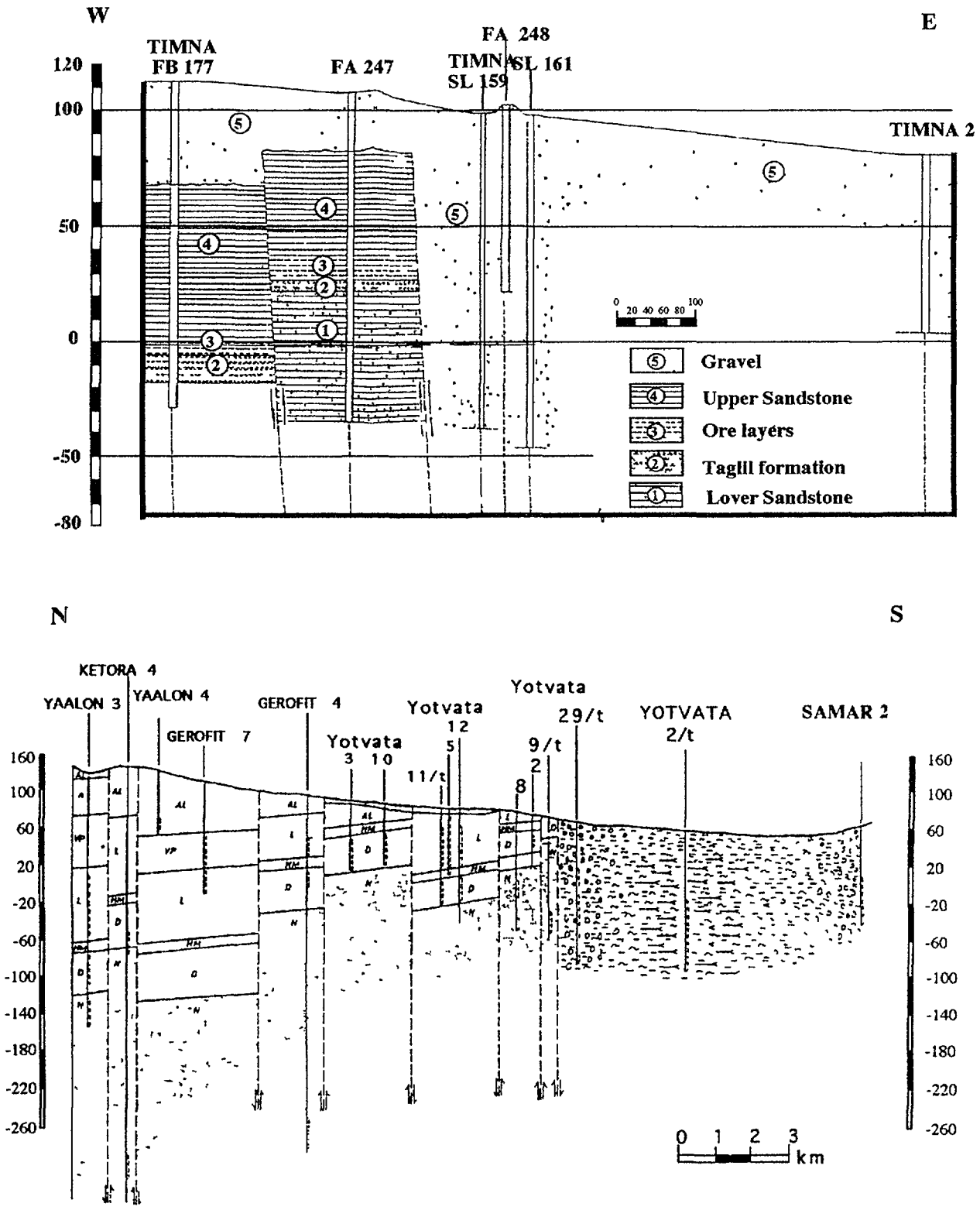

Figure 5 Complex hydrological structure along (A) and across (B) the southern Arava Rift Valley (After Adar et al. [28]).

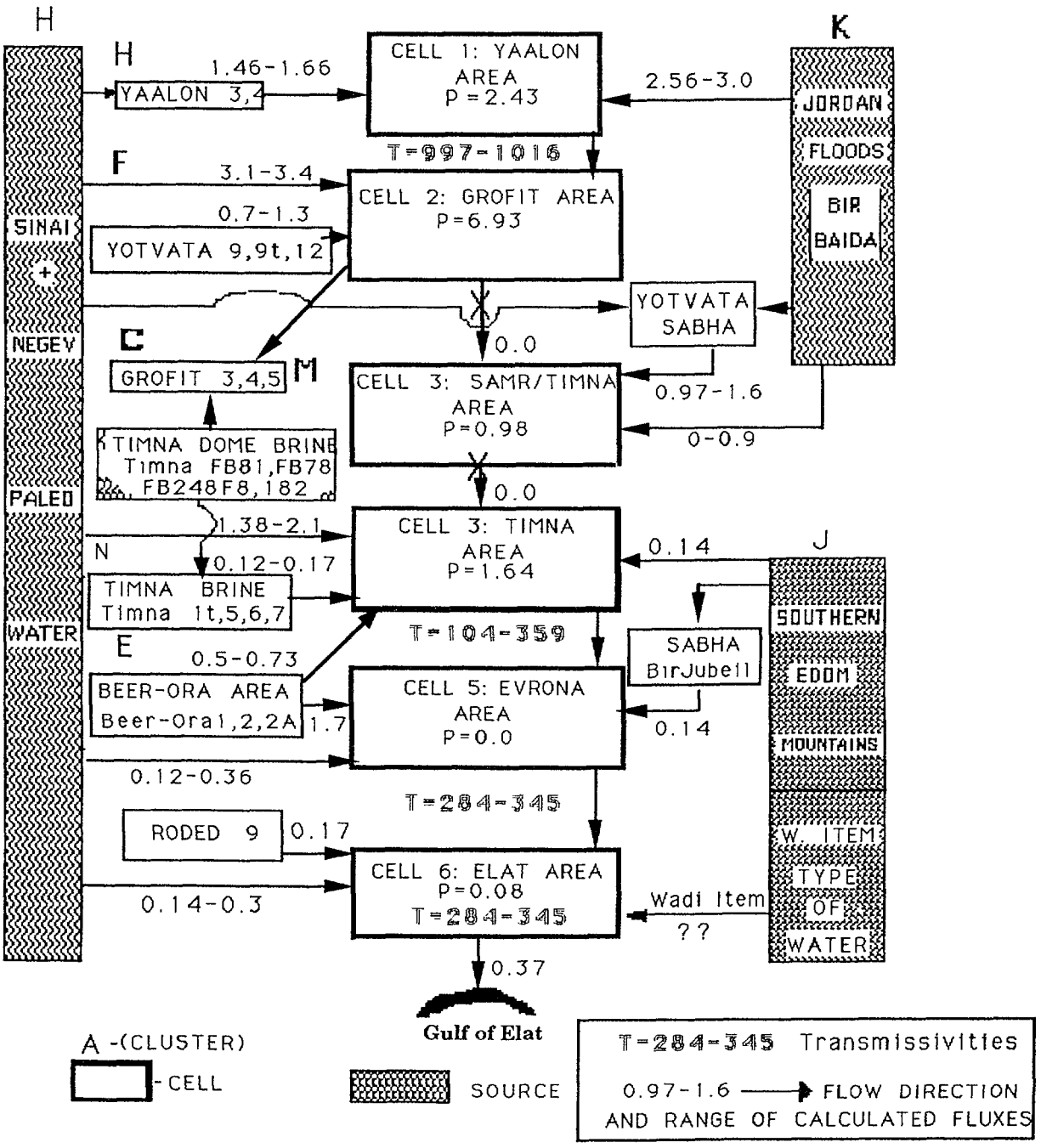

Figure 6. Schematic flow pattern for the southern Arava Valley (fluxes are given in 10^6 m^3/day transmissivities in m^2/day).

results obtained from a slightly modified set-up of the assigned concentrations to the end members. It also stems from the fact that the assigned pumping values were adjusted following the change in configuration of the cell. Only small non-significant changes could be implemented. A more notable modification caused an unbounded solution, in other words, no unique solution could be obtained. This issue will be further addressed when the sensitivity analyses are described in the following sections.

5. SENSITIVITY ANALYSIS : EFFECT OF ERRORS IN THE INPUT DATA

In real field situations the input data are not known with accuracy and the assumptions behind the model are not always satisfied. The model, therefore, should not be expected to provide precise estimates of flow rates. To examine the effect of erroneous input data on the quality of such estimates, the optimization scheme with synthetic input data was repeated after corrupting with various levels of uncorrelated Gaussian noise. The data was corrupted according to a certain realistic hydrochemical and isotopic constraints which is further discussed in this chapter. Adar and Neuman [30] examined the effect of erroneous chemical and isotopic input data with 250 noisy data sets on the assessment of flow rates. Results show that the stricter the constraints, the closer the average to the true flow rates. The fact that the model yields good results when noisy data satisfy constraints similar to those that real data usually satisfy suggests that the model should be applied to real hydrologic conditions in the field. In the following the sensitivity analysis is extended in order to account for uncertainties which are associated with vague geometry and the configuration of the cell.

The rationale for the particular method used to generate our noise stems from the assumption that the major cause of errors are (1) laboratory errors in isotopic and hydrochemical analysis, and (2) inaccurate assessment of the compartmental configuration and the cell's geometry. The first step is to generate normal errors of zero mean and unit variance $\mathbf{N_{(0,1)}}$ by means of the following formula (Box and Muller, 1958, as cited in Bard, [43]:

$$\mathbf{N_{(0,1)}} = \left(-2\log_{10}\mathbf{U_1}\right)^{0.5}\cos\left(2\pi\mathbf{U_2}\right) \tag{12}$$

where $\mathbf{U_1}$ and $\mathbf{U_2}$ are independent random variables drawn from uniform distribution. For perturbation of hydrochemical and isotopic values, each "true" $\mathbf{C_k}$ value entering into the model is transformed into a noisy concentration $\mathbf{C_k^*}$ according to:

$$\mathbf{C_k^*} = \mathbf{C_k}\left[\mathbf{1} + \beta_k \mathbf{N_{(0,1)}}\right] \tag{13}$$

where β_k is a weighting parameter controlling the magnitude of the corrupted concentration $\mathbf{C_k^*}$ relative to that of the "true" concentration $\mathbf{C_k}$. This causes the error to increase linearly with concentration in a manner similar to that assumed by Woolhiser, et al. [40]. This seems to be realistic for laboratory data. When the noise was made independent of concentration, the Wolf algorithm at times failed to converge. It appears that errors in dissolved components have greater effect than errors associated with the measuring of sink or sources when the number of flow rate equations in the model is less than the number of chemical balance equations.

The sensitivity test was performed in which different β_k values had been assigned to the various isotopic and chemical species k according to:

$$\beta_k = \frac{\sigma_k}{\mu_k} \tag{14}$$

Here μ_k is the mean of a large number of concentrations determined for laboratory standards of the k species, and σ_k is the associated standard deviation. In this manner β_k becomes the coefficient of variation of the error in determining the laboratory standard for the k species. The β values for each of the K tracers used in this test are listed in Table 1.

Table 1. coefficient of variation (β_k) values for ions, TDI, ^{18}O and D constituents. The data is an average from five laboratories in Israel, USA, Austria and Germany.

TDI	HCO_3	SO_4	Cl	Ca	Mg	Na	^{18}O	D
0.0122	0.0315	0.0622	0.0163	0.0411	0.0520	0.0855	0.0231	0.0647

When applied even to a simple flow system, results with the aforementioned algorithm for data corruption, seldom yield an optimal solution. Most of the difficulty stems from having neglected to maintain the ionic balance between the chemical species and the fixed empirical ratios between D and ^{18}O, or if electrical conductivity does not vary linearly with the total dissolved ion (TDI). We had to do the same with the artificial concentrations obtained when generating our noise. To do so, the ionic balance was maintained within 5%, the ratio between electrical conductivity and TDI ranged from 35 to 55, and the ratio between D and ^{18}O from 6.5 to 8.5, which is close to the mean world meteoric line. Results of this type of test with a simple synthetic cell configuration are illustrated in Adar et. al. [30] (Figures 5 and 6). These figures show the mean computed value of fluxes vary with the number of realizations, and converge toward the "true" value.

The same error generator (equation 12) is also used for introducing noise to the geometry of the flow system. for this, equation 13 is modified accordingly:

$$L_m^* = L_m\left[1 + \lambda_m N_{(0,1)}\right] \tag{15}$$

where λ_m is a weighting parameter controlling the magnitude of the corrupted length or width L_m^* of the m^{th} active cells' boundary relative to that of the "true" length L_m. The flow configuration of the synthetic, 3-D compartmental aquifer presented in Figure 1 was used to examine the sensitivity of both calculated fluxes and transmissivities to expected errors in the input data. Errors such as the cell's concentrations and the length and width of an active boundaries were introduced in the form described by equations 13, 14 or 15 for fluxes and transmissivities, respectively. For this purpose, the used β values are listed in Table 1, and λ was equal to 0.10 to assign a 10% maximum error.

Figure 7 shows the mean computed fluxes between cells obtained by a Monte-Carlo simulation applied to two types of perturbed data. The solid lines illustrate the variations of fluxes versus increasing number of realizations derived by perturbation of chemical and isotopic data. The dashed line was derived when

the error generator was also applied to perturb the assigned length of active boundaries and distances between cells. Results show that under severe, but nevertheless realistic chemical and isotopic constraints, the average inflow estimates are almost identical to the assigned (true) flux values. Some deviations are due to the non negativity requirement of the optimizer algorithm. Figure 8 shows the variations in the mean computed transmissivities obtained by the above mentioned tests. Solid lines represent results obtain from perturbed tracers, while the dashed lines are the results from perturbed tracers and geometry of cells. The true values for both fluxes and transmissivities are posted in Fig. 1. Figure 9 illustrate the distribution of mean values of inflows (recharge) for random errors employed to the ionic and isotopic concentrations (solid lines) as well as to the geometry and the magnitude of the compartments (dashed lines). It is important to note that although the mean values of fluxes, transmissivities and inflows are presented in a separate figures, results were obtained from a single Monte-Carlo type of simulation with 500 realizations. Results indicate that fluxes and transmissivities converge into stable values close to the "true" (assigned) solution after 50 to 100 realizations. Also, the later the unknown variable is solved by the optimization scheme and the higher is the magnitude of the variable, the effect of the errors is more significant. Therefore, the mean calculated values converge after more realizations with higher deviation from the "true" value. The last three figures also demonstrate that increasing the computation effort by introducing further errors associated with cell's boundaries, has only a minor effect on the final solution. In general, the mean values converge even faster toward a stable solution. The fact that the model yields good results when noisy data satisfy constraints similar to those that real data usually satisfy, suggests that the model should be applied to real hydrologic conditions in the field.

5.1 **Sensitivity test for the Southern Arava Valley.**

Sensitivity analysis was performed on results obtained from the southern Arava Rift Valley on the same flow configuration presented in Figure 6. Results with 1992/93 rates of pumping as presented in Table 2 (see the following section) were used in the sensitivity test which was performed in two stages: (1) Random errors were applied to tracers associated with external sources of inflows and to concentrations of cells; (2) Random errors were employed also to the geometry and the magnitude of the cells' boundaries. The effect of random errors on inflows (components of subsurface recharge), fluxes within the alluvial aquifer and on the evaluated transmissivities were studied. In all simulations β_k values equal to coefficient of variation evaluated from laboratory standards and λ is equal of 0.15 to account for up to 15% error in the length of the flowing boundaries and cell's magnitude.

Figure 10 shows the effect of the above mentioned errors on recharge components (1, 3, 4 and 12). Figures 11 and 12 show the same error effects on internal fluxes between cells and on the associated transmissivities respectively. Those figures show that similar to results obtained with synthetic data, the average computed fluxes (inflows) converged after 40 to 150 realizations. It took

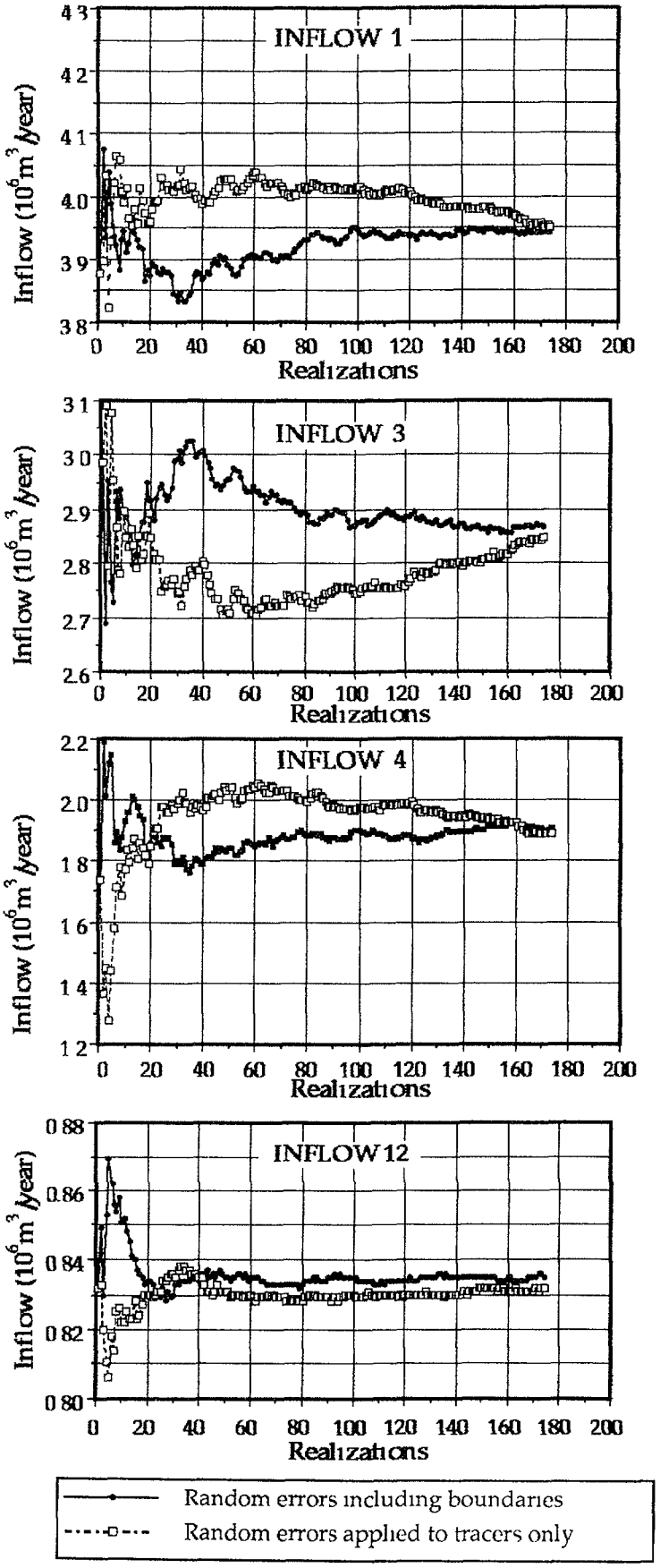

Figure 7. Results of Monte Carlo simulation for inflows calculated for the southern Arava Valley:

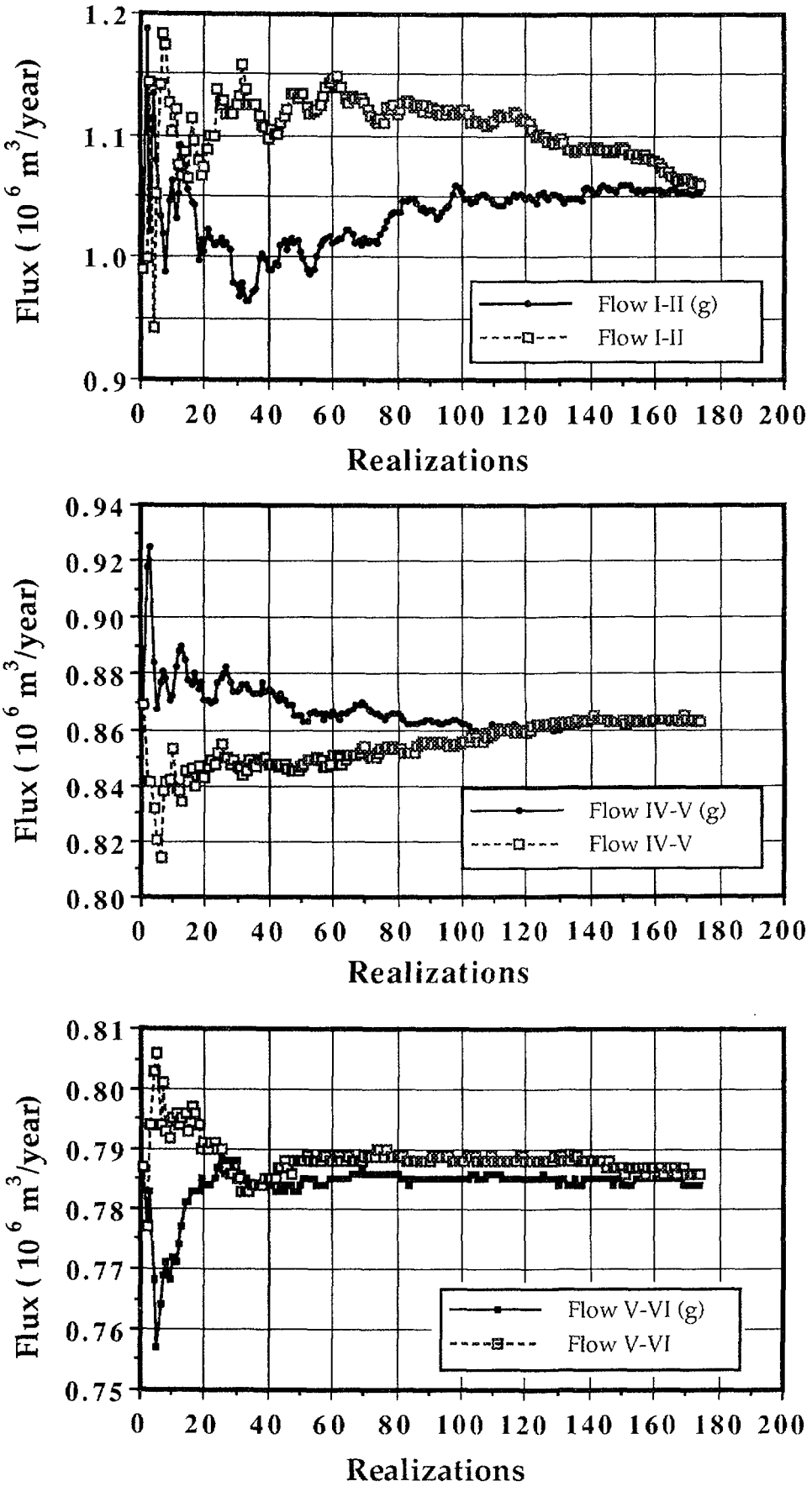

Figure 8. Results of Monte Carlo simulation for fluxes calculated for the southern Arava Valley:

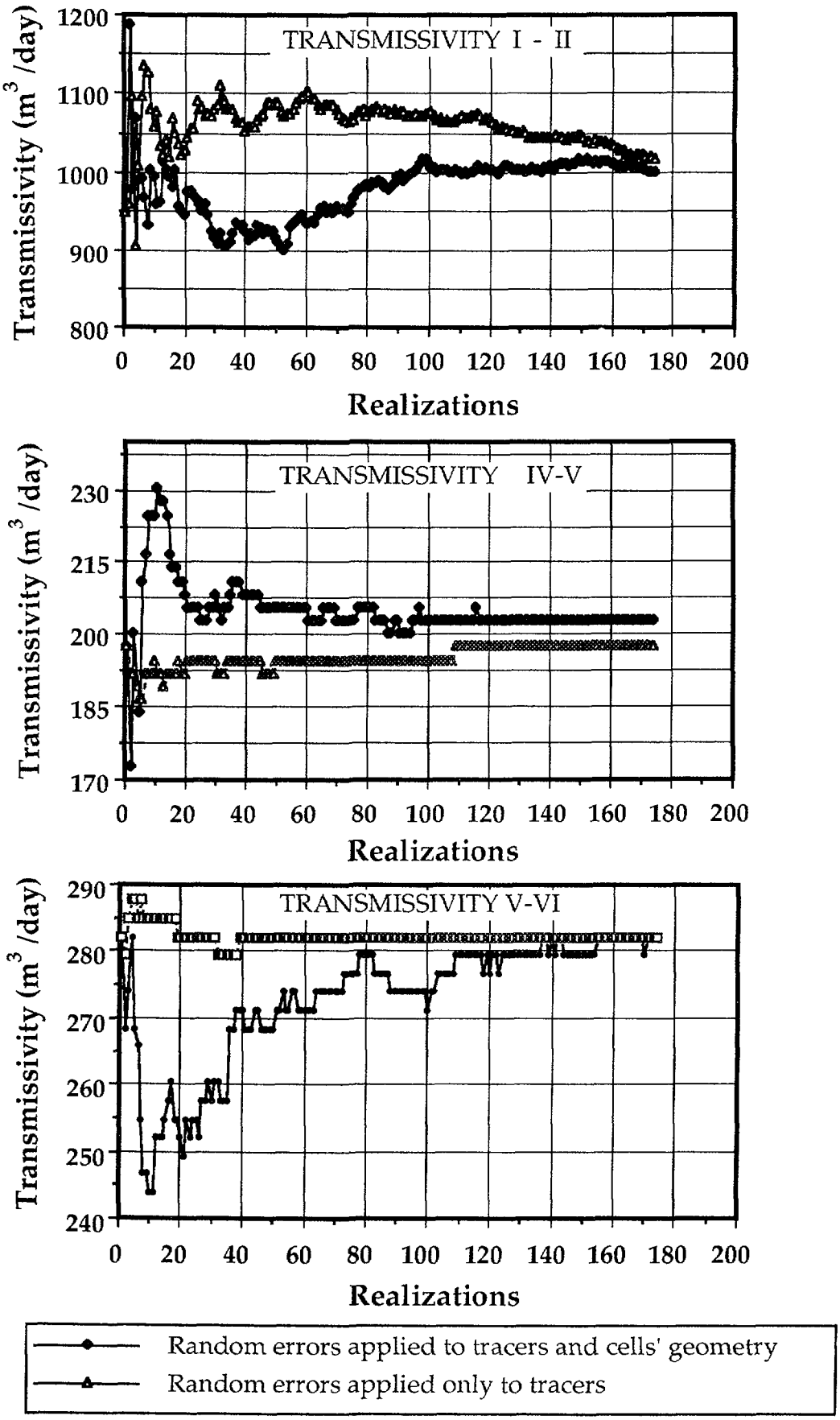

Figure 9. Results of Monte Carlo simulation for transmissivities calculated for the southern Arava Valley:

Table 2 Results obtained for 12 unknowns with weight factor W=1 for oxygen-18 and deuterium and W=0.5 for ions. A-Inflows for steady rates of pumping until 1990; B- Estimated inflows for expected pumping rates for 1992/1993

The unknown inflows are:

	Name of inflow		A Pumping	A Rate of inflow (in 10^6 m^3/y)	B Pumping	B Rate of inflow (in 10^6 m^3/y)
Cell 1			2.433		2.72	
	BIR BAIDA	=		3.0131		3.877
	YAALON 3/4	=		0.0000		0.000
Cell 2			6.93		7.75	
	YOTVTA 9t	=		1.7687		2.986
	YOTVTA 12	=		2.7656		1.736
	YOTVTA 9	=		0.4490		2.525
Cell 3			0.979		1.10	
	YOTVTA 9t	=		1.6349		1.143
Cell 4			1.64		0.90	
	YOTVTA 9t	=		1.7297		1.256
	BEER ORA 1	=		0.5245		0.387
	TIMNA 6	=		0.1183		0.033
Cell 5			0.00		1.00	
	BEER ORA 1	=		0.1788		0.298
	YAALON 3	=		0.0765		0.503
Cell 6			0.08		1.09	
	YAALON 3	=		0.2220		0.832

Total estimated inflows 12.4811 10^6 m^3/y (100.0%)
Qout + Total pumpage: 12.4307 10^6 m^3/y; Absolute difference: 0.0504 (0.4054%)

more realizations until the average values converged into the "true" value for the first unknowns to be solved. However, when random errors were applied to concentrations and to boundaries, the perturbed realizations converged faster than those applied only to cell's concentrations. The additional errors employed to the flowing boundaries of the cells simply further perturbed the results. However, the solutions converged into the same values as obtained when errors had applied only to the concentrations. The same was found for the calculated internal fluxes and transmissivities (Figures 11 and 12 respectively). For cells with relatively short flowing boundaries (i.e. V-VI in Figure 12) the effect of errors on the cell's geometry is more pronounced. In such alluvial aquifer, the width of the flowing boundaries were assigned bases on the surface contact between the alluvium and the side base rocks as taken from maps and air photos. This is a rough estimation of the true magnitude of the flowing boundary. Results indicate that when transmissivities are simultaneously calculated with internal fluxes and recharge components, the solution is quite stable. It is important to notice, however, that the deviation of transmissivities between the assessed values and the assigned transmissivities are heavily dependent upon the rates assigned to the known outflows. The absolute values of these deviations have no real meaning aside from the fact that for more reliable flow configurations, one may expect to obtain lower deviations.

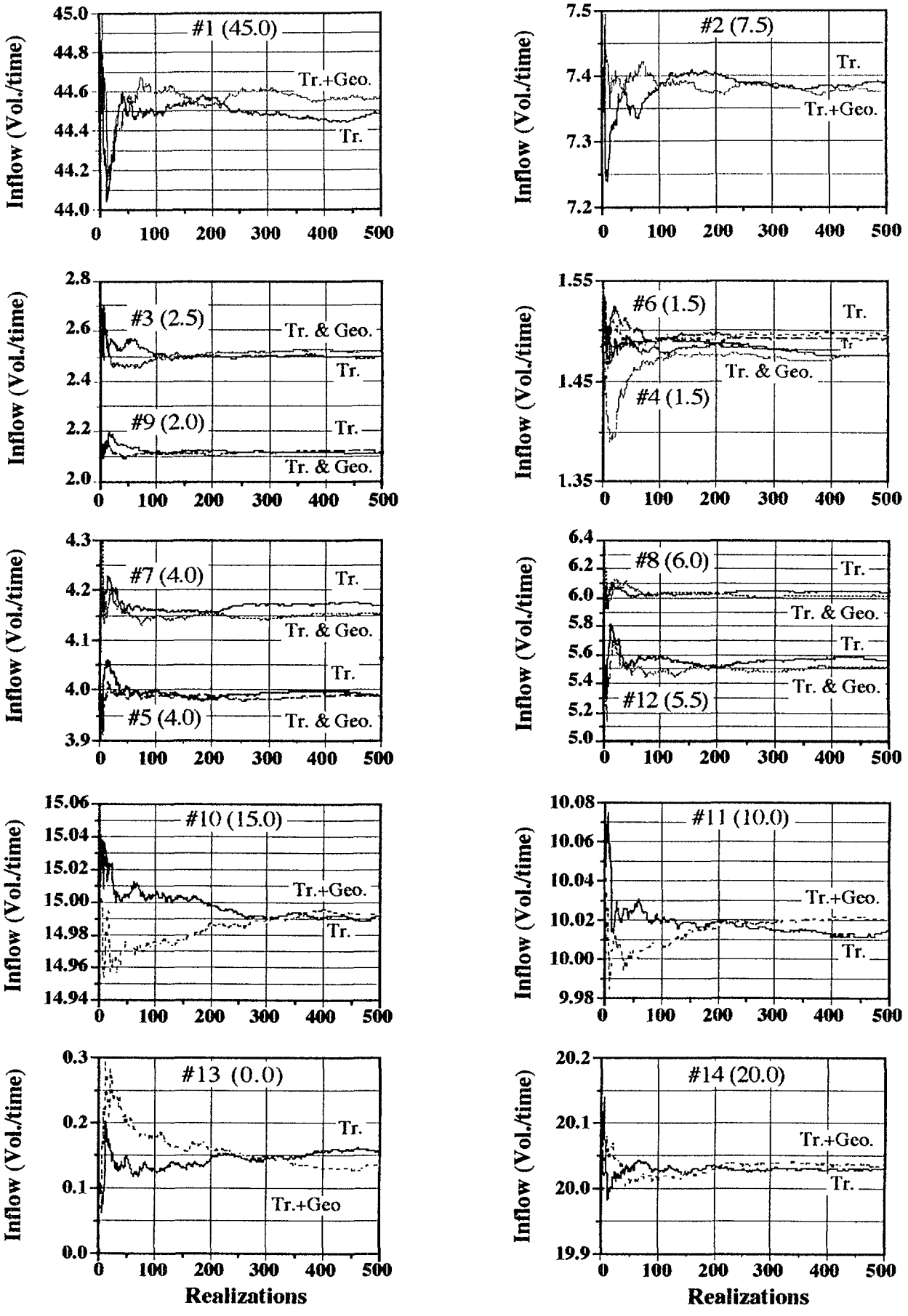

Figure 10. Results of Monte Carlo simulation for inflows calculated for the southern Arava Valley:

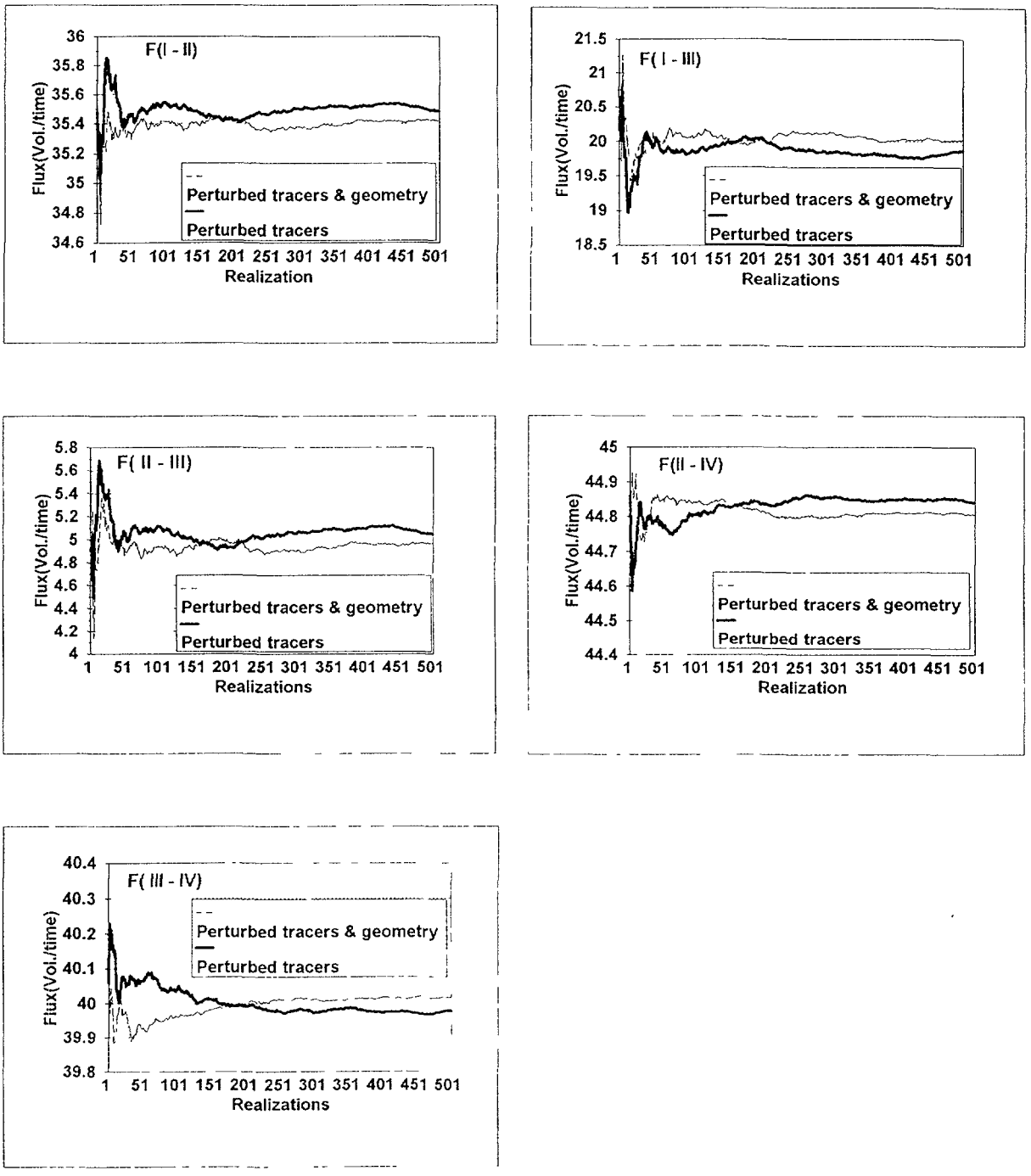

Figure 11 Results of Monte Carlo simulation for fluxes calculated for the southern Arava Valley:

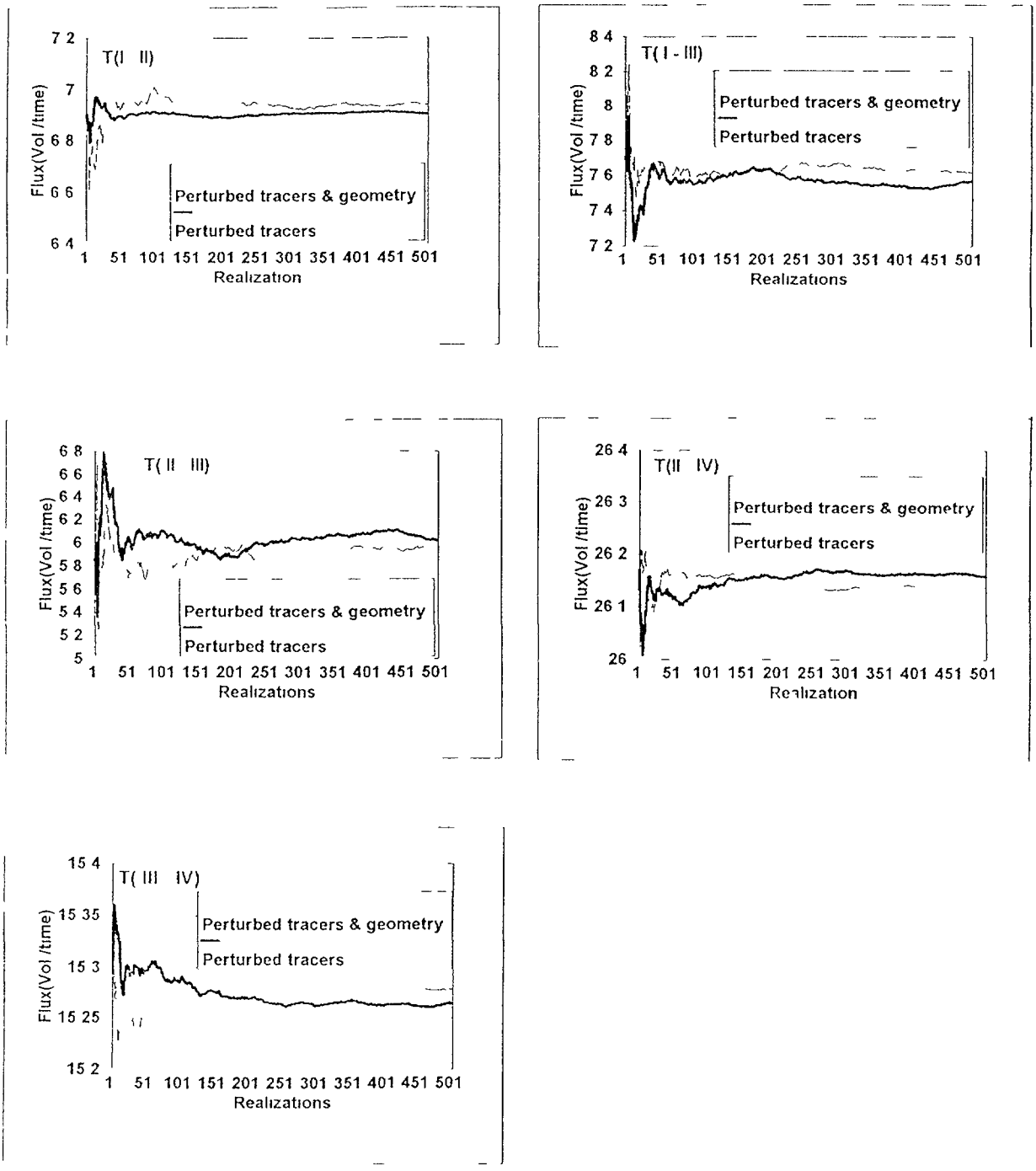

Figure 12 Results of Monte Carlo simulation for transmissivities calculated for the southern Arava Valley:

6. SUMMARY AND DISCUSSION.

In this model, the only data that is required aside from the qualitative knowledge of the flow system for solving the time-averaged fluxes are the spatial distribution of environmental tracers. However, for the calculation of transmissivities, one should obtain the distribution of hydraulic heads, as well as the dimensions of the cells; mainly the size of active boundaries. The combination of head distribution and cell configuration suggests which of the boundaries is a flowing boundary (active boundary); as boundary which is situated parallel to a stream line normal to the piezometric surface, should be considered as no flow boundary.

The concentrations and the hydraulic heads which represent each compartment are assigned to the geometric center of the cell. In other words, an imaginary well is posted at the geometric center of a cluster of observation holes presenting a similar type of water. Therefore, in a real case, the actual location of boundaries between cells is not precisely known. In fact, the most one can say is that the boundary should be somewhere between the extreme (marginal) wells of nearby clusters forming the cells.

The location of the representative imaginary wells are assigned arbitrarily to the geometric center of the well's cluster (not to the center of the entire cell's area). Therefore, the exact location of the cells' boundaries has no effect on the distance l_{in} between the centers of the cells. However, the position of the boundaries, which are always normal to the flow trajectory, affects the width w_{in} of permeable boundaries (Equation 5). The width of the boundaries in the southern Arava Valley were assigned according to the contact between the alluvium and the surrounding hills, as determined from satellite images and air photos.

Sensitivity analyses show that the model is extremely sensitive to the assigned concentration values associated with potential inflows and internal fluxes. It is less sensitive to the exact cell's geometry mainly for active (flowing) boundaries with high rates of fluxes. As long the water and mass balance are maintained a unique solution can be obtained. This implies that the optimized solution is highly related to the assigned known fluxes, mainly sinks and/or sources. Those assigned fluxes have a direct effect on the water balance within each cell. Therefore, in order to maintain the water balance, an increase in pumping rate must be adjusted by an appropriate increase in inflows and internal fluxes. This issue is further demonstrated in Table 2 where two sets of calculated fluxes with different sets of pumping values are compared. In (A), the inflows were assessed for an average steady rates of pumping prevailed until 1990. In (B), the same set of tracers were used with higher rates of pumping assumed for 1992/93. Due to an increase demand for water, pumping was increased in Cell I, II, III, V and VI. The pumping rate was decreased in Cell IV due to a local increase of water salinity. Table 2 shows that following the increase in pumping rates a respective increase of inflows and internal fluxes were predicted for all cell but Cell No. III. It seems that the increasing pumping in Cell III, attracts more water from Cell II than from external inflow.

Transmissivity values that were obtained by various types of pumping tests in wells along the valley are listed in Table 3. The transmissivity values assessed by the above-mentioned model are in fairly good agreement with the values found from the pumping tests. As listed in Table 3, the measured transmissivity value were obtained by different methods such as draw down (DD) test, recovery (R)

Table 3. Calculated versus measured (*) transmissivities in three sections along the southern Arava Valley (m^2/day).

Section		Measured	Calculated
Yaalon-Grofit area.			**997-1016**
	Ketora 4 (DD)	1849	
	" (R)	1209	
	Yotvata 2 (R)	2665	
	" 2 (IT8)	1400	
	Yotvata11 (DD)	980	
	" 11 (DD)	1000	
	" 11 (R)	1060	
	Yotvata12 (R)	2010	
Samar-Timna area			**104-350**
	Samar 2 (?)	400	
	Timna 4 (R)	370	
	Timna FC (IT?)	807	
	Timna 4 (IT3)	4600	
	" (IT1)	2800	
Eilat area			**284-345**
	Eilat 10 (R)	496	
	Eilat m.s. (R)	105	
	Eilat 16 (R)	273	

*(R) - Recovery test ; (DD) - Draw down test ; (IT) - Interference test

and interference (IT) tests. Data were obtained from the Water Commissionery - Hydrological Service, Jerusalem. Also in Table 3, for those wells where two or more methods were employed, up to 50% differences were found. It is important to notice, however, that this model allows the evaluation of transmissivities for flowing segments of the aquifer with steady fluxes. Though the transmissivity is a physical property of the aquifer independent of the hydraulic head, in this model transmissivities can not be assessed unless there are head gradients between cells. Therefor, for cells with heavy rates of pumping, as in the central section of the southern Arava basin (Fig. 6), transmissivities can not be evaluated since the inter-cell fluxes are zero. Consequently, it is necessary to assess simultaneously both transmissivities and fluxes. Similar to results obtained with the inverse numerical solution, the calculated transmissivities are average values between the nodes. Due to difference in magnitude in a compartmental scheme, these values are assort of conductances across permeable boundary between cells. In other words, it describes the ability of the boundary to transmit a certain volume of water per unit length of the boundary per unit time.

REFERENCES

[1] THEIS, C.V., The relation between the lowering of piezometric surface and the rate and duration of discharge of well using groundwater storage, Trans. AGU 16 (1935) 519-524.

[2] KRUSEMAN, G.P., DE RIDDER, N.A., Analysis and Evaluation of Pumping Test Data, Inter. Inst. for Reclamation and Improvement/ILRI, Wageningen, The Netherlands, Bul. 11 (1976) 200 p.

[3] CARRERA, J., NEUMAN, S.P., Estimation of aquifer parameters under transient and steady-state conditions. I. Maximum likelihood method incorporating prior information, Wat. Resour. Res. 22(2) (1986a) 201-211.
[4] CARRERA, J., NEUMAN, S.P., Estimation of aquifer parameters under transient and steady-state conditions. II. Uniqueness, stability and solution algorithms, Wat. Resour. Res. 22(2) (1986b) 211-227.
[5] WITTMEYER, G., NEUMAN, S.P., Monte Carlo experiments with robust estimation of aquifer parameters. Adv. Water Resources 14 (1991) 252-272
[6] HOFFMAN, K.H., KNABNER, P., SEIFERT, W., Adaptive methods for parameter identification in ground water hydrology, Adv. Water Resources 14 (1991) 220-239
[7] CARRERA, J., GLORIOSO, L., On geostatistical formulation of the groundwater flow inverse problem, Adv. Water Resources 14 (1991) 273-283
[8] WHI, H.F., LEDOUX, E., MARSILY, G.DE., Regional modelling of groundwater flow and salt and environmental tracer transport in deep aquifers in Paris basin. J. Hydrol. 120 (1990) 34-355.
[9] VERHAGEN, B. TH., SELLSCHOP, J. P. F., JENNINGS, C. M. H., contribution of environmental tritium measurements to some geohydrological problems in South Africa, Isotope Hydrology 1970, IAEA, (1970) 289-313.
[10] GAT, J.R. AND DANSGAARD, W., Stable isotope survey of the fresh water occurrence in Israel and the Northern Jordan Rift valley, Israel, J. Hydrol. 16 (1972) 177-212.
[11] MAZOR, E., VAUTAS ,F.D., AND JAFFE, F.C., Tracing groundwater components by chemical, isotopic and physical parameters, example: Schinziach, Switzerland, J. Hydrol. 76 (1985) 233-246.
[12] LEVIN M., GAT J. R., AND ISSAR, A., Precipitation, flood and groundwaters of the Negev highlands: An isotopic study of desert hydrology., Arid Zone Hydrology: Investigations With Isotope Techniques, IAEA, Vienna, (1980) 3-23.
[13] ROSENTHAL, E., ADAR, E.M., ISSAR, A.S. & BATELAAN, O., Definition of groundwater flow pattern by environmental tracers in the multiple aquifer system of southern Arava Valley, Israel, J. Hydrol. 117, (1990) 339-368.
[14] ERIKSSON, E., The possible use of tritium for estimating ground water storage, Tellus, 10 (1958) 472-478.
[15] BREDENKAMP, D.B., SCHULTE, J.M., DU TOIT, G.J., Recharge of a dolomite aquifer as determined from tritium profiles, International Symposium on Isotope Hydrology, IAEA-SM-182, Vienna, (1974) 73-94.
[16] VOGEL, J.C., THILO, L., VAN DIJKEN, M., Determination of groundwater recharge with tritium. J. Hydrol. 23 (1974) 131-140.
[17] ALLISON, G.H. HUGHES, M.W., The use of environmental tritium to estimate recharge to the South-Australian aquifer, J. of Hydrol. 26 (1975) 245-254.
[18] MALOSZEWSKI, P., ZUBER, A.. Determining the turnover time of groundwater systems with the aid of environmental tracers, I. Models and their applicability, J. of Hydrol. 54 (1982) 207-231.

[19] MALOSZEWSKI, P., ZUBER, A., Principles and practice of calibration of mathematical models for interpretation of environmental tracer data in aquifers. Advances Wat. Resour. (1993) (in press).

[20] ZUBER, A., MALOSZEWSKI, P., STICHLER, W., HERRMANN, A., Tracer relations in variable flow, 5th International Symposium on Groundwater Tracing, Athens (1986) 355-360.

[21] NIR, A., Role of tracer methods in hydrology as a source of physical information. Basic concepts and definitions, Mathematical Models for Interpretation of Isotope Data in Groundwater Hydrology, IAEA-TECDOC-381,IAEA,Vienna, (1986) 7-44.

[22] ZUBER, A., Mathematical models for the interpretation of environmental isotopes in groundwater systems, Handbook of Environmental Isotope Geochemistry, P. Fritz and J. Ch. Fonts, Eds., Elsevier, Amsterdam (1986) 1-59.

[23] ZUBER, A., Review of existing mathematical models for interpretation of tracer data in hydrology, Mathematical Models for Interpretation of Tracer Data in Groundwater Hydrology, IAEA-TECDOC-381, IAEA, Vienna, (1986) 69-116.

[24] GOBLET, P., General review of methodology and approaches in mathematical models for interpretation of tracer data in hydrological systems, IAEA-TECDOC-381, IAEA, Vienna, (1986) 45-68.

[25] GORELICK, S.M., EVANS, B. & REMSON, I., Identifying sources of groundwater pollution: an optimization approach, Wat. Resour. Res. 19 (3) (1983) 779-790.

[26] WAGNER, B.J. AND GORELICK, S., Optimal groundwater quality management under parameter uncertainty, Wat. Resour. Res. 23 (1986) 1162-1174.

[27] LAWRENCE, F.W. AND UPCHURCH, S.B., Identification of recharge areas using geochemical factors analysis., Ground Water 20(6) (1982) 260-287.

[28] ADAR, E.M., ROSENTHAL, E., ISSAR, A.S., BATELAAN, O., Quantitative assessment of flow pattern in the southern Arava valley (Israel) by environmental tracers and a mixing cell model. J. Hydrol. 136 (1992) 333-354.

[29] SIMPSON, E.S. AND DUCKSTEIN, L., . Finite state mixing-cell models. In: V. Yevjevich (Editor), Karst Hydrology and Water Resources. Vol. 2. Water Resource Publications, Ft. Collins, Co., (1976) 489-508.

[30] ADAR, E.M., NEUMAN, S.P., WOOLHISER, D.A., Estimation of spatial recharge distribution using environmental isotopes and hydrochemical data. I. Mathematical model and application to synthetic data. J. Hydrol. 97 (1988) 251-277.

[31] ADAR, E.M., NEUMAN, S.P., Estimation of spatial recharge distribution isotopes and hydrochemical data. II. Application to Aravaipa Valley in Southern Arizona, USA. J. Hydrol. 97, (1988) 297-302.

[32] ADAR, E. & SOREK, S., Multi-compartmental modelling for aquifer parameter estimation using natural tracers in non-steady flow. Advances Wat. Resour. 12(2) (1989) 84-88.

[33] YURTSEVER, Y. AND PAYNE, B.R., A digital simulation approach for a tracer case in hydrological systems: Multi compartmental model, Finite Elements in Water Resources, Brebbia, Gray and Pinder Eds., London, (1978).

[34] CAMPANA, M.F. & SIMPSON, E.S., Groundwater residence time and discharge rates using discrete-state compartment model and ^{14}C data. J. Hydrol. 72 (1984) 171-185.

[35] CAMPANA, M.E., MAHIN, D.A., Model derived estimates of groundwater mean ages, recharge rates, effective porosities and storage in a limestone aquifer, J. of Hydrol. 76 (1985) 247-264.

[36] VAN OMMEN, H.C., The mixing-cell concept applied to transport of non reactive and reactive components in soil and groundwater, J. of Hydrol. 78 (1985) 201-213.

[37] YURTSEVER, Y., PAYNE, B.R., Mathematical models based on compartmental simulation approach for quantitative identification of tracer data in hydrological systems, 5th International Symposium on Groundwater Tracing, Athens, (1986) 341-353.

[38] YURTSEVER, Y., PAYNE, B.R., GOMEZ, M., Use of linear compartmental simulation approach for quantitative identification of isotope data under time variant flow conditions, Mathematical Models for Interpretation of Isotope Data in Groundwater Hydrology, IAEA-TECDOC-381,IAEA,Vienna, (1986) 203-231.

[39] YURTSEVER, Y. BUAPENG, S., Compartmental modelling approach for simulation of spatial isotopic variations in studding groundwater dynamics: A case study of a multi-aquifer system in Bangkok Basin, Thailand, Isotope Techniques in Water Resources Development, IAEA, Vienna (1991) 291-308.

[40] WOOLHISER, D.A. & GARDNER, H.R., Estimation of multiple inflows to a stream reach using water chemistry data. Trans. ASAE, 25(3) (1982) 616-622

[41] ADAR, E. & SOREK, S., Numerical method for aquifer parameter estimation utilizing environmental tracers in a transient flow system, MODELCARE 90, International Conference on Calibration and Reliability in Groundwater Modelling, The Hague, Holland, K. Kovar, Ed. IAHS No. 195 (1990) 135-148.

[42] WOLF, P. Methods of Non-linear Programming, Chap. 6. In: Interscience J. Wiley, New York, (1967) 97-131.

[43] BARD, Y., 1974. Nonlinear parameter estimation (Appendix D). Academic Press, (1974) 332 p.

FLUID FLOW AND SOLUTE TRANSPORT IN FRACTURED MEDIA

L. MORENO, I. NERETNIEKS
Royal Institute of Technology,
Stockholm, Sweden

Abstract

A model is proposed to describe flow and transport in fractured rocks. It is based on the concept of a network of channels. This approach is backed by observations in drifts and tunnels that flow in fractured rocks takes place in sparse narrow effluent locations with widths typically less than 10 cm and a channel frequency of one channel per a few square meters to one channel per more than a hundred square meters. Observations in boreholes also indicate that there are large distances, tens to hundreds of meters, between the most conductive sections in boreholes.

For visualization purposes the model is displayed on a rectangular grid. The individual channels are given stochastically selected conductances. Flowrate calculations have been performed in grids of sizes 20*20*20 channels in most cases but larger grids have also been used. For large standard deviations in conductances, greater than 1.6 in the log normal distribution (base 10), channeling becomes pronounced with most of the water flowing in a few paths. The effluent patterns and flowrate distributions obtained in the simulations have been compared to three different field measurements of flowrate distributions in drifts and tunnels. Standard deviations of channels conductances were between 1.6 and 2.4 or more in some cases. Channel lengths were found to vary between 1.2 m and 10.2 m in the different sites.

A particle tracking technique was used to simulate solute transport in the network. Nonsorbing as well as sorbing tracer transport can be simulated and by a special technique also tracers that diffuse into the rock matrix can be simulated.

Tracer measurements in one site, Stripa, were used to compare dispersivities. These were large, Peclet numbers less than 5 both in simulations and the field results. From the Stripa tracer data it was also found that the tracers were taken up into the rock matrix by molecular diffusion.

INTRODUCTION AND BACKGROUND

In this paper we develop a model for solute transport in sparsely fractured rock. We also show some properties of the model that affect solute migration. Furthermore, we attempt to estimate values for the important parameters from large-scale field experiments and observations. Solute transport is also calculated for solutes that diffuse into the rock matrix.

Flow and solute transport in fractured rock has been found to be poorly described by the advection-dispersion concept and equations. Field observations show that there are strong channeling effects and that when attempts are made to evaluate the dispersion coefficient, it appears to increase with distance (Neretnieks et al., 1987). Field observations in drifts and tunnels also show that flow channels are sparse and that the

flow-rate distribution is very large among channels. For short distances, it has been proposed that the flow and solute transport might better be described as taking place in a bundle of independent channels (Neretnieks et al., 1987). For longer distances, channels have a greater chance of meeting and a network concept seems more appropriate. For very long distances, it is conceivable that the mixing between channels is large enough for the transport to behave as described by the advection-dispersion model. This does not seem to have been observed in fractured rocks so far.

Fracture network models have been proposed and tested on field data (Robinson, 1984; Long et al., 1985; Dverstorp and Andersson, 1989) for flow calculations and in some cases also for tracer transport (Dverstorp, 1991; Cacas et al., 1990b). These models need information on fracture trace lengths, orientations, frequencies, and transmissivities, plus some assumptions, that are difficult to prove. In the end, they have to be calibrated to field observations.

In this paper we attempt a simpler approach, and assume that flow and solute transport can be described as taking place in a network of channels. This simplification allows us to develop a simple model that does not need very detailed information. Data can be obtained from borehole transmissivity measurements and observations on fracture widths. Calibrations can be made with observations in drifts and tunnels. One important aspect of the model is that it is simple enough to accommodate the transport of solutes that diffuse into the rock matrix. This is very important when assessing retardation of these solutes. Below, we summarize some observations that have been the basis for the formulation of this model.

Abelin et al. (1985) analyzed flow and solute movement in three natural fractures intersecting tunnels in the granite in the Stripa mine. They found that the fractures were closed or very tight, with few open parts between the areas where two fracture surfaces are in contact. Observations in drifts and tunnels strengthen this impression (Neretnieks et al., 1987). In two investigations (Neretnieks, 1987; Abelin et al., 1991a.b) it was found that fracture intersections often make up high flow-rate conduits.

In the 3-D tracer test experiment performed in the Stripa mine by Abelin et al. (1991a,b), it was found that water flows into the drift with a very uneven spatial distribution. The results also show that the tracers are unevenly distributed in the drift. Very different concentrations were found in sheets near each other. Low values alternate with high values in nearby locations. In some cases, much of the tracer was found in locations far away from the injection hole.

Detailed observations of flow distributions in two other long drifts and tunnels, Kymmen (Palmqvist and Stanfors, 1987) and SFR (Neretnieks et al., 1987), show that the water outflow occurs in narrow channels, most of them less than 10 cm wide. The channel density is about 1 per 20 to 100 m^2. Experiments that specifically aim to study channeling in individual natural fractures on the scale of 2-2.5 m in the Stripa mine (Abelin et al., 1990) also show that water is conducted in only a small part of a fracture. Channels have typical widths of less than 10 cm. Hydraulic conductivities measured in the fracture planes show that there are very strong variations in conductivity in the plane of the fractures.

Network models have been used to describe the flow rate distribution in the Stripa experiment (Geier et al., 1990; Dverstorp, 1991). They describe the stochastic nature of

the areal flow distribution but do not account for the channeling nature of the flow. None of the models have addressed the question of the interaction of solutes with the rock surfaces. Nor have any of the models accounted for the observations (Abelin et al., 1990; Neretnieks, 1987) that fracture intersections play an important role in conducting the water solutes.

In a recent study, it was assumed that the flow in fractures that intersect each other can be described as the flow through channels in the planes of the fractures (Cacas et al., 1990a). These channels connect the centres of the fractures through a point at the intersection line between the fractures. The fracture network may then be simplified to a network of connected channels.

One drawback of these models is that they need a large amount and very detailed data on fracture orientations, fracture size distributions and fracture conductivity distributions. Some assumptions must also be made in interpreting the field observations to translate them into the data used in the models. Many of the assumptions are difficult to validate. The models with all their built-in assumptions must finally be validated by comparison with field data. The model described here needs much less data but also needs to be validated by field observations.

CONCEPTUAL MODEL

In this approach a three dimensional channel network model is developed. It can account for the stochastic nature of the flow distribution, the channeling nature of the flow and the interaction of reactive solutes with the flow-wetted rock surfaces. The solutes in the channels can also diffuse into and out of the rock matrix.

To avoid many of the difficulties that fracture networks exhibit, we choose a different starting approach. It is assumed that the flow paths make up a channel network in the rock. Every channel member can connect to any number of other channel members, but we choose an upper limit of six members intersecting at a point, for reasons that are described below.

The use of six channel members is partly based on the observation that both fracture intersection and channels in the fracture planes play an important role in conducting flow. For two fractures that intersect, there will be one channel in every fracture plane that may continue over the intersection line with the other fracture. In this way, up to four members in the fracture plane may intersect at one node. For those intersections where the fracture intersection itself is conducting, two more members may be added, forming a six-member intersection.

Although the model concept is based on the above considerations, this does not mean that we consider a channel to lie only in one fracture or at a fracture intersection. A channel in our concept may have been formed by individual channel members in series. Thus a channel may consist of 1, 2, 3 or even more channel members. The actual number is not very important, as the properties of the channels will be obtained by calibration to field measurements.

For visualization purposes, the network is depicted as a rectangular grid. The hydraulic properties of the members can be generated by including the effects of channel

members of different lengths, different hydraulic conductivities and other properties of interest. It is easy to vary the channel member density in different regions (e.g., along fracture zones) and to include effects of anisotropy in a simplified manner. In this paper, we develop and show some important basic properties of the model. They include the ability to describe the uneven spatial distribution of flow, the residence time distributions of tracers, and the retardation due to matrix diffusion and sorption in the rock matrix.

We do not think of the channels as necessarily being clearly identifiable physical features. In a fracture with varying apertures, the water will trace out different paths, depending on the gradient that exists at a given moment. When the conductivity variations are large, there will only be one or a few paths where most of the water flows. This has been found in simulations (Moreno et al., 1988) as well as in the field (Abelin et al. 1990). The flow paths may also be actual physical channels along fracture intersections or where dissolution processes have formed channels. They may have properties that vary along the flow path, but an average conductivity, volume and flow-wetted surface may be assigned to every channel member in the model.

All properties of the channel members used in our model are thought to have a stochastic nature. The average transmissivity along a member and its length define the conductance. This is the only entity needed to calculate the flow, if the pressure difference between the two ends of the member is known. If the residence time is to be calculated for non-interacting solutes then the volume of the channel members is needed as well. For solutes that can sorb on the rock, the "flow-wetted" surface area is also needed (Neretnieks 1980). If the rock matrix is porous and the solutes have access to the interior porosity, the matrix diffusion properties must be known as well. We assume that it is possible to average these properties along a channel member. We also assume, in the present paper, that there is ideal mixing at channel intersections. Other mixing modes will be explored in later work.

The residence time distribution (RTD) is often described in terms of a mean residence time and dispersion. These are obtained from the first and second moments of the RTD. Higher moments, which describe exceptionally long tails or early arrivals, are usually not considered.

There are several mechanisms that cause dispersion of tracers: dispersion in the individual members of the network, dispersion caused by increase in the spread of residence times due to different velocities in the channels, and spreading caused by matrix diffusion effects. In preliminary calculations, we found that the dispersion in the individual members is negligible compared to the two other causes, and will not be used further in this study.

Mixing at intersections will also influence the RTD of the network. Several possible reasonable assumptions can be made of the mixing processes but none have been actually tested in real networks. We will only use the full mixing assumption in this paper. Matrix diffusion effects and sorption in the interior of the matrix are assumed to be active.

Fluid flow and solute transport are simulated. For tracer transport, additional information on channel volumes and flow-wetted surfaces is needed. No independent data on this are available, and therefore various assumptions are used and compared with the field results.

SOLUTE TRANSPORT IN A CHANNEL

The equation for solute transport in one channel, neglecting longitudinal dispersion is:

$$R_a \frac{\partial c}{\partial t} + u \frac{\partial c}{\partial z} = \frac{2D_e}{\delta} \frac{\partial c_p}{\partial x}\Big|_{x=0} \quad (1)$$

The first term is the accumulation of solute and includes the accumulation in the water in the channel and the solute sorbed on the channel walls. R_a is a retardation factor defined as

$$R_a = 1 + \frac{2}{\delta} K_a \quad (2)$$

The second term in Equation (1) accounts for the advection in the channel. The third term accounts for the exchange rate of solute with the rock matrix by molecular diffusion.

The diffusion of the solute in the rock matrix is described by

$$K_d \rho_p \frac{\partial c_p}{\partial t} = D_e \frac{\partial^2 c_p}{\partial x^2} \quad (3)$$

where the first term accounts for the accumulation of solute in the pore water in the matrix as well as on the micropore surfaces. The sorption capacity of the solid and the pore water is $K_d \rho_p$.

For the situation where there is no solute in the system initially, and the input concentration of the solute is constant, the solution is (Carslaw and Jaeger, 1959)

$$c = c_o \operatorname{erfc}\left(\frac{(D_e K_d \rho_p)^{0.5}}{(t - t_N)^{0.5}} \frac{LW}{Q}\right) \quad (4)$$

where t_N is the travel time for a solute that does not diffuse into the rock matrix. Equation (4) shows that the outlet concentration from one channel is a function of the channel volume, matrix properties, flow-wetted surface and flow rate.

If the diffusion into the rock matrix is pronounced, the travel time for the solute is much longer than that for a solute that does not interact with the matrix. So, the outlet solute concentration is almost independent of the channel volume. The concentration is then mainly a function of the matrix properties and the ratio between the flow-wetted surface and the flow rate.

CALCULATION PROCEDURES

Generation of network

The use of a rectangular network does not mean that the channel members are of equal length or that they form such a network: it is only a simple way of visualizing the

network. Each member of the network is assigned a hydraulic conductance. For tracer transport, a volume and surface are also needed. The orientation and location of the members only become important when they are compared with real geometry.

The flow calculations only need the information on the conductances of the channel members and the boundary conditions. The conductance the ratio between the flow in a channel member and the pressure difference between its ends. When solute transport is included, the volume of the member has to be known. If sorption onto the fracture surface or diffusion into the matrix will be included in the model, the surface area of the flow-wetted surface must also be included. Then some properties of the rock are needed as well, such as rock matrix porosity, diffusivity, and sorption capacity for sorbing species.

The individual channels are given stochastically selected conductances. In the present simulations, the conductances of the channel members are assumed to be lognormally distributed, with mean μ_0 and standard deviation σ_C. It is also assumed that the conductances are not correlated in space. The volume will be estimated by using various assumptions, owing to the lack of data.

Figure 1 shows a schematic view of the mesh used in this report. An outline of the approach used to calculate the fluid flow and solute transport through the network of members is presented below. The method is described in more detail in Moreno et al. (1988).

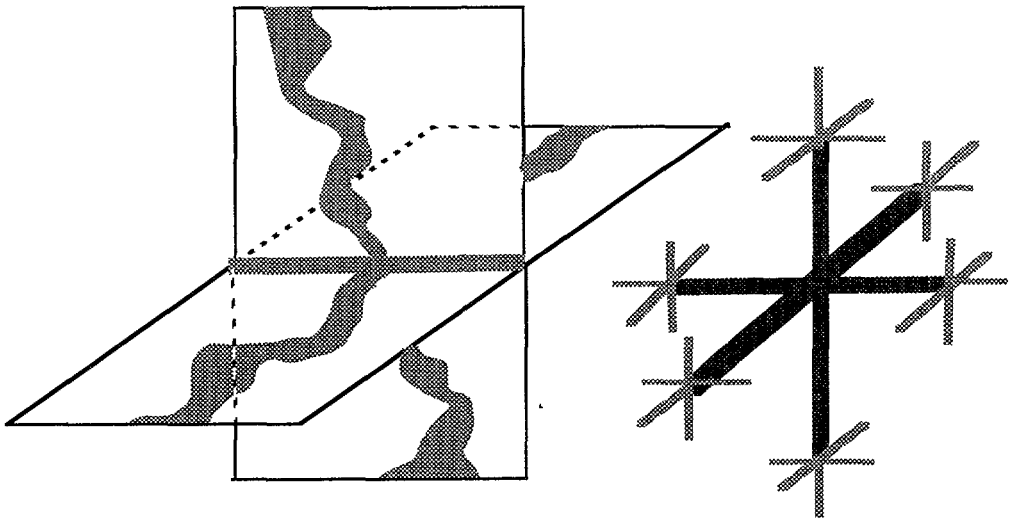

Figure 1 At a fracture intersection up to six channel members may intersect.

Fluid flow calculations

For laminar conditions, the flow through a channel member is proportional to the pressure gradient. The flow between two points "i" and "j" may be written as

$$Q_{ij} = C_{ij}(P_j - P_i) \tag{5}$$

where C_{ij} is the conductance connecting the nodes "i" and "j." The pressure field is calculated by writing the mass balance at each intersection point

$$\sum_j Q_{ij} = 0 \quad \text{for all i} \tag{6}$$

The solution of this system of equations yields the pressure at each node. The flow between adjacent nodes is then calculated by using Equation (5).

Solute transport calculations

The solute transport is simulated by using a particle-following technique (Robinson, 1984; Moreno et al., 1988). Many particles are introduced, one at a time, into the known flow field at one or more locations. Particles arriving to an intersection are distributed in the outlet channel members with a probability proportional to their flow rates. This is equivalent to assuming total mixing at the intersections. Each individual particle is followed through the network. The residence time in a given channel for non-sorbing tracers is determined by the flow through the channel member and by its volume. The residence time of an individual particle along the whole path is determined as the sum of residence times in every channel member that the particle has traversed. The residence time distribution is then obtained from the residence times of a multitude of individual particle runs.

From the RTD, the mean residence time and variance can be calculated. They may be used to determine the Peclet number, which is a dimensionless measure of the dispersivity (Levenspiel, 1972)

$$\frac{2}{Pe} = \frac{\sigma_t^2}{t_w^2} \tag{7}$$

When dispersion in the channel and/or diffusion into the rock matrix are considered, different particles in the same channel member will have different residence times. Here, residence times for the particles may be described by the RTD of the particles, expressed as a probability density function, pdf. It may be thought of as the outlet concentration for a pulse injection. If this curve is integrated over all the possible residence times, the cumulative distribution of the residence times is obtained.

When diffusion from the moving water into and out of the rock matrix takes place, a particle may reside in the matrix for some time in addition to its residence time in the water in the channel member. For a flat channel from which the diffusion is perpendicular to the channel surface, a simple analytical solution is available for the RTD. The cumulative curve, F, for the residence times is obtained as

$$F = \text{erfc}\left(\frac{(K_d D_e \rho_p)^{0.5} t_w}{(t - t_w)^{0.5} \delta}\right) \tag{8}$$

for times greater than the water-plug-flow residence time t_w. Otherwise the value is zero. Equation (8) considers only advection in the channel and diffusion into the rock matrix. Longitudinal dispersion is neglected.

For a rectangular channel member, the water-plug-flow residence time is obtained from the ratio between the channel volume and the flow rate through it. It may be calculated by LWδ/Q. Introducing this expression into Equation (8) yields

$$F = \text{erfc}\left(\frac{(K_d D_e \rho_p)^{0.5} L W}{(t - t_w)^{0.5} Q}\right) \tag{9}$$

For particle following, we follow the technique used by Yamashita and Kimura (1990). The travel time for each particle in a channel member is determined by choosing a uniform random number in the interval [0,1]. The travel time for the particle, t, is then calculated by solving for t in Equation (10).

$$[R]_0^1 = \text{erfc}\left(\frac{(K_d D_e \rho_p)^{0.5} L W}{(t - t_w)^{0.5} Q}\right) \tag{10}$$

SOME PROPERTIES OF THE MODEL

The simulated domain was a cubic grid with 20 channel members in each direction. The pressure gradient is imposed perpendicularly to one side. No-flow conditions were imposed on the four sides parallel to the pressure gradient. The outflow is through the 400 channels in the low-pressure side. Grids with a larger number of channel members were also simulated.

Flow rate distributions

Figure 2 shows the number of channels, of the 400 at the outflow face of the cubic grid, which carry a given flow rate (relative) for two σ_C. Note that the flow rate decreases to the right in the graph. The flow rates have been grouped in "bins" with the upper bound twice as large as the lower bound. This forms a geometric progression with a factor of 2 between the bins. This mode of representation has been chosen because in practice the larger channels will always be seen, whereas the measurement limit will determine the smallest flow rates that can be observed. In field observations, only the flow rates in the 6-8 bins with the largest flow rates may be used for calibration purposes. This means flow rates in 2-3 orders of magnitude. In histograms showing the fraction of flow in a given interval, only the largest flow rates contribute significantly to the total flow. Figure 3 shows the cumulative fraction of flow for flow rates less than a given value, for two σ_C. The total flow is normalized to the total flow in the 8 largest intervals. The contribution of the interval with the smallest flow rate is very small for both σ_C. This type of graph will later be used to calibrate the model with field data.

As shown in Figure 2, the distribution of the flow rates from the grid, on a logarithmic scale, shows an asymmetric tail extending out to smaller flow rates. This tail is not observed at the field observations because the very small flows are not measured. The flow rates cover 2 - 3 orders of magnitude at most.

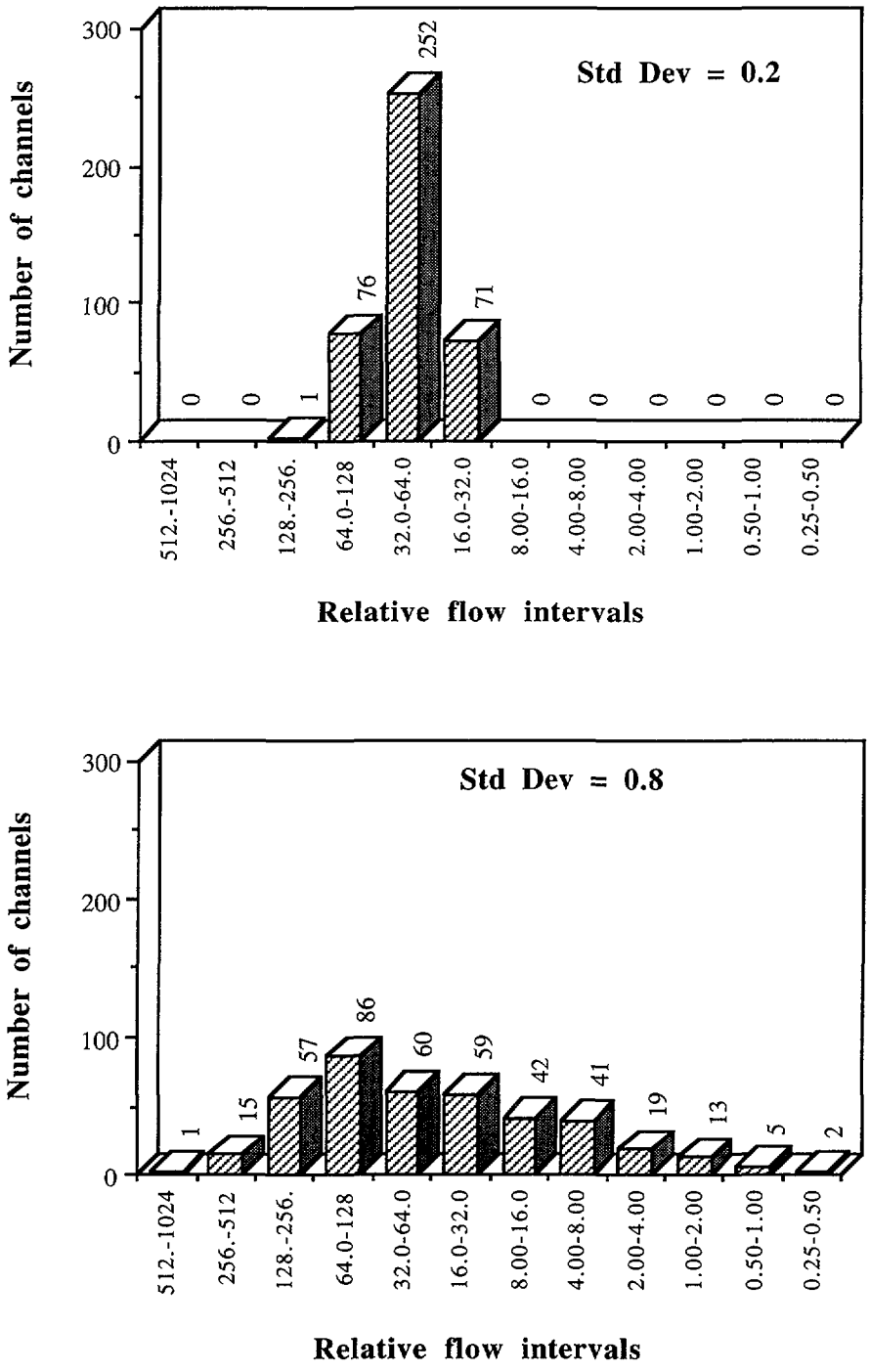

Figure 2 Histograms for the number of channels with flow rate in a given interval, for values of 0.2 (a) and 0.8 (b) in the standard deviation of the conductance σ_c. The flow at the left is large, and decreases towards the right.

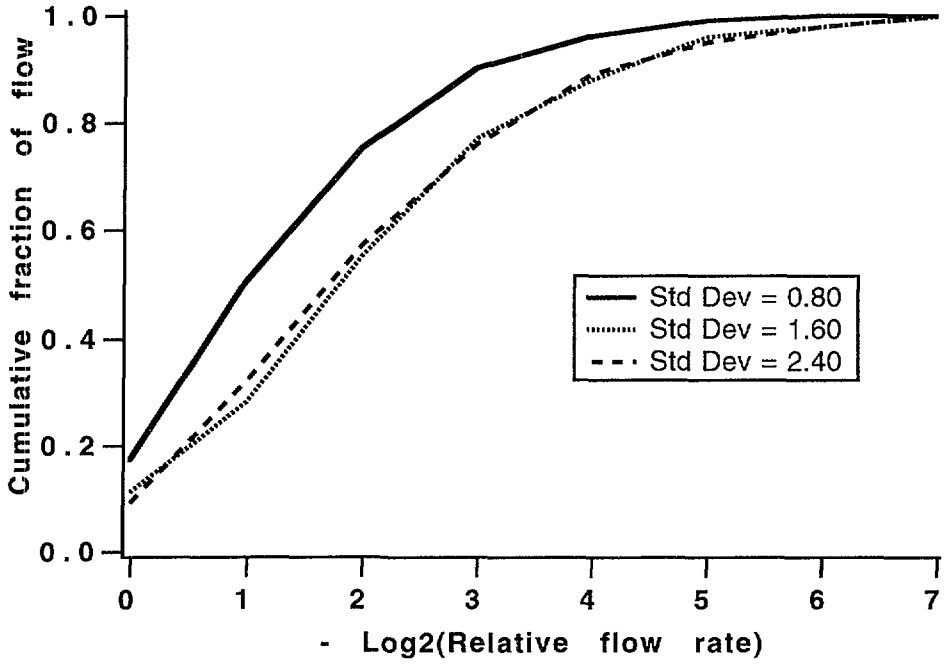

Figure 3 Cumulative curve for fraction of flow with flow rate less than a given value for different standard deviation in conductances

Solute residence time distributions for non-interacting solutes

It will later be shown that the RTD for non-interacting solutes is not and cannot be related to the RTD of sorbing solutes. Nevertheless, non-interacting solutes are commonly used for tracer tests. Information on spacial distribution of flow and of mixing and spreading processes in the network can however be obtained. For this reason, the RTD properties for non-interacting solutes are discussed here, and some of the limitations in our understanding are pointed out.

Although a few flow paths carries most of the flow all channel members contribute to some extent. This implies that the distribution of the residence time may become very broad. The fastest paths will be those with large flows, but the tail of the RTD will be determined by low-flow channel members. For large values of σ_c, it may be expected that the difference in residence times between the fast and the slow paths is considerable. The RTD is influenced not only by the flow rates in the channel members but also by their volume.

There are no reliable relationships known, at present, between the conductance and the volume. Several approaches were explored. The main difficulty in determining which of the possible approaches may represent the volume is the lack of field data. We have tested some approaches between conductance and volume. From these simulations, we expect to find which approach(es) could be used, by comparisons with field observations of the distribution of tracer residence times.

Four approaches were chosen:

- Volume is *proportional* to the hydraulic conductivity.
- Volume is *constant.*
- Volume is proportional to *cubic root* of channel conductance.
- Volume is determined from an *independent* random distribution.

To test these approaches, solute transport was simulated. Two types of injection were used. First, a large number of particles was injected on the high-pressure side of the block and collected on the opposite side. The number of particles that flow into each inlet channel is proportional to the flow rate in these channels. This type of injection was chosen because results are independent of the injection location (Moreno et al., 1990).

For the second injection type, many particles are injected at a point in the mesh, and the particles reaching the outlet side are collected at their respective locations. The relative concentration is determined from the number of particles per unit time that arrive at a collection point, divided by the flow rate in the same location. This type of injection was used to compare the data with those from the 3-D tracer test experiment done in Stripa (Abelin et al., 1991a,b).

As will be shown later, values of σ_C obtained from comparisons with field observations are between 1.6 and 2.4.

Peclet numbers and mean residence times are calculated from the particle residence time distribution. Peclet numbers when the particles are injected in one of the block sides are shown in Table 1 for different volume approaches. There is insufficient information to accept or reject any of these approaches. However, if we consider that a very large dispersion (Peclet numbers much less than 1.0) is uncommon in field observations,

Table 1 Peclet number as a function of the standard deviation σ_C for different assumptions used for channel volume. Average values from 20 simulations.

Assumption for channel volume	Standard deviation σ_C 0.80	1.60	2.40
Proportional to Cond	2.63	0.19	0.13
Constant volume	3.90	0.56	0.09
Prop. to $Cond^{1/3}$	10.45	4.41	1.13
Prop. to $Cond^{2/3}$	8.41	0.79	0.20
Random with $\sigma = \sigma_C/3$	3.19	0.28	0.80
Random with $\sigma = \sigma_C$	0.41	0.04	0.06

then some approaches seem less likely, e.g. when the volume is chosen from a new distribution or when the volume of the channel is proportional to the channel conductances. The other approaches give residence time distributions found in field experiments. The largest Peclet number (or the smallest dispersion) is obtained when the channel volume is taken to be proportional to the cubic root of the conductance. The same results are obtained when point injection is used.

Solute transport for matrix interacting solutes

If the solutes also have access to the matrix porosity by diffusion, the residence times of the solute particles are larger than the residence time without diffusion into the matrix. For low flow rates, Q, in relation to the flow-wetted surface, LW, in a channel member, the solute can be very much retarded compared to the water flow residence time, t_W. In the flow and tracer experiments in Stripa (Abelin et al. 1991a,b), where water flow residence times for the different tracers varied from months to years, they found that matrix diffusion may have contributed noticeably to the retardation of the tracers. We have therefore incorporated this mechanism in our model for use in later studies of tracer transport.
The residence time for each particle that passes the channel member is stochastically determined by Equation (10). The capability of the particle following method to describe the diffusion in the rock matrix was tested by generating a network with equal channel members (zero standard deviation). In these channels, we used the stochastic process to simulate the diffusion in the rock matrix. The results agree very well when compared with the analytical solution if a few thousand particles are used. The procedure was found to be fast and accurate in network calculations as well.

CALIBRATION AND COMPARISON WITH FIELD OBSERVATIONS

The calibration of the model, to a given site, involves the determination of the conductance distribution used to generate the channel and the channel length. If a lognormal distribution is used, then the mean and standard deviation would be determined. The mean works as a scale factor for flowrate, so if the flux is known the mean may be evaluated. Procedures to determine the standard deviation are shown below.

To determine these parameters, observations of water inflow to tunnels or drift may be used. Borehole data may be also used to estimated channel lengths (Moreno and Neretnieks, 1993. The water inflow to tunnels will be at isolated points on the tunnel walls. This will look like a number of "channels" being cut by the rock faces of the tunnel. The outflow face of the network model will also have a number of "channels" with flowing water.

The flow rates out from the simulated cubic grid cover a very wide interval, if a large value of σ_C is used. On the other hand, the field results often show variations of only a few orders of magnitude in flow rates. This aspect is schematically presented in Figure 4. The histogram shows the number of channels with flow rates in a given interval, if even the channels with a very small flow rate could be monitored. From field observations, only data for 6 - 8 bins may be obtained. They are shown with gray bars in the figure. The white bars represent the unknown data. The whole histogram could also represent the results of a simulation.

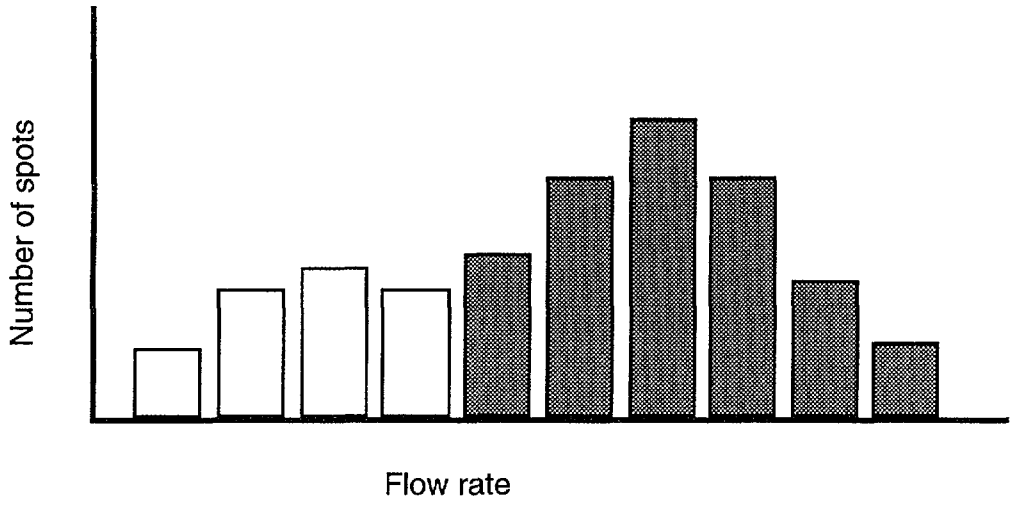

Figure 4 Histogram showing the number of channels with a flow rate in a given interval. The gray bars represent hypothetical data from field observations. The white bars represent channels with a flow rate below the detection limit.

The calibration procedure is as follows. The inflow measurements to the drift are compared with the simulated results. With the available data (the gray bars) the standard deviation σ_C may be estimated. Then, when the value of σ_C is known, the number of channels in the observable flow rate interval for the field data is compared with that of the model for the same interval. The total number of channels in the field (observable and non-observable channels or gray and white bars in the histogram) is obtained by comparing the field data with the results from simulations.

$$\frac{\text{Total number of channels in rock}}{\text{Total number of channels in simulations}} = \frac{\text{Number of channels observed in rock above a chosen flowrate}}{\text{Number of channels in the simulations spanning the same flowrate range}} \qquad (11)$$

The same procedure can be used for the packer test data in boreholes if these are analysed for the number of intersections, provided channel widths and the borehole diameter are known. This will be described later.

The channel network model gives no inherent information on channel member widths or lengths. Nor is the distribution function for the conductances known a priori. If the latter is assumed to be lognormal, then the mean and standard deviation can be found by fitting them to measured data. It has been found, by several investigators, that the standard deviation of transmissivities obtained in boreholes often is between 1 and 3 on a logarithmic (base 10) scale (Cacas, 1990a; Geier et al., 1990). Dverstorp (1991) used σ_C values ranging from 0.4-2.4 in simulations of the Stripa experiments with the best results for $\sigma_C = 1.7$. Cacas et al., (1990a,b) found a value of $\sigma_C = 3.2$ for the Fannay Augère experiments in their fracture network model calibration.

Using data from drifts and tunnels

At the SFR site, there are flow rate measurements available for individual spots over an area of 14 000 m^2 (Neretnieks, 1987). Table 2 summarizes the data. The flow rate ranges have been chosen as a decreasing geometrical progression, such that each range "bin" is half the previous one. The reason is that one will undoubtedly observe the largest flow rate spots, but will have a decreasing accuracy in detecting spots with lower flow rates. It is also generally not possible to know the total inflow to the low-flow rate spots, so that a cumulative flow rate curve cannot be constructed to start at the low-flow end. However, a cumulative curve can be started from the high-flow end and

Table 2 Flow rate distribution at the different spots at SFR.

Flow rate range, l/min	Number of spots	Cumulative number of spots	Fraction of Flow rate
>=1.6	2	2	0.13
0.8-1.6	4	6	0.15
0.4-0.8	12	18	0.21
0.2-0.4	41	59	0.30
0.1-0.2	38	97	0.13
< 0.1	67	164	0.08

can be compared to the model results. If graphs with the cumulative fraction of flow rates are used and the experimental results plotted in those, an estimate of the standard deviation of conductances can be made. The cumulative flow rate increases little when more than 5-6 "bins" are used. The method can thus be expected to be robust, in the sense that the most important paths have been accounted for. For the SFR data, σ_C is found to be about 1.6 with this method. The cumulative flow rate curves obtained from the simulations and the cumulative curve from the field observations are shown in Figure 5. The choice is not totally clear, because the differences between the curve obtained with the SFR observations and the curves for σ_C = 1.6 and 2.4 are small. For this reason, an alternative procedure is discussed below.

In Table 3, the cumulative numbers of channels for three σ_C are given. If the ratio of the cumulative number of channels in the model to the number of channels in the SFR observations is calculated, the model and observed results agree best for σ_C = 1.6. The agreement is based on obtaining the same ratio along the various flow rate intervals. This is shown in Figure 6, where this ratio is plotted as a histogram. The figure shows that the bars for σ_C = 1.6 are of a more even height than for the other σ_C, meaning that the observed and model distributions agree best for this σ_C. This confirms the value of σ_C obtained with the cumulative flow rates. The values used in Table 3 correspond to average values for 20 realizations.

Once σ_C has been established, the number of channels can be found by "aligning" the two columns, "Number of channels in the model" and "Observed number of channels," starting with the highest flow rate range, see Table 3. The ratio of the number of channels in the model to the observed number of channels was about 0.99, which means that the model has 1 % fewer channels than the real drifts and caverns at SFR.

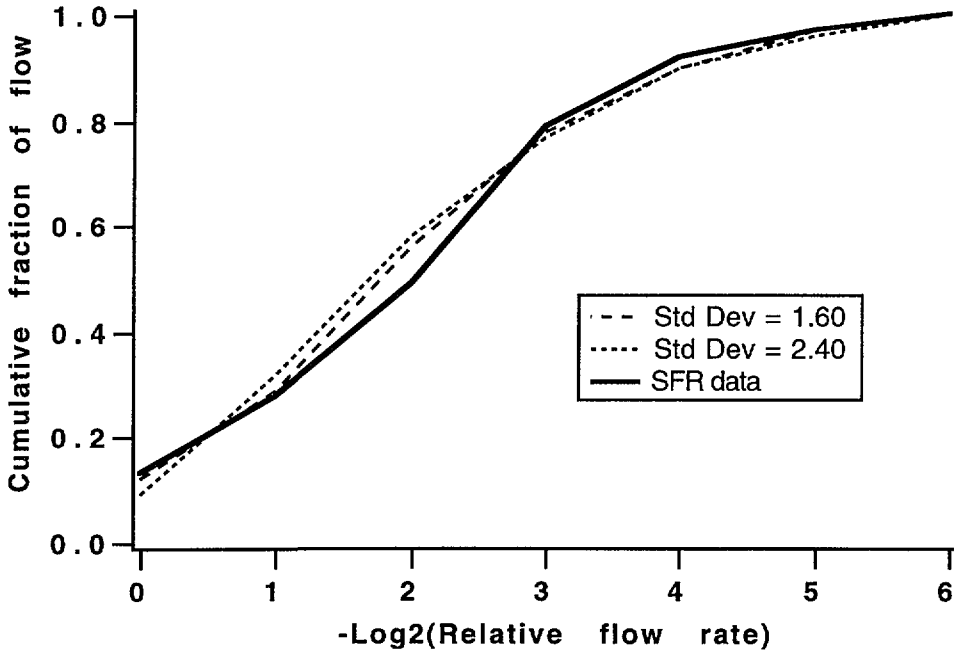

Figure 5 Cumulative fraction of flow. Solid line shows values for SFR data, dashed lines show simulated results.

Table 3 Match of model and observed flow rates at SFR, for a grid with 20 channels in each direction.

	Cumulative number of channels from model for			Observed channels
σ_C	0.8	1.6	2.4	at SFR
Flow rate category				
1	11	2	1	2
1/2	53	8	6	6
1/4	119	27	17	18
1/8	194	57	34	59
1/16	258	90	56	97
1/32	351	163	103	164
0	400	400	400	

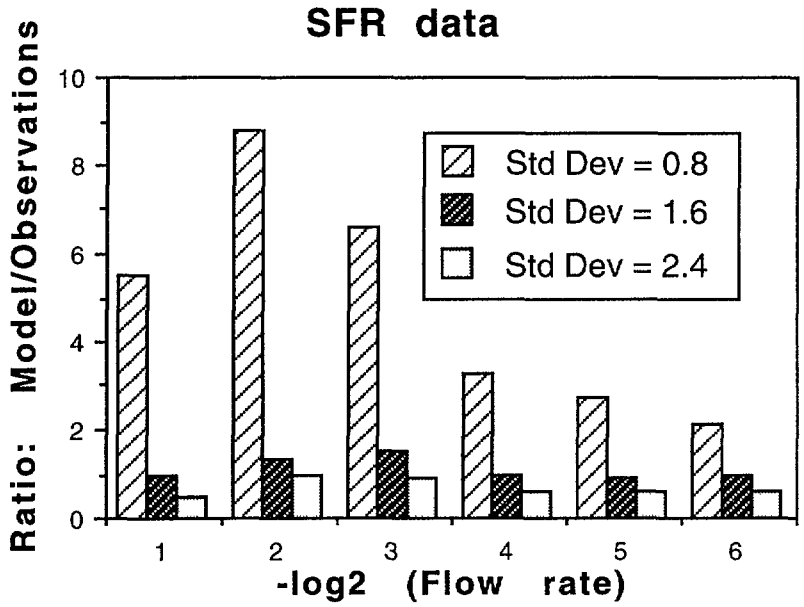

Figure 6 Ratio of model to observed number of channels in SFR for different standard deviations, σ_C.

The model in the present simulations had 400 channels at the outflow face. The SFR thus has 400/0.99 = 404 inflow channels. In this figure all the channels are included. These 404 channels are found on a surface area of 14 000 m^2. This means that every channel has 35 m^2 on average, and the average length of the channel members is the square root of this figure, Z = 5.9 m. When the simulations were done using a grid with 40 channels in each direction, the ratio of the number of channels in the model to the observed number of channels was 4.1. As the total number of channels in the model is 1600, the SFR has 1 600/4.1, or 390 inflow channels. This gives a density of 1 channel per 36 m^2 and a length of 6.0 m. The results not are only influenced by the grid size.

The same method can be applied to the observations in Stripa, by assuming that every sheet has only one channel. The best agreement is obtained for σ_C = 2.4. The channel density is found to be one channel per 2.7 m^2 and the channel length 1.6 m. Besides the quite detailed Stripa and SFR measurements, there are flow rate estimates at spots in a drilled tunnel at Kymmen in western Sweden (Neretnieks, 1987). The Kymmen tunnel is a face-drilled tunnel with a length of 4.5 km and a diameter of 4.6 m. 63 fractures zones were identified, which make up a total length of 672 m. Within the rock mass, the channel density is found to be one channel per 105 m^2 and the channel length 10.3 m. For the zones, the area per channel is 21 m^2 and Z is 4.5 m. Table 4 summarizes the results for the three sites.

Channel widths have been measured in drifts and tunnels. Recently Palmqvist and Lindström (1991) analysed earlier observations in the Kymmen tunnel and found that 99.7 % of the channels have a width smaller than 0.1 m. Channel widths at SFR were also a few tens of centimetres, at most, with a few exceptions. A large number of them was point spots, found at fracture intersections and as small holes (Neretnieks 1987). In the 3D drift at Stripa, they also found that the water collection sheets collected more

water in areas where there were more fracture intersections (Abelin et al., 1991a,b). A recent experimental investigation that specifically measured channeling at Stripa (Abelin et al., 1990) also found that channels were typically a few centimeters to a few tens of centimeters wide. We use 20 cm as a "typical" width for channels in this paper.

Table 4 Summary of the results for SFR, Stripa and Kymmen

	σ_c	A m^2	Z(drift) m
SFR	1.6	35	5.9
Stripa	2.4	2.7	1.6
Kymmen rock mass	2.4	105	10.3
Kymmen zones	2.4	21	4.5

Using borehole data to estimate channel lengths

In practice, the measurement limit in packer tests determines when a packer section is assumed to be "non-conducting." Typically, the transmissivity of the most conducting sections in the rock mass is 4-6 orders of magnitude more transmissive than the measurement limit. The measurements are usually available in the form of a number of packer intervals with measured transmissivities for the borehole tests. These measurements can be used to estimate the total number of conductive fractures (channels) intersected by the borehole(s). This has been done on data from Stripa (Geier et al., 1990). The information then needs to be translated into the number of channels of a given width W and length Z per rock volume. A method for doing this is developed below.

The rock contains a large number of channels randomly orientated, with an average length Z and an average width W. If there are several of such channels in a volume of rock, a borehole that is drilled in the rock may intersect some of them. In this analysis, we assume that the aperture of the channels is very small compared to the other dimensions of the channels and that the widths of the channels are small in relation to the average distance between channels.

Consider a borehole with diameter D_{bh} and how a channel must be located in order to be in contact with the hole. Figure 7 shows a vertical borehole and a channel with different angles to the horizontal. The average distance, W_{av}, is obtained by integrating over all angles α

$$W_{av} = \frac{1}{\pi/2}\int_0^{\pi/2} W \sin\alpha \, d\alpha = W\frac{2}{\pi} \qquad (11)$$

In the same way the average distance at which a channel will intersect the hole in the other direction, Z_{av}, can be obtained.

$$Z_{av} = \frac{1}{\pi/2}\int_0^{\pi/2} Z \sin\beta \, d\beta = Z\frac{2}{\pi} \tag{12}$$

Thus the average area in which a channel must lie to contact the hole is

$$A_{av} = \frac{\pi}{4} D_{bh}^2 + 2 Z_{av} (D_{bh} + 2 W_{av}) \tag{13}$$

If the average distance between channels intersected by the borehole has been shown to be H, then the rock volume containing one channel is $H \cdot A_{av}$. In a system with a cubic grid of channels, every cube with sides Z is delimited by 12 channels. Every channel is shared by four other cubes, so there are three channels per volume of size Z^3. Thus

$$Z^3 = 3 H A_{av} = 3 H \left(\frac{\pi}{4} D_{bh}^2 + 2 Z_{av} (D_{bh} + 2 W_{av})\right) \tag{14}$$

Substituting Equations (11) and (12) into (14) gives

$$Z^3 = 3 H \left(\frac{\pi}{4} D_{bh}^2 + 4\frac{Z}{\pi}\left(D_{bh} + 4\frac{W}{\pi}\right)\right) \tag{15}$$

If H, D_{bh} and W are known from independent measurements, then Z is obtained from equation (12). When $Z >> D_{bh}$, the first term in equation (12) can be neglected and Z is obtained from

$$Z^2 = H \frac{12}{\pi}\left(D_{bh} + 4\frac{W}{\pi}\right) \tag{16}$$

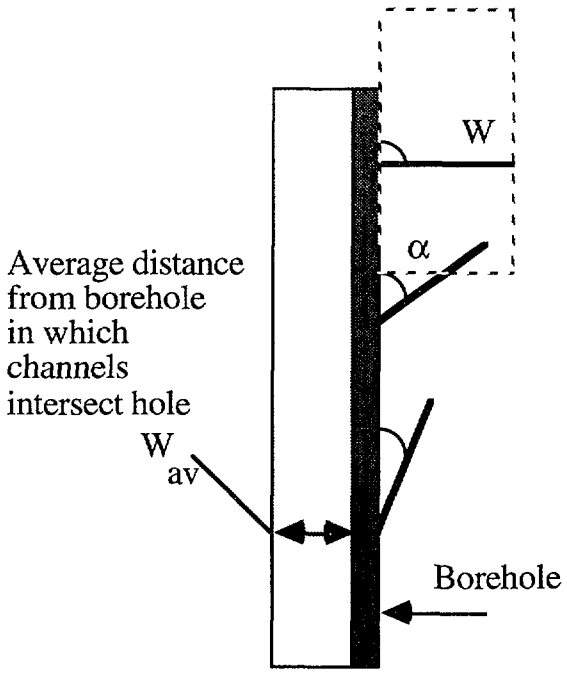

Figure 7 View of borehole from above, indicating at what distance from the borehole a channel must lie, on average, in order to be in contact with a borehole.

Geier et al., (1990) found that in three horizontal north-south orientated boreholes, drilled nearly parallel to the 3-D drift in Stripa, the standard deviation of transmissivities was 1.5 a logarithmic (base 10) scale and the conductive fracture frequency was 0.57 m^{-1}. This fracture frequency corresponds to the total number of conductive fractures. In two horizontal east-west orientated boreholes, starting at the 3-D drift, the same values were found for the fracture density and the standard deviation. The mean transmissivity, however, was 10 times higher in the latter holes.

With a width W = 0.1 m and a borehole diameter of 0.076 m, Equation (13) above gives an average channel grid length Z of 1.2 m. This agrees reasonably well with the results obtained from the observations of flow rate distribution in the 3D drift, where Z was 1.6 m.

Thus measurements from drifts and tunnels as well as from boreholes can be used to estimate the channel lengths. To use borehole information, channel widths are needed. However, the results are not very sensitive to the channel widths if they are of the same magnitude as the borehole diameter. This can be seen from Equation (13). If W is taken to be equal to D_{bh} (although it is much less in reality), Z would have been overestimated by 51 %. This is not a very large error compared to many other entities used for the simulation of flow in the network. However, W has a large effect on the interacting tracers, because it directly influences the flow-wetted surface. It must, for this reason, be determined accurately. We have found very few measurements, beyond those mentioned, that could be used to determine the flow-wetted surface or channel width more precisely.

In the next subsection, an attempt is made to use some tracer data to at least check if the value $W \approx 0.1$ m is at all reasonable.

SAMPLE CALCULATIONS FOR SOLUTE TRANSPORT

To illustrate the potential impact of matrix diffusion on the transport, some sample calculations are presented. The data are chosen to cover a wide interval, from species that do not diffuse into the rock matrix to species that have a small sorption capacity. Simulations were done on a mesh of 20x20x20 nodes. The member length was assumed to be 5 m; this means a travel distance of 100 m. A channel width of 0.2 m and a channel aperture of 0.1 mm are chosen. The Darcy velocity through the mesh is assumed to be 0.0001 m^3/m^2a. Therefore is the water mean residence time 2.4 years.

For the species that diffuse into the rock matrix, three values were chosen for $D_e K_d \rho_p$. This product describes the diffusion and sorption properties of the rock. For species that are not sorbed within the matrix the term $K_d \rho_p$ is equal to the porosity. In the first simulation, small values are assumed for the porosity and the effective diffusion coefficient for the rock matrix (0.003 and 10^{-13} m^2/s respectively). These values are similar to those found in crystalline rock. In the second simulation large values are used (0.03 and 10^{-12} m^2/s). In the last simulation, transport of a slightly sorbing species is calculated. Here, a value of 3.0 is assumed for the term $K_d \rho_p$.

The simulations were done with a standard deviation, σ_c, of 1.6. Figure 8 shows the breakthrough curves for these realizations. The transport of species that interact with the matrix is thus determined mainly by the diffusion and sorption properties of the rock, the flow distribution, and the flow-wetted surface area of the channels. The impact of the channel volume is negligible since the residence time of interacting solutes in a channel is usually much longer than the water residence time, see Equation (4).

In an earlier paper, simulations were done for sorbing species using different volume-conductance relations (Moreno and Neretnieks, 1993). The breakthrough curves had the same shape irrespective of the volume-conductance relations used. This suggests that the RTD of tracers that have access to the rock matrix will be determined by the conductance distribution and the flow-wetted surface of the rock, and not by its flow porosity. For this reason the calculations were carried out with a constant aperture.

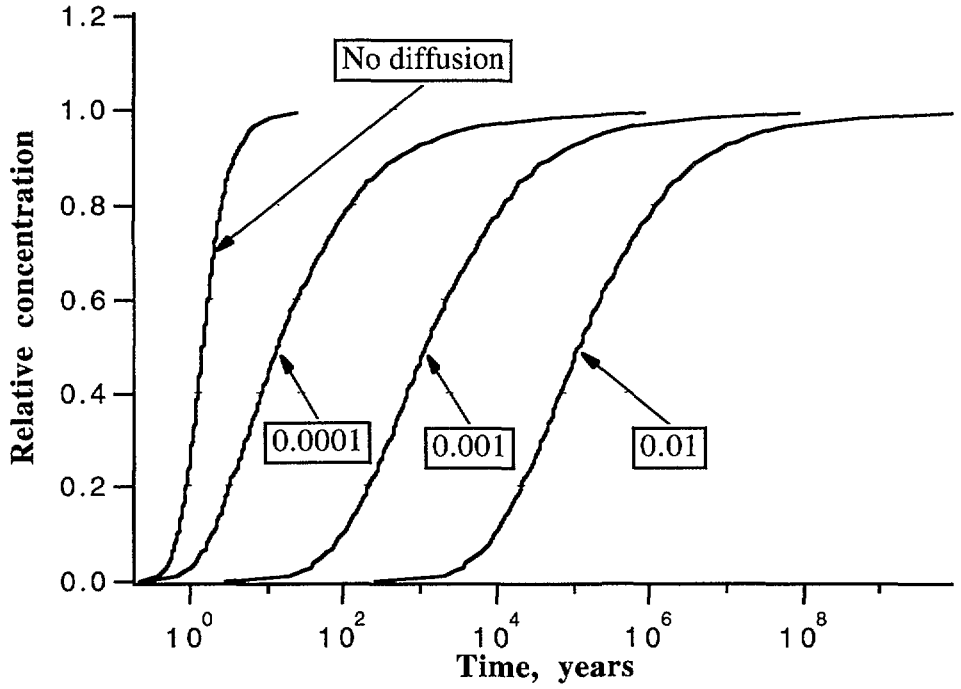

Figure 8 Breakthrough curves for solutes that interact with the matrix. The water residence time is 2.4 years. The figures attached to the curves correspond to the values of $(D_e K_d \rho_p)^{0.5}$

So, to simulate the transport of species that diffuse into and out of the rock matrix, the following data are primarily needed in the model:

- conductance distribution (μ, σ_c)
- channel lengths (L)
- channel widths (W)

The conductance distribution, together with the average hydraulic gradient, gives the flow rate distribution in the channel network. The channel lengths and widths determine the flow-wetted surface of the channel members. This is sufficient for the simulation of

the migration over the distance of interest. Note that no information is needed on flow porosity or "dispersion". The data needed can be obtained from field observations and experiments.

DISCUSSION AND CONCLUSIONS

The model proposed is intentionally made simple so that it is easy to incorporate tracer transport and to accommodate interacting tracers. The model must be calibrated to field measurements. Borehole transmissivity data obtained by "narrow" packer intervals should, in principle, suffice to obtain the effective channel lengths, provided channel widths can be determined independently. The comparisons and calibrations with field observations are rather straightforward and have shown that the model can exhibit the properties of channeling observed in the field. Tracer residence time distributions and patterns also agree.

It has been shown that the flow-wetted surface area is of prime importance for the migration of solutes that diffuse into the rock matrix. There are not enough detailed in situ observations that can be used to assess the flow-wetted surface area. Special techniques and tests must be developed and applied to obtain more accurate information.

NOTATION

A	Area	m^2
a	Wetted surface	m^2/m^3
C	Conductance	m^4s/kg
c	Concentration	mol/m^3
D_e	Effective diffusion coefficient	m^2/s
D_{bh}	Hole diameter	m
K_d	Sorption coefficient	m^3/kg
L	Length	m
P	Pressure	$kg/(m \cdot s^2)$
Pe	Peclet number	
R	Retardation factor	
Q	Water flow rate	m^3/s
W	Channel width	m
r	Radial distance	m
t_w	Water residence time	s
Z	Channel length	m
α	Angle	
δ	Aperture	m
ε	Porosity	
μ_o	Mean logarithm of conductance	
ρ_p	Density of bulk rock	kg/m^3
σ	Standard deviation in the lognormal distribution of conductances	
σ_t	Standard deviation in the residence time distribution	s

REFERENCES

Abelin, H., I. Neretnieks, S. Tunbrant, and L. Moreno, Final Report of the Migration in a Single Fracture - Experimental Results and Evaluation, Stripa Project Technical Report 85-03, OECD/NEA, SKB 1985.

Abelin, H., L. Birgersson, H. Widén, T. Ågren, L. Moreno, and I. Neretnieks, Channeling experiment to study flow and transport in natural fractures, Stripa Project Technical Report 90-13, OECD/NEA, SKB 1990.

Abelin, H., L. Birgersson, J. Gidlund, and I. Neretnieks, A large-scale flow and tracer experiment in granite, 1. Experimental design and flow distribution, Water Resour. Res., 27, 3107-3117, 1991a.

Abelin, H., L. Birgersson, L. Moreno, H. Widén, T. Ågren, and I. Neretnieks, A large-scale flow and tracer experiment in granite, 1. Results and interpretation, Water Resour. Res., 27, 3119-3135, 1991b.

Cacas, M.C., G. de Marsily, B. Tillie, A. Barbreau, E. Durand, B. Feuga, and P. Peaudecerf, Modelling fracture flow with a stochastic discrete fracture network: calibration and validation - 1 The flow model, Water Resour. Res., 26, 479-489, 1990a.

Cacas, M.C., E. Ledoux, G. de Marsily, A. Barbreau, P. Calmels, B. Gaillard, and R. Margritta, Modelling fracture flow with a stochastic discrete fracture network: calibration and validation - 2 The transport model, Water Resour. Res., 26, 491-500, 1990b.

Carslaw, H. S. and J. C. Jaeger, Conduction of Heat in Solids. Oxford University Press, 1959.

Dverstorp, B., Analyzing flow and transport in fractured rock using the discrete fracture network concept. Ph.D. Thesis, Royal Institute of Technology, Dept. of Hydraulic Engineering TRITA-VBI-151 Stockholm 1991.

Dverstorp, B. and J. Andersson, Application of the discrete fracture network concept with field data: Possibilities of model calibration and validation, Water Resour. Res. 25(3), 540-550, 1989.

Geier, J., W. Dershowitz, and G. Sharp, Prediction of inflow into the D-holes in the Stripa mine. Stripa Project Technical Report 90-06. OECD/NEA, SKB April 1990.

Levenspiel, O., Chemical Reaction Engineering, 2nd ed., p 275. John Wiley and Sons, New York, 1972.

Long, J.C.S., H.K. Endo, K. Karasaki, L. Pyrak, P. MacLean, and P.A. Witherspoon, Hydrological Behavior of Fracture Networks. Hydrogeology of Rocks of Low Permeability, IAH Conference Jan 7-12, 1985, Tucson Arizona. Volume XVII, p 44-468, 1985.

Moreno, L., Y.W. Tsang, C.F. Tsang, F.V. Hale, and I. Neretnieks, Flow and tracer transport in a single fracture. A stochastic model and its relation to some field observations, Water Resour. Res., 24, 2033-3048, 1988.

Moreno, L., C.F. Tsang, Y.W. Tsang, and I. Neretnieks, Some anomalous features of flow and solute transport arising from fracture aperture variability, Water Resour. Res., 26, 2377-2391, 1990.

Moreno, L. and I. Neretnieks, Fluid flow and solute transport in a network of channels, Journal of Contaminant hydrology, accepted for publication, 1993

Neretnieks, I., Diffusion in the Rock Matrix: An Important Factor in Radionuclide Retardation? J. Geophys. Res. 85, 4379-4397, 1980.

Neretnieks, I., Channeling effects in flow and transport in fractured rocks - Some recent observations and models, Paper presented at GEOVAL symposium, Stockholm, Proceedings, 315-335, 1987.

Neretnieks, I., H. Abelin, and L. Birgersson, Some recent observations of channeling in fractured rocks. Its potential impact on radionuclide migration, In DOE/AECL conference Sept 15-17, 1987, San Francisco, Proceedings p 387-410, 1987.

Palmqvist, K. and R. Stanfors, The Kymmen power station TBM tunnel. Hydrogeological mapping and Analysis, SKB Technical Report TR 87-26, 1987.

Palmqvist, K. and M. Lindström, Channel widths, SKB Technical Report TR 91-14, 1991.

Robinson, P.C., Connectivity, flow and transport in network models of fractured media, Ph. D. Thesis, St. Catherine's College, Oxford University, Ref TP 1072, May 1984.

Yamashita, R. and H. Kimura, Particle-tracking technique for nuclide decay chain transport in fractured porous media, Journal of Nuclear Science and Technology, 27, 1041-1049, 1990.

KBS/SKB - Technical Reports can be obtained from: INIS CLEARING HOUSE, International Atomic Energy Agency, P.O. Box 100, A-1400 VIENNA, AUSTRIA.

SYNTHESIS OF GEOCHEMICAL, ISOTOPIC AND GROUNDWATER MODELLING ANALYSIS TO EXPLAIN REGIONAL FLOW IN A COASTAL AQUIFER OF SOUTHERN OAHU, HAWAII

C.I. VOSS, W.W. WOOD
United States Geological Survey,
Reston, Virginia,
United States of America

Abstract

Regional geohydrologic characterization of the flow field in the coastal stratified basalt aquifer of the Pearl Harbor area in southern Oahu, Hawaii, is provided by a synthesis of geochemical and isotopic information, collected in vertical profiles, and numerical simulation of the variable-density ground-water flow. The uppermost water layer, 75 m to 125 m thick, consists of water recharged from local rainfall and irrigation over the past few decades. Below this is the core of the freshwater lens, 100 m to 150 m thick, containing waters with an apparent carbon-14 age of 1800 years. The freshwater lens floats on a third saltwater layer that likely extends to the bottom of the aquifer. The apparent carbon-14 age of the saltwater is between 6000 years and 9000 years, and the difference in ages between an inland well and a coastal well suggests that before aquifer development began in the 1880s, saltwater flowed inland at a velocity of about 2 m/yr. Assuming a constant lateral velocity in the saltwater body, the saltwater recharge area may thus be estimated to be 11 km to 24 km from the observation wells, in an area located between 1 km and 14 km offshore of the southern Oahu coast. Post-bomb carbon-14 and tritium data indicate a residence time of water within the freshwater lens of no more than a few tens of years. If total recharge estimates assumed here are correct, the 1800-year apparent age of this water can only be explained by long residence time in recharge area compartments the central plateau of Oahu and the dike zone in the Koolau Mountains before entering the lens, although the storage volume is not sufficient to account for the entire delay. In addition, some of the great apparent freshwater age may be accounted for by a component of old organic carbon introduced in the ground-water recharge area.

The simple geochemical reactions in this aquifer system allow clear interpretation of water chemistry and isotopic data. The chemical and stable isotope composition of all samples is well-explained by simple mixing of the three types of water. The major reaction in the saltwater is sodium-calcium exchange, which increases calcium concentration over that of seawater, but which has negligible effect on carbon-14 dating. There is no evidence of calcite dissolution affecting the freshwater. Extrapolated aquifer saltwater carbon-13 content is somewhat lighter than oceanic values, probably indicative of oxidation of organic carbon. Assuming this organic carbon was devoid of carbon-14, measured carbon-14 values for saltwater must be adjusted upward by at most a factor of 1.24. Thus, carbon-14 values with or without adjustment give similar absolute ages and travel times of water flow between measurement points. Unfortunately, a number of samples collected show a high degree of scatter suggesting the possibility of contamination by modern carbon-14 during handling or analysis, reducing the quantity of vertical age data available from profiling.

The characterization of both the freshwater and saltwater flow field obtained from geochemical analysis is consistent with regional hydrologic behavior of the Pearl Harbor area represented by the cross-sectional variable-density flow and solute transport model of Voss and Souza (1993). This model was based only on analysis of hydraulic data and vertical salinity profiles through the freshwater lens and saltwater transition zone. Thus, the simply-structured numerical model, which included an estimate of regional effective porosity for flow (0.04) that could not be verified on the basis of data existing at that time, can explain all currently-available geochemical and hydraulic field information. This may be the first analysis in which it was possible to corroborate ground-water model-calculated density-driven saltwater velocities in a coastal aquifer with flow velocity determined from chemical and isotopic field data.

1. INTRODUCTION

Hydrologic, geologic, geochemical and other information can be synthesized to obtain a satisfactory explanation of the occurrence and large-scale behavior of

subsurface fluids in complex hydrogeologic environments. The most satisfactory explanation is the simplest one that simultaneously describes all types of available data. Solute geochemistry constrains the possible interpretations of the hydrogeology of a system and adds direct measurement of flow velocity and identification of the source of water often unavailable in hydrologic investigations.

Most regional ground-water flow systems are three-dimensional, exhibiting not only areal variability, but vertical variability as well. It is a challenging task to satisfactorily explain the vertical variations in such systems; most wells provide data over a limited depth interval, and the cost of drilling a well makes the definition of vertical variability even more sparse than of areal variability. Vertical variations are important because ground-water systems are highly stratified; recharge from a higher-elevation area generally is found at greater depth than locally-recharged water. Thus, vertical variations contain information on recharge areas and flux of water from these areas.

In coastal aquifer systems, vertical variations are generally better characterized because of the threat of seawater intrusion from below. In Hawaii, coastal aquifers have been characterized in a vertical sense primarily in terms of salinity-depth profiles in deep observation wells. This information, together with hydraulic information collected since aquifer development began in 1880, has been used in numerical simulations by Souza and Voss (1987) and Voss and Souza (1993), to explain the vertical distribution of regional groundwater flow in the Pearl Harbor area of the southern Oahu aquifer, near Honolulu. For these studies, vertical profiles of isotopic and other geochemical field data yielding information on fluid velocities and source areas was unavailable, and thus it was not possible to directly test these aspects of the model.

However, the areal distribution of stable and radioactive environmental isotopes as well as major ion chemistry in southern Oahu aquifers was well-characterized in a comprehensive series of studies by Hufen and others (1972), Hufen (1974), Hufen and others (1974a), Hufen and others (1974b), and Hufen and others (1980). The results demonstrated significant differences in source areas and ages of freshwater pumped from various aquifers in southern Oahu. Hydrologic explanation of the findings concerned mainly the areal differences in isotopes, as most data was collected by pumping water from existing wells. Three generic layers of water in the aquifers were postulated to explain some of the areally-measured variations: water recharged from irrigation, (apparent age of tens of years), freshwater lens core (age ranging from tens of years to hundreds of years), and intruded seawater (age as great as ten-thousand years).

In the immediate vicinity of the Waipahu monitor well where one profile was collected for the present work, Hufen and others (1980) found carbon-14 concentrations from 87 pmC to more than 100 pmC in samples collected from water pumped from active supply wells. It will be seen in this paper that the vertical profile collected for this study at the Waipahu well showed a relatively smooth carbon-14 variation from more than 100 pmC in the uppermost water, to values as low as 90 pmC in the core of the freshwater lens, to 30 pmC in the saltwater. This illustrates the difficulty of hydrologic interpretation of isotope data collected as single-depth samples at or near active wells. On the other hand, it will be seen that our analysis confirms much of Hufen's general view of vertical structure. Further, because our analysis is based on continuous vertical geochemical and isotopic profiles, it refines the proposed structure and allows explanation of the hydrogeologic origin of the vertical structure to be proposed on a quantitative basis.

In the present study, vertical profiles of geochemical and isotopic information extending through the freshwater lens into saltwater, were collected in two observation wells located approximately along a flow line (in the areal plane) in the Pearl Harbor area. Analysis of these data and corroboration with the existing vertical hydraulic model of the system (Souza and Voss, 1987; Voss and Souza, 1993) allows a quantitative explanation of water occurrence and flow at the regional scale that satisfies all data types to be proposed.

2. HYDROGEOLOGY

The major population center of the volcanic Hawaiian island chain located in the north Pacific Ocean as well as the city of Honolulu is on the island of Oahu (FIGURE 1). Oahu was built by lavas extruded from two shield volcanoes and their associated rift zones (FIGURE 2), the Waianae on the west (approximately 3 million years old) and the younger Koolau on the east (approximately 2 million years old). See MacDonald and others (1983) for a complete discussion of Oahu geology. The rift zones are characterized by a concentration of sub-vertical dikes through which basalts were extruded at the surface. The bulk of the island mass is composed of dike-free basalts formed by sub-aerial lava flows which make up a gently-dipping stratified aquifer fabric extending from land surface to considerable depth. These layers rest upon a base of submarine extruded pillow basalts, which, because of subsidence of the island, are now at a depth of over 2 km below sea level (Andrews and Bainbridge, 1972). Although some interfingering of Waianae and Koolau basalts is thought to have occurred, the bulk of Koolau basalts rest upon the weathered flank of the older Waianae volcano. While the eastern side of the Koolau volcano and both sides of the Waianae volcano are severely eroded, the Koolau basalt flows in the central saddle of the island have not been eroded extensively. Much of the coastal portions of the island are covered by a sedimentary wedge (referred to as 'caprock') composed of layers of marine and terrestrial sediments and clays as well as coral reef and organic debris. The largest caprock extends 30 km to 40 km south of Oahu (FIGURE 3).

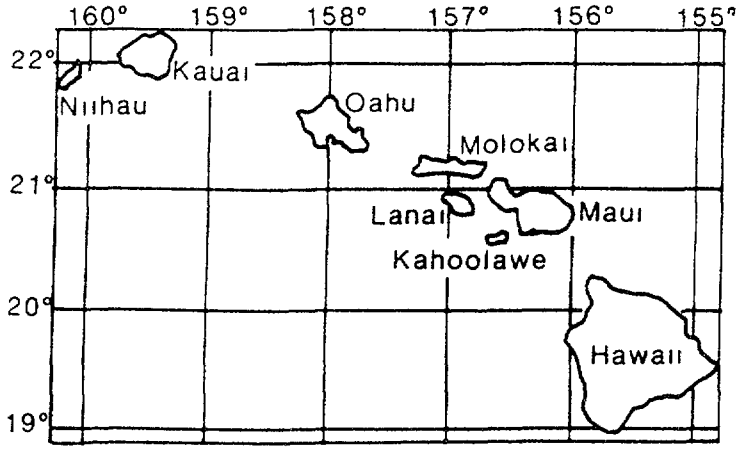

Figure 1 - Map showing location and relative positions of Hawaiian islands (after Hunt and others, 1988).

The layered basalts are highly transmissive to ground water with hydraulic conductivity typically on the order of 500 m/d. They are also highly vesicular and porous (up to 50%) but connected porosity through which significant water flow can occur is less than 10%. The largest lava flows can be tens of kilometers long, up to 1 km wide and up to 10 m thick. Current examples of such flows may be found on the volcanically-active island of Hawaii (e.g. see Lockwood and Lipman, 1987, and Holcomb, 1987). The well-connected highly conductive zones occur in rubbly material between overlapping lava flows, while the body of the lava flows themselves are relatively impermeable. The stack of tabular units may be 100 to 1000 times less conductive vertically than horizontally and the caprock is 1000 to 10000 times less conductive than the layered basalts (Souza and Voss, 1987).

A number of geologic barriers control the regional flow of ground water on Oahu (FIGURE 2). The rift zones contain swarms of intersecting vertical dikes cutting across layered basalts which have low permeability and which impound water in numerous compartments (Takasaki and Mink, 1985; Hunt and others, 1988). Sediment-filled valleys scoured into the layered basalts also act as barriers to flow through the layered basalts, as does the contact zone between Waianae and Koolau basalts, wherein the weathered surface of the Waianae basalts likely have lower conductivity than unweathered layered basalts. The caprock acts to impede ground-water discharge near the coast, raising hydraulic heads in the layered basalt aquifers. Except beneath the caprock, aquifers are unconfined. Two other barriers to flow are inferred from precipitous drops in groundwater levels (discussed in the following) below the central saddle of Oahu (Dale and Takasaki, 1976). To date, it has not been determined whether these barriers are dikes, weathered ridges of the Waianae volcano, or some other low-permeability structures.

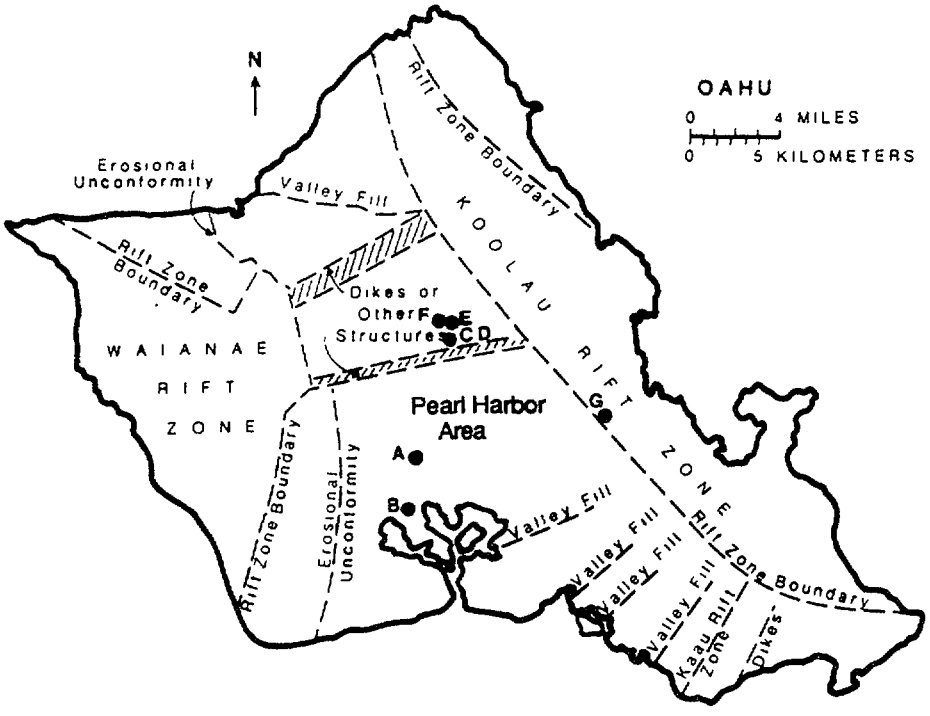

Figure 2 - Map showing hydrogeologic barriers on Oahu (after Hunt and others, 1988). Map also shows location of measurement points (A: Waipio monitor well, B: Waipahu monitor well, C,D,E,F: Soil-gas samples, G: Waihee high-level water and soil-gas samples.)

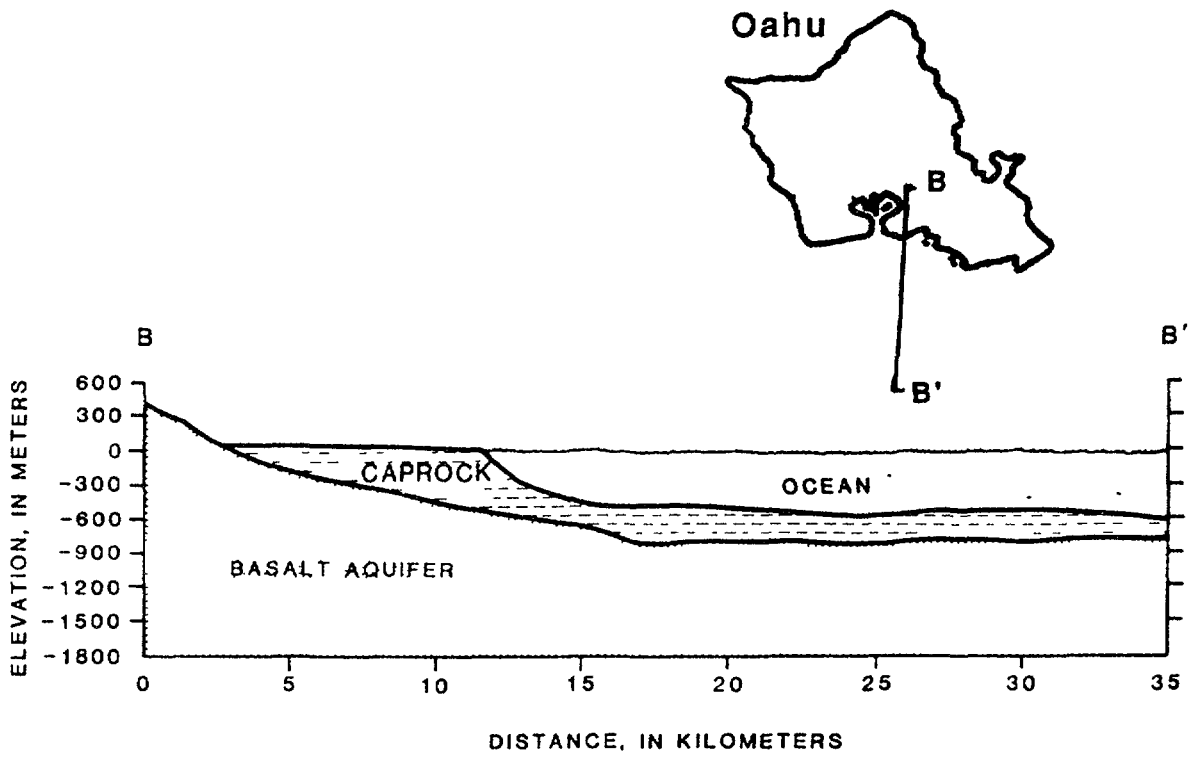

Figure 3 - Generalized geologic cross-section of southern Oahu showing offshore extent of caprock (modified from Gregory, 1980).

Ground-water recharge is concentrated in the high rainfall areas along the eroded volcanic ridges (FIGURE 4). In areas where rainfall is more than 1.3 m/yr, roughly half of the rainfall may recharge the aquifers (Dale and Takasaki, 1976). The high-recharge areas are thus coincident with the rift zones and central saddle area of Oahu. The resulting ground-water levels display sharp elevation changes at geologic barriers (FIGURE 5). In the Waianae rift zone the highest measured water level is 490 m, in the Koolau rift zone the highest level is 300 m, the central saddle area has a water level of 85 m, while between the coast and inland geologic barriers, water levels rarely exceed 10 m. Within compartments formed by barriers, water levels are nearly flat and each compartment is referred to as an 'isopiestic area'. Thus, various water bodies and barriers have been delineated on Oahu largely on the basis of water level (FIGURE 6).

The geohydrologic relations of compartmentalized and basal water bodies are shown in cross-section in FIGURE 7. The coastal water bodies with low-elevation water tables are called 'basal-water bodies'. A basal-water body is a freshwater lens that freely floats on intruded seawater (FIGURE 8), with an intervening zone of transition containing a mixture of freshwater and saltwater. The Honolulu water bodies are separated from each other and from the Pearl Harbor body, the largest continuous water body on Oahu, by valley-fill barriers resulting in partial compartmentalization (FIGURE 2, FIGURE 5, FIGURE 6). The compartmentalized waters are the Koolau and Waianae dike-impounded water bodies in the rift zones, and the Schofield high-level water body in the central saddle. Because of the high water elevation in the rift zones and Schofield water body, saltwater would be expected only at depths of several kilometers (Dale and Takasaki, 1976); and thus, these compartments must contain freshwater to the aquifer bottom. This study focusses on relations in the Pearl Harbor basal-water body.

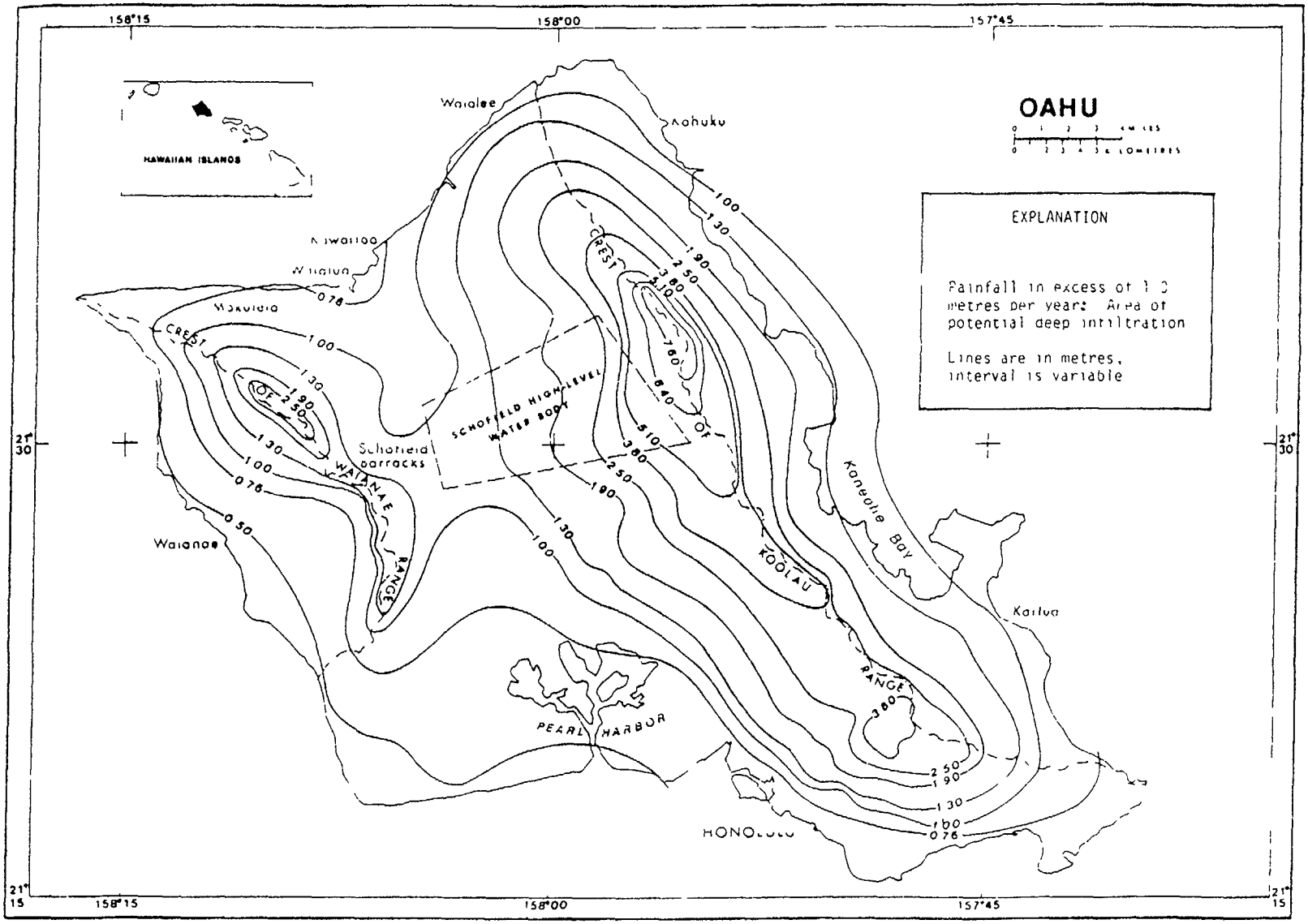

RAINFALL MAP FOR THE ISLAND OF OAHU, 1931-60

Figure 4 - Rainfall map for Oahu (after Dale and Takasaki, 1976).

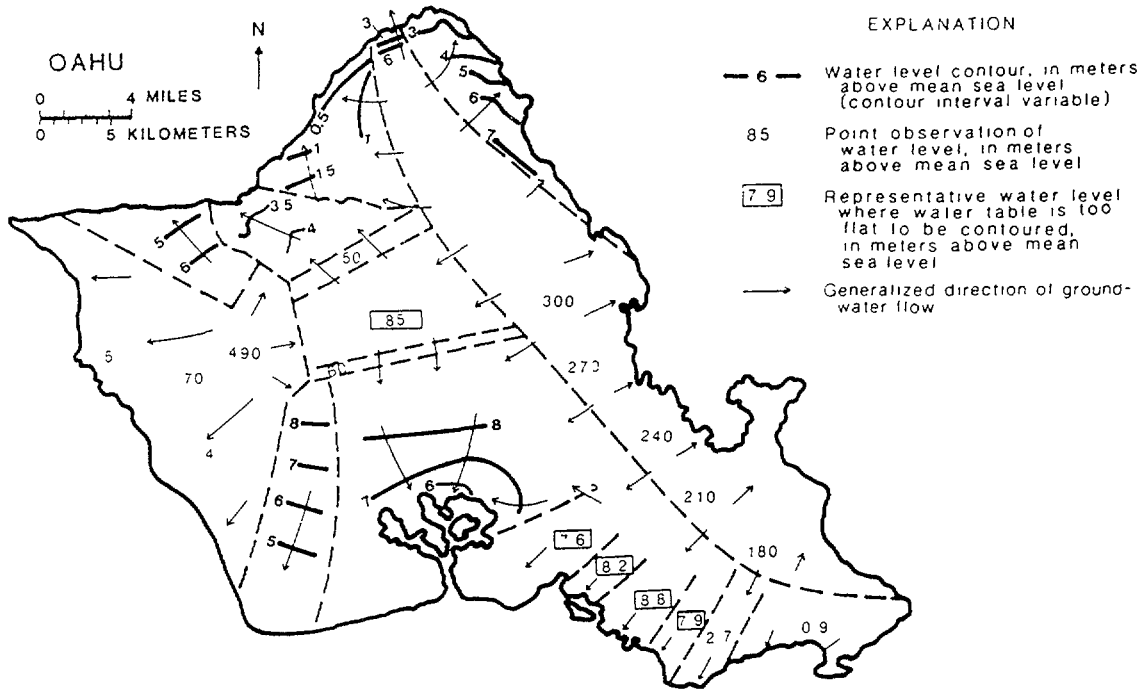

Figure 5 - Water levels in principal Oahu aquifers and inferred freshwater flow directions (after Hunt and others, 1988).

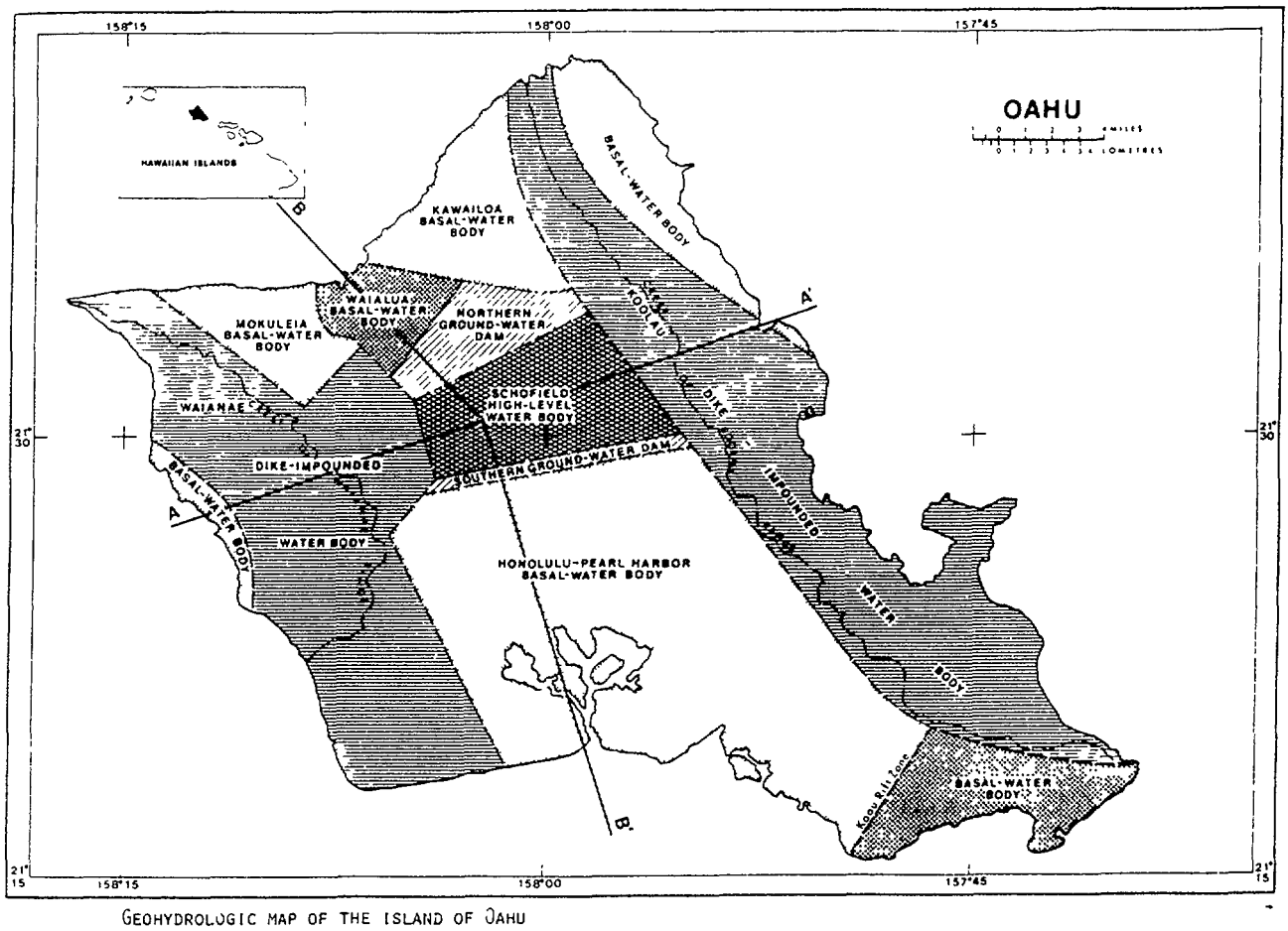

GEOHYDROLOGIC MAP OF THE ISLAND OF OAHU

Figure 6 - Major water bodies on Oahu defined from water levels (after Dale and Takasaki, 1976).

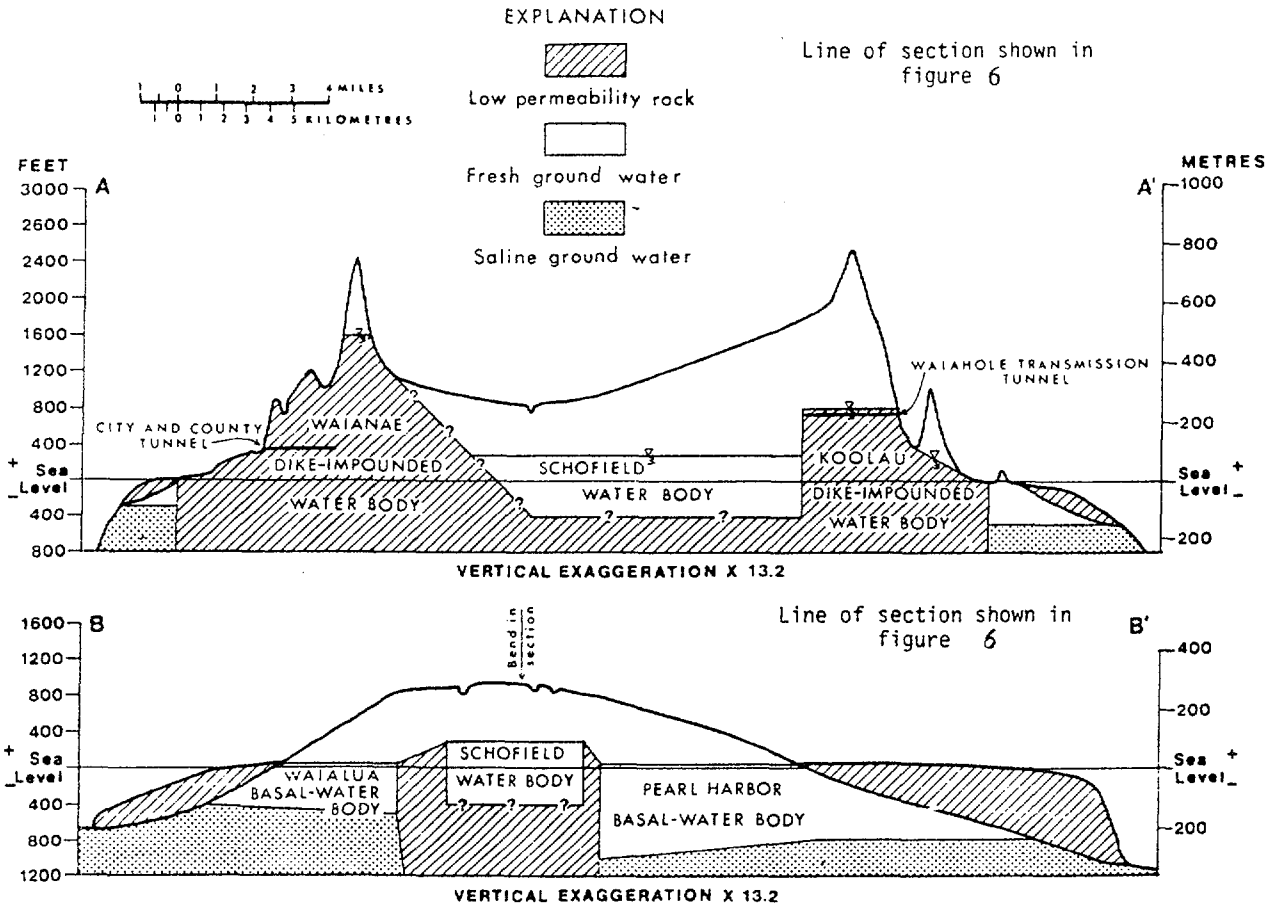

Figure 7 - Schematic cross-sections of ground-water bodies on Oahu (after Dale and Takasaki, 1976; see Figure 6 for locations of sections).

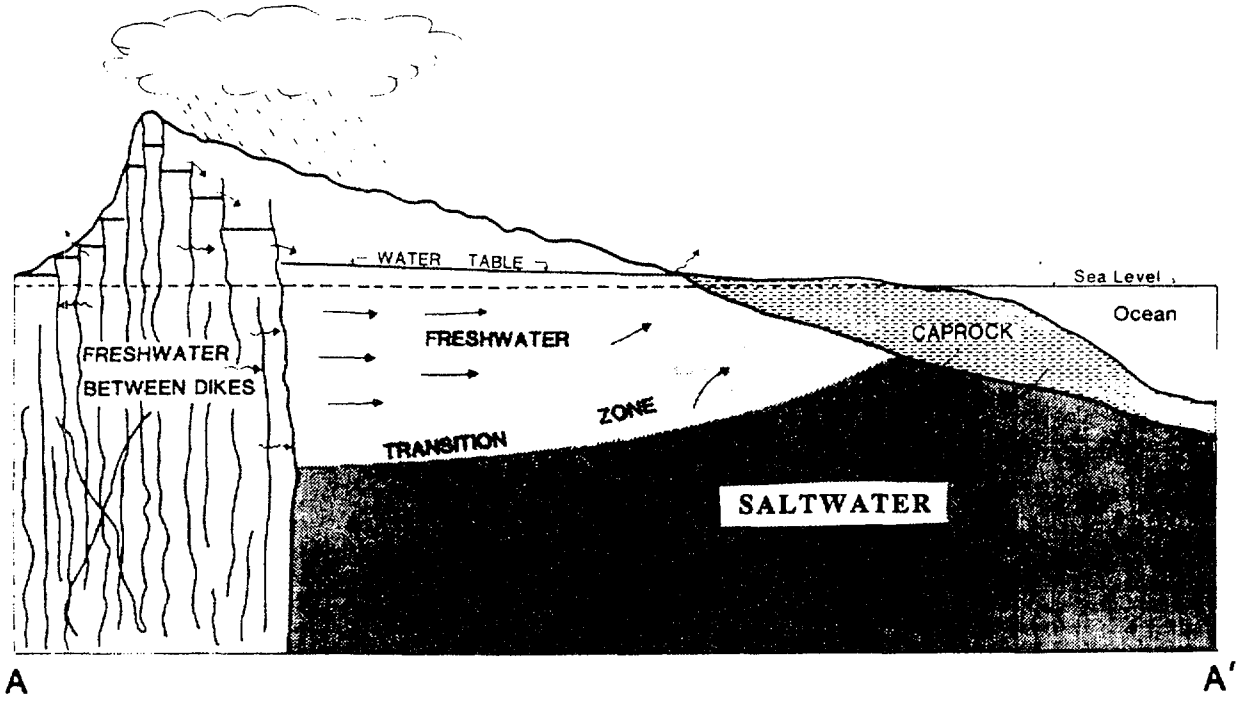

Figure 8 - Typical cross-section of basal and dike-impounded water bodies showing occurrence and movement of ground water (modified from Souza and Voss, 1987).

Natural recharge to the Pearl Harbor area aquifer occurs mainly in the upper-elevation areas as a result of direct infiltration, discharge from the Schofield high-level water body, and discharge from the Koolau dike-impounded water body (FIGURE 5). Total recharge to the Pearl Harbor area is about 9 x 10^5 m^3/d (240 Mgal/d) (Mink, 1980). Natural discharge occurs along a line of springs at the inland boundary of the caprock near Pearl Harbor, and likely as diffuse leakage through the caprock to Pearl Harbor. Saltwater discharge likely occurs diffusely through the caprock (FIGURE 8). Pumping from the aquifer began in the early 1880's for the purposes of sugar cane irrigation. Rates of withdrawal increased continuously from the early 1900's to 1980 with resultant reductions in head and upward and landward movement of the transition zone between freshwater and saltwater. Most wells for public and irrigation supply are located in a band near the coast (FIGURE 9). Some wells were abandoned as a result of increasing salinity. Pre-development heads in the Pearl Harbor aquifer measured about 10 m near the spring discharge area, and are estimated to have been over 12 m near the upstream boundary. The pre-development freshwater lens in the Pearl

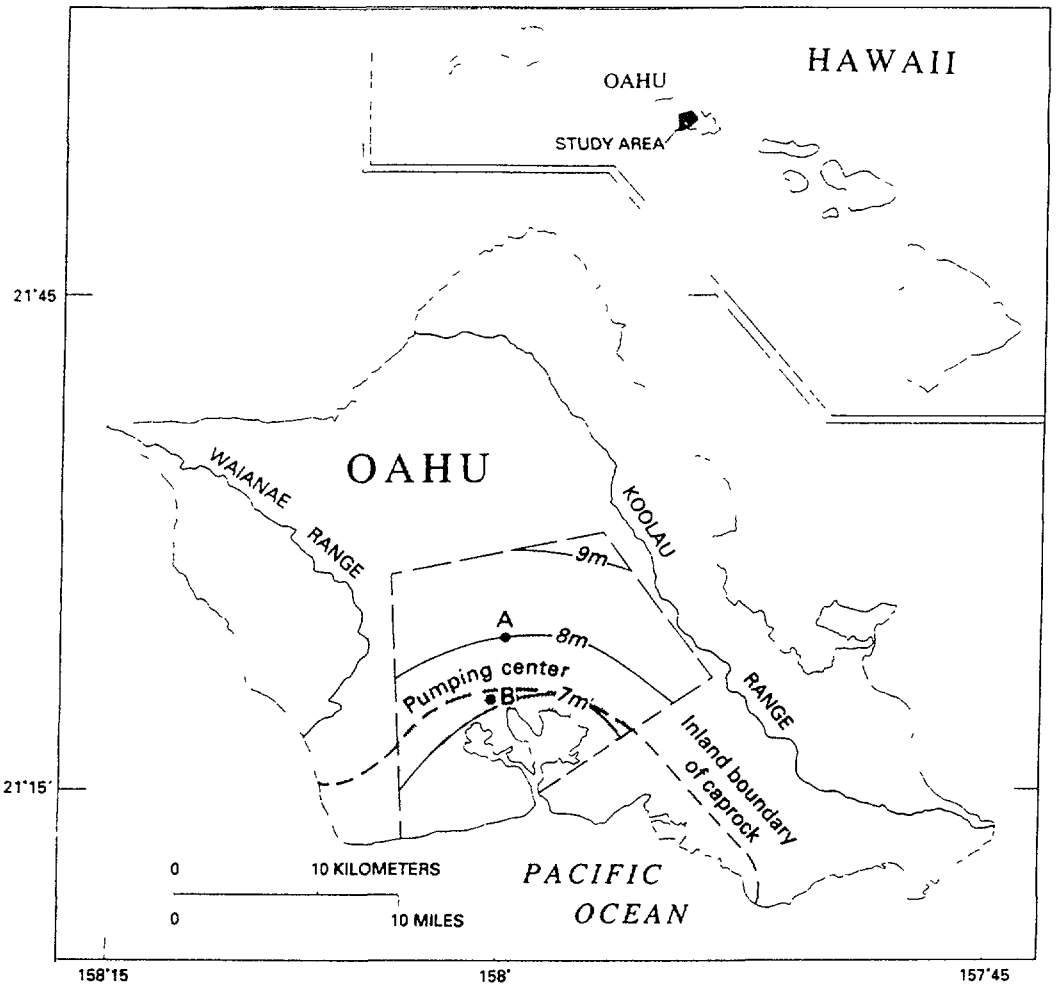

Figure 9 - Map showing Pearl Harbor area aquifer with hydrogeologic boundaries, hydraulic heads from 1958 (after Mink, 1980), location of monitor wells (A: Waipio, B: Waipahu), and location of coastal band of pumping (modified from Souza and Voss, 1987).

Harbor area was thus 400 m to 500 m thick (Mink, 1980) assuming conditions of static equilibrium with seawater. In 1990, freshwater heads in the aquifer ranged from about 5 m to 7 m above sea level, and measured salinity profiles showed the freshwater lens to be only 200 m to 300 m thick (Voss and Souza, 1993).

3. SAMPLE COLLECTION

Vertical profiles of solute and isotopic chemistry in the aquifer located within Koolau basalts were obtained for two observation wells 4.5 km apart located approximately along a regional flow line (Well A and Well B, FIGURE 2, FIGURE 9). The well bottom at Waipio (21◦ 26' 16" N, 157 59' 41" W) is 370 m below sea level. The well bottom at Waipahu (21 23' 40" N, 158 01' 20" W) is 296 m below sea level.

Samples were collected from open uncased holes. The well water is representative of the aquifer water at each sample depth because there is little commingling of water from over or underlying zones at any sample point in the well. This condition is clearly satisfied in the large scale view as shown by temperature in FIGURE 10 (Voss, unpublished data extracted from continuous log) and chloride in FIGURE 11 (this study) which change in a regular manner. Vertical flow measurements in the wells (Voss, unpublished data) show that water enters and leaves the boreholes through conductive zones approximately every 20 m. This may be seen in FIGURE 10, where temperature changes abruptly at a number of points, located where outflow occurs from the well bore. Points of inflow are located along smooth sections of the profile, between the sharp shifts. Thus, there is a local disturbance by vertical borehole flow on the order of about ±20 m. On the scale of the entire profile, however, the resulting data adequately describes the vertical distribution of fluid composition.

Samples were collected sequentially from the top down in the uncased wells by a 4.5-liter down-hole motorized sampler attached to the cable of a borehole logging system. The sampler had a valve at the top that could be opened and closed from the surface. Samples were collected every 50 m in 1990 and every 25 m in 1992. The chamber of the sampler was filled with nitrogen gas prior to each descent in the hole.

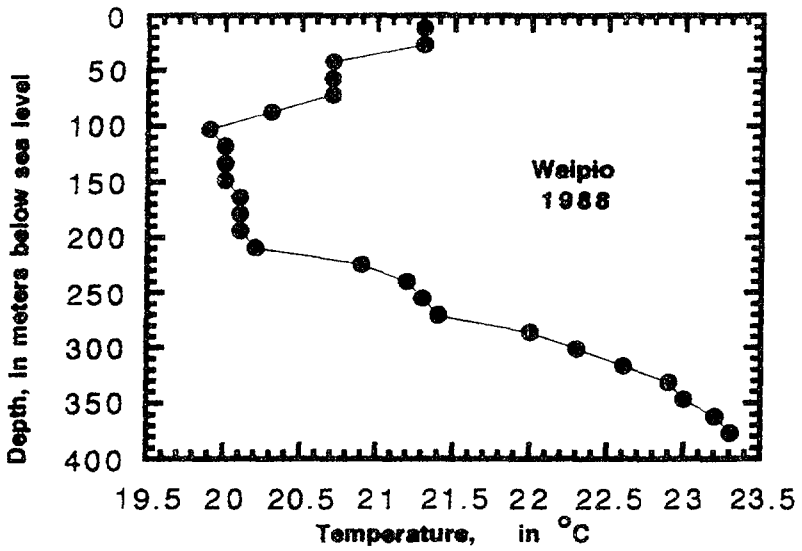

Figure 10 - Depth profile of fluid temperature, Waipio monitor well, 1988.

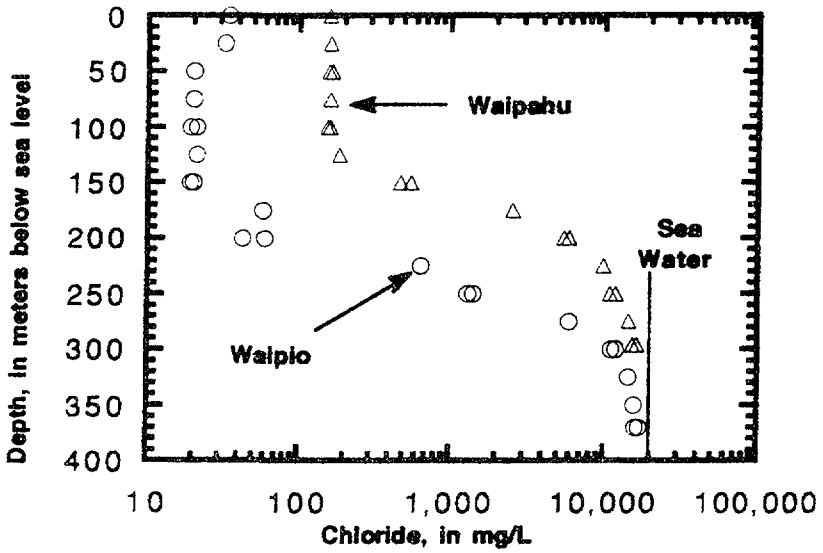

Figure 11 - Depth profiles of chloride concentration in ground water, Waipio and Waipahu monitor wells, based on two rounds of sample collection, 1990 and 1992, also showing seawater chloride concentration.

Motion in the hole was less than 7 m/min, and less than 2 m/min in the vicinity of the sampling depth. After lowering the closed nitrogen-filled sampler to the desired depth, it was opened for ten minutes and occasionally shaken or closed and re-opened to release trapped bubbles from the sampler chamber. The water-filled chamber was then closed and brought to the surface. The top sampler valve was then opened and the water was drained downwards by a pump through a manual valve and fitting at the sampler bottom to a nitrogen-filled 3.9 liter glass container fitted with a two hole rubber stopper for carbon isotope analysis. The inlet side of the rubber stopper was connected to a 20 cm length of 1 cm diameter polyvinyl chloride tubing that connected to the motorized sampler (pump) and was closed by a pinch clamp. The discharge end of the inlet tube was placed at the bottom of the sample bottle to allow gentle filling and thus minimizing potential degassing. The outlet hole of the rubber stopper was fitted with a 20 cm x 1 cm glass tube filled with granular CO_2-sorbing material (Askerite) and connected to 2 cm of polyvinyl chloride tubing and a pinch clamp at the end. This arrangement was designed to prevent any atmospheric CO_2 from entering the sample bottle during the filling process. The inlet was connected to the sampler, the inlet and outlet pinch clamps were removed and the sample bottles were completely filled. The stopper assembly was removed and the bottle quickly capped with a conical-shaped "poly-seal" cap. Additionally, the following samples were collected: a one-liter sample in a plastic bottle for tritium, two 250 ml (milliliter) filtered samples (.45 micron) in plastic bottles for standard inorganic chemical analysis (one sample was acidified), and a 60 ml sample in a glass bottle for deuterium and oxygen-18. The caps were taped, then bottles were wrapped with bubble wrap, stored in ice chests and shipped overnight express to our home office in Reston, Virginia. Specific conductance, temperature, pH and alkalinity determinations were made at the time of collection on the remaining 100 ml of sample. In 1992, samples for organic carbon analyses were removed from the glass bottles.

Carbonate for carbon-14 analyses was precipitated under a nitrogen atmosphere as $SrCO_3$. The precipitating solution of $Sr(OH)_2$ was prepared by dissolving 2.2 kilograms of $SrCl_2$ in 5 liters of NH_4OH. After overnight settling, any precipitate was removed by filtration in a nitrogen glove box using 0.45 micrometer filter. One hundred ml of the clear stock solution was added to 3 liters of the sample. After overnight settling, the solution was filtered through a 0.45 micrometer filter designed for high pH solutions, washed with one liter of carbonate-free deionized water, dried, placed into plastic Petri dishes and shipped overnight express to the laboratory for ^{13}C and carbon-14 determination. Methods of inorganic analyses are those given in Skougstad and others (1989).

4. GEOCHEMISTRY

Based upon the solute and isotopic analyses of the collected samples (TABLE 1), the vertical profiles of the aquifer can be divided into three zones: an uppermost zone of irrigation-return water, a middle zone of pristine freshwater, and a lower mixing zone grading from freshwater to seawater. The relative position and thickness of each zone can be inferred at Waipio (FIGURE 10) in which the ground water temperature profile illustrates the presence of warmer irrigation return water (0 to 100 m below sea level) on top of the freshwater (100 to 200 m). The top of the saltwater mixing zone occurs at approximately 200 m and extends to the bottom of the well. This analysis is consistent with the chloride concentration in Waipio (FIGURE 11).

The higher concentrations of chloride, nitrate, dissolved solids, alkalinity, isotopically-heavier deuterium and oxygen-18, and some tritium activity in the water above 100 m at Waipio (TABLE 1) are consistent with the presence of return irrigation water. Local ground water is pumped for irrigation and reapplied to the ground surface. When freshwater is withdrawn for irrigation, evaporation increases the concentration of solutes and dissolves fertilizers and any soil conditioners applied to the fields and the water is warmed. Thus, irrigation-return water has a distinct isotopic signature from interaction with the atmosphere and biosphere making the 2H, ^{18}O and $\delta^{13}C$ isotopically heavier and increasing tritium and carbon-14 activity. At Waipahu, the irrigation return water has completely masked the pristine water zone and return irrigation water merges directly with the saltwater mixing zone.

The solutes in the transition zone between freshwater and seawater result largely from a simple conservative mixing of seawater and water from the freshwater lens. This is clearly indicated in FIGURE 12 which illustrates the strong correlation between chloride and $\delta^{18}O$ (VSMOW). The scatter in the upper portion of this diagram is the result of return-irrigation water which has experienced some evaporation.

In addition to simple mixing, ion exchange occurs in the saltwater moving beneath the island (Mink, 1961; Visher and Mink, 1964), altering solute ratios somewhat from that expected according to simple mixing. FIGURE 13, based on data from Waipahu, illustrates that sodium, and to a lesser degree, potassium, in seawater has exchanged with calcium and magnesium from the caprock resulting in an increase in calcium and magnesium and a decrease of sodium and potassium in solution. The data in FIGURE 13 are plotted relative to the zero line generated by conservative mixing of the freshwater and seawater end members.

To carry out age-interpretation of carbon-14 data, it is necessary that potential sources of dissolved carbon be considered. In the freshwater, possible dissolved carbon sources to the Pearl Harbor area aquifer are: plant respiration (soil gas), dissolved organic carbon from decaying vegetation, and calcite dissolution. Solutes

TABLE 1

Sample ID	Depth	Date	Ca	Mg	Na	K	Sr	Li	Alk as	Cl	SO4	Br	NO3	H4SiO4	pH
	m BSL	m/d/y							CaCO3						
PIO-410	0	5/27/92	9.9	8.9	29	1.9	0.07	0.01	58	34	8 1	0 18	6.2	105	7.36
PIO-495	25	5/27/92	9 6	8.9	29	1.9	0.07	0.01	59	32	7.6	0.16	3.5	105	7.37
PIO-577	50	4/17/90	7.8	6.7	18	1.3	0.02		59	20	4.7	0 10	4.3	90	7.92
PIO-577	50	5/27/92	7.2	6.8	19	1.5	0.04	0.01	45	20	5.0	0.12	2.4	95	7.56
PIO-659	75	5/27/92	7.0	6.6	19	1.6	0.04	0.01	45	20	5.0	0.10	3.2	95	7.51
PIO-741	100	4/17/90	7.0	6.2	16	1.2	0		50	19	4.1	0.09	3.0	88	7.53
PIO-741	100	5/28/92	5.2	4.9	17	1.5	0.03	0.01	32	21	3.3	0.08	<0.01	70	7.85
PIO-823	125	5/28/92	5.3	4.8	17	1.5	0.04	0.01	33	21	3.3	0.09	<0.01	70	7.97
PIO-905	150	4/17/90	6.0	5.1	16	1.2	0		43	19	2.9	0.07	0.27	74	7.85
PIO-905	150	5/28/92	5.1	4.7	17	1.5	0.03	0.01	33	20	3.2	0.10	<0.01	70	7.91
PIO-987	175	5/28/92	7.9	7.3	35	2.4	0.70	0.02	32	58	8.0	0.27	<0.01	65	7.89
PIO-1069	200	4/17/90	7.0	6.1	26	1.9	0		37	43	5.4	0.15	<0.01	66	8.15
PIO-1069	200	5/28/92	8.4	7.2	36	2.4	0.70	0.02	33	60	8.0	0.27	<0.01	60	7.80
PIO-1151	225	5/28/92	42	49	335	15	0.50	0.14	34	650	88	3.3	<0.01	55	7.99
PIO-1233	250	4/17/90	97	112	640	18	0.70		42	1310	176	4.7	<0.01	61	7.88
PIO-1233	250	5/28/92	95	115	670	23	1.1	0.31	40	1420	200	6.9	<0.01	60	7.86
PIO-1315	275	5/28/92	465	580	2530	110	5.0	1.7	53	5930	790	28	<0.01	60	7.59
PIO-1397	300	4/17/90	560	900	5530	140	6.0		81	11100	1290	38	<0.01	70	7.45
PIO-1397	300	5/29/92	600	885	5700	195	9.0	2.2	74	11840	1630	54	<0.01	65	7.61
PIO-1479	325	5/29/92	610	1065	7410	220	9.0	2.5	80	14380	2000	62	<0.01	65	7.52
PIO-1561	350	5/29/92	675	1160	8100	240	10	2.4	87	15800	2010	64	<0.01	65	7.33
PIO-1627	370	4/17/90	720	1200	8100	211	7.2		97	16000	1820	54	<0.01	45	7.50
PIO-1627	370	5/29/92	670	1190	8710	260	10	2.5	94	16850	2150	70	<0.01	65	7.39
AHU-28	0	5/30/92	19	17	75	3.9	0.15	0.090	52	158	22	0.82	<0.1	14	8.22
AHU-110	25	5/30/92	24	21	67	3.3	0.16	0.090	49	160	22	0.80	0.22	85	7.62
AHU-192	50	4/19/90	26	21	65	3.1	0.1		52	157	21	0.80	1.3	78	7.54
AHU-192	50	5/30/92	24	21	68	3.5	0.16	0.094	48	165	22	0.69	3.5	85	7.48
AHU-274	75	5/30/92	25	22	68	3.3	0.16	0.097	47	160	21	0.70	1.28	85	7.50
AHU-356	100	4/19/90	26	21	64	3.1	0.1		47	153	20	0.80	5.1	77	7 56
AHU-356	100	5/30/92	24	21	68	3.3	0.16	0.097	48	160	21	0.68	2.47	85	7.53
AHU-438	125	5/30/92	27	23	73	3.5	0.20	0.109	45	185	24	0.83	2.14	85	7.51
AHU-520	150	4/19/90	64	54	180	8.8	0.4		28	476	58		<0.01	67	7.54
AHU-520	150	5/30/92	74	67	195	8.9	0.50	0.241	29	560	75	2.4	<0.01	70	7.56
AHU-602	175	5/31/92	315	345	815	30	3.5	1.1	34	2550	350	11	<0.01	75	7 36
AHU-648	200	4/19/90	560	650	2100	60	4.9		47	5490	650		<0 01	67	7 35
AHU-648	200	5/31/92	580	720	2410	79	6.0	2.3	50	5920	980	32	<0.01	70	7 36
AHU-766	225	5/31/92	640	875	4280	112	8.0	2.4	61	9840	1365	43	<0.01	70	7.31
AHU-848	250	4/19/90	670	910	5300	135	6.0		68	10900	1500		<0.01	34	7.32
AHU-848	250	5/31/92	665	960	5700	150	9.0	2.8	67	11870	1600	56	<0 01	70	7.31
AHU-930	275	5/31/92	765	1160	6850	185	11	3.0	79	14450	1960	62	<0.01	75	7.26
AHU-1000	296	4/19/90	980	1300	7700	150	8.0		85	15310	2200		<0 01	70	7.35
AHU-1000	296	5/31/92	1000	1340	7770	200	14	3.9	85	16340	2200	71	<0.01	75	7.22
		SOIL GAS							PACIFIC OCEAN 21°24'20"N 158°18'40"W						
Sample ID	13C	Date	Lat.		Long.				Depth	13C	14C	2H	18O		
PIO-1 C	-20.4	6/1/92	21°30'00"	N	157°58'12"	W					pmC				
PIO-2 D	-20.4	6/1/92	21°30'00"	N	157°58'12"	W			250m	-7.1	103.0 ± 0.6	3.9	0.09		
PIO-3 E	-21.4	6/1/92	21°30'40"	N	157°57'30"	W			500m	-10.1	92.8 ± 0.5	1.1	-0.12		
PIO-4 F	-13.9	6/1/92	21°30'45"	N	157°58'08"	W			1000m	-5 5	83.5 ± 0.6	1 4	-0.15		
HEE-5 G	-26.7	6/2/92	21°26'42"	N	157°52'08"	W			1500m	-7.6	88.3 ± 0.5	0.9	-0.04		

TABLE 1 (continued)

Sample ID	Depth	Dissolved	DO	TOC	Temp.	Density	del 2H	del 18O	del 13C	Tritium	14C
	m BSL	solids			°C	at 20°C				TU	pmC
PIO-410	0	186	7 5	1 2	21.3	0 9981	-10.5	-2 90		0.39 ± 0 11	
PIO-495	25	181	2.0		21.0	0 9981	-14.0	-3.15		0.36 ± 0.11	
PIO-577	50	144			20.7		-13.5	-3.15	-18.9	0.03 ± 0 17	112.7± 2.7
PIO-577	50	137	5.0	2.2	20.7	0.9982	-10.5	-3.05		0.08 ± 0.14	
PIO-659	75	137	3.2	1.8	20.7	0.9981	-9.0	-3.00		0.37 ± 0.13	
PIO-741	100	130			19.9	0.9979	-15.0	-3.20	-19.3	0.21 ± 0 17	98.4 ± 2.3
PIO-741	100	107	3.0	14	19.9	0.9981	-8.5	-3.00	-16.4	0.04 ± 0.13	73.4 ±.58
PIO-823	125	108	2.8	3.6	20.0	0.9981	-10.5	-2.75	-21.8	0.13 ± 0.13	80 ± .61
PIO-905	150	113			20.0	0.9980	-10.0	-3.30	-21 2	0.27 ± 0.17	96.4 ± 2.3
PIO-905	150	106	2.8	2.5	20.0	0.9981	-9.5	-2.80	-21.1		82.7 ± .63
PIO-987	175	171	3.4	9.2	20.1	0.9981	-9.0	-2.95	-22.0		79 ± .59
PIO-1069	200	144			20.1	0.9988	-10.0	-3.10	-20.8	0.12 ± 0.11	84.9 ± 2.3
PIO-1069	200	173	2.6	5.7	20.1	0.9982	-9.5	-2.90	-22.0		79.2 ± 1.29
PIO-1151	225	1231	3.1	5.4	20.9	0.9986	-7.0	-2.60	-19.7		75.6 ± .59
PIO-1233	250	2414			21.2		-9.0	-2.95	-19.3	0.11 ± 0.13	76.6 ± 1.8
PIO-1233	250	2585	2.4		21.2	0.9996	-6.5	-2.60	-20.9		70 ± .84
PIO-1315	275	10501	2.2		21.8	1.0057	-5.0	-2.00	-17.2		53.4 ± .56
PIO-1397	300	19648			22.3	1.0129	-3.5	-1.10	-9.5	0.11 ± .13	58.3 ± 1.5
PIO-1397	300	20992	1.0		22.3	1.0132	0.5	-0.65	-12.5		68.1 ± .50
PIO-1479	325	25839	1.0		22.7	1.0165	0.0	-0.60	-11.4		40.7 ± .59
PIO-1561	350	28146	1.2		23.1	1.0188	3.0	-0.10	-9.6		41.2 ± .38
PIO-1627	370	28193			23.2	1.0189	1.5	-0.35	-7.3	0.14 ± 0.16	26.0 ± 1.0
PIO-1627	370	30001	0.6		23.2	1.0201	1.5	-0.05	-11.9		64.4 ± .60
AHU-28	0	334	1.0	1.2	24.8	0.9981	-6.0	-2.35		0.72 ± 0.11	
AHU-110	25	370	2.2	0.54	22.5	0.9981	-10.5	-2.90		0.32 ± 0.10	
AHU-192	50	365				0.9985	-11.0	-3.25	-16.7	0.19 ± 0.17	109.4 ± 3.8
AHU-192	50	379	2.3	0.85	23.1	0.9980	-10.5	-2.65			
AHU-274	75	372	2.2	0.54	22.5	0.9981	-11.0	-3.00		0.22 ± 0.10	
AHU-356	100	360				0.9985	-13.0	-3.30	-16.7	0.22 ± 0.16	99.2 ± 4.1
AHU-356	100	372	2.3	0.47	23.0	0.9981	-10.0	-2.90		0.42 ± 0.11	
AHU-438	125	408	2.5	0.46	23 5	0.9983	-10 5	-2.80		0.30 ± 0.12	
AHU-520	150	891				0.9980	-9.5	-3.15	-22.2	0.05 ± 0.17	94.4 ± 2.1
AHU-520	150	1035	2.3	0.44	23.0	0.9986	-9.5	-2.85	-19.4		88.3 ± 1.35
AHU-602	175	4478	2.1		23.2	1.0015	-7.5	-2.45	-22.0		75.1 ± .68
AHU-648	200	9577				1.0052	-7.0	-2.30	-17.2	0.04 ± 0.13	60.5 ± 1 5
AHU-648	200	10794	1.7		23.0	1.0061	-2.5	-1.75	-17.3		58 ± .48
AHU-766	225	17237	1.4		23.5	1.0105	-1.5	-1.15	-14.0		62.05 ± .85
AHU-848	250	19479					-3.5	-1.30	-11.1	0.08 ± 0.15	38.9 ± 1.2
AHU-848	250	21088	1.0		24.5	1 0139	-0.5	-0.80	-12.3		40.0 ± .38
AHU-930	275	25531	1.0		24.0	1.0170	2.5	-0 30	-14 1		75.0 ± .63
AHU-1000	296	27734				1.0196	-2.0	-0.45	-12.3	0 03 ± 0.16	34.9 ± 1.0
AHU-1000	296	29027	1.0		24.0	1.0195	2.5	0.05	-12.8		59.6 ± .49

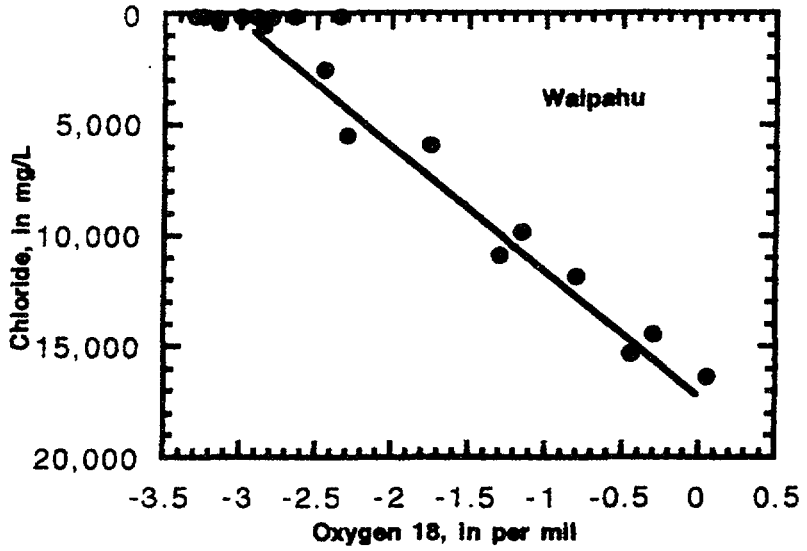

Figure 12 - Mixing diagram showing oxygen-18 and chloride for Waipahu monitor well; based on two rounds of sample collection, 1990 and 1992.

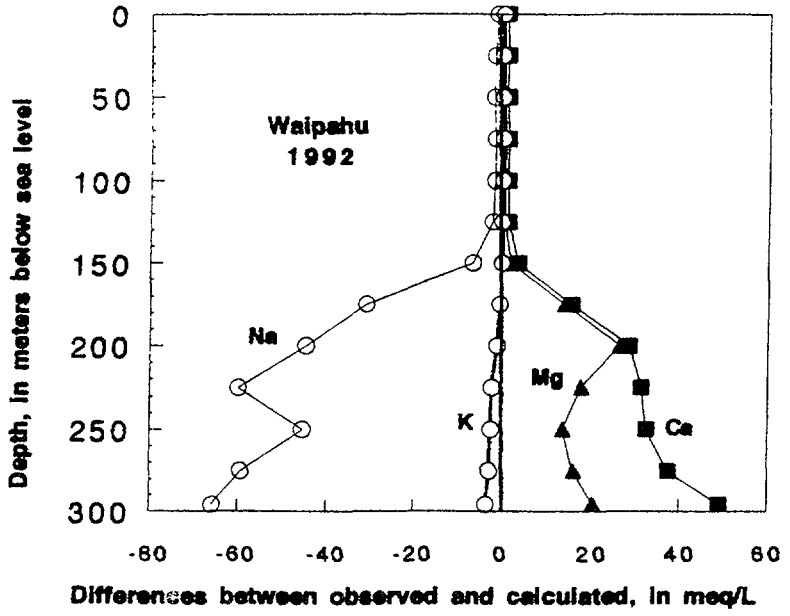

Figure 13 - Cation imbalance depth profile for samples collected at Waipahu monitor well in 1992.

in the freshwater zone are generated by carbonic acid weathering of the silicate minerals in the volcanic rock. The result is a dilute sodium-calcium-magnesium-bicarbonate type water and high silica with dissolved solids of approximately 110 mg/L (milligrams per liter) (PIO-741 to PIO-987, TABLE 1). The low concentration of calcium (~5 mg/L, TABLE 1) in the freshwater zone is consistent with weathering of plagioclase and pyroxene and not calcite, as described below. The $\delta^{13}C$ (PDB) of the freshwater

(-20 ‰) is in approximate equilibrium with the soil gas observed (-26 ‰) in the probable recharge zone, discussed below, suggesting the absence of calcite dissolution. However, there is indication of dissolved organic carbon (TABLE 1) which may add old carbon to the freshwater. Unfortunately, the $\delta^{13}C$ value does not allow discrimination of this source from plant-respiration-derived carbon.

Delineation of recharge area is an important consideration in the hydrology of aquifer systems. Because of the flat and high water levels it has been proposed that the Schofield dike free area is a large reservoir from which water enters the Pearl Harbor aquifer (Dale and Takasaki, 1976). However, it is not clear if most water is recharged within the Schofield area or to dike compartments in the adjacent Koolau Range which has a higher topographic position and higher rainfall. We attempted to gain some insight into the location of recharge area by sampling the soil gas for $\delta^{13}C$. The $\delta^{13}C$ of shallow (~0.5 m) soil gas in the Schofield area averages -19 ‰ on four samples (SOIL GAS: C,D,E,F, TABLE 1, see FIGURE 4 for locations). Rainfall in this area is approximately 2.5 m/y. A soil gas sample collected near the crest of the Koolau Range has a $\delta^{13}C$ of -26.7 (SOIL GAS HEE-5 G, TABLE 1, see FIGURE 4 for location). This sample is from an area that has approximately 4 m/y of rainfall. The pristine-water zone at Waipio has $\delta^{13}C$ values that average -20.6 (PIO-741 to PIO-1151, TABLE 1). Because of the approximately 6 ‰ isotopic fractionation in $\delta^{13}C$ between bicarbonate in ground water and soil gas, it is suggested that the water was recharged in an area in which soil gas $\delta^{13}C$ is approximately -26 ‰. This is consistent with water recharged in the Koolau Range rather than in the Schofield area. Clearly, there is need of further soil-gas reconnaissance in both areas to confirm this.

Additional support for the absence of calcite dissolution in the freshwater may be obtained through evaluation of solutes. It is indeed possible to explain all of the calcium (~5 mg/L) by the weathering of feldspars and pyroxens rather than by dissolution of calcite. If we assume that chloride and an equivalent amount of sodium enter the aquifer from rainfall, then approximately 0.18 meq/L (milliequivalents per liter) of sodium comes from weathering of plagioclase. If we conservatively assume a plagioclase composition of 0.5 Ca and 0.5 Na typical of tholeitic basalts (0.65 Ca and 0.35 Na may be more typical), then approximately 0.18 meq/L of Ca will be derived from weathering of plagioclase. As the total Ca is 0.25 meq/L, then it follows that 0.07 meq/L of Ca must come from another source. It is likely that most of the additional 0.07 meq/L Ca is derived from weathering of pyroxene known to be present in the rock. Thus, adjustment to the samples for the presence of dead carbon from calcite dissolution is unnecessary.

A further argument for the lack of calcite dissolution based on consideration of carbon mass balance in the system can also be made. Both the pristine and the return irrigation water indicate significant thermodynamic undersaturation with respect to calcite (determined with PHREEQE, Parkhurst and others, 1980) and calcite would dissolve if present (see FIGURE 15). Analyses of a fresh sample of basalt from the island of Hawaii indicate approximately 75 ppm (parts per million) of carbon present (USGS Rock Standard BHVO-1, from the June 1919 lava flow in Kilauea crater, Island of Hawaii, Flanagan and others, 1976) thus suggesting low initial concentration of calcite. If we assume that the ground-water hydrology of the Pearl Harbor aquifer has been active for approximately a million years at the present rate and composition, it can be readily shown that the small amount of calcite present originally (based on 75 ppm carbon) would have long since been dissolved. Thus, we conclude from the above discussion, that weathering of calcite is not a likely source of calcium or carbon in this system and no adjustment from this source is necessary for carbon-14 dating of the core of the freshwater lens.

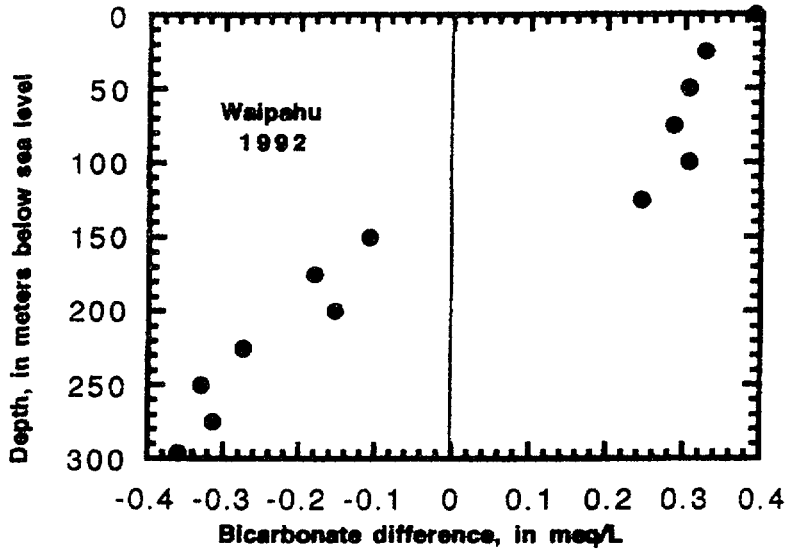

Figure 14 - Bicarbonate imbalance depth profile for samples collected at Waipahu monitor well in 1992.

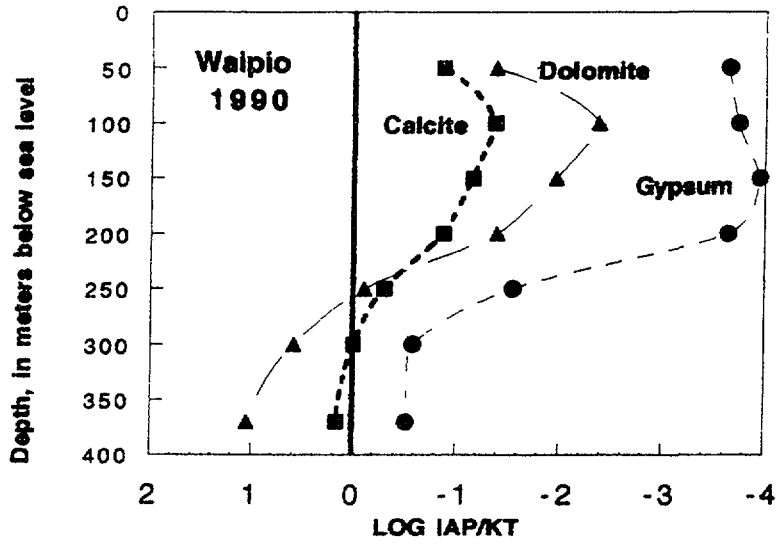

Figure 15 - Saturation index depth profiles for calcite dolomite and gypsum, for samples collected at Waipio monitor well in 1990. Saturation indices calculated using PHREEQE (Parkhurst and others, 1980).

In the saltwater, probable dissolved carbon sources to the Pearl Harbor area aquifer are: bicarbonate from calcite equilibrium in seawater, and organic carbon in sea-bottom sediments and within the caprock though which recharging seawater flows. In the saltwater, a small amount of calcite precipitation results from the ion exchange mentioned above. The addition of calcium to the solution from exchange caused precipitation of calcite, thereby removing calcium and an equivalent amount of bicarbonate from solution, as seen in FIGURE 14. The actual amount of calcite precipitated is small, as only a few milliequivalents per liter of bicarbonate are lost from

solution. The expectation of calcite precipitation is supported by thermodynamic calculation using the code PHRQPITZ (Plummer and others, 1988). FIGURE 15 shows that the log of the saturation indices for calcite is near zero, indicating equilibrium. The $\delta^{13}C$ of saltwater reaching both the Waipio and Waipahu wells is isotopically lighter (-6 ‰) than seawater. It is hypothesized that this results from dissolution of organic material in the caprock (with a $\delta^{13}C$ value of about -25 ‰) through which the seawater is believed to infiltrate.

5. CARBON-14 CHEMISTRY AND DATING

Ideally we would like to obtain different residence times in this hydrologic system: 1) time required from saltwater to move from the ocean to each of the wells, 2) time required for freshwater to move from the recharge area to each of the wells. These times would also provide: 3) time for freshwater and saltwater flow between the two wells which are approximately on the same flow path. Based on an initial hydrologic model of the system, our belief was that carbon-14 dating of the dissolved bicarbonate would be a suitable method by which to attempt dating for items 1 and 2 above. It was felt that difference in freshwater residence time between wells might be so low as to preclude obtaining a freshwater time for item 3 from carbon-14. Additionally, the lack of a clearly-defined pristine-water zone at the Waipahu well precludes any chemical or isotopic dating technique for freshwater travel time between the wells.

The $SrCO_3$ precipitate, described earlier, was analyzed for carbon isotopes. The samples collected in 1990 were analyzed using a specially designed miniature cell and long counting times (Mebus Geyh, NLB, Hannover, Germany, personal communication) and those collected in 1992 were analyzed using accelerator mass spectroscopy (AMS) methods at the University of Arizona. Accuracy of analyses are about ±2 pmC for samples dominated by freshwater and about ±1 pmC for samples dominated by seawater for both methods. $\delta^{13}C$ values were obtained from the same samples.

Unfortunately the 1992 AMS carbon isotope data (both $\delta^{13}C$ and pmC) show a large degree of scatter relative to the traditional counting method and depth. Our AMS control sample, an Ordovician age marble, was dissolved in acid under nitrogen atmosphere and precipitated at the same time with the same reagents as the other samples, gave the expected values of greater then 45,000-year age and $\delta^{13}C$ of +1.6 ‰. We would expect as smooth a change in carbon isotope values with depth as exists with chloride and other species concentrations. Moreover, all other species measured gave nearly identical results at the same depth and chloride concentration in 1990 as in 1992. (Note that we found a slight but consistent upwards shift of the transition zone of roughly five to ten meters between 1990 and 1992 in both wells based on most species, which may be indicative of a shrinkage of the freshwater lens.) At this time, we are unable to explain the carbon-isotope AMS data scatter as the samples were collected and treated in exactly the same way for both methods.

In the freshwater, we find no evidence of calcite dissolution based on $\delta^{13}C$ values and thus carbon-14 values do not require adjustments for apparent age determination. We must keep in mind, however, that there may be a component of old organic carbon causing an increase in apparent age in the freshwater that we cannot quantify using $\delta^{13}C$ values.

Saltwater carbon-14 content is not altered significantly by the calcite precipitation resulting from ion exchange because of the small amount of calcite precipitated and the relatively small fractionation factor (2 ‰). Thus, no carbon-14 correction for

apparent age determination is necessary for calcite precipitation and there can be no dissolution of the caprock to add dead carbon to the system. However, assuming that the organic carbon added during seawater recharge is dead and seawater has a $\delta^{13}C$ of 0 ‰, the pmC values for carbon-14 in the saltwater must be increased by a factor of 1.24 based on extrapolation of observed $\delta^{13}C$. It is assumed that the small amount of calcite precipitation occurs after the addition of organic carbon and does not significantly affect the isotopic ratios.

6. AGE RELATIONS

The objective here is to date the three water types and to determine travel times of these waters between the points where the two profiles were collected. As is common in hydrologic systems, each sample is a mixture of water types (or 'end members'), in this case, up to three types. To date each water type occurring in a mixture, it would be necessary to theoretically unmix the sample, a calculation that would require knowledge of a number of unknown quantities. To avoid this dilemma, an assumption can be made that every sample collected is a simple mixture of distinct water types, or end members, and that samples collected along each observation well differ only by the relative amounts of each water type in the mixture. In the Pearl Harbor area, a different set of end members may be defined for each of the two profiles. This may be motivated as follows.

Of the three water types, only irrigation-return water contains finite (but small) amounts of tritium. Simultaneously, this water has high carbon-14 levels (up to 110 pmC). Thus, the water contains post-bomb carbon and tritium, and must be less than 50 years old. The low tritium content in this young water may be due to the use of already-old ground water as irrigation water (Hufen and others, 1972) which is imprinted by modern carbon during percolation through the soil zone.

The second water type, the core of the freshwater lens, contains no tritium. This implies that the water must be greater than 50 years old. However a hydrologic calculation based on accepted values of recharge and pumping records implies that water must travel through the entire lens in only a few tens of years. Rough calculation with recharge of 10^6 m^3/d, aquifer width of 26 km, lens thickness of 300 m, and porosity of 10%, gives a freshwater velocity of 1.3 m/d, where: velocity = recharge / (porosity x width x thickness). The resulting travel time through a 10 km long aquifer is only about 20 years and some tritium activity would be expected in this water. This hydrologically-determined residence time in the freshwater lens conforms with the brief residence time of the irrigation-return water determined geochemically. A similar velocity of irrigation-return water and lens water would indeed be expected because the hydraulic gradient affecting both is the same. This apparent contradiction between isotope dating (age of more than 50 years) and hydrology (residence time less than 20 years) is resolved when the significant storage of ground water in high-level dike compartments is recognized. Ground-water flow through a large compartment could take hundreds or thousands of years, resulting in a large component of old water recharging the freshwater lens. Moreover, acceptance of a brief residence time of freshwater implies that the carbon-14 content of freshwater is practically constant throughout the lens.

Inspection of carbon-14 values for deep samples predominantly composed of seawater (20 to 30 pmC), indicates residence times up to about two half-lives, or 10^4 years. Thus, the saltwater ages as it moves inland, and for the purposes of a simple mixing model is assumed to move inland in a uniform manner, with depth-independent age.

For the simple mixing model applied to carbon-14 content, there is only one end member for irrigation water and for freshwater for both profiles. For saltwater, a different end member must be allowed for each profile, as a significant travel time between the points would result in a different carbon-14 value at each location. Based on the mixing fraction defined by chloride content of each sample, the carbon-14 content as pmC of a binary mixture is defined as follows:

$$pmC = \frac{C_F pmC_F + \omega \Delta C14}{C_F + \omega \Delta C}$$

where:

$$\Delta C14 = C_S pmC_S - C_F pmC_F$$

$$\omega = \frac{Cl - Cl_F}{Cl_S - Cl_F}$$

$$\Delta C = C_S - C_F$$

and pmC, pmC_F and pmC_S are the mixture, freshwater and saltwater end-member percent modern carbon, respectively, C_F and C_S are the freshwater and saltwater end-member inorganic carbon concentrations. ω is the saltwater end-member fraction in the mixture, Cl_F and Cl_S are the freshwater and saltwater end-member chloride concentrations, 20 mg/l and 19,350 mg/l, respectively, and Cl is the chloride concentration of the mixture. Because pmC is a relative concentration and the total carbon of the mixture depends on seawater fraction, a mixing line on a plot of pmC vs. ω is non-linear (FIGURE 16a).

This mixing relation is used to estimate end-member carbon-14 concentrations for each profile collected. To do this, alkalinity profiles in each well are first extrapolated to obtain freshwater and saltwater end members. Because of the pH of these waters, the alkalinity is assumed to be equivalent to the total inorganic carbon concentration. Thus, total inorganic carbon values for Waipahu are C_F=3.1 mg/l and C_S=12.0 mg/l, and for Waipio are C_F=4.0 mg/l and C_S=12.4 mg/l. Then the mixing curve for each well is moved upwards on the carbon-14 vs. saltwater fraction plot (FIGURE 16ab) by adjusting end-member pmC values in the above mixing relation, until the curve rests against the largest possible number of the lowermost data points. This results in end-member carbon-14 values for Waipahu of pmC_F=100 and pmC_S=30, and for Waipio of pmC_F=80 and pmC_S=23.

Use of only the lowermost points may be justified as follows. The scatter relative to the simple mixing curves may be due to contamination of samples with atmospheric carbon dioxide, as all of the other isotopic and chemical species collected in the same water samples closely follow simple mixing lines between end members, and did not vary significantly between the 1990 and 1992 sampling rounds (TABLE 1) except for the small upwards shift in 1992 described earlier. Rather, the variability may be due to contamination of samples during handling by modern carbon which would raise

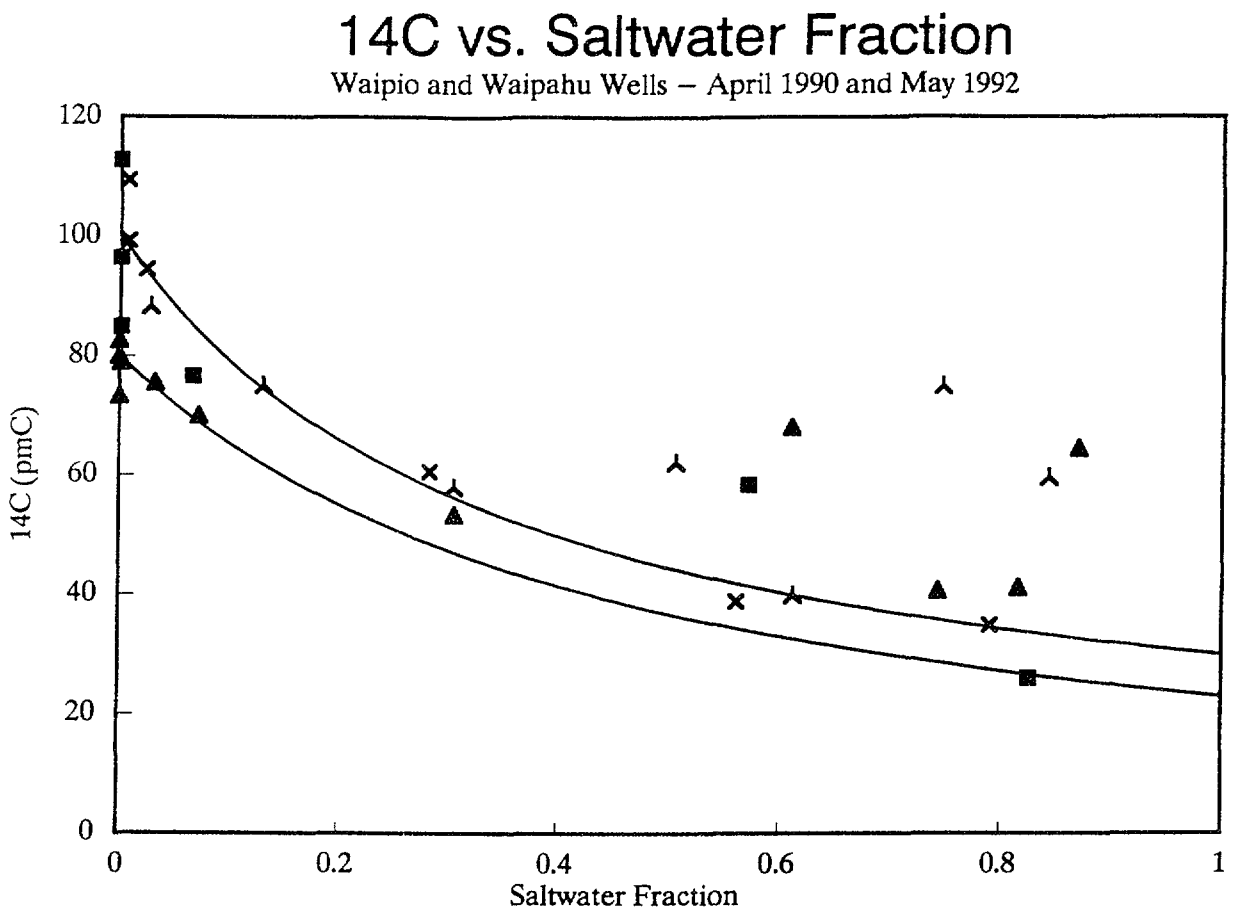

Figure 16a - Carbon-14 (pmC) relation to saltwater fraction for Waipahu monitor well profile (X is 1990, inverted-Y is 1992) and for Waipio monitor well (Square is 1990, and Triangle is 1992).

values above 'true values' which would fall close to the simple mixing curve in FIGURE 16ab. Indeed, in this system, there does not appear to be a reasonable mechanism for lowering carbon-14 measurements below actual aquifer values; thus, interpretation may be most soundly based on the lowest values in relation to the mixing curve. Considering the addition of dead carbon by oxidation of organic carbon indicated by end-member carbon-13 values for saltwater, the maximum possible adjustment to carbon-14 of the saltwater end members is the increase in pmC_S by a factor 1.24, as discussed earlier. This adjustment results in values for Waipahu of $pmC_S = 37$ and for Waipio of $pmC_S = 28$.

Using a half-life of carbon-14 of 5730 years, the Waipio freshwater carbon-14 has undergone decay from 100 pmC at recharge to 80 ±2 pmC, giving an apparent age ranging from 1600 to 2100 years. The Waipahu freshwater end member (FIGURE 16) has a higher carbon-14 content of about 100 pmC, which would suggest that waters are getting 'younger' along the flow line from Waipio to Waipahu. However, as discussed earlier, the freshest water at Waipahu is a mixture of irrigation-return water and pristine freshwater; thus, this high value is due to irrigation-return component of the mixture and is not a true freshwater end member.

In contrast, the saltwater end-member carbon-14 content at Waipahu is relatively well-constrained by data (FIGURE 16b) to be 30 ±1 pmC within the binary-mixing model. Seawater recharge to the aquifer system occurs offshore likely through the

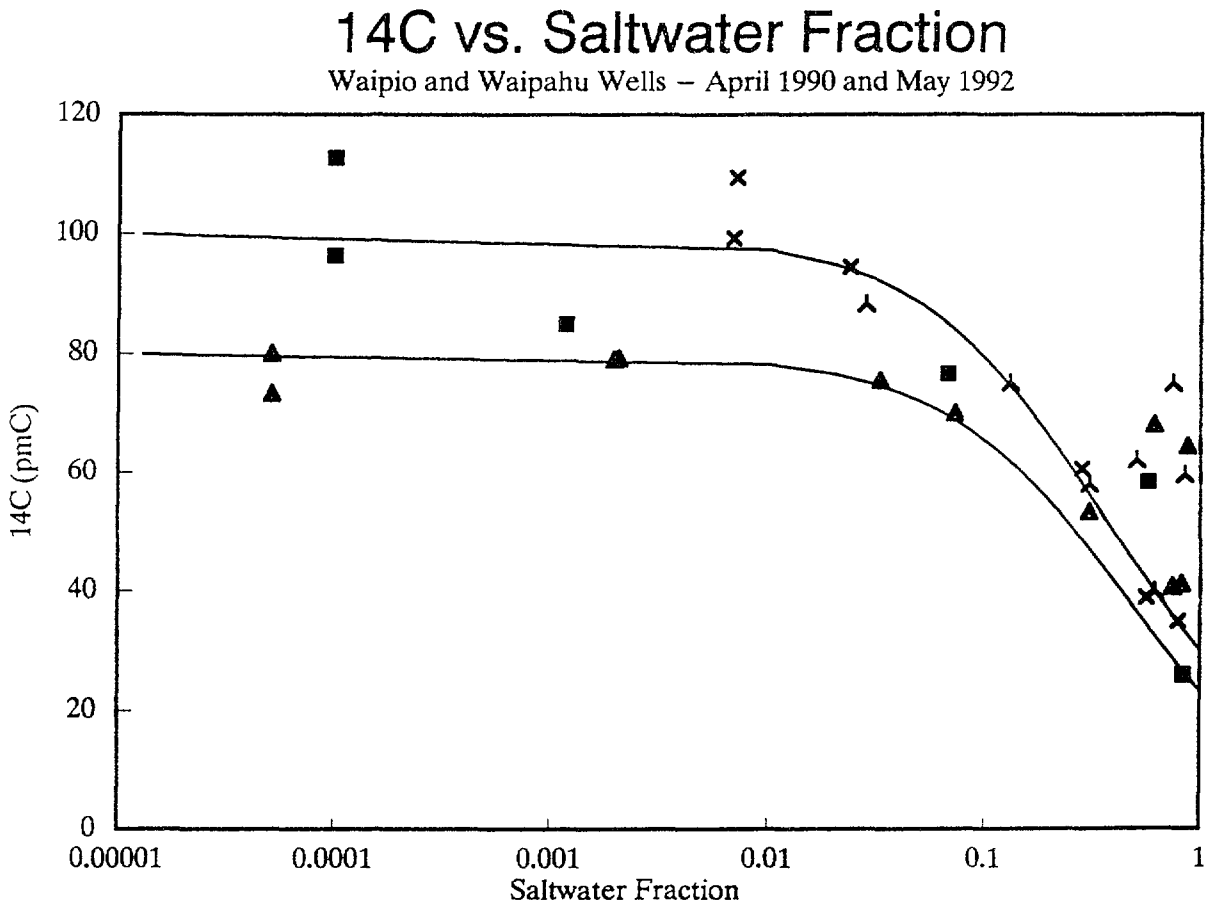

Figure 16b - Carbon-14 (pmC) relation to log10 of saltwater fraction for Waipahu monitor well profile (X is 1990, inverted-Y is 1992) and for Waipio monitor well (Square is 1990, and Triangle is 1992).

caprock, which is at a depth of about 500 m south of Oahu. An initial seawater carbon-14 content is required in order to estimate the age of saltwater under Oahu. In order to characterize the recharging seawater, a vertical profile of seawater was collected for this project at the Kahe-1 station roughly 25 km west of Pearl Harbor by GOFS (Global Ocean Flux Study) in October 1992. Carbon-14 and other isotope analyses are presented in TABLE 1 (carbon analyses by AMS at University of Arizona, stable isotopes by USGS, Reston, Virginia). A deeper oceanic GEOSECS profile (Östlund and others, 1979) collected about 1000 km southwest of Oahu (FIGURE 17) may give additional guidance regarding an initial carbon-14 content of seawater that entered the aquifer thousands of years ago. In the GEOSECS profile, the minimum ocean carbon-14 value is about 80 pmC and we may guess that in the pre-bomb profile, this value may have existed up to a depth as shallow as 500 m (which is the approximate submarine depth of the caprock, see FIGURE 3). The greatest possible value at 500 m depth at the time of recharge would be the present value, about 90 pmC. Thus the range of possible initial seawater activities at recharge is roughly from 80 to 90 pmC based on both the GEOSECS profile and the GOFS profile. The resulting apparent saltwater age at Waipahu is between 7800 and 9400 years. Using $\delta^{13}C$ values and adjusting for dead organic carbon input, the resulting saltwater age at Waipahu is between 6200 and 7600 years.

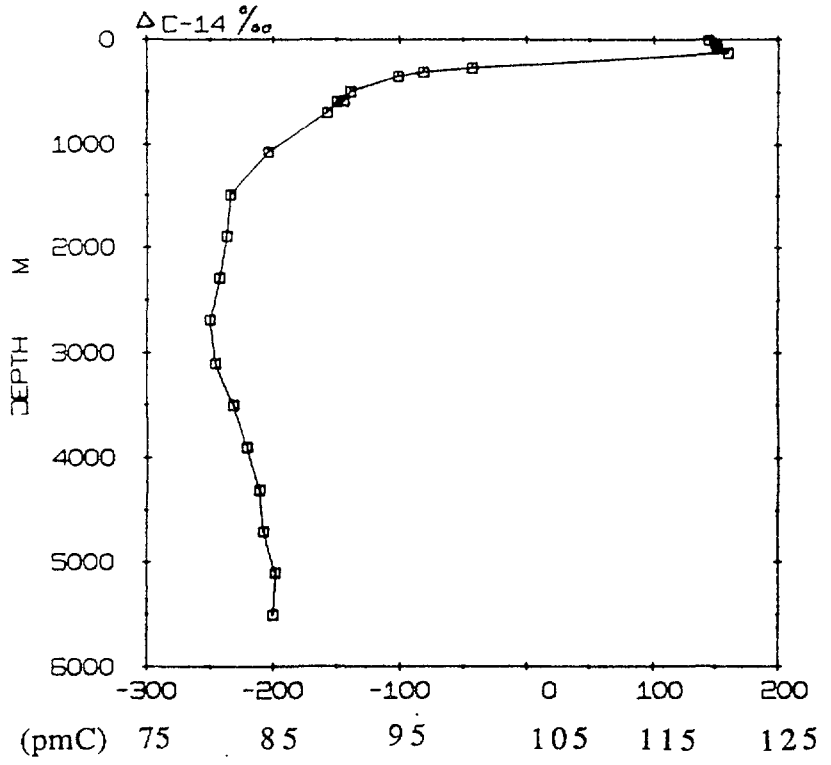

Figure 17 - Profile of carbon-14 in open ocean south of Oahu, Hawaii (Station 235). After Östlund and others (1979).

The end-member saltwater carbon-14 content at Waipio (23 ±1 pmC) is less than at Waipahu (30 ±1 pmC) consistent with an inland flow of the saltwater. Because the change in carbon-14 content is due to radioactive decay only, the associated saltwater travel time between the wells is between 1600 and 2800 years. This travel time is unaffected by the saltwater $\delta^{13}C$ adjustment which only changes both end-member carbon-14 values by the same fraction.

The associated estimate of saltwater velocity to travel 4.5 km from the Waipahu well to the Waipio well is between 1.6 m/y and 2.8 m/y. Note that this velocity actually describes conditions in the aquifer before development began 100 years ago. Considering that the age of the saltwater is much greater, the difference in radiocarbon age between the two profiles was established well before aquifer development began. Present-day saltwater velocity may be as much as five times greater than before development (Voss and Souza, 1993) due to the ongoing shrinkage of the lens. The simple assumption that the predevelopment velocity was constant between the Waipahu well and the recharge area for seawater allows estimation of a distance to the recharge area. Using the above saltwater age range at Waipahu, the distance is between 14 km and 24 km (or with the adjusted ages, between 11 km and 19 km). From Oahu's southern coast, the seawater recharge area is therefore 1 km to 9 km offshore (or 4 km to 14 km offshore using $\delta^{13}C$-adjusted ages).

The 1800-year radiocarbon age of freshwater in the Pearl Harbor area lens is in apparent contradiction to the brief residence time spent in the lens of only a few tens of years. A possible explanation for a freshwater age greater than the residence time in the Pearl Harbor area is that the high-level ground-water compartments contain large volumes of fresh ground water which is impounded for long times before the water

enters the freshwater lens. This water becomes a significant amount of the total lens recharge, quickly flows to the coast and discharges. This idea is not without precedent.

Dale and Takasaki (1976) evaluated the possible effects of increased pumpage in the Schofield high-level water body in reducing recharge to the Pearl Harbor area aquifer. Takasaki and Mink (1985) evaluated the water resources of the Oahu dike zones and discussed significant discharge to adjoining basal aquifers. Hufen and others (1980) found in an areal sampling program of shallow waters that some Pearl Harbor area waters in the western portion of the aquifer were a few-hundred years old. They suggested that some older recharge water may derive from the Schofield high-level water body. They also found waters in some Honolulu aquifers separated by valley fills with apparent ages of nearly 1000 years and suggested that some recharge may have been impounded in dike compartments. Lacking vertical profiles through the freshwater lens, however, Hufen and others (1980) were led to conclude that most ground water in the Pearl Harbor area had experienced short residence times and was young water, in contrast with the older freshwater lens found in this study.

The total compartment volume available to impound ground water before it enters the Pearl Harbor area freshwater lens does not, according to a simple calculation, suffice to create a delay as long as 1800 years. The largest possible volume of the Koolau rift zone that may contribute recharge to the Pearl Harbor area begins alongside the Schofield high-level water body and continues southeast along the upstream boundary of the area. The total length of this maximal zone is about 20 km and width is about 10 km. A maximum thickness of subaerial basalts intruded by dikes in this area is about 2 km. Allowing that the maximum possible volumetric porosity of vesicular basalts, about 50 %, can participate in water storage, gives a total absolute maximum stored water volume of about 2×10^{11} m^3. With the earlier-mentioned natural recharge rate to the Pearl Harbor area aquifer of about 9×10^5 m^3/d (240 Mgal/d), the mean residence time in the rift-zone compartment would thus be, at most, 600 years. This is equivalent to a considerable ground-water recharge rate of about 1.7 m/y over the rift-zone area. Considering an additional compartment volume in the Schofield high-level water body in an 8 km by 4 km area, 2 km deep, provides only an additional 100 years to the maximum compartment residence time should all rift-zone water flow through the Schofield area before entering the Pearl Harbor area lens. The two to three times discrepancy between apparent freshwater radiocarbon age (1600 years to 2100 years) and maximum possible residence time in the compartments (700 years) may be presently explained in two ways. Either the natural recharge to the Pearl Harbor water body is less than assumed by up to a factor of two to three, or the carbon-14 activity in the freshwater lens has been decreased by an undetermined source of old carbon during recharge. A possible carbon source is addition of old organic matter in recharge areas discussed earlier. We have not, at this time, further considered this discrepancy, elucidation of which requires additional field reconnaissance in recharge areas to determine initial carbon-14 activity and carbon sources.

7. COMPARISON WITH MODEL

The numerical model of the system was discussed by Voss and Souza (1993) and by Souza and Voss (1987) to which the reader is referred for details on the model development. Only a brief review sufficient to demonstrate model results applicable to the present geochemical and age relationship analysis is given here. The 20 km long

two-dimensional cross-sectional model (based on the finite-element method) represents the entire Pearl Harbor area aquifer from the dike-zone boundary and Schofield high-level water body boundary to the inland edge of the caprock (10 km) and an additional distance into the ocean south of Oahu (10 km). The width of the section is 26 km, and depth is 1.8 km. The numerical model simulates variable-density ground-water flow and solute transport (of total dissolved solids) in the section. Note that the rift zone and Schofield water body are not included in this model.

The inland and bottom model boundaries are impermeable (FIGURE 18), and the vertical sea boundary is held at hydrostatic seawater pressure allowing either inflow of seawater or outflow of aquifer water. The upper boundary is a water table with a specified amount of recharge inland of the caprock, and is held at a specified pressure of zero above the caprock to reflect the presence of the Pearl Harbor water and the ocean with concomitant inflow or outflow. Along the inland portion of the water table, time-independent natural recharge (from rain or compartment spillage) is specified as increasing linearly towards the inland boundary. The natural recharge is assigned a seawater concentration (dissolved solids) of zero. Between this area and the caprock edge, spatially-constant recharge from irrigation is specified to occur on a time-varying schedule from 1880 to 1990 as determined from pumping records. In a departure from the previously-published modeling results, the irrigation recharge is arbitrarily assigned a non-zero concentration in order to track the movement of this water in the section.

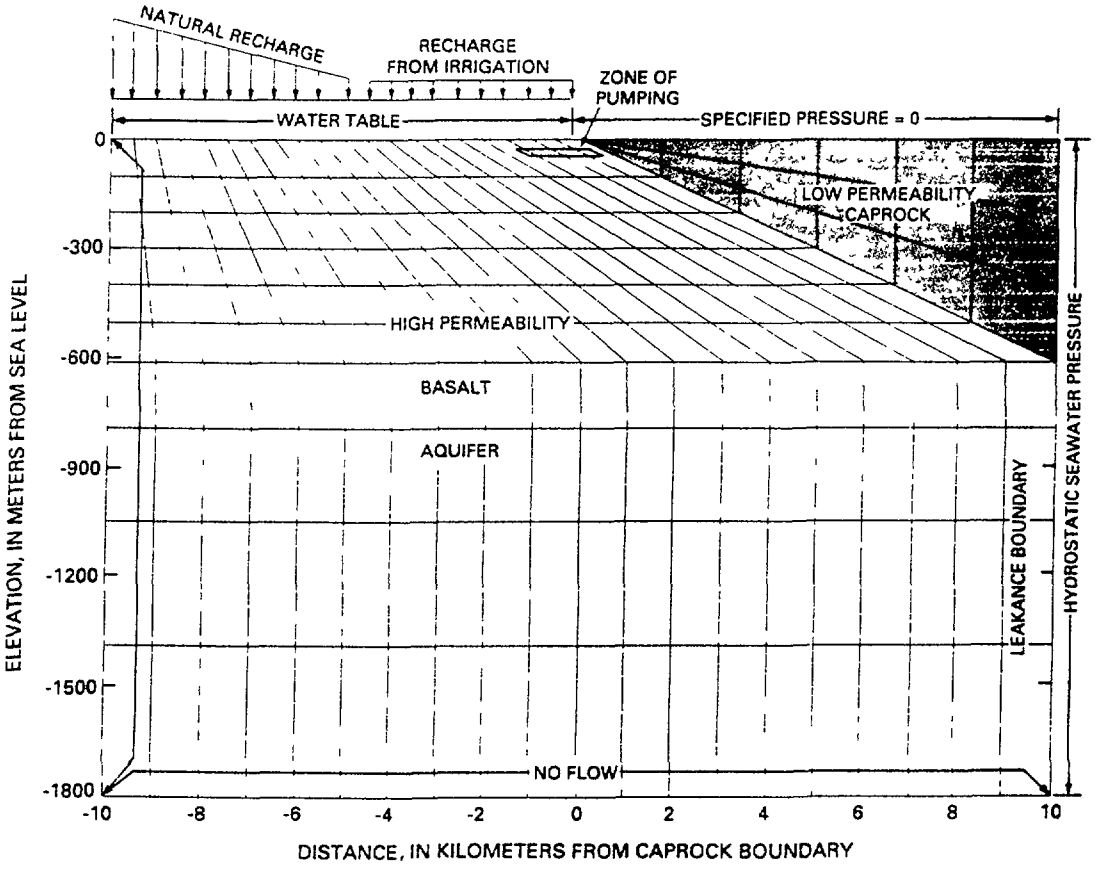

Figure 18 - Pearl Harbor aquifer cross-sectional model showing finite-element grid (schematic), boundary conditions, pumping region, basalt and caprock regions (after Voss and Souza, 1993).

Near the caprock edge at a depth of 40 m below the water table in the basalt aquifer, the coastal band of wells is specified to pump water from the aquifer at a time-varying rate from 1880 to 1990 as determined from pumping records.

The model structure is very simple. The layered-basalt aquifer is anisotropic with horizontal conductivity of 457 m/d and 200 times lower vertical conductivity. The caprock is isotropic with conductivity 10^4 times less than the basalt (horizontal). Specific yield and porosity (and effective porosity) are 0.04, and there is considerable compressive storage in the layered basalts (matrix compressibility of 2.5×10^{-9} Pa^{-1}, or equivalently, specific storage of 2.37×10^{-5} m^{-1}). In the model, longitudinal dispersivities for horizontal flow and vertical flow are respectively, 250 m and 50 m, while transverse dispersivity is only 0.25 m. The following model results derive from new simulations with the earlier-reported numerical model (Voss and Souza, 1993) without change with the exception noted above to trace the irrigation-return water.

The modeled distribution of the three water types and the flow field for predevelopment conditions (1880) and for 1990 is shown in FIGURE 19abcd. The shrinkage of the freshwater lens in this period is apparent, and even given constant recharge and pumping after 1990, the shrinkage would continue (Souza and Voss, 1989). In the 1990 simulation, the upstream monitor well (Waipio) intercepts all three water types, while at the downstream monitor well (Waipahu) the irrigation-return water and the saltwater overlap and mix across the freshwater lens (FIGURE 19c). This conforms with the spatial distribution found in the geochemical analysis.

To further compare the field-measured age distribution and the model, isochrones (lines of equal residence time) were calculated in the model. Using the 1880 steady-state flow field, an extra simulation was run at steady state for an imaginary species having zero concentration at inflow, but with a zero-order production of this species in the fluid (see Voss, 1984, for definition of this source) with a value of one per year. This numerical trick produces isochrones directly from the transport model, accurately indicating residence time in the model section for regions with low

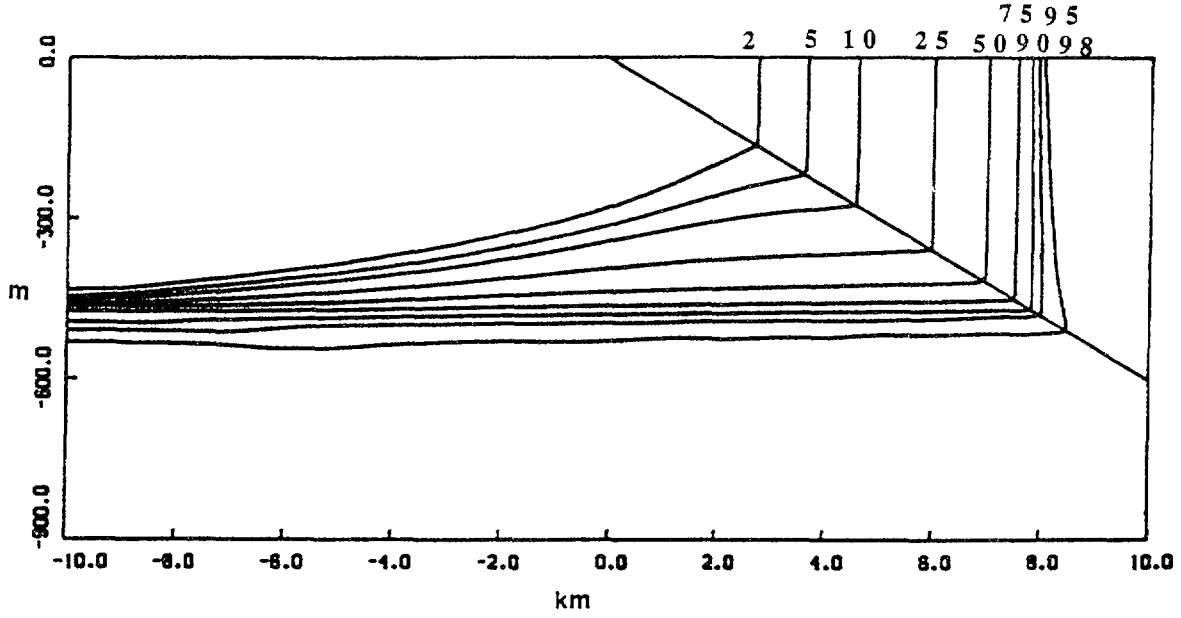

Figure 19a - Modeled cross-section of Pearl Harbor area aquifer showing seawater distribution in 1880. Contours are in percent seawater. Upper half of model section is shown.

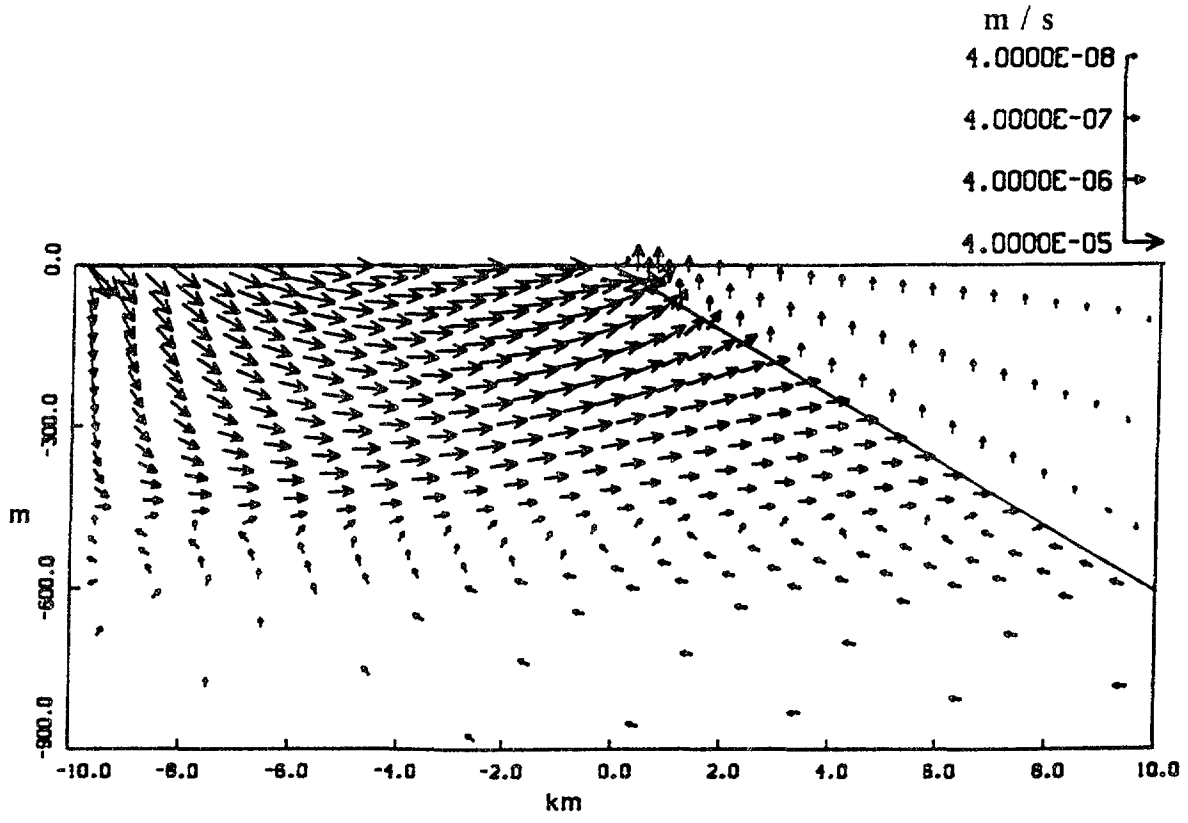

Figure 19b - Modeled cross-section of Pearl Harbor area aquifer showing velocity distribution in 1880. Upper half of model section is shown.

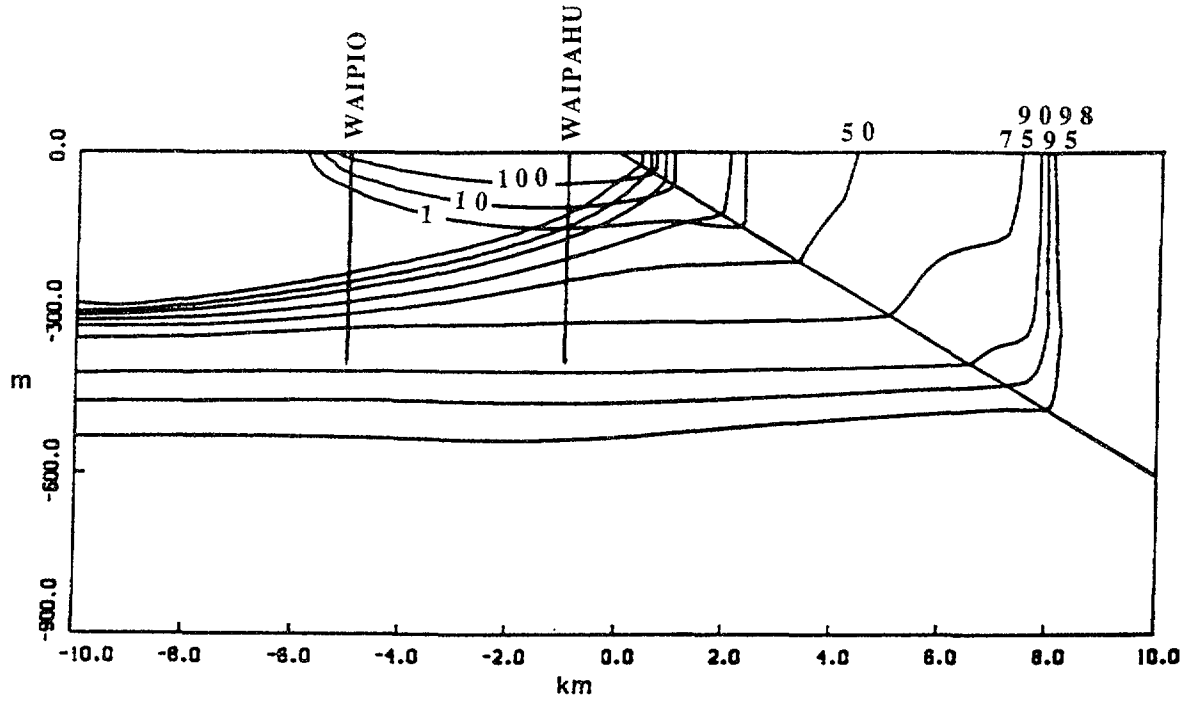

Figure 19c - Modeled cross-section of Pearl Harbor area aquifer showing seawater distribution (lower set of contours), and irrigation recharge water distribution (upper set of contours) in 1990 in units of percent of irrigation water, and location of monitor wells. Contours are in percent seawater. Upper half of model section is shown.

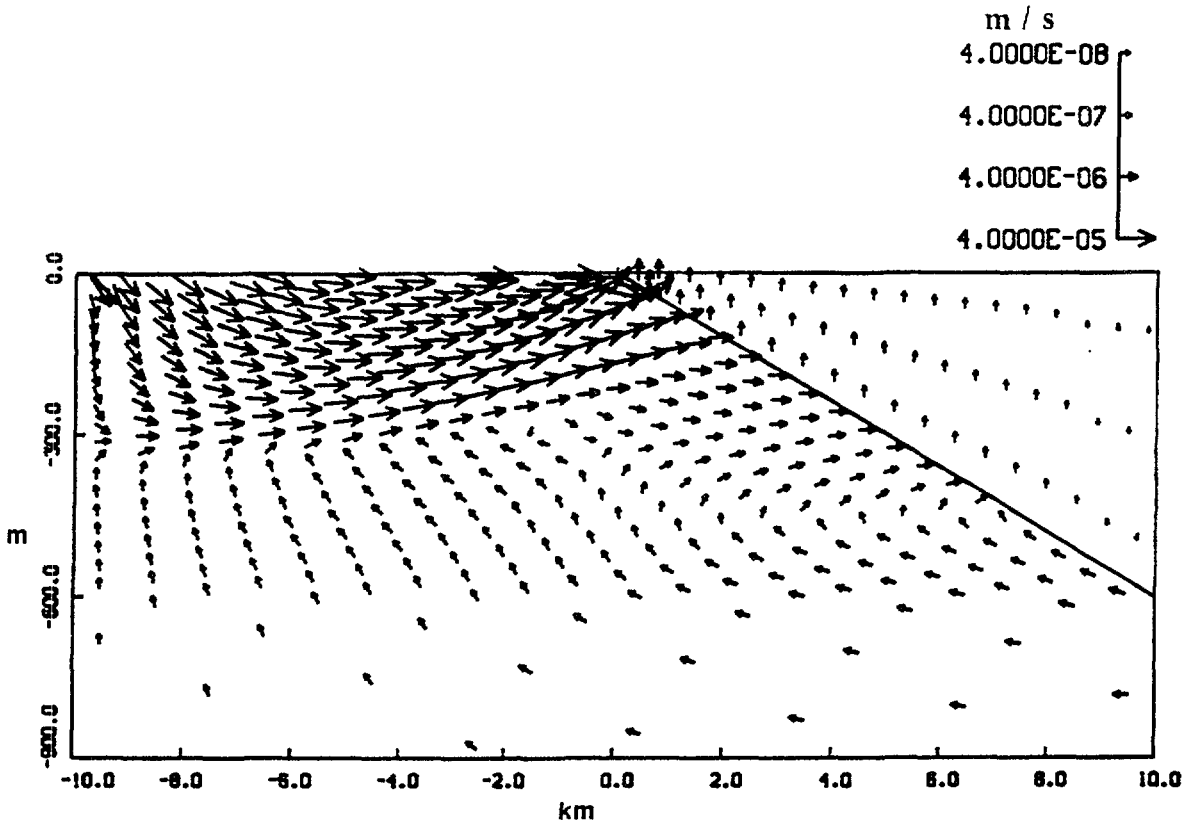

Figure 19d - Modeled cross-section of Pearl Harbor area aquifer showing velocity distribution in 1990. Upper half of model section is shown.

solute dispersion. The result (FIGURE 20) in both the freshwater lens and the deep saltwater gives model residence times. Isochrones within the zone of mixing between freshwater and seawater are ignored. Total residence time of water in the freshwater lens is less than 20 years, in conformance with the tritium findings for irrigation-return water, and the freshwater would exhibit a constant carbon-14 age throughout. The saltwater takes approximately 6000 years to flow 20 km from the sea boundary to the inland boundary in the model, equivalent to a velocity of about 3.3 m/y. This is somewhat greater than but similar to the carbon-14-based saltwater transit velocities from the Waipahu well to the Waipio well of between 1.6 m/y and 2.8 m/y.

The inland flow of saltwater in a steady-state system is driven by the amount of salt entrained in and subsequently discharged with the freshwater flow towards the coast. This, in turn, depends on two factors, the flux of freshwater and the dispersion process. To slow down the modeled saltwater inflow to better conform with the isotope-based velocity would require either a decrease in the model recharge to the aquifer by up to one half, or a decrease in the model dispersion coefficients used to reproduce the seawater transition zone. Another factor, not considered in the model calculations, is that the effective porosity experienced by the slow-moving saltwater may be greater than the value of 0.04, assigned to the entire aquifer, a value which had been determined mainly by data on the freshwater zone. In slow-moving saltwater the entire volumetric porosity, up to about 0.40, may participate in solute transport by both solute diffusion and advection through blocks of basalt alongside the well-connected conductive rubbly beds for which the regional effective porosity is

apparently only 0.04. In the case of an effective porosity of 0.40, the same saltwater flux as determined in the simulations can be obtained with a ten-times lower saltwater velocity. Thus there is ample flexibility in this process to account for the discrepancy in modeled and isotope-determined saltwater velocities even with only a small portion of the less-conductive basalt porosity participating in saltwater zone solute transport.

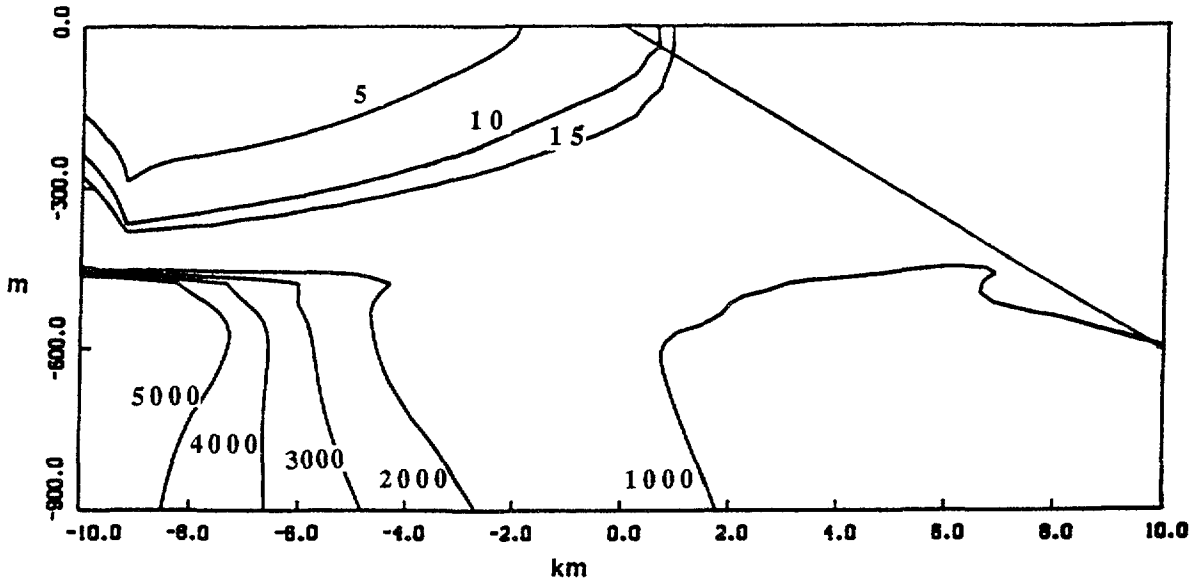

Figure 20 - Modeled cross-section of Pearl Harbor area aquifer showing contours of equal travel time (note: NOT absolute ages) from entry into model area for conditions in 1880. Upper half of model section is shown. Travel times are in years.

8. CONCLUSIONS

Sampling in vertical profile in two wells along a regional ground-water flow line and geochemical and isotopic analysis has resulted in proposal of a hydrologic model of the Pearl Harbor area aquifer in southern Oahu, Hawaii. The hydrologic model includes ages and flow velocities of the three major water types found. These have been compared with the predictions of a numerical variable-density ground-water solute transport model developed independently of the present geochemical analysis from hydraulic data and from vertical profiles of salinity through the freshwater lens and into seawater. Within margins of uncertainty in the chemical data and age interpretations, the flow behavior represented by the numerical model is in good agreement with the geochemically-derived model. This agreement was not necessarily expected at the outset of the study, as our experience was that most numerical models need to be revised significantly as new data becomes available. Perhaps most interesting is the similarity in the velocity of saltwater moving inland as determined by carbon-14 dating (about 2 m/y) and that occurring in the numerical model (about 3 m/y). While this agreement may at worst be only a coincidence, to our knowledge, it is the first time that a numerical variable-density ground-water model prediction of saltwater circulation in a coastal aquifer has been independently corroborated by geochemical field data.

The uppermost water consisting of recharge from irrigation is found to be only a few tens of years old and moves through the aquifer at a velocity on the order of 1 km/y. The freshwater core of the freshwater lens has a great apparent age of about 1800 years. From hydrologic considerations, once this water enters the coastal system from the compartments, it must move through the aquifer as quickly as the irrigation recharge water. The great apparent freshwater age may be satisfactorily explained as being due to long storage in ground-water compartments in the recharge areas of the island. Simple volumetric calculations show, however, that this storage can account for considerably less than one-half of the apparent age. The excess apparent age may be partly due our present inability to quantify and remove any possible contribution of old dissolved organic carbon added during recharge, which would tend to make the water appear older than it is. The deepest water is intruded seawater with an apparent age of about 6000 years to 9000 years near the inland edge of Pearl Harbor. Older saltwater is found further inland, and from the difference in ages, the approximate velocities mentioned above were calculated.

It would have been difficult to propose a quantitative model of the hydrologic system on the basis of an areal geochemical distribution of vertically-mixed or shallow samples collected from springs and active pumping wells. Mixed samples would have obscured much of the primary information on water type, recharge area and age, while shallow samples would only characterize the uppermost layer of water. This points to the importance of vertically-stratified geochemical sampling through the entire aquifer section.

In our view, it is of utmost importance to understanding of regional aquifer systems to collect hydrogeologic, geochemical as well as hydraulic information. Further, we believe that these data must be analyzed simultaneously, with the objective being the discovery of a descriptive model that gives a consistent description of all data types in as simple but quantitative a manner as possible. In the present investigation, the corroboration of hydrogeologic, geochemical and isotopic data with predictions of a numerical ground-water flow model has lent credence to the viability of a simply-structured quantitative model to describe the Pearl Harbor area aquifer system.

ACKNOWLEDGEMENTS

The analysis of carbon-13 and carbon-14 for the 1990 data was provided by Prof. Dr. Mebus Geyh, and the Niedersächsisches Landesamt für Bodenforschung, Hannover, Germany, as a contribution to the Coordinated Research Program of the International Atomic Energy Agency on "Mathematical Models for Quantitative Evaluation of Isotope Data in Hydrology", of which this study was a part. We are most indebted to Dr. Geyh for this gracious support. We thank Dr. Gordon Tribble of the U.S. Geological Survey, Hawaii District office, for providing a core sample of Oahu caprock, and for leading a windward Oahu reconnaissance trip. Tyler Coplen, USGS provided ^{2}H and ^{18}O analyses, and Robert Michel, USGS provided tritium analyses for which we are most grateful. We also thank the Hawaii District office for logistical and equipment support, and both the State of Hawaii and Board of Water Supply, City and County of Honolulu for providing access to monitor wells. Finally, we thank the Global Ocean Flux Study (GOFS) through David Karl and Dale Hebel at the University of Hawaii for generous support in arranging special sampling and for collecting the seawater isotope profile reported in this project.

REFERENCES

Andrews, J.E. and C. Bainbridge, Submarine Canyons off Eastern Oahu: Pacific Science, vol. XXVI, no. 1, 108-113, 1972.

Dale, R.H. and K.J. Takasaki, Probable effects of increasing pumpage from the Schofield ground-water body, Island of Oahu, Hawaii, U.S. Geological Survey Water-Resources Investigations Report 76-47, 45 pp., 1976.

Flanagan, F.J., J.C. Chandler, I.A. Breger, C.B. Moore, and C.F. Lewis, The carbon contents of USGS volcanic rock standards, in Flanagan, F.J. ed., Descriptions and analyses of eight new USGS rock standards, U.S. Geological Survey Professional Paper 840, 123-126, 1976.

Gregory, A.E., Reflection profiling studies of the 500-meter shelf south of Oahu: Reef development on a mid-oceanic island, M.S. Thesis, University of Hawaii, Honolulu, Hawaii, 68 pp., 1980.

Holcomb, R.T., Eruptive history and long-term behavior of Kilauea volcano, in Decker, R.W., T.L. Wright and P.H. Stauffer, eds., Volcanism in Hawaii, U.S. Geological Survey Professional Paper 1350, Chapter 12, 261-350, 1987.

Hufen, T.H., R.W. Buddemeier and L.S. Lau, Tritium and radiocarbon in Hawaiian natural waters- Part I, Technical report No. 53, Water Resources Research Center, University of Hawaii, 54 pp, 1972.

Hufen, T.H., A geohydrologic investigation of Honolulu's basal waters based on isotopic and chemical analyses of water samples, Doctoral Dissertation, University of Hawaii, 160 pp., 1974.

Hufen, T.H., R.W. Buddemeier and L.S. Lau, Isotopic and chemical characteristics of high-level groundwaters on Oahu, Hawaii, Water Resources Research, 10-2, 366-370, 1974a.

Hufen, T.H., L.S. Lau and R.W. Buddemeier, Radiocarbon 13C and tritium in water samples from basaltic aquifers on the Island of Oahu, Hawaii, in Isotope Techniques in Groundwater Hydrology 1974 - Proceedings of a symposium organized by the International Atomic Energy Agency and held in Vienna, 11-15 March 1974, Volume II, IAEA-SM-182/33, 111-127, 1974b.

Hufen, T.H., P.R. Eyre and W. McConachie, Underground residence times and chemical quality of basal groundwater in Pearl Harbor and Honolulu aquifers, Oahu, Hawaii, Technical report No. 129, Water Resources Research Center, University of Hawaii, 75 pp, 1980.

Hunt, C.D., C.J. Ewart and C.I. Voss, Region 27, Hawaiian Islands, in Back, W., Rosenshein, J.S. and Seaber, P.R. eds., The Geology of North America, Vol. O-2, Hydrogeology, The Geological Society of America, Chapter 30, 255-262, 1988.

Lockwood, J.P. and P.W. Lipman, Holocene eruptive history of Mauna Loa volcano, in Decker, R.W., T.L. Wright and P.H. Stauffer, eds., Volcanism in Hawaii, U.S. Geological Survey Professional Paper 1350, Chapter 18, 509-535, 1987.

MacDonald, G.A., A.T. Abbott and F.L. Peterson, Volcanoes in the Sea - The Geology of Hawaii, University of Hawaii Press, Honolulu, 517 pp., 1983.

Mink, J.F., Some geochemical aspects of sea water intrusion in an island aquifer, Internat. Assoc. Sci. Hydrology Comm. of Subterranean Waters Pub. 52, p. 424-439, 1961.

Mink, J.F., State of the groundwater resources of southern Oahu, Board of Water Supply, City and County of Honolulu, 83 pp., 1980.

Östlund, H.G., R. Brescher, R. Oleson and M.J. Ferguson, GEOSECS Pacific radiocarbon and tritium results (Miami), Tritium Laboratory Data Report #8, Rosenstiel School of Marine and Atmospheric Science, University of Miami, Florida, 1979.

Parkhurst, D.L., D.C. Thorstenson, and N. Plummer, PHREEQE - A computer program for geochemical calculations, U.S. Geological Survey Water-Resources Investigations Report 80-96, 195 pp., (revised August 1990), 1980.

Plummer, L.N., D.L. Parkhurst, G.W. Fleming and S.A. Dunkle, PHRQPITZ - A computer program incorporating Pitzer's equations for calculation of geochemical reactions in brines, U.S. Geological Survey Water-Resources Investigations Report 88-4153, 310 pp., 1988.

Skougstad, M.W., M.J. Fishman, L.C. Friedman, D.E. Erdmann and S.Duncan, eds., Methods for determination of inorganic substances in water and fluvial sediments, Techniques of Water-Resources Investigations of the U.S. Geological Survey, Book 5, Chapter A1, 626 pp., 1989.

Souza, W.R. and C.I. Voss, Analysis of an anisotropic coastal aquifer system using variable-density flow and solute transport simulation, Journal of Hydrology, 92, 17-41, 1987.

Souza, W.R. and C.I. Voss, Assessment of potable groundwater in a freshwater lens using variable-density flow and transport simulation, in proceedings of NWWA conference on Solving groundwater problems with models, Feb 7-9, Indianapolis, Indiana, National Water Well Association, 1023-1043, 1989.

Takasaki, K.J. and J.F. Mink, Evaluation of major dike-impounded ground-water reservoirs, Island of Oahu, U.S. Geological Survey Water-Supply Paper 2217, 77 pp., 1985.

Visher, F.N. and J.F. Mink, Ground-water resources in southern Oahu, Hawaii, U.S. Geological Water-Supply Paper 1778, 39 pp., 1964.

Voss, C.I., SUTRA: A finite element simulation model for saturated-unsaturated, fluid density dependent ground-water flow with energy transport or chemically reactive single species solute transport. U.S. Geological Survey Water-Resources Investigations Report 84-4369, 409 pp., 1984.

Voss, C.I. and W.R. Souza, Dynamics of a regional freshwater-saltwater transition zone in an anisotropic coastal aquifer system, Journal of Hydrology, in press, 1993.

CALIBRATION AND VERIFICATION OF A REGIONAL GROUNDWATER FLOW MODEL BY COMPARING SIMULATED AND MEASURED ENVIRONMENTAL ISOTOPE CONCENTRATIONS

An application to the Alnarp aquifer system in southwestern Sweden

G. BARMEN
Lund Institute of Technology,
Lund University,
Lund, Sweden

Abstract

Environmental isotope studies and computerized groundwater flow modelling and radioisotope transport modelling have been applied to the large system of reservoirs in the sedimentary deposits of southwestern Scania, Sweden.

The stable isotopes ^{2}H, ^{18}O and ^{13}C and the radioactive ^{3}H and ^{14}C have been measured and the results obtained can improve the estimations of the periods of recharge and the average circulation times of the groundwater reservoirs studied.

A groundwater flow model based on finite difference techniques and a continuum approach has been modified by data from traditional hydrogeological studies. A calibration against piezometric records has been made for 1970, assuming steady-state conditions, and also for the transient evolution from 1840 to 1988. The computer code NEWSAM has also been used to simulate steady-state and transient isotope transport in the area studied, taking into account advective transport with radioactive decay. The interacting groundwater reservoirs studied have been represented by a three-dimensional grid in the numerical model.

A major merit of this combination of isotope hydrogeology and regional flow and transport modelling is that the isotope transport simulations help to demonstrate where zones particularly vulnerable to pollution are situated. However, there are several difficulties concerning the detailed, quantitative interpretations of the results, and these difficulties must be the focus of future work. Even if the aquifer system studied here can be classified as unusually homogeneous and well-defined, the number of isotope measurements is small compared to the extension of the system. Furthermore, the calculated concentrations are similar over large areas. Therefore, it is at present not possible to calibrate the isotope transport model by measured isotope concentrations in order to verify or reject the results of the underlying groundwater flow model.

1. INTRODUCTION

Environmental isotope techniques and computerized mathematical flow and transport modelling have become relatively widespread and frequently used. Yet, these tools have been developed side by side with very little interaction. Recent years, however, have witnessed a tendency towards greater collaboration and interaction among the different techniques and disciplines dealing with groundwater. One major reason for this is an expectation that the knowledge about a system of aquifers will often increase and become more reliable if the results from many independent methods of investigation and interpretation are used in combination. This is of particular interest when little information is available. Data from one method can then be expected to compensate to some extent for the lack of data from another method.

It follows, therefore, that it would be of special interest to try to use environmental isotope techniques together with computerized distributed parameter, conceptual flow and transport modelling of regional aquifer systems. To the author's present knowledge, Robertson (1974) is

the only one who has published a scientific paper on the application of such an approach. In addition, Markussen, Möller, Villumsen, Mortensen & Selchau presented a report founded on a similar idea in 1991.

2. PURPOSES AND DELIMITATIONS

The main purpose of this work is to investigate whether a combination of the results from deterministic flow and advective transport modelling with observations of environmental isotope contents can improve the understanding of a chosen regional groundwater system. The investigation should be carried out with the overall objective to improve the basis for maintaining a quantitatively and qualitatively safe long-term use of the groundwater resources studied. The main purpose can be broken up into a few interacting and subordinate aims.

It should be investigated whether comparisons between observed temporal and spatial isotopic variations and corresponding calculated values can be used as an independent way of verifying the results of the numerical, groundwater flow model, which underlies the isotope transport model used. Another aspect of this combination of results is that isotope data might improve estimations of the properties relevant to the flow and transport processes which are active in the groundwater system modelled. Therefore, the potential contribution of environmental isotope data to the identification of the physical parameters of the hydrogeological system to be studied, should also be investigated.

A second subordinate aim is to obtain a better knowledge concerning the hydrogeological system chosen for the application of the methodology outlined. The selected system is situated in the sedimentary rocks and glaciofluvial sediments of southernmost Sweden (see figure 1) and includes the Alnarp valley aquifer. The major reasons for choosing this system are that it has been the subject of comparatively thorough investigations and observations over more than a century, that all parts of it are situated at moderate distances from Lund and that the volumes of groundwater withdrawn for this region are substantial (see for example Brinck, Leander & Winqvist, 1969, and Hydén, Leander & Voss, 1980).

Financial and temporal restrictions have set limits also for this work. In general, priority has been given to equipment and techniques which were easily available and cheap, but which satisfied basic requirements of quality and performance. The following is an account for the most decisive delimitations.

The use of only one hydrogeological system obviously implies an important restriction concerning the generality of the conclusions. In principle, it is possible to draw conclusions related only to this particular system or to very similar ones. Though a great amount of information exists about the groundwater system of southwestern Scania compared to other aquifers, only a small and unequally distributed number of useful data in relation to the extension of the system have been to hand for the calibration work. This is of course a general and realistic situation, but it limits the possibility of drawing methodological conclusions concerning the combination of environmental isotope investigations with regional flow and transport modelling.

The deterministic flow and transport model applied assumes an environment equivalent to a porous medium. Moreover, the main modelling work has been done by means of only one computer code, NEWSAM (Ledoux, 1986b). This finite difference computer code has its limits in simulating groundwater flow and isotope transport phenomena as quasi-three-dimensional and only taking into account advective transport with radioactive decay. Thus, the numerical representation of the regional hydrogeological system used does not admit an accurate simulation of the isotope concentration in every point.

3. PREVIOUS WORKS

In this work a deterministic continuum approach with distributed parameters is followed to combine environmental isotope data with a numerical flow and transport model for a regional

system of aquifers. This approach comprises a very conceptual representation of isotope transport through hydrogeological systems. All physical and/or chemical phenomena which can occur can be included and are described as being continuous and deterministic. That is, advection, molecular diffusion, hydrodynamic dispersion, adsorption, ion-exchange and other forms of retention as well as chemical reactions and radioactive decay can be considered.
In many real, field situations the spatial variations of the properties of the studied groundwater system make the mathematical representation too complex to be solved analytically. Instead a numerical method for solving the transport equation has to be applied. There exist several numerical methods which are suitable for solving the governing equation for solute transport, i.e. the advection-dispersion equation. For instance, finite differences, finite elements, the method of characteristics, including the methods of particle in cells (PIC) and random walk, and also combinations of these, have been most commonly used. A large number of computer codes for application of these methods have been developed during the past two decades. However, only a few results of the application of these models for comparison with environmental isotope data have been published.

Robertson (1974) seems to have been the first to document an isotope-verification of a two-dimensional, deterministic groundwater flow and transport model based on numerical techniques. He solves the flow equation by means of the finite difference method. The calculated groundwater velocities are subsequently used to simulate advective transport, two-dimensional dispersion, radioactive decay and ion exchange by the method of characteristics. The results of the model were compared with measured concentrations of tritium, strontium-90 and chloride in the Snake River Plain aquifer and proved to be satisfactory. The isotopes and solutes studied originate from a radioactive waste disposal and are thus not environmental.

Herweijer, van Luijn & Appelo (1985) have applied a similar approach to calibrate a one-dimensional vertical flow and transport model with measured concentrations of environmental tritium. They used the random walk method for the solution of the transport equation instead (see, e.g., Kinzelbach, pp. 227-245 in Custodio, Gurgui & Lobo Ferreira, 1987). The calibrated model was subsequently used for the simulation of contamination originating from heavily manured areas.

Markussen, Möller, Villumsen, Mortensen & Selchau (1991) have applied the computer code SHE, European Hydrological System, to simulate the three-dimensional flow and transport of environmental tritium in a system of aquifers below Copenhagen, Denmark. This code solves the flow and transport equations by means of finite difference techniques and the version applied has been developed by the Danish Hydraulic Institute. Markussen et al. have compared the simulated and the measured tritium concentrations in the main aquifer of the studied area and they have adjusted the porosity values of the model to obtain a better fit. The resulting average circulation times of the groundwater in the vicinity of some wells producing drinking-water have subsequently been used to estimate the propagation of various pollutants threatening the groundwater quality in the Copenhagen area.

4. HYDROGEOLOGICAL CONDITIONS

The investigated area is situated in southwestern Scania (see figure 1) at the edge of a geological border zone between archaean rocks in the north and thick layers of sedimentary rocks in the south. The Fennoscandian Border Zone, as it is called, forms a tectonic buffer zone between the essentially rigid Fennoscandian Shield and a large area of subsidence, which comprises the Danish-Polish Trough. The border zone crosses Scania in a northwest-southeast direction and includes several crystalline horsts. One of them, the Romeleås horst, constitutes the northeastern limit of the area of interest.

The geological evolution of southwestern Scania has been characterized by considerable tectonic movements. Most of the faults and flexures follow the northwest-southeast trend of the border zone. Faults in other directions do also occur and the bed-rock can be divided into blocks, defined by tectonic zones of weakness. In general, the blocks southwest of the Fennoscandian Border Zone have subsided as a consequence of alternating downward tectonic

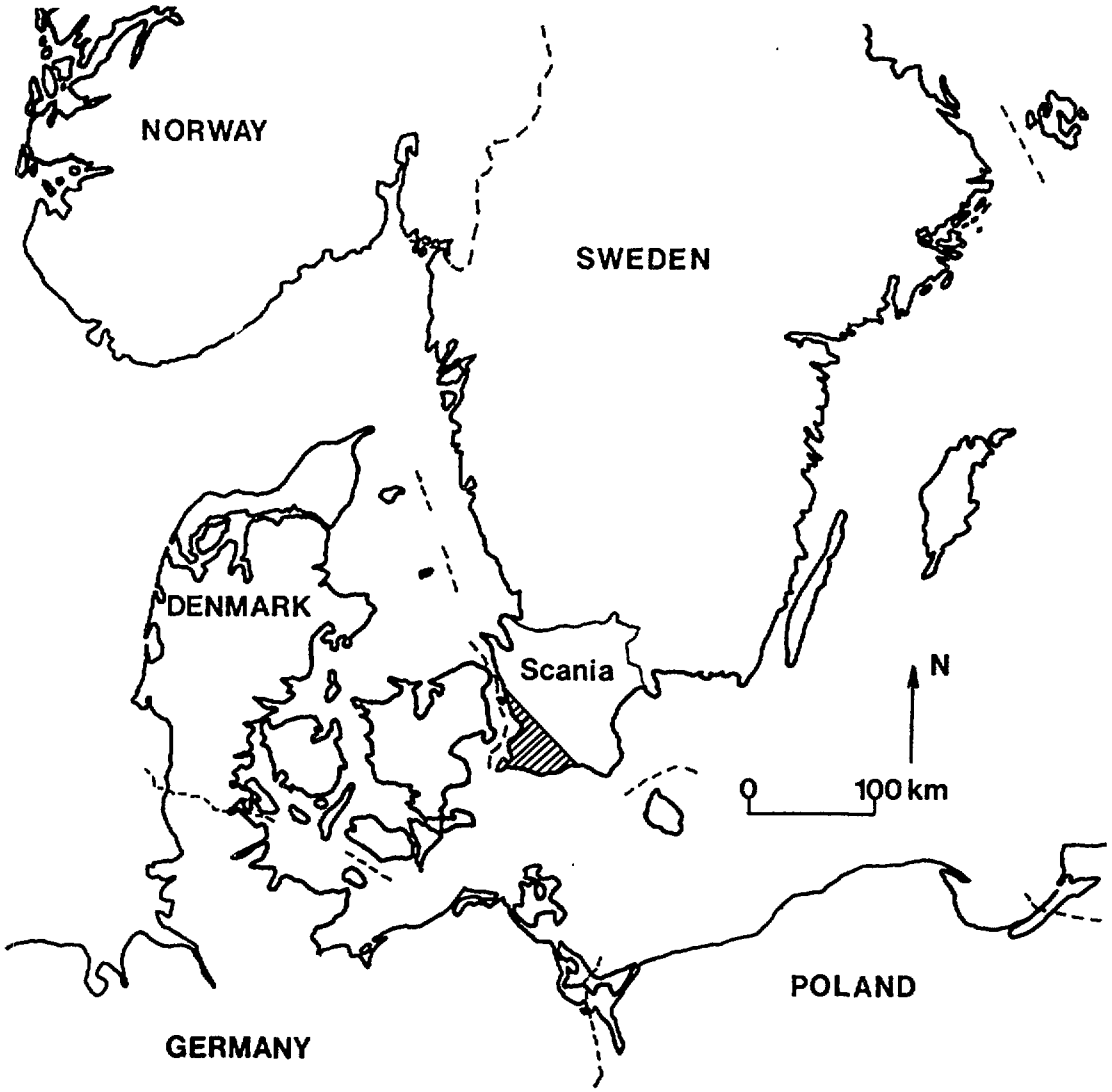

Figure 1: *The hatched domain in southwestern Scania, the southernmost province of Sweden, is the area being investigated.*

movement, marine transgression and sedimentation. Today, these sediments have been petrified and form a sequence of sedimentary rocks up to three kilometres thick. This sequence is dominated by deposits from the Upper Cretaceous, probably due to a comparatively rapid subsidence and sedimentation during this period (Bjelm, Hartlén, Röshoff, Bennet, Bruch, Persson & Wadstein, 1977). The upper bed-rock consists mainly of Danian limestone.

The morphology of the upper bed-rock, shown in figure 2, is almost completely masked by Quaternary deposits. These deposits are only a few metres thick at the Romeleås horst and along the coasts. Towards the Alnarp valley the Quaternary deposits become thicker and the observed maximum is 183 m at Lemmeströtorp, situated in the southeastern part of this depression (Gustafsson, 1978).

The deep sediments within the Alnarp valley consist mainly of fluvial deposits, called Alnarp sediments. At the bottom of the depression they consist predominantly of gravel and sand. The sediments become progressively more fine-grained upwards and the main part of the Alnarp sediments is made up of fine sand and silty fine sand. It is assumed to have been deposited by a big river flowing from the south-east in the Alnarp depression (Holst, 1911). This happened about 25000 to 30000 years ago, during an interstadial, a warmer substage, of the latest glacial period (Weichselian). At that time the sea-level is assumed to have been about 60 m lower than today, which would explain the position of the sediments. Later, silt and clay have been deposited on top of the layers of fine sand (Ringberg, 1980).

Figure 2: *Map showing the relief of the upper surface of the bed-rock in southwestern Scania (after Gustafsson & Teeling, 1973). All values in metres above sea-level.*

The Alnarp sediments, as well as the bed-rock on both sides of the Alnarp depression, are in general overlain by Late Weichselian tills (see figure 3). The composition of the different beds of till and the total thickness of till vary markedly, both vertically and horizontally. This variation is an effect of the complex glacial history in this area. Ice masses probably arrived from the north as well as from the east and the south only during the last part of the Weichselian, approximately 25000 to 13000 years ago. Furthermore, there are sometimes fluvial or glaciofluvial sediments between the different beds of till. These sediments have been deposited during ice-free periods when temporary deglaciation occurred.

The main groundwater reservoir within the hydrogeological system of southwestern Scania is formed by the uppermost part of the limestone bed-rock, which is relatively fissured. The comparatively coarse-grained Alnarp sediments are hydraulically connected with the limestone reservoir and they are therefore also included in this confined aquifer. The principal inflows to

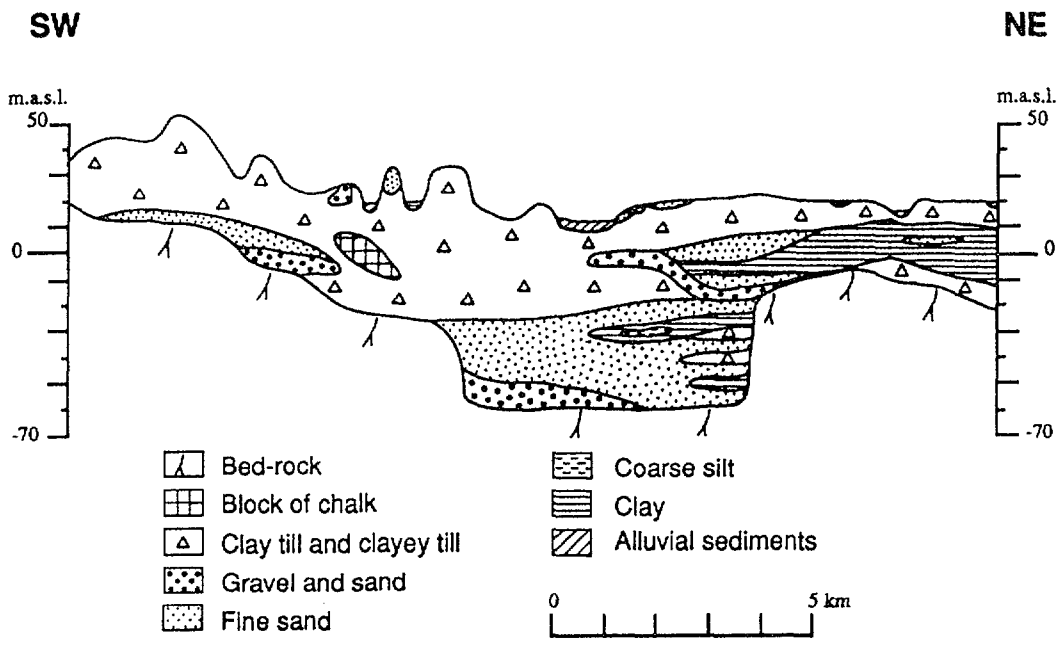

Figure 3: *Simplified geological cross-section (SW-NE) in the northwestern part of the Alnarp valley close to Staffanstorp (after Ringberg, 1980).*

and outflows from the main aquifer of the area of investigation are shown schematically in figure 4. The aquifer is chiefly supplied by:

1) Infiltration on and along the Romeleås horst. It is probably the relatively high altitude, the thin cover of comparatively permeable till, the fractured nature of the rocks and the steeply tilted sedimentary layers which together make this area one of the major zones of recharge.

2) Vertical leakage from small and shallow aquifers situated in the uppermost deposits of the hummocky moraine region in the centre of the area of interest. Here, the altitude is relatively high, the hummocky morphology reduces the surface run-off and the uppermost Quaternary deposits consist mainly of comparatively permeable sandy or clayey sandy tills. All these features facilitate the recharge of the main aquifer in this region.

3) Vertical leakage from small and shallow aquifers in the lowlands outside the two zones of recharge mentioned above. However, in these areas the rate of infiltration towards the main aquifer is very sensitive to changes in groundwater exploitation and it has therefore varied greatly with time. Nevertheless, most of the recharge of the main aquifer seems to occur here today.

The principal aquifer chiefly discharges by:

1) Groundwater extraction in wells situated in the Alnarp sediments and in the upper part of the limestone bed-rock. Apart from a few fluctuations, the exploitation has increased since the beginning of this century. Today, this exploitation causes the biggest outflows of groundwater from the main aquifer.

2) Upward leakage from the main aquifer towards shallow, phreatic aquifers, which gives rise to marshy tracts or springs in local depressions. This phenomenon was relatively common in large parts of southwestern Scania at the beginning of this century. Today, this type of outflow occurs only in small zones of the flat lands north, west and south of the hummocky central area.

3) Groundwater discharge into the Baltic Sea and the Sound, as the gradient of the hydraulic head in the main aquifer causes a flow directed towards the coast and the semipervious layers overlying the aquifer are usually relatively thin in off-shore coastal areas.

As mentioned above, the size of some of the inflows to and outflows from the main aquifer have varied a lot with time. The major reason for this is the increase of groundwater extraction last century, which has resulted in a corresponding decrease of the hydraulic heads.

However, the head of the main reservoir has chiefly been lowered in the vicinity of the wells exploited, that is, in particular around the northwestern part of the Alnarp valley, but also in the western and southern lowlands. About one hundred years ago, there was mainly upward leakage from the main aquifer in these areas. Today, most of the recharge of the aquifer in the Alnarp sediments and the uppermost Danian limestone seems to occur here. The lowered hydraulic heads have probably also reduced the groundwater discharge into the sea.

In the central parts of the area of investigation the long-term piezometric records concerning the main aquifer display only relatively small fluctuations. Consequently, the recharge conditions have probably not changed very much here.

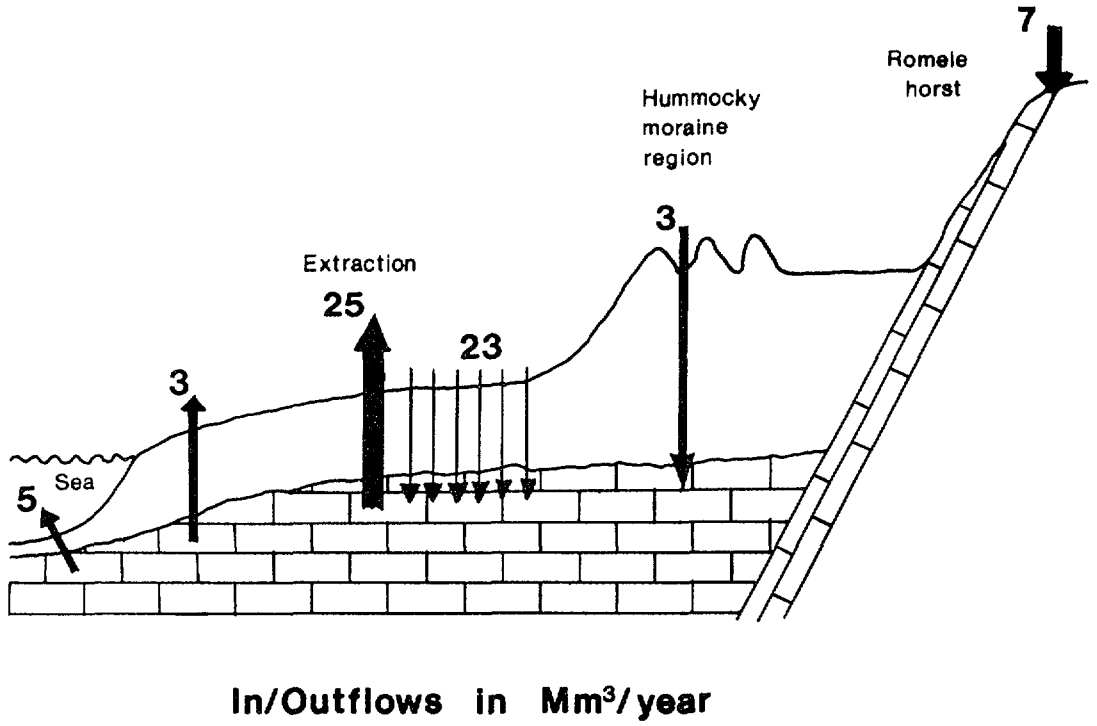

Figure 4: *Schematic representation of the principal inflows to and outflows from the main aquifer in southwestern Scania, approximating the situation in about 1970.*

5. ENVIRONMENTAL ISOTOPE CONCENTRATIONS

5.1 Oxygen-18 and deuterium

37 samples of groundwater from 32 wells have been analysed with respect to the stable isotopes of oxygen-18 and deuterium (Barmen, 1989). 25 of the sampled wells yield groundwater from the main aquifer.

Burgman, Calles & Westman (1987) and Calles & Westman (1989) have studied the isotopic composition of precipitation in Sweden. They have recorded mean annual values of about -9.7‰ for $\delta^{18}O$ and -69‰ for $\delta^{2}H$ at Arup, some ten kilometres northeast of the investigation area. The major part of this area has a more maritime climate than at the sampling station. Therefore, the isotopic composition of the precipitation in the area of interest is probably slightly heavier than at Arup.

Burgman, Eriksson & Westman (1983) claim that the isotopic composition of the groundwater in southern Sweden should essentially reflect that of the mean annual precipitation. The major recharge in the area of interest is assumed to take place during the autumn, when the

isotopic composition of precipitation is usually close to the annual mean and the evapotranspiration loss is relatively small.

The isotope contents of the analysed groundwaters agree very well with this argumentation. Almost all $\delta^{18}O$ values are close to -9‰ (see figure 5) and the $\delta^{2}H$ values are about -65‰. The spatial variations and the differences between the reservoirs are very small. Therefore, the stable isotope contents do not seem to be very suitable for regional groundwater flow modelling in southwestern Scania. This was to be expected as there are comparatively small variations in the area of interest as regards climate and altitude.

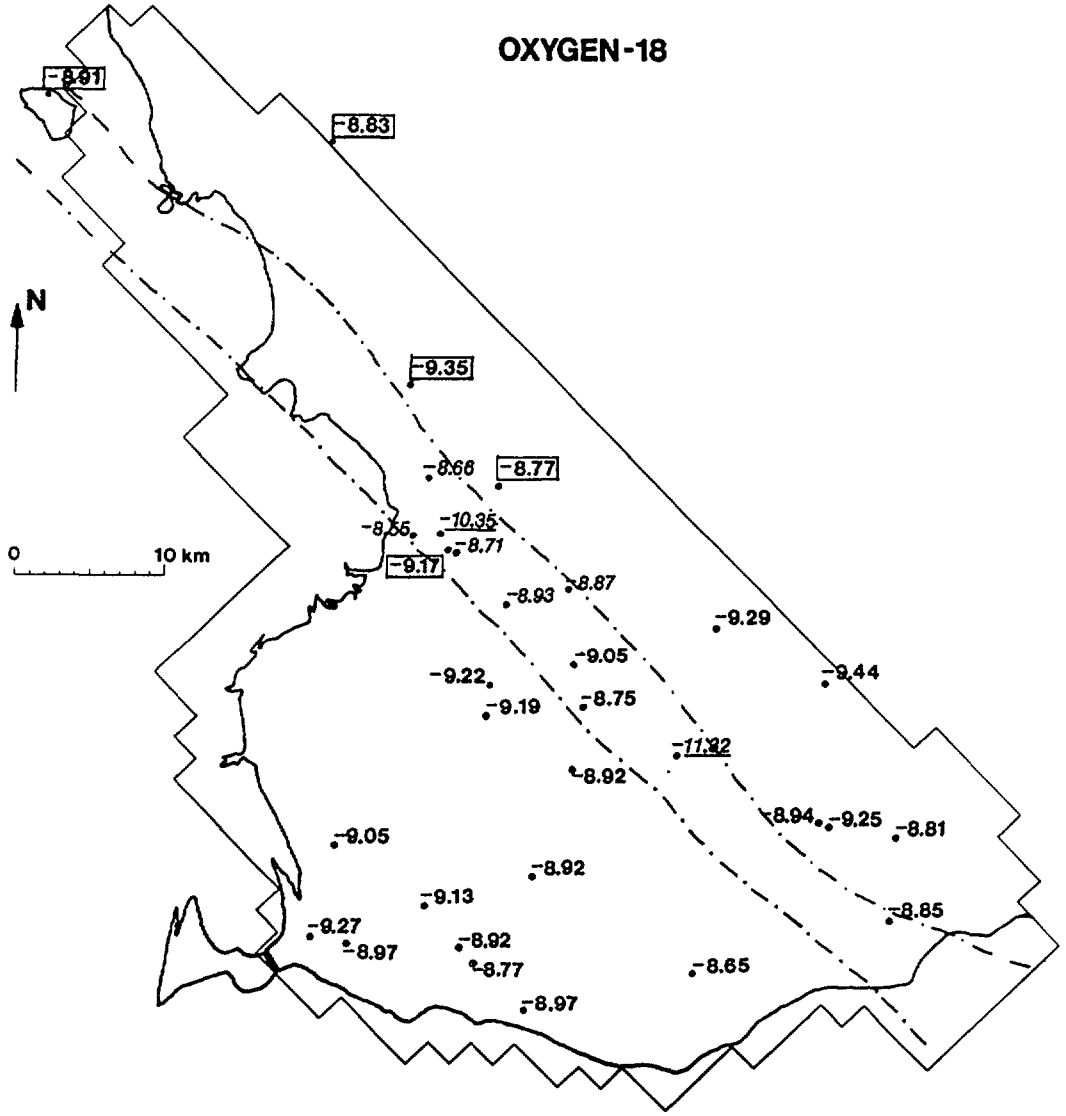

Figure 5: *Distribution of the oxygen-18 contents in groundwaters sampled by Barmen (1989). Figures in boxes represent shallow aquifers, while figures in italics represent groundwater from the Alnarp sediments. Two very low values are underlined and discussed in section 5.4. The other values are for water from the rest of the main aquifer. All values are given as $\delta^{18}O_{SMOW}$ in per mil.*

5.2 Tritium

There are very few measurements of the natural tritium contents in precipitation from before 1952. Since that year, the tritium from nuclear weapon tests has overshadowed the natural production by some orders of magnitude. However, it can be assumed from the general data presented in Fritz & Fontes (1980) that the background level in southwestern Sweden should be

about 20 TU. Perers & Johansson (1980) and Sevel, Kelstrup & Binzer (1981) have carried out hydrogeological investigations in or in the vicinity of the area of interest. They claim that the tritium concentration in precipitation was probably relatively constant before 1952, with an average close to 10 TU. Saxena (1990) is of the opinion that these pre-bomb values might have been as low as about 2-4 TU, according to estimates based on analyses of old wines.

In this study an average tritium concentration of 18 TU in precipitation before 1952 has been adopted. In a few cases an alternative value of 10 TU has also been used. According to the references mentioned, both of these values might be somewhat too high. However, whether 4, 10 or 20 TU is adopted as an average for the period before 1952 has a comparatively small influence on the interpretation of today's tritium concentrations in the main aquifer.

Also as regards the tritium contents in precipitation after 1952 in the area being studied, unfortunately only relatively few measurements exist. The only ones available for this work have been undertaken on precipitation collected at Skurup in the southeastern part of the investigation area. Nevertheless, it is usually possible to make highly valid extrapolations from other sampling sites with similar geographical conditions. By means of such extrapolations the annual average tritium concentrations in precipitation in southwestern Scania have been estimated. The estimations are based on correlations between records from the sampling stations Skurup and Huddinge in Sweden and Taastrup and Odum in Denmark. Values for years without measurements in those places have been extrapolated from the long tritium records in Ottawa and Vienna.

Groundwaters in the area being studied have been sampled and analysed with respect to tritium since the early sixties, as reported by Nilsson in 1966. The general results of these analyses and the detailed results of some 100 other tritium analyses have been available for this work. Most of the latter data have been collected in the hydrogeological mapping of southern Sweden (Gustafsson, 1972, 1978, 1981 and 1986) or as a part of the groundwater monitoring program of the Swedish Geological Survey (SGU). In addition, a further 22 wells in southwestern Scania have been sampled for tritium content (Barmen, 1989). Finally, samples from three wells at Grevie, taking groundwater from the Alnarp sediments for the Malmö water-works, were analysed in 1991. As before, the conditions within the main aquifer were the main focus and the vast majority of the sampled wells yield groundwater from this aquifer.

A comparatively large number of samples for tritium analyses were collected in about 1971. The results of the analyses regarding groundwater from the main aquifer are shown in figure 6. Tritium data also from shallow aquifers are available in the archives of the Swedish Geological Survey. 24 samples were collected in 9 wells in the southeastern part of the investigation area over the years 1973-1975. In most of the samples the tritium concentration exceeds 50 TU. The maximum tritium content is 209 TU and the average of these samples is about 75 TU. Furthermore, the Danish Geological Survey (DGU et al, 1975) have also collected samples for tritium analysis around the Danish part of the Alnarp valley. They have found no measurable tritium in groundwater from the Alnarp sediments and the limestone below it. On the other hand, the tritium concentration in the water of Lake Esrum has been determined to be 104 TU.

The data on the distribution of tritium in groundwater may be summarized and interpreted as follows. The outlines of this interpretation are more or less in accordance with the opinions of, among others, Nilsson (1966), Gustafsson (1972, 1978, 1981 and 1986), Perers & Johansson (1980) and Brinck & Leander (1981). The mentioned average groundwater circulation times are roughly estimated by a one-dimensional piston flow model, usually leading to under-estimates. The concentrations are comparatively high in samples from lakes and shallow aquifers. High tritium values have also been found in groundwater from the main aquifer along the coasts and along the northeastern boundary of the area in question. In these zones the Quaternary deposits are comparatively thin and in the southwestern coastal district the extraction of groundwater from the main aquifer is extensive. Some samples from the central zone southwest of the Alnarp valley also showed somewhat enhanced tritium contents, in particular in 1971, but also in 1982. At most of these sampling points the Quaternary deposits were locally comparatively thin and also permeable. In the cases mentioned the tritium concentrations were at least 5-10 TU and often more than 20-30 TU.

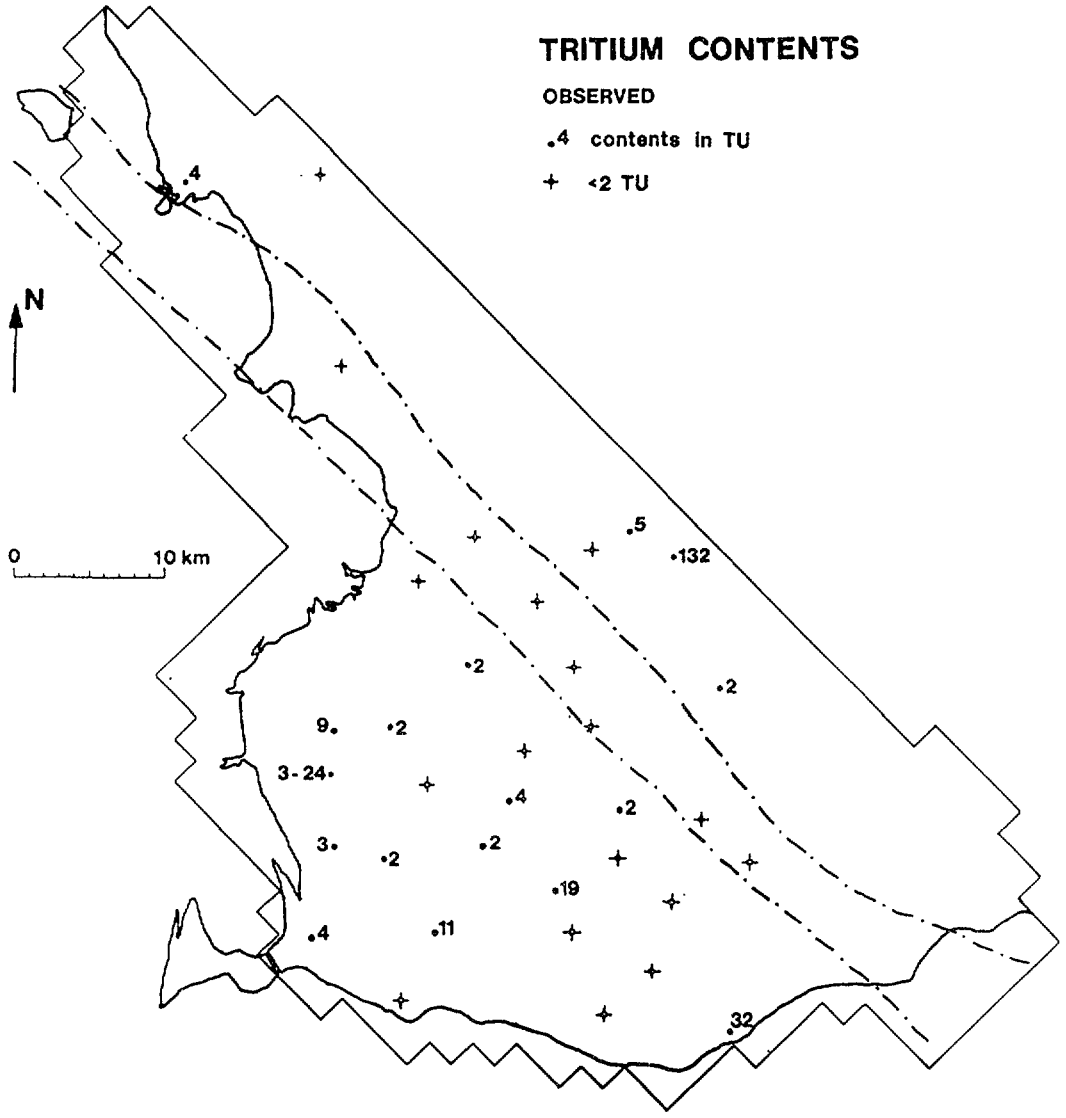

Figure 6: *Tritium contents measured in groundwater from the main reservoir in southwestern Scania in 1970 and 1972 (from Gustafsson, 1972 and 1978). Four values from 1974 and three from 1975 are also included (data from Gustafsson, 1978 and 1981, and also unpublished data from the Swedish Geological Survey). The interval 3-24 TU, marked for a sampling site in the southwestern part of the area, indicates that the tritium contents have varied between these values in seven samples taken between 1970 and 1975.*

The conclusions to be drawn from observations of enhanced tritium contents in the main aquifer may be developed further at places where the local hydrogeological conditions are well known. In certain zones, it is plausible that the high tritium values indicate that groundwater withdrawals have led to a more rapid turn-over due to a stimulation of recharge from shallow aquifers and surface waters.

5.3 Carbon-14

There are many processes which can affect the carbon budget of a groundwater. Consequently, it is usually not a straight-forward and trivial task to interpret the results of carbon-14 analyses of groundwater samples. Several attempts to overcome these problems have been made during

the past thirty years and a number of possible correction procedures have been presented by different authors.

Methods for carbon-14 corrections are usually applicable on either "closed-" or "open system" conditions and in some cases also on mixed conditions, which is perhaps the most realistic description of many real systems. In an open system with respect to $CO_2(g)$, carbonate dissolution occurs while the solution remains in contact with an abundant gaseous environment of constant pCO_2, such as the atmosphere. In contrast to this, the dissolution proceeds in the absence of $CO_2(g)$ in a closed system. Consequently, the equilibrium pCO_2 of the groundwater will decrease, when carbonic acid is consumed in this latter case.

The main aquifer of southwesternmost Sweden can generally be characterized as a closed system consisting of, or in close contact with limestone. According to Fontes (1985), the correction methods presented in Pearson & Hanshaw (1970) and in Fontes & Garnier (1979) should be the most suitable ones in this type of situation. The two methods give similar results for most samples collected in the area of investigation. ^{14}C activities estimated by the method of Fontes & Garnier with feasible input parameters are presented in figure 13. A few values from wells penetrating deep into the limestone and with very high carbon-13 contents have been calculated by the correction process outlined by Wigley, Plummer & Pearson (1978). More information on the input values for these figures, as well as some alternative results, are presented in Barmen (1992).

Some of the sampled wells penetrate deep into the limestone of the main reservoir and show high contents of ^{13}C. These features may indicate that incongruent dissolution and reprecipitation of calcite occur in very slowly circulating groundwater. In such a situation the correction procedure presented by Wigley, Plummer & Pearson (1978) would be adequate and a slightly simplified version of it has been applied to the samples here. To estimate the effects of incongruent dissolution and reprecipitation better, more detailed geochemical information on the groundwater system being studied is needed. If the influence of such processes is substantial, many of the corrected ^{14}C activities presented in figure 13 are likely to be too low.

The effect of fractionation on the isotopic composition of the CO_2 in the soil and the carbon dissolved in the groundwater has probably not reached equilibrium in the water recharging the main aquifer, according to general descriptions by Pearson & Hanshaw (1970). As a consequence, the activities obtained by the method of Fontes & Garnier (1979) and presented in figure 13 may be slightly too low.

Finally, another few words of caution. The increased exploitation of the main aquifer in southwestern Sweden over the past century has in general changed the direction of flow through the aquitardeous layers. Therefore, the groundwater extracted may first have been moving slowly upwards for a very long time and then increased withdrawal has caused a principally downward migration towards an exploitation well. This means that the measured ^{14}C activities in the sampled groundwaters do not reflect today's hydrogeological situation. The activities are lower and the estimated "ages" are older than they would have been had they represented the actual average circulation times of the main aquifer. This problem is most severe for the interpretation of radioisotopes with relatively long half-lives, a point which has been well described by Geyh & Backhaus (1978) and Sudicky & Frind (1981).

These authors also treat the related difficulty that water with very low ^{14}C activities in stagnant groundwater bodies may diffuse into a relatively young groundwater. Such relatively old water might reside in the smallest pores or fissures of the clay tills and limestones. Thereby, the groundwater velocities will seem to be lower than what could be assumed from the hydrodynamic conditions and the kinematic porosity.

However, these problems should not affect the comparisons between the corrected, measured ^{14}C activities and the simulated ones discussed in the following. The simulations of the transient evolution of the flow and transport phenomena will start by calculating a steady-state situation in 1840, prior to any exploitation of the main reservoir. Furthermore, the simulations should use property sets with porosities higher than normally estimated as being kinematic ones, to compensate for diffusion effects from groundwater residing in the smallest pores and fissures of the clay tills and limestones of the area being studied.

5.4 General results from the isotopic investigations

Very shallow aquifers are likely to have short, mean turn-over times, perhaps of a few years, and contain recently recharged water. The average circulation times in aquifers in inter-morainic sediments are estimated to be somewhat longer, of the order of a few hundred years.

The groundwaters in the main aquifer in the upper part of the limestone outside the Alnarp valley and in the Alnarp sediments usually seem to have a much lower rate of renewal. Mean turn-over times range from more than 40 years, estimated from tritium measurements, to 500 - 2500 years, according to corrected carbon-14 activity. Nevertheless, in coastal zones, along the northeastern boundary and also in a few other localities in the area being investigated, where the Quaternary deposits are relatively thin and permeable, recently recharged groundwaters have been detected in the major aquifer. These high contents of radioisotopes may indicate that groundwater withdrawals have led to a more rapid turn-over due to a stimulation of recharge from shallow aquifers and surface waters and that the risk of pollution of the main aquifer has increased. Conclusions based on data from locations where the hydrogeological conditions are better known could obviously be further elaborated.

Groundwater sampled in deep wells, penetrating at least several tens of metres of the Danian limestone, often seem to represent reservoirs with very long circulation times. The chemical contents are high and the concentration of radioisotopes is very low. Estimates based on ^{14}C activity indicate average turn-over times of 4000 - 12000 years. Moreover, two samples from this type of reservoir below the Alnarp valley have very low contents of ^{2}H and ^{18}O (see figure 5). This feature indicates that these groundwaters, at least partly, have been recharged during a period with generally colder climate. The number of observations is too small and the interpretation tools are not accurate enough to make these observations convincing. Nevertheless, one can speculate whether groundwater influenced by recharge during the final stage of the latest glaciation might have been retained in hydrogeological "pockets" within the main aquifer.

The contrasts between the ^{2}H and ^{18}O concentrations in the groundwater from different parts of the aquifer system are too small to be suitable for the following regional transport modelling. There is not even an indication of an admixture of sea-water, rich in these stable isotopes, in groundwater from wells situated close to the coasts.

As regards tritium, there are significant contrasts between the different parts of the investigated groundwater system. However, the contrasts within large areas of the main aquifer are small. Due to the short half-life of tritium and to the usually, long mean turn-over time of this aquifer, most samples from it show very low contents of tritium. This may reduce the possibilities of drawing reliable conclusions from a comparison with the results of the transport modelling. Furthermore, it would be very valuable to collect samples for tritium analysis from several different levels within the aquitardeous layers. Such results could probably elucidate the recharge processes in the main aquifer.

Finally, it has been emphasized that it is not a trivial task to interpret ^{14}C contents from a system including limestones and clay tills comparatively rich in lime. In spite of the many uncertainties related to such an interpretation, contrasts in the concentrations of the same type as for tritium may be detected. Using both of these radioisotopes in comparisons with the subsequent isotope transport modelling is probably the best way to benefit from the results of isotope investigations.

6. GROUNDWATER FLOW MODELLING

The computer code NEWSAM is founded on a classical phenomenological, macroscopic description of groundwater flow through porous media. It is assumed that the flow within an aquifer takes place only in a quasi-horizontal plane, and that water passes aquitards only in the perpendicular direction. With this approximation one can avoid treating a real three-dimensional flow problem, which is a much more laborious task. NEWSAM may be used to obtain an

approximate solution by means of finite difference techniques. The code utilises nested squares of variable size for the subdivision of the area of interest into discrete cells. The mean value of the hydraulic head is calculated for each cell or mesh and for each time step considered. For a given distribution of aquifer properties and defined initial and boundary conditions, there exists only one solution to the flow equation above. The reader is referred to Ledoux (1986a and b) and Marsily, Ledoux, Levassor, Poitrinal & Salem (1978) for a more detailed description of the principles behind the finite difference computer code NEWSAM.

6.1 Subdivision into layers and discrete meshes

The major aquifer of the studied hydrogeological system is confined and situated in the upper part of the limestone bed-rock and in the Alnarp sediments. This groundwater aquifer is in general separated from surface water and local, shallow aquifers by thick layers of till, which function as aquitards. The shallow reservoirs are represented by layer no. 1 of the model, while the bottom layer, no. 2 of the model, corresponds to the main aquifer. The elements of layer no. 2 are assigned leakage coefficients, which govern the vertical exchange of water between the two strata. In this manner the variable thickness and vertical hydraulic conductivity of the almost impervious clayey tills and clay tills are taken into account.

The two superposed layers of the model have been subdivided into meshes of up to four different sizes. In general, the small mesh sizes have been used in zones where the available information is relatively dense and/or where it is of particular interest to obtain comparatively detailed and reliable results from the model calculations. The big meshes, on the other hand, have chiefly been positioned in zones where the existing hydrogeological data are relatively scarce and/or where it is less important to obtain detailed results from the model calculations.

As regards the bottom stratum, the grid-net has been designed with the situations of wells with big groundwater withdrawals and wells with long piezometric records as a basis. In the first case, big piezometric gradients in the vicinity of the pumped wells motivate small elements. In the second case, the meshes have to be small to make possible relatively reliable comparisons between the measured piezometric levels and those derived from the model. Areas without the above types of wells are subdivided into big meshes (see figure 7).

6.2 Assumptions and boundary conditions

Average values of transmissivity, the leakage coefficient and storage coefficient concerning each mesh in the model are required for the numerical calculations. In addition, an estimate of the real, mean piezometric level of each mesh and for each time step considered is necessary for comparison with the corresponding, calculated values and to make possible the calibration of the flow model. However, the number of measurements of hydrogeological properties and variables of state is very small compared to the number of elements in the model. Therefore, it is necessary to make considerable assumptions and approximations so as to be able to estimate the mentioned input data for each mesh. A general problem is that the size and complexity of the hydrogeological system demands a dense subdivision of the model into small elements, while the existing density of observations is not sufficient to permit such a high mesh frequency.

The estimations of input data for each mesh have mainly been done by hand in a somewhat subjective manner. As the measurements of hydrogeological properties are relatively few, the estimates have been based on qualitative hydrogeological information, mainly derived from Gustafsson (1972, 1978, 1981 and 1986). Another major source of information are the almost 3000 drilling records of wells in southwestern Scania, which are stored in the Well Archives of the Swedish Geological Survey. They usually comprise a fairly good description of the geological stratification along the bore-holes. Piezometric observations and results from well capacity tests are also often included. Assisted by this additional information all meshes of the model have been assigned tentative and approximate, but hydrogeologically reasonable values of transmissivity, leakage coefficient, storage coefficient and initial piezometry. The assessments of the boundary conditions have been made in a corresponding way.

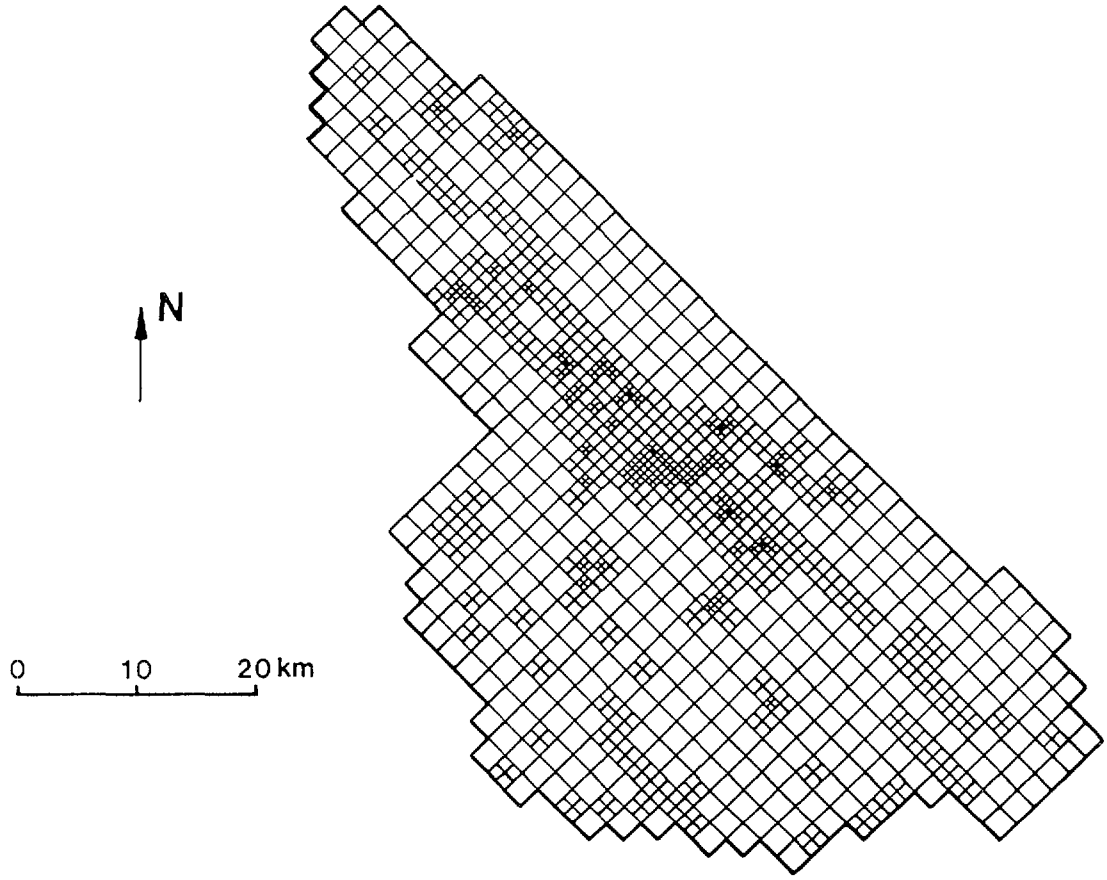

Figure 7: *Subdivision of the bottom layer into 1238 meshes of four sizes. This stratum of the numerical groundwater flow model represents the main aquifer in the area of interest.*

Another simplification in the model is that no seasonal variations of, for instance, pumping rates, infiltration and piezometric levels are taken into consideration. Only annual averages have been judged as relevant for this investigation, which mainly considers long-term hydrogeological processes on a regional scale. In addition, detailed information about seasonal variations is available only for a limited number of places and variables over relatively short periods.

As will be discussed below, the recharge processes are highly simplified in this model. The piezometric level of the uppermost layer is regarded as constant with time. Therefore, apart from the leakage coefficients, it is only the difference between this constant value and the calculated piezometric level of the main aquifer, which determine the amount of recharge to the bottom layer of the model.

Interactions between surface water and groundwater is almost neglected in the flow model. Nevertheless, the piezometric levels are prescribed where there are lakes and rivers.

It should also be mentioned that the bottom layer of the model does not have any hydraulic contact with reservoirs situated below it. In reality, a certain groundwater exchange of this type may take place, in particular along fissured fault zones. The reservoirs situated at great depths have been neglected, as their global influence on the system of interest is most likely relatively small. Moreover, there is hardly any information available on their hydraulic properties and hydrogeological status.

One of the major boundary conditions of the groundwater flow model is that the water table of the upper layer is prescribed in each mesh. The piezometric level of this layer varies spatially but it is regarded as stationary. The average ground surface level of every element has been

approximated by means of the topographical maps on the scale 1:50000. The mean piezometric level has been determined somewhat subjectively to be located 1 - 6 m below the ground surface level of the mesh. No horizontal flow occurs in the local phreatic aquifers due to the completely prescribed piezometry of the upper layer.

In fact, the main purpose of layer no. 1 of the model is to simulate the recharge of the principal aquifer. If the hydraulic head on the bottom stratum is situated below the water table in a certain place there will be a downward vertical flow in the model, that is, recharge. The prescription of the piezometric levels of the upper stratum means that a mesh of layer no. 1 will be supplied with water from "outside" until flow and mass balance is obtained within the whole system of meshes. If the hydraulic head on the bottom stratum is situated above the prescribed water table in a certain position, groundwater will be transported upwards and leave the model from the upper layer in the same manner. The magnitude of the recharge or discharge will be proportional to the vertical piezometric gradient and also to the leakage coefficient representing the aquitardeous layers between the two strata of the model.

While the piezometric levels of all the meshes of the upper layer are prescribed, there are no meshes with completely prescribed piezometric head in the bottom layer. The northeastern limit of the bottom layer is defined as a boundary where no horizontal groundwater flow may pass the border. However, the area on and along the Romeleås horst is a preferred zone of infiltration and recharge. The hydrogeological situation along this border, with a relatively big vertical inflow to the main aquifer, is reproduced by the model by means of a high elevation of the prescribed piezometric levels of layer no. 1. In addition, the meshes at the boundary are assigned big leakage coefficients to take into account the fact that the aquitardeous layers are comparatively thin and permeable there.

6.3 Results from groundwater flow modelling

Boundary conditions with prescribed piezometric levels and drainage meshes in accordance with the previous description have been applied in the following. Furthermore, the storage coefficients of the main aquifer were assumed to be uniform and equal to $5 \cdot 10^{-4}$ in the transient simulations. After various tests, an initial time-step of 168 hours has been found to give a satisfactory convergence of the non-stationary numerical calculations. The time-step has been increased progressively by the square root of two in the calculations for each period - normally a year.

After some adjustments of the estimated tentative transmissivities and leakage coefficients, the resulting distribution of values was assumed to represent the real groundwater system relatively well, as a fairly good correspondence between model-derived and observed steady-state and transient piezometric values was obtained in most parts of the area of the investigation, as can be seen in figures 8 and 9. The difference between calculated and observed values is usually less than two metres in these figures. However, as mentioned earlier, several different distributions of transmissivities and leakage coefficients could probably have led to an acceptable piezometric fit, due to the complexity of the modelled system and the relatively small number of observations. Nevertheless, the alternating calibration procedure considering steady-state as well as transient conditions, significantly limits the number of adjusted combinations possible.

It is also interesting to compare the piezometric map representing steady-state conditions in 1970 derived from the model, with the corresponding one obtained after a transient simulation of the piezometric evolution 1840-1970. The two maps are very similar, which strengthens the conclusion that the groundwater flow model is fairly well adjusted.

Another way to try to verify the results of the flow model is to compare the different components of the water balance of the groundwater system with the corresponding estimates. However, these estimates are relatively rough and it is therefore not possible to make a very accurate verification. Nevertheless, the figures presented in table I indicate that the adjusted groundwater flow model gives reasonable results and also that the results from steady-state and transient simulations are similar. The modelled outflows into the sea are perhaps slightly too

small, while the modelled inflows at the northeastern boundary seem to be slightly too big. This type of flow result can also be used to illustrate how the overall inflow-outflow pattern and magnitude have changed over the past century.

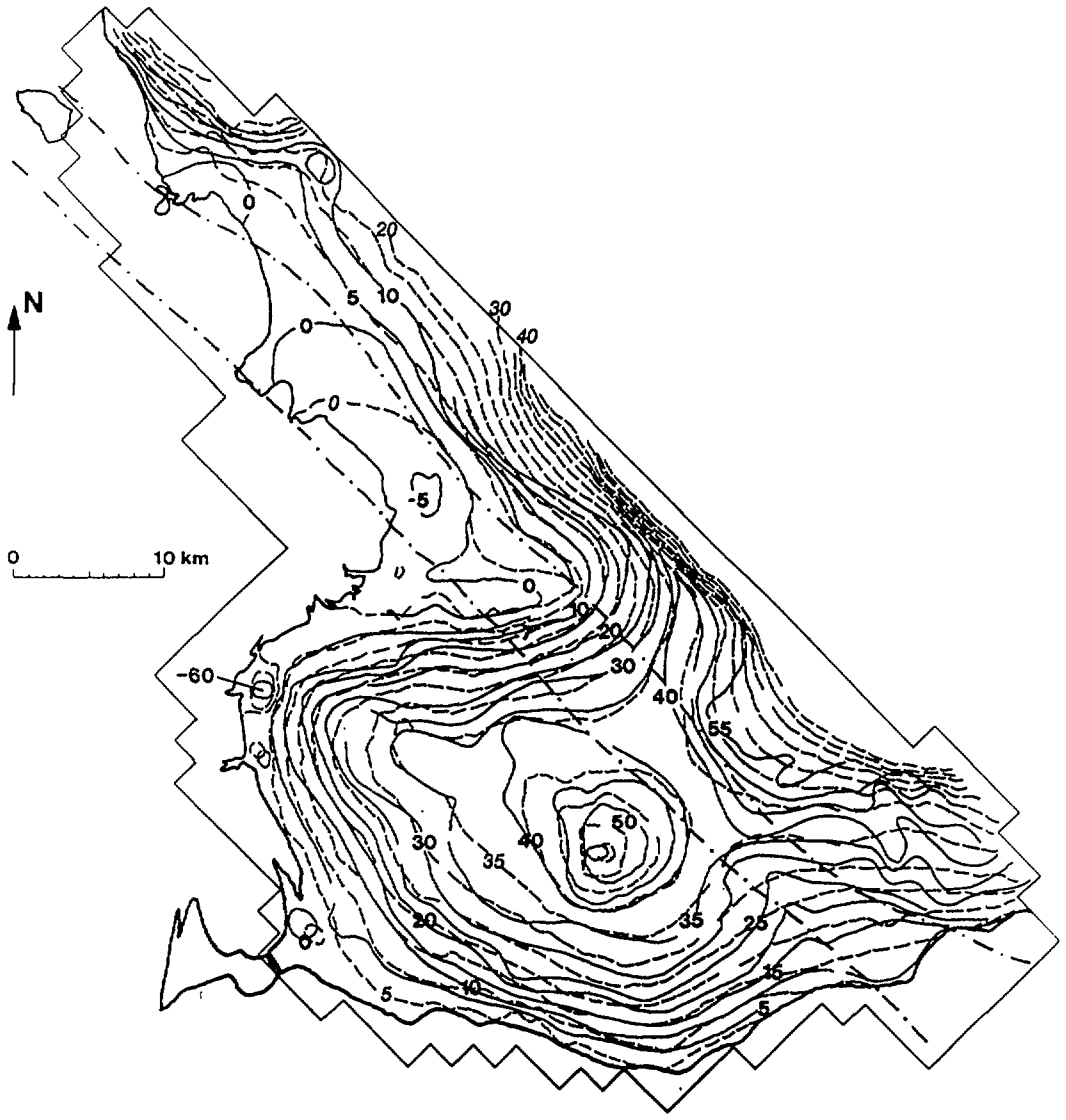

Figure 8: *Piezometric map of the main aquifer, corresponding to the situation in 1970. The dashed lines with figures in italics show the results obtained by steady-state calculations with the adjusted groundwater flow model. They are compared to the piezometric map based on observations (continuous lines). All piezometric values are given in metres above sea-level. The calculated piezometric curves are interrupted at the shore-line to make the presentation clearer.*

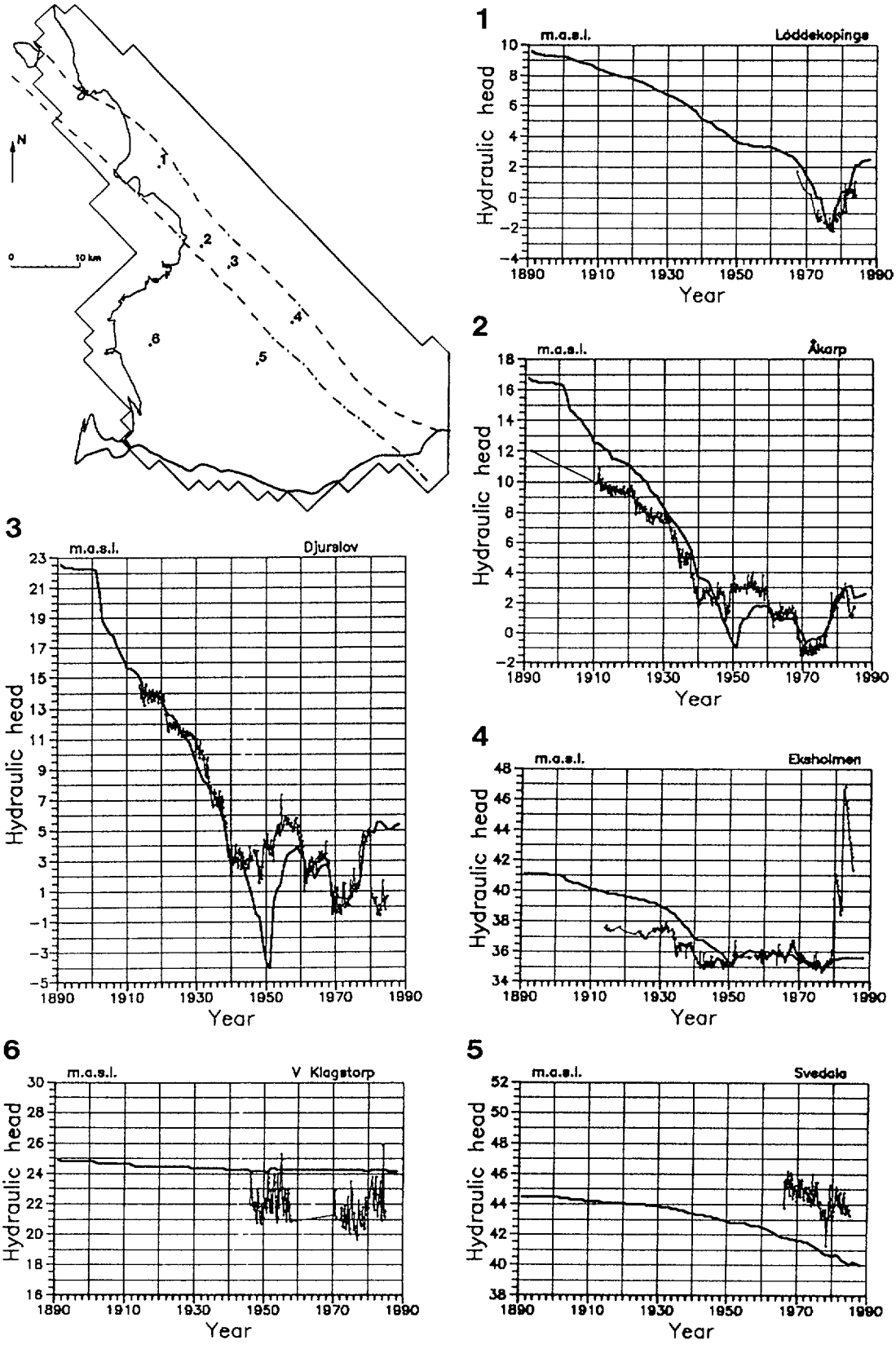

Figure 9: *Piezometric variations in some selected observation wells (thin lines) compared with values obtained by transient model calculations (thick lines). Measurements are marked as small filled squares.*

TABLE I

Calculated and estimated magnitudes of the different componenets of the water balance concerning the main aquifer. All figures are given in Mm^3/year.

Components of the total water balance of the main aquifer	Steady-state model results for 1970	Transient model results for 1970	Estimated values
Limhamn limestone quarry	1.2	1.2	1.2 - 1.5
Klagshamn limestone quarry	0.3	0.3	0.3
Outflow to the sea	5.3	5.4	5 - 8
Extraction from wells	26.8	26.8	26.8
Total outflows	33.6	33.7	33.3 - 36.6
Northeastern boundary	8.0	7.9	6 - 8
Net recharge elsewhere	25.6	25.8	21 - 33
Total inflows	33.6	33.7	27 - 41

7. GROUNDWATER TRANSPORT MODELLING

According to the objectives of this work and the conclusions of section 5.4 our interest will be focussed on the transport of the radioactive isotopes tritium and carbon-14 through a regional groundwater system. It is reasonable to assume that commonly occurring concentrations of tritium and carbon-14 neither change the density of the groundwater, nor modify the groundwater flow. Consequently, the flow equation and the transport equation may be solved one after the other and not with full interaction between the two phenomena.

In general, tritium is assumed not to be subject to any changes, exchanges, or reactions during migration, other than radioactive decay. On the other hand, carbon-14 is known to be influenced by several physical, geochemical, radiological and biological mechanisms. An attempt to correct the measured ^{14}C concentrations for these effects has been made as mentioned in section 5.3.

Ala-Eddin & Magnusson (1991) have shown that in a hydrogeological environment like the one of southwestern Scania, variations in the dispersivity have a relatively big influence on solute transport on the local scale. However, the author's experience from preliminary tests with the computer code METIS (Goblet, 1985) is that the sensitivity to variations in the dispersivity is relatively small on a regional scale. Solute transport is more sensitive to variations of such properties as hydraulic conductivity and porosity. Dispersivities are likely to differ very much among the different geological materials in the area of interest. Furthermore, dispersion coefficients are very difficult to measure or estimate on a regional scale of tens of kilometres. This is particularly true when the time span of interest covers more than 150 years and the groundwater flow pattern has changed markedly during this period. As a consequence, omitting explicitly dispersion from the transport equation will probably give a satisfactory representation of the transport phenomena if our interest is focussed on the major characteristics and behaviour of the regional hydrogeological system over the past century.

The simplifications mentioned will result in the following transport equation:

$$- \mathrm{div}\,(c\,\vec{V}) = n\,(\partial c/\partial t + \lambda c)$$

where c = concentration, as mass of solute per unit volume of solution
$\vec{V}$ = Darcy velocity vector
n = porosity
t = time
λ = radioactive decay constant

According to this description, the transport of the dissolved substances will be in the same direction and with the same velocity as the transport of the groundwater molecules, that is, via advective transport. The isotopes will decrease by radioactive decay as they are transported.

The computer code used for the groundwater flow calculations may also be used for simplified transport simulations. In principle, the code calculates solute transport in accordance with the equation above, approximated by finite differences. Ledoux (1986b) argues that NEWSAM gives a satisfactory representation of transport phenomena if the purpose is to study regional hydrogeological characteristics. In general, it does not provide an accurate simulation of the solute concentrations at every point of an aquifer system. Nevertheless, calculations with this computer code may help to gain an understanding of the regional transport mechanisms. In general, finite difference approximations of solute transport equations may cause a relatively large numerical dispersion. Therefore, it should be emphasized once again that the results presented in the following are to be regarded only as a first approximation of the regional solute transport phenomena.

7.1 Subdivision into layers and discrete meshes

The subdivision used earlier has been extended to a somewhat more fully three-dimensional representation in order to model the transport of isotopes through the groundwater system being studied. The shallow reservoirs are represented by layer no. 1 of the model, in the same way as in the previous sections, while the almost impervious clayey tills and clay tills are now modelled as 14 strata, no. 2 - 15, each 5 metres thick. They are of various sizes to take into account the variable total thicknesses of the aquitards in southwestern Scania. The bottom stratum, layer no. 16 of the model, represents the main aquifer. It is 30 metres thick, which corresponds to the fissured, upper part of the limestone bed-rock and the sandy sediments at the bottom of the Alnarp valley. The positions of some of the 16 layers are shown schematically in figure 10.

It must be emphasized that the model representation of the variable total thicknesses of the aquitard layers is very much simplified and schematized. Only strata classified as clay, clay till and clayey till from drill-hole records are taken into account, for the determination of the above-mentioned number of layers. The transport through other geological materials situated within and below these strata is assumed to occur instantaneously compared to the transport times through the aquitard layers. This assumption is strengthened by the results of more detailed, finite-element calculations executed by Ala-Eddin & Magnusson (1991) for a similar environment. However, the dilution effects on the isotope concentrations of vertical transport run the risk of being under-estimated, as the volume of "old" groundwater remaining in the more coarse-grained layers is neglected by the model.

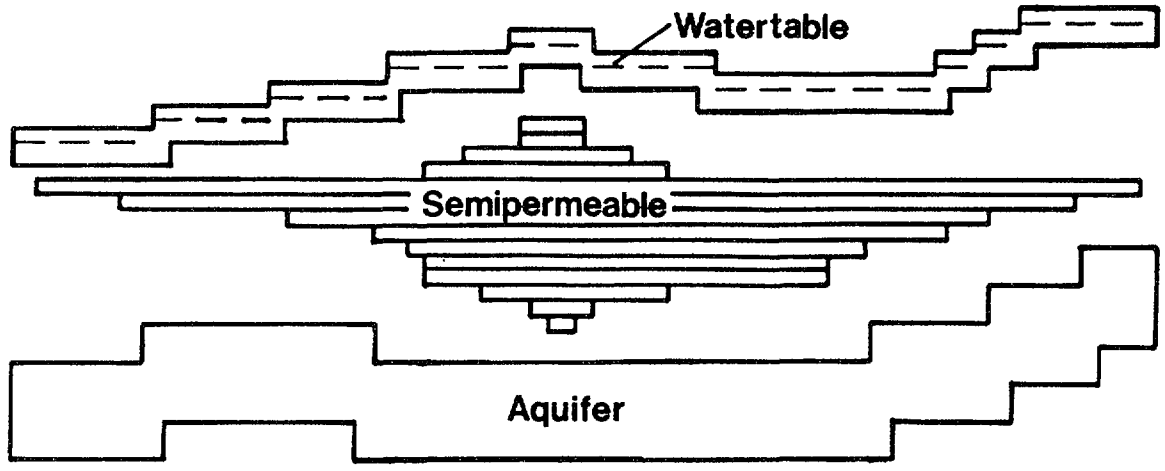

Figure 10: *Schematic positions of the 16 layers of the numerical model of groundwater flow and transport model.*

Leakage coefficients are assigned to all meshes of layers no. 2 - 16, regarding leakage from or to the layer situated above. Their values have been chosen to give the same leakage through the 14 aquitard layers as between the two aquifer layers used earlier. Furthermore, the coefficients have been assumed to be equal in meshes overlying each other. Thus, vertical variations in the leakage properties have not been modelled. However, zones with relatively thin and/or permeable aquitardeous layers in the real geological environment have been represented by few layers with big leakage coefficients in the numerical model.
In addition to the prescribed piezometric levels of the uppermost layer, also the isotopic concentrations are prescribed when simulating transport. The tritium concentrations in the meshes of the uppermost layer have been fixed at 18 TU before 1952. As regards the period after 1952, the tritium concentrations of the uppermost layer have been set equal to the average concentrations in precipitation as estimated in section 5.2. The carbon-14 concentrations in the meshes of the uppermost layer have been fixed at 100 pmc in most of the simulations.

The simulations of isotope transport in the aquifer system of interest have been done under more or less identical conditions as were applied in the groundwater flow simulations. In general, the "adjusted" property set mentioned in section 6 has been used. A situation corresponding to long-term steady-state conditions in 1840 has been estimated. The steady-state calculations have been initialized with zero-concentrations of isotopes in all meshes except for those of the uppermost layer. From the resulting situation the changes until 1988 have been simulated by transient calculations. After 1952 the prescribed isotopic concentrations in the uppermost layer have been changed annually.

7.2 Results from transport modelling

When simulating isotope concentrations in accordance with the equation given above, only the porosity and the radioactive decay constant will be additional input properties compared to the groundwater flow simulations. The latter is in general determined satisfactorily. On the other hand, the porosity values of interest as regards isotope transport are usually much more difficult to determine.

Most porosity measurements concern the total porosity. However, it is the kinematic porosity which is often judged to be the most adequate for solute transport. Unfortunately, it is more complicated to determine this porosity. For instance, it is plausible that the kinematic porosity varies with the hydraulic gradient.
In principle, there is a big difference between the total porosity and what is usually assessed as the kinematic porosity of clay till. The groundwater flow crosses this material relatively slowly. Thus, there will probably be time for equilibration between the truly mobile water and those water molecules, which are, for instance, fixed to the surfaces of geological material or are stagnant in dead-end pores. Consequently, a much bigger fraction of the porosity than the strictly kinematic one will probably be "effective" in the migration of substances. This latter porosity value is believed to be the one which is most reasonable for use in simulations of isotope transport.
On the whole, this discussion shows that it is very difficult to assign porosity values to the meshes of the transport model. Therefore, the sensitivity of the model to variations in the porosity has been investigated. Due to the lack of detailed information and also for simplicity, the porosities have been assumed to be uniform within both the aquitards and the main aquifer. Values within a comparatively wide interval have been tested in the simulations of isotope transport in the area of interest.

Moreover, the calculated tritium contents are close to 0 TU and the calculated carbon-14 contents are between 80 and 100 pmc at almost all sampling points. Therefore, plots of the calculated isotope values against the observed ones give very little information (see Barmen, 1990).

Due to these difficulties, the results of the transport model will be presented mainly as maps of the calculated tritium and carbon-14 distributions in the main aquifer for the selected years.

The corresponding, observed values will also be shown for general comparison. The maps will concern the years around 1971 and 1988, when the isotope measurements were comparatively frequent (see figure 11 and 12).
The general patterns are very similar in the tritium distributions presented in figures 11a-c. Both the calculated and the measured values are enhanced in certain zones along the coasts and along the northeastern boundary, where the aquitard layers are thin. The tritium values are also relatively high here and there in the central areas. However, in the latter case the positions of the high, measured and of the high, calculated concentrations, do not correspond very well. The majority of both the measured and calculated values are much lower than 2 TU. Due to these features, the figures do not make it possible to determine which of the sets of effective porosities used, best correspond to reality. Nevertheless, results from simulations with other sets of properties make it likely that effective porosities of 30% in the clay till and 15% in the main aquifer are the smallest ones which would result in relatively reasonable simulated tritium

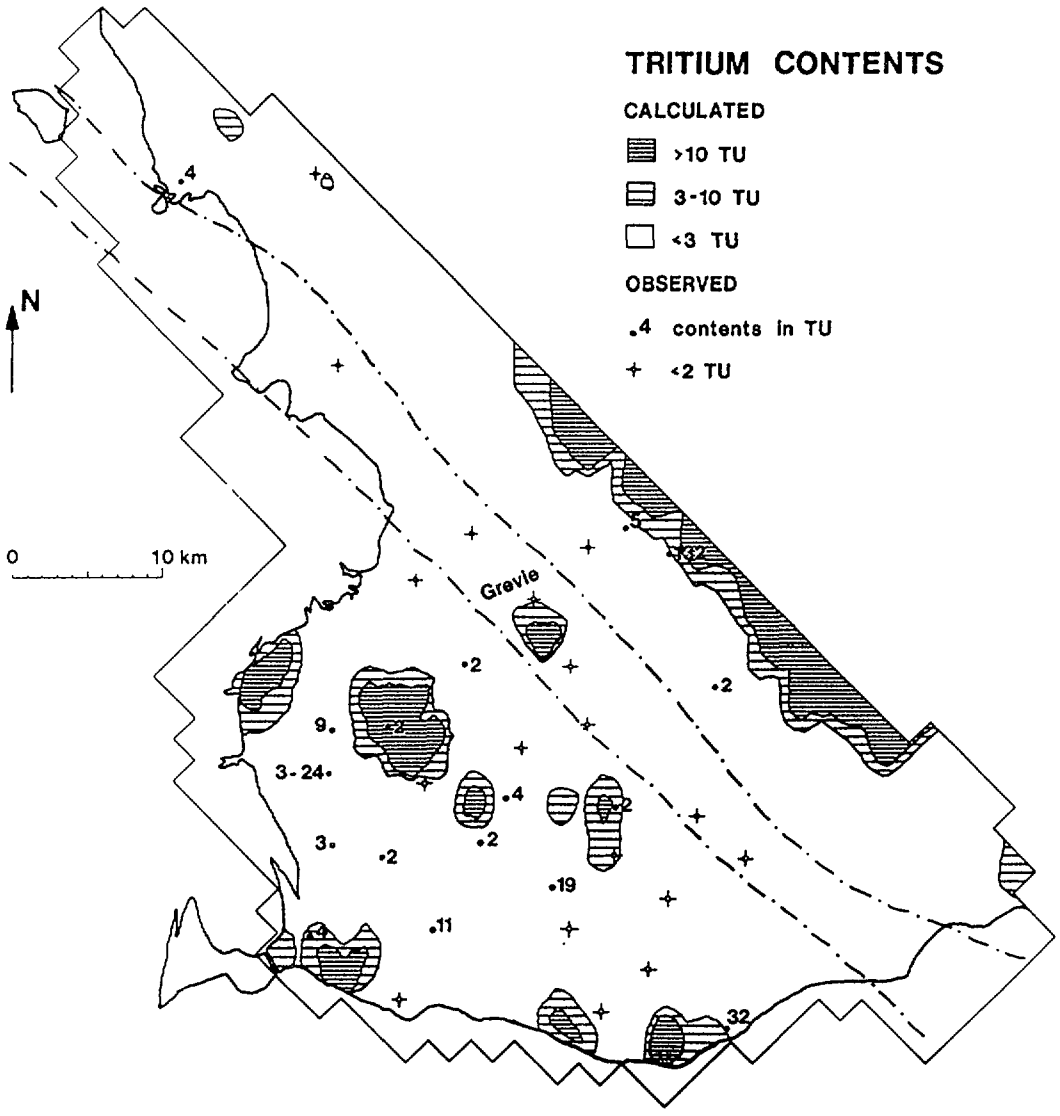

Figure 11a: *Calculated and observed tritium contents in the main aquifer corresponding to the situation in about 1971. The effective porosities in the calculations are 30% in the clay till and 15% in the main aquifer.*

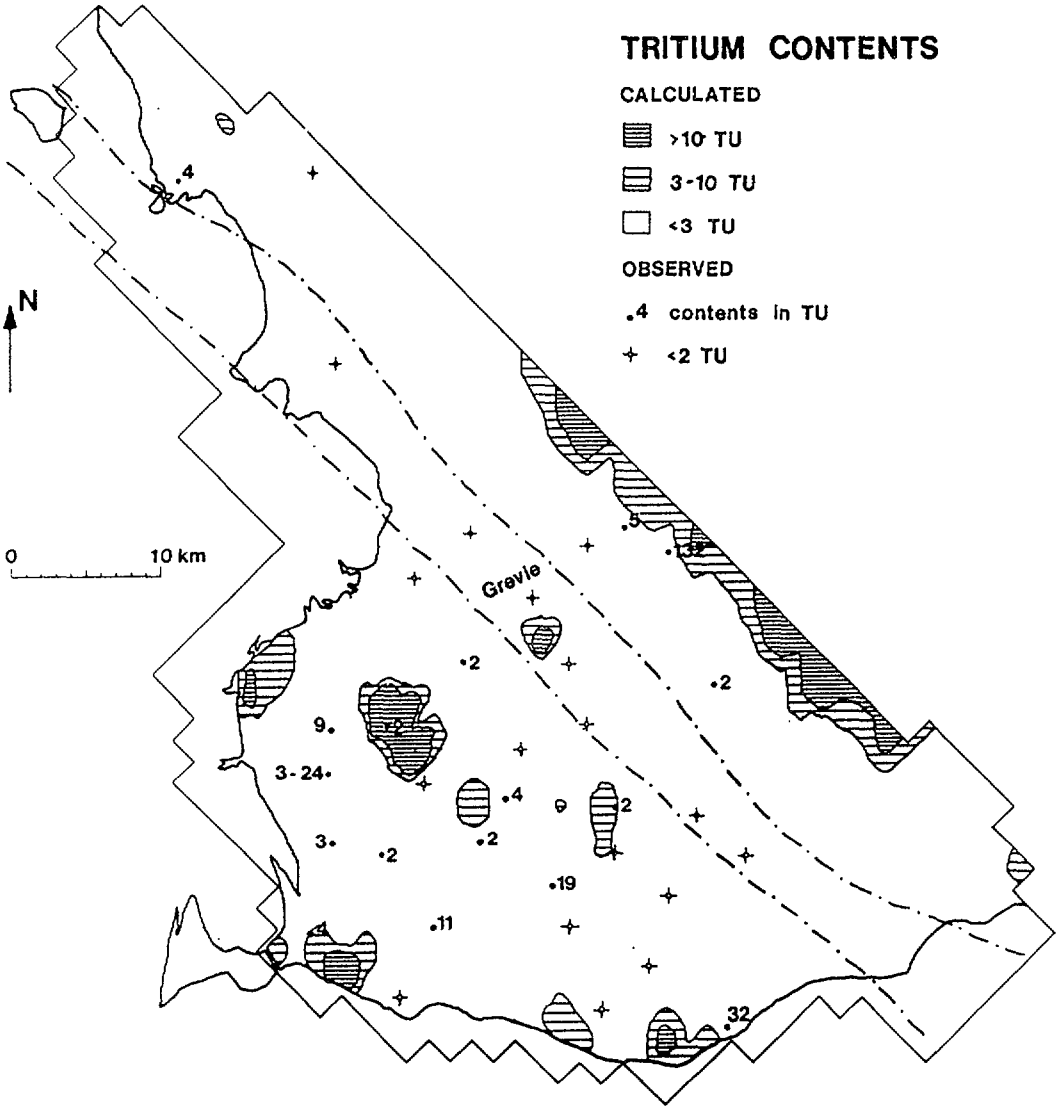

Figure 11b: *Calculated and observed tritium contents in the main aquifer, corresponding to the situation in about 1971. The effective porosities in the calculations are 30% in the clay till and 30% in the main aquifer.*

concentrations. However, there are also some clear differences between the results presented in figures 11a-c. When any of the effective porosities is increased, the zones with enhanced, calculated tritium contents in the main aquifer become smaller and less numerous.

The general patterns in figure 12 are very similar to those in figures 11a-c. However, the zones with enhanced, calculated tritium contents in the main aquifer have become larger and more numerous in 1988. The smaller the porosities are, the stronger this tendency is.

Similar conclusions can be drawn from the results of simulations for the transport of carbon-14 with varying effective porosities. Both calculated and measured isotope concentrations are enhanced in certain zones along the coasts and along the northeastern boundary. Increased effective porosities in the numerical model imply that the areas of the zones with high isotope concentrations in the main aquifer decrease.

It is also difficult to determine which of the porosity sets used in the simulations result in the best agreement with observations. The main reason for this problem is once again the small number of measured isotope concentrations. In particular, there are hardly any measured ^{14}C values in the large areas southwest of the Alnarp valley with enhanced, calculated activities.

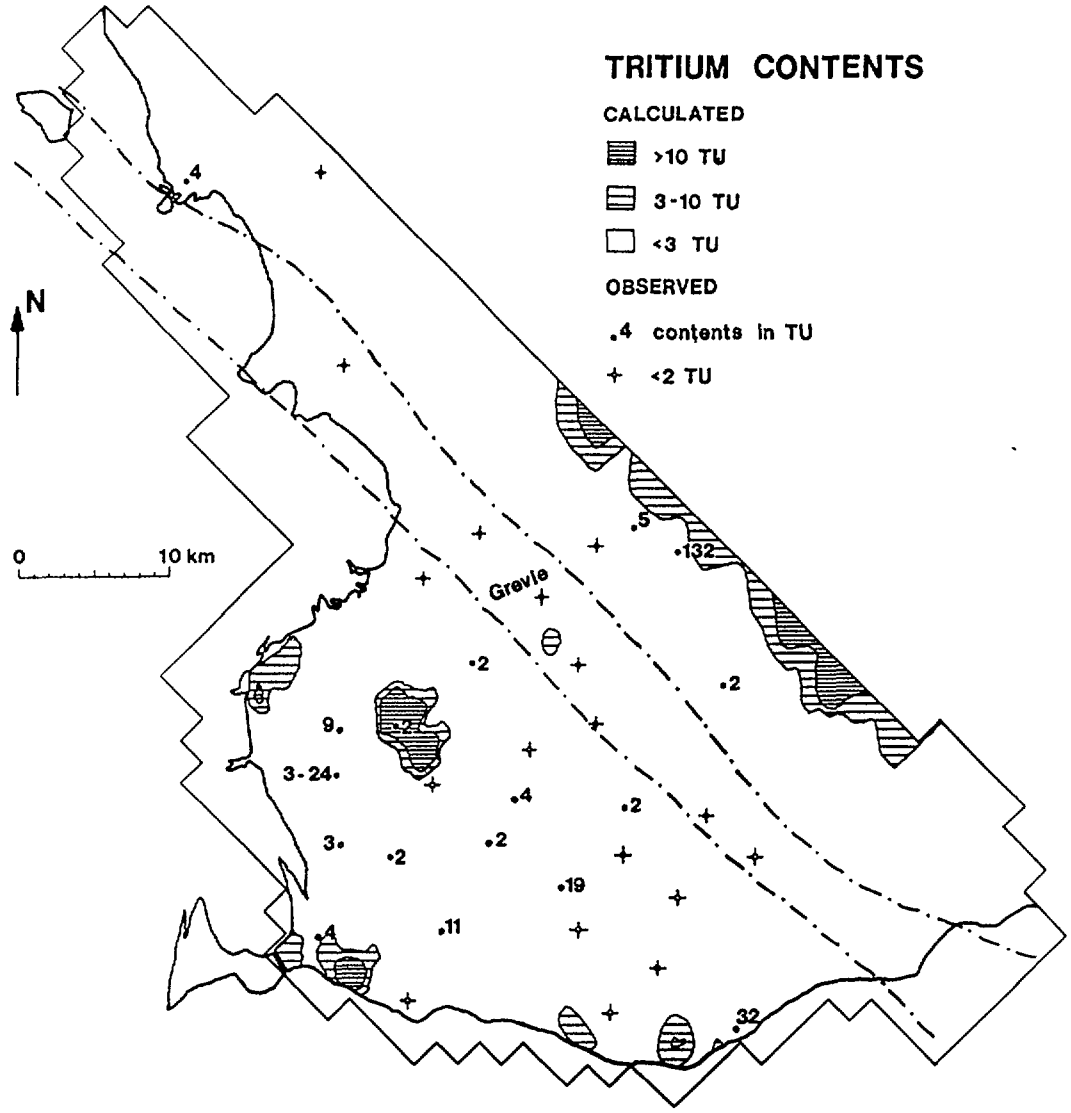

Figure 11c: *Calculated and observed tritium contents in the main aquifer, corresponding to the situation in about 1971. The effective porosities in the calculations are 50% in the clay till and 30% in the main aquifer.*

These peculiarly high concentrations may at least partly be due to an overestimation of the leakage coefficients and/or transmissivities in the numerical model.

On the other hand, the measured contents of ^{14}C in the central part of the Alnarp valley are much lower than any of the calculated values. Here it should be repeated that the measured activities have been corrected for various dilution effects. These figures may thus be unreliable, especially the very low ones. The reason for the discrepancy may also be that the leakage coefficients and/or transmissivities are overestimated in this area.

There are very small differences between the simulation results concerning ^{14}C activities in 1840 and in 1988. Figure 13 has its origin in a flow and transport situation before any exploitation of the main reservoir had started in southwestern Scania. In other words, the low isotope concentrations in large areas probably do not reflect the present circulation times in this groundwater system.

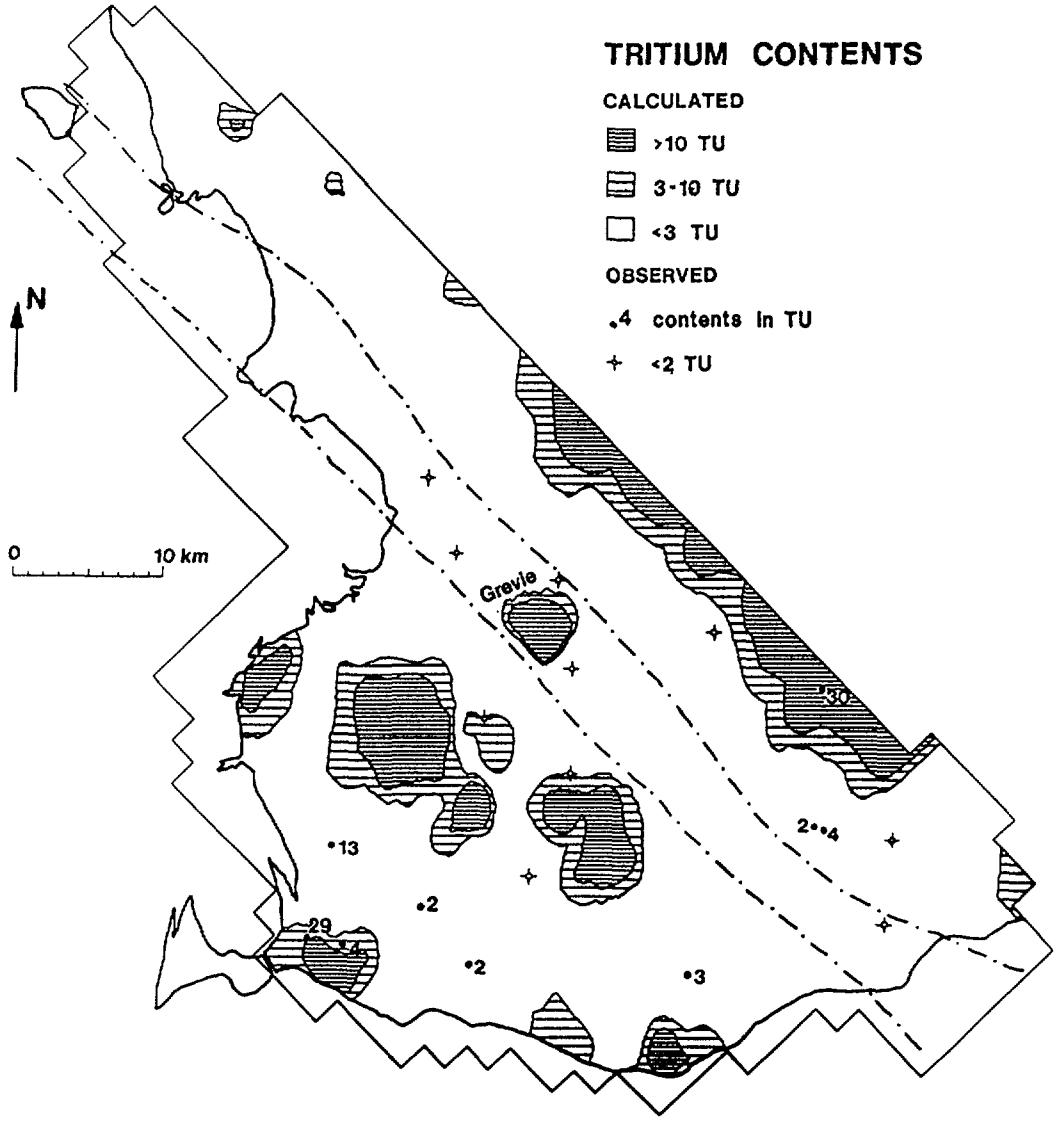

Figure 12: *Calculated and observed tritium contents in the main aquifer, corresponding to the situation in about 1988. The effective porosities in the calculations are 30% in the clay till and 15% in the main aquifer.*

8. GENERAL CONCLUSIONS AND RECOMMENDATIONS

A major merit of this combination of isotope hydrogeology and regional flow and transport modelling is that the isotope transport simulations help to demonstrate where zones particularly vulnerable to pollution are situated. These locations are chiefly the result of hydrogeological characteristics traditionally examined, but they are revealed by means of the transport model. Subsequent, more detailed investigations can then be focussed primarily on these vulnerable zones.

The groundwater flow and transport model applied can be updated progressively as results of further investigations become available. The deterministic model can at any time be used to judge the quantitative and qualitative effects of, for instance, increased groundwater extractions or an inflow of a pollutant, on the basis of the present state of knowledge about the groundwater system of interest.

There are also several difficulties concerning the detailed, quantitative interpretations of the results, and these difficulties must be the focus of future work. Even if the aquifer system

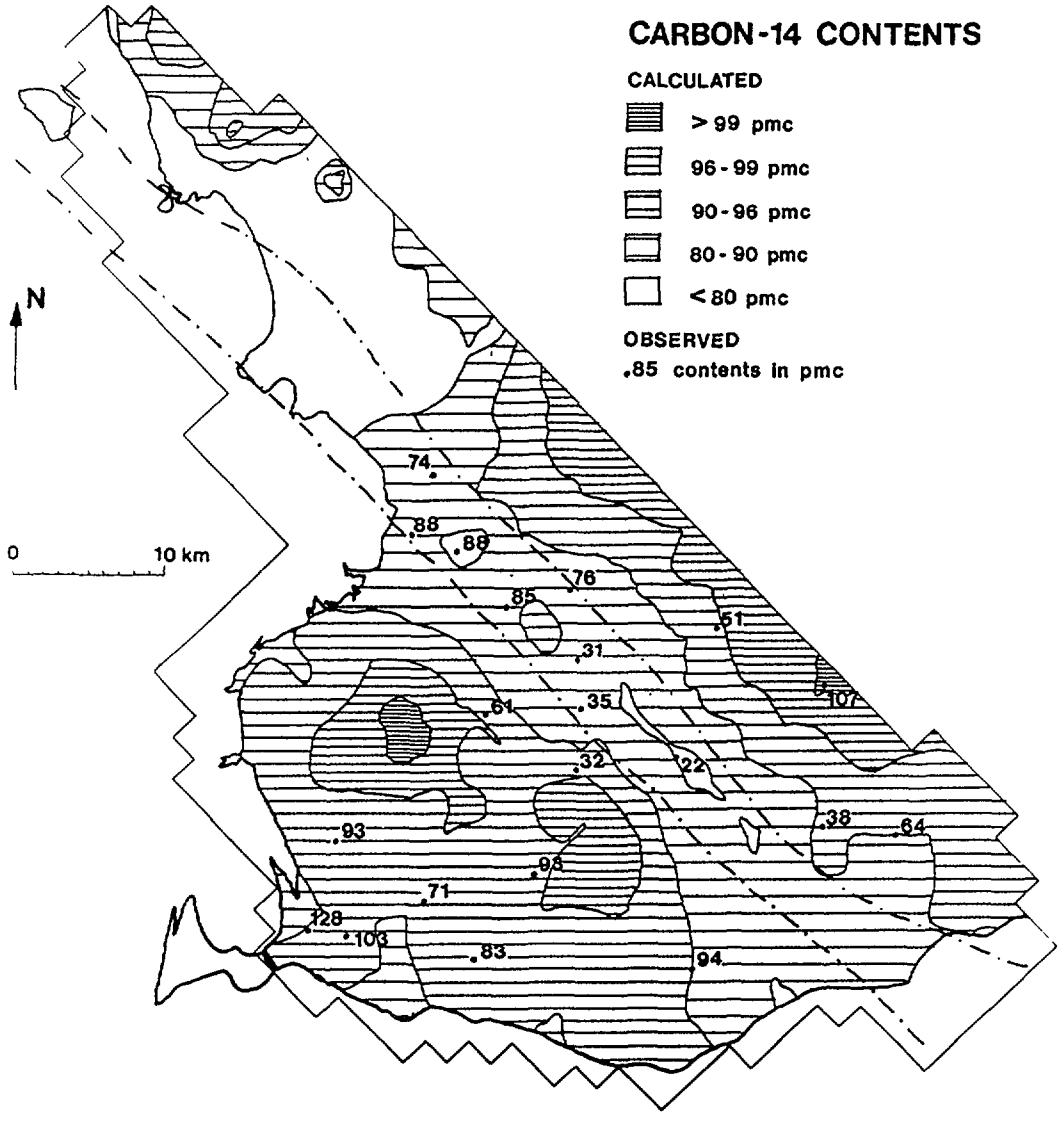

Figure 13: *Calculated and observed carbon-14 contents in the main aquifer, corresponding to the situation in about 1988. The effective porosities used in the calculations are 50% in the clay till and 30% in the main aquifer.*

studied here can be classified as unusually homogeneous and well-defined, the number of isotope measurements is small compared to the extension of the system. Furthermore, the calculated concentrations are similar over large areas. The concentrations observed in sampling wells often represent mixtures of groundwaters from different depths and with different average circulation times, while the calculated concentrations correspond to the average in an element of the model at a certain level. Occasionally, the measured isotope contents may represent a smaller portion of the groundwater reservoir than the calculated mean value for an entire element. Peak concentrations will be smoothed out during the vertical transport due to the relatively rough subdivision into layers. Therefore, it is at present not possible to verify or reject the results of the flow model by a calibration of the isotope transport model.

Furthermore, the isotopic investigations included in this work can improve the general estimations of the properties relevant to the flow and transport processes, but it is not possible to make any reliable, detailed quantitative determinations. The contrasts between the ^{2}H and ^{18}O concentrations in different parts of the aquifer system are too small to be suitable for transport modelling. As regards ^{3}H, there are significant contrasts between the different parts of the

investigated groundwater system, but within large areas of the main reservoir the concentrations are usually very small, due to a long, average, circulation time. The measured ^{14}C values have to undergo a substantial correction before they can be compared with the simulation results. In spite of the many uncertainties related to such an interpretation, contrasts of the same type as for tritium can be detected.

It is recommended that the combination of isotope hydrogeology with regional flow and transport modelling should be developed further to improve the fundamental knowledge and the investigation methods essential for maintaining a quantitatively and qualitatively safe, long-term use of groundwater resources. Other modelling concepts and techniques and also other areas for application should be tried.

In general, the applied combination of various investigation methods will result in a wider understanding of the flow and transport conditions within a studied groundwater system. Zones which seem to be particularly vulnerable to pollution or where a small amount of additional information could improve the hydrogeological survey substantially, can easily be identified. Detailed investigations with measurements and more accurate modelling should be conducted at these locations. The information gained from the detailed studies should be used for adjustments of the regional flow and transport model. The recalibrated regional model will serve to detect other zones in which additional, detailed investigations should be carried out, etc. This iterating procedure will gradually lead to improved knowledge about the groundwater system studied.

The treatment and interpretation of the available data, concerning, among other things, geological logs from drill-holes, groundwater hydraulics and hydrochemistry, have been undertaken mainly without automatization. The spatial and temporal distributions have been determined by hand and by means of simple statistical methods. It is recommended that data are treated by more advanced methods, such as computerized kriging and factorial analysis, to obtain a starting-point for the calibration of flow and transport models more swiftly. However, the results of such operations have to be checked against qualitative information from stratigraphic descriptions, drill-hole logs, local hydrogeological experience, etc.

Most samples from the main groundwater reservoir of southwestern Scania show very low contents of tritium, reducing the possibility of drawing reliable conclusions from a comparison with the results of the transport modelling. It would be very valuable to collect samples for tritium analysis from several different levels between the shallow aquifers and the major aquifer to better elucidate the vertical transport processes in this groundwater system.

It is also recommended that future research should be devoted to estimations of porosities suitable for isotope transport simulations, in general as well as in southwestern Scania in particular. The relationship between the isotope composition of precipitation and water recharging the main aquifer must be studied further. Additional attempts to estimate the ^{14}C contents of the water recharging the main reservoir after all types of dilution mechanisms and processes should also be carried out.

ACKNOWLEDGEMENTS

This study has partly been financed by grants from the Swedish Environmental Protection Agency, the Swedish National Board for Technical Development and the Swedish Natural Science Research Council, which hereby are gratefully acknowledged. The author is also very grateful to professor G. de Marsily, Paris School of Mines, and professor J. Ch. Fontes, Paris University XI, for their generosity and benevolent guidance during his stays in their laboratories for mathematical modelling and isotope analysis respectively.

REFERENCES

Ala-Eddin, M. and Magnusson, E. (1991): FE-modellering av ämnestransport i grundvatten. Master of Science Thesis, Department of Engineering Geology, Lund Institute of Technology, LUTVDG/TVTG-5029, Lund, Sweden, 55pp.

Barmen, G. (1989): Transport av lösta ämnen och isotoper i grundvattensystemet kring Alnarpsdalen. Mätning och modellering. Report LUTVDG-TVTG-7013, Department of Engineering Geology, Lund Institute of Technology, Lund, Sweden, 23pp.

Barmen, G. (1990): Combining environmental isotope investigations with flow and transport modelling of regional groundwater systems. NHP report no. 26 from the Nordic Hydrological Conference 1990 in Kalmar, edited by Gun Sigurdsson, Nordic Hydrological Association, ISBN 91-87996-02-2 Norrköping, Sweden, pp. 104-113.

Barmen, G. (1992): On the combination of isotope hydrogeology with regional flow and transport modelling. An application to the groundwater system of southwestern Sweden. Doctoral Thesis, Department of Engineering Geology, Lund Institute of Technology, LUTVDG/ TVTG-1006, ISBN 91-628-0587-8 Lund, Sweden, 201pp.

Bjelm, L, Hartlén, J, Röshoff, K, Bennet, J, Bruch, H, Persson, P-G. and Wadstein, P. (1977): Geotermisk energiutvinning i Skåne. Slutrapport Etapp 1. Förutsättningarna för utvinning i Skåne. Department of Engineering Geology and Department of Soil Mechanics and Foundation Engineering, Lund Institute of Technology, LUTVDG/TVGL-5013, Lund, Sweden, 60pp.

Brinck, S. and Leander, B. (1981): Alnarpsströmmen. Sammanställning av utredningar 1970-1980. The Alnarp committee, VBB 10520, Malmö, Sweden, 45pp.

Brinck, S, Leander, B. and Winqvist G. (1969): Alnarpsströmmen. Utredning rörande vattentillgång och dess lämpliga utnyttjande. The Alnarp committee, VBB, Malmö, Sweden, 56pp.

Burgman, J.O, Calles, B. and Westman, F. (1987): Conclusions from a ten year study of oxygen-18 in precipitation and runoff in Sweden. In the proceedings of an international symposium on Isotope techniques in water resources development, International Atomic Energy Agency, Vienna, Austria, pp. 579-590.

Burgman, J.O, Eriksson, E. and Westman, F. (1983): A study of oxygen-18 variations in river waters and monthly precipitation in Sweden and determination of mean residence times. Internal report, Division of Hydrology, University of Uppsala, Uppsala, Sweden, 19pp.

Calles, B. and Westman, F. (1989): Oxygen-18 and Deuterium in precipitation in Sweden. Report series A, no. 47, Division of Hydrology, University of Uppsala, Uppsala, Sweden, 20pp.

Custodio, E, Gurgui, A. and Lobo Ferreira, J.P. (editors, 1987): Groundwater Flow and Quality Modelling. Proceedings of the NATO Advanced Research Workshop on Advances in Analytical and Numerical Groundwater Flow and Quality Modelling, Lisbon, June 2-6, 1987. NATO ASI ser. C: Mathematical and Physical Sciences, vol. 224. D. Reidel Publishing Company, Dordrecht, Netherlands, 843pp.

DGU and Kemp & Lauritzen (1975): Nordvand. Grundvandsundersogelse ved Esrum sö. The Danish Geological Survey and Kemp & Lauritzen A/S, Frederiksborg Amtskommune, Denmark, 88pp.

Fontes, J.Ch. (1985): Some considerations on groundwater dating using environmental isotopes. Memoirs of the 18th congress of the International Association of Hydrogeologists, Hydrogeology in the service of man, Cambridge, Great Britain, pp. 118-154.

Fontes, J.Ch. and Garnier, J-M. (1979): Determination of the initial activity of the total dissolved carbon. A review of existing models and a new approach. Water Resources Research, vol. 15, no. 2, pp. 399-413.

Fritz, A.P. and Fontes, J.Ch. (editors, 1980): Handbook of Environmental Isotope Geochemistry, Volume 1, The Terrestrial Environment, A. Elsevier, Amsterdam, Netherlands, 545pp.

Geyh, M.A. and Backhaus, G. (1978): Hydrodynamic aspects of carbon-14 groundwater dating. In the proceedings of an international symposium on Isotope Hydrology, vol. II, International Atomic Energy Agency, Vienna, Austria, pp. 631-643.

Goblet, P. (1985): Programme METIS. Notice d'utilisation. Centre d'Informatique Géologique, Ecole Nationale Supérieure des Mines de Paris, LHM/RD/85/41, Fontainebleau, France, 68pp.

Gustafsson, O. (1972): Beskrivning till hydrogeologiska kartbladet Trelleborg NV och Malmö SV (Description of the Hydrogeological Map Trelleborg NV and Malmö SV). Swedish Geological Survey, SGU, ser. Ag, no. 4, Stockholm, Sweden, 37pp.

Gustafsson, O. (1978): Beskrivning till hydrogeologiska kartbladet Trelleborg NO/Malmö SO (Description to the Hydrogeological Map Trelleborg NO/Malmö SO). Swedish Geological Survey, SGU, ser. Ag, no. 6, Stockholm, Sweden, 72pp.

Gustafsson, O. (1981): Beskrivning till hydrogeologiska kartbladet Malmö NV (Description to the Hydrogeological Map Malmö NV). Swedish Geological Survey, SGU, ser. Ag, no. 13, Uppsala, Sweden, 51pp.

Gustafsson, O. (1986): Beskrivning till hydrogeologiska kartbladet Helsingborg SV (Description to the Hydrogeological Map Helsingborg SV). Swedish Geological Survey, SGU, ser. Ag, no. 14, Uppsala, Sweden, 58pp.

Gustafsson, O. and Teeling, M. (1973): Sydvästra Skånes geologi: Jordlager - Berggrund - Grundvatten. Swedish Geological Survey, SGU, Lund, Sweden.

Herweijer, J.C, van Luijn, G.A. and Appelo, C.A.J. (1985): Calibration of a mass transport model using environmental tritium. Journal of Hydrology, vol. 78, pp. 1-17.

Holst, N.O. (1911): Alnarps-floden. En svensk "Cromer-flod". Swedish Geological Survey, SGU, ser. C, no. 237, Stockholm, Sweden, 64pp.

Hydén, H., Leander, B. and Voss, C.I. (1980): The Alnarp Groundwater System. A Mathematical Model Study. VBB Special Report 02:80.1, Stockholm, 25pp.

Ledoux, E. (1986a): Modèles mathématiques en hydrogéologie. Centre d'Informatique Géologique, Ecole Nationale Supérieure des Mines de Paris, LHM/RD/86/12, Fontainebleau, France, 120pp.

Ledoux, E. (1986b): Programme NEWSAM. Simulation des aquifères multicouches en mailles de taille variable. Note de présentation. Centre d'Informatique Géologique, Ecole Nationale Supérieure des Mines de Paris, Fontainebleau, France, 33pp.

Markussen, L.M, Möller, H-M.F, Villumsen, B, Mortensen, J.K. and Selchau, T. (1991): Frederiksberg Kommune. Sikring av drikkevandsressourcen. Ramböll & Hannemann Bulletin, no. 27, Copenhagen, Denmark, 85pp.

Marsily, G. de, Ledoux, E, Levassor, A, Poitrinal, D. and Salem, A. (1978): Modelling of large multilayered aquifer systems: Theory and applications. Journal of Hydrology, vol. 36, pp. 1-34.

Nilsson, K. (1966): On the ground water conditions in the sedimentary rocks of Scania. In the proceedings of an international symposium held in Stockholm, Wenner-Gren Center International Symposium Series, vol. 11. Ground Water Problems, edited by E. Eriksson, Y. Gustafsson and K. Nilsson. Pergamon Press, Great Britain, 1968, pp. 43-56.

Pearson, F.J. Jr and Hanshaw, B.B. (1970): Sources of dissolved carbonate species in groundwater and their effects on carbon-14 dating. In the proceedings of an international symposium on Isotope Hydrology, International Atomic Energy Agency, Vienna, Austria, pp. 271-286.

Perers, J. and Johansson, I. (1980): Trelleborgs och Vellinge kommuner. Grundvatten. Utredning över tillgång, behov, utnyttjande och skydd. Sammanfattning. VIAK 5812.1518, Malmö, 29pp.

Ringberg, B. (1980): Beskrivning till jordartskartan Malmö SO (Description to the Quaternary map Malmö SO). Swedish Geological Survey, SGU, ser. Ae, no. 38, Uppsala, Sweden, 179pp.

Robertson, J.B. (1974): Application of digital modelling to the prediction of radioisotope migration in groundwater. In the proceedings of an international symposium on Isotope Techniques in Groundwater Hydrology, vol. II, International Atomic Energy Agency, Vienna, Austria, pp. 451-478.

Saxena, R.K. (1990): Personal communication. Researcher at the Division of Hydrology, Uppsala University, Uppsala, Sweden.

Sevel, T, Kelstrup, N. and Binzer, K. (1981): Nedsivning. Suså hydrologi. Danish Hydrological Committee, Report no. Suså H6, Copenhagen, Denmark, 59pp.

Sudicky, E.A. and Frind, E.O. (1981): Carbon -14 dating of groundwater in confined aquifers: Implications of aquitard diffusion. Water Resources Research, vol. 17, no. 4, pp. 1060-1064.

Wigley, T.M.L, Plummer, L.N. and Pearson, F.J. Jr (1978): Mass transfer and carbon isotope evolution in natural water systems. Geochimica et Cosmochimica Acta, vol. 42, pp. 1117-1139.

APPLICATION OF HYDROGEOCHEMICAL MODELLING FOR VALIDATION OF HYDROLOGIC FLOW MODELLING IN THE TUCSON BASIN AQUIFER, ARIZONA, UNITED STATES OF AMERICA

R.M. KALIN
University of Georgia,
Athens, Georgia

A. LONG
University of Arizona,
Tucson, Arizona

United States of America

Abstract

This work examined the hydrogeochemical evolution of Tucson basin groundwater, including isotope hydrology, geochemistry and age determinations. Results of mineralogic investigation on basin fill constrain water-rock geochemical reactions. Examination of 45 years of water quality data shows that groundwater mining has affected water quality. Stable isotopes of carbon, oxygen, hydrogen, sulfur, and chlorine and radiocarbon, tritium [1] and radon determinations [2] refine the interpretation of hydrogeochemical evolution of Tucson basin groundwater as modelled with NETPATH [3]. Two distinct sampling periods, the first in 1965 [4] and the second between 1984 and 1989, resulted in the determination of groundwater ages for water mined two decades apart. Isotope hydrology and geochemical modelling suggest that much of the water presently mined from the Tucson basin has a component recharged during the last 50 years. Increased sulfate concentrations suggest that heavy pumping in the northeastern basin induced increased leakage from lower units. Results of geochemical modelling indicate an average of 5 percent mountain-front recharge to the Ft. Lowell fm. along the northern aquifer margin. An increase in dissolved solids along the basin margin implies that this component to recharge has increased in the past decade.

The radiocarbon age of the basin groundwater was compared with the temporal movement of water as modelled with MODFLOW and PATH3D [5]. In general, the hydrologic simulation agrees with both the distribution of tritium and the exponentially modelled water age, as determined with bomb-derived radiocarbon, for areas of the Tucson basin that contain water less than 50 years in age. Hydrologic modelling failed to predict the antiquity of recently sampled water in the central basin but is similar to age determinations on waters collected in 1965.

INTRODUCTION

Groundwater chemistry is determined by the initial chemistry of water entering a groundwater system and subsequent chemical reactions with minerals comprising the aquifer materials. It is possible to model chemical reactions (water-rock) that control the chemical composition of groundwater if the following are known: A) basic knowledge of the hydrology of the aquifer system, B) initial chemistry of recharge waters, C) knowledge of minerals most prevalent in the aquifer and D) chemical analyses of major and minor chemical constituents in groundwater.

Tucson City, Pima County and Arizona State planning is based on estimates of population growth, economic growth, national trends and other factors such as availability of an ample water supply. The metropolitan Tucson area will continue to depend on ground water as a natural resource. The Central Arizona Project (CAP) can supply up to an estimated 18 million m^3 of Colorado river water to Tucson annually, but the long-term master-plan for Tucson projects continuous growth, and consequently, the use of CAP water will only be a stop-gap solution to the mining of Tucson basin groundwater.

The quantity of water recharged to the Tucson basin from infiltration of local precipitation has been estimated at 6.3 million m^3 per year [6]. The volume of water recharging the basin as leakage along the mountain front has been estimated by Davidson [6] at 13,000 to 25,000 m^3 per kilometer of perimeter per year.

Marra [7] applied the finite difference model MODFLOW to movement of groundwater in the Tucson basin. Mathematical models are based on estimates of aquifer parameters and may not fully represent the actual hydrology. This study of the hydrogeochemical evolution and isotope hydrology of Tucson basin groundwater is used to validate our understanding of the movement of water in the subsurface independent of hydrologic modelling.

SIGNIFICANCE OF HYDROGEOCHEMICAL MODELLING

The Tucson basin is well studied with both hydrological and geochemical methods [6 - 57], yet a full understanding of the temporal and spatial flow of water in the Tucson basin is not fully realized. This is due, in part, to a high degree of large-scale inhomogeneity of the aquifer, chemistry of the water and boundary conditions as well as severe anthropogenic impact on the hydraulic system.

Understanding the chemical evolution of groundwater requires identification of chemical reactions and subsequent mass-transfer. Use of mass-balance calculations in conjunction with water-mineral equilibria calculations allow identification of controlling geochemical reactions along a flow path. Knowledge of reactant and product phases constrains geochemical reactions. Proposed mass-transfer reactions are examined to determine which reaction path best predicts the mass of dissolving and precipitating phases occurring.

Isotope balances are used to validate mass-balance calculations. Isotopes are particularly well suited for this problem because of the almost unique solutions required to reproduce the measured values. These isotopic constraints can be applied to the mass-transfer models of Wigley *et al.* [58] and Plummer *et al.* [3] to calculate the $^{13}C/^{12}C$ and ^{14}C of the original water, place limits on the possible admixture and reactions along the flow path and to accurately estimate of the age of the water.

PHYSIOGRAPHIC SETTING

The Tucson basin, southeastern Arizona, USA (Figure 1) is part of the Basin and Range geological province of the southwestern United States [59]. It is a broad northwest trending alluvial valley. The basin is bounded by mountains that range in elevation from 900 to 2800 meters (mean sea level, m.s.l.). The elevation of the basin floor ranges from 610m in the northwest to 1070m m.s.l. in the southeast. The entire Tucson basin covers approximately 3600 km^2.

The Tucson basin drains to the northwest. Major rivers consist of the Santa Cruz river, which flows generally northward along the western edge of the basin; the Pantano river, which drains the eastern basin mountain-front along the Rincon mountains and joins Tanque Verde creek and Rillito river which drains the Catalina mountains along the northern basin edge (figure 1). All major drainage features are currently intermittent but may have been perennial during the Holocene [60,61].

Recharge to the basin occurs mainly as leakage through riverbeds (figure 2). Additional recharge to the groundwater system occurs as recharge along the mountain-front. These components of recharge flow toward the basin center. Water leaves the aquifer system through evapotranspiration, flow out of the basin to the northeast and by mining of groundwater. Mining of groundwater is defined here as an excess of water removed over water recharged resulting in a net loss of water in the aquifer.

Modern precipitation consists of 2 major rainfall patterns. Winter rainfall arrives as frontal storms that pass eastward over Arizona from October to May. Summer precipitation occurs as intense local convective "monsoon" storms that form as moist air moves into Arizona from Mexico. Periodically "cut-off" lows, intense low pressure storms that form in the low latitudes of the pacific ocean, move across Arizona and bring significant rainfall. The occurrence of these events may be related to the El Nino/Southern Oscillation (ENSO) [62].

Rainfall average is 300 mm per year over the basin and as high as 650 mm of rain and snow (water equivalent) on the surrounding mountains [63,64]. The potential evaporation, ca. 2000 mm per year [19,45], currently far exceeds precipitation in the basin.

Metropolitan Tucson lies within the north-central one third of the basin. Tucson's population is continuously growing (Table 1) and is expected to exceed 1.5 million by the year 2025 [46-49]. Tucson presently depends on groundwater as a water supply. Groundwater mining has resulted in water table declines exceeding 50 meters in some portions of the Tucson basin. As the aquifer is dewatered, there is the potential for basin subsidence [50]. The arrival of CAP water can offset groundwater mining but will not provide all of the water resources needed.

The Tucson Water Resources Plan [17] calls for a decrease in groundwater withdrawals from 123 million m^3 in 1991 to approximately 18 million m^3 in 1995. With population growth, groundwater mining will increase to 56 million m^3 per year by the year 2030. Fifty percent of Tucson's water needs are expected to be met by CAP water. Non-potable effluent is presently used for irrigation of parks and golf courses to offset water demands. Effluent is presently recharged to the groundwater system and, with recharged CAP water, is expected to be recovered, treated and used as drinking water before 2050. These plans have been made without detailed evaluation of the fate of recharged water or the temporal movement of water in the Tucson basin aquifer system. Results of this study should be used to consider the fate and reclaimation of recharged water.

GEOLOGY AND HYDROGEOLOGY

The basin consists of Oligocene to Pleistocene age alluvium [65-69] deposited in the deep grabens produced from high-angle normal faulting during Basin-and-Range crustal extension (figure 2). The most

centrally-located grabens within the Tucson basin extend to over 3000 meters depth below land surface. The location of these graben faults as mapped by Anderson [68] are in figure 3.

The lowest unit of Tucson basin sediments is the Pantano formation [66]. This formation is consolidated and contains few clasts of Catalina gneiss suggesting that the uplift of the Catalina and Rincon core complexes is post-Oligocene [65]. It is interbedded with volcanic flows which have potassium-argon dates ranging from 31.4 to 24.9 million years (m.y.) [67]. The Pantano fm. outcrops on the periphery of the basin as up-thrown blocks of the Basin-and-Range faulting.

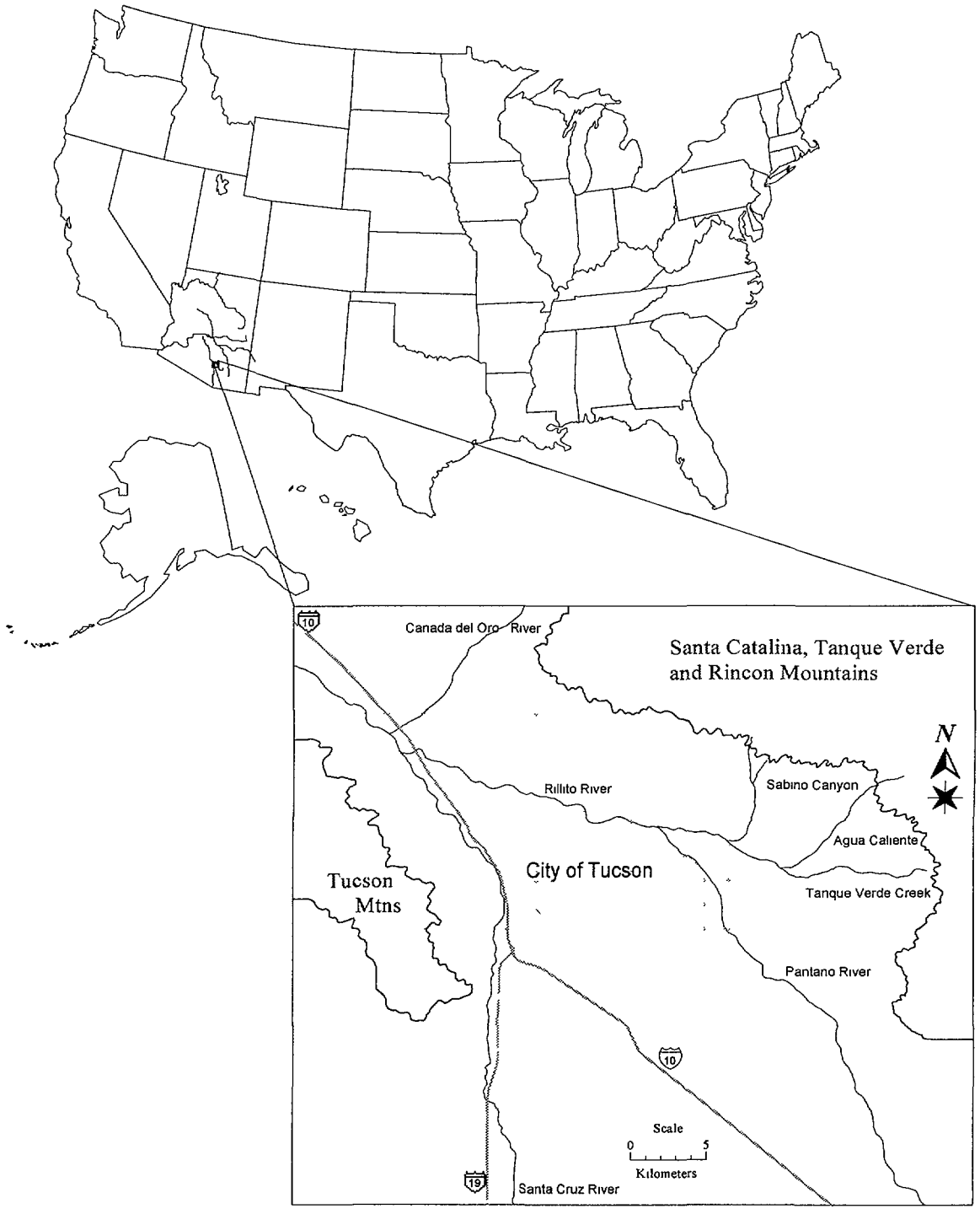

Figure 1. Geographical location of study area

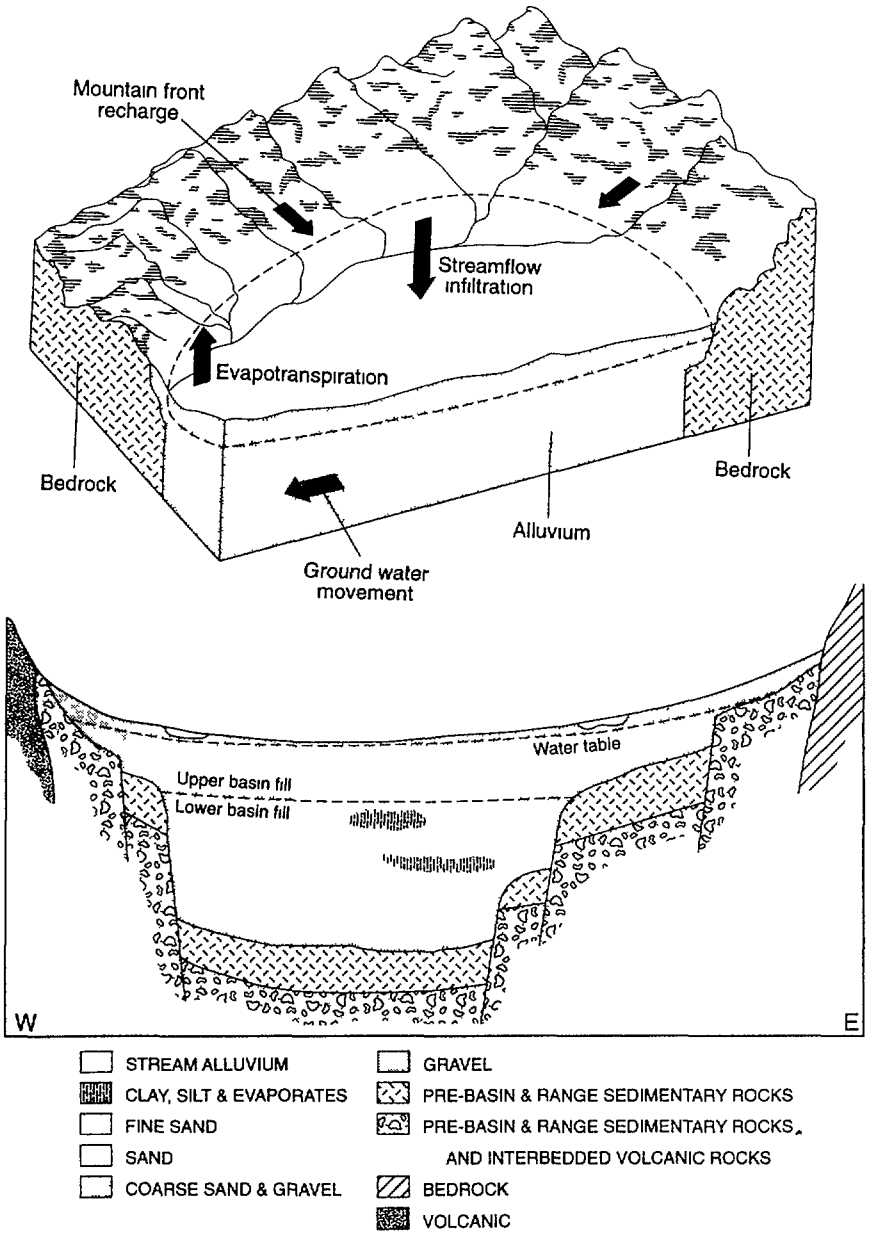

Figure 2. Idealized hydrologic system of Tucson basin and cross-section of aquifer system

Table 1. Projected population for the Tucson Metropolitan Area after Arizona Department of Economic Security, December 1981

Year	Population Projection [46] Low Growth - High Growth	Projected Water [46] Use (millions m^3)
2000	829,000 - 851,600	183.3 - 188 3
2010	1,019,700 - 1,101,000	225.5 - 243.5
2020	1,176,000 - 1,316,600	260 0 - 301.1
2030	1,318,600 - 1,624,100	291 6 - 359.1
2040	1,433,600 - 1,891,700	317.0 - 418.3
2050	1,525,600 - 2,146,060	337.4 - 474.6

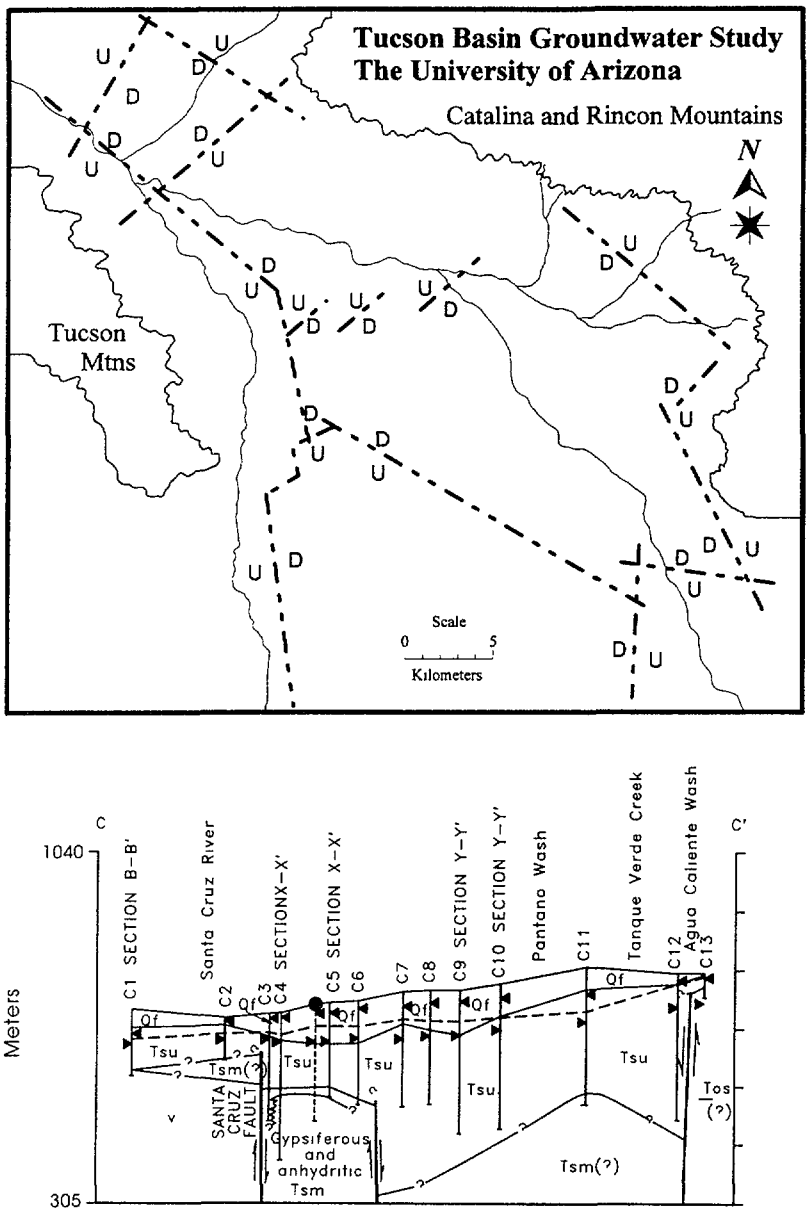

Figure 3. Estimated location of graben faults in the Tucson basin and east-to-west cross section

The central units of sediments, the Tinaja beds [18,68], are Miocene to Pliocene in age and range from 100 meters thickness along the basin perimeter to 600 meters thickness in the basin center. The sediments comprising these units include clasts from the Tucson Mountain volcanic and the Catalina and Rincon metamorphic core complexes interbedded with clay-rich anhydrite/gypsum beds. Anderson [68] subdivided the Tinaja fm. into three unconformable units, the upper Tinaja, middle Tinaja and lower Tinaja beds. Some production wells penetrate the upper Tinaja fm. but few penetrate the middle and lower units.

Most wells in the Tucson basin draw water from the upper geologic unit, the Ft. Lowell fm., which unconformally overlies the upper Tinaja beds [68]. The Ft. Lowell fm. was deposited during the early to mid-Pleistocene. Sediments of the Ft. Lowell fm. range between 60 and 125 meters thick and consist of gravel to clayey silt. Overlaying the Ft. Lowell fm. is a veneer of Pleistocene and Holocene alluvial sediments which are generally above the water table. These deposits are typically very coarse sand and gravel and therefore can allow significant recharge along the intermittent rivers.

Rogers [25] reported the hydraulic conductivities of the Middle and Upper Tinaja beds at between 0.3 and 10 m/d while transmissivity ranges between 16 and 1500 m^2/d. The average saturated thickness of the Ft. Lowell fm. is 30m. The reported hydraulic conductivity of this formation ranges between 0.3 and 60 m/d [25,7]

with transmissivities between 270 and 15,500 m^2/d. Regions of high transmissivity and "shoestring" aquifers act as recharge conduits of mountain-front recharge water [9] and are hypothesized here as paleo-alluvial channels and fans from the streams and rivers that drain the surrounding mountains. Figure 4 shows the percent clay for the Tinaja and Ft. Lowell fms. respectively (after Anderson [68]). It is envisioned that during the closed-basin formation of the Tinaja beds, a series of alluvial fans stretched across the northern basin (Agua Caliente, Tanque Verde, Bear Canyon, Sabino Canyon and Ventana Canyon) depositing sediments of high transmissivity. This trend can also be seen in the Ft. Lowell fm. which contains very little clay at the pediment-basin interface,

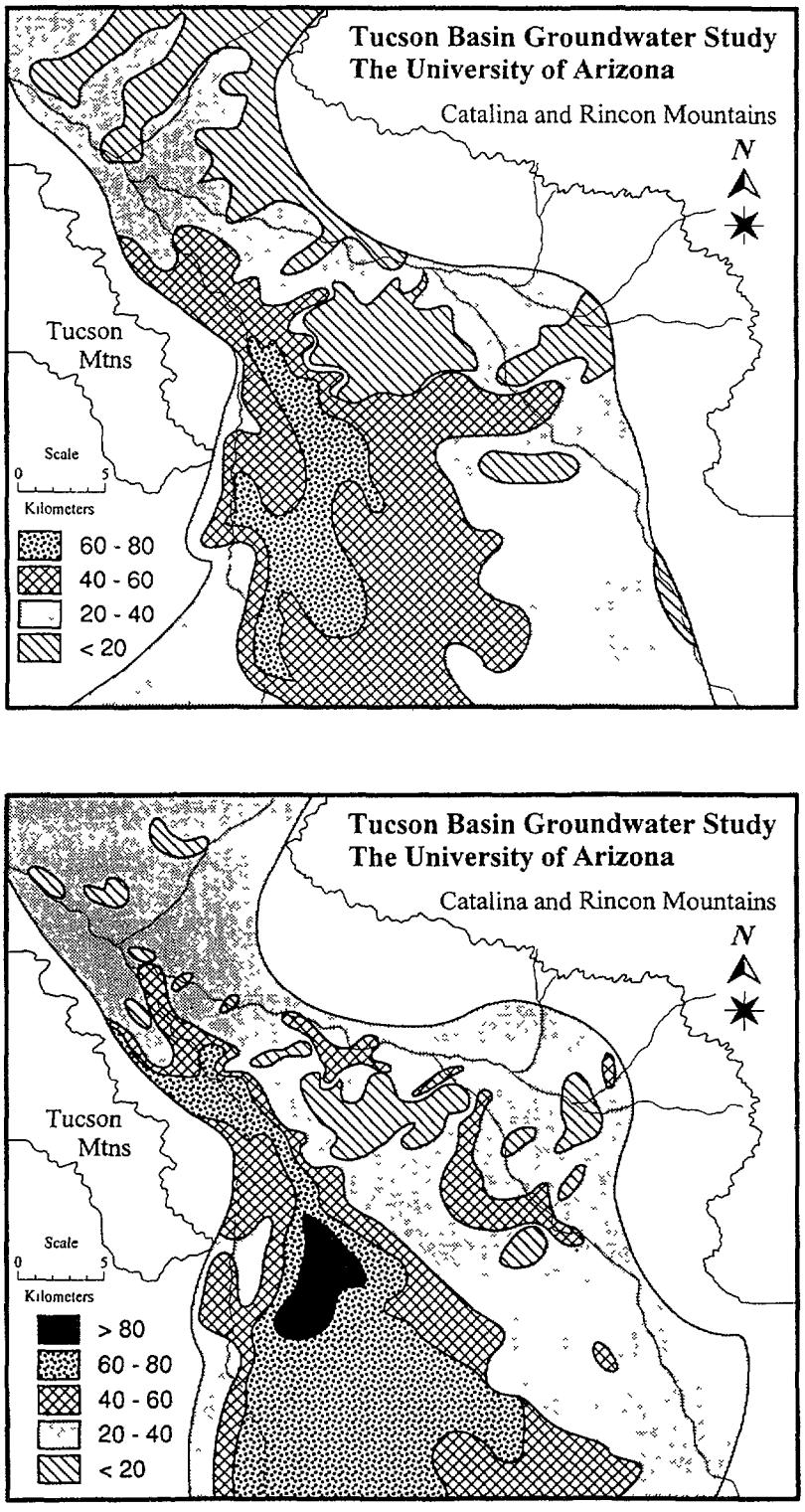

Figure 4. Percent clay in Tinaja (lower confined) and Ft. Lowell (upper unconfined) aquifers

suggesting a high-energy depositional environment. The hydrogeology and hydrogeochemistry suggest that water presently recharging and flowing in these zones of higher transmissivity travel at greater velocity than in regions of lower transmissivity. This boundary must be taken into consideration when choosing the flow path for geochemical reactions. Mixing of older with younger waters should be considered along these boundaries.

Figures 5 shows the head distribution in the Tucson basin for the years 1940 and 1988 respectively. The effect of pumping can be seen in the west-central portion of the basin where hydrologic head has lowered significantly in the last 50 years of population growth and expansion of water mining. This extensive

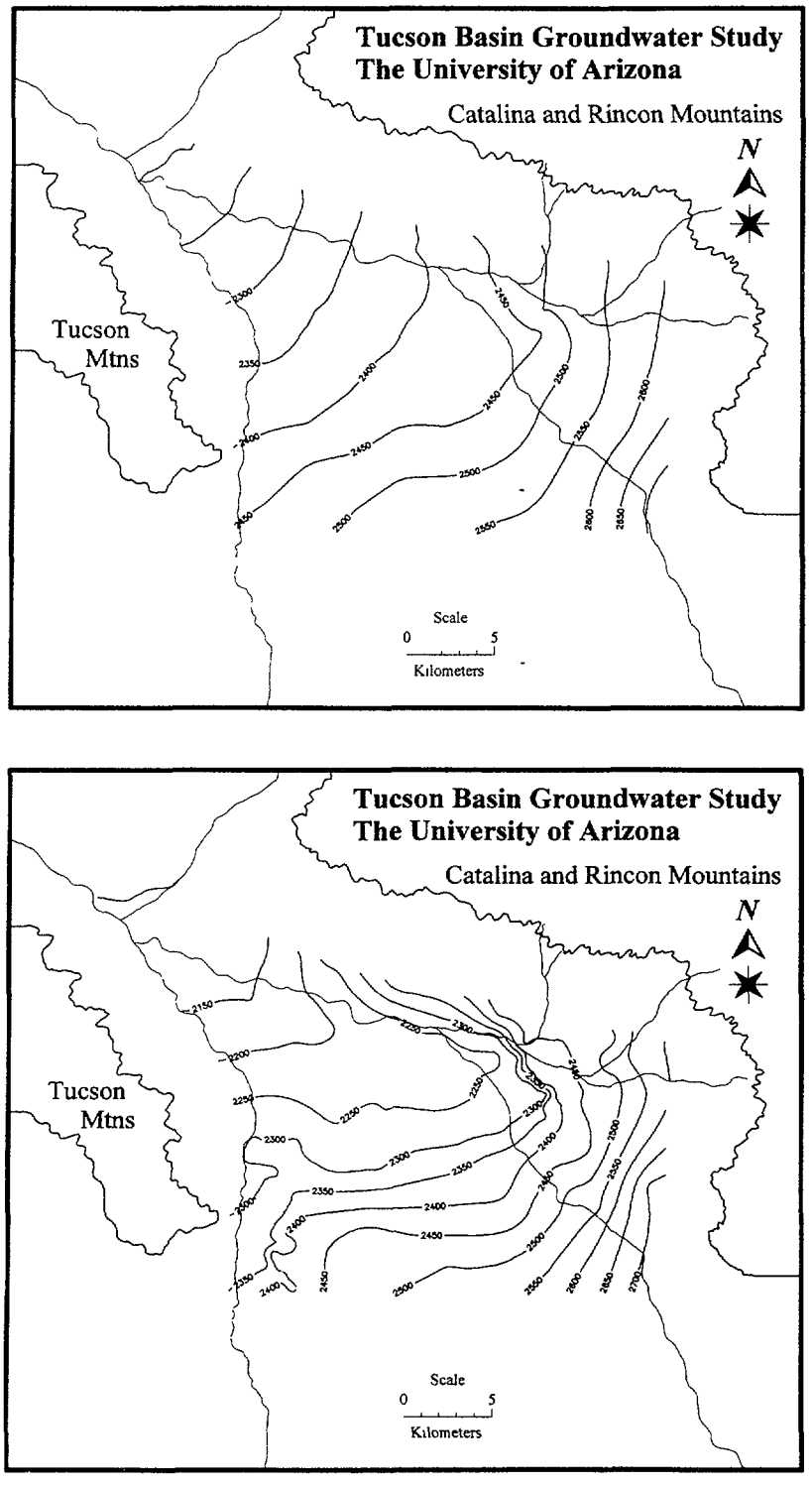

Figure 5. Potentiometric surface of unconfined aquifer during 1940 and 1988

perturbation of the natural groundwater system increases the complexity of groundwater resource analysis by both hydrogeological and hydrogeochemical methods. However, this strong transient state also provides the opportunity to examine changes in the hydrogeology and hydrogeochemistry of the system as it accentuates changes in recharge sources, mixing and the groundwater flow characteristics near transmissivity boundaries.

ISOTOPIC COMPOSITION OF BASIN PRECIPITATION

The stable isotopic composition of water can be used for identification of different sources of water [70-87]. Samples of most precipitation events in Tucson have been collected by A. Long and R. Kalin during the time period 1981 until present. The majority of these samples were analyzed for stable oxygen and hydrogen isotopes [88-94] through the combined efforts of many individuals, most notably Christopher Eastoe. The number of samples represented in this data set are far greater than those in the work of Simpson *et al.* [33], but the same basic interpretation of the seasonality of recharge applies.

Figure 6 plots the summer (May through October) precipitation events and winter (November through April) respectively. The average δD values of these samples are -58‰ $_{SMOW}$ for winter and -38‰ $_{SMOW}$ for summer. These values are close to the values of -61‰ and -42‰ reported by Simpson *et al.*. [33] in 1970. Oxygen and hydrogen isotopic information defines local meteoric water lines for winter and summer precipitation.

Figure 7 plots the d-parameter [95] of these samples against the rainfall amount. A value of d = 10 indicates a sample population that lies on the globally averaged meteoric water line. A d-parameter greater than 10 may indicate, among other effects, a source of precipitation that originated as a solid precipitate (snowfall). Values of d less than 10 indicate local/regional evaporative processes acting upon the precipitation. The sources of moisture for the Tucson basin are winter cyclonic storms that are expected to produce precipitation with d-parameters equal to or greater than 10, and for the summer, local convective storms that are expected to produce precipitation with d-parameters less than 10. The average d-parameter for summer rainfall is 4.98 and for winter rainfall is 11.14. These results confirm the hypothesized range of values. The coefficient of fit (r^2) for both graphs suggest no relationship of d-parameter with precipitation amount.

ISOTOPIC COMPOSITION OF MOUNTAIN PRECIPITATION

Summer and winter precipitation samples from the Santa Catalina mountains are plotted in figure 8. The values measured in this study compare favorably with those of Simpson *et al.* [33]. The summer mountain precipitation is similar to that at the basin floor with the exception that most of the mountain events lie near or above the global meteoric water line. The average d-parameter (12.6 +/- 5.3) of summer rainfall on the mountains is near the global average of 10. The apparent distribution of the d-parameter near the global average suggests that moisture for summer convective storms does not undergo exchange with local evaporative moisture. The discrepancy between the d-parameter of high elevation precipitation and the low d-parameter of rainfall on the basin floor may reflect "below cloud" evaporative effects that occur as raindrops evaporate during their travel to the basin floor. This distribution may also reflect the sparse nature of rainfall events collected on the mountains. The winter precipitation is isotopically lighter than summer precipitation and has an average d-parameter (24.0 +/- 4.4) above the global meteoric average, consistent with the source of moisture.

The seasonality of the sources of precipitation, and the effect of the El Nino - Southern Oscillation Index SOI on regional precipitation patterns [62] prompted an investigation of seasonal differences reflected in the stable isotopic composition of rainfall. Figure 9 shows a spline-fit to the δD of the monthly averaged precipitation, and the monthly average values for δD, $\delta^{18}O$ and d-parameter. An annual cycle in the data shows the effect of differing sources of moisture. Figure 10 shows the frequency distributions of the oxygen and hydrogen stable isotopic compositions of rainfall events. The distribution of values suggest 4 different precipitation patterns for the rainfall events. Pattern 1 is cyclonic storms that originate in the North Pacific and are swept across Arizona by the jet stream. Months that represent this pattern are October, November, February, March, April, and possibly May. The isotopic composition of these events is characterized by light isotopic values and an average d-parameter near 10.

Precipitation pattern 2 is dominated by "cut-off" low pressure systems that originate in the low latitudes of the Pacific and move across Arizona from the southwest. These storms generally occur during the months of December and January. Figure 9 shows distinct differences for precipitation during these months. The average δD and $\delta^{18}O$ are heavier and the d-parameter for this pattern averages 7.5.

Pattern 3 is from local convective systems that begin to appear in June and are fully represented during the months of July, August and September. The δD and $\delta^{18}O$ are isotopically heavier and the average d-parameter, 4.98, is lower than other precipitation. The source of this moisture is the lower latitudes of the Pacific and/or the Gulf of California.

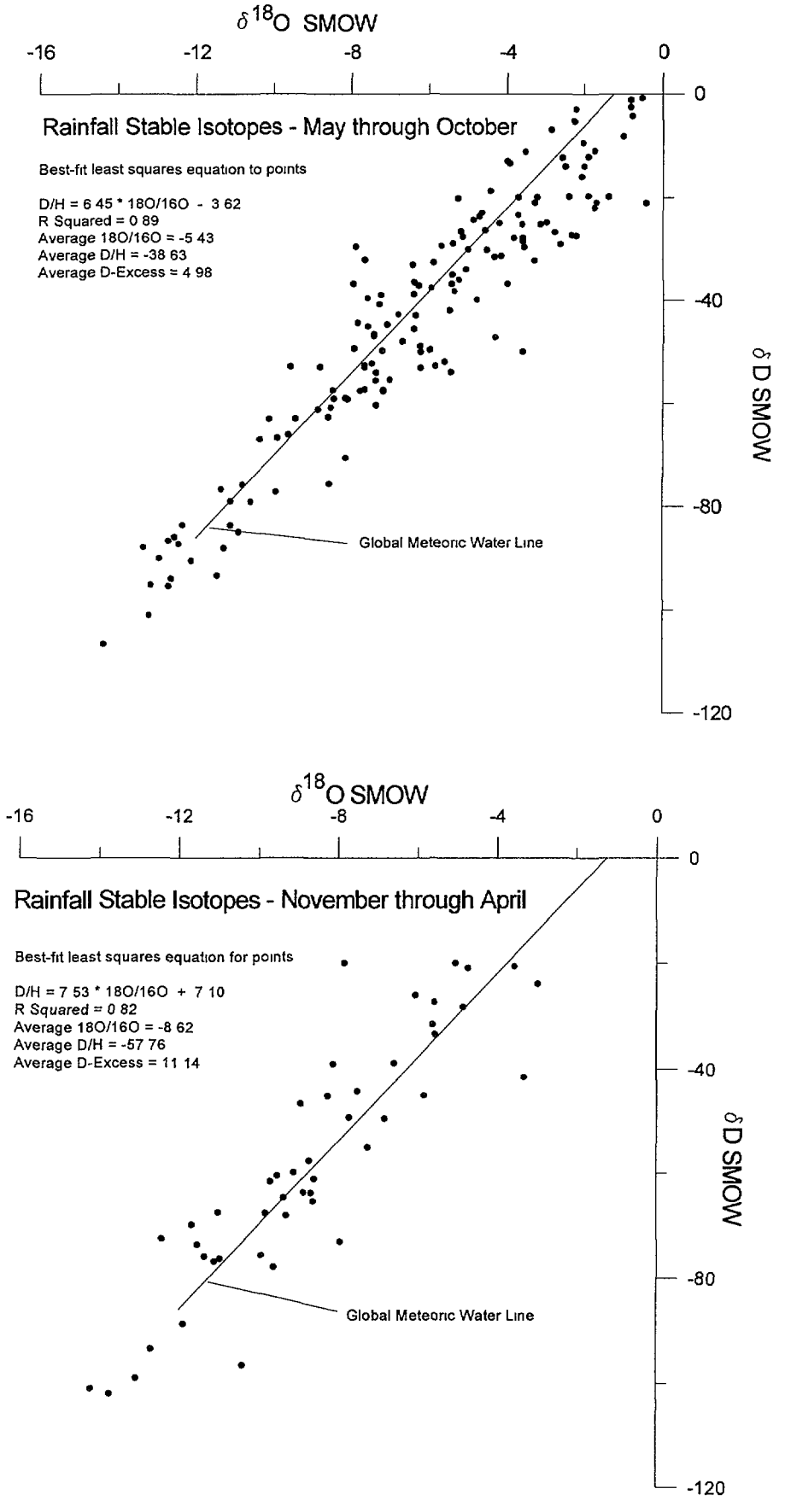

Figure 6. Stable isotopic composition of summer and winter precipitation 1981 - 1992

Pattern 4 is represented as a series of precipitation events during the summer months that are isotopically lighter than most summer convective events. These events also have d-parameters near and above 10. The isotopic signature of this pattern is similar to the precipitation events of pattern 1. The source of moisture for these events is cyclonic storms that move across Arizona during the summer months.

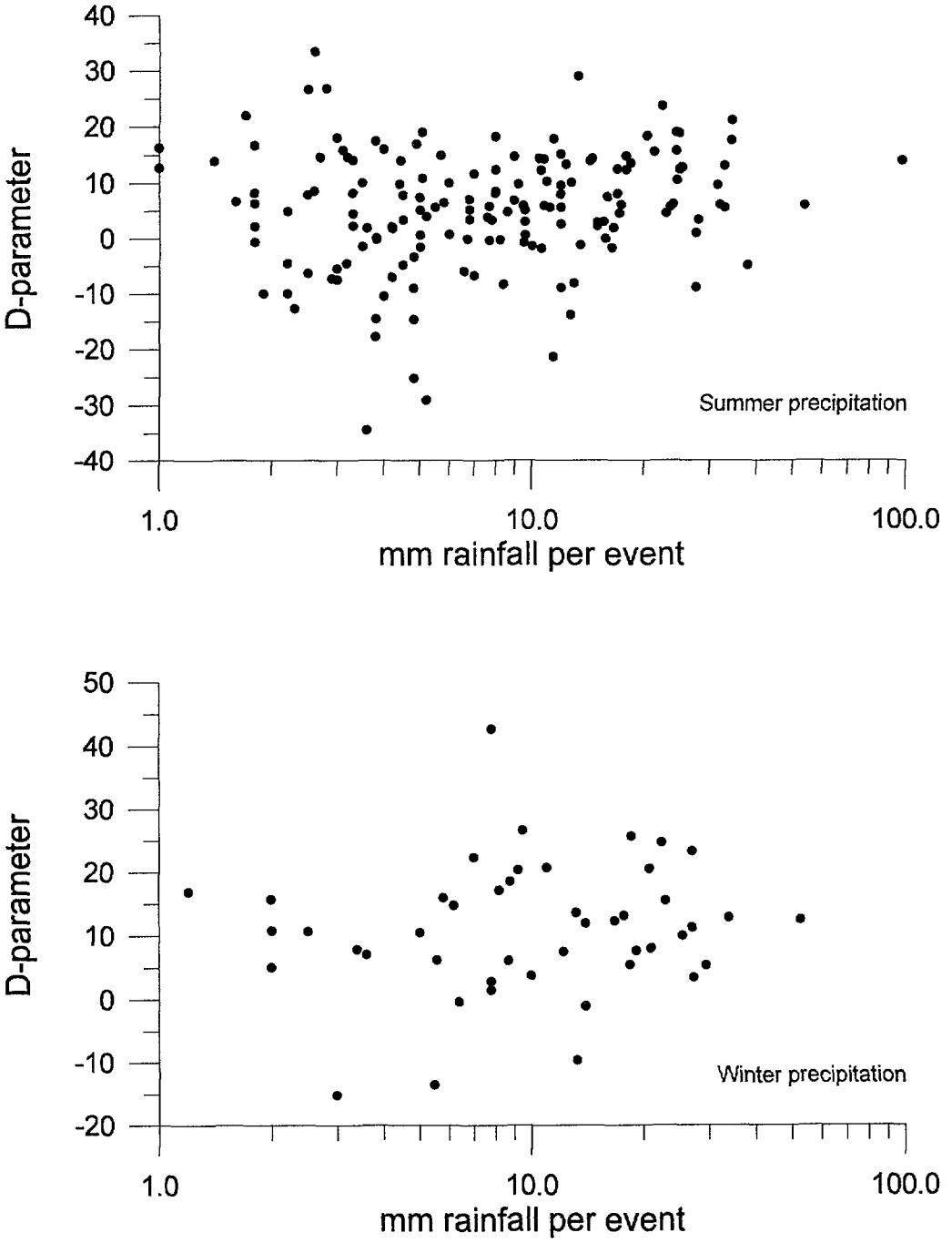

Figure 7. d-parameter of summer and winter precipitation against rainfall (mm)

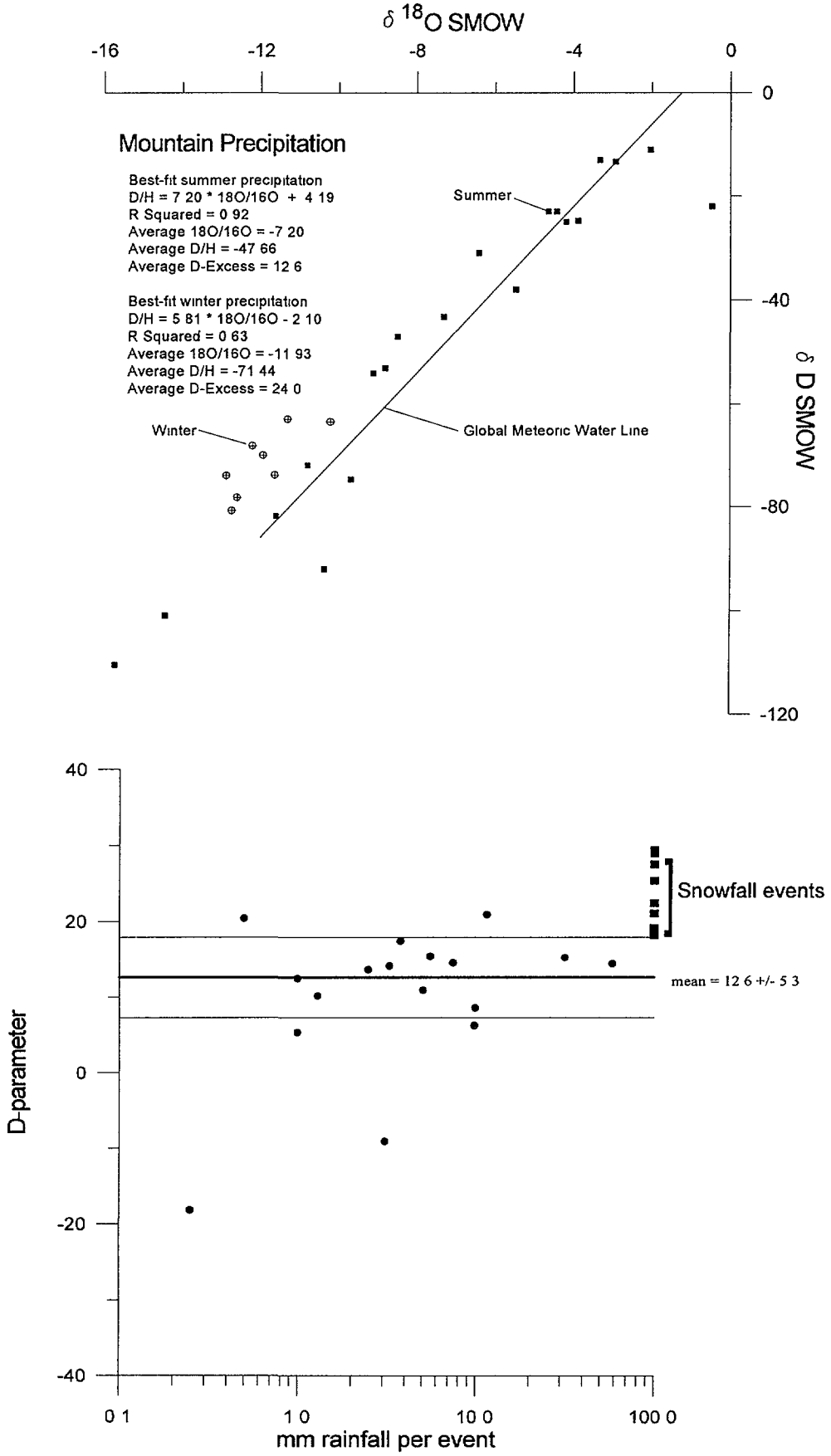

Figure 8. Stable isotopic composition of mountain precipitation and d-parameter against rainfall (mm)

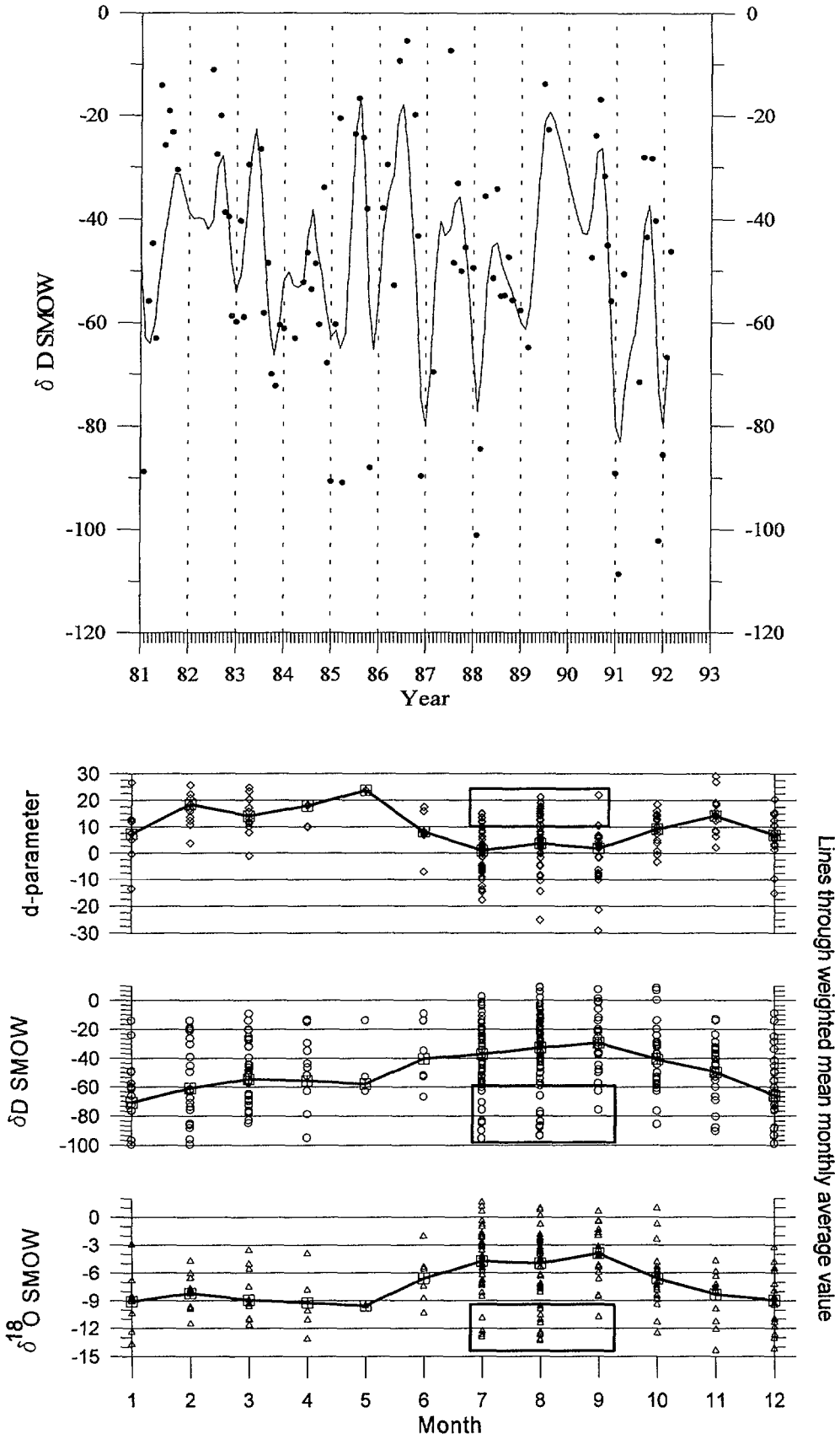

Figure 9. Seasonal variations in the δD, $\delta^{18}O$ and d-parameter of Tucson basin precipitation

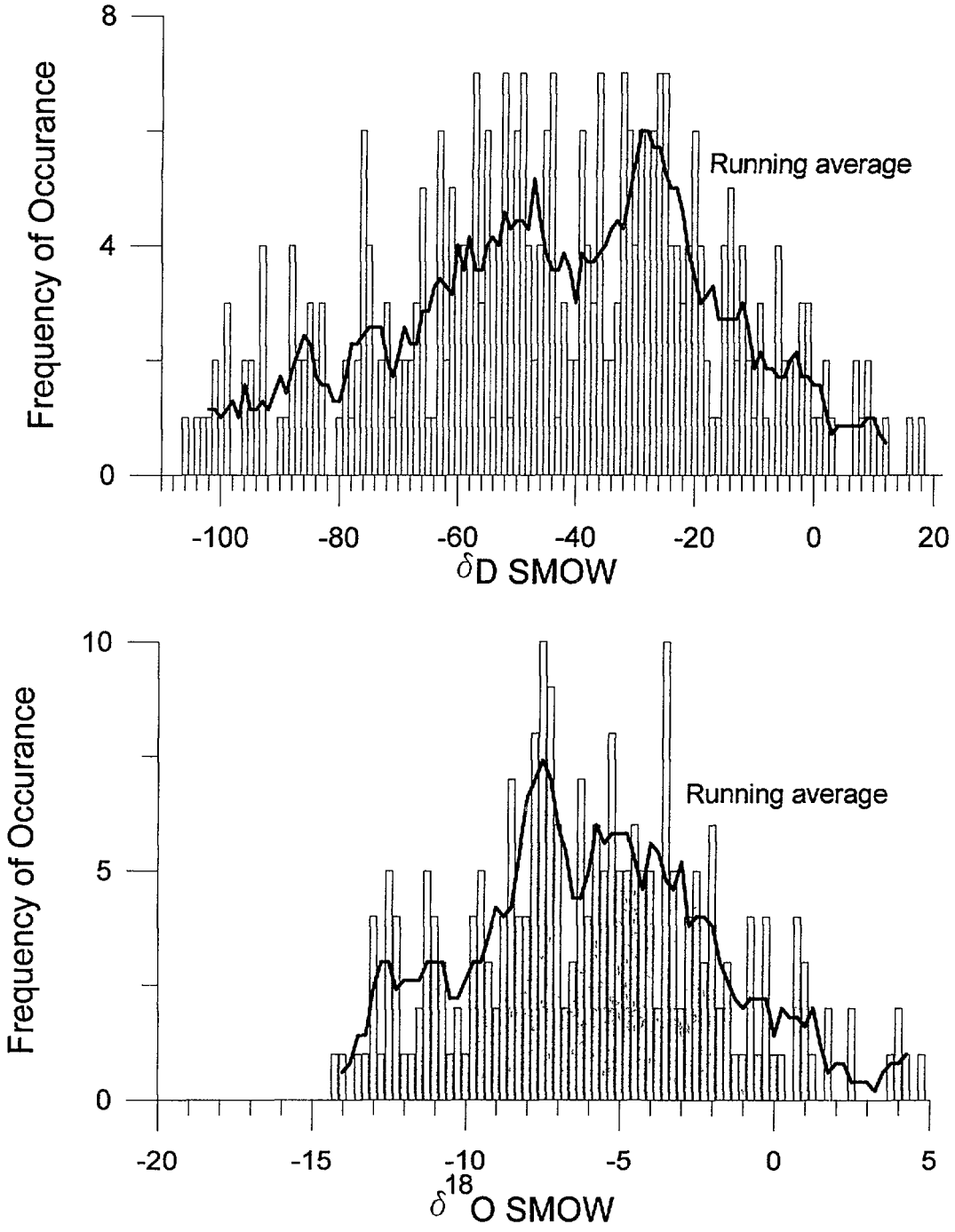

Figure 10. Frequency distribution of δD and $\delta^{18}O$ of precipitation 1981 - 1992

ISOTOPIC COMPOSITION OF RIVER WATER

River water samples were aperiodically collected from major rivers in the Tucson basin. The results of these samples are plotted in figure 11. The findings of this study are similar to those of Simpson *et al.* [33] for the Rillito River system that drains the Santa Catalina, Tanque Verde and Rincon mountains along the eastern and northern boundary of the basin. Winter precipitation and snow on the mountains provide most of the water sampled from the Rillito River and its tributaries. The result is isotopically light waters with an average d-parameter slightly above the global meteoric water line. The Santa Cruz River samples are significantly more enriched in heavy isotopes than those of the Rillito, and have an average d-parameter below the global meteoric line. This suggests that summer rainfall and precipitation from lower elevations comprise the greater proportion of water sampled from the Santa Cruz River. Infiltration through river bottoms is the primary mechanism of

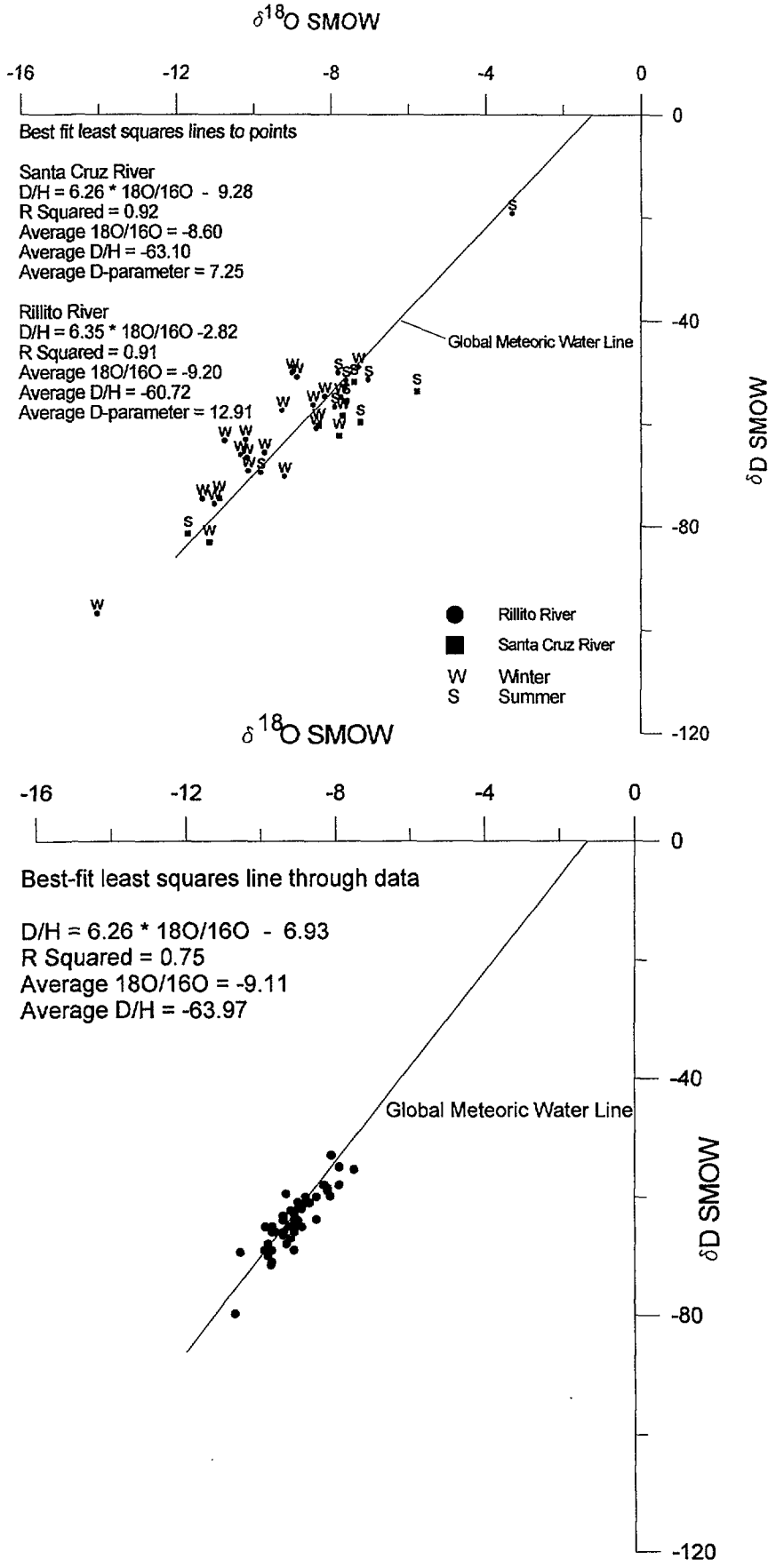

Figure 11. Stable isotopic composition of Tucson basin river water and groundwater samples

recharge to the Tucson basin aquifer. From these data, the stable isotopic composition of groundwater recharged along the Rillito River and its tributaries is expected to average $\delta^{18}O$ = -9.2 and δD= -64, and for groundwater that recharged along the Santa Cruz River, $\delta^{18}0$ = -8.6 and δD = -56.

STABLE ISOTOPES OF OXYGEN AND HYDROGEN IN GROUNDWATER

Simpson *et al.* [33] reported δD values of groundwater samples in the Tucson basin and concluded that most recharge to the system was from winter precipitation. An additional 142 samples of Tucson basin groundwater were analyzed for this study. Figure 11 also shows a plot of $\delta^{18}O$ vs δD of groundwater along with the global meteoric water line. Figure 12 shows the distributions of $\delta^{18}O$ and δD in the basin groundwater. The isotopic composition of groundwater is in general agreement with the mean isotopic signatures of River

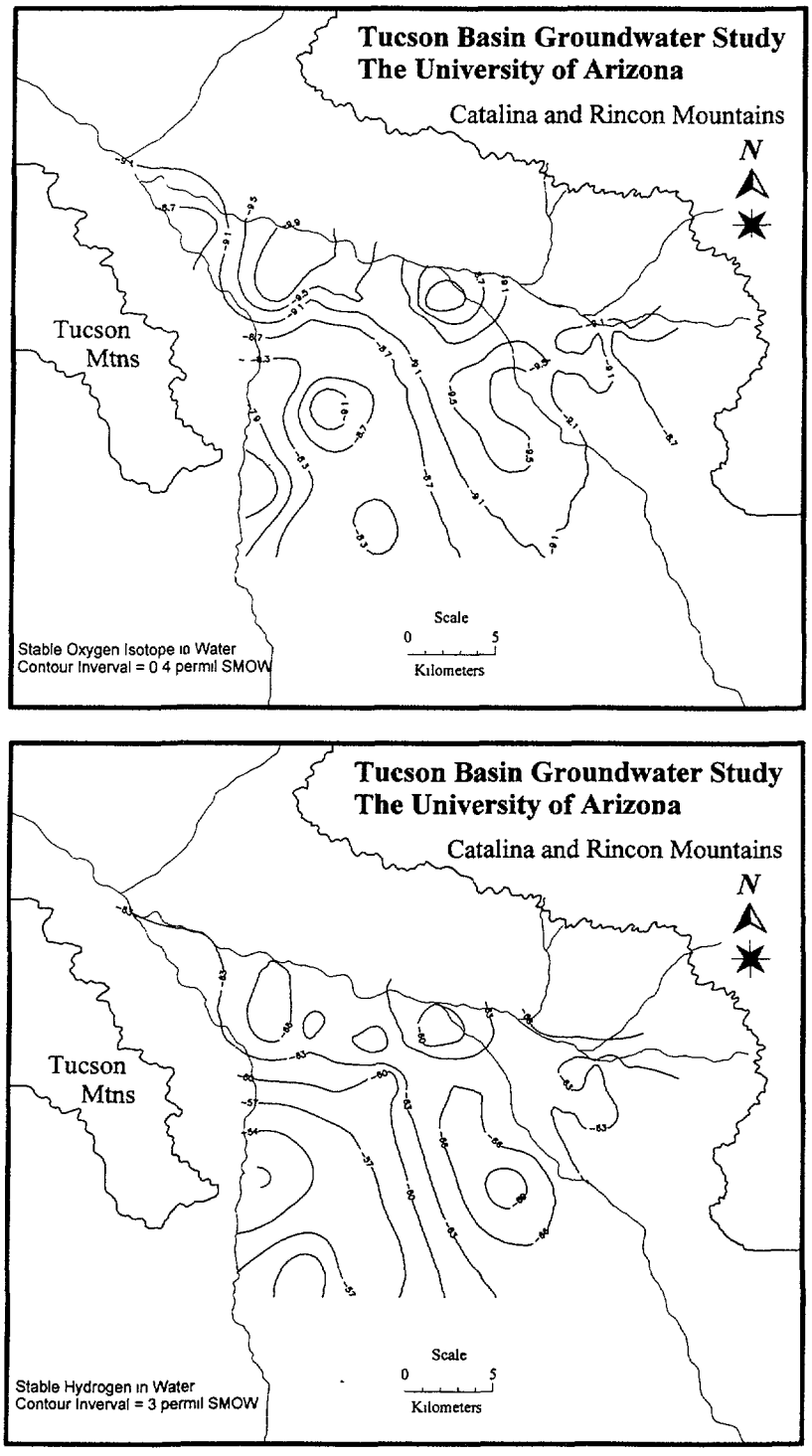

Figure 12. Spatial distribution of δD and $\delta^{18}O$ in Tucson basin groundwater

waters recharging the basin. Isotopic values are heaviest along the lower Santa Cruz River, $\delta^{18}O$ = -8.0 and δD= -57, where summer precipitation and precipitation from lower elevations dominate recharge. Some distinct zones of groundwater are isotopically lighter than River waters. These zones either represent a relatively large proportion of mountain-front recharge (high elevation mountain precipitation) or represent paleowaters. Only samples used for determining the geochemical evolution of groundwater are plotted. The least-squares line calculated through these points is similar to the local meteoric water line of all precipitation events analyzed.

Figure 13 plots of the frequency and cumulative frequency of these values. The distributions imply that for most wells sampled, recharge is derived from winter precipitation. There is, however, a small group of values indicative of summer precipitation or isotopically heavy "cut-off" low precipitation possibly related to ENSO activity [62]. These isotopically heavy values generally parallel the Santa Cruz River along the western edge of the Tucson basin. The Santa Cruz River has a large drainage system that extends into Mexico. It is plausible that summer rainfall does not greatly contribute to recharge of the basin groundwater system, but rather large-scale ENSO related storm events during October, November, and December produce significant recharge during high flow in the Santa Cruz drainage system.

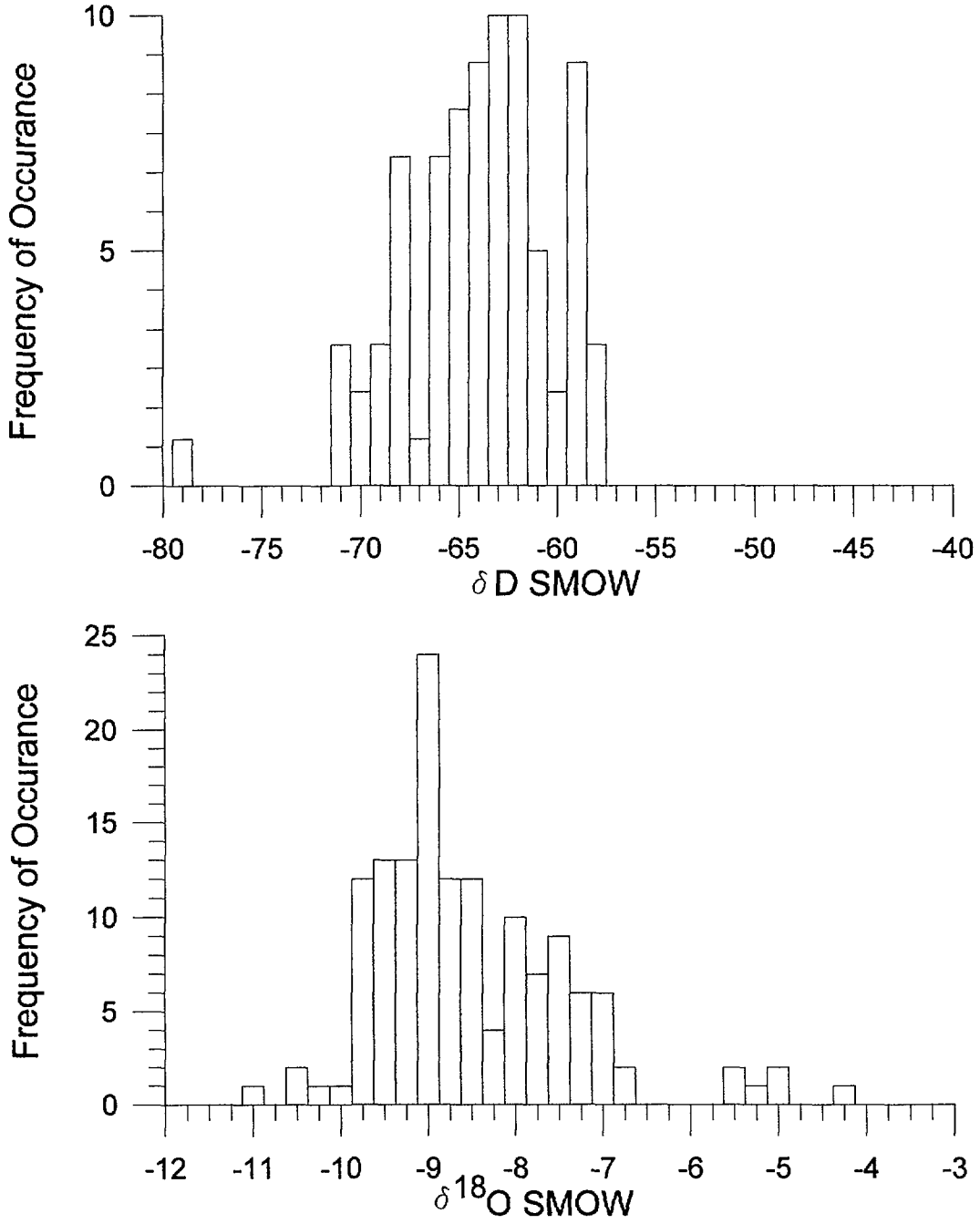

Figure 13. Frequency distribution Tucson basin groundwater δD and $\delta^{34}S$

RECHARGE ESTIMATES VIA TRITIUM

Figure 14 summarizes the results of Lindquist [1] and depicts the areal extent of detectable tritium in the near-surface groundwater of the Tucson basin. Areas of the basin suspected of having modern water containing detectable tritium, but for which we have no measurement, are represented with question marks in figure 14. Tritium is a naturally-occurring radioactive isotope of hydrogen with a half-life of 12.42 years. The concentration of naturally-produced tritium in precipitation prior to 1954 was estimated to be 5 to 24 tritium units (TU) [118]. (1 TU is defined as 1 ^{3}H in 10^{18} H atoms) During the 1950's and early 1960's, thermonuclear bomb testing injected tritium into the atmosphere. This "bomb pulse" increased tritium in Arizona precipitation

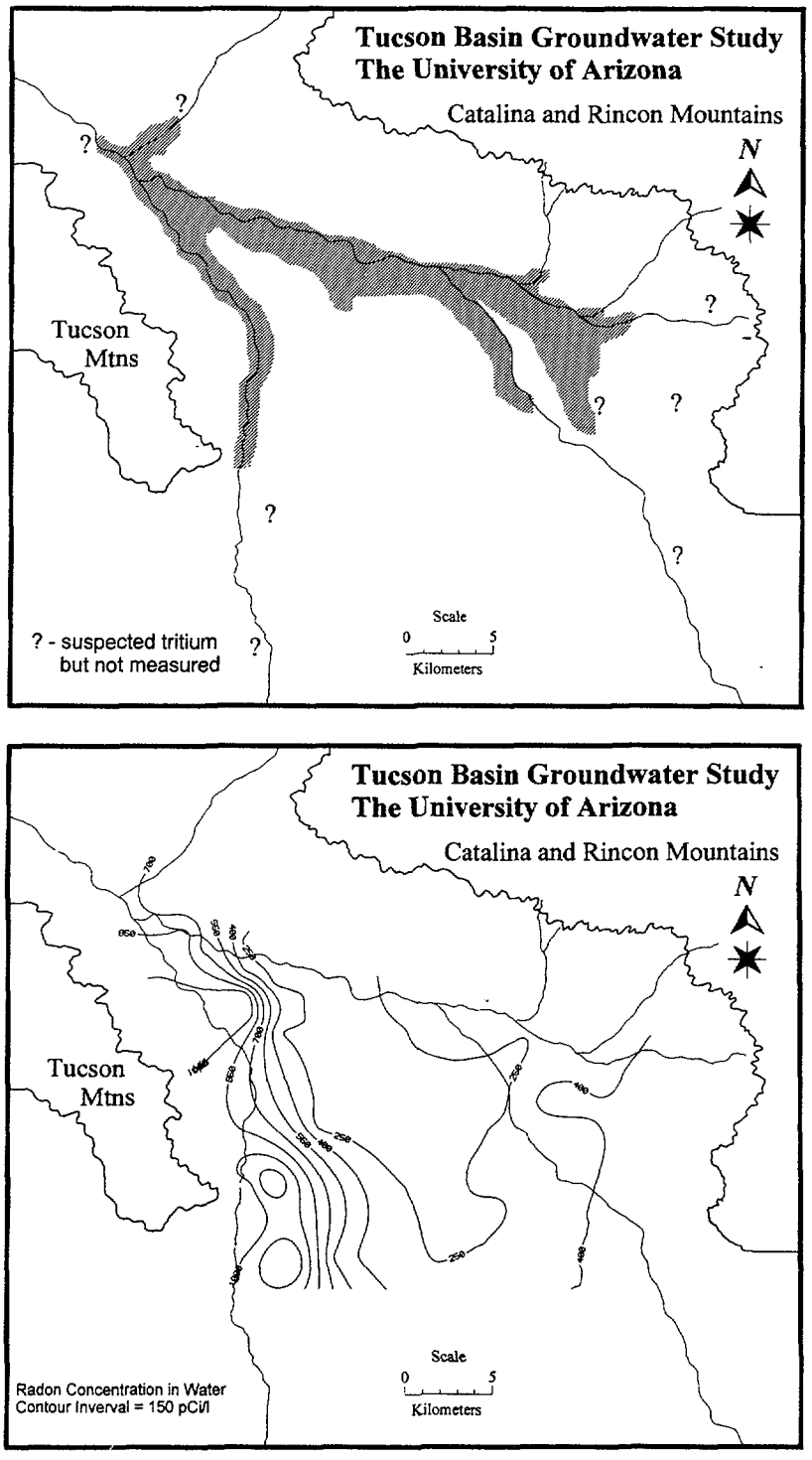

Figure 14. Spatial distribution of tritium and ^{222}Rn in Tucson basin groundwater

to levels as great as 4,400 TU. The average tritium concentration in Arizona precipitation for the period 1962-1965 was 1140 TU [119]. During the period since the cessation of atmospheric thermonuclear testing, the tritium concentration in precipitation has decreased due to radioactive decay and mixing in the hydrosphere. The tritium concentration in southwestern North American precipitation for the period 1983 - 1988 averaged 10.6 +/- 3.8 TU [119]. Post-1954 recharge to groundwater can be distinguished from older waters by the presence of measurable tritium.

Recharge rates were calculated from location of the post-1954 recharge front (samples containing measurable quantities of tritium) [3] using the following equation:

$$R = V * W * \eta * (b*C_m/C_i)$$

where R is the average annual recharge rate (m^3/yr), V is the average linear flow velocity in the hypothetical flow tube leading to the well (m/yr), W is the width of flow tube (m), η is the effective porosity of the aquifer (0.30), b (m) is the thickness of the aquifer sampled along the flow tube (total saturated thickness sampled as a results of perforations in the production well), C_m is the measured tritium concentration at the well and C_i is the 40-year decay corrected average input concentration of tritium (24 TU) (table 2). Burkham [12] estimated recharge rates (table 2) along the rivers in the Tucson basin using flow-duration curves that related infiltration rates to recharge during the period 1936 to 1963. Anderson [8] developed an electrical-analog model of the Tucson basin hydrologic system. Anderson's recharge estimates for the 1940 steady-state modelled period are in table 2. Hadj-Kaddour [54] calculated recharge rates along the Rillito Creek through deconvolution of the well-response function for 1960 data (table 2).

Table 2. Comparison of Recharge Rates from rivers in the Tucson basin Arizona

River Recharge	Average Recharge Rate (x 10^6 m^3 yr^{-1} km^{-1})		
Study	Rillito River	Tanque Verde River	Pantano Wash
Lindquist [1]	0.92	0.69	0.84
Burkham [5]	0.63	0.33	0.18
Anderson [1]	0.15	0.14	0.11
Hadj-Kaddour [61]	0.92 - 1.9	-	-

RADON IN TUCSON BASIN GROUNDWATER

The results of ^{222}Rn analyses [2] of basin groundwater are plotted in figure 14. The processes by which ^{222} Rn enters the groundwater from aquifer minerals are weathering, diffusion, indirect radioactive recoil and direct radioactive recoil. The effect of these processes are referred to as the emanation power of a radium-bearing mineral, defined by Tanner [120]. The relationship between the hydrogeology and radon concentrations in groundwater has been documented [120-133]. Semprini [128] and Kalin [2] focused on the relationship between radon concentration in groundwater and the hydrogeology of an alluvial aquifer. They concluded that radon concentrations in groundwater are derived directly from aquifer minerals and that radon concentrations increase with decreasing particle size of aquifer material. Fine grained sediments have greater surface area and shorter pathways of radon to the groundwater. Therefore, fine grained sediments have an enhanced potential that direct radioactive recoil will result in radon exiting the mineral and entering the groundwater. The spatial variability of radon in Tucson basin groundwater is most likely controlled by differences in lithology. Lithologic changes in the Tucson basin represent changes in the depositional environment, from high energy along the basin edges to low energy in the central basin. Graben faults have up-thrown lower stratigraphic units along the western and far eastern basin margins, and are suspected of producing very fine-grained fault breccia and gouge.

The interior well field of mid-Tucson represents background concentrations of ^{222}Rn, ranging from 125 to 483 pCi/l. The anomalous ^{222}Rn concentrations, approaching 2,000 pCi/l, along the western basin are hypothesized by Kalin [2] to be due to changes in lithology associated with the Santa Cruz graben fault. These results suggest that regional lithologic compositions control radon values. The chemical composition of groundwater will be in-part controlled by the lithology of the aquifer system. Therefore, the chemical composition of Tucson basin groundwater can be expected to change in the western basin.

STABLE ISOTOPES OF SULFUR AND OXYGEN IN DISSOLVED SULFATE

The distribution of the measured $\delta^{34}S$ values is presented in figure 15. The results of these analyses suggest multiple sources of sulfate in basin groundwater. The $\delta^{34}S$ values along the Rillito River show variable mixing between SO_4 sources. As the groundwaters evolve down-gradient, geochemical reactions and admixture of shallow water with water from deeper stratigraphic units progressively increase the $\delta^{34}S$ isotopic value.

An attempt was made to collect end-member sulfate phases from drill cutting archives, but during drilling of production wells in the basin, the cuttings are washed and contaminated with drilling mud, yielding samples of questionable value. The $\delta^{34}S$ values of the sulfate sources were estimated empirically using results on dissolved sulfate. Figure 15 shows the results plotted as $\delta^{34}S$ vs $1/[SO_4]$. There are three hypothesized

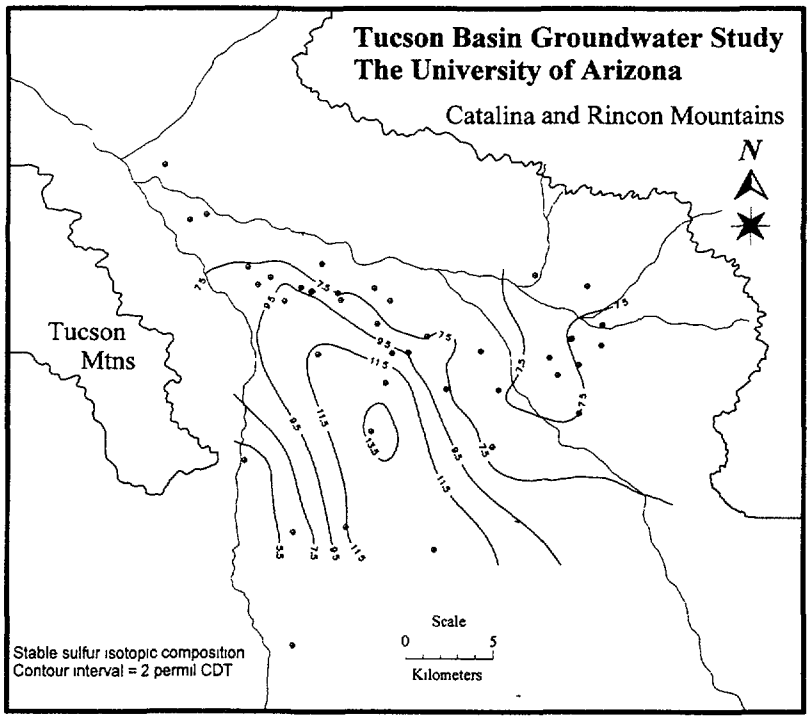

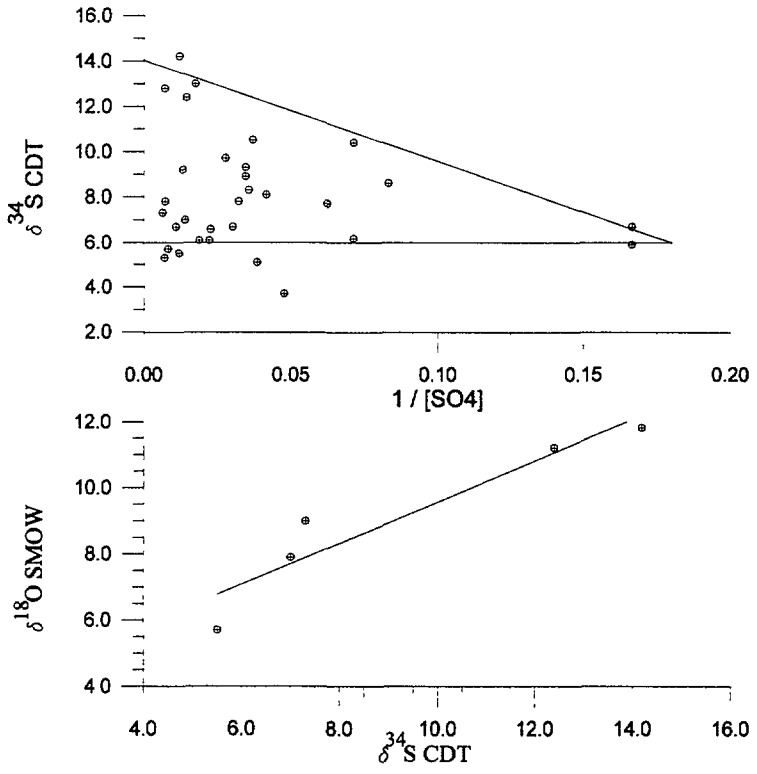

Figure 15. Distribution of $\delta^{34}S$ in Tucson basin groundwater and relationship of $\delta^{34}S$ with $[SO_4]$ and $\delta^{34}S$

mechanisms that produce the distribution of data, 1) reactions of river water or mountain-front water ($\delta^{34}S$ = 6 CDT estimated for both) with sulfate phases in basin minerals ($\delta^{34}S$ = 13 estimated); 2) mixing of recharge water (low sulfate $\delta^{34}S$ = 6 CDT) and mountain-front recharge water (high sulfate $\delta^{34}S$ = 6 CDT); and 3) values between the previous trends due to mixing of the two water types, either intrawell or along flow paths. The hypothesized values of $\delta^{34}S$ will be used when modelling the geochemical evolution using NETPATH.

Figure 15 also plots $\delta^{34}S$ vs $\delta^{18}O$ in dissolved sulfate for 6 groundwater samples. These waters were selected based on the results of the $\delta^{34}S$ analyses. These samples represent $\delta^{18}O$ in sulfate values of the sulfate mineral phases in the basin, recent recharge water to the basin, waters that may have anthropogenic sulfate and a water sample which is a mixture of $\delta^{34}S$ end-members. The $\delta^{18}O$ of sulfate is directly correlated to $\delta^{34}S$ and therefore, further study of the $\delta^{18}O$ in dissolved sulfate species may not enhance interpretation of the geochemical evolution of basin groundwater. $\delta^{18}O$ values of sulfate may help in tracking potential anthropogenic sources of sulfate for specific regions within the basin. Further study of this is warranted.

STABLE CHLORINE ISOTOPIC DATA

Six samples were collected for analysis of stable $\delta^{37}Cl$. Christopher Eastoe performed the analysis of these samples at the University of Arizona, Laboratory of Isotope Geochemistry. The results of these samples have an uncertainty of 0.09‰ and have been published by Long *et al.* [134] without interpretation.

The average chloride concentration of the groundwater in the basin is low, <30 mg/l. The sources of Cl^- are initial meteoric chloride in recharge water, fluid inclusions in minerals, stratigraphically controlled evaporite deposits and recharge of secondary treated effluent and CAP water. There is no compelling evidence that suggests what source produces the small increase in chloride during the hydrogeochemical evolution in the Tucson basin. If any halite existed in the Ft. Lowell fm., it has long since been dissolved. The selection of samples, representing different sources of chloride, was based on the preliminary geochemical model of the basin ground waters. Three samples were selected that represented post-bomb recharge waters. These waters all have either meteoric chloride or anthropogenic sources of dissolved salts and are all positive with respect to the Sea Water Standard defined as 0 permil $\delta^{37}Cl$. Three waters were selected and that represent waters in contact with lower stratigraphic formations. All of these water samples have negative $\delta^{37}Cl$ values. Long *et al.* [134] suggested that the isotopically light values for brines could potentially be used to identify leakage into potable groundwater supplies. It is inferred that $\delta^{37}Cl$ of recently recharged meteoric or anthropogenically derived chloride may be isotopically different from $\delta^{37}Cl$ of chloride in the mineral phases or deep, high TDS water.

Figure 16 shows a plot of $\delta^{37}Cl$ vs. 1/[Cl] and $\delta^{37}Cl$ plotted against $\delta^{34}S$. Given the uncertainty of +/- 0.09‰ $\delta^{37}Cl$ for these measurements, it is hypothesized that the data represents only two sources of chlorine isotopes, one isotopically heavier than sea water (meteoric or anthropogenically derived) and one isotopically depleted with respect to sea water (lithological source). The results of figure 16 generally support this hypothesis. The lighter values for $\delta^{37}Cl$ coincide with heavier values of $\delta^{34}S$. $\delta^{37}Cl$ isotopic values may be potentially useful when interpreting the geochemical evolution of groundwater in alluvial basins and the effects of anthropogenic contamination, but due to the high cost of analysis and small difference in values between chloride sources, other isotopic data should first be examined.

STABLE AND RADIOACTIVE CARBON ANALYSIS RESULTS

Over 100 analyses of ^{14}C from various groundwater and unsaturated zone studies in the Tucson basin are now available. The samples were collected and analyzed according to published methods [135-140].

The distributions of $\delta^{13}C$ and ^{14}C in the basin are presented in figure 17. The results of the stable carbon isotopic analyses of the DIC show the influence of active recharge/carbonate dissolution zones along the Rillito River system. As water moves down-gradient, the stable carbon isotopic value of groundwater approaches an average value between -10 and -11 permil PDB. This is due to reactions between recharge water and the carbonate and dissolved CO_2 phases in the recharge zone. Concentrations of dissolved organic carbon (DOC) in Tucson basin groundwater range between 0 and 7 mg/l. The influence of oxidation of DOC on ^{14}C and $\delta^{13}C$ values of DIC is estimated when modelling with NETPATH, but DOC has little effect due to the small mass-balance of carbon from this source in down-gradient wells. Further study of DOC in Tucson basin groundwater is needed. The distribution of radiocarbon in DIC is, in-part due to dilution with depleted carbon through reactions with carbonate phases and, in-part to radioactive decay of ^{14}C.

Constraint of end-member carbon phases is crucial for reconciliation of both radiocarbon and stable carbon isotopes during geochemical modelling of groundwater. Table 3 summarizes radiocarbon and stable carbon isotopic results on solid and gas phase carbon. The data are results of unpublished carbonate analyses from samples collected in recharge zones throughout southern Arizona. The average value of the $\delta^{13}C$ in recharge zone carbonates was -4.5 +/- 1.0 ‰. There is a large range of values in the ^{14}C content of carbonates from recharge zones. This study assumes a conservative estimate of 10 percent Modern Carbon (pMC), 1950 atmosphere ≡ 100.0 pMC, for carbonates in regions in the Tucson basin where rapid groundwater velocities and

geochemical evolution under open conditions exist. A value of 5 pMC was assigned to the carbonate phase in regions of the Tucson basin where groundwater ages are suspected to be less than 100 years and for where the movement of water parallels the recharge zone. Measured values of carbonate phases from well cuttings in the central basin have an average of -2.5‰ $\delta^{13}C$ and 1 pMC.

MINERALOGY OF BASIN SEDIMENTS

In an attempt to constrain controlling hydrogeochemical reactions in the Tucson basin groundwater the author reviewed the literature [4, 18, 21, 65-69, 142-157] and performed experimental analysis on basin fill sediments using X-ray diffraction, X-ray fluorescence, microscopic and petrographic analysis. Quartz, plagioclase, calcite, orthoclase, muscovite, biotite, chlorite, and clay are the dominant minerals in the bulk fraction. Garnet, epidote, pyroxenes and amphiboles were detected in some samples and x-ray florescence data suggested the presence of apatite, ilmenite and dolomite in some samples. Minerals identified in thin section are

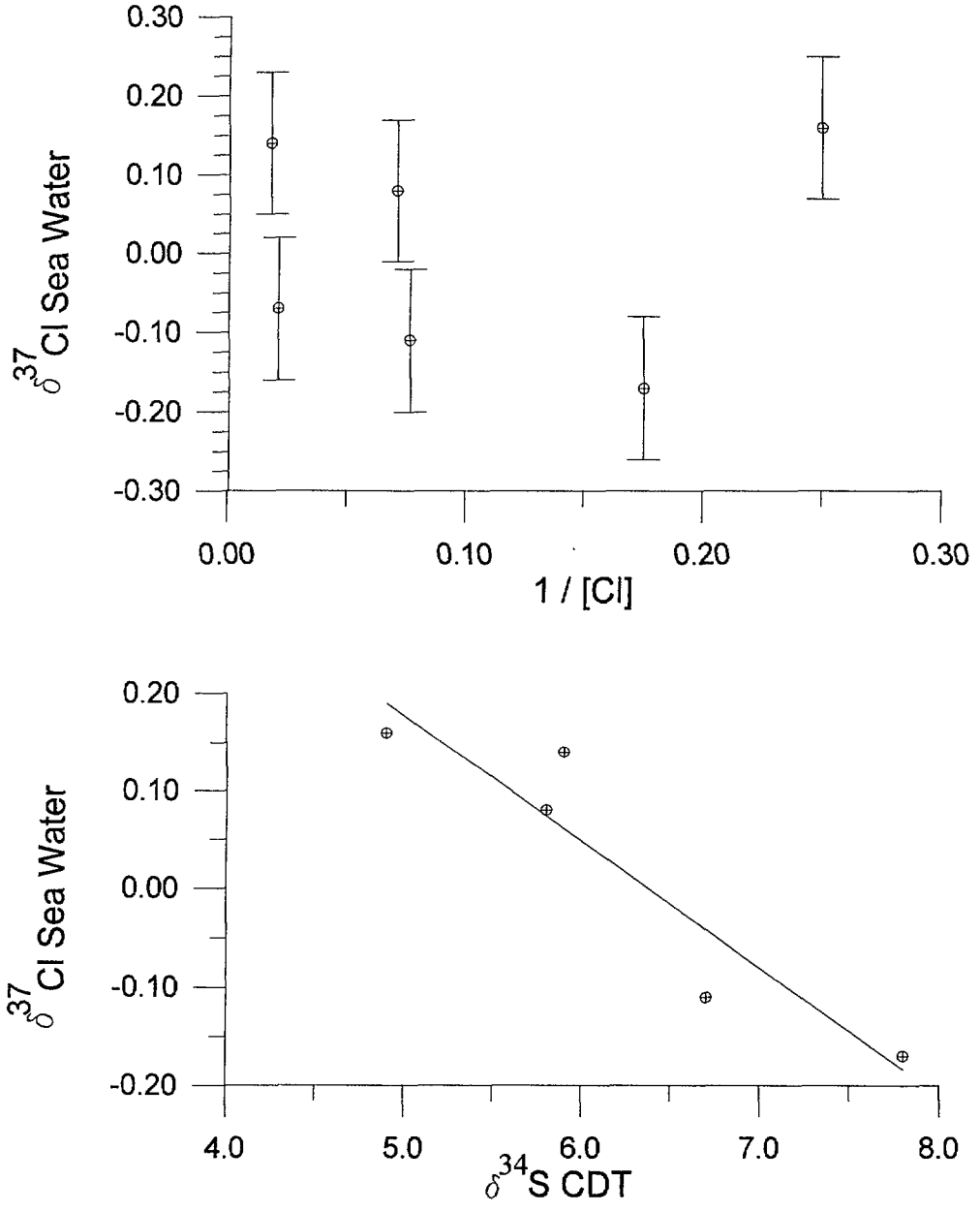

Figure 16. $\delta^{37}Cl$ relationship with [Cl] and $\delta^{34}S$

plagioclase, biotite, quartz, and calcite. Microscopic investigation of sand-size grains shows the presence of quartz, plagioclase, ferrihydroxides, orthoclase, chlorite, ilmenite?, biotite, and garnet. X-ray diffraction mineral identification on the less than 2-micrometer fractions of basin fill used the standard procedure of Dixon and Weed [156]. The samples were mounted on quartz slides and scanned at a rate of 2 degrees 2 theta. The samples were then treated with ethylene glycol and reanalyzed. Peaks that shifted after treatment with ethylene glycol indicate montmorillonite. Other peaks correspond to micas, calcite, illite and kaolinite [157]. As suspected, the major clay component was smectite.

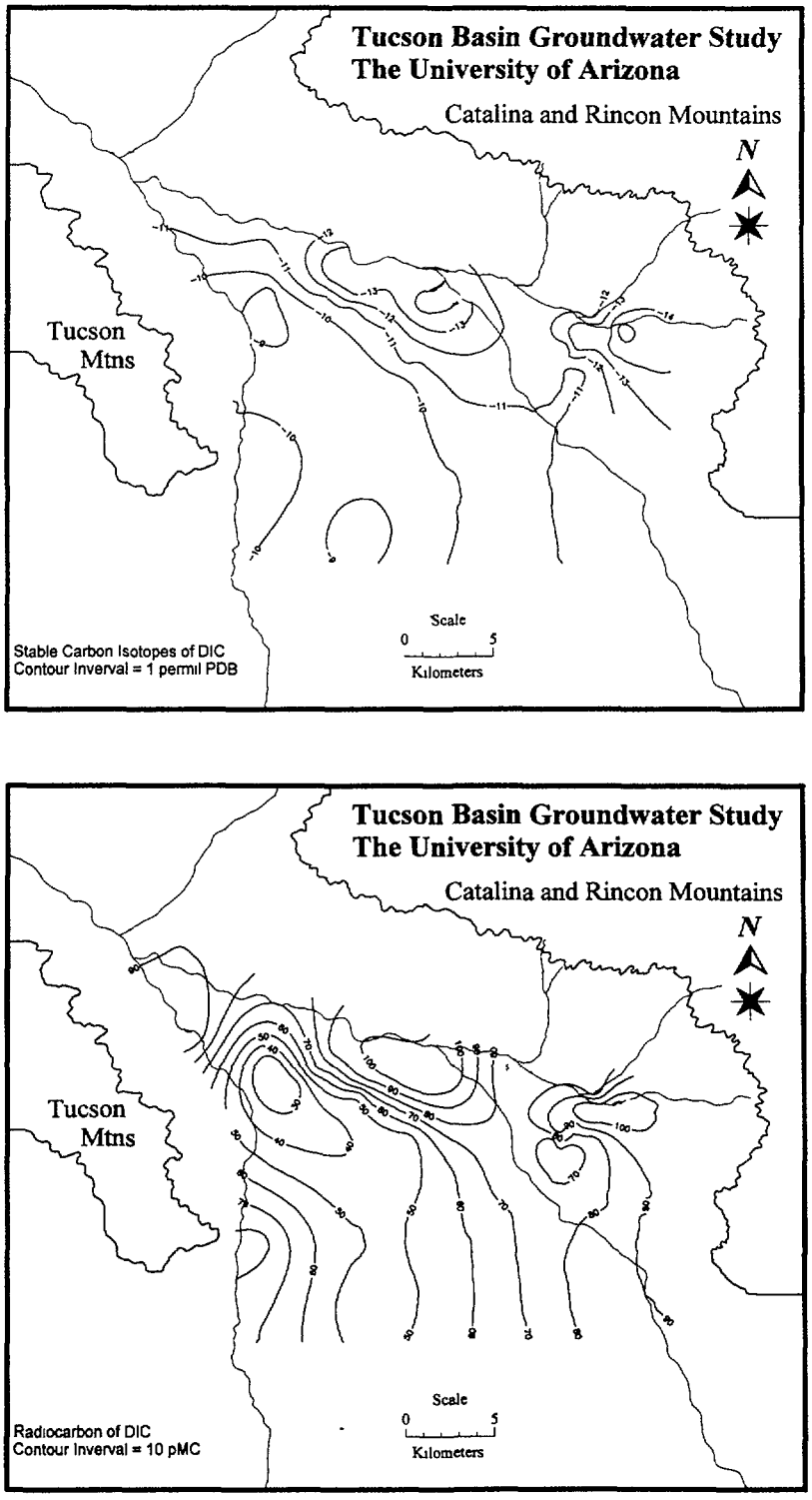

Figure 17. Spatial distribution of $\delta^{13}C$ and ^{14}C in Tucson basin groundwater DIC

Table 3. Values of carbon phases used to constrain reaction path modelling.

Carbon Phase	$\delta^{13}C$ Measured	^{14}C PMC Measured
Recharge Zone Carbonates[141]	Average Value = -4.5‰	Average Value = 10 pMC
Mixing Zone Carbonates	Estimated Value = -3.5‰	Estimated Value = 5 pMC
Deep basin Carbonates	Average Value = -2.5‰	Average Value = 1 pMC
Soil Gas CO_2[140] Deep Tucson basin	Average Value = -18‰	Range 115.9 - 61.6 pMC Surface - Depth
Soil Gas CO_2[140] Recharge Zones	Average Value = -19.1‰	Estimated Value = Modern
Soil Gas CO_2[141] Recharge Zones Southern Arizona	Average Value = -20.3‰	Estimated Value = Modern
River Water 1965	N/A	142.6 pMC

The author performed X-ray fluorescence analyses on 14 samples of both 120 mesh and less than 62 micrometer size fractions. The stoichiometric composition of each mineral is constrained by the X-ray florescence results, and is used in NETPATH when modelling water-mineral reactions.

CONTROLLING GEOCHEMICAL REACTIONS

Table 4 shows stoichiometrically determined plausible reactions that control the geochemical evolution of the basin groundwater based on the major minerals in basin-fill and the thermodynamic stability of each mineral. Selection of mineral phases and stoichiometry must agree with the chemistry of the groundwater, because the water chemistry is controlled, in part, by the chemistry of water-rock interactions. In the recharge zones, high pCO_2, ca. $10^{-2.0}$ [24], is a source of H^+ for the dissolution of calcite and the incongruent weathering of silicate minerals. Silica concentrations in the recharge zones are oversaturated with most silica mineral phases. The geochemical evolution of groundwater chemistry is controlled both thermodynamically and

Table 4. Plausible chemical reactions occurring during the geochemical evolution of groundwater in the Tucson basin.

(1) Congruent dissolution of Tucson basin high-magnesian calcite:
$Ca_{1.3}Mg_{0.7}(CO_3)_2 + 2H_2O \rightleftharpoons 1.3Ca^{+2} + 0.7\ Mg^{+2} + 2HCO_3^- + 2OH^-$

(2) Formation and dissociation of carbonic acid:
$CO_2 + H_2O \rightleftharpoons H_2CO_3 \rightleftharpoons H^+ + HCO_3 \rightleftharpoons H^+ + CO_3^=$

(3) Incongruent dissolution of Oligoclase and formation of Tucson basin smectite clay:
$Ca_{05}Na_{90}Al_2Si_3O_8 + 12H_2O \rightarrow [(Ca_{.167},Mg_{45},K_{1},Fe_{05})]Al_2Si_{3\ 67}O_{10}(OH)_2H_2O + (Ca^{+2}) + (Na^+)$

(4) Incongruent dissolution of Biotite:
$K(MgFe)_3(AlSi_3O_{10})(OH)_2 + 3H_2O + 8H^+ \rightarrow K^+ + 3\text{-}xMg^{+2} + x\text{FeOOH} + Al(OH)_3 + 3H_4SiO_4$

(5) Incongruent dissolution of Orthoclase and formation of Tucson basin Smectite clay:
$KAlSi_3O_8 + 7H_2O + H^+ \rightarrow K(Ca_{.167},Mg_{45},K_{1},Fe_{05})Al_2Si_{3\ 67}O_{10}(OH)_2H_2O + NH_2O + K^+$

(6) Hydrolysis of silica:
$SiO_2 + 2H_2O \rightleftharpoons H_4SiO_4$

(7) Congruent dissolution of Gypsum/Anhydrite:
$CaSO_4 \circ 2H_2O \rightleftharpoons Ca^{++} + SO_4^=$

(8) Formation of Goethite orFerrihydroxides:
$Fe + O_2 + H_20 \text{ --> } FeO(OH)_2$

(9) Ion Exchange:
$(Na,K)_2$ - clay + $(Ca,Mg)^{+2}$ --> (Ca,Mg) - clay + 2 $(Na,K)^+$

stoichiometrically. Reactant and product phases modelled in the groundwater system are constrained by the solubility of each phase. The speciation of dissolved constituents and the fugacity of gas phases are calculated to determine the mineral saturation index.

$$SI = Log\frac{IAP}{K_{eq}}$$

If SI is less than 0 the measured IAP is thermodynamically undersaturated with respect to the given phase. Conversely, if SI is greater than 0 the IAP is thermodynamically oversaturated. The IAP, K_{eq} or SI of a phase does not predict the reactions that will occur, but rather a potential for a given reactive phase. Kinetic hindrances or competing reactions may inhibit a phase from taking part in a chemical reaction.

Data required for the accurate determination of SI include accurate chemical analyses of major and minor dissolved constituents, field pH, temperature, alkalinity, and when electro-chemical reactions are expected, accurate Eh.

CHEMISTRY OF TUCSON BASIN GROUNDWATER

The City of Tucson, Water Department provided 45 years of chemistry data for many of the wells in the Tucson basin. The Flowing Wells water company, which operates a small nest of wells in the Tucson basin, provided this study with chemical analyses of wells sampled over the last decade. These data, with data from the literature [4,10, 16, 17, 20, 21, 23, 24, 26, 27, 33] were compiled for geochemical modelling. Rose [158] and Cheng [159] present descriptive discussions of the general chemical trends of Tucson basin groundwater. Complete discussion of the chemistry of all data is beyond the scope of this work. In general, the basin groundwater is rather dilute, suggesting that most water presently mined from the basin has undergone water-rock reactions in the unconsolidated Ft. Lowell fm; a minor amount of water mined has reacted with the Tinaja bed. The Tinaja fm. contains evaporites in lower stratigraphic units, but the Ft. Lowell fm. contains no evaporites.

The chemical composition of Tucson basin groundwater is controlled by the weathering reactions listed in table 4. These reactions refine our understanding of the source of dissolved constituents [160].

Hydrogen ion, H^+, required for the incongruent dissolution of silicate minerals and congruent dissolution of carbonates, derives from the dissociation of carbonic acid that is in equilibrium with the partial pressure of CO_2 in the unsaturated zone. Oxidation of pyrite/marcasite and the hydrolysis of Fe^{+3} to $Fe(OH)_3$ also produces H^+ in groundwater systems but is not a major contributor for the Tucson basin.

Sodium and calcium ions in Tucson basin groundwater, Na^+ & Ca^{+2}, originate from the incongruent dissolution of plagioclase to form clay minerals. Cation exchange of divalent cations for Na^+ and evaporite deposits are additional potential sources of Na^+. Where carbonate minerals exist, Ca^{+2} is controlled by the solubility of calcite or high magnesium calcite. Gypsum/anhydrite is also a source of Ca^{+2}.

Mg^{+2} and K^+ , magnesium and potassium ions, result from the incongruent weathering of biotite. Additional sources of Mg^{+2} include ferromagnesian minerals (pyroxenes and amphiboles) or dolomite/high magnesium calcite. Some K^+ originates from the incongruent weathering of feldspar.

Dissolved silica species derive from the incongruent dissolution of silicate minerals. Quartz, because of its near inertness, contributes insignificant dissolved silica even with the ubiquitous nature of quartz in basin fill material. Solubility constraints may be controlled by clay formation or perhaps chalcedony.

Naturally occurring chloride, Cl^-, is controlled by the concentration of chloride in meteoric precipitation, river water, release of fluid inclusions during the weathering of minerals and from discharge of waters in contact with evaporite minerals.

Sulfate, SO_4^{-2}, ions derive from meteoric precipitation, dissolution of gypsum/anhydrite or other sulfate minerals, and from the oxidation of sulfide minerals.

Bicarbonate, HCO_3^-, forms from the dissolution of calcite and other carbonate minerals as well as the dissolution of CO_2 gas and the dissociation of carbonic acid, H_2CO_3.

The concentration of aluminum in groundwater is kept low by the solubility constraints of gibbsite and other aluminum hydroxide species. The pH range of Tucson basin groundwater is between 6.7 and 7.9. The dissolved aluminum will be between 10^{-7} and 10^{-6} M. Measured aluminum concentrations were between 6×10^{-5} and 2×10^{-4} M. This range lies within the gibbsite stability field. Therefore, aluminum is considered conservative in the solid phase for all chemical weathering reactions that involve aluminum.

Likewise, the concentration of iron (Fe^{+3}) in Tucson basin groundwater is controlled by the stability of goethite and ferrihydroxides. Dissolved oxygen is ubiquitous in basin groundwater [158]. The Eh of Tucson basin groundwater is between 0.3 and 0.9 volts and the pH range is between 6.7 and 7.9. This places the water in the stability field of the mineral goethite. This concentration of iron, between 10^{-7} and 10^{-8} M, is in the range of values presented in tables 5a and 5b. Therefore, the dissolution of iron from biotite and ferromagnesian minerals can also be considered conservative as iron will stay in the solid phase.

SELECTED WATER CHEMISTRY

Table 5a gives typical chemical concentrations for different waters in the Tucson basin. Well C85 represents recharge water. Two chemical analyses of water from a well drilled by the USGS in 1966 were provided by Frederick Robertson of the USGS. These two analyses represent water from the unconsolidated Ft. Lowell fm. and the consolidated Tinaja fm. There is a difference in water chemistry between the two formations. Austin Long collected water from the Kelm well and the water was analyzed at the Laboratory of Isotope Geochemistry and the University Analytical Center.

Table 5a. Chemistry of selected waters in the Tucson basin

Well	Ft. Lowell fm. 40-160m Screen Depth 60m	Tinaja fm. 200-235m Screen Depth 220m	Tucson Well C85 Recharge Water	Mountain Front Kelm Well	Santa Cruz River [194]
Calcium (mg/l)	37	488	30	13.6	25
Magnesium (mg/l)	5.2	3.0	2.7	2.6	2
Sodium (mg/l)	40	482	32	155	20
Potassium (mg/l)	4.2	N/A	1.4	7.51	0.95
Alkalinity (mg/l)	174	30	110	146	98
Sulfate (mg/l)	41	2010	37	317	9
Chloride (mg/l)	10	105	10	34.3	7.9
Fluoride (mg/l)	0.4	5.4	0.3	-	0.4
Iron (mg/l)	0.02	0.06		-	0
Silica (mg/l)	30	17	40	29.8	0.5
pH	8.6	7.9	7.4	8.1	7.0

Table 5b. Chemistry of selected waters in the Tucson basin

Well	Flowing Wells #70 11/02/89	Flowing Wells #70 06/16/86	Flowing Wells #70 08/25/83	Flowing Wells #70 08/06/80	Effluent Recharge Ponds
Calcium (mg/l)	90	108	88	75	53
Magnesium (mg/l)	7.4	10.0	6.6	5.0	5.0
Sodium (mg/l)	57.9	61	56	46	120
Potassium (mg/l)	-	-	-	-	12.0
Alkalinity (mg/l)	117	112	68	90	150
Sulfate (mg/l)	336	154	155	81	105
Chloride(mg/l)	139	124	118	77	111
Fluoride (mg/l)	0.13	-	ND	0.12	0.6
Iron (mg/l)	0.07	ND	0.15	0.16	ND
Silica (mg/l)	-	-	-	-	-
pH	7.61	7.7	7.9	7.9	7.1

Table 5c. Chemistry of selected waters in the Tucson basin

Well	Rillito River	Tanque Verde River	Santa Cruz River	Pantano River	CAP Water
Calcium (mg/l)	32	18	47	74	53
Magnesium (mg/l)	5.0	3.0	7	15	27
Sodium (mg/l)	11	20	28	46	88
Potassium (mg/l)	0.5	0.5	-	-	6
Alkalinity (mg/l)	119	59	137	218	100
Sulfate (mg/l)	9	11	65	143	252
Chloride (mg/l)	4	10	16	14	70
Fluoride (mg/l)	0.3	0.3	0.5	0.6	0.4
Iron (mg/l)	-	-	-	-	-
Silica (mg/l)	-	-	-	-	-
pH	6.9	6.8	7.1	7.1	8.4

Table 5b presents changes in the chemistry of Flowing Wells Irrigation District well #70 over a decade of groundwater mining as well as chemical analyses of effluent presently infiltrating along the Santa Cruz River (Pima County Wastewater Management). The increase in dissolved sulfate and chloride over the decade 1980 - 1989 may represent a decreasing proportion of dilute water from the Ft. Lowell fm and an increase in higher TDS water from the Tinaja fm. (table 5a). The depth of this well, 230 m., suggests that the chemical composition of water from this well is a product of intrawell mixing between water from the Ft. Lowell fm. and the Tinaja fm.

Table 5c presents the average chemical composition of water infiltrating the groundwater system through riverbeds in the Tucson basin and the average chemical composition of Central Arizona Project (CAP) water delivered to Tucson. The major source of recharge to the basin aquifer system is the Rillito River and its tributaries. The composition of river water defines the chemistry of infiltrating water prior to water-rock reaction and modelling with NETPATH. The present chemical composition of water in the Pantano River suggests a component of anthropogenic sources of dissolved constituents. The CAP water has higher TDS than natural recharge water but is similar in chemistry to reclaimed effluent.

Mining of groundwater in the Tucson basin has affected the chemistry. Figure 18 shows the spatial distribution of $SO_4^=$ in groundwater measured in 1983 and 1992 along with contours of increased sulfate concentrations between 1983 and 1992. Three distinct areas of increase in sulfate are evident. Three hypothetical sources of increased sulfate concentrations are; 1) In the eastern basin, draw-down of the water table has increased the contribution of mountain-front recharge and water from the upper Tinaja fm. to water mined in this region. Intensive water mining has reduced the head in the Ft. Lowell fm. and may have induced increased leakage from the mountain-front. The structural geology also suggests that the Tinaja fm. is shallow along the up-thrown side of high-angle normal faults in this area. The reduced hydrostatic head above this unit may increase leakage of water upward from the lower units. The result would be an increased percentage of high sulfate water entering the Ft. Lowell fm. flow system. 2) In the western basin, the mining of groundwater continues to remove shallow waters from the Ft. Lowell fm. The deeper water that resides in up-thrown units of the Tinaja fm would then be an increasing (over time) percentage of water mined. Recharge of reclaimed sewage effluent at the City of Tucson Pilot Recharge Project ponds, at the Rodger road site, and in the Santa Cruz Riverbed also increased during this time period. The combination of these effects probably accounts for the observed increase. 3) In the southwestern extent of the study area, water residing in the Tinaja fm. may be an increasing (with time) contribution to mined water as a result of dewatering the Ft. Lowell fm. This, along with anthropogenic influence due to prescribed groundwater restoration, may account for the observed increased sulfate concentration.

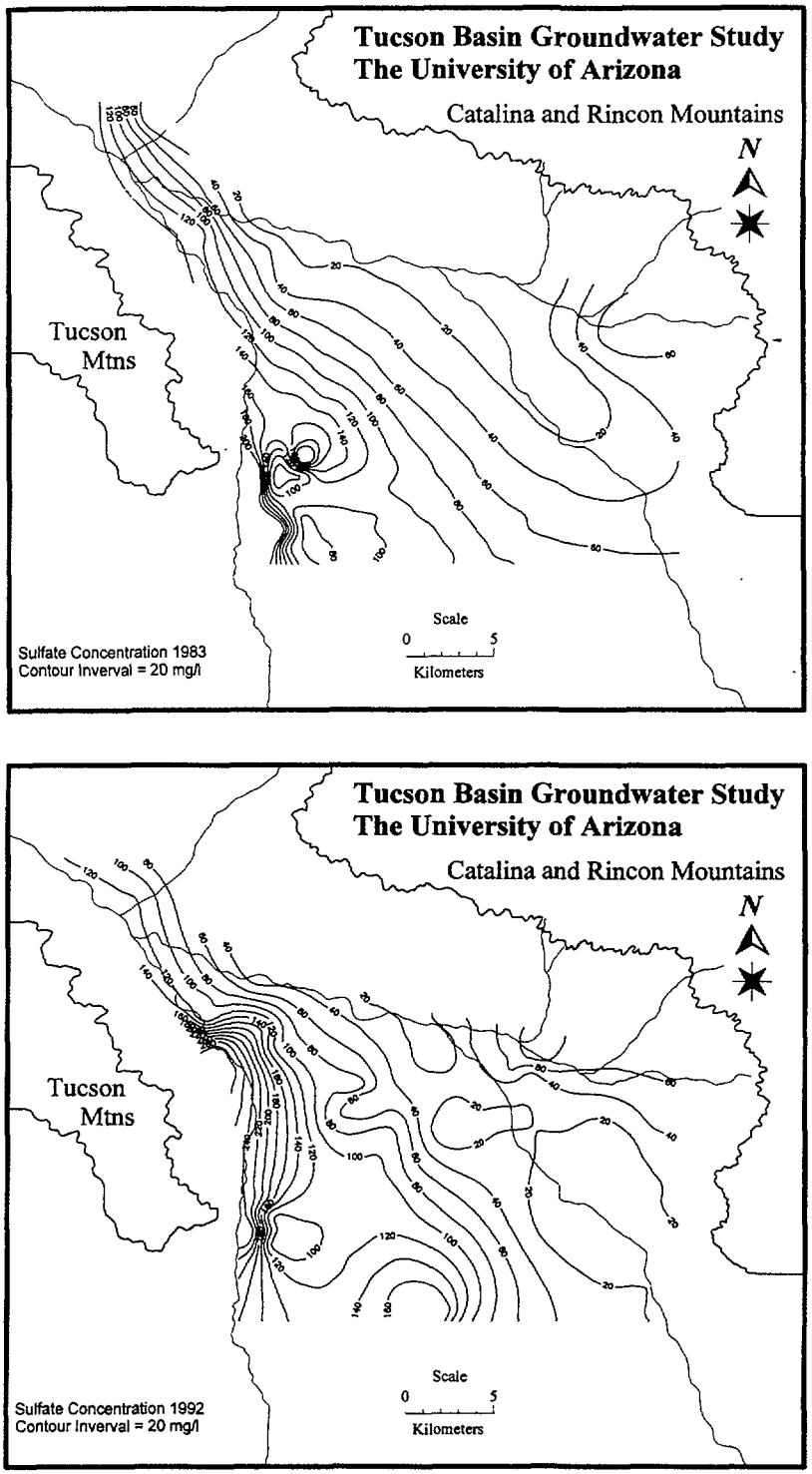

Figure 18. Affects of groundwater mining on [SO_4] in Tucson basin groundwater 1983 - 1989

GEOCHEMICAL MODELLING OF REACTION PATHS IN THE TUCSON BASIN AQUIFER

The conceptual model of hydrogeochemical reactions in the Tucson basin is similar to Robertson [142] where rather dilute recharge waters react with primary silicate minerals and incongruently form secondary mineral phases. This study differs from previous geochemical studies of Tucson basin groundwater [4, 10, 14, 16, 17, 18, 23, 26, 27, 34, 38, 158, 159] in that, for previous studies, either little mineralogic data was available to constrain and define water-rock reaction phases or the composition of mineral phases was speculative. In recharge zones, water-rock chemical reactions are controlled by the presence of soil CO_2 and carbonate species (open-system), and once water has moved down-gradient, there is no additional source of CO_2, and CO_2 is

consumed in the process of silicate weathering (closed-system). Though water in the Tucson basin ultimately enters a phase of geochemical evolution closed to CO_2, much of the water presently mined has not evolved to a aluminasilicate mineral phase boundary. Through examination of basin sediments and the chemical nature of water along selected flow paths, this study determined stoichiometrically correct reactions occurring in the subsurface that produce the observed changes in water chemistry from point to point along the flow path.

MASS TRANSFER MODELLING WITH NETPATH

Geochemical reaction paths and controlling geochemical reactions were modelled for 55 groundwaters, analyzed during 1984-1989 as part of this study. In addition, 13 groundwaters analyzed in 1965 were reevaluated. Many studies have been dedicated to the geochemistry of groundwater and the correction of radiocarbon ages on groundwater [167-193]. A number of models have been developed [3, 16, 166, 170, 172, 174, 175, 176, 184, 191] that can be used when correcting groundwater radiocarbon ages for geochemical mass-balance, isotope mass-balance and mass-transfer.

Hydrogeochemical modelling in this study considers two chemical systems: open-system, in which the aquifer chemistry is controlled by the availability of atmospheric gases, in particular, carbon dioxide down-gradient from the recharge point: closed-system, in which the aquifer chemistry is controlled only by water-rock interactions and is not influenced by atmospheric gases.

The new computer code, NETPATH [3], determines mass transfer between two waters when stoichiometric constraints are placed on reactive phases and initial and final water chemistry. NETPATH consists of 3 codes. The first, DB.EXE, is a database for the management of chemical and physical information about each sample. The second, WATEQ, is an aqueous speciation model modified after Plummer *et al.* [171]. The thermodynamic database for this version of WATEQ does not contain as complete a database as WATEQ4F [166]). This program was used in this study to determine the equilibrium state of aqueous solutes in water with respect to mineral phases. The third program is the NETPATH code which is an extension of BALANCE [177]. This code determines potential mixing ratios and mass-transfer reactions between initial and final water chemical and isotopic compositions. NETPATH is an interactive program that can be used to interpret the net geochemical mass-balance reactions along a hydrologic flow path. The program uses defined chemical and isotopic data for waters from a hydrochemical system to constrain the solution. NETPATH examines all possible geochemical mass-balance reaction models between selected waters for a set of chemical and isotopic constraints, and a set of plausible phases in the system. The results from NETPATH are useful in interpreting geochemical reactions, mixing proportions, evaporation and dilution of waters and mineral mass-transfer in the chemical and isotopic evaporation of groundwater. Rayleigh distillation calculations are applied to each mass-balance model that satisfies the constraints to predict carbon, sulfur and strontium isotopic compositions at the final water, including radiocarbon age calculations.

The chemical and isotopic data to be modelled were entered into DB, the equilibrium state with respect to mineral phases was determined automatically with WATEQ, and NETPATH was used to model reasonable hydrologic flow paths (constrained by the 1910, 1940 and 1988 potentiometric surfaces) in the basin. This entailed a series of permutations that resulted in the analysis of hundreds of potential reaction path models. Results of these models, coupled with the results of preliminary modelling efforts with WATEQ4F constrained a series of flow paths and resulted in convergence of reaction pathways.

HYDROGEOCHEMICAL EVOLUTION OF THE TUCSON BASIN

The flow of water across the entire basin is controlled by the potentiometric surface. The general flow path follows from recharge in the east basin to exit in the northwest basin. Riverbed infiltration and mountain-front recharge along the upper reaches of the Tanque Verde River flow between the confluence of this river and the Pantano River, under the Pantano River, to the center of the basin and then to the northwest exit of the basin. Hydrogeochemical modelling of this flow path included both open-system reactions, where carbon chemistry is controlling the geochemical evolution of water and closed-system reactions, where recrystillization reactions with carbonate phases and incongruent dissolution of silicates become the controlling reactions.

Figures 19 to 21 plot the chemical and isotopic trends that support the conceptual model of this flow path. A four-staged system (opened - closed - opened - closed) is evident along the flow path and is supported by figure 19. The pCO_2 and total carbon in groundwater at each point along the reaction path shows change as a result of the availability of soil CO_2. The open stages of the reaction path are zones of active recharge where water with high pCO_2 infiltrates through the soil zone to the groundwater system. pCO2 values are highest in water from well C75 and decrease down-gradient as dissolved carbon dioxide is used as a source of protons during the incongruent dissolution of primary silicate and carbonate phases. These reactions consume available CO_2 and the dissolution of calcite continues until saturation with respect to calcite is achieved at Well D-34 (1.0 km up gradient from Pantano wash). Between well D34 and D30, recharge to the groundwater system occurs from infiltration along the Pantano River. The influence of open-system conditions near the Pantano wash is

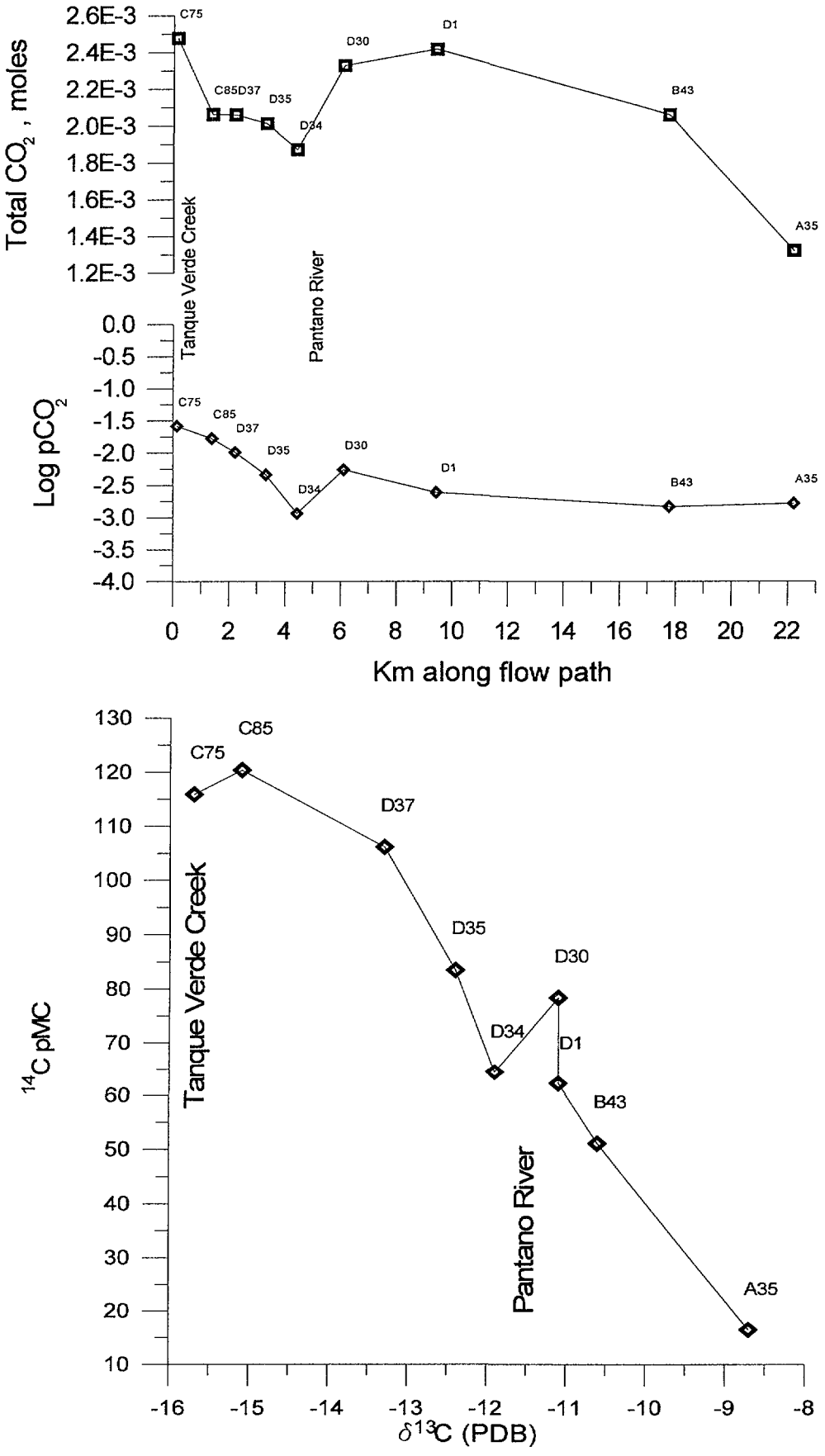

Figure 19. Changing carbon chemistry and isotopes during geochemical evolution of Tucson basin groundwater

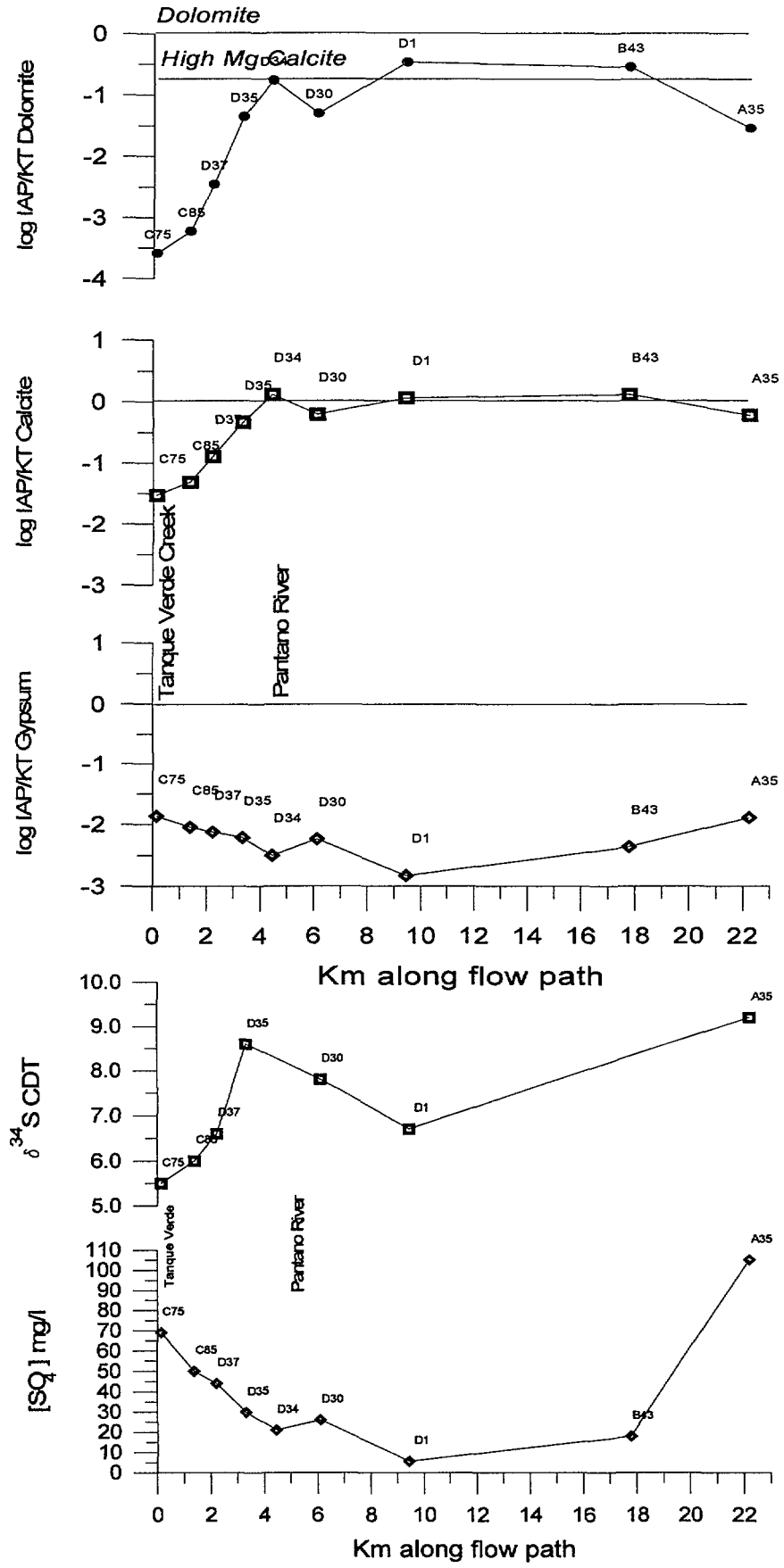

Figure 20. Changing sulfur chemistry and isotopes, and the staturation index of calcite, gypsum and dolomite during the geochemical evolution of Tucson basin groundwater

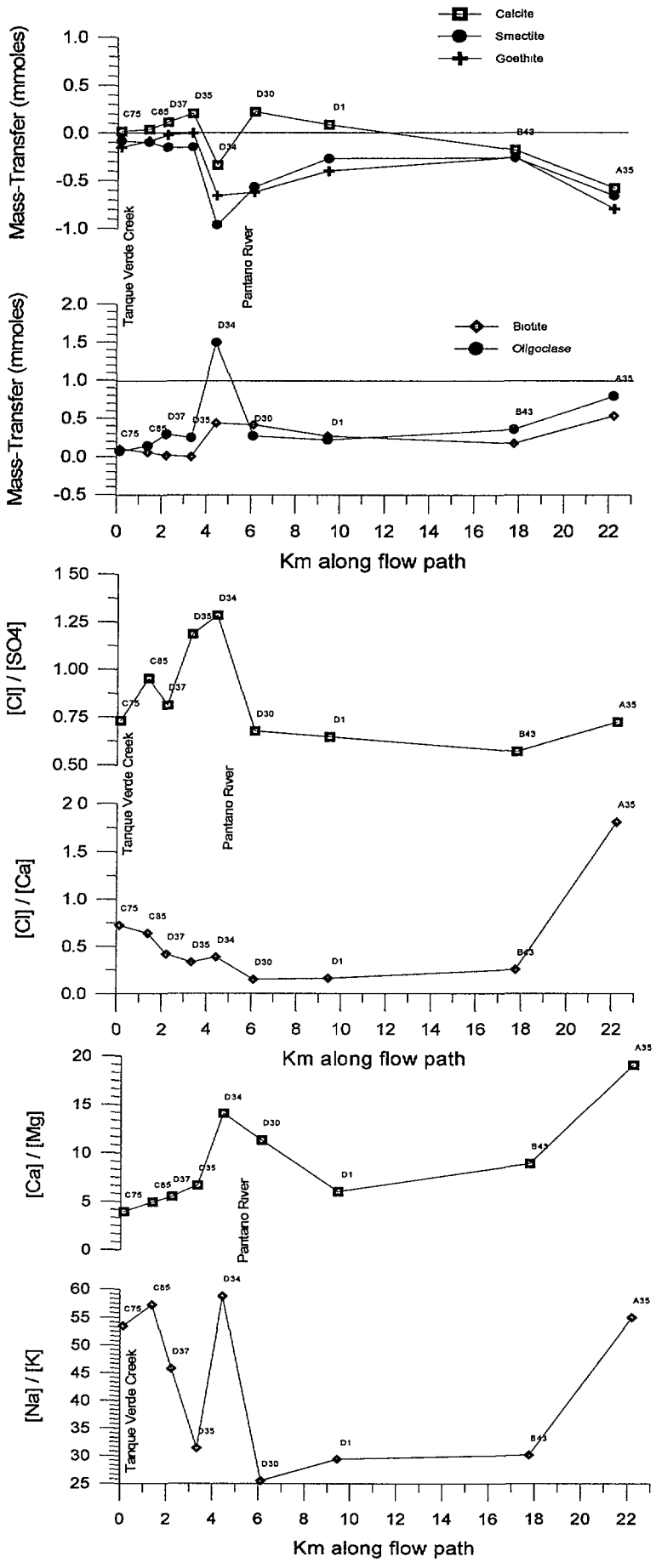

Figure 21. Changing ion ratios and mass-transfer during the geochemical evolution of Tucson basin groundwater

evident from the increase of pCO_2 in well D-30 (150 meters down-gradient from the Pantano wash). Down-gradient from the wash, the saturation index of calcite again falls below 0 and calcite dissolves as consumption of CO_2 takes place. The influence of the high-magnesian calcite discussed previously is evident in figure 20. Slow reaction kinetics produce hydrogeochemical controls on calcium and magnesium concentrations acting on the decade to century time scale.

This geochemical pathway has a striking influence on the ^{14}C and $\delta^{13}C$ as seen in figure 19. Plotting $\delta^{13}C$ values against ^{14}C values relate three reactions that control one or both of the isotopes. First, in open-systems, the dissolution of CO_2 in the gas phase controls the ^{14}C of the water (here, bomb carbon) and the dissolution of carbonate mineral phases controls the $\delta^{13}C$ of DIC. This results in a nearly constant ^{14}C of DIC and an increasingly heavy $\delta^{13}C$ trend. Second, in the closed-system, the dissolution of silicate minerals controls the carbon chemistry. The pH of water evolving in a closed-system increases, thereby oversaturating the water with respect to calcite and precipitating carbonate phases. Reactions in the closed-system have little effect on the $\delta^{13}C$ of DIC. As groundwater moves down-gradient, radioactive decay of ^{14}C occurs with time and decreases the ^{14}C of the water. Third, the effect of "recrystallization reactions" in a closed-system is a concurrent enrichment of the $\delta^{13}C$ due to exchange with the carbonate phase and a decrease in the^{14}C content due to dilution with carbon with much lower ^{14}C activity.

Three wells, C-75, C-85 and D-37, define the bomb pulse, open-system dissolution of calcite and consumption of CO_2. Wells D-37 to D-34 show evidence of ^{14}C decay. A trend toward heavier $\delta^{13}C$ values suggests that true closed-system conditions do not exist, but rather wells C-75, C-85 and D-37 represent a transition phase between open and closed. At well D-30, open-system conditions reappear, the pCO2 increases and water infiltrating at the Pantano River adds CO_2 with modern levels of ^{14}C and lighter $\delta^{13}C$ to the groundwater system. The increased pCO_2 provides H^+ for additional dissolution of calcite. The $\delta^{13}C$ becomes heavier as a result. Water flowing down-gradient undergoes the transition from open to close system reactions in the vicinity of well D-1, and when it reaches well B43, the system is essentially closed to pCO_2.

The relationship of $\delta^{34}S$ with distance along the reaction path suggests that the initial $\delta^{34}S$ of water averages 6.0 ‰ CDT (figure 20). Intrawell mixing of water from deeper stratigraphic units or dissolution reactions with sulfate mineral phases ($\delta^{34}S$ = 13‰ CDT) along the flow path increases the $\delta^{34}S$. The dissolved sulfate component has been diluted with isotopically lighter sulfate from active recharge (from the Pantano River at well D34 to well D1). The final $\delta^{34}S$ of the reaction path is a result of additional dissolution of sulfate mineral phases or again from intrawell mixing of water from lower stratigraphic units.

Chloride is conservative, increasing slightly along this flow path. The fluctuations in Cl^- concentrations are assumed to be due to variation in the mixing ratio of mountain-front recharge water, variable inputs of Cl^- from precipitation and rivers, or from possible leakage from lower stratigraphic units. The trend of increasing Cl/SO_4 along the flow path before the Pantano River indicates an increasing mountain-front component in more recently recharged groundwater (figure 21). Cl/Ca tracks the dissolution of carbonate phases during open-system conditions and is nearly constant in locations where closed-system reactions prevail. The large increase in Cl/Ca at well A35 indicates that this water has either a input from lower stratigraphic units or has undergone significant Ca/Na ion exchange.

Ca/Mg (figure 21) is low in active recharge zones due to the influence of the initial Ca/Mg of river and mountain-front waters. Dissolution of calcium carbonate phases in an open-system results in an increased Ca/Mg. This may be the mechanism affecting the Ca/Mg in well D34 near the recharge zone of the Pantano River. During closed-system reactions, the precipitation of calcite again decreases the Ca/Mg. The high ratio at well A35 again suggests a change in lithology or an increased input of water from lower stratigraphic units.

The Na/K is problematic (figure 21). Na is controlled by two reactions along the flow path; incongruent dissolution of oligoclase and Ca/Na and Mg/Na ion exchange on clays. The sources of K are incongruent dissolution of orthoclase, river water, mountain-front recharge water and intrawell mixing of water from deeper stratigraphic units. Illite and smectite clays are sinks of potassium. The interpretation of Na/K ratios is dependant on the reactions controlling [K]. Recently recharged water has a Na/K indicative of a substantial mountain-front recharge component. Na/K values decline to well D35. The rise in Na/K between wells D34 and D30 suggests an influx of river water, low in Na. Well A35 is again anomalous further substantiating potential intrawell mixing between two stratigraphic units.

Figure 21 also presents the mass of dissolving and precipitating mineral phases along the flow path in Case Study Four. The geochemical reactions involving groundwater between the confluence of the Tanque Verde and Pantano Rivers (well C75 to well D34) progress from an open-bicarbonate buffered system to a closed silicate-weathering controlled system. This is evident as change in mass-transfer of the Ca-Mg carbonate phase from dissolution to precipitation. Influx of recharge at the Pantano River changes mass-transfer reactions to open-system conditions at wells D30 and D1. Mass-transfer reactions are again controlled by silicate-weathering, closed-system conditions down-gradient. The mass-transfer of silicate phases increases when closed-system, silicate-weathering geochemical reactions dominate.

DETERMINATION AND DISTRIBUTION OF TUCSON BASIN GROUNDWATER AGES

35 of the 55 groundwater samples analyzed for ^{14}C and $\delta^{13}C$ resulted in values that contain water that is modern (<50 years) after carbon mass-balance modelling with NETPATH. A full description of the equations used to determine corrections to the^{14}C of DIC using the mass-balance approach are presented by Plummer *et al.* [3]. Analysis of ^{14}C and $\delta^{13}C$ involves considerable time and effort; therefore, this study will attempt to use all results of ^{14}C and $\delta^{13}C$ to place the recharge of each sample in time. Modelling of groundwater ages using bomb-derived ^{3}H has been used extensively in hydrology. The use of the exponential model has proven effective for the interpretation of ages from tritium. The application of the exponential model to bomb-derived radiocarbon has been problematic due to the complex chemical reactions that affect the^{14}C of DIC. The use of isotopes for validation of mass-transfer modelling and determination of geochemical evolution of groundwater has increased confidence in corrections to ^{14}C values. We present a simplified exponential model based on groundwater ^{14}C corrected with mass-transfer and geochemical modelling. This approach essentially simplifies the influx of ^{14}C into groundwater during the 1950's and early 1960's and the subsequent decline in this function after the atmospheric levels described by MacKay *et al.* [196].

To define the ^{14}C input function for recharge water, a minimum of three ^{14}C values are needed to represent groundwater ^{14}C in the recharge zone over time. The three years chosen to define the groundwater input function are 1956, 1965 and 1989. The 1956 value of ^{14}C in recharged groundwater was defined as 100 +/- 4 pMC. This represents an average ^{14}C of the atmosphere between 1954 and 1957. The maximum ^{14}C in recharge waters occurred during 1964 - 1965, the height of above-ground thermonuclear testing. Bennett [197] measured a sample of river water for ^{14}C during the early part of 1965. The result of this analysis was 142.6 +/- 4.0 pMC.

NETPATH was used to confirm the use of this value for the predicted maximum ^{14}C of recharge water in 1965. ^{14}C and $\delta^{13}C$ used for this prediction include: ^{14}C = 180 pMC and $\delta^{13}C$ = -20.3‰ PDB for soil CO_2 [141, 195]; ^{14}C = 10 pMC and $\delta^{13}C$ = -4.5‰ for carbonate mineral phases (table 3); ^{14}C = 180 pMC and $\delta^{13}C$ = -19 ‰ for river water and ^{14}C = 16.5 pMC and $\delta^{13}C$ = -10.7‰ for mountain-front recharge to the Ft. Lowell fm (table 3) and well C75-1984 chemistry. The ^{14}C of mountain-front recharge is considered valid because the source, Kelm Well, is less than 1km from the Agua Caliente Wash. These values are defined with the data of Bennett [197], Robertson [141], and results from this study. The ^{14}C of groundwater recharged in 1965 as predicted with NETPATH mass-transfer reaction modelling is 148.7 pMC.

The radiocarbon activity of DIC in groundwater recharged during 1989 was measured at well C75 as 115.9 pMC. This well is less than 500 meters from the Tanque Verde creek and represents open-system groundwater that receives infiltration from the Tanque Verde creek.

To determine the bomb-derived excess ^{14}C at each well, the carbon isotope values for NETPATH modelling of mass-transfer reactions were assigned pre-bomb values of ^{14}C = 100 pMC and $\delta^{13}C$ = -19‰ for river water, ^{14}C = 100 pMC $\delta^{13}C$ = -20.3‰ for soil CO_2 and ^{14}C = 100 pMC and $\delta^{13}C$ = -25‰ for dissolved organic carbon (DOC). The ^{14}C and $\delta^{13}C$ of carbonate mineral phases were previously defined. The ^{14}C concentration in the atmosphere for the year 1950 is assigned a value of 100 pMC by convention, thus 1950 is year 0 for radiocarbon ages. NETPATH was used to model the carbon mass-transfer during hydrogeochemical evolution of each groundwater sample based on the constraints described in Case Studies One to Four. The mass-transfer of carbon and the final carbon isotopic composition of each water sample was validated using the measured $\delta^{13}C$ of DIC. NETPATH uses mass-transfer, Rayleigh distillation and exchange reactions to predict the ^{14}C of water. All the wells that contain measurable tritium contain bomb-derived ^{14}C. The difference between the predicted pre-bomb ^{14}C value as determined by NETPATH and the measured ^{14}C content of the water is assumed to equal the excess bomb-derived ^{14}C above 100 pMC. Two lines through the three points define the bomb-derived ^{14}C input function to Tucson basin groundwater (figure 22). Parallel lines at $+1\sigma$ and -1σ represent the uncertainty of the input function. The predicted bomb-derived ^{14}C for each well results in two potential recharge years. The intercept year selected for each sampling point was based on a uniform relationship of increasing age down-gradient. Tritium values in figure 22 confirm the exponential radiocarbon function. Tritium measurements on water sampled for radiocarbon follow the same trend, and represent bomb-pulse tritium in basin groundwater.

Re-evaluation of samples analyzed in 1965 by Bennett [197] and interpreted by Wallick [4] were modelled with NETPATH using the same assumptions and mineral phases as for the 1989 data set. This set of data is interesting because it was collected before severe anthropogenic effects on the hydrological system had occurred. It is suspected that water in the Tucson basin aquifer system not only increases with age down gradient, but also increases in age with increasing depth in the basin. This vertical stratification of ages increases the complexity of interpretation of the isotope hydrology of the Tucson basin system. 13 of the samples collected by Bennett [197] were used for further study. Other samples were not evaluated due to a lack of $\delta^{13}C$ data, reproducible results, questionable laboratory notes or lack of complete chemical analysis of the water for the year 1965. The predicted ^{14}C of 8 of the 13 water samples suggests a component of water with bomb-derived radiocarbon. These water samples are considered recently recharged water (<50 years).

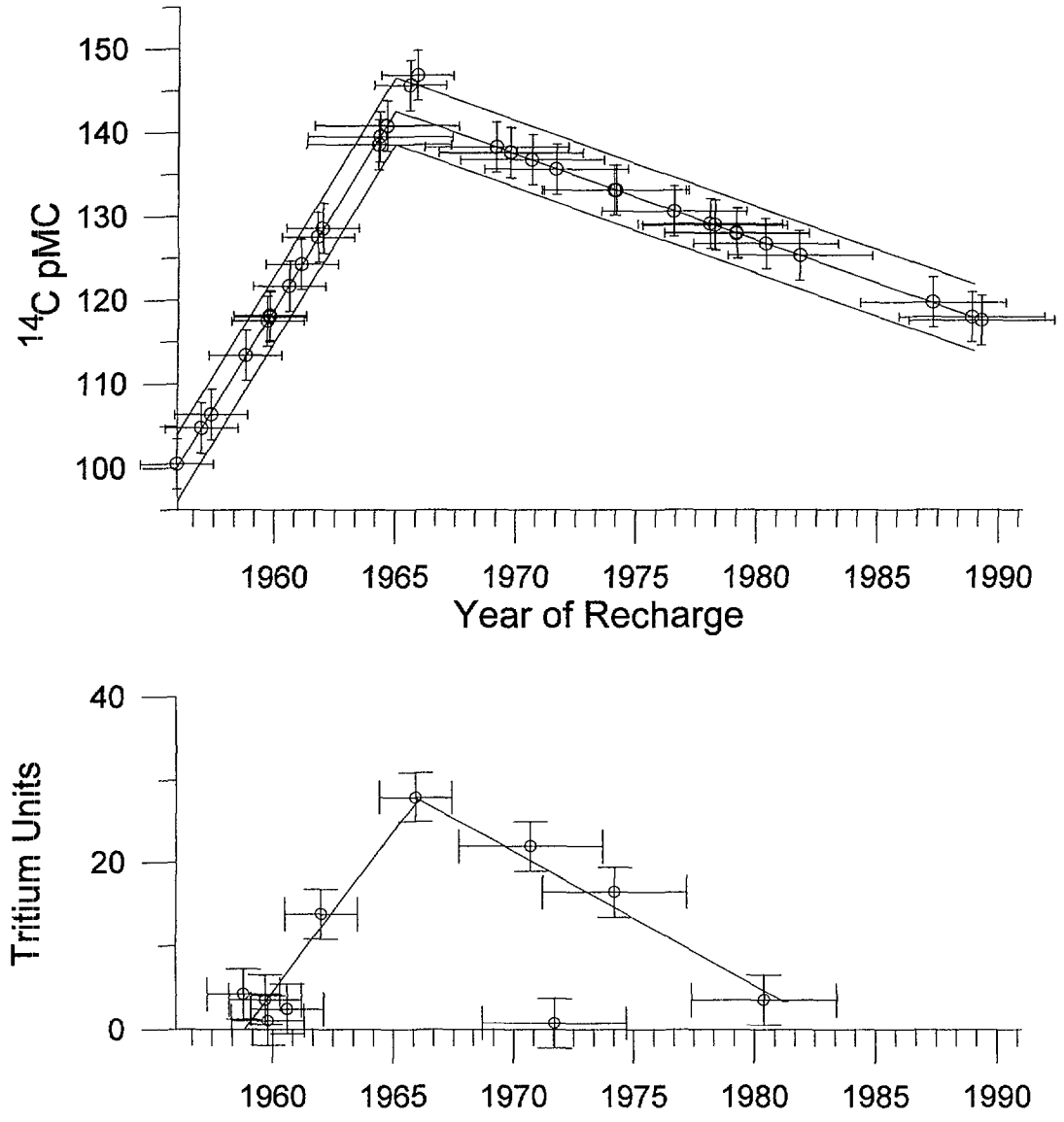

Figure 22. Exponetially modelled radiocarbon and tritium in Tucson basin groundwater

RADIOCARBON AGE ESTIMATES OF WATER

Figure 23 presents isochrons for water collected in 1989 that contained bomb-derived ^{14}C, isochrons of the radiocarbon age of groundwater collected in 1989 and the ages of water collected in 1965 respectively. Comparison of these figures suggests that groundwater withdrawals have increased the age of water mined parallel to recharge zones (rivers) in the basin. Vertical stratification of groundwater ages is consistent with this observation. The interpretation of these results may also be an artifact of sampling. Present groundwater mining extends over 100 meters into the aquifer resulting in less than ideal samples for age determination. The antiquity of some groundwater ages may reflect intrawell mixing between pleistocene and holocene groundwater. The distribution of young water, ages less than 50 years, determined from the 1989 dataset reflect the rapid turnover of this water component with time.

Hydrogeochemical modelling of samples yielded radiocarbon ages ranging from modern to 6300 years. Any inconsistencies between young (<50 years) and older water results from the effect of kriging data spaced at a decadal scale and data spaced at millennial scale. From figure 23 it is evident that much water in the basin is less than 250 years old. The antiquity of some water presently mined from the basin cannot be disputed given the results of the hydrogeochemical model. Potential intrawell mixing of younger and older waters suggests that water with the oldest radiocarbon age would have a component of mixing greater than the determined value.

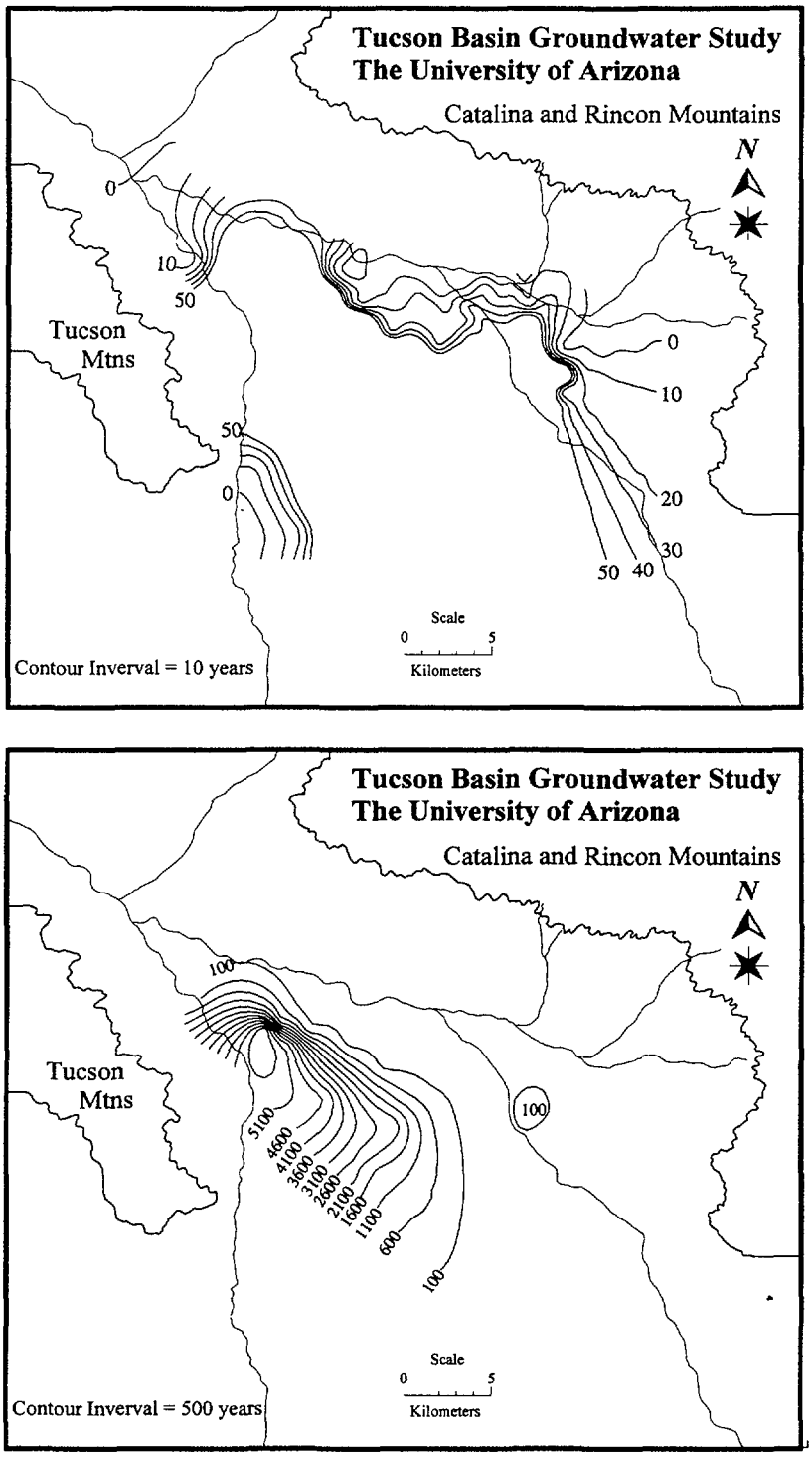

Figure 23. Isochrons of Tucson basin groundwater, 1989 radiocarbon ages

Reviewing figure 4 shows that the particle size distribution and transmissivity in the Tucson basin aquifer decreases from east to west. This change in transmissivity will slow water movement in the central Tucson basin. Shoe-string aquifers of high transmissivity run parallel to the Rillito River and act as high-velocity conduits for groundwater flow, bypassing the central basin. Recent recharge has not replaced water mined from the Ft Lowell fm. in the central basin. Thus, groundwater mined in the central basin will continue to increase in radiocarbon age. This hypothesis is supported by re-evaluation of samples analyzed by Bennett [197] and reinterpretation of Wallick [4] for groundwater for ^{14}C and $\delta^{13}C$ samples in 1965. Figure 24 presents isochrons of the radiocarbon age of water mined in 1965. Comparison of the 1989 data and 1965 data shows

that the radiocarbon age of groundwater mined in the central Tucson basin has increased 5000 years during the last two decades. The influence of vertical stratification of ages is further supported by measured radiocarbon ages at well A31 in 1965 and 1989, where the radiocarbon age for water mined during 1965 was 1000 years and in 1989 was 1500 years. These values represent a trend of increasing radiocarbon age of mined water over time. The result is that Tucson depends on water that was recharged many thousands of years in the past.

Parallel to the Rillito, Pantano and Tanque Verde Rivers, groundwater velocities are sufficiently high to offset the mining of the young water component and replace it with recently recharged water. However, in the central and southern basin, lower groundwater velocities and decrease in the potentiometric surface has depleted young, shallow water from the aquifer.

DETERMINATION AND DISTRIBUTION OF TUCSON BASIN GROUNDWATER AGES BASED ON MODFLOW AND PATH3D[tm] HYDROLOGIC MODELLING

The program PATH3D [5] was used in conjunction with the MODFLOW results of Marra [3] to relate the temporal flow of water as determined with ^{14}C to the mathematically defined temporal flow of water. Marra [7] chose MODFLOW, the Modular Three-Dimensional Finite-Difference Ground-Water Flow Model, to develop an extensive two-layer computer model of groundwater flow in the north-central Tucson basin aquifer system. The MODFLOW program, as released by the USGS, consists of many integrated packages that are used to represent recharge, water removal, spatial head and transmissivity variations in three-dimensions, evapotranspiration, rivers and boundary conditions. The model reported by Marra [7] used MODFLOW, as published by the USGS, to simulate the movement of water in the Tucson basin.

This study reconstructed the 1940 steady-state modelling efforts of Marra [7] from appendices and model output. Additional packages have been written for MODFLOW by both public and private organizations. The version of MODFLOW used to define the head distribution for 1940 steady-state in this study was purchased from S.S. Papadopolous and Associates. This version of MODFLOW overcomes some of the weaknesses of the original version, including the ability to re-wet dewatered cells during transient analysis.

Marra [7] describes the refined MODFLOW model of the north-central Tucson basin as a "fresh look" at layer geometry, aquifer parameters and previous hydrologic studies to reduce recycling of interpretations and circular reasoning. This model has a finer grid (figure 24) than many previous modelling efforts. The finer grid describes aquifer heterogeneities better and more specifically controls the locations of natural hydrologic boundaries. The mountain-front recharge boundary was constructed to be hydrologically connected to the flow system, but was placed a sufficient distance north of the Rillito River to dampen the effect on flux variations. The scarcity of both hydrologic and geochemical data along the basin-pediment interface severely limits the ability to model the hydrology and hydrogeochemistry of Catalina and Rincon mountain pediments. Two layers were incorporated into the MODFLOW model of Marra [7]. The upper layer represents the unconsolidated sediments of the Ft. Lowell fm. and overlying sediments. Layer two generally represents the consolidated sediments of the upper Tinaja fm. and is under variable semi-confined conditions. Leakage from stratigraphic units below the upper Tinaja fm. is considered negligible [7].

PATH3D was used to track the movement of particles in three dimensions and time based on the velocity vector field calculated from the potentiometric surface results of MODFLOW. PATH3D includes the hydrologic constraints used in the MODFLOW model and requires supplemental data arrays files needed for particle tracking. PATH3D consists of two major segments. The first is a velocity interpolator used to convert hydraulic heads calculated at nodal points into a velocity field for which the velocity in a given time step is determined as a function of position (x,y,z). The second is numerical solving routines used when tracking the movement of fluid particles in groundwater flow systems.

The effective porosity and saturated thickness of each layer/node is needed by PATH3D to calculate the mass-balance of water. The effective porosity of the Ft. Lowell fm. was assigned a value of 0.25 throughout the basin. The effective porosity of the consolidated upper Tinaja fm. was defined as 0.15 throughout the basin. The saturated thickness of each of the 5670 nodes for both layer I and layer II were calculated from the results of Marra [7]. Given these data, PATH3D was used to calculate the mass-flux passing each node with time as constrained by the transmissivity, heterogeneity, potentiometric surface and stresses on the aquifer system. The PATH3D model was based on the reconstructed MODFLOW model of Marra [7], with the revisions required for the expanded version of MODFLOW and for PATH3D. The grid for the MODFLOW model of Marra [6] was digitized at the same scale as all other work in this study. PATH3D was used to track the temporal movement of water based on both the measured head distribution for 1940 (from Marra [7] appendix e) and the modelled head distribution (from MODFLOW output) for the 1940 steady-state analysis.

The particles tracked with PATH3D in the Tucson basin flow system were introduced at the Santa Cruz, Rillito, Tanque Verde, Agua Caliente and Pantano Rivers. A sub-set of particles was also introduced along the southern boundary of the model to track the movement of water entering the grid from recharge sources not represented within the MODFLOW grid. The particles are envisioned here as specific water molecules that have

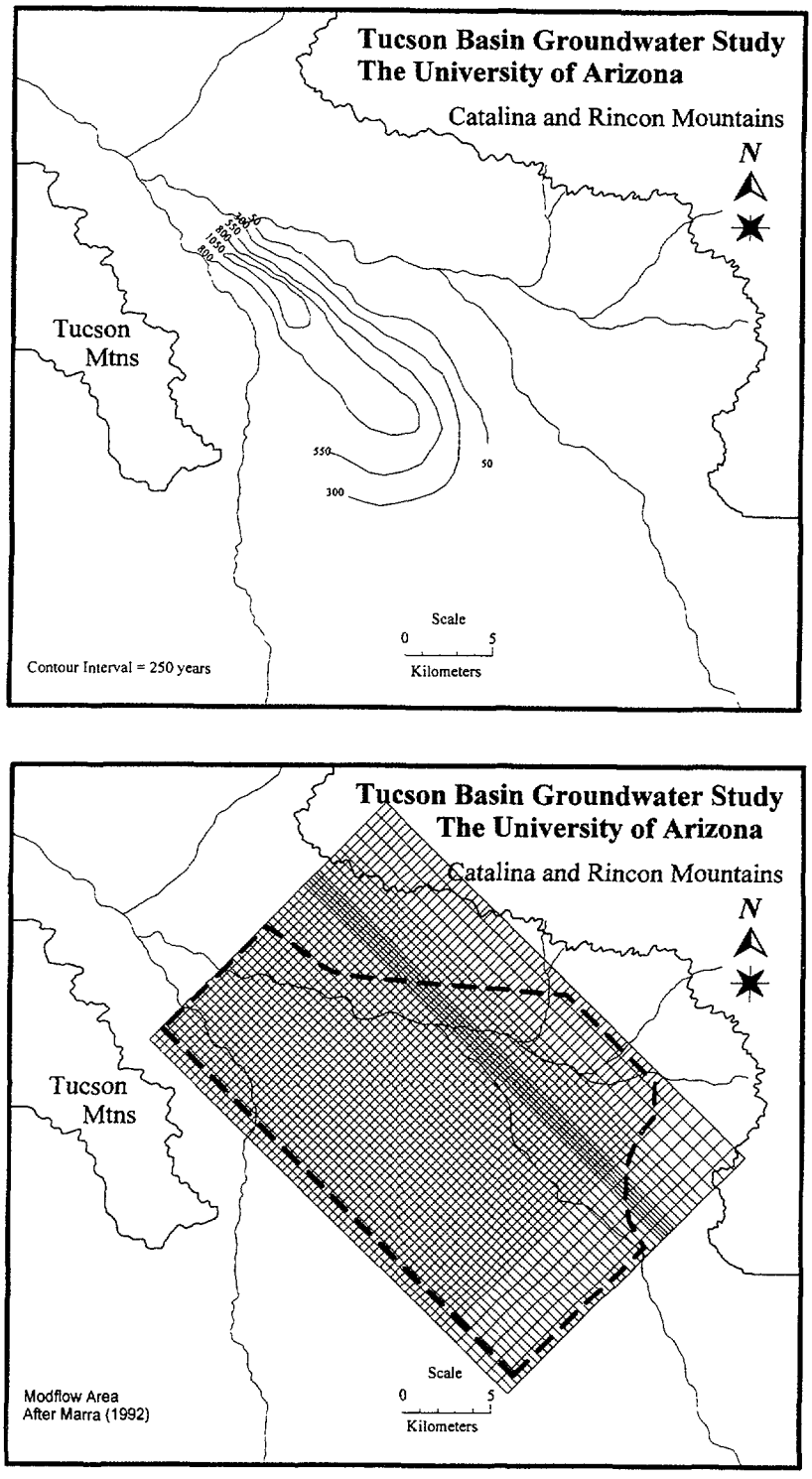

Figure 24. Isochrons of Tucson basin groundwater, 1965 radiocarbon ages and hydrological model grid

infiltrated through the riverbed to the groundwater system at any given time = 0, and move down-gradient affected only by hydrologic stresses defined by the mathematical model. Particle tracking represents forward modelling of groundwater flow. The results of hydrogeochemical modelling and the corrected exponential model of radiocarbon concentrations is an inverse model. To reconcile the two models, time = 0, is arbitrarily assigned the year 1989. Isochrons representing both the radiocarbon age and the movement of the recharge front over time are defined as years before 1989.

To represent the movement of water modelled with PATH3D, the location of each particle in three-dimensional space was projected onto the X-Y plane. The location of each particle was saved for each year the particle moved along flow paths constrained from MODFLOW and PATH3D. The isochrons resulting from

recharge along the Rillito, Tanque Verde and Agua Caliente Rivers and isochrons for water recharged in the Pantano and Santa Cruz Rivers are presented in figure 25. Different contour intervals denote spatial differences in groundwater flow-rates in the Tucson basin aquifer. Each isochron defines the front, in X-Y space, of recharge water in the Tucson basin system. The high-transmissivity regions that extend along the northern aquifer margin present a conduit for groundwater flow. Hydrologic modelling results show that 63 percent of water recharged (from mass-balance of particle tracking) along the northern aquifer margin has a residence time in the aquifer of less than 50 years. Only 30 percent of water recharged in the Santa Cruz and Pantano Rivers has a residence time less than 50 years (from mass-balance of particle tracking). Water recharged along the

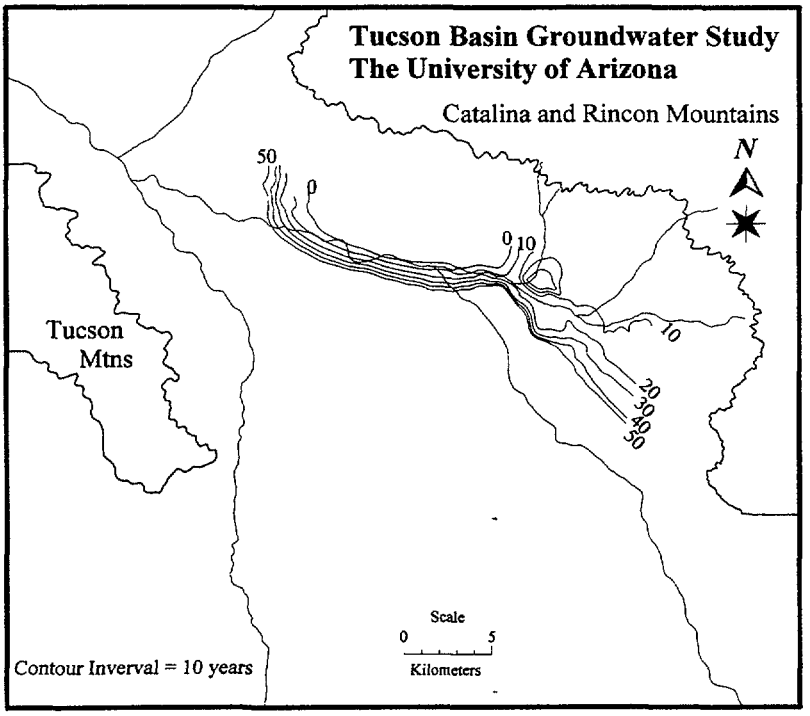

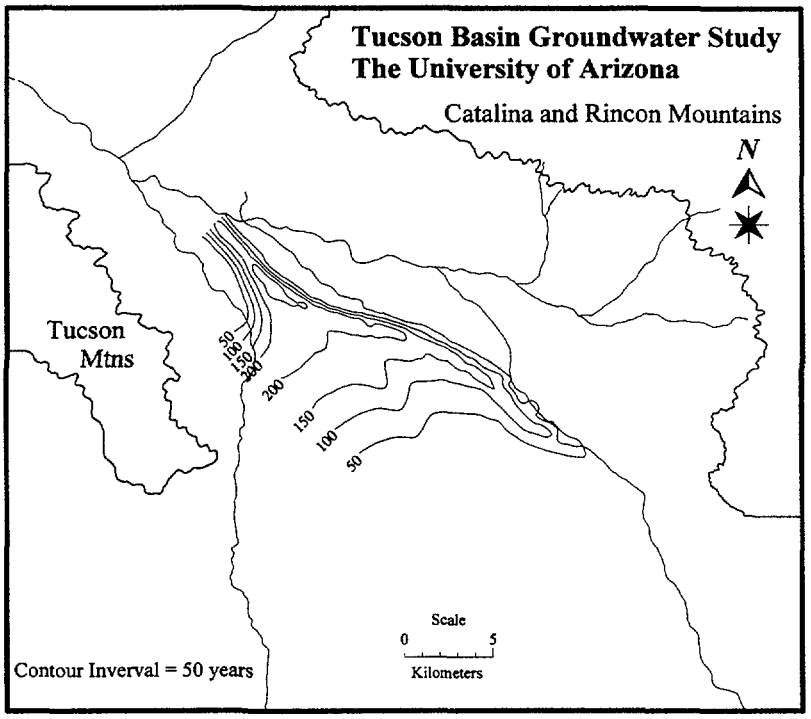

Figure 25. Isochrons of Tucson basin groundwater age modelled hydrologically

Pantano River near the confluence of this river and the Rillito River, flows in the high-transmissivity zones that parallel the northern basin margin. Water recharged in the Santa Cruz River flows parallel to the river and does not extend more than a few kilometers into the basin.

Comparison of figures 23, 24 and 25 show remarkably similar groundwater ages from both hydrological modelling and geochemical modelling. The front defining the spatial-distribution of groundwater recharged over the last 50 years, as derived by geochemical modelling, lies within a couple of kilometers of the front derived from hydrological modelling. The variations between the geochemical model and the hydrologic model may only reflect the uncertainty when contouring the results.

The convergence of the two methods for modern (<50 years) recharge water suggests that the steady-state hydrologic model reproduces the basic flow patterns of the basin flow system. However, MODFLOW and PATH3D modelling efforts failed to predict any waters greater than 300 years in age. The age of groundwater mined during 1989 approaches 6000 years as determined with radiocarbon dating. A more accurate undisturbed representation of the age of groundwater in the Tucson basin aquifer is shown the 1965 radiocarbon data. This data represents the spatial distribution groundwater radiocarbon ages on samples analyzed in 1965 and showed the maximum age of groundwater mined during 1965 was 1000 years. Comparison of the 1965 geochemical dataset with hydrological modelling of the temporal movement of water results in only a factor-of-three difference. This comparison again suggests that the steady-state hydrologic model reproduced the pre-stressed Tucson basin flow system.

Potential reasons as to why groundwater ages in the central basin did not completely converge include; 1) The MODFLOW model is an incomplete representation of the basin flow system. Extending the model to include a larger area by adding a longer reach of the Santa Cruz River will enlarge the convergence zone between flow from the Santa Cruz recharge and flow from the Rillito River recharge. At the convergence of flow paths there is a stagnation of the water movement. The waters that show antiquity in the central basin may reflect these stagnation points. 2) The mining of groundwater prior to 1965 removed groundwater originally less than 500 years old, and continual mining of groundwater removes water that increases in age over time. 3) The hydrogeochemical evolution model for central basin groundwater has flaws. The increasing radiocarbon age of water mined from the same well over time suggests vertical stratification of groundwater age. Geochemical modelling did not account for intrawell mixing of water having disparate radiocarbon ages. It is likely that a combination of 1,2 and 3 resulted in the discrepancies between results of the hydrologic flow-model and the hydrogeochemical model. The results of both modelling efforts suggest that a high degree of confidence can be applied to the 1940 steady-state simulation of Marra [7], and that bomb-derived radiocarbon can be effectively modelled if combined with a thorough geochemical investigation of the hydrological system.

SUMMARY AND CONCLUSIONS

This study included examination of isotope hydrology, hydrogeochemical changes in Tucson basin groundwater, mineralogic investigation of basin fill, and the relationship between radiocarbon age of groundwater and the temporal movement of water determined by hydrologic modelling. The collection of many new chemical and isotopic data combined with an already extensive geochemical and isotopic dataset makes the Tucson basin an intensively sampled aquifer system.

Tucson will continue to be dependant on groundwater as a water supply. The results of this study suggest that some water now used as a water resource in the Tucson basin has a component recharged in the last 50 years. The dilute, pristine water presently mined from much of the Ft. Lowell fm. has a finite limit. Water from deeper stratigraphic units has much lower water quality. Investigation of the change in water quality with time has shown that as water continues to be mined from the Tucson basin, the TDS has increased. The most plausible hypothesis for a rise in TDS is the gradual dewatering of the Ft. Lowell fm. and subsequent increased percentage of water mined from the Tinaja fm..

The study of isotope hydrology in the Tucson basin confirmed the results of Simpson *et al.* [33]. The new datasets of both stable isotopes in precipitation (1981-1992) and the stable isotopic composition of Tucson basin groundwater have expanded previous interpretations of recharge to the basin. Isotope hydrology confirms that recharge to the basin along the Agua Caliente, Tanque Verde, Rillito and Pantano rivers is dominated by winter precipitation and run-off from the surrounding mountain ranges. The western basin groundwater has a heavier isotopic composition than along the eastern and northern basin margins. These results reflect evidence of recharge from either low-elevation, large storm events (potentially related to ENSO activity) or from summer precipitation.

Evaluation of the mineralogy and stoichiometry of minerals that comprise the basin-fill has allowed for detailed mass-transfer modelling of the hydrogeochemical reactions occurring in the Tucson basin aquifer. This study was not conclusive in its investigation of the chemical composition, structure and spatial (3-D) distribution of the clay mineralogy within the Tucson basin aquifer. Mineralogic investigation was sufficient to constrain the major water-rock reactions occurring during the hydrogeochemical evolution of Tucson basin groundwater. As

expected, the dominant clay component was smectite. Recalculation and reevaluation of previously published activity diagrams substantiate this finding. The relationship of the cation exchange capacity with the structure of the Tucson basin clay mineralogy may increase the understanding of the relationship of dissolved constituents with particle size distribution in the basin. The clay mineralogy will also play an important role in the movement and fate of organics in the subsurface. Further study on this may be warranted.

Isotopes are very useful tools for validation of the conceptual understanding of groundwater movement, hydrogeochemical reaction-path modelling and as an age constraint on groundwater movement. Stable isotopes of carbon and sulfur were used to constrain potential mass-transfer reactions modelled with the USGS program NETPATH. The nearly unique solutions needed for convergence of mass-balance and isotope-balance constrained mixing and mass-transfer reactions modelled in the Tucson basin. The chemical and isotopic modelling indicated that groundwater mining may have increased leakage from lower stratigraphic units, or from mountain-front recharge into the Ft. Lowell fm. along the northern-eastern basin margin. This result is most apparent as an increase in sulfate with time. This trend may also result from an increase in intrawell mixing. The large screened interval within production wells results in less than ideal sampling for isotopic and chemical interpretation. This, combined with the inability of NETPATH to geochemically model a multi-component mixing system, may affect the interpretation of the results of this study.

NETPATH was used to correct radiocarbon determinations on Tucson basin groundwater DIC. The stable isotopic composition of carbon (DIC) and sulfur (SO_4) together with the chemical composition of groundwater, were used to constrain mixing and water-rock reactions. The stoichiometric composition of minerals that comprise the basin-fill were well defined. Of the 55 wells sampled for ^{14}C, 35 contained some component of bomb-derived radiocarbon. Correction of mixing and isotope-dilution reactions with NETPATH allowed the approximate year of recharge to be determined based on a simple exponential model. The spatial distribution of groundwater with a "young" recharge component (<50 years) follows zones of high transmissivity within the Tucson basin aquifer system.

The radiocarbon age of water sampled during 1989 from the central-basin approached 6500 years after mass-balance and isotope validation with NETPATH. Thirteen groundwater samples were collected and analyzed for ^{14}C by Bennett [197] in 1965. These samples were reanalyzed using the results and interpretations of this study. The radiocarbon age of groundwater mined during 1965 in the central basin only approached 1500 years. Analysis of well A-31 in both 1965 and 1989 resulted in an increase of the age of mined water by 500 years. Therefore, Tucson is becoming increasingly dependant on water that recharged many thousands of years in the past, and that much of this water cannot be easily replaced by recharge.

The results of the Tucson basin hydrogeochemical modelling effort were compared to results of hydrologic modelling of the same system. This allowed the evaluation of the temporal movement of water by two independent methods. The MODFLOW finite-difference hydrologic model of Marra [7] was extended for use with PATH3D, a particle tracking software package. Water-recharge was input along the Rillito, Pantano, Agua Caliente, Tanque Verde and Santa Cruz Rivers and tracked along the steady-state (1940 estimate) velocity vector field as determined from the results of the MODFLOW model. The movement of these recharge "fronts" with time compared favorably with the spatial distribution of the recharge "front" determined with bomb-derived ^{14}C. The age of water in the central basin determined with hydrologic modelling (1940 steady-state) and the radiocarbon age of water mined in 1965 have only a factor of 3 difference. The convergence of radiocarbon age and hydrologic age increases confidence in both the hydrogeochemical modelling effort and the steady-state analysis of Marra [7]. No attempt was made to reconcile the transient modelling effort of Marra [7] with the antiquity of groundwater ages for the 1989 isotopic dataset. This effort would require evaluation of a multi-component mixing/mass-balance geochemical model. No hydrogeochemical model is presently available for this. In addition, the results of Marra [7] suggest that transient modelling of the Tucson basin system is not well defined using the MODFLOW model. Refinement of the MODFLOW model is required before any attempt is made to reconcile both transient models. Further work to reconcile the transient data is warranted. Studies of bomb-derived ^{36}Cl, freons and noble gases, and the fate and movement of dissolved organic matter (^{13}C and ^{14}C isotope balances) in Tucson basin groundwater should provide additional constraints needed to hydrogeochemically model a multi-phase mixing system.

The hydrologic and hydrogeochemical modelling show that recharge along the rivers in the Tucson basin may have a relatively short mean residence-time (<50 years). Any artificial recharge to the aquifer system should consider the modelled movement and temporal fate of water in the aquifer. Artificial recharge may increase the velocity of water in certain regions of the basin, ultimately resulting in the loss of the recharged water from the basin system before it can be recovered.

Finally, climatic change will affect the present sources of recharge to the Tucson basin aquifer. A comprehensive evaluation of the paleohydrology of the Tucson and Avra Valley aquifers should be considered to assist in long-term planning of water resources. The results of this study should be further evaluated to provide information on century-to-millennia time scale recharge to the Tucson basin aquifer.

ACKNOWLEDGMENTS

The authors would like to acknowledge the dedication of the staff and graduate research assistants at the Laboratory of Isotope Geochemistry, University of Arizona, in particular the efforts of Christopher Eastoe. This work was funded by the State of Arizona, Geohydrology Program. We acknowledge helpful dicussions to this work made during cooperation with the IAEA Coordinated Research Program on Mathematical Models for the Evaluation of Isotope Data in Hydrology. Finally, we would like to acknowledge the contributions made by Jean-Charles Fontes, to the understanding of the radiocarbon dating of groundwater systems.

REFERENCES

[1] Lindquist, J.C., 1992, Tritium analysis of groundwater to determine stream-channel recharge rates in the Tucson basin, Southern Arizona, MS Thesis, University of Arizona, Tucson, Ariz., (unpublished)

[2] Kalin, R.M., Smith, B.D. and Long, A. (1994), 222Rn in the groundwater of the North-Central Tucson basin and its relationship to the hydrogeology, in review, Groundwater

[3] Plummer, L.N., Prestemon, E.C. and Parkhurst, D.L., 1991, An Interactive Code (NETPATH) for Modelling NET Geochemical Reactions along a Flow PATH, USGS Water Resource Investigations Report 91-4078

[4] Wallick, E.I., 1973. Isotopic and chemical considerations in radiocarbon dating of ground water within the arid Tucson basin aquifer, Arizona. Ph.D Dissertation, University of Arizona, Tucson, Ariz. (unpublished).

[5] Zheng, C., 1991, PATH3D, A Ground-Water Path and Travel Time Simulator, S.S. Papadapolous & Associates, Inc.

[6] Davidson, E.S., 1973, Geohydrology and water resources of the Tucson basin, Arizona, U.S. Geological Survey: Water -Supply Paper 1939 E.

[7] Marra, R.P. 1993, Preliminary Steady-State modelling calibrations of Tucson Water's central well field flow model Tucson basin, Southeastern Arizona, MS Thesis, University of Arizona, Tucson, Ariz (unpublished)

[8] Anderson, T.W., 1972, Electrical-analog analysis of the hydrologic system, Tucson basin, southeastern Arizona, U.S. Geological Survey: Water-Supply Paper 1939-C.

[9] Belan, R.A., 1972, Hydrogeology of a Portion of the Santa Catalina Mountains, Unpublished Master's Thesis, University of Arizona, Tucson, (unpublished)

[10] Bennett, R., 1965. Carbon-14 dating of ground water in an arid basin. Proc. 6th Int. Conf. on Radiocarbon and Tritium Dating, Washington State University, Pullman, Wash., 1965, pp, 590-596.

[11] Bitner, M.J., 1983, The effects of dispersion and mixing on radionuclide dating of groundwater MS thesis, University of Arizona, Tucson, Arizona, 101pp. (unpublished)

[12] Burkham, D.E., 1970, Depletion of streamflow by infiltration in the main channels of the Tucson basin, southeastern Arizona, U.S. Geological Survey: Water-Supply Paper 1939-B.

[13] Campana, M.E., 1975. Finite-state models of transport phenomena in hydrologic systems. Ph.D dissertation, University of Arizona, Tucson, Arizona (unpublished).

[14] Campana, M.E., and E.S. Simpson, 1984, Groundwater residence times and recharge rates using a discrete-state compartment model and 14C data. Journal of hydrology, V.72, pp. 171-185.

[15] Campana, M.E. 1987, Generation of ground-water ages, Groundwater, V. 25, No. 1, pp. 51-58.

[16] Cheng, S. and Long, A, 1984, Implementation of carbon isotope subroutine to computer program PHREEQE and their application to C-14 Groundwater dating, in Proceedings of AWRA symposium Hydrology and Water Resources in Arizona and the Southwest, April 1984, pp 121-135

[17] CH2M Hill, Errol L. Montgomery and Associates, and L.G. Wilson, 1988, Assessment of potential recharge sites for long-term storage and recovery, report prepared for Tucson Water Planning Division, Hydrology Section.

[18] CH2M Hill, 1992, Pantano Pilot Recharge Project: Progress Report, Prepared for Tucson Water's Planning and Technical Services Division.

[19] Fogg, G.E., E.S. Simpson, and S.P. Neuman, 1979, Aquifer modelling by numerical methods applied to an Arizona groundwater basin, Natural Resource Systems Technical Report No. 32, University of Arizona, Department of Hydrology and Water Resources.

[20] Gallaher, B.M., 1979, Recharge properties of the Tucson basin aquifer as reflected by the distribution of a stable isotope, MS thesis, University of Arizona, Tucson (unpublished)

[21] Hem, J.D. and Robertson, F.N. 1987, Hydrogeochemistry of ground water recharge in alluvial aquifers, southern Arizona, Third symposium on artificial recharge of groundwater in Arizona, Salt River Project symposium proceedings

[22] Keith, S.J., 1981, Stream channel recharge in the Tucson basin and it's implications for groundwater management, MS thesis, University of Arizona, Tucson (unpublished)

[23] Laney, L.R., 1972. Chemical quality of the water in the Tucson basin, Arizona. U.S. Geological Survey Water Supply Paper 1939-D, 46 pp.

[24] Parada, C.B., A. Long, and S.N. Davis, 1983. Stable isotopic composition of soil carbon dioxide in the Tucson basin, Arizona, U.S.A. Isotope Geoscience, V. 1, pp. 219-236.

[25] Rogers, Scott., 1987, Hydrogeologic investigation of the northeast area of the Tucson basin, structure and stratigraphy, Water Resources open-file report WRS 87-1, Tucson Water Planning Division. Hydrology Section.

[26] Rose, S. and Long, A., 1988. Dissolved oxygen systematics in the Tucson basin Aquifer. Water Resources Research, vol. 24, No. 1, pp. 127-136.

[27] Rose, S. and Long, A., 1989, Dissolved inorganic carbon in the Tucson basin aquifer, Groundwater, vol. 27, No. 1, pp 43-49.
[28] Schwalen, H.C., 1933, Water Supply of the Flowing Wells Irrigation District, Library of Special Collections, University of Arizona, Tucson.
[29] Schwalen, H.C., 1965, Progress report on study of water in the Santa Cruz Valley, Arizona, University of Arizona, Agricultural Experiment Station, Report No. 205.
[30] Schwalen, H.C., Collected papers 1916-1965, AZ 563: Boxes 22 and 23, Library of Special Collections, University of Arizona, Tucson.
[31] Schwalen, H.C., and R.J. Shaw, 1957, Groundwater supplies of Santa Cruz Valley of Southern Arizona between Rillito Station and the International boundary, Bulletin 288, University of Arizona Agricultural Experiment Station,Tucson.
[32] Schwalen, H.C. and Shaw, R.V., 1961. Water in the Santa Cruz Valley, Arizona: Univ. of Arizona, Ariz. Exp. Station, Report No. 205, 20 pp.
[33] Simpson, E.S., Thorud, D.B and Friedman, I., 1970, Distinguishing seasonal recharge to groundwater by deuterium analysis in southern Arizona, International association of hydrology publication no. 92, pp 112-121.
[34] Smoor, P.B., 1967. Hydrochemical facies study of ground water in the Tucson basin: Ph.D Dissertation, Univ. of Arizona, Tucson, Arizona (unpublished)
[35] Smith, G.E.P., 1910, Groundwater supply and irrigation in the Rillito Valley, University of Arizona: Agricultural Experiment Station, Bulletin 64.
[36] Streitz, R.S., 1962. Subsurface stratigraphy and hydrology of the Rillito Creek, Tanque Verde Wash Area, Tucson, Arizona. MS thesis, University of Arizona, Tucson. 60 pp.
[37] Supkow, D.J., 1971. Subsurface heat flow as a means for determining aquifer characteristics in the Tucson basin, Pima County, Arizona. Ph.D Dissertation, University of Arizona, Tucson, Ariz. (unpublished)
[38] Thorne, D.P., 1982, A chemical and isotopic study of groundwater flow in the Tucson Mountains, MS thesis, University of Arizona, Tucson (unpublished)
[39] Travers, B.C., and P.A. Mock, 1984, Groundwater modelling study of the upper Santa Cruz basin and Avra Valley in Pima, Pinal, and Santa Cruz Counties, southeastern Arizona, Arizona Department of Water Resources report.
[40] Wilson, L.G. and DeCook, J., 1968. Field observations on changes in the subsurface water regime during influent seepage in the Santa Cruz River, Water Resour. Res., 4(6), 1219-1234.
[41] Freethay, G.W., and T.W. Anderson, 1986, Predevelopment hydrologic conditions in the alluvial basins of Arizona and adjacent parts of California and New Mexico, U.S. Geological Survey: Hydrologic Investigation Atlas, Map HA-664 Sheet 3.
[42] Sigalove, J.J., 1968, Carbon-14 Content and Origin of Caliche, Masters Thesis, University of Arizona, Tucson
[43] Bedinger, M.S., Anderson, T.W., Langer, W.H., 1984, Maps Showing Ground-water Units and Withdrawal, basin and Range Province, Arizona, USGS Water-Resources Investigations Report 83-4114-A
[44] Babcock, J.A., and G. Hix, 1982, Annual static water level basic data report, Tucson basin and Avra Valley, Pima County, Arizona, 1981, City of Tucson, Tucson Water Planning Division, Hydrology Section.
[45] Boul, S.W., 1964, Calculated actual and potential evapotranspiration in Arizona, Agricultural Experiment Station, Technical Bulletin 162, University of Arizona, Tucson.
[46] Arizona Department of Water Resources, 1984. Management Plan for First Management Period, 1980-1990. Tucson Active Management Area, 147 pp.
[47] Brittain, R. and K.E. Foster, 1983. Residential Water Conservation System Design in Tucson Arizona. In: Proceedings, Symposium on Urban Water Management: Augmentation and Conservation, K.E. Foster and M.C. Escher (editors). University of Arizona, Office of Arid Lands Studies, Tucson, Arizona, pp.87-99.
[48] Foster, K.E and DeCook, K.J., 1986. Impacts of residential water reuse in the Tucson area, American Water Resources Association, Bulletin, v. 22, No. 5
[49] McNulty, M.F., 1983. A Water Issue Primer for the Tucson Active Management Area. Arizona Department of Water Resources, 61 pp.
[50] Anderson, S.R., 1991, Potential for Land Subsidence Pima County, Arizona, USA, U.S. Geological Survey: Water-Resources Investigations Report 91.
[51] City of Tucson, 1990, Tucson Water Resources Plan 1990-2100, Public Report
[52] Riddle, J.F., 1984, Isotopic Composition of Stable Carbon and Carbon Dioxide Concentration of Atmosphere in Stream Beds near Tombstone, Arizona, MS Thesis, University of Arizona, (unpublished)
[53] Hess, G.S., and A.N. Elder, 1990, Annual static water level basic data report, Tucson basin and Avra Valley, Pima County, Arizona, 1989, City of Tucson, Tucson Water Planning Division.
[54] Hadj-Kaddour, B. 1983, Recharge from ephemeral streams: case study in Arizona, MS Thesis, University of Arizona, Tucson, Arizona USA (unpublished)
[55] Vandemoer, C. 1988, The Hydrogeochemistry of Recharge Processes and Implications for Water Management in the Southwestern United States, PhD Dissertation, University of Arizona, Tucson (unpublished)
[56] Briggs, P.C., 1984, Arizona's Ground Water Pollution Control Program, Proceedings of the Specialty Conference Sponsored by Irrigation & Drainage Division ASCE, pp.35-43
[57] Foster, K. E., DeCook, K.J., 1986, Impacts of Residential Water Reuse in the Tucson Area, Water Resources Bulletin, Vol. 22, No. 5, pp. 753-757
[58] Wigley, T.M.L., L.N. Plummer, and F.J. Pearson, 1978. Mass transfer and carbon isotope evolution in natural water systems. Geochimica et Cosmochimica Acta. v. 42, pp. 1117-1138.
[59] Fenneman, N.M., 1931, Physiography of Western United States, McGraw-Hill Book Company, New York, 534 p.

[60] Webb, R.H. and Betancourt, J.L. 1990, Climatic variability and flood frequency of the Santa Cruz River, Pima County, Arizona, U.S., Geologic Survey: Open File Report, 90-553
[61] Hastings, J.R., 1958. Vegetative changes and arroyo cutting in southeastern Arizona during the past century-A historical overview. University of Arizona Desert Lands Colloquia, Tucson. pp. 24-39.
[62] Woolhiser, D.A., Keefer, T.O and Redmond, K.T, 1993, Southern Oscillation Effects on Daily Precipitation in the Southwestern United States, Water Resource Research, V 29, no. 4 pp 1287-1296
[63] Sellers, W.D. and Hill, R.H., 1974. Arizona climate. University of Arizona Press, Tucson, Ariz., 2nd rev. ed., 616 pp.
[64] Sellers, W.D., R.H. Hill, and M. Sanderson-Rae (eds.), 1985, Arizona Climate: The First Hundred Years, University of Arizona Press, Tucson.
[65]Pashley, E.F., 1966. Structure and stratigraphy of the central, northern, and eastern parts of the Tucson basin, Arizona. (Ph.D dissertation), University of Arizona, Tucson. 273 pp.
[66] Finnel, T.L., 1970, Pantano Formation, in Cohee, G.V., Bates R.G., and Wright, W.B., Changes in Stratigraphic Nomenclature by the U.S. Geological Survey 1968: U.S. Geological Survey Bulletin 1294_A, pp. A35-A36.
[67] Damon, P.E., 1964, Correlation and chronology of ore deposits and volcanic rocks, Annual progress report COO-689-42, contract AT(11-1)-689 to U.S. Atomic Energy Commission, Geochronology Labs., University of Arizona.
[68] Anderson, S.R., 1987, Cenozoic stratigraphy and geologic history of the Tucson basin, Pima County, Arizona, U.S. Geological Survey: Water-Resources Investigations Report 87-4195.
[69] Eberly, L.D., and T.B. Stanley Jr., 1978, Cenozoic stratigraphy and geologic history of southwestern Arizona, Geological Society of America Bulletin, vol. 89, p. 921-940.
[70] Barnes, C.J., Allison, G.B., 1988, Tracing of Water Movement in the Unsaturated Zone using Stable Isotopes of Hydrogen and Oxygen, Journal of Hydrology, Vol. 100, pp.143-176
[71] Benson, L., Klieforth, H., 1989, Stable Isotopes in Precipitation and Ground Water in the Yucca Mountain Region, Southern Nevada: Paleoclimatic Implications, American Geophysical Union, Geophysical Monograph 55,pp. 41-58
[72] Clark, I.D., Fritz, P. et al., 1982, Isotope Hydrogeology and Geothermometry of the Mount Meager Geothermal Area, Canadian Journal of Earth Science, Vol. 19, pp.1454-1473
[73] Ferronsky, V.I., Polyakov, V.A., 1982, Environmental Isotopes in the Hydrosphere, John Wiley & Sons, New York
[74] Fontes, J.C., Allison, G.B., 1986, Estimation of Long-term, Diffuse Groundwater Discharge in the Northern Sahara Using Stable Isotope Profiles in Soil Water, Journal of Hydrology, Vol. 86, pp.315-327
[75] Friedman, I., 1953, Deuterium Content of Natural Waters and Other Substances, Geochimica et Cosmochimica Acta, Vol. 4, pp. 89-103
[76] Friedman, I., Scholz, T.G., 1974, Isotopic Composition of Atmospheric Hydrogen, 1967-1969, Journal of Geophysical Research, Vol. 79, No. 6, pp. 785-788
[77] Geyh, M.A., Khouri, J., Rajab, R., Wagner, W., 1985, Environmental Isotope Study in the Hamad Region, pp. 1-15
[78] Gupta, S.K., 1983, An Isotopic Investigation of a Near-surface Groundwater System, Hydrological Sciences Journal, Vol. 28, No. 2
[79] Hoefs, J., 1980, Stable Isotope Geochemistry, Springer-Verlag, New York
[80] Ingraham, N.L., Taylor, B.E., 1991, Light Stable Isotope Systematics of Large-Scale Hydrologic Regimes in California and Nevada, Water Resources Research, Vol. 27, No. 1, pp. 77-91
[81] Leguy, C., Rindsberger, M., et al., 1983, the Relation Between the O-18 and Deuterium Contents of Rain Water in the Negev Desert and Air-mass Trajectories, Isotope Geoscience, Vol. 1, pp. 205-218
[82] McDonnell, J.J., Bonell, M., et al., 1990, Deuterium Variations in Storm Rainfall: Implications for Stream Hydrograph Separation, Water Resources research, Vol. 26, No. 3, pp. 455-459
[83] Schoch-Fischer, H., Rozanski, K., et al., Hydrometeorological Factors Controlling the Time Variation of D, O-18 and H-3 in Atmospheric Water Vapour and Precipitation in the Northern Westwind Belt, IAEA-SM-270/19
[84] Sofer, Z., Gat, J.R., 1975, The Isotope Composition of Evaporating Brines: Effect of the Isotopic Activity Ratio in Saline Solutions, Earth and Planetary Science Letters, Vol. 26, pp.179-186
[85] Vogel, J.C., Ehhalt, D., Roether. W., 1963, A Survey of the Natural Isotopes of Water in South Africa, IAEA Symposium (SM 38/41)
[86] Vogel, J.C., Lerman, J.C., Mook W.G., 1975, Natural Isotopes in Surface and Groundwater From Argentina, Bulletin of the International Association of Hydrological Sciences
[87] Craig, H., 1961, Stable Isotopes in Precipitation, Science V133, pp.1702-1703
[88] Coleman, M.L., Shepherd, T.J., et al., 1982, Reduction of Water with Zinc for Hydrogen Isotope Analysis, Analytical Chemistry, Vol. 54, pp.993-995
[89] Friedman, I., O'Neil, J.R., 1977, Compilation of Stable Isotope Fractionation Factors of Geochemical Interest, USGS Professional Paper 440-KK
[90] Kishima, N., Sakai, H., 1980, O-18 and Deuterium Determination on a Single Water Sample of a Few Milligrams, Analytical Chemistry, Vol. 52, pp. 356-358
[91] Sofer, Z., Gat, J.R., 1972, Activities and Concentrations of O-18 in Concentrated Aqueous Salt Solutions: Analytical and Geophysical Implications, Earth and Planetary Science Letters, Vol. 15, pp. 232-238
[92] Tanweer, A., 1990, Ultra Clean Surface of Metallic Zinc for D/H Isotope Analysis, Analytical Chemistry, Vol. 62, No. 19, pp.2158-2160
[93] Tanweer, A., Hut, G., Burgman, J.O., 1988, Optimal Conditions for the Reduction of Water to Hydrogen by Zinc for Mass Spectrometric Analysis of the Deuterium Content, Chemical Geology, Vol. 73, pp. 199-203
[94] Roether. W., 1970, Water-CO2 Exchange Set-up for the Routine O-18 Assay of Natural Waters, International Journal of Applied Radiation and Isotopes, Vol.21, pp. 379-387

[95] Gat, J.R., 1980, The isotopes of hydrogen and oxygen in precipitation. In: Fritz, P. and Fontes, J.C. (editors), Handbook of Environmental Isotope Geochemistry, Ch1, pp 21-47, Elsevier Scientific Publishing Co., Amsterdam, The Netherlands, 545 pp.
[96] Payne, B.R. 1972, Isotope Hydrology, Adv, Hydrosci, V 8, 95-138
[97] Weeks, E.P., Earp, D.E., Thompson, G.M., 1982, Use of Atmospheric Fluorocarbons F-11 and F-12 to Determine the Diffusion Parameters of the Unsaturated Zone in the Southern High Plains of Texas, Water Resources Research, Vol. 18, pp. 1365-1378
[98] Bassett, R.L., 1990, A Critical Evaluation of the Available Measurements for the Stable Isotopes of Boron, Applied Geochemistry, Vol. 5, pp. 541-554
[99] Davis, S.N., DeWiest, R.J.M., 1966, Hydrogeology, John Wiley & Sons, New York
[100] Desaulniers, D.E., Kaufmann, R.S., et al., 1986, Cl-37 and Cl-35 Variations in a Diffusion-controlled Groundwater System, Geochimica et Cosmochimica Acta, Vol. 50, pp.1757-1764
[101] Douthitt, C.B., 1982, The Geochemistry of the Stable Isotopes of Silicon, Geochimica et Cosmochimica Acta, Vol. 46, pp. 1449-1458
[102] Fabryka-Martin, J.T., Davis, S.N., et al., 1988, I-129 and Cl-36 in Uranium Ores, 2. Discussion of AMS Measurements, Chemical Geology, Vol. 72, pp. 7-16
[103] Graves, B., 1987, Radon in Ground Water, Lewis Publishers, Chelsea, Michigan
[104] Hoehn, E., von Gunten, H.R., 1989, Radon in Groundwater: A Tool to Assess Infiltration From Surface Water to Aquifers, Water Resources Research, Vol. 25, pp. 1795-1803
[105] Kaufmann. R., Long, A., et al., 1984, Natural Chlorine Isotope Variations, Nature, Vol. 309, pp. 338-340
[106] McMahon, P.B., Chapelle, F.H., 1991, Microbial Production of Organic Acids in Aquitard Sediments and its Role in Aquifer Geochemistry, Nature, Vol. 349, pp. 233-235
[107] Thurman, E.M., 1985, Organic Geochemistry of Natural Waters, Martinys Nijhoff/Dr. W. Junk Publishers, New York
[108] Phillips, F.M., Bentley, H.W., Elmore, D., 1986, Cl-36 Dating of Old Ground Water in Sedimentary basins, Proceedings of the Third Canadian/American Conference on Hydrogeology, pp. 143-150
[109] Bentley, H.W., Phillips, F.M., Davis, S.N. et al., 1986, Chlorine-36 Dating of Very Old Groundwater,1. The Great Artisan basin, Australia, Water Resources Research, Vol. 22, No. 13, pp. 1991-2001
[110] Striegl, R.G., Armstrong, D.E., 1990, Carbon Dioxide Retention and Carbon Exchange on Unsaturated Quaternary Sediments, Geochimica et Cosmochimica Acta, Vol. 54, pp.2277-2283
[111] Andres, G. and Egger, R. 1985, A new tritium interface method for determining the recharge rate of deep groundwater In the Bavarian Molasse basin., J. Hydrol. V82, pp27-38
[112] Colville, J.S., 1984, Estimation of aquifer recharge and flow from natural tritium content of groundwater, J. Hydrol, V67, pp 195-222
[113] Egboka, B.C.E., Cherry, J.A., Farvolden, R.N., and Frind, E.O. 1983, Migration of contaminants in groundwater at a landfill: a case study, 3. Tritium as an indicator of dispersion and recharge. In: J.A. Cherry, (guest editor), Migration of Contaminants in Groundwater at a Landfill: A Case Study, J. Hydrol, V63, 51-80
[114] International Atomic Energy Agency, 1992, Environmental Isotope Data: World Survey of Isotope Concentration in Precipitation (1953-1990), IAEA, Vienna
[115] Larson, G.J., Delcore, M.R. and Offer, S., 1987, Application of the tritium interface method for determining recharge rates to unconfined drift aquifers, I. Homogeneous Case, J. Hydrol, V91, pp59-72
[116] Munnich, K.O. 1968, Infiltration and deep percolation. In: Nuclear Techniques in Hydrology, IAEA Vienna, V-3a, pp 191-197
[117] Allison, G.B. and Hughes, M.W. 1975, The use of environmental tritium to estimate recharge to a south-Australian aquifer, J. Hydrol, V26, pp 245-254
[118] Doney, S.C., Glover, D.M. and Jenkins, William J., 1992, A model function of the Global Bomb Tritium Distribution in Precipitation, 1960-1986, J. Geophys Res., V97, no.C4, pp.5481-5492
[119] International Atomic Energy Agency, 1992, Environmental Isotope Data: World Survey of Isotope Concentration in Precipitation (1953-1990), Data supplied to Author on disk
[120] Tanner, A.B., 1964, Physical and chemical controls in distribution of Radium-226 and Radon-222 in groundwater near Great Salt Lake Utah, In: The Natural Radiation Environment, J.A. S. Adams and W.M. Lowder, Eds, Univ. Chicago, Press, pp 253-278
[121] Graves, W.B. (editor) 1987, Radon, Radium and other radioactivity in groundwater, Proceedings of the NWWA Conf, Lewis Publisher
[122] Hall, F, 1988, Geologic COntrols on Radon Gas in Groundwater, In: Radon and the Environment, W.J. Makofske and M.R. Edelstein (editors), Noyes Publications, pp 48-55
[123] Brutsaert, W.F., Norton, S.F., Hess, C.T. and Williams, J.S., 1982, Geologic and Hydrologic Factors controlling Radon-222 in Groundwater in Maine, Ground Water, V19, no. 4, pp 407-417
[124] Gilkeson, R. H. and J. B. Cowart. 1987. Radium, Radon and Uranium Isotopes in Groundwater from Cambrian-Ordovician Sandstone Aquifers in Illinois. In: Radon, Radium, and Other Radioactivity in Ground Water. Proceedings of the NWWA Conf. B. Graves, Ed. Lewis Publishers. pp. 423-436.
[125] Cech, I., M. Lemma, H. Prichard, and C.W. Kreitler. 1987. Radium-226 and Radon-222 in Domestic Water of Houston-Harris County, Texas. Ibid., pp. 377-402.
[126] Szabo, Z. and O. S. Zapecza. 1987. Relation Between Natural Radionuclide Activities and Chemical Constituents in Ground Water of the Newark basin. in: Radon, Radium, and Other Radioactivity in Ground Water. B. Graves, Ed. Proceedings of the NWWA Conf. Lewis Publishers. pp. 283-310.

[127] Cothern, R. C. 1987. Estimating the Health Risks of Radon in Drinking Water. J. AWWA. April, pp. 153-158.
[128] Semprini, L. 1987. Radon-222 Concentrations of Ground Water From a Test Zone in a Shallow Alluvial Aquifer in the Santa Clara Valley. In: Radon, Radium, and Other Radioactivity in Ground Water. B. Graves, Ed. Proceedings of the NWWA Conf. Lewis Publishers. pp. 205-218.
[129] Wei, C. and L. Yi-yao. 1984. Preliminary Study of the Application of Hydrogeochemistry to Earthquake Prediction, International Symposium on Earthquake Prediction. (Paris, France 1979) Terra Sci. Publ. Co. pp. 539-552.
[130] Smith A. R., H. A. Wollenberg and D. F. Mosier. 1980. Roles of Radon-222 and Other Natural Radionuclides in Earthquake Prediction. In: The Natural Radiation Environment III, NTIS, Springfield, Va, pp. 154-174.
[131] Lorenz, P. J., O. D. Rodenberg, L. G. Shadle, A. C. Antes, and W. D. Hess. 1961. Background Radioactivity in the Decorah Fault Region, Iowa Academy of Science. v. 68, pp.397-403.
[132] King, P.T., Michel, J., and Moore, W.S. 1982. Ground Water Geochemistry of ^{228}Ra, ^{226}Ra, and ^{222}Rn. Geochim. Cosmochim. Acta v. 46, pp. 1173-1182.
[133] Harvey, J.P. 1981. Groundwater Extraction and Radon Anomalies in the Picacho Area, South-central Arizona. Master's thesis, Dept. of Hydrology and Water Resources, Univ. of Arizona. 120 p.
[134] Long, A., Eastoe, C.J., Kaufman, R.S., Martin, J.G., Wirt, L and Finley, J.B., 1993, High-precision measurement of chlorine isotope ratios, Geochemica et Cosmochemica Acta, 57, pp 2907-2912
[135] Long, A. and Kalin, R.M., 1990, A Suggested Quality Assurance Protocol for Radiocarbon Dating Laboratories, Radiocarbon, V 32, no. 3, pp 329-334
[136] Feltz, H.R., Hanshaw, B.B., Preparation of Water Sample for C-14 Dating, pp.1-3
[137] Geyh, M.A., Wagner, R.H., 1979, Guideline for Groundwater Sampling for Isotope Analyses, C-14 & H-3 Laboratory, Hannover, Germany
[138] Mook, W.G., Bommerson, J.C., Staverman, W.H., 1974, Carbon Isotope Fractionation Between Dissolved Bicarbonate and Gaseous Carbon Dioxide, Earth and Planetary Science Letters, Vol. 22, pp.169-176
[139] American Public Health Association, 1981, Standard Methods for the Examination of Water and Wastewater, 15th ed. American Public Health Association, 1134pp
[140] Turin, J., 1986, Carbon Dioxide and Oxygen Profiles in the Unsaturated Zone of the Tucson basin, Masters Thesis, University of Arizona, (unpublished)
[141] Robertson, F.N., Personal communication
[142] Robertson, F.N., 1989, Geochemistry of ground water in alluvial basins of Arizona and adjacent parts of Nevada, New Mexico and California. U.S. Geological Survey Professional Paper 1406c.
[143] Robertson, F.N., Garrett, W.B., 1988, Distribution of Fluoride in Ground Water in the Alluvial basins of Arizona and Adjacent Parts of California, Nevada, and New Mexico, USGS Hydrologic Investigations Atlas
[144] Busby, J.F., Plummer, L.N., Lee, R.W., Hanshaw, B.B., 1988, Geochemical Evolution of Water in the Madison Aquifer in Parts of Montana, South Dakota, and Wyoming, USGS Professional Paper 1273-F
[145] Drever, J.I., 1982, The Geochemistry of Natural Waters, Prentice-Hall, Inc., Englewood Cliffs, N.J.
[146] Freeze, R.A., Cherry, J.A., 1979, Groundwater, Prentice-Hall, Inc., Englewood Cliffs, N.J.
[147] Garrels, R.M., MacKenzie, F.T., 1966, Equilibrium Concepts in Natural Waters (10-Origin of the Chemical compositions of Some Springs and Lakes, 151st Meeting of the American Chemical Society, pp. 222-242
[148] Henderson, T., 1984, Geochemistry of Ground-water in Two Sandstone Aquifer Systems in the Northern Great Plains in Parts of Montana, Wyoming, North Dakota, and South Dakota, USGS Professional Paper 1402-C
[149] Lettenmaier, D.P., Hooper, E.R., 1991, Trends in Stream Quality in the Continental United States, 1978-1987, Water Resources Research, Vol. 27, No. 3, pp. 327-341
[150] Muller, A.B., 1978, Determination of the Basement Complex Configuration in the Safford Valley, Arizona, by Bouguer Gravity Anomaly Techniques, Journal of the Arizona-Nevada Academy of Science, Vol. 13, pp. 3-6
[151] Murray, R.S., Quirk, J.P., 1980, Clay-water Interactions and the Mechanism of Soil Swelling, Colloids and Surfaces, Vol. 1, pp. 17-32
[152] Nordstrom, D.K., Munoz, J.L., 1986, Geochemical Thermodynamics, Blackwill Scientific Publications, Palo Alto
[153] Sherwonit, W.E., 1974. A petrographic study of the Catalina gneiss in the forerange of the Santa Catalina Mountains, Arizona. MS thesis, University of Arizona, Tucson (unpublished)
[154] Stumm, W., Morgan, J.J., 1981, Aquatic Chemistry, John Wiley & Sons, New York
[155] Todd, D.K., 1980, Groundwater Hydrology, John Wiley & Sons, New York
[156] Dixon, J.B and Weed, S.B., 1979, Minerals in soil environments, Madison, Wis, Soil Science Society of America, 948
[157] Chen, PY 1977, Tables of key lines in X-ray Powder Diffraction Patterns of minerals and clays and associated rocks, Dept. of Natural Res., Geological Survey Occasional Paper 21, State of Indiana
[158] Rose, S. 1987, Dissolved Oxygen Systematics in the Tucson basin Aquifer, Arizona, PhD Dissertation, University of Arizona, unpublished
[159] Cheng, S.L. 1984, Application of stable isotopes of oxygen, hydrogen and carbon to hydrogeochemical studies, with special reference to Canada del Oro Valley and the Tucson basin. PhD Dissertation, University of Arizona, Tucson
[160] Faure, G. 1991, *Principles and Applications of Inorganic Geochemistry*, MacMillan Publishing, 625pp
[161] Helgeson, H.C., 1969, Thermodynamics of hydrothermal systems at elevated temperatures and pressures, American J. Science, v267 pp729-804
[162] Tardy, Y. and Garrels, R.M., 1976, Prediction of Gibbs energies of formation - I. Relationships among Gibbs energies of formation of hydroxides, oxides and aqueous ions, Geochim. Cosmochim Acta, V 40, pp 1051-1056
[163] Tardy, Y. and Garrels, R.M., 1977, Prediction of Gibbs energies of formation - II. Monovalent and divalent metal silicates, Geochim. Cosmochim Acta, V 41, pp 87 - 92

[164] Norton, D. 1974, Chemical mass transfer in the Rio Tanama system, west-central Puerto Rico, Geochim. Cosmochim. Acta., V38, pp. 267-277
[165] Ball, J.W., Nordstrom, D.K., and Jenne, E.A., 1980, Additional and revised thermochemical data and computer code for WATEQ2 - A computerized chemical model for trace and major element speciation and mineral equilibria of natural waters: U.S. Geological Survey Water-Resources Investigations 78-116, 109p
[166] Ball, J.W. and Nordstrom, D.K., 1991, User's manual for Wateq4F, with revised thermodynamic data base and test cases for calculating speciation of Major, Trace and Redox elements in natural waters, U.S.G.S. Open-File Report
[167] Brinkmann, R., Munnich, K.O. and Vogel, J.C., 1959. 14C Altersbestimmung von grundwasser. Naturwissenschaften, 46: 10-12.
[168] Davis, S.N., and Bentley, H.W., 1982. Dating ground water: a short review. In: Nuclear and Chemical Dating Techniques (Lloyd, A.C., ed.), p.187-222.
[169] Deines, P., Langmuir, D. and Harmon, R.S., 1974. Stable carbon isotope ratios and the existence of a gas phase in the evolution of carbonate ground water. Geochim. Cosmochim. Acta, 38: 1147-1164.
[170] Fontes, J. Ch. and Garnier, J.M., 1979. Determination of the initial 14C activity of total dissolved carbon: A review of the existing models and a new approach. Water Resources Research, 15: 399-413.
[171] Ingerson, E. and Pearson, F.J., 1964. Estimation of age and rate of motion of ground water by the 14C method. In: Recent Research in the Field of Hydrosphere, Atmosphere, and Nuclear Geochemistry, Maruzen, Tokyo, p. 263.
[172] Mook, W.G., 1976. The dissolution exchange model for dating ground water with 14C. In: Interpretation of Environmental Isotope and Hydro-chemical Data in Ground Water Hydrology. IAEA, Vienna, p. 213-225.
[173] Munnich, K.O., 1957. Messung des C-14-Gehaltes von hartem Grundwasser. Naturwissenschaften, 44: 32-33.
[174] Reardon, E.J. and Fritz, P., 1978. Computer modelling of ground water 13C and 14C isotope compositions. J. Hydrol., 36: 201-224.
[175] Tamers, M.A., 1967. Radiocarbon ages of ground water in an arid zone unconfined aquifers. In: Isotope Techniques in the Hydrologic cycle. Amer. Geophys. Union, Geophys. Monogr. Ser., 11: 143-152
[176] Wigley, T.M.L., 1976. Effect of mineral precipitation on isotopic composition and 14C dating of ground water. Nature, 263: 219-221.
[177] Parkhurst, D.L., L.N. Plummer and D.C. Thorstenson, 1982. BALANCE--A computer program for calculation of chemical mass balance. U.S. Geological Survey Water-Resources Investigation 82-14, 33 p.
[178] Parkhurst, D.L., Thorstenson, D.C., and Plummer, L.N., 1980. PHREEQE-A computer program for geochemical calculations. U.S. Geol. Surv., Water-Resour. Investigation. 80-96, 210 p.
[179] Plummer, L.N., B.F. Jones and A.H. Truesdell, 1976. WATEQF-a Fortran IV version of WATEQ, a computer program for calculating chemical equilibrium of natural waters. US Geological Survey, Water-Resources Investigation 76-13
[180] Fontes, J.C., 1990, Chemical and Isotopic Constraints on C-14 Dating of Groundwater, Taylor, RE, Long, A and Kra, R eds, Radiocarbon After Four Decades, Springer-Verlag, New York, pp. 242-261
[181] Fontes, J.C., Andrews, J.N., et al., 1991, Paleorecharge by the Niger River (Mali) Deduced From Groundwater Geochemistry, Water Resources Research, Vol. 27, No. 2, pp. 199-214
[182] Geyh, M.A., Frohlich, K., Verhagen, B., 1990, Numerical Modelling with Groundwater Ages, Taylor, RE, Long, A and Kra, R eds, Radiocarbon After Four Decades, Springer-Verlag, New York, pp. 276-287
[183] Leaney, F.W., Allison, G.B.,1986, Carbon-14 and Stable Isotope Data for an Area in the Murray basin: Its Use in Estimating Recharge, Journal of Hydrology, Vol. 88, pp. 129-145
[184] Pearson, F.J., 1990, Effects of Parameter Uncertainty in Modelling C-14 in Ground Water, Taylor, RE, Long, A and Kra, R eds, Radiocarbon After Four Decades, Springer-Verlag, New York, pp. 262-276
[185] Spiker, E.C., Rubin, M., 1975, Petroleum Pollutants in Surface and Groundwater as Indicated by the Carbon-14 Activity of Dissolved Organic Carbon, Science, Vol. 187, pp. 61-64
[186] Thatcher, L., Rubin, M., Brown, G.F., 1961, Dating Desert Ground Water, Science, Vol. 134, No. 3472, pp. 105-106
[187] Vogel, J.C., Ehhalt, D., 1963, The Use of the Carbon Isotopes in Groundwater Studies, IAEA Symposium (SM 38/40)
[188] Hem, J.D., 1985. Study and interpretation of the chemical characteristics of natural water, 3rd ed. U.S. Geological Survey Water-Supply Paper 2254, 263 p..
[189] Mangold, D.C., Tsang, C., 1991, A Summary of Subsurface Hydrological and Hydrochemical Models, Reviews of Geophysics, Vol. 29, No. 1, pp. 51-79
[190] White, A.F., Chuma, N.J., 1987, Carbon and Isotope Mass Balance Models of Oasis Valley-Fortymile Canyon Groundwater basin, Southern Nevada, Water Resources Research, Vol. 23, No. 4, pp.571-582
[192] Wigley, T.M., 1973, Chemical Evolution of the System Calcite-Gypsum-Water, Canadian Journal of Earth Sciences, V 10, No. 2, pp 306-315
[193] Wigley, T.M., 1973, The Incongruent Solution of Dolomite, Geochimica et Cosmochimica Acta, Vol. 37, pp. 1397-1402
[194] Yonge, C.J., Ford, D.C., et al., 1985, Stable Isotope Studies of Cave Seepage Water, Chemical Geology, Vol. 58, pp. 97-105
[195] Stuiver, M., Long, A. and Kra, R., 1993, Radiocarbon Calibration Issue, Radiocarbon, V34, no.2
[196] Niel Plummer, USGS Personal Communication
[197] McKay, C.P., Long, A., Friedmann, E.I., 1985, Radiocarbon Dating of Open Systems with Bomb Effect, Journal of Geophysical Research, V no. pp
[198] Bennett, R. 1965, Unpublished results, Radiocarbon Laboratory, University of Arizona

CYCLIC MODEL FOR SEASONAL RECHARGE AND DISCHARGE OF GROUND AND SPRING WATER IN THE VALDAY EXPERIMENTAL BASIN (HUMID ZONE) USING ENVIRONMENTAL ISOTOPE DATA

V.I. FERRONSKIJ, V.V. ROMANOV, L.S. VLASOVA
Water Problems Institute,
Russian Academy of Sciences,
Moscow

G.P. KOLESOV, S.A. ZAVILEISKIJ
State Institute of Hydrology,
St. Petersburg

V.T. DUBINCHUK
Research Institute of Hydrogeology and
Engineering Geology,
Moscow

Russian Federation

Abstract

The seasonal recharge and discharge of ground and spring water within a small experimental basin in humid zone near Lake Valday (56N, 33E) was studied using environmental tritium. The contribution and transit time of different sources of recharge and discharge of ground and spring water were identified. The sources appeared to be as follows: precipitation and direct surface runoff with zero transit time, sandy layer with a transit time of 0.25yr, the morain sandy loam with water age of 20 yr, and the local swamp with time of water exchange of 5 yr.

The process of seasonal recharge and discharge of ground and spring water as a whole and by source components has cyclic regime. In this connection the cyclic model for description of the process is proposed and discussed.

1. Introduction

The problem of groundwater formation through infiltration recharge is of permanent interest to hydrologists and soil researchers because of its practical importance. The other aspect of the task is the regime of groundwater discharge towards surface springs and rivers. The consideration of both the infiltration recharge and the surface spring discharge of groundwater within a catchment area and elaboration of corres-

ponding physical and mathematical models sets up the complete formulation of the problem. But there is no universal solution of this problem because of the variety of natural hydrogeological and climatic conditions. Therefore, an experimental approach is searched for generalized but typical hydrogeological and geographical conditions.

The present work was carried out on Valday experimental station of the State Institute of Hydrology. The station is situated near Lake Valday, at a distance of 350 km from Moscow, in the direction to St.Peterburg, in a humid zone typical for the North-West Russia,

The scope and goals of experimental and analitical work are as follows:

- to estimate seasonal infiltration recharge and discharge of groundwater within the studied catchment basin;
- to determine the parameters of soil moisture transport through the unsaturated zone;
- to build up the physical picture of the runoff formation during the flood and non-flood seasons;
- to comprehend the mechanism of groundwater discharge into local springs;
- to elaborate physical and mathematical models of groundwater regime for the studied basin taking into account its infiltration recharge and discharge into springs.

2. Hydrological conditions of the basin

The Valday hydrological station is representative of the North-West region of the European part of Russia. It is located in the central part of the Valday Upland (56N, 33E). The studied area covers a small meadow catchment basin within the field of the station and is called the Hollow Usadievsky. The spring on the bottom appears to be left-bank of the local Ponika River flowing into the Lake Valday (Fig. 1). The catchment of the Hollow Usadievsky is elliptic in shape and has an area of 0.44 km^2, stretching from the North to the South and being 0.8 km long and 0.45 km width. The area is characterized by moraine hilly landscape. The exess of the hill tops over the Hollow thalweg does not exceed 4 m. The only part exceeding 18-20 m is its western region. The mean slope of the catchment is equel to 4‰. The slope of the Hollow bed is 26‰. Positive forms of the landscape are formed by solid moraine loam coverd by a layer of sandy lo-

am from 0.3 to 0.5 m thick. An exception to this general picture occurs on the most northern and southern parts of the catchment which are composed by sand varying in grain size and including pebble and gravel of 3-4 m thick.

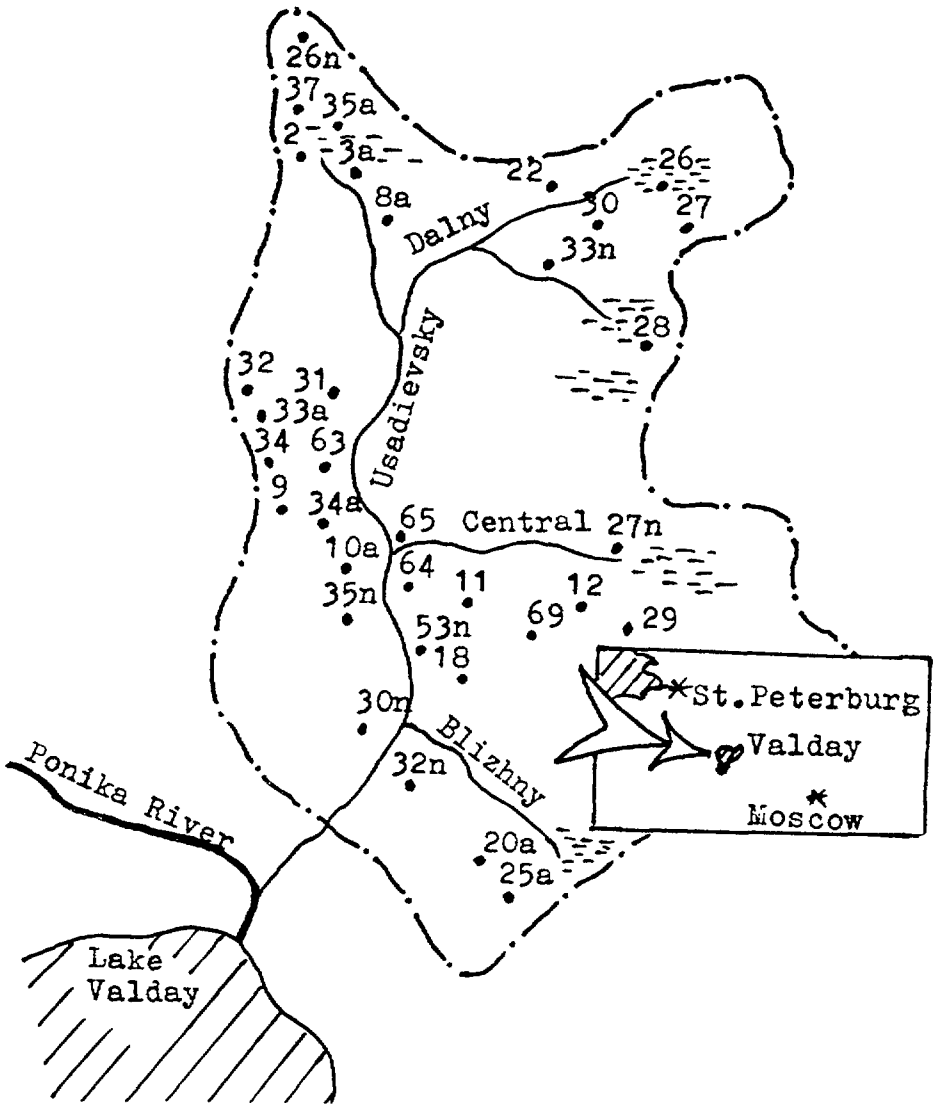

Fig. 1 Scheme of experimental basin Usadievsky and sampling point location. The figures indicate borehole numbers.

The podzolic soils make up 75% of the basin area. The peat layer on the swamp is of 1-2 m thick. More than 80% of the catchment is occupied by a field and a meadow. A patch of forest is located in the North-East of the basin and occupies no more than 2% of the area. The swamp constitutes 11% of the area and is located in the North-East and the East parts.

The annual runoff of the Hollow Usadievsky is equal to 120 000 m^3 while the total precipitation reaches 600-700 mm/yr. The mean monthly flow rate varies from 0.1 to 25 l/sec. The total duration of the runoff absence due to winter freezing and summer dry seasons is close to 250 days. The floods occur in late March or early April every year.

3. Methodology

The collection and accumulation of experimental isotope and conventional data on infiltration recharge and discharge conditions of the basin was the main goal of the first stage of the work. The environmental tritium was used as a tracer of the study process. The tracer carries both genetic and time information and is the best tool for this particular purpose. Periodic but systematic sampling of water was carried out at fixed points. Fig. 1 shows a sketch of the location of observational boreholes, streams and other points of sampling.

The geological structure of the studied basin is shown in Fig.2.

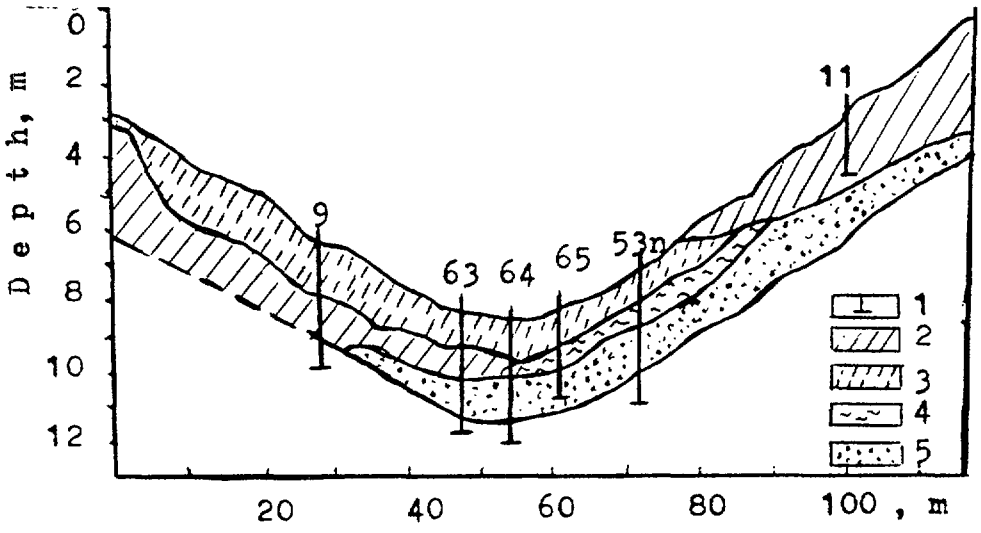

Fig. 2 Geological section of the experimental basin: (1) borehole end its number, (2) sandy loam, (3) clayish sand, (4) clay, (5) sand.

The data on tritium content in precipitation and its variation in time are needed for hydrogeological interpretation of the tracer behaviour and for the elaboration of physical and mathematical models. The collection of those data in the region was started at the beginning of 1985, mainly on the monthly basis. The long-term mean annual values of tritium in precipita-

tion are determined by the data of the near located meteorological stations of European Russia where such observations have taken place, namely in Arkhangelsk, Tver, Vologda, Minsk and Moscow. Those particular data are presented in Table 1. The reported results of the previous years were recalculated relative to 1986 taking into account the radioactive decay of tritium.

Table 1 Mean annual concentration of tritium in precipitation over Central European Russia and recalculated figures relative to 1986

Year	Tritium measured in T.U.	Tritium relative to 1986 in T.U.	Year	Tritium measured in T.U.	Tritium relative to 1986 in T.U.
1960	207	48	1974	127	65
1961	246	61	1975	127	68
1962	1340	349	1976	101	58
1963	3963	1090	1977	99	60
1964	2325	678	1978	99	63
1965	934	288	1979	77	52
1966	752	245	1980	52	37
1967	404	139	1981	75	43
1968	274	100	1982	49	39
1969	296	114	1983	52	44
1970	198	81	1984	41	40
1971	137	58	1985	36	35
1972	155	71	1986	38	38
1973	90	43	1987	33	
1990	27		1988	35	
1991	31		1989	28	

During 1986-1987 the sampling was carried out from all the boreholes and springs at the time of spring-summer and autumn-winter recharge seasons. The data were used for identification of the age and genetic type of waters which take part in the recharge of the springs and groundwater of different soil layers. The data were also interpreted with respect to water dynamics in the various seasons of the year.

Starting from 1988, the monitoring was continued using limited number of a representative borehole within the basin and in the mouth ranges of the spring and its tributaries. The samples were collected during spring-autumn floods, after individual rainfalls and during the winter thaws.

4. Genesis and age of recharged-discharged water

Fig. 3 demonstrates the results of summer 1986 observations. One can see that the main part of the surface and subsurface samples have tritium content close to its concentration in the mean annual precipitation varying from 25 to 40 T.U. Besides, there are three places where tritium values are different from the above. One is in the North-East part of the basin within the upper swamps and is characterized by higher concentrations which vary from 52 to 54 T.U. This fact indicates that meteoric water of the previous years has stored here. Taking into account the data reported in Table 1, it is possible to calculate the time of water delay which is equal to 6-7 years and the measured values of tritium in groundwater represent precipitation of 1979.

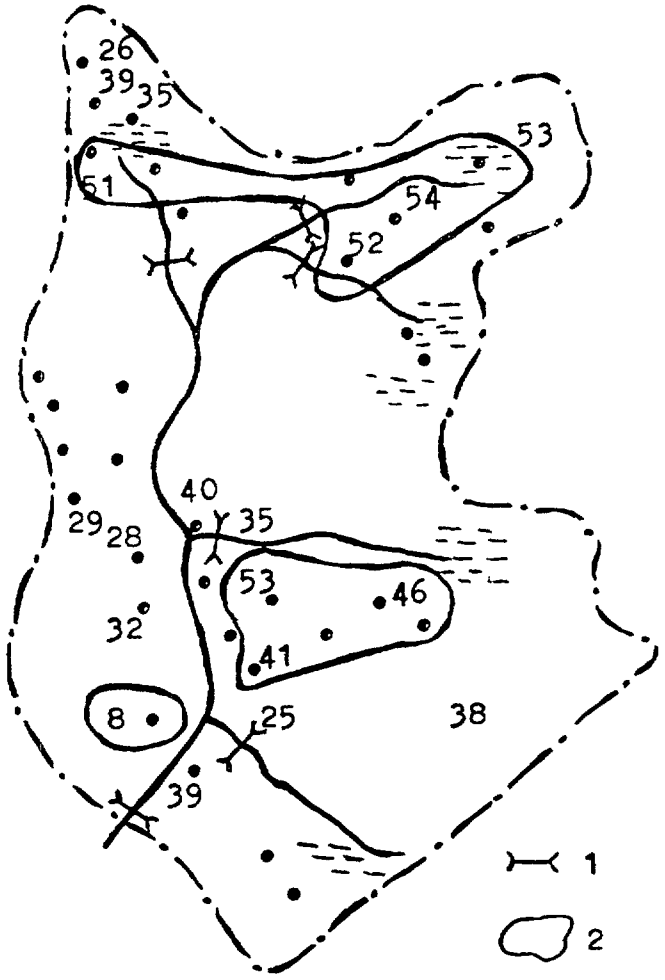

Fig. 3 Mean values of tritium measured in 1986: (1) stream sampling place, (2) areas with higher concentrations relative to precipitation.

The second place with higher tritium concentration (from 41 to 53 T.U.) was discoverd over sandy loam in the boreholes 11, 12, and 18. Here the average time of delay in groundwater movement is equel to 3 or 4 years and related to moraine sandy loam.

The third area is characterized by lower concentration of tritium (7 to 8 T.U.) and was fixed in borehole 30n where artesian water of the carboniferous sediments are discharged. This water is not involved into the ground and surface water discharged to the springs. A histogram in Fig. 4 shows the frequences of tritium concentrations in all the water samples taken in 1986 and 1987 and confirms the above mentioned statement.

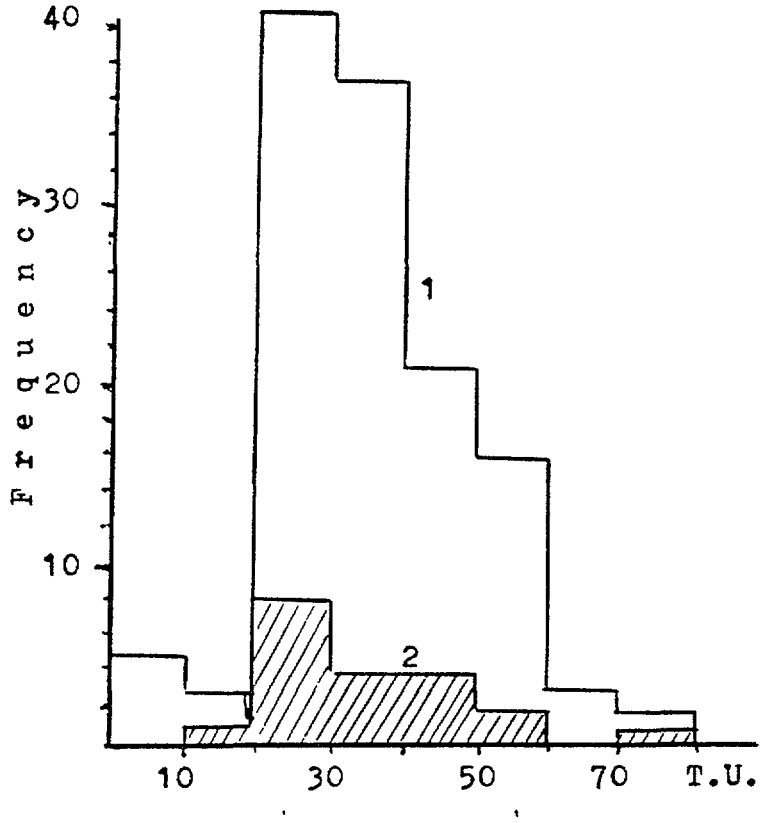

Fig. 4 Histogram of tritium concentration distribution in ground and surface waters of the Hollow Usadievsky (1) and in precipitation over the experimental area (2) in 1986 and 1987.

The main part of the ground and surface waters (78%) are recharged from precipitation of sampling year. And water with tritium concentration higher than 50 T.U. (16%) is related to the origin

of previous seasons. The water with tritium content less than 10 T.U. forms distribution maximum which is not connected with the main mass of water.

Let us consider time variation of tritium concentration in two groups of water: the "young" and the "old" ones.

Borehole 53n is the most representative of the first group. It is located on the east slope of the spring bed, and its depth is 4.4 m from the surface. The borehole reveals groundwater in the covering sandy loam and sandy lens below (see Fig. 2).

Fig. 5 shows the time variation of tritium concentration in water from the borehole 53n which is in accordance with the water level changes and with tritium values variation in the monthly precipitation during all the periods of observation. The average tritium content in the both types of water is the same and equals to 34 T.U.

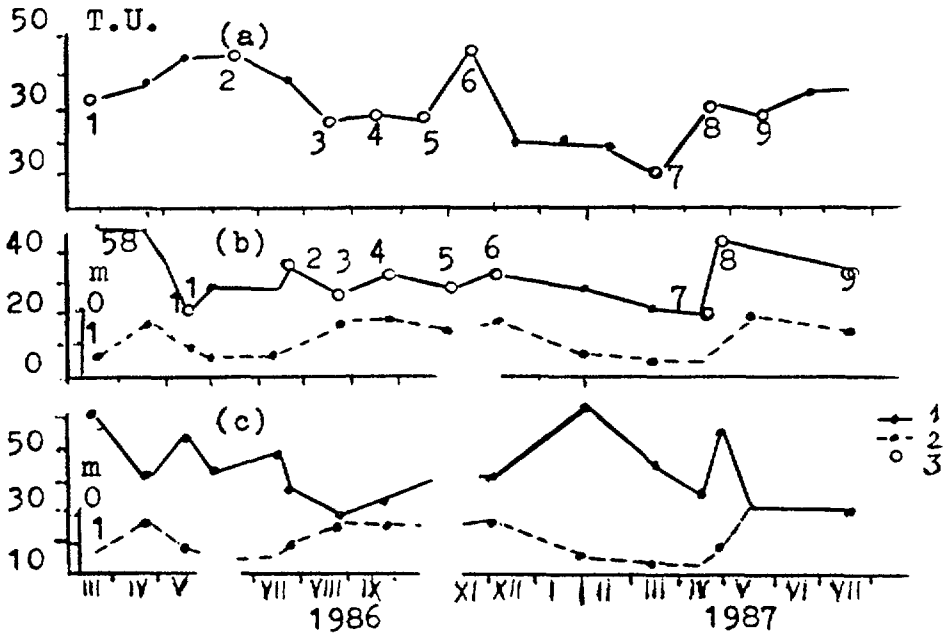

Fig. 5 Variation of tritium concentration in precipitation (a), borehole 53n (b), and borehole 11 (c) relative to vater table variation. (1) tritium concentration, (2) water table relative to the surface, (3) the peak of concentration.

But any correlation between tritium concentration in groundwater C_g and water table H_w, as well as between C_g and precipitation C_p calculated by the least square method is practically absent (r=0.2 and 0.01 respectively). It follows from this

that despite of the fact that groundwater is recharged by precipitation of the same year, there is a delay in time between the fallout and appearance in the borehole. One can see from the plot that the delay does not exceed one season, i.e. three months. For more correct estimation of infiltration delay we compared the time of occurence of all the successive monodirectional extremes of the both curves (a) and (b) in Fig. 5 and calculated difference in time. For the parallel extreme series 1 - 9 from the spring of 1986 to the summer of 1987 the value time difference is equal to 60, 37, 7, 10, 18, 16, 27, 10 and 62 days, accordingly. The maximum values of time delay equal to 1 and 2 months are related to the period of May and June when winter precipitation appears in groundwater with maximum delay.For the rest of the year the average time delay is close to 12 days. Taking into account the depth of the perforated casing of the borehole, it was found that the average velocity of vertical infiltration in the sandy loam and sandy section is close to 21 cm/day.

Groundwater of the second group with higher tritium concentration is studied in detail together with precipitation in borehole 11 (see Fig. 2 and 3). The borehole is located in 30 m up to the slope from borehole 53n and intersects only sandy loam. Its depth from the surface is 2.76 m, and the lower end of the perforation is situated at the depth of 2.64 m. The tritium concentration and water table variation are demonstrated in Fig. 5c. The mean value of tritium concentration in the water during the period of observation is equal to 53 T.U. It exceeds the mean value of tritium in precipitation for the same period by 9 T.U. We note an interesting fact that the tritium content change has reverse run with water table in the borehole. The rise of water table is accompaned by lowering of tritium content and vice versa. At the lower water table at the depth of 135 cm from the surface the mean value of tritium content in water is equal to 60.4 T.U., and at a higher level, at the depth of 27 cm, the tritium concentration drops to 46.8 T.U. This fact allows to assume that there are two sources of water recharge of different age feeding the borehole. One of them supplies the lower sandy loam layer with retardation of movement and the other is connected with the upper layer where the modern water is moving along the moraine sandy loam. We assume that the upper source has tritium concentration similar to

that of the water in borehole 53n, i.e. equal to 33.6 T.U., which is similar to the mean value during the time of observation, and this water is mainly responsible for the water table variation in borehole 11. Then it is possible to write a system of balance equations whose solution allows to find the proportion of mixing water components and its tritium concentration in the lower layer of sandy loam.

We write the system:

$$C_{up.w.t.} = C_1 x + C_2 y$$
$$C_{low.w.t.} = C_1 fx + C_2 y$$
$$X + y = 1$$

or

$$C_{up.w.t.} = C_1 x + C_2(1 - x)$$
$$C_{low.w.t.} = C_1 fx + C_2(1 - x)$$

where $C_{up.w.t.}$ and $C_{low.w.t.}$ are the mean values of tritium concentration in water of boreholes 11 at the upper and lower water table, respectively; C_1 and C_2 are tritium concentrations in the both water sources, i.e. in the "young" water similar to that of borehole 53n, and in the sandy loam of the lower layer; x and y are portions of both waters; it is the coefficient of variation of water proportion of the first source which is proportional to the variation of water level in borehole 11 and equal to 0.57 : (276 - 135)/(276 - 27) cm.

The numerical form of the system is as follows:

$$46.8 = 33.6\ x + C_2(1 - x)$$
$$60.4 = 33.6 \cdot 0.57\ x + C_2(1 - 0.57\ x)$$

The solution of the system gives the following figures:

$$x = 0.71; \quad y = 0.29; \quad C_2 = 78.5 \text{ T.U.}$$
$$(x' = 0.57\ x = 0.4; \ y' = 1 - 0.57\ x = 0.60)$$

The calculated figures show that during the flood period (higher water table) borehole 11 is filled up to 2/3 by "young" water. In the dry season 60% of the borehole water is represented by the "old" one from the lower layer of sandy loam. In order to estimate the age of this "old" water, we can compare the calculated value of 78.5 T.U. of tritium concentration with the input function of tritium in precipitation corrected by radioactive decay relative to 1986 (see Table 1). In this case we use

piston flow approximation. The precipitation with tritium content of 80 T.U. corresponds to 1970. So, water age from the loam sediments of 2.76 m depth is close to 16 year, and the vertical velocity of infiltration in sandy loam is 276 : 16 = 17.2 cm/yr.

Additional soil samples near borehole 11 were taken by means of auger in November 1986 and in June 1987. The boring depth was 4.23 m and sampling was fulfilled at interval of 0.5 - 1.0 m. The pore water was evaporated at the temperature of 300°C and tritium content was measured (Fig. 6). Variation of tritium concentration in the pore water can be explained only by piston emplacement of the "old" meteoric water. If one takes into account the diffusion washing of tritium and its radioactive decay in time, in this case the maximum value of 120 T.U. in pore water at a depth of 3 m can be connected with penetration of meteoric water to the depth since 1963 when thermonuclear tests took place in the atmosphere.

This gives a time interval of 23 years relative to 1986 year of observation. From this the velocity of water infiltration is 300 : 23 = 13 cm/yr. One can see from both calculations that the order of figures is the same and the water movement in the sandy loam is by 2.5 orders lower than in sand.

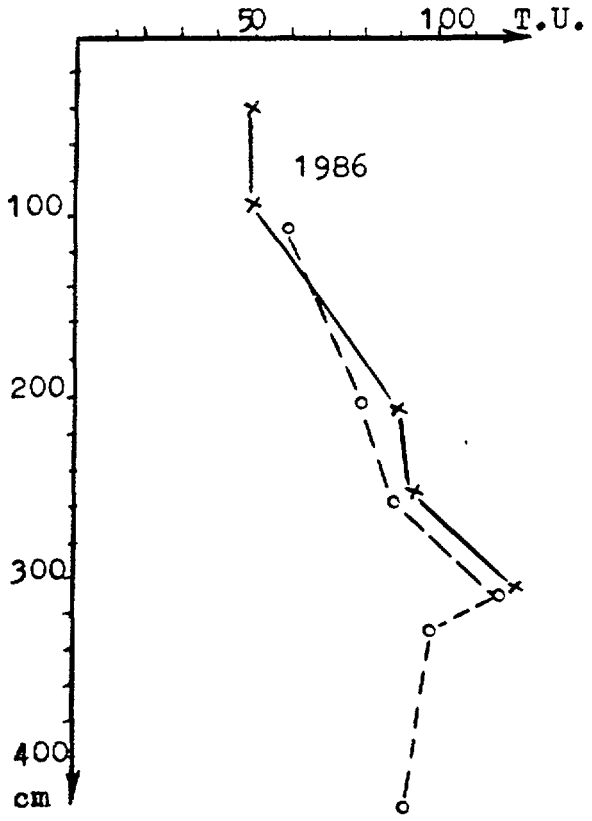

Fig. 6 Tritium profile of pore water in sandy loam near borehole 11 measured in Nov. 1986 and June 1987.

The calculated values of filtration velocity seem to be limited for infiltration properties of the waterbearing sediments. For example, the velocity of filtration in carbonate and fractured rocks estimated by analogous isotope methods is 63 cm/yr. This correlates with the same interval and by 4 times exceeds the velocity in the sandy loam.

One can see from the above data that tritium age of groundwater in two different deposits varies from 0 to 3 months in sand and from 0 to 23 years in the moraine sandy loam.

Using experimental results, it is possible to estimate seasonal age variation of water within a year. Table 2 contains initial data and calculation results of water proportions of different age (a,x,y) for the groundwater of sandy lens sampled from borehole 53n and from Spring Usadievsky. The calculation was carried out relative to the seasonal balance of water which was accepted as unity. Fig. 7 demonstrates the same data in absolute values of of water amount of the particular age . The relative data of Table 2 represent the formation conditions of water in a season while Fig. 7 shows their changes during the year.

The age characteristics of water properties were selected from the calculations on the basis of the previous analysis of isotope data. In fact, water with t = 0 within the season transit time and seasonal delay t = 3 months relative to the time of precipitation is taken as a basic fallout. The water with t = 0 in principle can be specified as the surface runoff.

It follows from Table 2 that the maximum precipitation proportion with t = 0 in the groundwater appears in spring and summer, and the minimum one - in autumn and winter. Accumulation of groundwater in the cold half of the year by 70 or 80% takes place at the expense of previous year precipitation. Groundwater recharge in a warm season goes from the surface runoff.

It was found that groundwater balance in the spring of 1986 and 1987 does not fit if one uses only two fractions. Evidently, the third component from the deep sandy loam takes part in this process. The old water is displaced into the sandy lens by the pressure of flood water. Tritium content in such water is equal to 78.5 T.U., on the average. In the case of three-component task, for the calculation of three ages it is possible to combine two balance equations of spring seasons and general water balance equation assuming small hydrological difference between the same

seasons of two years. The result of the calculation shows that the fraction of "old" groundwater with the age of from 16 to 23 years in the sandy lens in a spring season does not exceed 10%.

By analogy, the balance of the main surface spring Usadievsky at the closing range was calculated (Table 2 and Fig 7). Contrary to the grounwater, the isotope balance for spring does not fit given that two components are used for spring as well as for autumn. The attempt to use tritium concentration of

Table 2 Seasonal variation of ages of ground and spring waters of the basin in 1986-1987

Season	Discharge, mean value in l/s	Tririum content in the components C	C_a	C_x	C_y	Portion of water a t=0	x t=0.4	y t=20	Mean age in yr
		Groundwater, borehole 53n							
1986									
Spring	0.93	43	40	37.5	78.5	0.57	0.33	0.1	2.13
Summer	1.01	41	38	43	-	0.4	0.6	-	0.24
Autumn	0.49	31	36	30	-	0.2	0.8	-	0.32
Winter	1.03	29	24	31	-	0.3	0.7	-	0.28
Mean weited value		36	-	-	-	0.37	0.61	0.025	0.77
1987									
Spring	1.20	32	26	29	78.5	0.57	0.33	0.1	2.13
Summer	0.75	35	37.5	32	-	0.55	0.45	-	0.18
		Spring Usadievsky							
1986									
Spring	11.32	41	40	38	43	0.28	0.23	0.49	2.54
Summer	0.6	40	38	43	-	0.6	0.4	-	0.16
Autumn	7.45	37	36	30	39	0.49	0.05	0.46	2.32
Winter	1.92	29	24	31	-	0.29	0.71	-	0.28
Mean weited value		38.5	-	-	-	0.36	0.22	0.42	2.19
1987									
Spring	10.45	35	26	29	43	0.28	0.23	0.49	2.54
Summer	4.26	26	37.5	32	22	0.19	0.12	0.59	3.0
Autumn	-	26.5	15	35	39	0.49	0.05	0.46	2.32

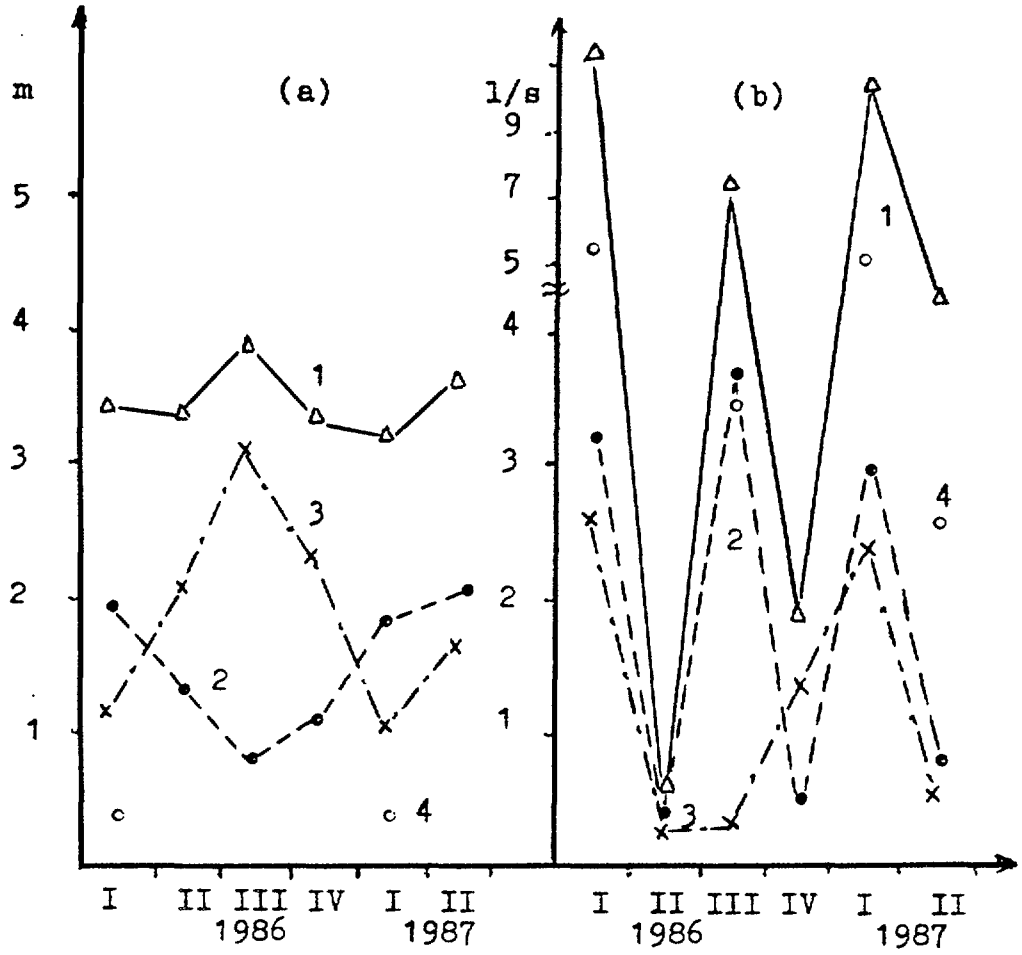

Fig. 7 Seasonal variation of different age water for groundwater (a) and spring water (b) of the basin: (1) water table and discharge, (2) surface runoff (t=0), (3) groundwater with t=3 months, (4) "old" water with t=20 yr (a) and t=5 yr (b).

sandy loam (78.5 T.U.) with a longer delay time (20 yr) as the third component does not provide the balance and the equation system is to be unsolved. From the physical point of view, it is understandable due to the fact that the proportion of the "old" water in the soil does not exceed 2% during the year, and because of dilution of this water its tritium concentration appears to be within analytical errors. In this particular case it is possible to assume that in addition to precipitation (portion "a") and groundwater (portion "x"), the third component can be the water from the swamp of the upper part of the basin. Isotope characteristic of the swamp is represented by borehole 26n and the Spring Dalny and the drainage trench. The mean value of tritium concentration here is close to 43

T.U. for the spring and 39 T.U. in automn (t=5 yr from piston flow model). The results of the calculation are presented in Table 2 and Fig. 7.

The formation of the runoff withn the basin is characterized by the opposite tendencies relative to those of the groundwater. Increase in contribution of the runoff (t=0) in the groundwater leads to decrease in the spring, i.e. at continuous saturation of porous media of the unsaturated zone by precipitation or melted snow the proportion of this "young" water in the runoff is lower and vice versa. For instance, in the similar spring season of 1986 and 1987 and the rainy summer of 1987 the minimum proportion of the surface runoff of the spring and its maximum for the soils are characteristic. Maximum of the surface runoff occurs in autumn when 80% of soil pours are filled with water of the previous precipitation (t=0.4 yr, see Table 2). And winter is the only season when there is close agreement of water component ages for the spring and the soil.

During the rainy seasons of 1987 the percentage of swamp water in the spring runoff is high (42% of the mean annual runoff). But this water is completely absent in the sandy lens. The runoff from the swamp is discontinued in dry seasons of the year (the summer and the winter of 1986). Because of high proportion of swamp water with t=5 yr the groundwater component with t=0.4 yr in the spring runoff is lower than in the unsaturated zone and its mean annual value is 22%. But mean annual surface runoff of the spring and soil water is the same (37%). On the basis of the first two years of observation it was found that water of four ages is balancing in the recharge and discharge within the basin: surface water of precipitation origin (t=0), groundwater of sandy deposits with residence time of up to 0.25 yr, swamp water with 5 yrs of exchange time, and water of morain sandy loam with mean age of 20 yrs. The contribution of different age waters to the recharge of Spring Usadievsky is varied seasonally. Mean values of the components in 1986-1987 were 36, 22, 41.8 and 0.2 accordingly.

The mechanism of groundwater discharge into the spring is well identifiend by simple piston model of displasement of water accumulated in the sediments under pressure of the entered precipitation water. The box model gives mean age of spring water equal to 2.2 yr.

5. Seasonal cycling of recharged and discharged basin water

The results of tritium measurements of groundwater in boreholes 11, 18, 26, 26n and 53n obtained in 1989-1991 are presented in Fig. 8.

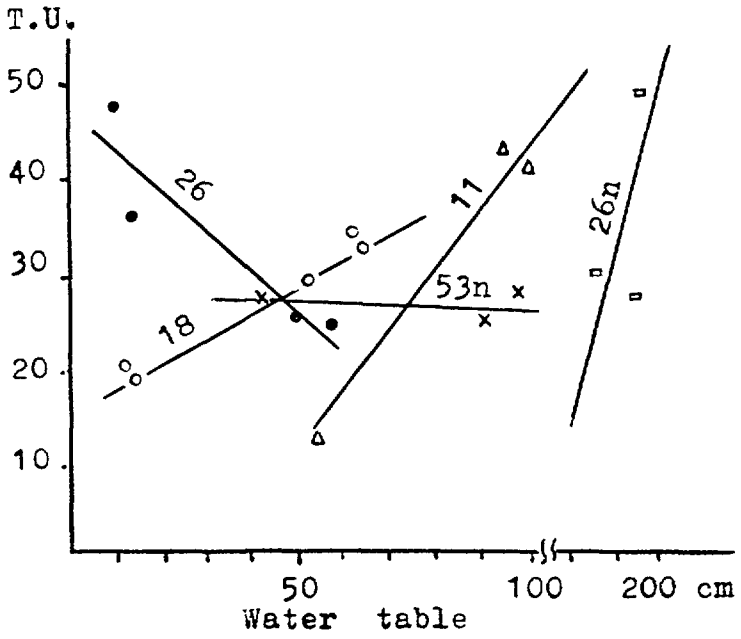

Fig. 8 Relationship between tritium concentration of groundwater and its water table (mean values for 1989-1991)

The depth of boreholes varies from 3 to 5 m. Perforation of the boreholes 18 and 26n was accomplished on all the length. The borehole 11 reaches only sandy loam, 53n comes to sandy layer and 26 locates in the swamp area and opens peat water.

One can see from Fig. 8 that the sandy loam profile (26n, 18) tritium concentration of water increases with decrease of groundwater table. This relation demonstrates the fact that after flood water has gone the recharged into the borehole water appears to be of the previous years origin with higher tritium concentration. It was found earlier by the data of borehole 11 that mean water age of this is about 20 yrs. For sandy sediments in borehole 53n tritium concentration practically does not depend on the water table. This is because of high value movement velocity of water in sands.

A reverse picture is observed in the swamp borehole 26, where tritium concentration of water is sharply droped with water table decrease and vise versa. As a consequence the peat water on the depth has very low tritium concentration. On the contrary upper part of the section peat water has higher tritium concentration of the previous years precipitation. Fig. 9 shows this phenomenon more clearly.

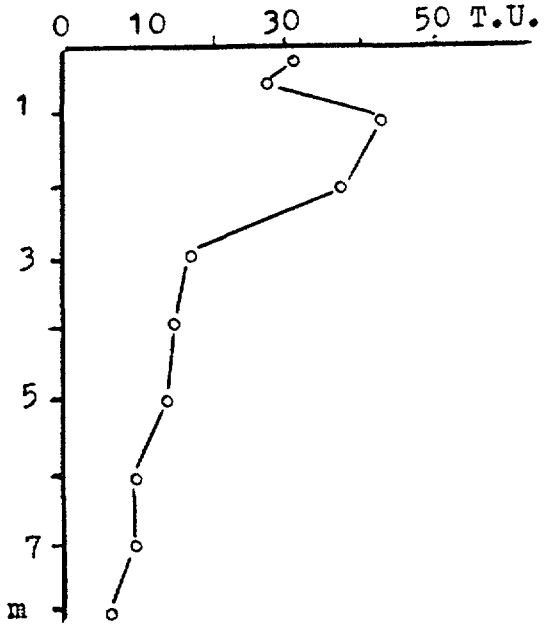

Fig. 9 Distribution of tritium concentration in swamp borehole (mean value for 1990)

The plot was built up using 1990 observational data of one more borehole set up in an upstream swamp of the near located Tver region. The profile of tritium concentration is divided into two parts. The upper one up to 2 m has high concentration for which the mean age obtained by box model is about 5 yrs. The lower part from 2 to 8 m of the depth shows that its water age is not less then 100 yrs due to diffusion process of transfer. The same character of water dynamics seems to be responsible for for tritium distribution in the borelole 26 relative to the water table. So, relationship between tritium content and water level shows that after spring floods and rainfalls process of replacement of previous year water in sandy loam and peat soils takes place. Sandy soil does not retain old water.

Taking into account distribution of the observational boreholes within the basin it is assumed that the mean tritium concentra-

tion of all the samples in the same month can be accepted as mean isotope characteristic for groundwater of the basin. In this case isotope variation of groundwater from month to month is applied as indicator of its dynamics. Fig. 10 shows this variation and dynamics.

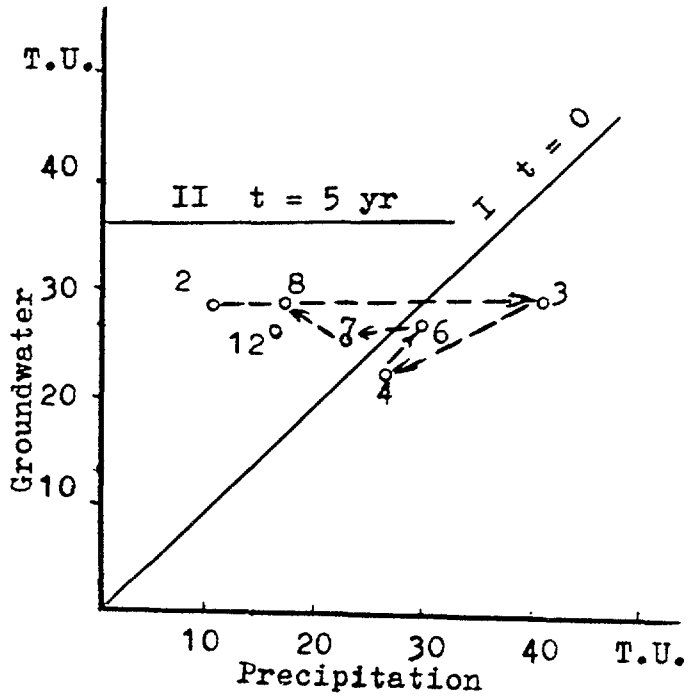

Fig. 10 Relationship between tritium concentration in groundwater and precipitation (monthly mean values for 1989-1991). Figures indicate the month and t is residence time.

Theoretical lines reflecting general directions of tritium content changes in the groundwater in connection with its variation in precipitation are also drawn. The line I defines tritium distribution in groundwater of zero age. This is possible when tritium content in groundwater is equal to that in precipitation. Theoretical line II corresponds to the groundwater age of t=5 yrs. Isotopic composition of this water reveals weak reaction with respect to seasonal variation of tritium in precipitation and the line of its tritium concentration passes in parallel with the abscissa axis.

Let us consider seasonal distribution od tritium concentration in groundwater shown in Fig. 10. During winter time tritium content does not depend on its concentration in precipitation. this is because of frozen soil and snow cover. But concentration of tritium here equal to 31 T.U., what is lower then in groundwater during 1988 (34 T.U.) in average. This can be explained by infiltration of small portion of water of 1989 winter precipitation with low tritium concentration (10 T.U.) into

groundwater. Perhaps it has happend during winter thaws and due to variation of freezing depth of the soil in connection with winter temperature variation. The mean value of this thaw influece winter water in soil is estimated by tritium balance (31 = 9a + 34(1 - a), where a is portion of the thaw water of 1989), and equal to 12%.

From March to April tritium content in groundwater sharply dropped from 34 T.U. to 24 T.U. due to the spring flood. The amount of thaw water in the soil in April was 32% (24 = 9a + 31(1-a). In June tritium concentration in groundwater was 29.5 T.U. while in precipitation its mean monthly content was 31 T.U. From isotope balance it follows that in the beginning of Summer only 7% of Spring flood water presented in the groundwater. The remaining 93% did not manage to mix with the older water and discharged into the spring. During Summer variation of tritium concentration was in small range (28-31 T.U.) in comparison with broad changes in mean monthly precipitation of these months (17-31 T.U.). The mean monthly tritium content of groundwater in summer was 30 T.U. and in precipitation was about 24 T.U. It means that the groundwater content of tritium is weakly dependent on summer precipitation. Using tritium balance and taking into account tritium content of groundwater in winter as 31 T.U., one can find that summer precipitation here forms portion of 14% of water. At the same time summer precipitation in that region set up 35-40% of the annual one. This is due to the surface runoff and evaporation-transpiration process.

In December when negativ temperature is set up, tritium content in the groundwater was close to the summer value (29 T.U.) but with small shift relative to the preautumn flood of 1989 (31 T.U.).

The value of mean annual tritium content in grounwater of the basin is close to 29 T.U. and in the precipitation is 24 T.U. From this using isotope balance equation the portion of precipitation in the groundwater is equal to 29%. It means that one third of old groundwater was replaced by this year precipitation water. Mean residence time of groundwater here is close to 3 years.

It is worth to draw attention that this is mean residence time. It varies from close to zero for sand to some tenth of years for sandy loam. One may obtain from the equation of isotopic

balance that only 16% of groundwaters are represented by water from the sandy loam and loamy sediments.

Let us consider now seasonal variation of isotopic composition of Spring Usadievsky in its mouth range. Fig. 11 shows tritium content changes relative to the seasonal water discharge in 1989-1991. Fig 11a demonstrates the regime of Spring discharge for a long in time thaw in February 1989. In the beginning of the thaw the discharge was increased from 1.5 l/s to 7 l/s. The tritium content reached the value of 38 T.U. exceeding its level in the groundwater (31 T.U.) and much more in the snow pack (9 T.U.). That time tritium content of water in tributary Blizhny flowing out of swamp was 43 T.U., and in the borehole 26 (on the swamp) was 49 T.U. So that the possible source of high tritium concentration was swamp water with that of about 46 T.U. With the increased flood up to its maximum of 9 February the portion of melting snow water in accordance with proportion $33 = 38a + 9(1 - a)$ increased up to 17%. But the portion of swamp water is still high because the tritium content of spring water was 33 T.U. which is higher then that of groundwater (31 T.U.). In the end of February when the thaw was finished the discharge of spring dropped to 33 l/s, the tritium concentration in its water was decreased lower of its value in the groundwater and reached the figure of 23 T.U. The calculations show that this was a stage of maximum portion of melted snow water in the spring (42%). In general during the thaw the decrease of tritium content in spring water due to melting water discharge is observed. But in this particular case the main contribution belonged to the swamp water discharge.

Fig. 11b shows the same distribution during the spring flood in March-April 1991. In the end of March when melting started the value of tritium content in the spring water was 27 T.U. This is close to that of mean monthly content of groundwater (26 T.U.). The mean tritium concentration in snow water of winter precipitation was 16 T.U. With the increase of discharge of spring water its tritium content decreased due to dilusion by melting water, but after 23 March started slowly to increase. After 4 April the discharge dropped from 107 l/s to 50 l/s but tritium concentration started to increase and reached maximum value of 45 T.U. on 6 April. And to the end of flood both parameters returned to the initial values making a cycle.

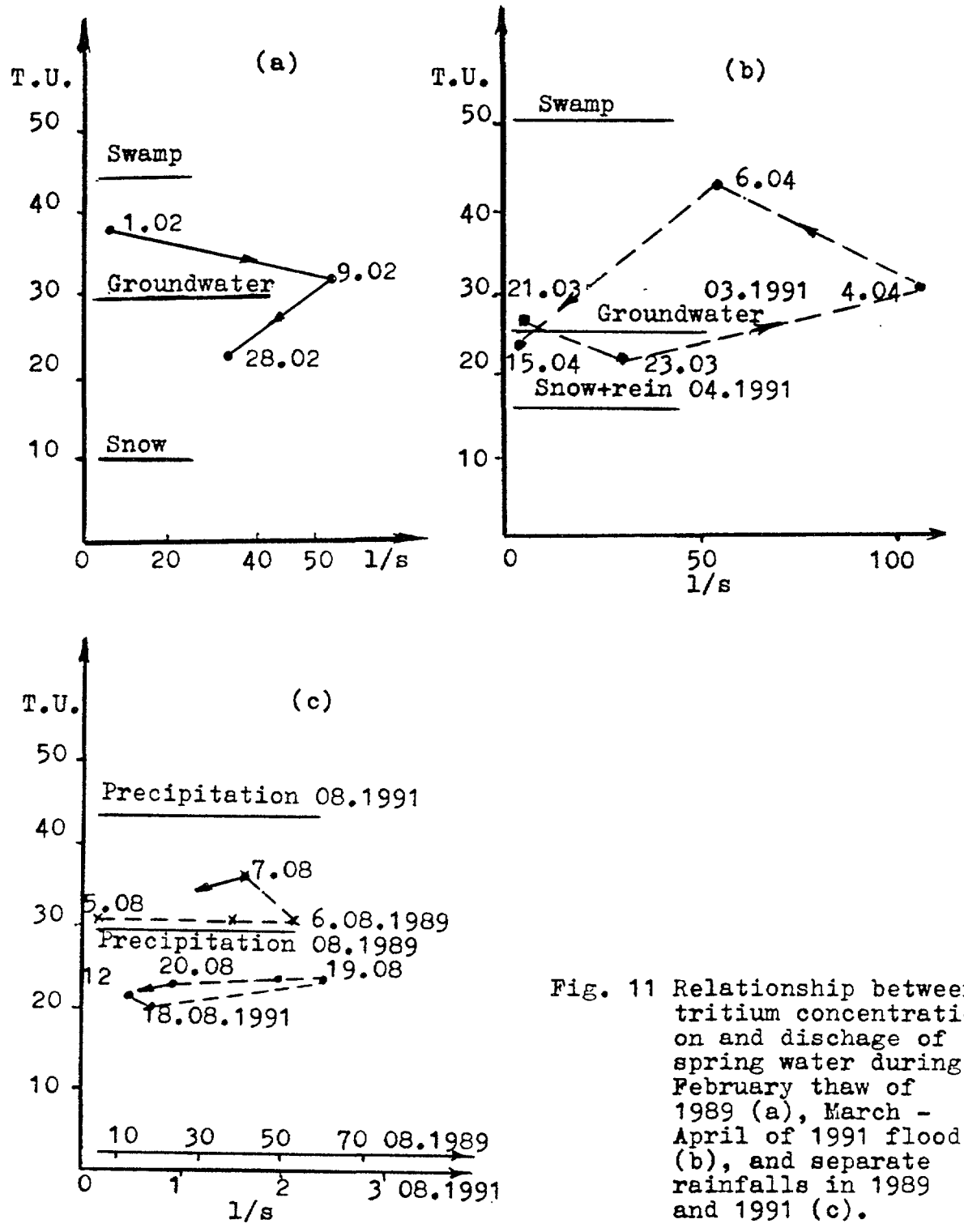

Fig. 11 Relationship between tritium concentration and dischage of spring water during February thaw of 1989 (a), March - April of 1991 flood (b), and separate rainfalls in 1989 and 1991 (c).

Between the results of numerous analyses the maximum tritium concentrations were observed in the water in the water of Sprins Dalny and Blizhny from 4 to 9 April with values of 44-60 T.U. So that the maximum concentration of tritium during the period has swamp water with value of around 52 T.U. In this connection the increase of tritium values may be explaned by increase of discharged swamp water, If it is true then the swamp

contribution to the droped discharge of the spring water from proportion 45 = 52a + 26(1 - a) can be determined by figure of 73%.

Fig. 11c demonstrates the spring dynamics during separate rainfalls of different intensity. The intensive rainfall during 5-7 August 1989 increased the spring discharge up to 50 l/s. The precipitation water had tritium concentration of 29 T.U. The mean value of that of groundwater in August was 39 T.U., and the spring water at mouth range showed 30 T.U. It follows from that the surface runoff of the rainfall in this situation reached 70%. Later on tritium content in the spring increased to 38 T.U. and water discharge in the spring decreased to 35 l/s. It is assumed that the tritium content increase corresponds to swamp water of Spring Dalny with concentration of 42 T.U. Its amount is accounted by figure of 66%.

Some different picture was observed during a poor but long rainfall in 17-20 August. The precipitation tritium had concentration of 43 T.U., and the spring water with discharge of 0.5 l/s had 24 T.U., and groundwater content showed 24 T.U. The increase of spring discharge up to 2.5 l/s was accompanied by weak increase of tritium content to 25 T.U. By isotope balance only 14% of the spring discharge was determined by surface runoff. In the first case the spring discharge was increased by 16.3 times, and in the second by 5.6 times. But portion of the surface runoff was equal to 66% in the first case and to 14% in the second one. It follows from those that during weak but long rainfall the water saturates the soil. During heavy rainfall the water runs off on the surface and may overflow the swamp which discharges with some delay to the spring.

In order to have more representative picture of isotope dynamics in the spring water the mean tritium data of the basin from 1986 to 1991 are presented on Fig. 12. Tritium concentrations of the spring water here in January-February are exceeded that in precipitation, The spring recharge occured mainly at the expense of groundwater with higher tritium content.

During the spring flood which starts in the region in the end of March or beginning of April tritium concentration of the spring - water is decreased due to their dilution by melting water with low tritium content. The process of mixing of snow, swamp and groundwater of zero, five and three year age is observed on the plot.

The main experimental results are as follows:

- residence time of groundwater in sandy loam is determined by 3 yrs and every year fresh precipitation water displaces one

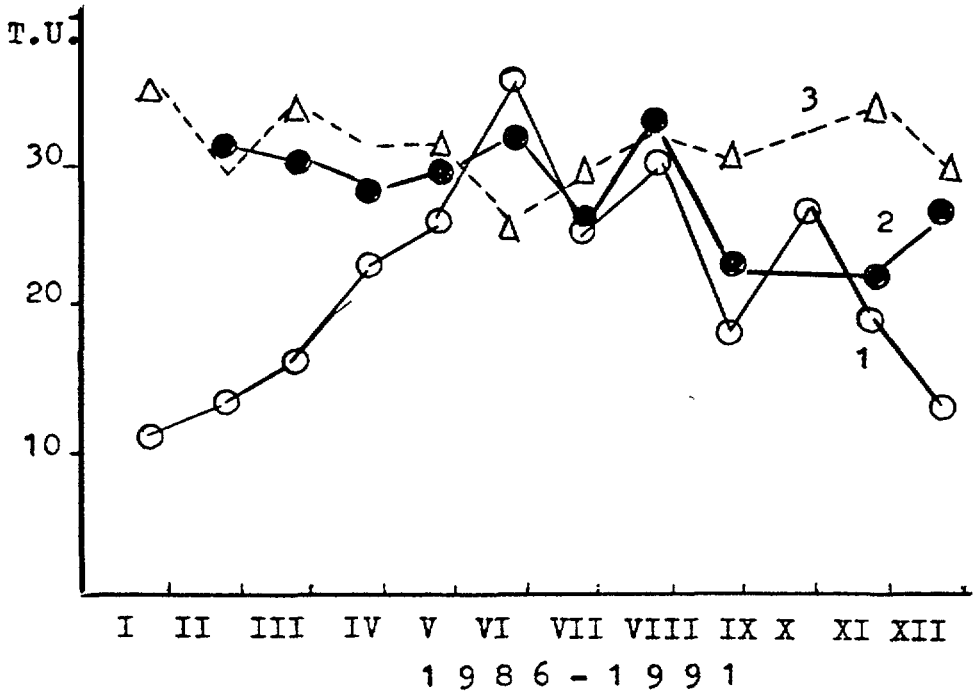

Fig. 12 Variation of tritium concentrations in precipitation (1), in spring water (2), and in groundwater (3). Mean values for 1986-1991 are normalised to 1986.

third of old water;

- residence time of groundwater in swamp is equal to 5 yrs and it discharges during the spring and autumn floods;
- during winter thaw groundwater is recharged by melting water and its portion is accounted by 12-17%;
- the recharge of springs is performed by surface runoff, groundwater and swamp water;
- during 6 yrs of observation the water balance of spring discharge is accounted by 50% of precipitation, 30% of groundwater, and 20% of swamp water. The mean residence time of spring water is close to 2 yrs.

6. Cyclic model for seasonal recharge and discharge of ground and spring water using the approach of maltycompartmental hydrological systems

Seasonal variation of water cycle is sinchronous with variation of isotopic composition of precipitation. In this connection a cyclic model is to be the best for description and simulation of natural processes like cyclic recharge and discharge of ground and spring water.

Fig 13 represents a block-scheme model of the system under consideration. In order to preserve a symmetry of the analytical presentation of the model and, in turn, avoid an over complication of equation to be derived we suppose that all blocks (compartments,

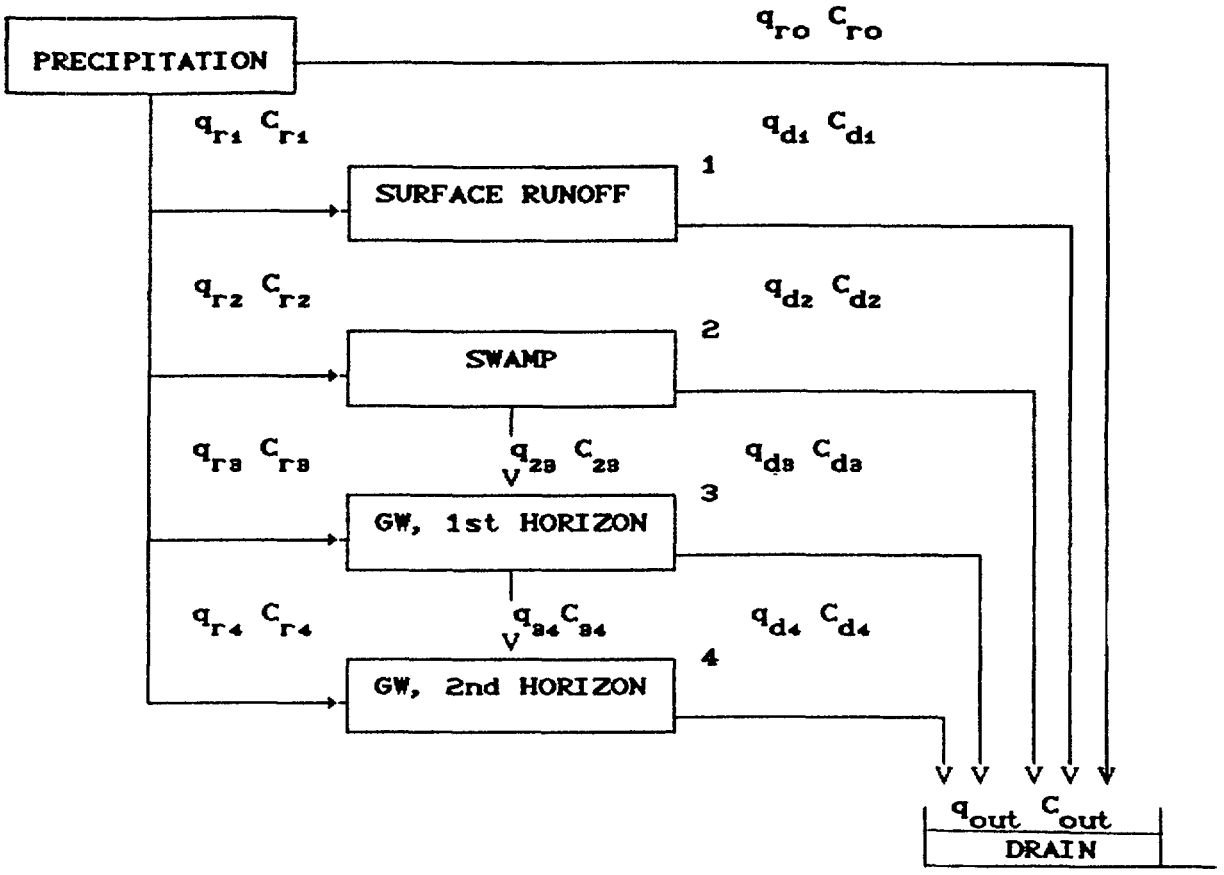

Fig 13 A block-scheme of the multi compartment model of a hydrological dranaige system with sinusoidal inputs:

$$q_{ri}(t)=q_{ai}\sin\omega t + \overline{q_{ri}}$$

$$C_{ri}(t)=C_{ai}\sin(\omega t+\phi_i) + \overline{C_{ri}}$$

$$C_{out}=\frac{q_{d1}C_{d1}+q_{d2}C_{d2}+q_{d3}C_{d3}+q_{d4}C_{d41}+q_{ro}C_{ro}}{q_{d1}+q_{d2}+q_{d3}+q_{d4}+q_{ro}}$$

$$q_{out}=q_{d1}+q_{d2}+q_{d3}+q_{d4}+q_{ro}$$

reservoirs) of the system are interconnected each with others and back-feeded itself. Then a basic model equations can be written as follows:

water mass balance

$$(1)\quad dV_i/dt=\sum_{k=1}^{n} q_{ki} - \sum_{i=1}^{n} q_{ik}+q_{ri}-q_{di}$$

isotope tracer mass balance

$$(2)\quad dV_iC_i/dt=\sum_{k=1}^{n} q_{ki}C_{ki} - \sum_{i=1}^{n} q_{ik}C_{ik}+q_{ri}C_{ri}-q_{di}C_{di}-\lambda_a V_i C_i$$

where

i, k indexes of particular compartments,

n total number of the compartments,

C_i, C_k isotope tracer concentration in the i-th and k-th compartment respectively, i.e. variables to be sought,

V_i water volume (storage) of i-th compartment,

q_{ik}, q_{ki} water flow rates from the i-th into k-th compartment and vice versa respectively,

q_{ri} recharge flow rate to the i-th compartment from the external systems (input, a precipitation share used to recharge the i-th compartment),

q_{di} discharge flow rate of the i-th compartment to external systems (output, discharge into a main drain of the watershed, i.e into a creak, river, lake, etc.),

λ_a isotope tracer decay constant.

To this equation some initial conditions concerning the water storages and tracer concentrations in every compartments must be added, for instance:

(3) $V_{oi}=V_i(t=0)$,

(4) $C_{oi}=C_i(t=0)$,

Generally speaking, the set of the model equations (1) and (2) appear to be non-stationary ones as all variables incorporated are depended on time.

Opening the derivative in the right side of (2) gives

$$(5)\quad V_i dC_i/dt+C_i dV_i/dt=\sum_{k=1}^{n} q_{ki}C_{ki} - \sum_{i=1}^{n} q_{ik}C_{ik}+q_{ri}C_{ri}-q_{di}C_{di}-\lambda_a V_i C_i$$

Further substituting dV/dt from (1) into (5) yields (here and farther the summation indexes are omitted as they have been fixed)

$$(6)\quad V_i dC_i/dt+C_i\left[\Sigma q_{ki} - \Sigma q_{ik}+q_{ri}-q_{di}K\right] = \Sigma q_{ki}C_{ki} - \Sigma q_{ik}C_{ik}+q_{ri}C_{ri}- -q_{di}C_{di}-\lambda_a V_i C_i$$

where

$$(7)\quad V_i=\int_o^t \left(\Sigma q_{ki} - \Sigma q_{ik}+q_{ri}-q_{di}\right)dt + V_{oi}$$

Thus, the general set of the basic model differential equations has been get.

It is seen that an analytical solution to such a set is not so easy to be directly solved especially if it is taken into account a real dependence of input functions q_{ri} and interrelation functions q_{ki} and q_{ik} on the current time.

Generally, there might be used any relevant known calculation techniques. Due to a huge complexity the general solution to this problem in an explicit form is practically impossible to be given in this short communication. There is a reason to give here some approaches how this solution could be get and demonstrate some illustration of more simplified cases.

The first simplification can be made assuming that water and an isotope tracer in each compartment is fast and completely mixed less during a time period which is to be much less than a mean residence time of water and the component respectively. This is so-called a perfect mixing model (PMM).

In that case, a current output concentration in any i-th compartm is to be equaled to that inside of this compartment. It means that

(8) $C_{ki}(t)=C_k(t)$

(9) $C_{ik}(t)=C_i(t)$

(10) $C_{di}(t)=C_i(t)$

Using this relationships in (6) gives us

(11) $$V_i dC_i/dt+\left(\Sigma q_{ki} - \Sigma q_{ik}+q_{ri}-q_{di}\right)C_i = \Sigma q_{ki}C_k - \Sigma q_{ik}C_i+q_{ri}C_{ri}- -q_{di}C_i-\lambda_a V_i C_i$$

or

(12) $$V_i dC_i/dt+\Sigma q_{ki}C_i-\Sigma q_{ik}C_i+q_{ri}C_i-q_{di}C_i = \Sigma q_{ki}C_k - \Sigma q_{ik}C_i+q_{ri}C_{ri}- -q_{di}C_i-\lambda_a V_i C_i$$

where the similar members are underlined. Further rearranging yields

(13) $$V_i dC_i/dt+\Sigma q_{ki}C_i+q_{ri}C_i = \Sigma q_{ki}C_k +q_{ri}C_{ri}-\lambda_a V_i C_i$$

or

(14) $$V_i dC_i/dt + \left(\Sigma q_{ki} + q_{ri} + \lambda_a V_i\right)C_i - \Sigma q_{ki}C_k = q_{ri}C_{ri}$$

Nevertheless, this variant of the general equation has yet been stayed non-stationary one and indefinite relating to the water storages $V_i(t)$ depended on current time. Its solution is principally possible if there is data on current temporal variations of water flow rates related (see eq (7)).

Making the second simplification we assume now that temporal changes of all water storages V_i are negligible compared with their mean averaged values, i.e. it is supposed that definitely or, as less approximately

(15) $V_i(t)=\text{const}$

and consequently

(16) $dV_i/dt=0.$

It is clear that for confined ground water aquifer, this supposition is rather reliable, as to surface reservoirs and unconfined shallow horizons it is likely a strong supposition to be controlled by the experimental data.

In such and only in such a case the general model equation can be convoluted to the stationary one with respect to the storages related:

(17) $$dC_i/dt + \left(\Sigma(q_{ki}/V_i) + q_{ri}/V_i + \lambda_a\right)C_i - \Sigma(q_{ki}/V_i)C_k = (q_{ri}/V_i)C_{ri}$$

Introducing the following constant kinetic coefficients

(18) $\lambda_{ki}=q_{ki}/V_i$

(19) $\lambda_{ik}=q_{ik}/V_i$

(20) $\lambda_{ri}=q_{ri}/V_i$

eq (17) can be rewritten in a new more symmetrical form

(21) $$dC_i/dt + \left(\Sigma\lambda_{ki} + \lambda_{ri} + \lambda_a\right)C_i - \Sigma\lambda_{ki}C_k = \lambda_{ri}C_{ri}$$

Opening sums contained in (21) gives

(22) $$dC_i/dt+\left(-\lambda_{1i}C_1-\lambda_{2i}C_2-\ldots-\left(\lambda_{ii}-(\Sigma\lambda_{ki}+\lambda_{ri}+\lambda_a)\right)C_i-\ldots-\lambda_{ni}C_n\right)=\lambda_{ri}C_{ri}$$

furthermore introducing the following denotation for ii-th kinetic coefficients

(23) $\Lambda_{ii}=\lambda_{ii}-\Sigma\lambda_{ki}+\lambda_{ri}+\lambda_a$

it can be derived a very symmetric and convenient equation

(24) $dC_i/dt-\lambda_{1i}C_1-\lambda_{2i}C_2-\ldots-\Lambda_{ii}C_i-\ldots-\lambda_{ni}C_n=\lambda_{ri}C_{ri}$

Moreover, applying the Laplace transformation to this set of differential equations we can derive a set of algebraic equations which can be solved immediately. Indeed, in the Laplace transformation (24) is written as

(25) $sC_i(s)-C_{oi}-\lambda_{1i}C_1(s)-\lambda_{2i}C_2(s)-\ldots-\Lambda_{ii}C_i(s)-\ldots-\lambda_{ni}C_n(s)=\lambda_{ri}C_{ri}(s)$

where s is a parameter of the Laplace transformation.
One yet rearranging all similar members in (25) we obtain

(25) $-\lambda_{1i}C_1(s)-\lambda_{2i}C_2(s)-\ldots(s-\Lambda_{ii})C_i(s)-\ldots-\lambda_{ni}C_n(s)=C_{oi}+\lambda_{ri}C_{ri}(s)$

or in matrix form

(26) $\left|\lambda_{ki}\right|\left|C_k(s)\right| = \left|C_{oi}+\lambda_{ri}C_{ri}(s)\right|$

Thus, we have obtained a matrix presentation of eq (17) in term of the Laplace transformation by Vi=const..

In order to get a solution to this matrix equation one has to multiply both its side by the inverse matrix of the kinetic coefficient matrix as follows

(26) $\left|\lambda_{ki}\right|^{-1}\left|\lambda_{ki}\right|\left|C_k(s)\right| = \left|\lambda_{ki}\right|^{-1}\left|C_{oi}+\lambda_{ri}C_{ri}(s)\right|$

As a product of the direct and inverse matrix is a unit matrix the final solution in the Laplace form is given by

(27) $\left|C_k(s)\right| = \left|\lambda_{ki}\right|^{-1}\left|C_{oi}+\lambda_{ri}C_{ri}(s)\right|$

It is seen that to reach the final solution to the problem we have

- to assume an explicit dependence of the input concentrations $C_{ri}(t)$ on time and find out their Laplace presentations as well,
- to define or nominate all kinetic coefficients λ_{ri} and λ_{ki} rememberi that ii-th values are determined by the eq (23),
- to construct a matrix equation in accordance with (27) which represent a solution to be sought in the laplace form, then
- to make an inverse Laplace transition to the explicit original functions being sought.

It is known that the tritium concentration as well as precipitation flow rate recharge q_{ri} can be represented as a periodical functions versus current time t. In the simplest case, it might be assumed that there exist an annual periodicity in form

(28) $q_{ri}(t)=q_{ai}\sin\omega t + \overline{q_{ri}}$

(29) $C_{ri}(t)=C_{ai}\sin(\omega t+\phi_i) + \overline{C_{ri}}$

where q_{ai} and C_{ai} represent amplitudes of the water flow rate and isotope tracer concentration changes, $\overline{q_{ri}}$ and $\overline{C_{ri}}$ reflects mean annual values of the water flow rate and tritium concentration in the i-th compartment external input respectively, furthermore, Φ_i denotes a phase deviation angle of the concentration input function relatively to the flow rate function which is considered as synchronizing one.

Thus, the total input mass flow rate of tritium is

$$(30)\quad q_{ri}(t)C_{ri}(t) = (q_{ai}\sin\omega t + \overline{q_{ri}})(C_{ai}\sin\omega t + \overline{C_{ri}}) =$$

$$= q_{ai}C_{ai}\sin(\omega t+\Phi_i)\sin\omega t + \overline{q_{ri}}C_{ai}\sin(\omega t+\Phi_i) + q_{ai}\,\overline{C_{ri}}\sin\omega t + \overline{q_{ri}}\,\overline{C_{ri}} =$$

$$= q_{ai}C_{ai}\left[(1/2)[\cos(\omega t+\Phi_i-\omega t)-\cos(\omega t+\Phi_i+\omega t)\right] + \overline{q_{ri}}C_{ai}\sin(\omega t+\Phi_i) +$$

$$+ q_{ai}\,\overline{C_{ri}}\sin\omega t + \overline{q_{ri}}\,\overline{C_{ri}} = q_{ai}C_{ai}\left[(1/2)[\cos\Phi_i-\cos(2\omega t+\Phi_i)\right] +$$

$$+ \overline{q_{ri}}C_{ai}\sin(\omega t+\Phi_i) + q_{ai}\,\overline{C_{ri}}\sin\omega t + \overline{q_{ri}}\,\overline{C_{ri}} =$$

$$= q_{ai}C_{ai}\left[(1/2)[\cos\Phi_i-\sin(90^\circ+2\omega t+\Phi_i)\right] + \overline{q_{ri}}C_{ai}\sin(\omega t+\Phi_i)$$

$$+ q_{ai}\,\overline{C_{ri}}\sin\omega t + \overline{q_{ri}}\,\overline{C_{ri}}$$

It is completely evident that

$$(31)\quad \overline{q_{ri}(t)C_{ri}(t)} = \overline{q_{ri}}\,\overline{C_{ri}})$$

Thus, the last member in the right side matrix in eq (27) can explicitly be written in form

$$(32)\quad \lambda_{ri}C_{ri}(t) = (q_{ai}/V_i)C_{ai}\left[(1/2)[\cos\Phi_i-\sin(90^\circ+2\omega t+\Phi_i)\right] +$$

$$+ (\overline{q_{ri}}/V_i)C_{ai}\sin(\omega t+\Phi_i) + (q_{ai}/V_i)\,\overline{C_{ri}}\sin\omega t + (\overline{q_{ri}}/V_i)\,\overline{C_{ri}}$$

The Laplace transformation can be taken from the standard Laplace transformation tables and used to solve the matrix eq (27).

Even at the present level of consideration, it is evident that output concentrations of an isotope tracer exiting a hydrogeological system with the atmospheric precipitation can consist of several periodical components having different phase angle deviations each of other and different amplitude of variations caused by

- non-synchronized variations of recharge water flow rates, on one hand and isotope tracer concentration variations, on another hand,
- differences of residence times of water and tracer in particular compartments of the system under interest, the latter fact has already been demonstrated in recent publications [1,2,3].

The superposition of all these sinusoidal components can be analyzed in the future on the base of the approach developed and relative long-term observational data of both isotope and common hydrology character.

By the way, in the publications mentioned obove, some total solutions to a stationary one compartment model with a sinusoidal tracer input was given and analyzed.

1. Kusakabe M. et al., J. Geoph. Res..vol. 75, No. 30., (1970), 5941-5950.
2. Isotope Techniques in Ground Water Hydrology, 1974. IAEA, (1974), Vol. 1, 399-428. Dubinchuk V.T. et al.
3. Radioisotope Techniques in Engineering Geology and Hydrogeology, (1977), Atomizdat, Moscow, pp. 304, (in Russian)

LIST OF PARTICIPANTS

Adar, E.M.	Jacob Blaustein Institute for Desert Research, Ben-Gurion University of the Negev, Water Resources Center, Sede-Boker Campus, 84993 Israel
Barmen, G.	Lund Institute of Technology, Department of Engineering Geology, P.O. Box 118, S-221 00 Lund, Sweden
Ferronskij, V.	Water Problems Institute, Isotope Hydrology Laboratory, Sadovaja-Chernogriazskaja 13/3, 103064 Moscow, Russian Federation
Herrera, I.	Institute of Geophysics, UNAM, Ap. Postal 22-582, CP 14000, Mexico City, Mexico
Kalin, R.	Laboratory of Isotope Chemistry, University of Arizona, Building 77, Gould-Simpson Building, Tucson, AZ 85721, United States of America
Limic, N.	Department of Physics, Energy and Applications, Ruder Bošković Institute, P.O. Box 1016, 41001 Zagreb, Croatia
Maloszewski, P.	Institute of Hydrology, Ingolstaedter Landstrasse 1, D-85758 Neuherberg, Germany
Moreno, L.	Chemical Engineering Deparment, Royal Institute of Technology, Teknikringen 26, S-100 44 Stockholm, Sweden
Voss, C.I.	US Geological Survey, Water Resources Center, 431 National Center, Reston, VA 22092, United States of America
Yurtsever, Y. *(Scientif Secretary)*	Division of Physical and Chemical Sciences, International Atomic Energy Agency, P.O. Box 100, A-1400 Vienna, Austria
Zuber, A.	Institute of Nuclear Physics, Radzikowskiego 152, 31-342 Cracow 23, Poland